Aspects of the sedimentology, diagenesis and palaeomagnetism of the Capitan shelf margin (Upper Permian), Guadalupe Mountains, West Texas/New Mexico, U.S.A.

by

Gillian Darke

A thesis submitted for the degree of

Doctor of Philosophy

at the

University of Newcastle upon Tyne

Geology Department

January 1990

This thesis is dedicated to my Mamgu and Dadcu

my parents

and Bob.

Table of contents page

Chapter 6: Discussion

List of tables:

List of figures

Chapter 3

Acknowledgements

I would like to thank my supervisors, Gill Harwood and Don Tarling, for originally conceiving the project and asking me to do the research, along with Kevin Schofield and Max Coleman of BP.

Several people have helped with the practical aspects of this research: David Collinson, Marie Summersby, Trond Torsvik and Bill Rutherford helped with the 'magnetic' side of things; Brian Richardson and Len Rhodes helped on the 'geology' side of things. Particular help came from Trevor Whitfield who made most of the thin sections and Pete Hill who assisted with electron microprobe analysis at Edinburgh. Christine Jeans improved my understanding and skill in producing visual-aids/diagrams and Elizabeth Walton and Ann Thwaites helped with many administrative aspects. The burden of typing most of the manuscript was relieved by John and Betsi Darke.

My understanding of the magnetic properties of rocks and their uses, developed with the benefit of discussions with Bill Owens, Alan Stephenson, Pete Turner, Helen Turnell, George Thompson and Don Tarling. Discussions with Gill Harwood, Alan Kendall, Kevin Schofield, Max Coleman and Sal Mazzullo, as well as many other students of the Capitan 'reef complex', helped advance my understanding of the sedimentology and diagenesis of the Capitan shelf margin and the evolution of the Delaware Basin. I am also grateful to Mitch Harris and George Grover of Chevron for assembling students of the Capitan reef complex at the thirteenth SEPM core workshop in San Antonio, 1989, and for permission to use a photograph from that workshop. I also thank Rick Sarg for the loan of a rock sample.

This work would not have been possible without generous funding from BP, and the help and co-operation of the Guadalupe Mountains and Carlsbad Caverns National Parks Service, particularly John Roth and Ron Kerbo. Fieldwork would have been more difficult and more dangerous, and considerably less fun, without the cheerful assistance and company of Bob McBlane and who is my ally.

I declare that the contents of this thesis have not previously been presented for a degree at this, or any other, University.

Gillian Darke

Geology department

The University

Newcastle upon Tyne

Abstract

Petrographic, palaeomagnetic and outcrop studies of limestones and dolostones from the Capitan reef complex, Guadalupe Mountains, west Texas and New Mexico, have provided time constraints on diagenetic events, and demonstrated the crucial role of calcium sulphate in the history of these strata. This thesis is divided into six chapters: chapter 1 gives an introduction to the scope of the study and the geology of the study area; chapters 2, 3, 4 and 5 give the results and interpretations of sedimentological, diagenetic, magnetic fabric and palaeomagnetic/magnetic mineralogy studies respectively. Chapter 6 presents a discussion of the interplay of these results and interpretations, and conclusions.

Emplacement of anhydrite in the strata of the Capitan shelf margin, took place at an early stage, post-dating syn-depositional marine cementation by aragonite and high-magnesian calcite, and minor syn-sedimentary dolomitisation. Desiccation of the Delaware Basin in late-Upper Guadalupian times exposed the Capitan shelf margin. Consequently, evaporatively-concentrated brines migrated from the shelf into the Delaware Basin *via* the strata of the Capitan shelf margin. Anhydrite cement occluded all porosity and fractures in the strata of the Capitan shelf margin which remained after marine cementation, and this cementation was accompanied by fabric-selective dolomitisation. Continued movement of brines during early burial, due in part to compactional dewatering of the Castile Formation, caused the growth of replacive anhydrite and concomitant pervasive, fabric-destructive dolomitisation, particularly in the lower foreslope facies.

Bacterial sulphate reduction accompanied the input of meteoric water into the Capitan shelf margin during periods of uplift and erosion, and caused the calcitisation of some anhydrite and the growth of minor diagenetic magnetite, pyrrhotite and other sulphide minerals. These *magnetic* minerals have been palaeomagnetically dated and indicate Jurassic and late-Cretaceous to Tertiary ages. These ages are consistent with the periods of uplift and erosion indicated by the burial history of these strata.

Rapid uplift and faulting, associated with the development of the basin-and-range province of the southwestern USA, caused the wholesale dissolution of anhydrite, and established a meteoric aquifer in the Capitan shelf margin. Significant volumes of calcite spars were precipitated into the pore space and fractures which remained after the dissolution of anhydrite. Oxidation of most sulphides to haematite and the development of new magnetic phases *i.e.*, goethite and haematite, occurred during this stage. These magnetic minerals have been dated palaeomagnetically, and indicate times of formation of 80 Ma to present-day. These ages are consistent with the period of rapid uplift and erosion which formed the Guadalupe Mountains during late-Cretaceous times to the present day.

Chapter 1: Introduction

"and if we succeed in recovering this buried landscape, and wish to communicate to others the pleasure it gives us, how difficult it is to do so without intruding the unpalatable jargon of the geologist or the economic historian or some other learned trade." W.G. Hoskins; 'The making of the English landscape', published by Hodder and Stoughton.

1.1 Introduction

The overall aim of this research project was to establish the relationships, if any, between the magnetic properties of some carbonate rocks and their geological history. In order to do this most effectively certain variables had to be excluded from further consideration. For this reason, a study area was chosen in the so-called 'Capitan Reef Complex, because i. there is excellent stratigraphic control and the strata are well-exposed (King, 1948); ii. this area has had an uncomplicated structural history; iii. this area has not been affected by glaciations and consequent weathering processes; iv. the climate is semi-arid and the effects of weathering are not as great as for rocks from a humid, temperate climate; v. these strata are geologically related to an area which produces economically significant hydrocarbons and for this reason is relatively well-known (King, 1948; Hileman and Mazzullo, 1977; section 1.2).

The project was subdivided into several parts. The first was to determine whether these carbonate rocks posessed any magnetic fabric and to determine whether these rocks posessed any natural remanent magnetism. The second part was to examine the sedimentological and diagenetic processes that had affected these rocks and determine the diagenetic history. The third and final part was to relate the geological processes which had controlled the development of the magnetic and geologic features observed, by integrating the information derived from the magnetic and geological studies.

Despite the fact that magnetic fabric analysis had proved a useful tool in many other rocks, it became clear, as the investigations proceeded, that a magnetic fabric was not well-developed/present in *these* rocks (chapter 4). Furthermore, it became clear that an investigation of the geological significance of magnetic fabric would not be possible unless the properties of the minerals which were contributing to the fabric were more clearly understood and quantifiable. More specifically, the intrinsic properties of many rock-forming minerals, the relative contributions of dia-, para- and ferro-magnetic minerals to the net fabric and the relative importance of magnetic,

kinetic, gravitational and hydraulic forces to the net fabric, were either not well-established or were not quantifiable and therefore could not be separated (Owens and Rutter, 1978; Collinson, 1983). Thus, in order to proceed with understanding the geological controls on magnetic fabric development, some further studies of the *intrinsic* properties of rock-forming minerals were considered pre-requisite. However, initial studies of thermally enhanced fabrics and acquisition of isothermal remanence (Stephenson *et al.*, 1986) by these rocks gave more promising results (chapter 4). Furthermore, it became clear that study of the palaeomagnetic properties and magnetic mineralogy of these rocks was a potentially useful tool, and could constrain aspects of the timing of the evolution of the Delaware Basin as long as the diagenetic history could be related to the timing of acquisition of the natural remanent magnetism. Consequently, after considerable time had been devoted to examination of the magnetic fabric of these rocks, the emphasis of the research changed and became more *geologically* orientated *i.e.*, towards the relationships between magnetic mineralogy and palaeomagnetism and the diagenetic history of the Capitan shelf margin.

Palaeomagnetic studies have been carried out on carbonates, particularly limestones, since the initiation of palaeomagnetism in the 1940's, because biostratigraphic and palaeogeographic controls can be independently obtained from limestones. However, in-depth studies of the rock-magnetic and palaeomagnetic properties of carbonates were prohibited by the lack of technology sufficiently sensitive to be able to measure the typically low natural remanent magnetisations of limestones, until the late 1970's when the advanced spinner and cryogenic magnetometers were developed (Goree *et al.*, 1976). Since these technological advances, many palaeomagnetic studies have been undertaken (see Lowrie and Heller, 1982, for a general review). Despite these studies much remains to be investigated, particularly concerning the post-depositional, biological and diagenetic processes which affect the origins of the magnetic particles and their magnetisations in sedimentary rocks. Such fundamental aspects have often been neglected by palaeomagnetists and the magnetic minerals were commonly assumed to be detrital or their origins simply not considered at all. Until recently, it has been a basic assumption that, once acquired, the natural remanence and the magnetic mineralogy remains unchanged. In sedimentary rocks, it is critical to ascertain when and where the remanence was acquired and whether the remanence and/or the mineralogy has been changed since deposition *e.g.*, by processes such as bioturbation, or during diagenesis.

The degree of grain reorientation as a result of bioturbation has been investigated (Karlin and Levi, 1983; Ellwood, 1984). Blakemore (1975) reported the occurrence of a bacterium in a salt marsh environment which contained within its cell wall several

ultra-fine-grained magnetite crystals. Since then, many other workers have reported and investigated the occcurrence of these magnetotactic bacteria in many sedimentary environments. However, the environmental factors controlling their distributions are still not well known (Blakemore 1975; Frankel *et al.*, 1979 and Stolz *et al.*, 1986). Lovley *et al.*,(1987) reported bacteria which synthesised extracellular magnetite under anaerobic conditions and interest and research into the occurrence of biogenic magnetite is growing. The implications for the origins of magnetic particles in comparable ancient sediments are huge and, as yet, few studies have been undertaken in ancient rocks (Chang and Kirschvink, 1987; McCabe *et al.*, 1983; Horton *et al.*, 1984 and Blakemore *et al.*, 1985; Stolz *et al.*, 1987).

Karlin *et al.* (1987) undertook some integrated geochemical and magnetic work on a sediment core from the East Pacific Rise to investigate early diagenetic processes. Their magnetic and chemical results taken together suggest that fine-grained magnetite is precipitating at the top of the iron reduction zone (about 20 cm deep within the sediment). This observations is consistent with microbially mediated extracellular magnetite production (Lovely *et al.*,1987).

The timing of the diagenesis of detrital iron oxides (Turner and Archer, 1975; Turner and Ixer, 1977) and the diagenesis of ferroan carbonates (Elmore *et al.*, 1985; Loucks and Elmore, 1986) has been constrained by palaeomagnetic dating of the haematite/goethite which formed as a consequence of this diagenesis. Bacterial or thermo-chemical sulphate reduction may cause the formation of sulphide minerals and magnetite which may acquire a remanence and be dated palaeomagnetically (*e.g.*, Vaughan and Turner, 1980). Pyrrhotite (and pyrite) have also been reported in cap-rock associated with salt domes and anhydrite (McManus and Hanor, 1987; Sassen *et al.*, 1987; Gose and Kyle, 1988). In both instances the sulphide formation is related to bacterial sulphate reduction. Pyrite related to thermochemical sulphate reduction, is reported from Upper Smackover carbonates (Heydari *et al.*, 1988) due to sulphate reduction and comncomitant hydrocarbon oxidation.

Other later diagenetic factors may cause the formation of secondary magnetic minerals capable of carrying a remanence. Carbonates which contain hydrocarbons or bitumen may have associated magnetite and magnetite associated with bitumen has been observed in Silurian reef carbonates (McCabe *et al.*,1985; McCabe *et al.*,1987) Similar associations are reported from the Permian Phosphoria Formation of Wyoming where magnetite formation is dated as Cretaceous (Benthien and Elmore, 1987). Other magnetic minerals such as pyrrhotite (Reynolds *et al.*, 1985) and haematite (Cisowski *et al.*, 1987 and Benthien and Elmore, 1987) have also been reported as accessory in the hydrocarbon association. Several possibilities exist as to the origin of these

minerals. Bitumen is commonly derived from the microbial degradation of liquid crude oil and it has been suggested (Elmore *et al.*, 1987; McCabe *et al.*, 1987) that the magnetite results from microbial activity though no direct evidence has been found. However the discovery of a dissimilatory iron-reducing anaerobic bacterium which produces magnetite as a metabolic by-product (Lovley *et al.*, 1987), and the discovery that this bacterium can oxidise an aromatic hydrocarbon anaerobically (Lovley *et al.*, 1989), makes this proposed association more plausible. Other alternatives are the oxidation of iron sulphides such as framboidal pyrite or the reduction of precursor oxides, or the release of iron from iron-rich carbonate phases as a result of diagenetic changes; (McCabe *et al.*, 1987).

Thus, the use of palaeomagnetic studies when integrated with sedimentological and diagenetic studies had been demonstrated by previous studies. However, no similar studies had been undertaken in an area where several facies belts were juxtaposed adjacent to a major hydrocarbon-producing basin, such as are exposed in the Guadalupe Mountains. Furthermore, no detailed examination of these facies belts had been undertaken, although particular facies had been examined *e.g.*, the reef facies (Yurewicz, 1977; Schmidt, 1977), the back reef facies (Sarg, 1977; Neese and Schwartz, 1977) and the foreslope facies (Reeckmann, 1985).

This thesis is subdivided into five chapters, following this introductory chapter. Chapters 2 and 3 concern the sedimentology and diagenesis respectively; chapter 4 concerns magnetic fabric, and chapter 5 concerns the magnetic mineralogy and palaeomagnetism of these rocks. The sixth and final chapter integrates the information and interpretations derived from the studies reported in the previous four chapters, and relates them to the evolution of the Guadalupe Mountains.

1.2 Geological setting

The Guadalupe Mountains lie across the New Mexico/West Texas border in the south-western United States of America (fig. 1.1) and are one of the eastern-most expressions of 'basin and range' activity. Excellent outcrops of the so-called 'Capitan Reef Complex' (Upper Permian) are exposed, particularly on the eastern escarpment of the mountains, where canyons dissect the Capitan shelf margin. The study area was located in this region (fig. 1.2) and in McKittrick Canyon (104.8°W, 32°N) in particular.

Palaeogeography

Regional gravity and magnetic surveys indicate that the break-up of North America in the late Precambrian caused rifting of the crust in the area which is now West Texas and New Mexico (Erdlac, 1984). This rifting controlled the development of the Permian Basin which in turn comprises the Delaware, Midland and Val Verde basins (fig. 1.3). The Capitan Reef developed around the margins of the Delaware Basin (fig. 1.4) in Guadalupian times (258-251 Ma). During this time, this part of the North American continent had an equatorial position, latitude 5° North (Scotese *et al.*, 1979). The carbonate strata of the Capitan reef, foreslope and back reef facies, form a very narrow belt several 100 km in length and 10 - 20 km in width, in an area dominated by siliciclastics and evaporites. This study concentrated on strata of upper-Middle and Upper Capitan age *i.e.* Upper Guadalupian (fig. 1.6).

Burial history (fig. 1.5)

During most of the Permian there was little structural activity in the Permian Basin area and broad carbonate shelves developed on structural highs. In Guadalupian times the Capitan Reef developed and prograded until reef growth terminated with the onset of evaporite-dominated conditions in the Ochoan (see Garber *et al.* (1989) and section 1.3). During the Triassic continental conditions continued with deposition of further evaporitic and clastic red bed sequences causing further burial of the Guadalupian strata. The opening of the Gulf of Mexico and the Tethys seaway in the Jurassic caused a major palaeogeographic change which resulted in the northward drift of the Permian Basin area of the North American craton from its equatorial position. Regional subsidence stopped in the Permian Basin at around this time.

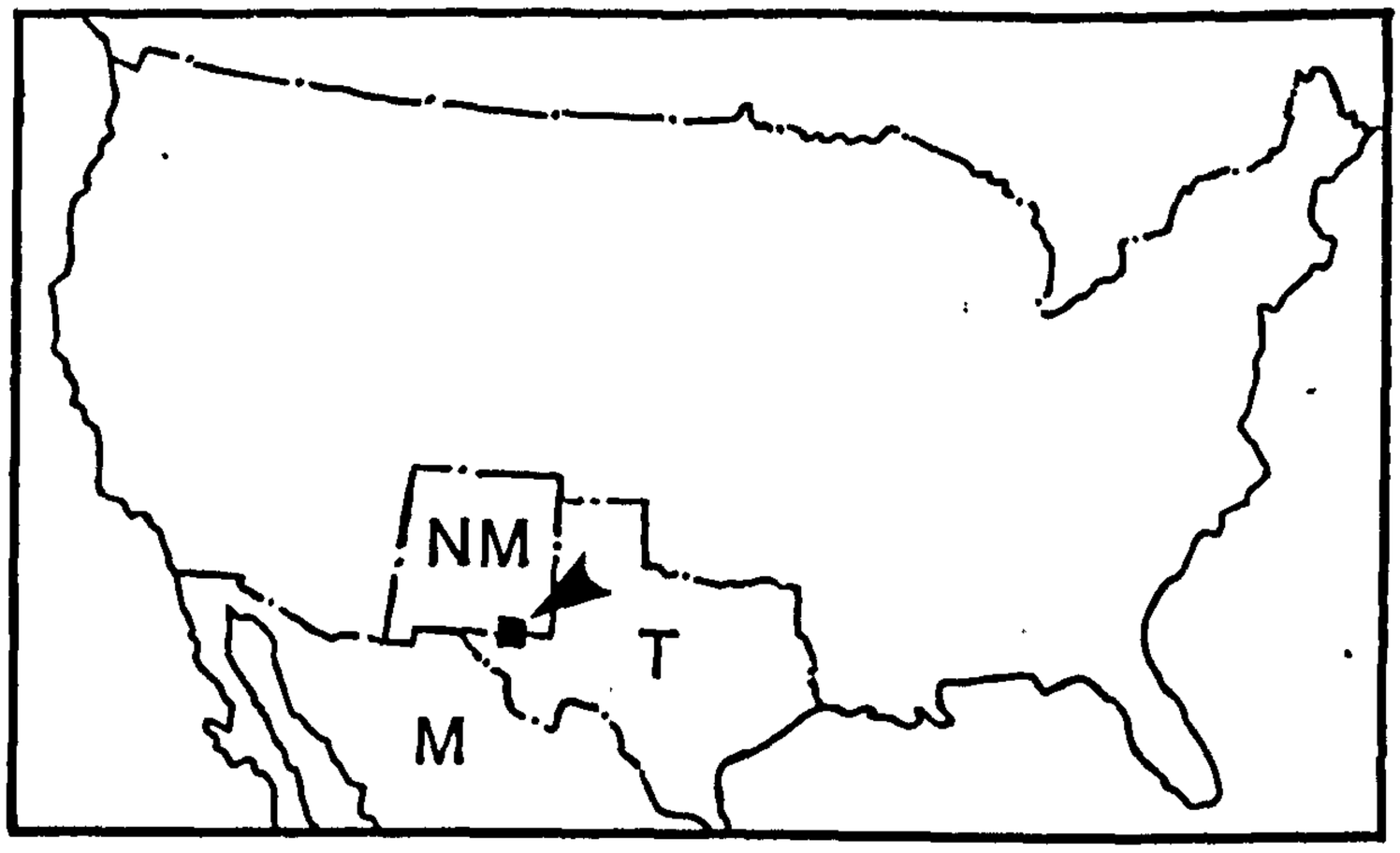

fig. 1.1 Location map of the Guadalupe Mountains in West Texas/New Mexico, south - western USA.

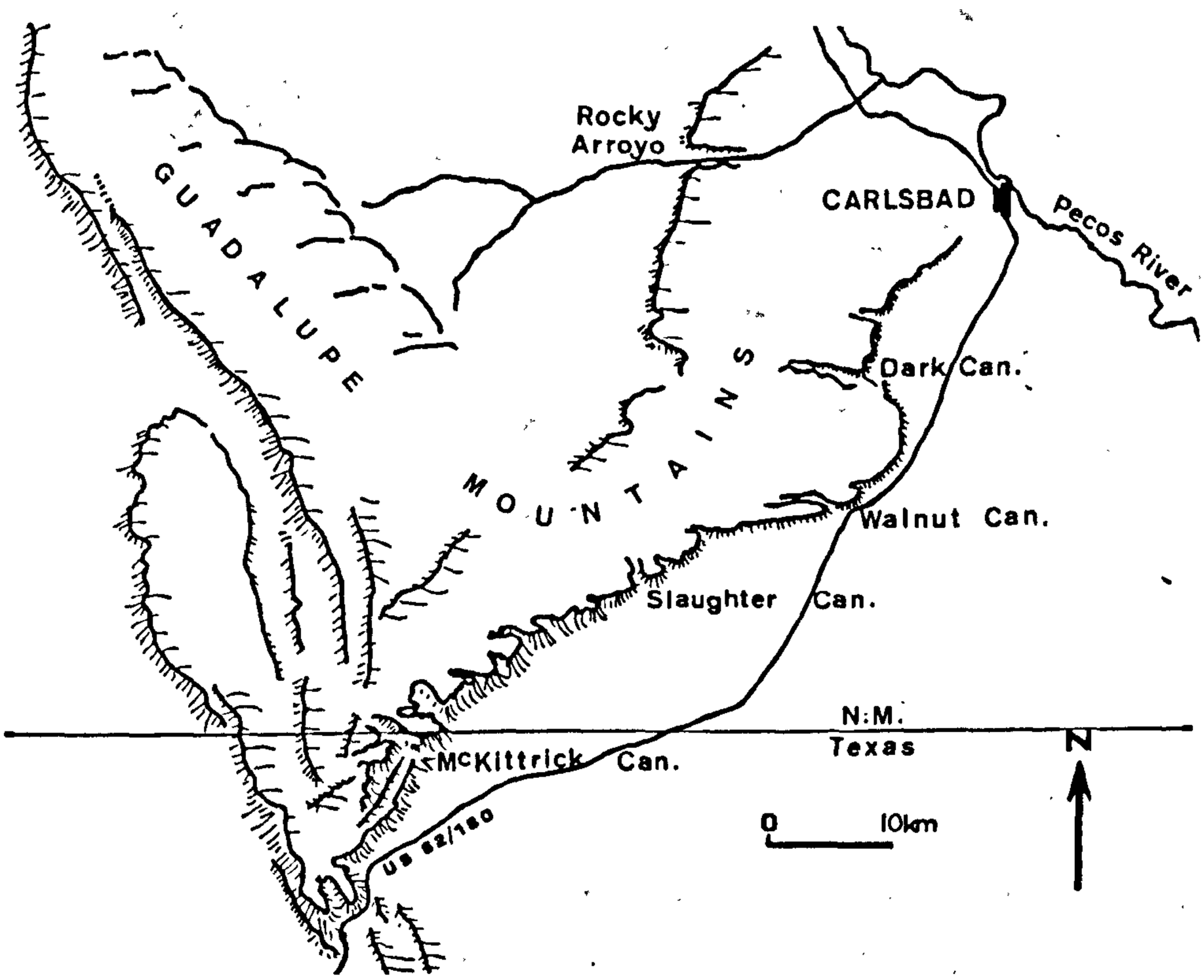

fig.1.2 Map showing the fault-controlled V-shape of the uplifted fault block of the Guadalupe Mountains. The block tilts at 5° NE causing the reef escarpment to dip gradually into the subsurface (from King, 1948). The locations of the principal canyons which dissect the eastern escarpment are shown, as well as the main highway US62/180.

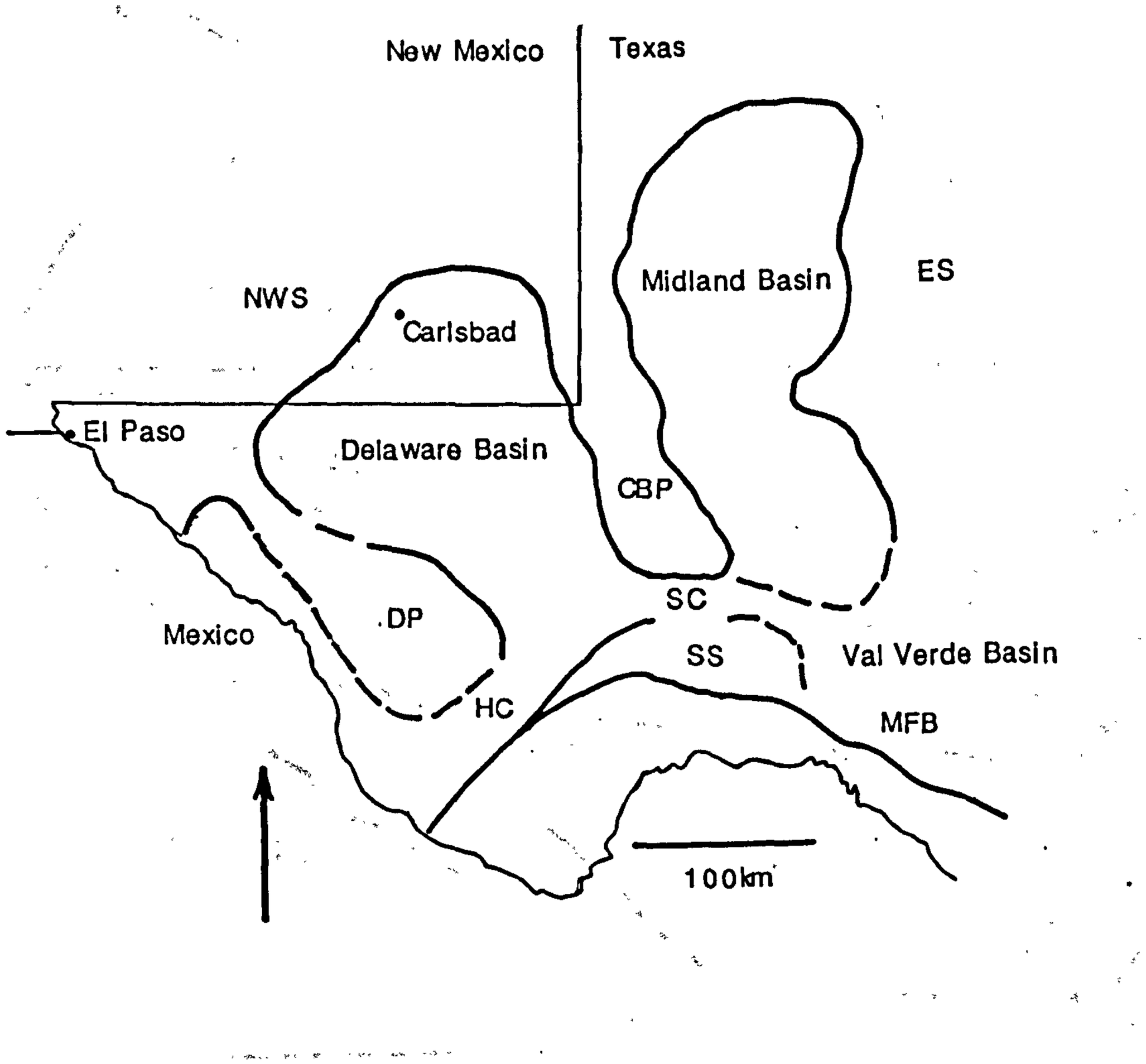

fig. 1.3 Map showing the main structural features of the Permian Basin which in turn comprises the Delaware, Midland and Val Verde Basins. **CBP** Central Basin Platform; **DP** Diabolo Platform; **NWS** North-Western Shelf; **ES** Eastern Shelf; **SS** Southern Shelf; **HC** Hovey Channel, **SC** Sheffield Channel; **MFB** Marathon Fold Belt; **GM** Guadalupe Mountains; **AM** Apache Mountains; **GI M** Glass Mountains (modified from King, 1948).

fig. 1.4 Map showing the limits of the Capitan Reef around the Delaware Basin. Dashed lines indicate where the reef is in the subsurface; solid lines indicate outcrops in the Guadalupe, Apache and Glass Mountains (modified from King, 1948). The Guadalupe Mountains outcrop across the New Mexico-Texas border.

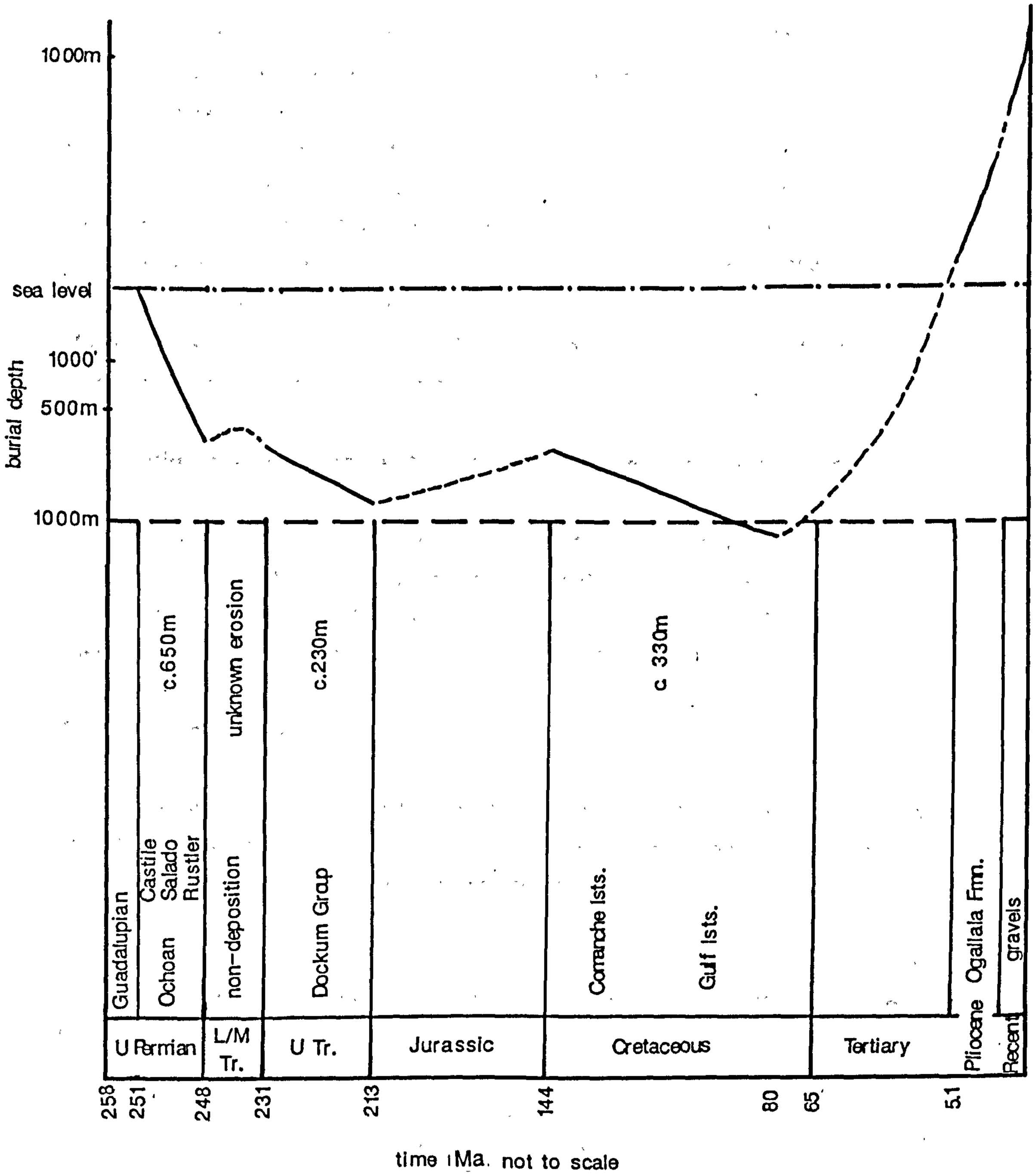

fig. 1.5 Burial curve for the Mid-Upper Capitan strata exposed in the Guadalupe Mountains, illustrating burial during the Upper Triassic and Cretaceous and uplift and erosion during Lower-Middle Jurassic and Tertiary times (Jones, 1953; Harland *et al.*, 1982; Hills, 1984; Horak, 1985 and Mazzullo, 1986).

The first stage of uplift of the Permian Basin took place during Jurassic times, during the Laramide orogeny, due to erosion/non-deposition. This caused erosion of the strata overlying the Guadalupian strata. Deposition resumed during the Cretaceous. A second period of uplift and erosion began in the Miocene, associated with the extensional tectonic regime of the 'basin and range' province which lies to the west of the Guadalupe Mountain region. This movement, possibly along Precambrian lines of weakness (Horak, 1984), may have opened joints which allowed circulation of groundwaters into Permian evaporites (Hills, 1984). These stresses also enhanced hydrocarbon reservoirs by allowing recent migration into newly opened fractures (Horak, 1984) which has significant implications for diagenesis. This tectonic activity uplifted the Guadalupe Mountains as a tilted fault block which dips uniformly at 5° to the north-east, and so forms the characteristic v-shaped plan of the mountains (fig. 1.2).

1.3 Stratigraphy and sedimentary geology of the Guadalupe Mountains

Detailed field studies were first carried out by King (1942, 1948), who investigated the tectonic setting, stratigraphy and sedimentology of the Guadalupe Mountains. Newell *et al.* (1953), Hayes (1964), and Dunham (1972), did further overview studies and established the sedimentological importance of this region.

1.3.1 Stratigraphy

The stratigraphic relationships of the north-western shelf of the Delaware Basin are complex due to the facies variation across the shelf margin and the evolution of the shelf margin through time. These relationships are now well known (fig. 1.6).

Newell *et al.* (1953) first used the term 'Permian Reef Complex' to describe the rocks in the Guadalupe Mountains. This term is now considered "undesirable" (Pray, 1989) because the large amount of research undertaken in the last 30 years or so, has shown that the 'Permian Reef Complex' actually comprises more than one 'complex' of Upper Permian age. The oldest part consists of two carbonate *bank* complexes; the Victorio Peak *bank* of Leonardian age, and the Grayburg-San Andres *bank* of Guadalupian age. The overlying *reef* complex of Mid-Upper Guadalupian age, comprises the Goat Seep *reef* complex and the Capitan *reef* complex. A major unconformity, with relief of several hundreds of feet, separates the bank complex from the reef complex (Pray, 1989). This study concentrates on the Capitan reef complex of Upper Guadalupian age.

Recent subsurface and outcrop studies of the Capitan-age shelf margin (Harris *et al.*, 1988; Garber *et al.*, 1989) subdivide the reef complex into two growth phases

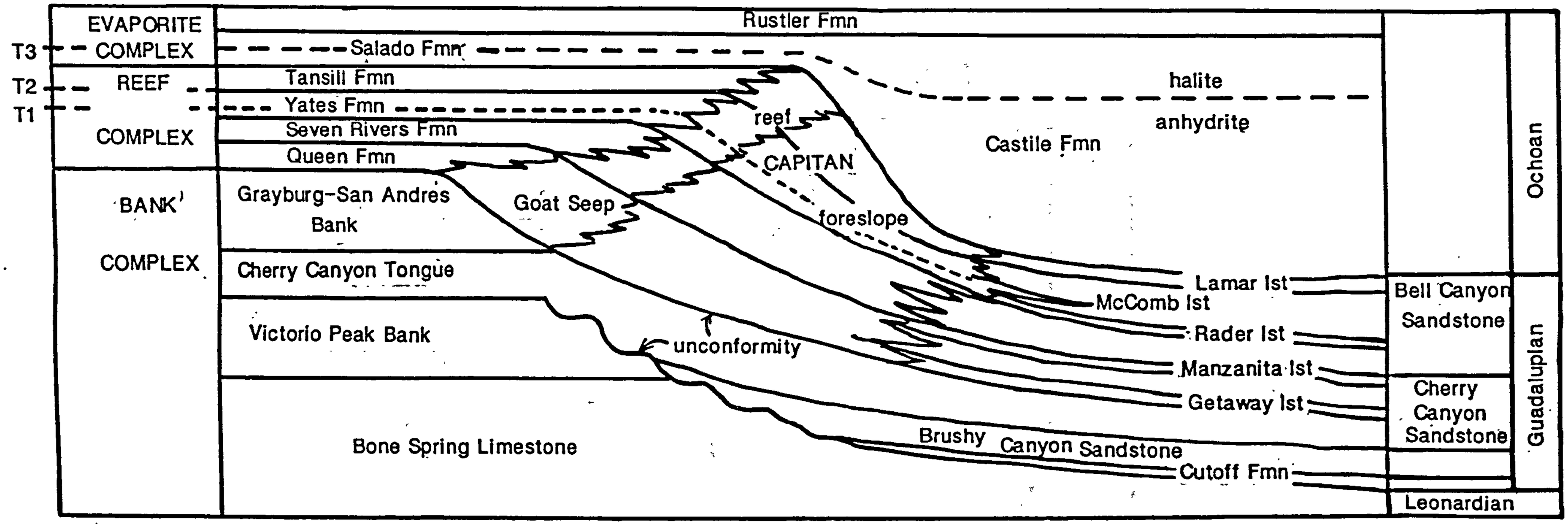

fig. 1.6 Schematic cross-section through the 'Permian Reef Complex' illustrating stratigraphic relationships between shelf to basin facies. T_1 the Yates bentonite correlates with the McComb limestone member (Harris and Grover, 1989); T_2 Yates-Tansill-Lamar correlation (Tyrrell, 1962); T_3 Halite-anhydrite transition in the Salado and Castile formations (Harris and Grover, 1989). Relationships have also been determined from outcrop (Pray *et al.*, 1977 and Pray, 1989).

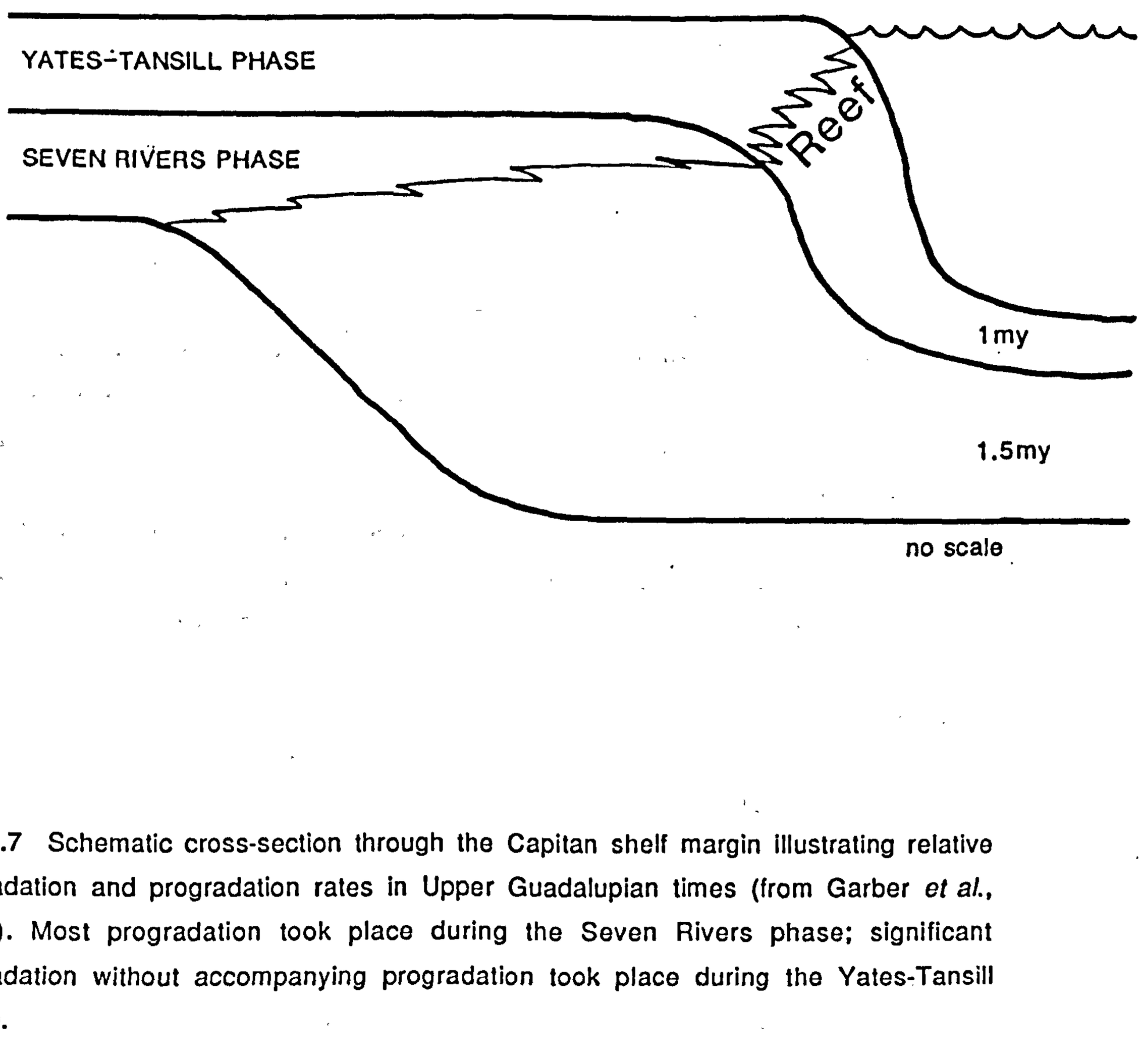

fig. 1.7 Schematic cross-section through the Capitan shelf margin illustrating relative aggradation and progradation rates in Upper Guadalupian times (from Garber *et al.*, 1989). Most progradation took place during the Seven Rivers phase; significant aggradation without accompanying progradation took place during the Yates-Tansill phase.

according to aggradation and progradation rates (fig.1.7). These growth phases were primarily controlled by eustatic fluctuations (Garber *et al.*, 1989). During the first growth phase (Seven Rivers age, 1.5 my duration), more than 80% of the progradation occurred. This was controlled by and associated with abundant deposition of carbonate debris along the basin margin and deposition of virtually all of the allochthonous carbonate debris present in the basin. In the second growth phase (Yates-Tansill, 1 my duration) the style of accretion of the shelf margin was mainly aggradational; yet nearly 70% of the siliclastics of the Bell Canyon Formation were deposited during the time-interval when 75-85% of the aggradation in this phase occurred (Garber *et al.*, 1989). This relationship between carbonate production and siliciclastic deposition contradicts the prevailing concept of reciprocal sedimentation. However, Garber *et al.* (1989) account for this by proposing that carbonate sdimentation took place during sea level high stands, and that carbonate production ceased during low stands when the majority of siliciclastic deposition occurred in the basin.

1.3.2 Terminology

In this study the terms *back reef*, *foreslope*, *basin margin* and *basin* have been used in a palaeogeographic sense, relative to the position of the reef. The term *reef* has been used to describe the massive facies of the Capitan Formation at the seaward margin of the shelf. The term *back reef* is used to describe the rocks landward of the reef. This facies is divided into two areas: i. the area closest to the reef which consists mainly of carbonates and ii. the area further from the reef which is evaporite dominated. The term *foreslope* is used to define the dipping strata seaward of, and topographically below, contemporaneous reef. This facies is divided into two; *upper* and *lower* according to topographic position. The term *basin margin* is used to describe the transitional facies between foreslope and basin facies. The term *basin* is used to define the facies away from the toe of slope. The main characteristics of these facies divisions are summarised in table 1.1. Facies relationships are illustrated in block diagram form (fig. 1.8).

1.3.3 Shelf margin profile

The general profile of the shelf margin in Capitan times is apparent at outcrop as the north-east escarpment of the Guadalupe Mountains is essentially an exhumed palaeotopography. The whole uplifted Guadalupe Mountain block now dips gently to the northeast. The general profile of the shelf margin is clearly visible in the mouths of the

Back reef		Reef	Foreslope		Basin margin	Basin
distal	proximal		upper	Lower		
Evaporitic shelf; mainly emergent, periodic fooding.	Shallow marine shelf; islands and flats; periodic emergence.	Shallow marine, below wave-base.	Submarine talus.	Submarine talus.	Talus/flow deposits.	600m depth, distal flows and slow continuous sedim-entation.
Alternating sand/ siltstones with (dolomitised) mud-wacke- and pack-stones and evaporites.	Alternating fine-grained sand/silt-stones and skeletal/ peloidal (dolomitised) fenestral grainstones. Teepees and pisolites common.	Massive sponge-algal, aragonite cemented bound-stone; some pack-stones and peloidal grainstones. Mainly non-dolo-mitised.	Skeletal/peloidal grainstones, with some reef blocks. Partial-pervasive dolomitisation	Reef boundstone blocks in grain-wackestone matrix Partial-pervasive dolomitisation.	Wacke- and pack-stones, non-dolomit-ised	Alternating beds of mud- and wacke-stones, and silt/ sandstones.

table 1.1 Summary table of the characteristics of the main facies

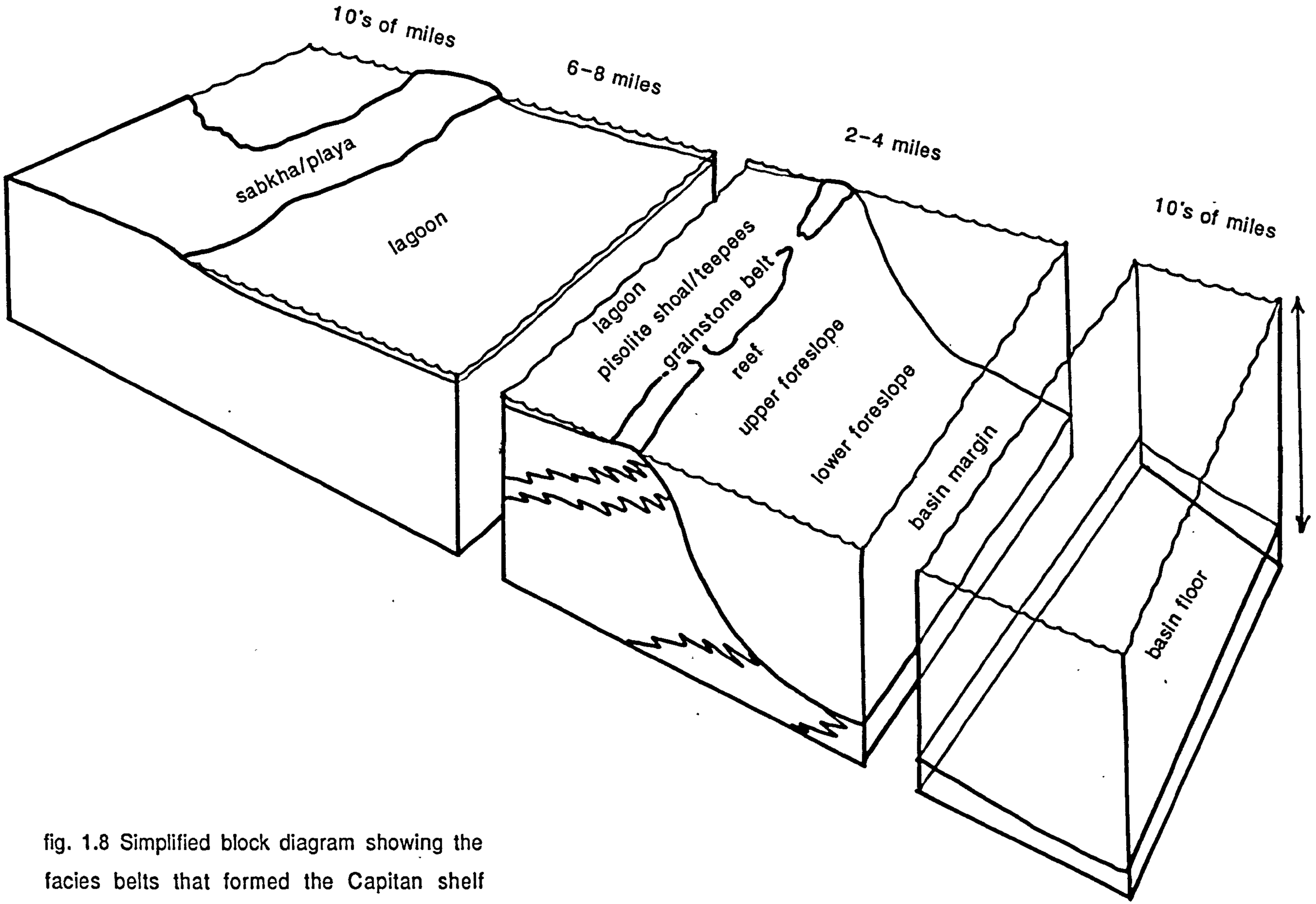

fig. 1.8 Simplified block diagram showing the facies belts that formed the Capitan shelf margin. Modified from Garber *et al.* (1989).

fig. 1.9 Photograph and overlay tracing of the mouth of McKittrick Canyon (north side), showing relationships of back-reef, reef, foreslope and basin facies. The route of the 'Permian Reef Trail' is shown. Stratigraphic boundary interpreted from Tyrrell (1969).

fig. 1.9

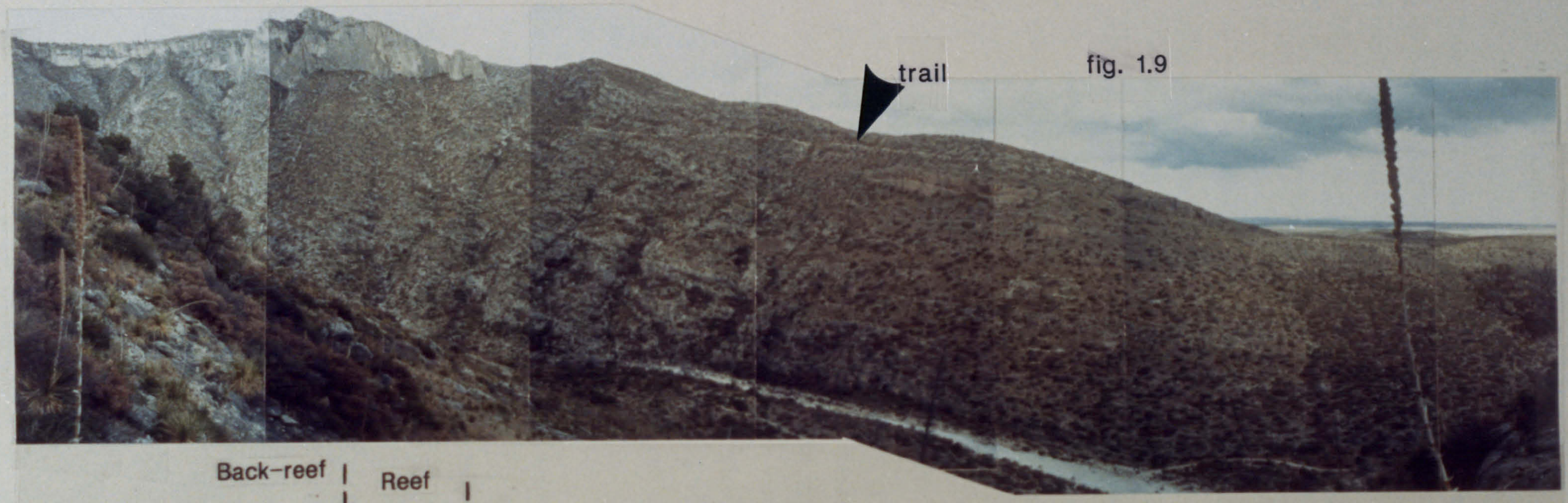
trail

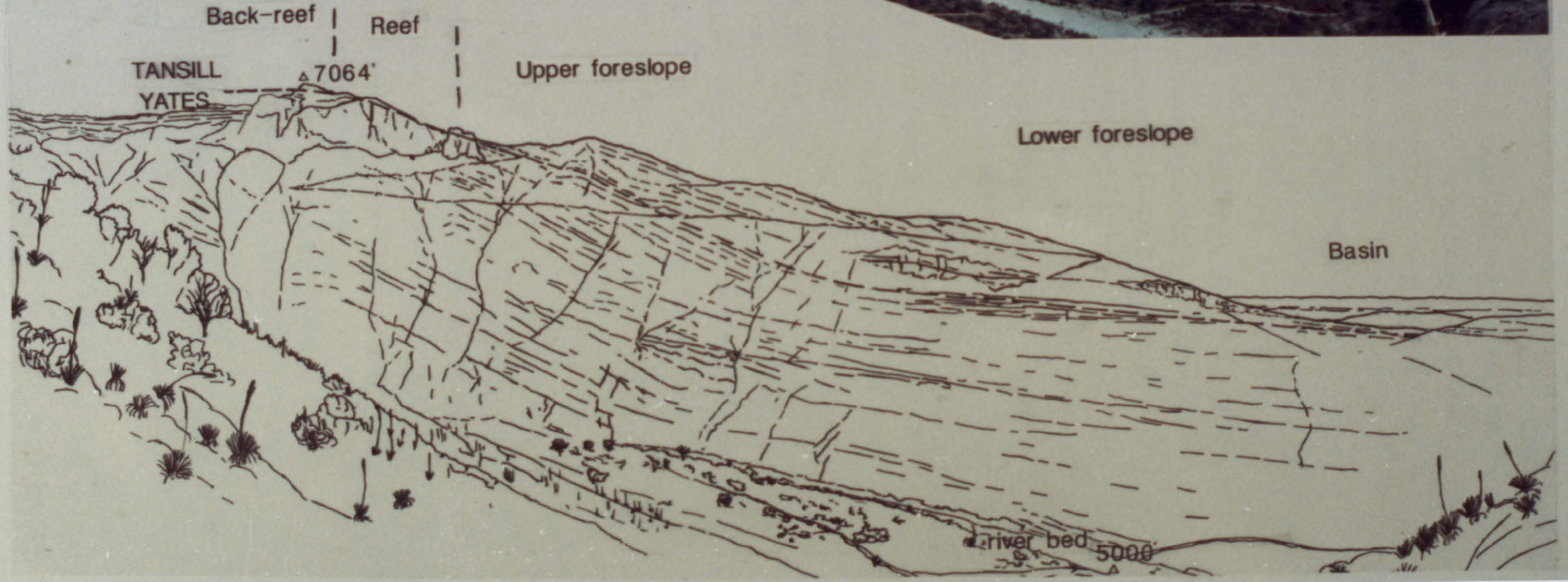
Back-reef
Reef
TANSILL
YATES
7064'
Upper foreslope
Lower foreslope
Basin
river bed
5000'

canyons which dissect the reef front and is particularly well exposed in McKittrick Canyon (fig. 1.9).

There has been much discussion concerning the precise location of the shelf crest. Four profiles have been proposed (Lang, 1937; King, 1948; Newell *et al.* 1953; Handford *et al.*, 1984). The first three are discussed at some length by Cys *et al.* (1977) and Dunham (1972). The four profiles proposed are; 1. the uninterrupted slope model; 2. the barrier reef model; 3 (*a* and *b*), the marginal mound model (fig. 1.10). The main *pros* and *cons* of these various models are summarised below:

Uninterrupted slope model This was first proposed by King (1948) who suggested that the back reef facies had a gentle, unbroken slope from the shoreline to the shelf edge. The reef was at some depth below wave base. This model explains the abundance of silt- and clay-sized particles within the reef and is agreed with by the interpretation of Yurewicz (1976) and Babcock (1974). This model does not explain the occurrence and location of the prominent teepee/pisolite shoal shelfward of the reef nor does it explain the restricted evaporitic facies of the distal backreef.

Barrier reef model This model was first proposed by Newell *et al.* (1953) and invokes the reef as a wave-resistant barrier at sea level composed of sediment- and reef-building organisms. It was influenced by analogies with modern reefs such as the Great Barrier Reef. It adequately explains the restricted circulation of the back-reef and the generation of the foreslope talus. Recent studies by Kirkland and Chapman (1989) on *Dasyclad* algae support this model. However, palaeo-depth estimates made in the reef, the great diversity of the reef biota and the lack of exposure surfaces In the reef are not explained. Neither does it agree with stratigraphic relationships observed at outcrop.

Marginal mound model This model, corroborated by Esteban and Pray (1983), was originally proposed by Lang (1937) and developed by Dunham (1972). Model **3a.** places the shelf crest behind the reef in the teepee/pisolite shoal complex. The restricted back-reef facies and features of the reef, as well as the cyclic nature of the back reef strata, are accounted for. However, this model does not provide a workable hydrologic mechanism for the formation of the teepee/pisolite belt.

Model **3b.** proposed by Handford *et al.* (1984), is a variant of the marginal mound model described above. The shelf crest is placed in the grainstone belt just behind the reef. This grainstone belt is proposed as being narrow, possibly with breaks in it. This model explains all the features described in 3a and also provides a hydrologically workable

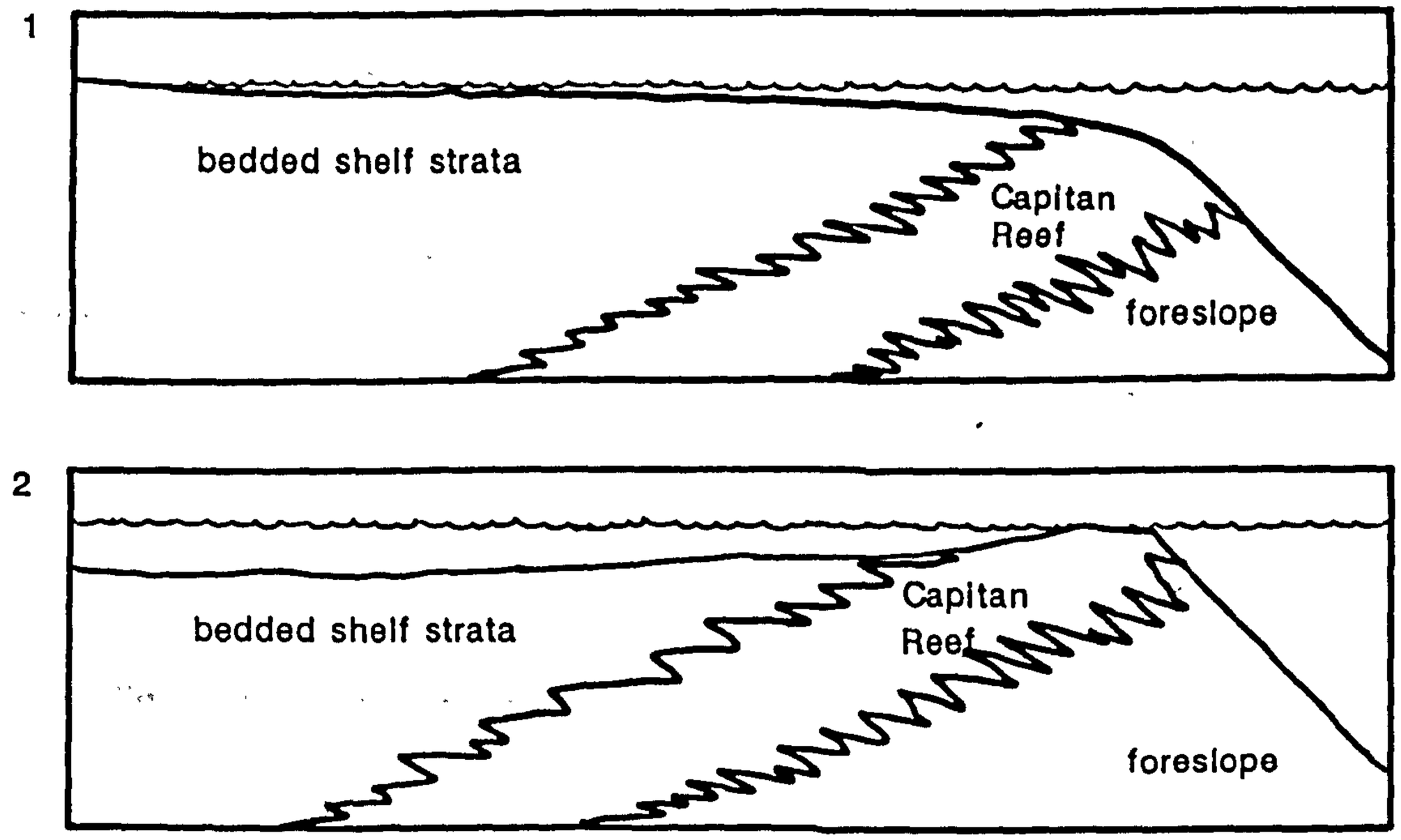

fig. 1.10 Schematic cross sections showing the four alternative profiles proposed for the Capitan shelf and shelf margin. 1. uninterrupted slope from shelf to basin; 2. barrier reef defining shelf crest; 3*a*. marginal mound, pisolite shoal defines shelf crest; 3*b*. marginal mound grainstone belt defines shelf crest. Adapted from King (1948), Newell *et al.* (1953), Lang (1937), Dunham (1972) and Handford *et al.* (1984).

mechanism for the formation of the teepee/pisolite belt, except where breaks in the grainstone belt are inferred. It is supported by the observations of Mazzullo (1985) and Mazzullo *et al.* (1989) who describe the presence of emergent, stacked-island facies in the grainstone belt a few hundred metres shelfward of the reef in Dark Canyon (Tansill Formation). This model has the disadvantage that the grainstone belt was narrow (less than 50m wide in some places (pers. comm., G.M. Harwood, 1989)) and may have been inadequate as a barrier.

Sedimentological and diagenetic studies, together with studies on the sedimentological response to relative sea level changes are discussed in more detail in chapter 3 (diagenesis).

1.4 Sampling

Sampling for palaeomagnetic study

In order to minimise the chances of collecting recently magnetised and weathered rocks, outcrops which were prominent, weathered or where water seepage was evident, were avoided and fresh surfaces were sampled where possible. Oriented core samples were taken in the field in preference to hand sampling and between 15 and 20 samples in varying orientations, were taken at each site (except sites M22 and M29 where this was not possible). These steps were taken in order to minimise any error that would possibly be incurred due to sampling method.

Samples, which were cores of 2.5cm diameter, were drilled using non-magnetic drill bits attached to a portable (but heavy and cumbersome), petrol-driven chain-saw motor. The drill-bit was water lubricated. Samples were oriented by using either a sun compass (Creer and Sanver, 1967), or by using a Brunton compass on the suncompass table. Local declination of the Earth's field of 11°W was taken into account. On return to Newcastle, cores were sliced into 2.1cm lengths (fig. 1.11). These dimensions were chosen in order to minimise the effects of sample shape on measurements of magnetic properties (Addison, 1982). Each sample was labelled 1 at the base of the core (least weathered portion) to 3 at the outermost part of the core. The first sample was then used preferentially in futher studies.

Samples were initially collected from a variety of lithologies and localities, including Dark Canyon, Rocky Arroyo, Slaughter Canyon, McKittrick Canyon and roadcuts on US 62/180 (fig. 1.2) These were used mainly for magnetic fabric studies. After preliminary magnetic fabric and palaeomagnetic analysis of these samples, a

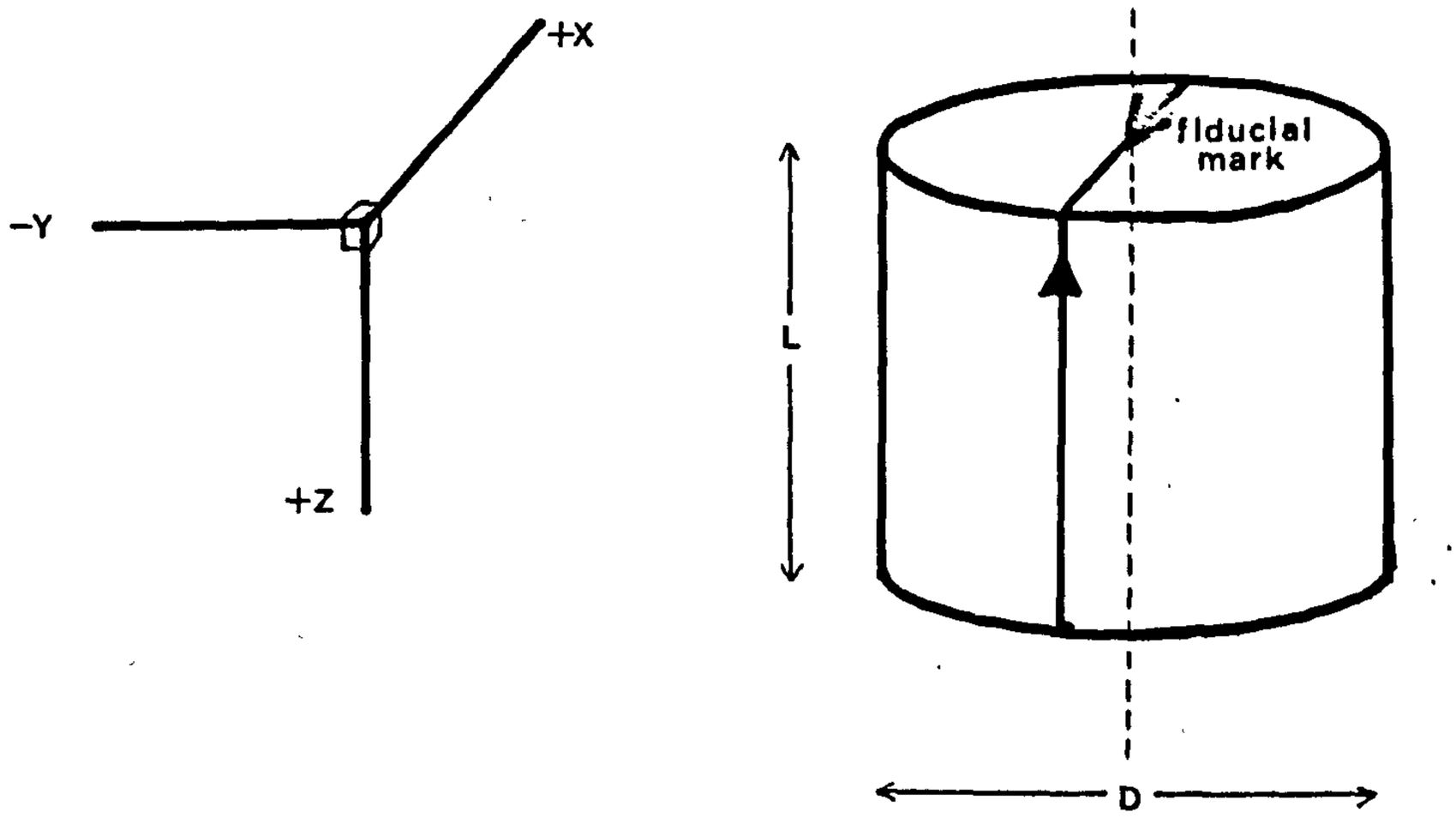

fig. 1.11 The relationship between the fiducial mark (reference direction) and the mutually perpendicular X, Y and Z measurement directions for cores used in palaeomagnetic studies.

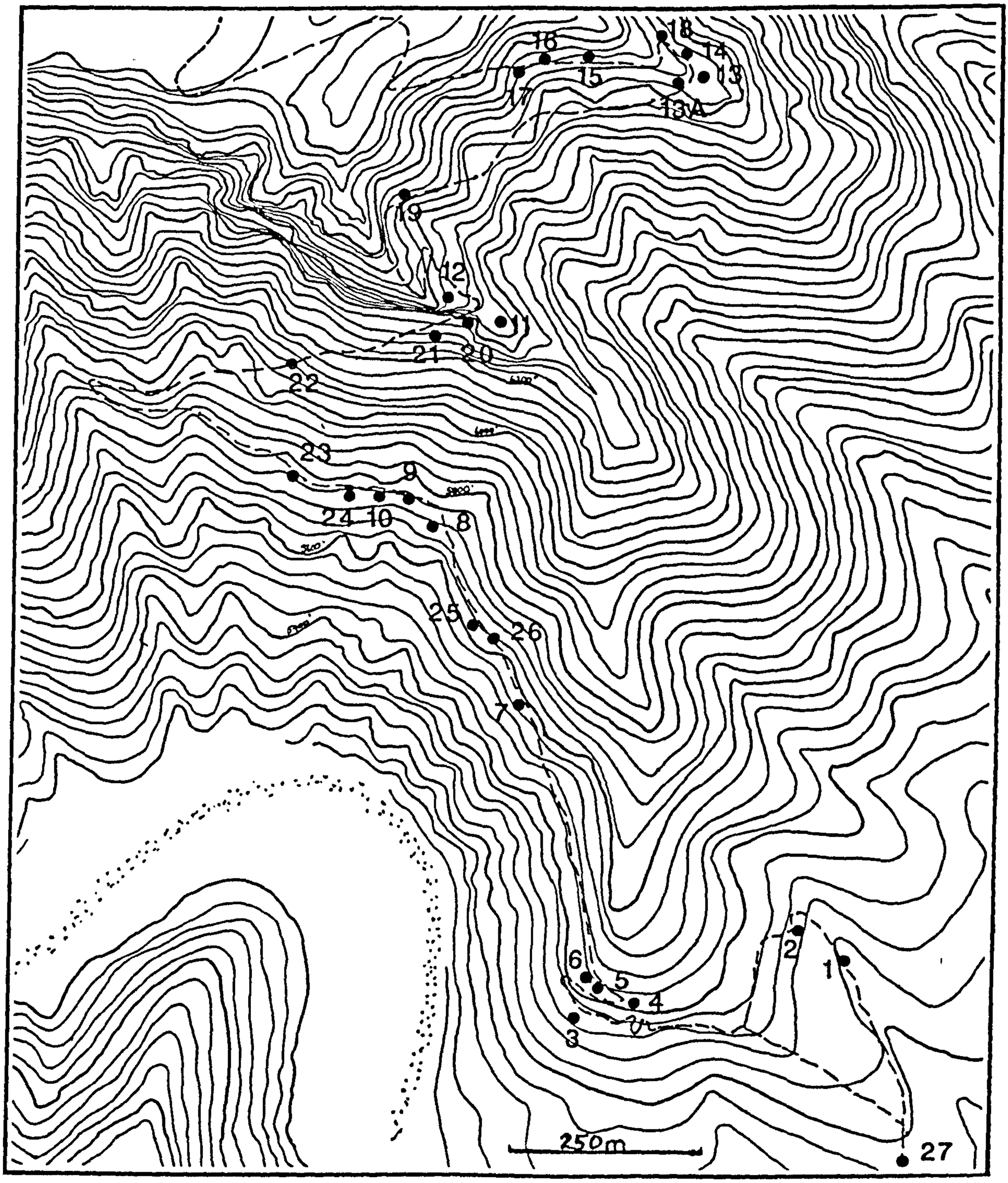

fig. 1.12 New map of the mouth of McKittrick Canyon showing the route of the 'Permian Reef Trail' and sampling locations. Modified from published trail map, Guadalupe Mountains National Parks (1985).

second set of samples were collected in McKittrick Canyon where stratigraphic and facies relationships are explicit. These explicit relationships constrained the age of the rocks (samples are of Upper-Middle and Upper Capitan age) and allowed a comparison of magnetic results from differient facies to be attempted. Samples were collected from 30 sites in a transect from basinal facies through foreslope and reef facies into back reef facies from US Highway 62/180 into the mouth of McKittrick Canyon. A summary of sample details for each site is listed in table 1.2. These samples were collected close to the so-called 'Permian Reef Trail' (fig. 1.12) because the trail allowed relatively easy access and fresh rock surfaces were available on the trail due to recent blasting. All traces of sampling activity were subsequently removed in accordance with the sampling permission granted by the US National Parks Service.

Sedimentology and diagenesis

One hundred and twenty two hand samples were collected from a range of facies and lithologies in order to supplement the samples collected for palaeomagnetic study, in order to log and describe the sedimentological and diagenetic features of the basin to back-reef transition. This was particularly important as much of the outcrop is coated with a caliche crust which prevents adequate field logging in many places.

site	facies	age (Capitan)	lithology	%dolomite	orientation	no. of cores	no. of samples
M1	basin margin	Upper	lime-micrite	0	magnetic	17	21
M2	basin margin	Upper	lime-wackestone	5	magnetic/sun compass	15	8
M3	basin margin	Upper	lime-packstone	5	sun compass	16	14
M4	lower foreslope	Upper	lime-boundstone	0	sun compass	18	12
M5	lower foreslope	Upper	dolo-grainstone	20	sun compass	15	10
M6	lower foreslope	Upper	dolo-grainstone	100	sun compass	18	12
M7	upper foreslope	Upper-Mid	dolo-grainstone	20	magnetic	18	13
M8	upper foreslope	Upper-Mid	lime-grainstone	5	magnetic	18	12
M9	upper foreslope	Upper-Mid	dolo-siltstone	100	magnetic	17	12
M10	upper foreslope	Upper-Mid	dolo-grainstone	100	sun compass	18	14
M11	upper foreslope	Upper	lime-grainstone	10	sun compass	17	10
M12	reef	Upper	lime-grainstone	10	sun compass	14	12
M13	back reef	Upper	lime-grainstone	10	magnetic	18	12
M13A	back reef	Upper	dolo-grainstone	50	sun compass	16	14
M14	back reef	Upper	dolo-siltstone	10	magnetic	19	18
M15	back reef	Upper	dolo-grainstone	60	sun compass	16	14
M16	back reef	Upper	lime-grainstone	5	magnetic	18	4
M17	back reef	Upper	dolo-grainstone	60	magnetic	16	16
M18	back reef	Upper	dolo-grainstone	60	magnetic	12	13
M19	reef	Upper-Mid	lime-grainstone	5	magnetic	16	15
M20	upper foreslope	Upper-Mid	dolo-grainstone	100	magnetic	17	12
M21	reef	Upper-Mid	dolo-grainstone	100	magnetic	16	11
M22	upper foreslope	Upper-Mid	dolo-grainstone	100	magnetic	5	3
J	upper foreslope	Upper-Mid	dolo-siltstone	10	magnetic	1	1
M23	upper foreslope	Upper-Mid	dolo-siltstone	10	magnetic	19	16
M24	upper foreslope	Upper-Mid	dolo-siltstone	0	magnetic	17	14
M25	upper foreslope	Upper-Mid	lime-grainstone	0	magnetic	17	13
M26	lower foreslope	Upper-Mid	dolo-grainstone	100	magnetic	19	23
M27	basin margin	Upper-Mid	lime-packstone	5	magnetic	17	17
L1	basin	Upper-Mid	lime-micrite	0	magnetic	11	15
CC1	basin	Mid	siltstone	5	sun compass	10	11
BC1	basin	Lower	siltstone	5	sun compass	11	19

table 1.2 Summary of sampling data for sites in palaeomagnetic sampling scheme

Chapter 2: Sedimentology

2.1 Introduction

In this chapter the sedimentology of the Capitan shelf margin is described with reference to outcrops at the mouth of McKittrick Canyon. Each facies has been described in detail and the facies are discussed separately in different sections, working from the back reef facies, down the foreslope and into the basin facies. Each section describes in some detail the sedimentological features seen at outcrop, such as lithology and bedding, and is illustrated with reference to summary lithological logs and photographs. This overview approach was used because the relationships *between* the facies have been largely neglected by previous workers who have tended to concentrate their attentions on particular facies (*e.g.*, Sarg, 1977; Reeckmann, 1985).

The separation of sedimentology and diagenesis in two chapters is difficult, especially as much cementation occurred contemporaneous with sedimentation. Accordingly, features which are visible or prominent at outcrop are introduced in *this* chapter, including those which have diagenetic as well as sedimentologic significance. Features of *primarily* diagenetic significance are discussed in chapter 4.

2.2 Methods

Fieldwork was carried out in McKittrick Canyon (fig. 1.2) where the so-called 'reef trail' allows relatively easy access to the facies belts of the Capitan shelf margin. Lithological logs were compiled in the back reef, reef, foreslope and basin margin facies, in order to document variations and enable comparison of features between the different facies. Outcrops of basinal facies rocks *i.e.*, the Lamar limestone and Brushy Canyon and Cherry Canyon sandstones were examined in disused road cuts close to the highway, US62/180 (fig. 1.2).

Dunham's (1962) carbonate classification is used to describe carbonate lithologies as follows: *grainstone* - a grain-supported rock without mud; *packstone* - a grain-supported rock with mud; *wackestone* - a mud-supported rock with >10% grains; *mudstone* - a mud-supported rock with <10% grains; *boundstone* - a rock showing signs of being bound during deposition.

2.3 Data presentation

The lithological logs have been compiled from field observations and laboratory observations of thin sections and cut surfaces. Lithology and sedimentary and diagenetic structures are shown on the left side of the logs. A standard key (fig. 2.1) is used for all logs. In all cases the vertical scale is 1cm = 1m, unless otherwise specified (*N.B.*, that logs jump across non-outcrop sections). A breakdown of components, type and relative proportions, is given in the middle columns and a brief verbal description and interpretation is given on the right side of the log. Colour is described using colour names as defined in the Geological Society of America's standard rock colour chart (1984). Heights from the base of the logs are given to facilitate cross-referencing between the logs and the text and these heights are given in brackets where they are included in the text. Sites, where hand samples and drill sites for palaeomagnetic study were collected, are also shown on the left hand side.

2.4 Facies descriptions

2.4.1 Back reef facies

The strata exposed at the top of the 'reef trail' (fig. 2.2) are of Upper Yates - Lower Tansill age. These strata dip gently at 5° in a basinward direction and are well-bedded. The transition from reef boundstones to the grainstones typical of the back reef facies, is illustrated in the first 5 metres of the log (fig. 2.3). Most strata of the back reef facies are well-bedded (fig. 2.4a) and the rocks are usually pinkish to light olive grey. A two-and-a-half metre-wide vertical fracture system parallel to the reef front (strike 206°) cross-cuts reef and back reef rocks here (fig. 2.4 b, c and d). The blocks of grainstone within the fracure appear to be *in situ*. Several generations of vertical fractures are visible (fig. 2.4 d) and dolomitisation and coarse calcite spar are associated with these fractures. The blocks of rock within the fracture and the rocks adjacent to the fracture are most affected by dolomitisation; the degree of dolomitisation decreases away from the fractured zone.

The succeeding sequence (5-14m) consists of interbedded, skeletal and peloidal wackestones and grainstones, the micritic components of which have been selectively dolomitised. In thin section these micritised areas are dark brown (fig. 2.5a). These grainstones contain *in situ* heads of a stromatolitic form, 6-10 cm in diameter, which is probably *Collenella*.

lithology

clay

silt grains

siltstone

limestone

dolostone

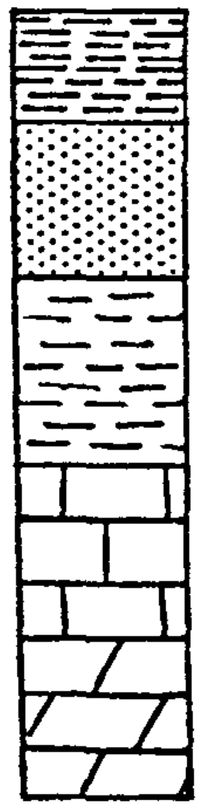

structures

cross-stratification

algal lamination

fenestrae

replacive anhydrite

stylolites

bioturbation on bedding plane

bioturbation

breccia

geopetal

components

Mizzia

pisoid

ooid

peloid

coated grain

sponge

crinoid

bivalve

brachiopod

bryzoan

Archaeolithoporella

trilobite

lithoclast

fusulinid

ostracode

coral

Collenella

scaphopod

contacts

planar

gradational

erosional

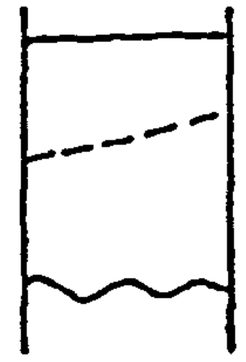

abbreviations

imc	isopachous marine cement
cc spar	calcite spar
ALP	*Archaeolithoporella*
k	kaolinite

fig. 2.1 Key to all lithological logs

fig. 2.2 Panoramic view and overlay sketch of bedded back reef strata overlying massive reef facies. The 'reef trail' zigzags through the reef facies and passes into the back reef facies. The dip of the foreslope strata is visible on the far side (south side) of McKittrick Canyon mouth (extreme left of picture). Sample sites for palaeomagnetic study are indicated: sites M12 and M19 in the reef facies; and sites M13, M13a, M14, M15, M16, M17 and M18 in the back reef facies.

back reef strata
siltstone
M17
M16
M15
siltstone
siltstone
M14
M18
M19
M13
M13a
foreslope
massive reef
reef trail
M12

fig. 2.2

fig. 2.4 *a.* Bedded back reef strata dipping basinward at 5°, the direction of dip is indicated by the pencil. Beds appear massive although bedding is on a decimetre scale. *b.* Fracture system, 2 and 1/2 metres wide, cross-cutting reef boundstone (left of photo) and back reef grainstones. The fracture contains dolomitised blocks in a calcite spar matrix. *c.* Close-up view of dolomitised blocks of grainstone in fracture. The blocks appear to be largely *in situ* and are supported in a matrix of smaller, angular fragments and coarse calcite spar (c). *d.* Several vertical, parallel fractures (strike 206°) in dolomitised back reef grainstones are associated with the fracture system illustrated in *b and c.* These fractures are about 10 cm wide and represent several generations of fracturing. McKittrick Canyon. Lens cap 6cm, clip board 30cm, long dimension.

fig. 2.4

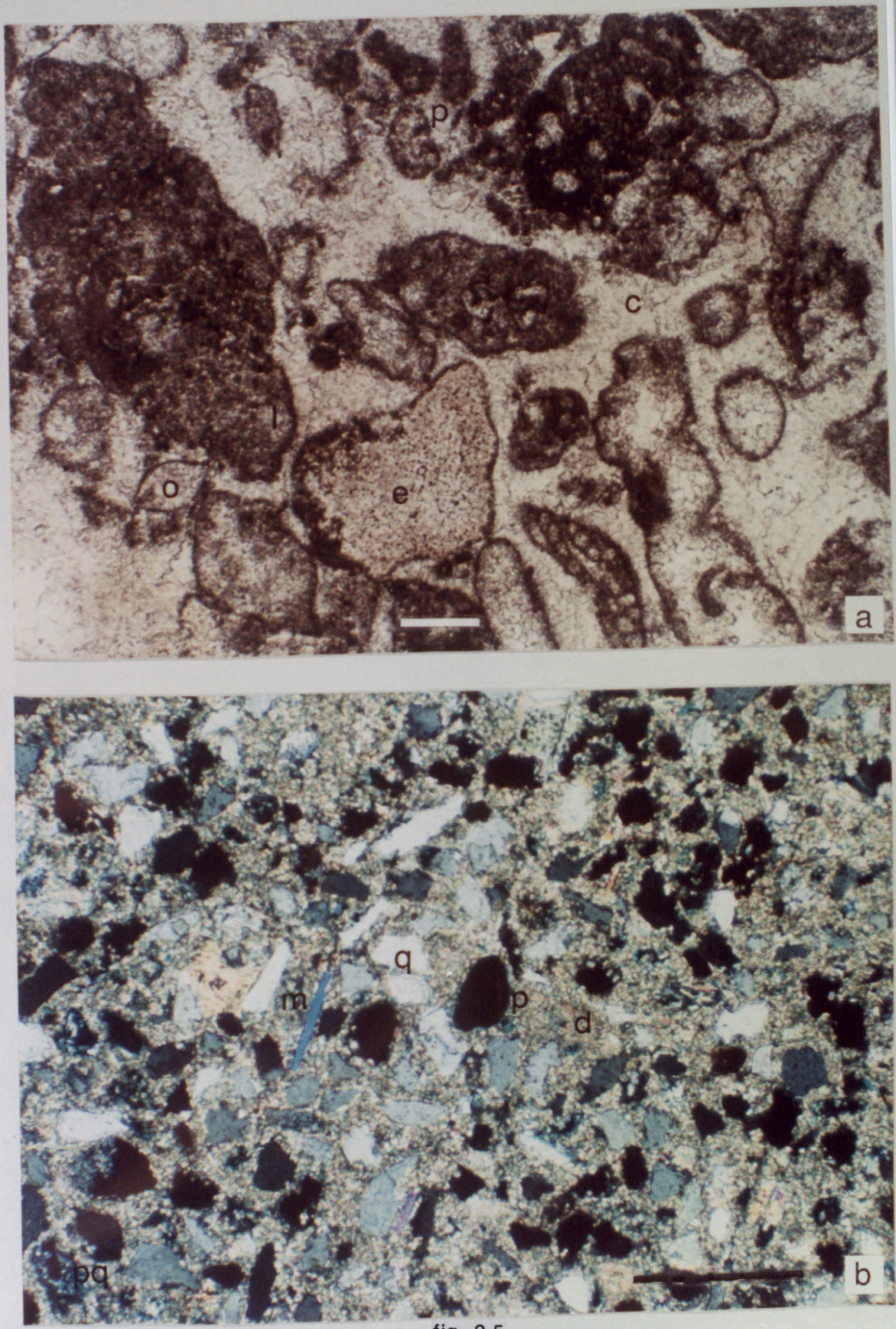

fig. 2.5

fig. 2.5 Immediate back reef facies. *a.* Photomicrograph (plane polarised light) of a grainstone composed of echinoid fragments (e), lithoclasts (l), peloids (p), ostracodes (o), and early radial acicular marine cements (c). Most components are surrounded by micrite envelopes (arrowed). McKittrick Canyon. Scale bar 250 µm. *b.* Photomicrograph of siltstone composed mainly of detrital monocrystalline quartz (q), and also mica (m), polycrystalline quartz (pq), and pyrite (p). A finely crystalline dolomite matrix (d) surrounds the grains. McKittrick Canyon. Scale bar 250 µm. Cross-polarised light.

A massive siltstone bed follows (6 - 11 m) which weathers to form a recessive smooth slope (fig. 2.2). It contains no obvious sedimentary structures, but this may be a reflection of the uniformity of the grain-size of the silt. The siltstone is composed mainly of sub-rounded to angular quartz grains, many of which have quartz overgrowth cements, and minor quantities of mica, staurolite, polycrystalline quartz and pyrite (fig.2.5b). No feldspar is present. The siltstone matrix is finely crystalline dolomite (fig. 2.5 b) which could originally have been carbonate mud or alternatively could have been isopachous marine cements. Mixed skeletal debris, including complete 10cm diameter gastropod shells *(Bellerophon)*, scaphopods and articulated crinoid stems, occur in this siltstone bed (fig. 2.6 b,c,d). Silt grains also occur dispersed throughout most carbonate rocks of the back reef facies (fig. 2.6a) and geopetal fabrics of siliciclastic silt and carbonate grains (fig. 2.6a) are also common as pore-fills and fracture-fills.

A unit composed of selectively dolomitised 'clasts' and which contains *Collenella* fragments in a grainstone matrix outcrops at the base of a sequence of grainstones from 16-20m (fig. 2.7 a) The 'clasts' range in size from 1cm to 35cm and are sub-angular to sub-rounded. No fractures are visible and the unit is not laterally continuous. The 'clasts' have clearly defined margins and are preferentially dolomitised. A similar exposure occurs in the same facies and stratigraphic position at the mouth of Walnut Canyon (fig. 2.7 b), where the dolomitised clasts are imbricated, and overlie a truncated surface. The outcrop in Walnut Canyon is overlain by the lower 'triplet sandstone', an informal term for sandstones in the Upper Yates (Neese and Schwartz, 1977). The lower part of these sandstones contains stromatolitic forms several decimeters in height (G.M. Harwood, pers. comm., 1989). In this respect this outcrop differs from the outcrop in McKittrick Canyon, which is overlain by a grainstone sequence (15-20m) containing marine fauna (foraminifers, ostracodes, echinoid fragments), and peloids, lithoclasts and coated grains. These grainstones are homogeneous, contain no obvious sedimentary structures other than bedding, and have not been significantly dolomitised.

Above this sequence of grainstones (21-31m) the strata *are* dolomitised and contain laminations, fenestrae and bedding is locally disrupted. Cement-lined fractures are associated with the disrupted bedding (fig. 2.7 c) where the beds are locally tilted up to around 45°. Fining-upward sequences, a few centimetres thick, are present in these strata; the mudstones are preferentially dolomitised and appear whitish at outcrop (fig. 2.7d). These mudstones contain some calcite spar-filled pores which have squarish outlines and castellated margins (fig. 2.7d). This calcite spar fills all porosity in these dolostones. Wispy laminations, which have a few milimetres relief and are preferentially dolomitised, are present in some of the mudstones (fig. 2.8a). Some

fig. 2.6 Back reef facies. *a.* Photomicrograph of geopetal fill (g), composed of peloidal grains inside a skeletal fragment. Silt grains are visible as bright, angular grains. Scale bar 500 μm. *b.* Articulated crinoid stems, aligned perpendicular to the shelf edge, in a siltstone unit. *c.* *Bellerophon* moulds weathered out on the surface of a siltstone outcrop. *d.* Scaphopods and other coarse skeletal debris in wackestone. McKittrick Canyon. Lens cap 6cm.

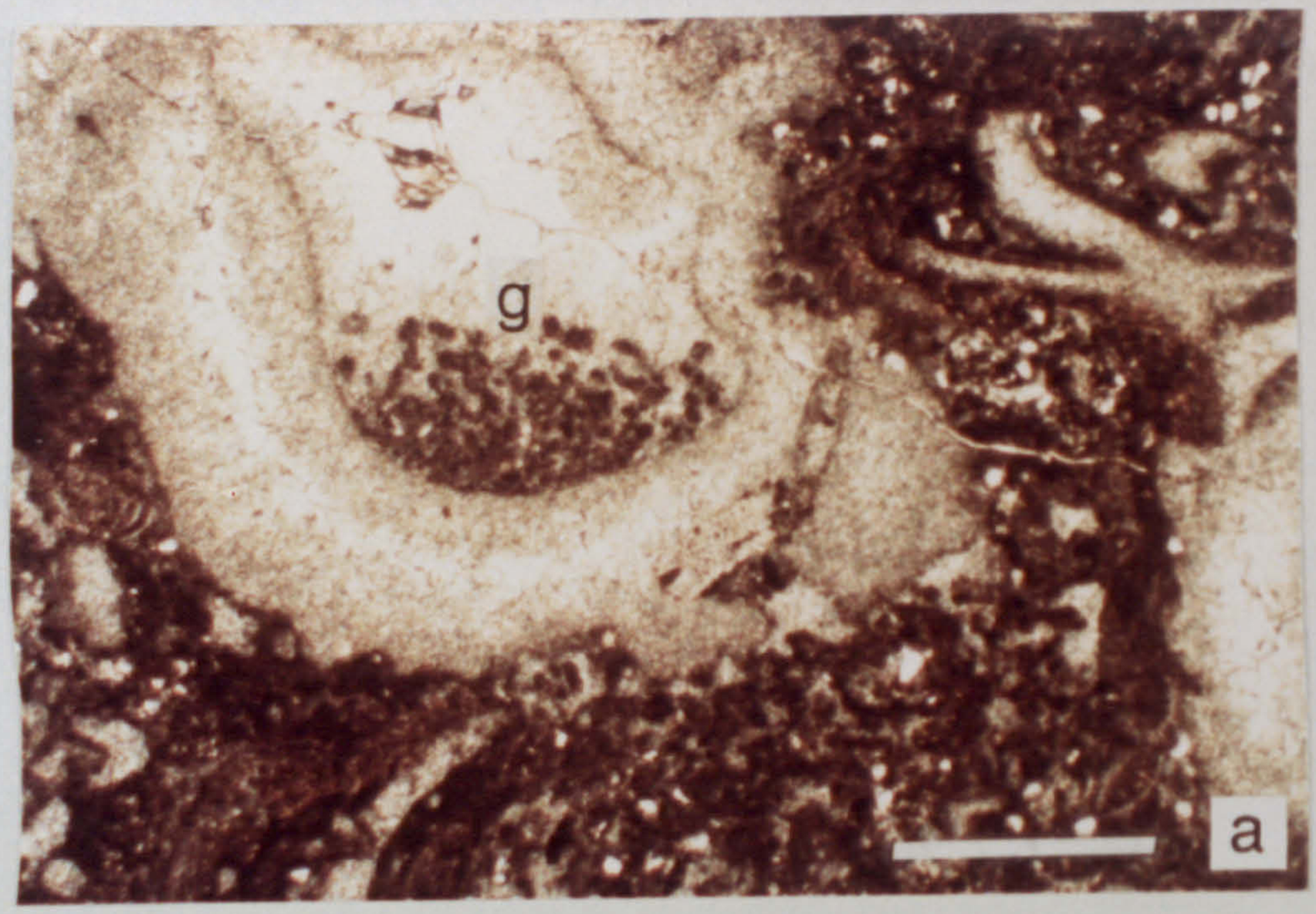

fig. 2.6

fig. 2.7 Back reef facies. *a.* Selectively dolomitised 'clasts' in wackestone matrix. 'Clasts' are subangular to subrounded and tend to be elongate and of variable size. Examination of thin sections shows no evidence of abrasion or truncation of grains, suggesting that these 'clasts' are a product of selective dolomitisation. *b.* Reworked, lithified and imbricated dolomitised clasts overlying an erosion surface (possibly representing exposure), in Walnut Canyon. These clasts are overlain by a well-bedded sandstone. *c.* Cement-lined fractures in dolomitised grainstone in which bedding has been locally disrupted and which are possibly associated with teepee formation. *d.* Disrupted bedding in laminated, fining upwards grain/mudstones. McKittrick Canyon. Lens Cap 6cm.

fig. 2.7

fig. 2.8 Back reef facies. *a.* Preferentially dolomitised lamination, of possible algal origin, associated with peloidal wackestone/mudstone layers. *b.* Vertically orientated, dolomitised grainstone areas, possibly filling burrows or cracks in a grainstone. *c.* Variable dolomitisation in a unit of grainstones. Dolomitisation is pervasive in the upper part of the unit (above the lens cap) and gives the unit a pale, pinkish colour; whereas the lower part remains limestone and is an olive-grey colour. McKittrick Canyon. Lens Cap 6cm.

fig. 2.8

vertical, grainstone-filled features cross-cut finer-grained grainstones (fig. 2.8b). The grainstone-fill is composed of coated grains up to 5mm in diameter. These outcrops are about 200m shelfward from the reef.

A silt-filled dyke, several decimetres wide, cross-cuts the overlying carbonate strata (30m). This is difficult to trace, because outcrops are inaccessible, but may join with a 1 metre thick siltstone unit which follows (33m). This siltstone is similar to others in the back reef facies and contains skeletal fragments. Fenestral fabric is associated with this siltstone in some places. It is overlain by 5 metres of variably dolomitised grainstones and packstones (34-39m). This sequence, of a siltstone followed by grainstones, is repeated once again (39-49m). The grainstone strata are composed mainly of peloids and coated grains (up to 6mm diameter), with a smaller contribution from skeletal grains (shell fragments, echinoid plates and bryzoa). Metre scale cross-bedding is visible on some inaccessible outcrop surfaces. These carbonate sequences tend to vary from limestone to dolomite over a vertical distance of less than 1 metre (fig. 2.8c) and this variable dolomitisation appears to be laterally continuous. The dolomitised strata have a paler, pinkish colour than the non-dolomitised strata which are an olive-grey colour. Where the dolomitisation is pervasive, there are no signs of previous isopachous cements and all porosity is occluded by a single calcite spar. This succession of carbonates and siltstones contains small dispersed 1cm diameter calcite-filled nodules, and many calcite-filled hairline fractures.

A fenestral, dolomitised grainstone sequence containing brecciated areas and fractures (fig. 2.9a), outcrops over the next 2 metres (49-51m). Some fractures are lined by isopachous cements (fig. 2.9b). The breccias are composed of a variety of angular clasts of backreef facies lithologies *i.e.*, dolomitised grainstones and fenestral dolostones, and have a siltstone matrix. A similar siltstone also fills fractures which cross-cut the grainstones. The silt predates a calcite spar which fills remaining space in fractures and in the breccias (fig. 2.9c).

Interpretation

The back reef strata exposed at the top of the 'reef trail' in McKittrick Canyon represent deposition in a shallow, offshore to nearshore marine setting. *Collenella* is found only in the shelfward Upper Capitan massive reef (J.A. Babcock, 1977) and its presence *in situ* indicates that the strata of the immediate back-reef inter-digitate with the reef here. Shallow agitated waters are indicated by several features, such as: the large amount of carbonate sediment produced and deposited adjacent to the reef; the presence of coated grains, which are indicative of grain reworking and abundant direct

fig. 2.9 *a.* Back reef facies. A brecciated grainstone cut by fractures which are filled with grainstone (g), silt (s) and calcite spar. *b.* Early fracture in fenestral dolomites, lined by isopachous early cements (c') and subsequently filled with silt *c.* Breccia composed of a variety of angular clasts of back reef lithology in a silt (s) matrix; remaining porosity is occluded by calcite spar (c). McKittrick Canyon. Lens Cap 6cm.

fig. 2.9

carbonate precipitation; the lack of carbonate mud in these strata which indicates winnowing; disarticulated skeletal fragments *e.g.*, individual crinoid ossicles, which indicate that the sediment supply need not necessarily have been local and that currents may have brought sediment from other areas such as further back on the shelf; and the cross-bedding present in some strata. Not all strata are composed of disarticulated skeletal fragments and coated grains, but are composed of grains which are not coated. Grains which have not been coated also imply that they may have been rolled about before deposition or deposited rapidly and without significant transport before they could become coated. Articulated crinoid stems and other skeletal fragments *e.g.*, the criniods and *Bellerophon* found in the siltstone units, also suggest rapid deposition of these organisms close to their life environment. The variety of skeletal and peloidal grains is consistent with that observed by Schmidt (1977) and Toomey and Cys (1977) (fig. 2.9). The skeletal component dominates seaward, whilst the peloidal and coated-grain component dominates landward.

The lack of sedimentary structures in the three massive siltstone units and the presence of articulated crinoid stems and other complete skeletal components implies that these sediments were not reworked much and that they may have been rapidly deposited under marine conditions. The apparent paucity of grain contacts suggests that the original rock was silty grainstone cemented by isopachous marine cement, or alternatively that the matrix was carbonate mud, which was subsequently obliterated by finely crystalline dolomite; no vestiges of isopachous cement remain. The occurrence of the lowest siltstone almost directly over the reef (massive reef boundstones and the grainstones containing *Collenella)* disagrees with the observation of Neese and Schwartz (1977) that the siliciclastic component pinches out at the shelf edge 100-300 metres away from the massive reef facies. The occurrence in most carbonate strata of dispersed silt grains suggests that some silt was wind-blown. The silt which was deposited in the massive siltstone units and in the geopetal fabrics, could have been transported by a combination of aeolian and marine processes but were deposited in marine conditions, as suggested by the presence of complete marine fossils in the siltstones.

Several lines of evidence suggest that there may have been periods of exposure of the back reef facies within a few hundred metres of the reef. The habit of the laminations and the fenestrae suggest that algal mats were once present in the mudstones and grainstones. Disrupted bedding, fractures and algal fenestrae suggest that these strata were deposited in shallow to emergent conditions associated with teepee formation. The unit containing selectively dolomitised 'clasts', which outcrops in McKittrick Canyon, may also represent the action of surface processes and/or soil formation. The imbricated clasts, which outcrop in Walnut Canyon, were interpreted as overlying an erosion

carbonate precipitation; the lack of carbonate mud in these strata which indicates winnowing; disarticulated skeletal fragments *e.g.*, individual crinoid ossicles, which indicate that the sediment supply need not necessarily have been local and that currents may have brought sediment from other areas such as further back on the shelf; and the cross-bedding present in some strata. Not all strata are composed of disarticulated skeletal fragments and coated grains, but are composed of grains which are not coated. Grains which have not been coated also imply that they may have been rolled about before deposition or deposited rapidly and without significant transport before they could become coated. Articulated crinoid stems and other skeletal fragments *e.g.*, the criniods and *Bellerophon* found in the siltstone units, also suggest rapid deposition of these organisms close to their life environment. The variety of skeletal and peloidal grains is consistent with that observed by Schmidt (1977) and Toomey and Cys (1977) (fig. 2.9). The skeletal component dominates seaward, whilst the peloidal and coated-grain component dominates landward.

The lack of sedimentary structures in the three massive siltstone units and the presence of articulated crinoid stems and other complete skeletal components implies that these sediments were not reworked much and that they may have been rapidly deposited under marine conditions. The apparent paucity of grain contacts suggests that the original rock was silty grainstone cemented by isopachous marine cement, or alternatively that the matrix was carbonate mud, which was subsequently obliterated by finely crystalline dolomite; no vestiges of isopachous cement remain. The occurrence of the lowest siltstone almost directly over the reef (massive reef boundstones and the grainstones containing *Collenella)* disagrees with the observation of Neese and Schwartz (1977) that the siliciclastic component pinches out at the shelf edge 100-300 metres away from the massive reef facies. The occurrence in most carbonate strata of dispersed silt grains suggests that some silt was wind-blown. The silt which was deposited in the massive siltstone units and in the geopetal fabrics, could have been transported by a combination of aeolian and marine processes but were deposited in marine conditions, as suggested by the presence of complete marine fossils in the siltstones.

Several lines of evidence suggest that there may have been periods of exposure of the back reef facies within a few hundred metres of the reef. The habit of the laminations and the fenestrae suggest that algal mats were once present in the mudstones and grainstones. Disrupted bedding, fractures and algal fenestrae suggest that these strata were deposited in shallow to emergent conditions associated with teepee formation. The unit containing selectively dolomitised 'clasts', which outcrops in McKittrick Canyon, may also represent the action of surface processes and/or soil formation. The imbricated clasts, which outcrop in Walnut Canyon, were interpreted as overlying an erosion

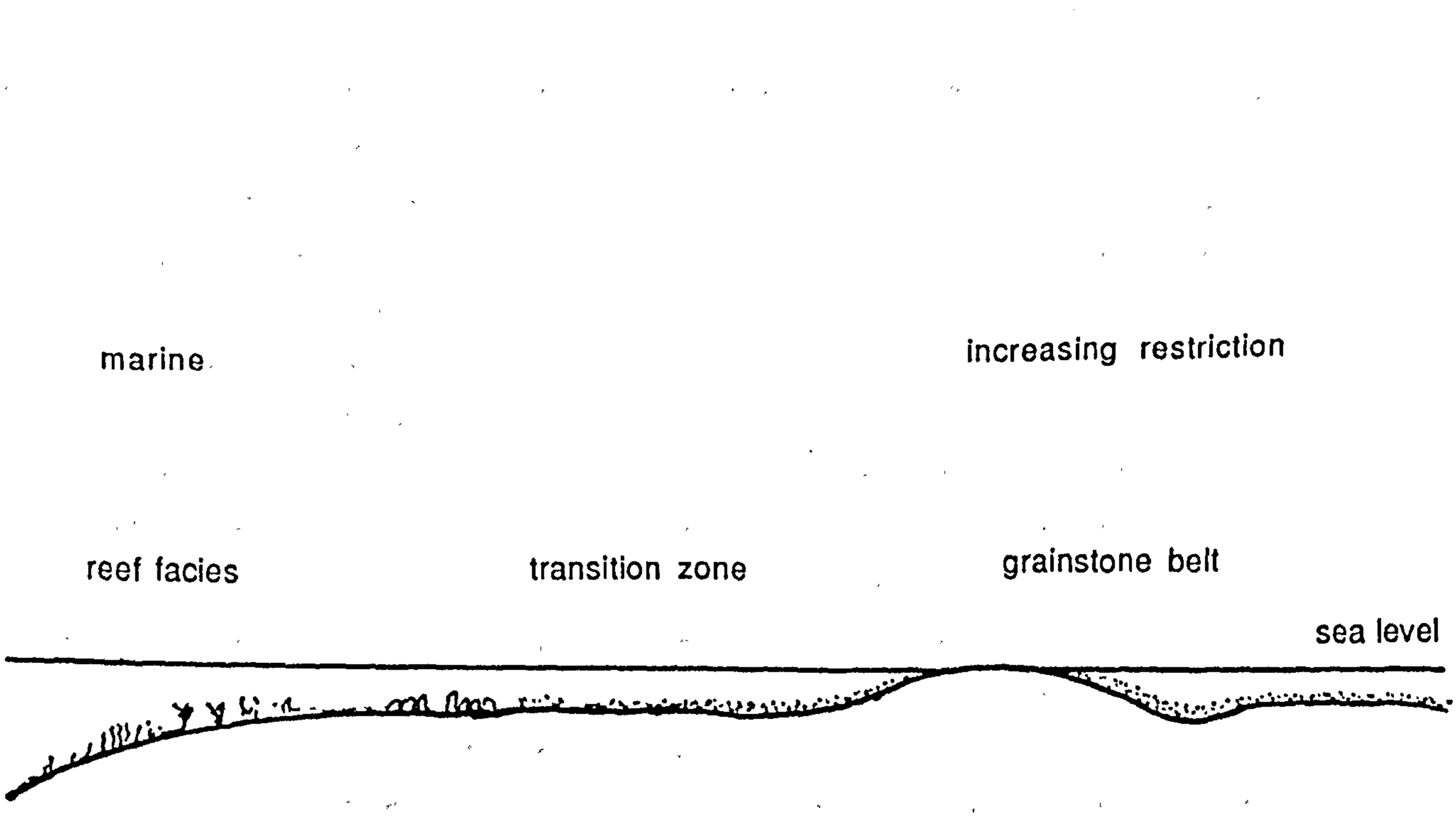

fig. 2.10 Summary diagram of the distribution of the main components present in the reef-back reef facies transition. Based on diagram from Schmidt (1977) and Toomey and Cys (1977) with additional observations from this study underlined.

surface (Dunham, 1972) and later as representing an exposure surface and sequence boundary (Sarg and Pray, 1984 and Mutti 1989). The unit containing selectively dolomitised 'clasts', which outcrops in McKittrick Canyon, is unlikely to have resulted from erosion and redeposition of clasts, as no erosion surface is visible. A diagenetic origin for the selective dolomitisation is more likely, related to surface processes and/or soil formation (pers. comm., A.C. Kendall, 1989) or possibly related to other diagenetic processes (chapter 3). If surface processes *were* responsible for the development of this selective dolomitisation, then the timing of these processes is equivocal, but may be related to present-day exposure or possibly to exposure in the Permian. The occurence of a non-dolomitised grainstone sequence over-lying the selectivley dolomitised unit in question, implies that this selective dolomitisation is not related to present-day processes, by instead took place prior to the deposition of the over-lying grainstone. Some outcrops, which are in a similar palaeogeographic position relative to the reef in Dark Canyon, have been interpreted as being of island origin (Mazzullo *et al.*, 1985, 1989) *i.e.*, of representing sequences deposited in shallow to exposed conditions.

Fractures, partially filled by geopetal silts and carbonate sediments and partially filled by isopachous cements, indicate that some fracturing took place contemporaneous with sedimentation (chapter 3). Re-fracturing, dolomitisation and brecciation suggest that such early fractures may have formed planes of weakness which were re-activated during subsequent tectonic movements and possibly acted as conduits for fluid flow. The Tertiary has been the most active period of tectonic activity in this area, so it seems likely that some fracturing and brecciation took place during this time. This implies that some infilling of fractures by silt and calcite spar was also likely to be Tertiary.

The sequence exposed on the 'reef' trail in McKittrick Canyon represents a grainstone belt which displays features which indicate a shallowing upward trend and increasing restriction, possibly to the point of exposure of some parts of the grainstone belt, and tends to support model 3b (1.3.3) for the topographic profile of the shelf margin.

2.4.2 reef facies

The reef exposed on the 'reef trail' in McKittrick Canyon is of Mid-Capitan age (figs. 1.6 and 1.9) and is a massive unit which commonly crops out as cliffs. The reef is homogeneous on a large scale and for this reason a lithological log is not given. The main organisms present have been studied in detail (J.A. Babcock, 1974; Yurewicz, 1977)

and were *Archaeolithoporella* (Endo, 1959), which resembles modern red algae in its structure, habit and state of preservation; *Tubiphytes* (Maslov, 1956), which was an ovoid encrusting organism; and *Collenella* (Johnson, 1942), which was a skeletal organism that resembles algal stromatolites (J.A. Babcock, 1977). *Collenella* boundstones and *Tubiphytes* boundstones are most abundant in the 'shallowest' (*i.e.*, palaeogeographically landward) parts of the Upper Capitan reef, whilst phylloid algal boundstones and *Archaeolithoporella* nodular boundstones are most abundant in the 'deeper' parts (*i.e.*, palaeogeographically seaward) of the Upper Capitan reef (J.A. Babcock, 1977) (fig. 20).

Large volumes of the reef are composed of *Archaeolithoporella* which is commonly intimately associated with botryoidal, radiating fans of brown early marine cement (fig. 2.12a). The brown colour of these botryoidal cements is quite distinctive and is a useful field guide to their presence; the remainder of the reef rock is an olive grey colour. Botryoidal cements also occur without *Archaeolithoporella* laminae (Mazzullo and Cys, 1977, 1978). Cementation will be discussed in Chapter 3 (diagenesis). Sponges are the most obvious organic component visible at outcrop, and tend to be a whitish colour. These commonly form the substrate onto which botryoidal cements precipitated (fig. 2.12b).

Cavities are more common in boundstones of the reef and become larger and more abundant towards the top of the 'reef trail' in McKittrick Canyon. Geopetal sediments are not obvious in all cavities in the reef, but they are common throughout the reef where sediments fill, or partially fill, cavities (fig. 2.12c) and fractures (fig. 2.12d). These geopetals are not always horizontal but do act as a guide to the depositional orientation of *in situ* reef and allochthonous reef boulders of the foreslope facies. The sediments in the geopetals vary in composition from fine grained laminated mudstones to coarse-grained wackestones and siliciclastic silts (fig. 2.12d). Many of the internal sediments are intimately associated with botryoidal and isopachous cements.

More than one generation of fractures in the reef is demonstrated by cross-cutting relationships (fig. 2.13a). These fractures are sometimes lined by isopachous cements and can also contain internal sediments. Early fractures in the reef have also been reported from exposures at the mouths of Walnut and Dark Canyon (J.A. Babcock, 1977). These fractures are lined by numerous laminae of botryoidal cement and *Archaeolithoporella.*

Grainstones are abundant in the reef and in these areas cavities are less common than in areas of boundstone. In the grainstones, the cavities have flat-floors which are emphasised by later cavity-fill of calcite spar (fig. 2.13b) and which dip basinwards. It is not clear at outcrop whether the dip of these cavities represents a primary dip and

fig 2.11 Panoramic view and overlay sketch of the reef facies, which forms high cliff faces, particularly at canyon mouths (extreme left of picture) and a uniform slope elsewhere, and overlying back reef strata. The 'reef trail' ascends through the reef facies. Sample sites for palaeomagnetic study of the reef (sites M12 and M19) are indicated.

fig. 2.11

fig. 2.12 Reef facies. *a.* Botryoidal masses of radiating, acicular brown cements which have coalesced to form the entire reef rock. *b.* laminated geopetal (g) mudstones, intimately associated with, and overgrown by, early marine botryoidal cements (c). Sponges formed the substrate onto which the cements precipitated (pale areas). *c.* grey silts forming geopetal structures which have varying dip, in a cavity surrounded by botryoidal cements. The dip initially steepens from the bottom of the cavity, and then becomes more shallow towards the top of the cavity. *d.* Mixed siliciclastic/carbonate grain-fill in a vertical fracture in the reef, nearly a metre wide. The silt has a dark colour and the carbonate grains are a pale grey. Lens cap 6cm or finger-tip for scale. McKittrick Canyon.

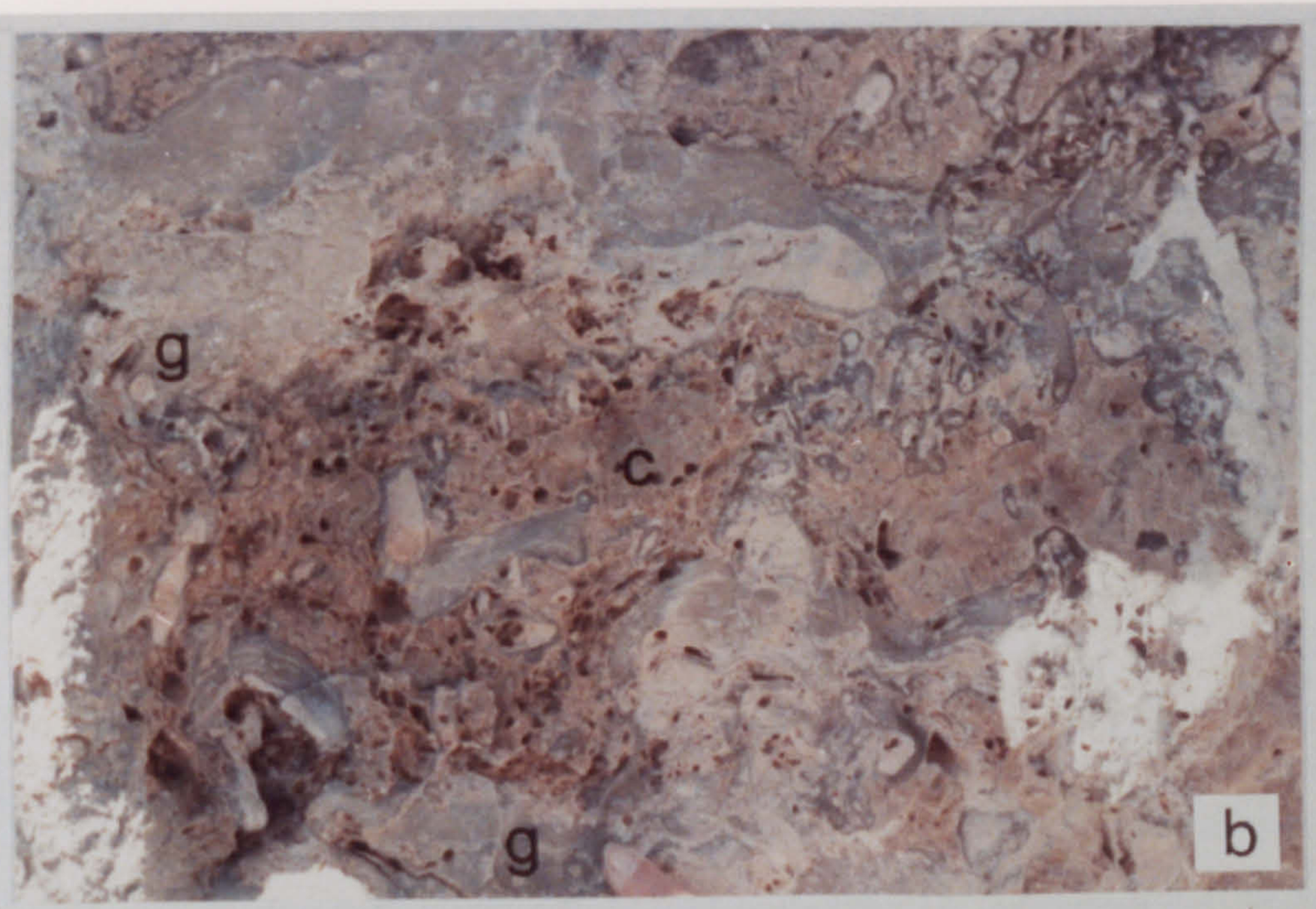

fig. 2.12

fig. 2.13 *a.* Reef cavity cross-cut by a cement-lined fracture and a grain-filled fracture illustrating that cementation and fracturing were contemporaneous with reef formation. *b.* Gently dipping, flat-floored cavities, now filled by calcite spar **(c)**, within a grainstone pocket. *c.* Dark grey geopetal silts **(s)** below coarse calcite spar **(c)** in a tightly cemented grainstone. *d.* Intimate association of yellow siliciclastic silt **(s')** and calcite spar **(c)** in a reef void. The silt overlies the calcite spar which indicates that the deposition of the silt post-dates the precipitation of the calcite spar. McKittrick Canyon. Lens cap 6cm, or finger-tip for scale.

fig. 2.13

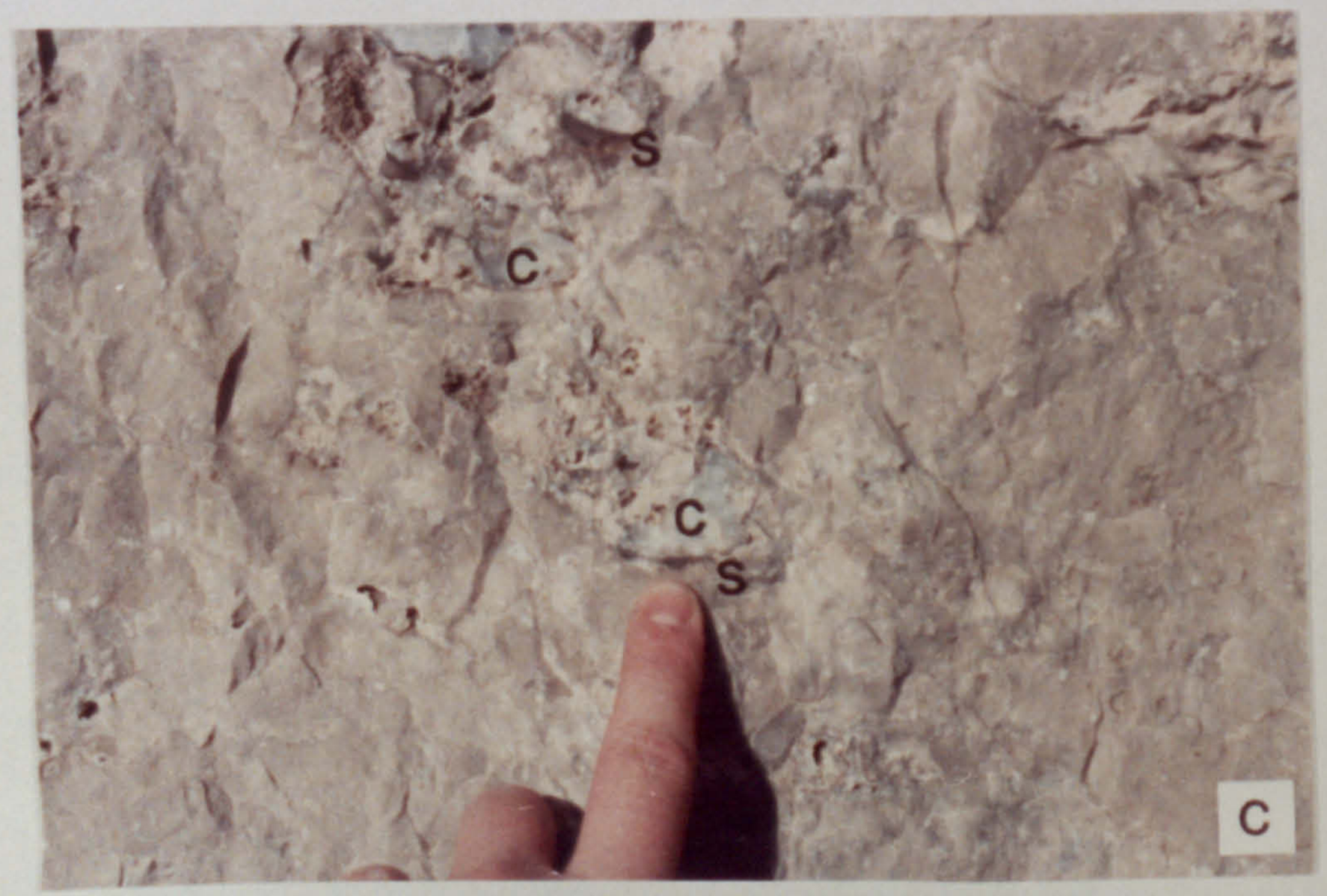

fig. 2.14 Reef facies; *a.* late silt filled fracture **(f)** which cuts through both the reef fabric and the coarse calcite spar **(c)**. *b.* Isopachous marine cements **(i)** and botryoidal, fibrous cements **(c')** lining reef cavity which has been subsequently filled with calcite spar **(sp)**. *c.* Large crystals of calcite spar **(sp)**, up to 10cm across, filling a void in reef boundstones. *d.* Calcite spar filling a fracture which cuts across early botryoidal, fibrous marine cement. McKittrick Canyon. Lens cap 6cm.

fig. 2.14

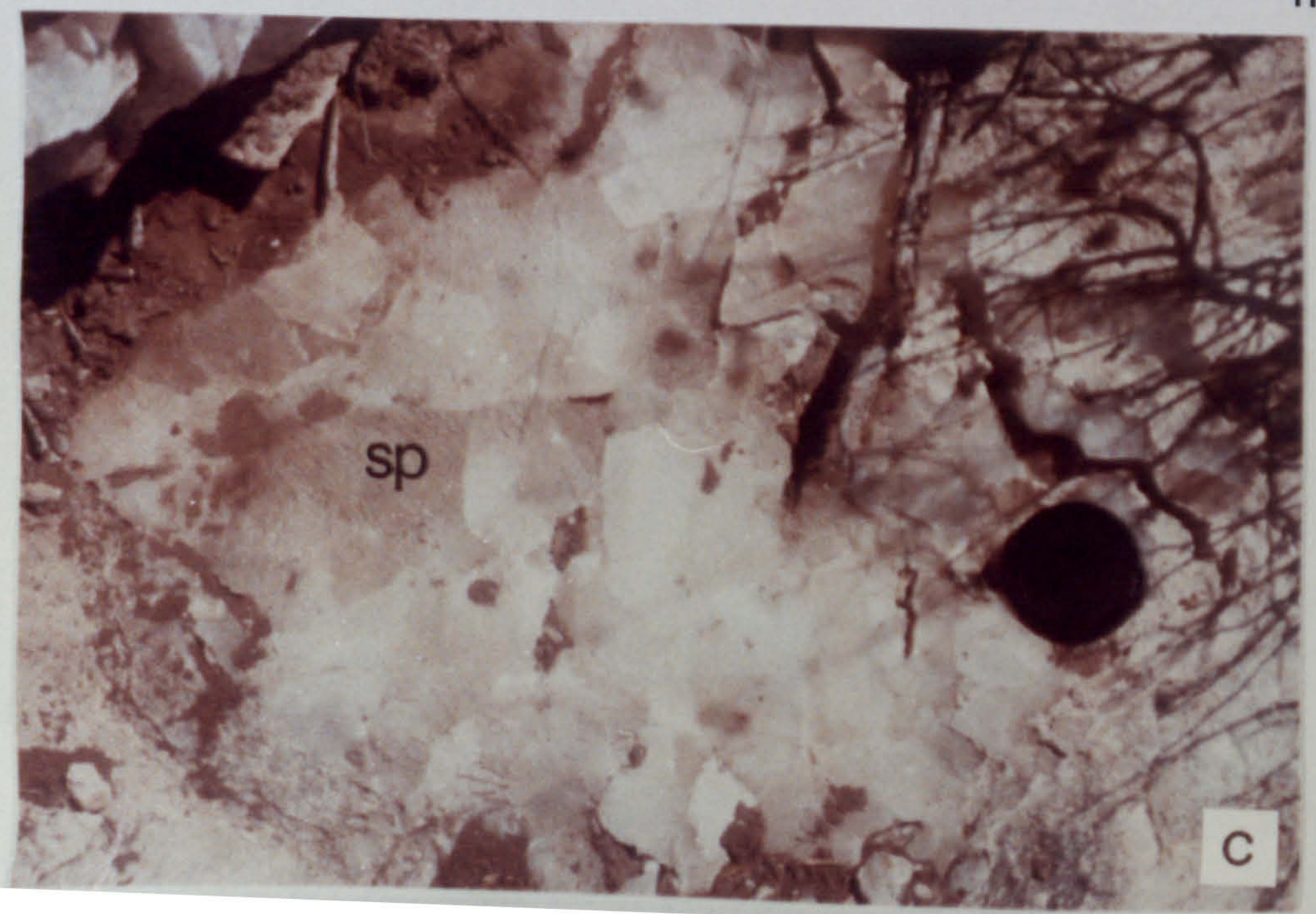

represents interdigitation with the foreslope facies, or whether it represents differential compaction.

Horizontal geopetals of black silt are common in cavities which now contain coarse calcite spar (fig. 2.13c). These black silts are never more than a few milimetres in thickness and are always associated with calcite spar. Yellow silts are also found in cavities (fig. 2.13d) and fractures (fig. 2.14a), again associated with this calcite spar. However, the silt overlies the calcite spar in the cavities and cross-cuts the spar in fractures, and must therefore post-date the precipitation of this calcite spar.

This calcite spar post-dates the fibrous botryoidal and isopachous cements as it fills porosity remaining after the precipitation of isopachous and botryoidal cements (fig. 2.14b,c) and fractures which cut these cements (fig. 2.14d). It is present throughout the reef but is more common and fills larger voids in the reef towards the top of the 'reef trail'.

Interpretation

It is clear from relationships between organic components, cements, fractures and geopetal infills, that cementation was early within the reef and that it was mainly boundstone. The reef formed by inorganic binding of sediment by carbonate cement, inorganic growth of a crystalline carbonate framework and inorganic lithification of attached skeletal organisms. Sediment was baffled by organisms such as phylloid algae before the precipitation of large volumes of cement filled most remaining porosity (fig. 2.15a). Encrusting organisms, such as *Archaeolithoporella*, coated the surfaces of organic and inorganic substrates, such as botryoidal cements (fig. 2.15b), alike.

Much discussion has taken place in the course of development of ideas and understanding of the Capitan Reef, concerning the relative importance of organic and inorganic processes (Schmidt, 1977; Cys *et al.*, 1977). Sponges were the major non-algal, non-encrusting organisms in the reef and various algae and problematic organisms (namely *Archaeolithoporella* (Endo, 1959), *Tubiphytes* (Maslov, 1956) and *Collenella* (Johnston, 1942)) were the other main organic components. Although these organisms were not framebuilding organisms, such as those recognised in modern reefs like the Great Barrier Reef, they played a major part in the growth and development of the reef. These organisms and carbonate sediment were cemented by early marine cements which bound the components together to form a massive structure which is now generally thought to have formed below wave base.

Grainstone also occurs in the reef, in 'pockets' within the boundstone and as massive areas. The reef rock was cut by fissures which were also filled with siliciclastic

fig. 2.15 *a.* Photomicrograph of phylloid algal blades **(p)** with similar orientation, which have been micritised, leached (and impregnated with blue epoxy) and which baffled peloidal sediment and then were entirely surrounded by early marine cement **(c)**. Scale bar 250 µm. *b.* Photomicrograph of botryoidal acicular cement **(c)**, encrusted by isopachous *Archaeolithoporella* laminae **(A)**. Plane polarised light. Scale bar 500 µm. McKittrick Canyon.

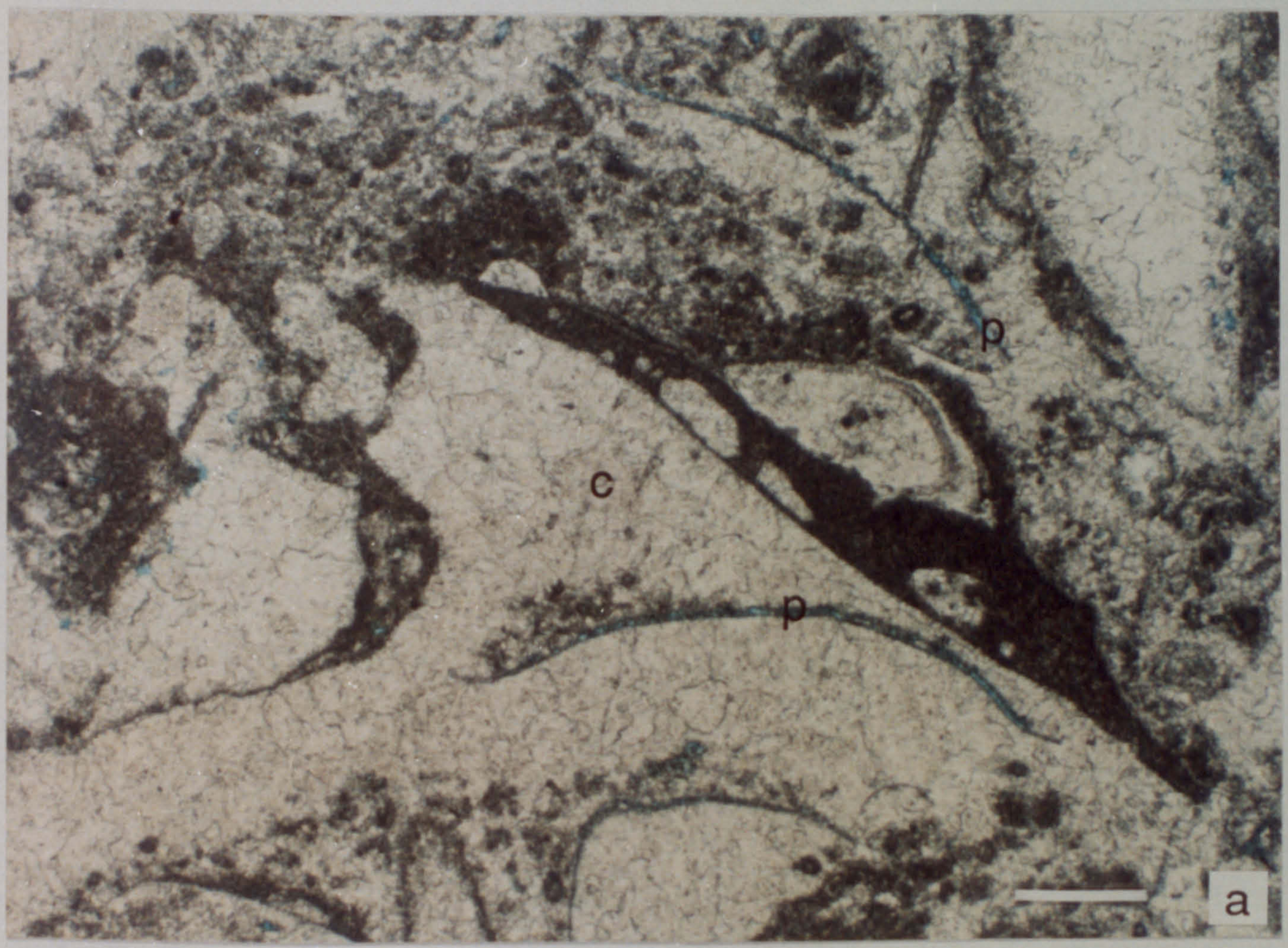

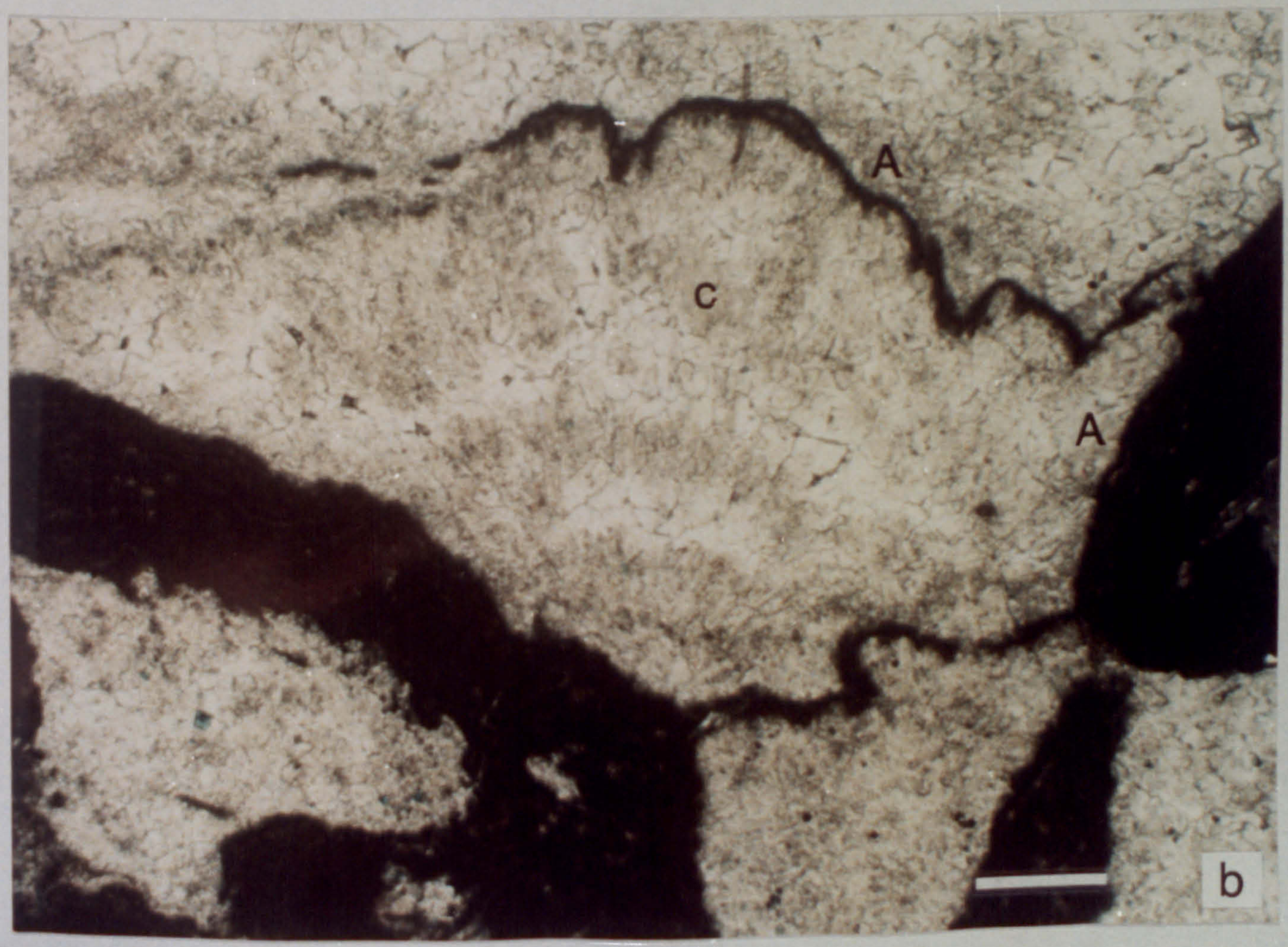

fig. 2.15

silts as well as grainstones and cements. The formation of fissures was probably one of the mechanisms which generated some of the large boulders of boundstone which occur on the foreslope.

2.4.3 Foreslope facies

The foreslope facies varies in character with distance downslope from the reef, and will therefore be described in three parts, upper, mid and lower foreslope. The rocks of this facies were examined in vertical traverses above and below the 'reef trail' (fig. 1.9 and 2.16). The section examined in the upper foreslope facies is of upper Mid-Capitan age and the section examined in the lower foreslope is of Upper Capitan age. This progressive younging downslope is a reflection of the eroded topography of the foreslope facies; strata of Upper Capitan age are largely removed in the upper foreslope, reef and back reef facies. Also, the 'reef trail' ascends into progressively older strata (fig. 2.16).

Upper foreslope Near the top of the slope, reef boundstones and grainstones interdigitate and grainstones commonly fill 'pockets' surrounded by boundstones. However, most of the strata of the upper portion of the slope (fig. 2.17) are grainstones and packstones which dip at 30° - 40° in a basinward direction; although dips of up to 45° - 50° are found in places. The main components of the grainstones are skeletal fragments and include bryzoans, sponges, *Mizzia*, brachiopod and crinoid ossicles, but also include some lithoclasts and peloids. Micrite envelopes are common around the grains and these envelopes are usually selectively dolomitised.

Some areas are selectively and/or pervasively dolomitised (chapter 3); a process which seems to be controlled to some extent by bedding (fig. 2.18a). The pervasively dolomitised areas are always grainstones as opposed to interdigitated boundstones. Flat floored, dipping cavities are common within the grainstones. These cavities are elongate downslope, dip in a basinward direction and are generally filled with calcite spar (fig. 2.18b). Where boundstones inter-digitate with the foreslope strata, botryoidal cements partially fill cavities and are preciptated onto grainstone layers within the boundstone (fig. 2.18c). The remaining pore space is always filled with calcite spar.

Aligned and unbroken fusulinids, of the genus *Polydiexodina*, form a prominent outcrop amongst grainstones of the upper foreslope facies (fig. 2.18d). Most grainstones are well-sorted, but it is unusual that individual units are dominated by a single grain type. Most grainstones are composed of a variety of fragmented skeletal

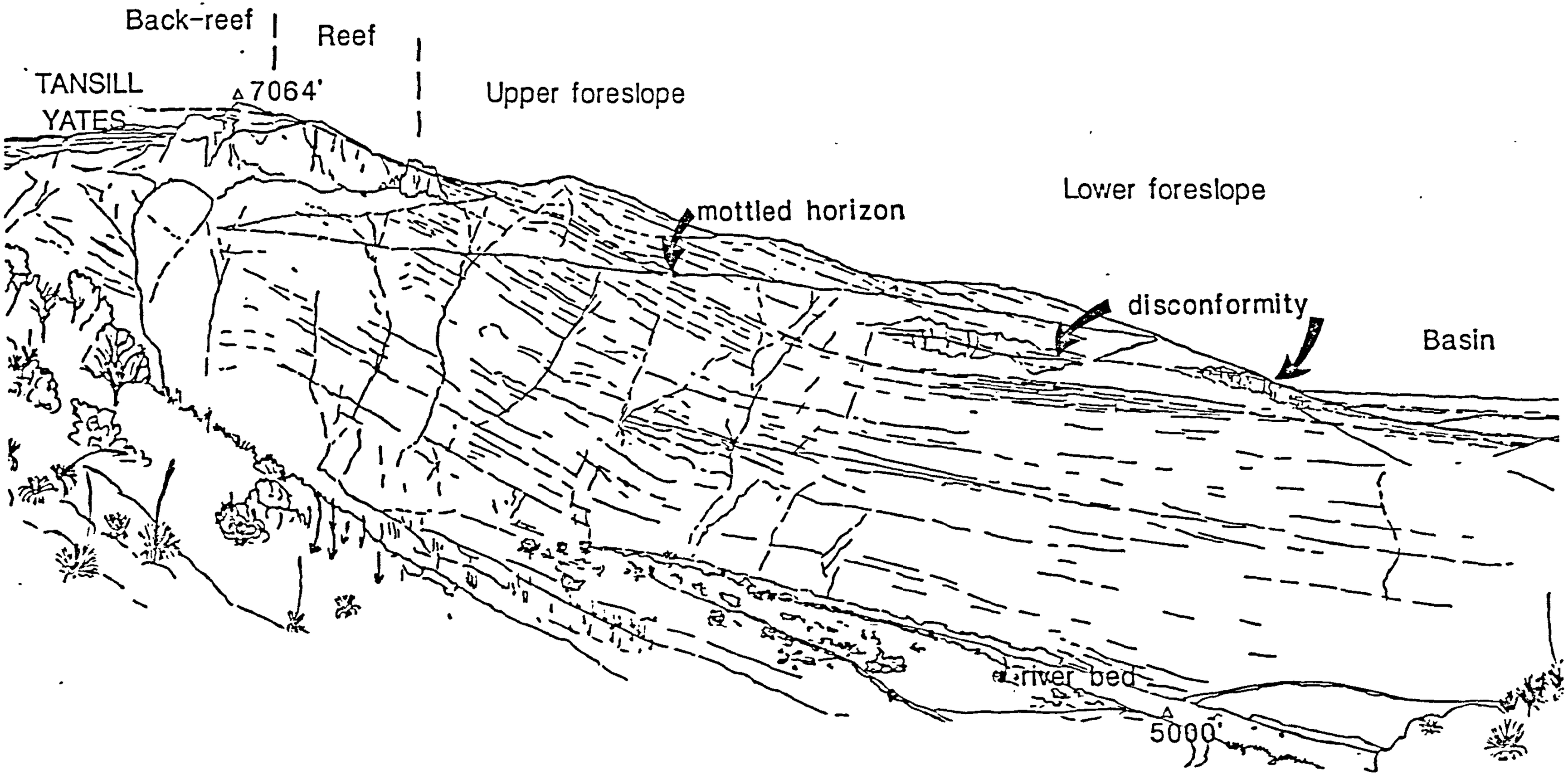

fig. 2.16 Sketch (from overlay of photographs, see fig. 1.9) of the facies exposed on the north-east wall of the mouth of McKittrick Canyon and their age relationships. In the foreslope facies, the 'reef trail' ascends into progressively older strata, and erosion has removed the upper foreslope, reef and back reef facies rocks of Upper Capitan age *i.e.*, Tansill equivalent strata (Tyrrell, 1969). Correlation of the disconformity identified in the basin margin facies, with the bioturbated horizon in the mid-foreslope facies is also shown.

Location: McKittrick Canyon 'reef trail'

Formation: Capitan limestone upper foreslope facies

Age: upper Mid- Capitan

height	sample	lithology	structures sed.	structures diag.	grain size m	w	p	g	b	particles	%	components cements	%	dolomite%	colour	description	interpretations
117	M11															bryzoa still articulated	not much reworking
116																	
115	MT61 MT14														greyish pink		patchy dolomitisation
114	MT13											cc spar	5	matrix 50		calcite spar replacing shell fragments	
113	MT112										60	imc	40		light olive		
112															grey	reefy	early cementation
111											50	imc cc spar	5 45			ALP nodular boundstones and grainstones with dip of 35-45 degrees	intertonguing reef
110																	
109	MT60										50	imc	45	selective		dip 48/192	intertonguing reef
108	M21											cc spar	5	10	light olive	flat-floored cavities	
107												imc	15	selective	grey	dip at 6 degrees	grains washed over reef
106	MT59 - MT48											cc spar	15		pinkish grey	mainly skeletal debris mixture of grain sizes	inter bedded with massive reef facies
105																	
65m																	
41																occasional reef boulders compactional drapes	
40	M8															dip 27/228	
39																	
38	MT47											cc spar	20	pervasive		1 generation of calcite spar dip 30/225	
15m																	
12	MT114 MT113																
11															pinkish		
10	M9										50	cc spar k	50 5	pervasive in matrix	grey	uniform grain size recessive weathering no obvious sedimentary structures leached silt grains	
9																	
8	M24										50	cc spar k	40 2	selective		siliciclastic grains replaced by calcite	
7																	
6	MT16 MT107									silt	45	cc spar	5	pervasive		angular silt grains rubbly outcrop	inter bedded siltstones and carbonate strata
5	- MT102											cc spar	30	pervasive	grey orange	difficult to sample	
4	M23															replacive anhydrite?	
3										silt	40 10			matrix			
2	M22																
1	MT112 MT111 MT110										50	cc spar	50	selective 50	pinkish grey	replacive anhydrite calcite-filled fractures reef boulders	
0																	

fig. 2.17 Summary log of upper foreslope facies exposed above the 'reef trail' in McKittrick Canyon.

fig. 2.18 Upper foreslope facies; *a.* Dip of the upper foreslope strata. The strata apparently controls dolomitisation; the whitish coloured bed is pervasively dolomitised (**d**) and the grey bed is still limestone (**l**). *b.* Cavities containing dolomitised botryoidal, acicular cements (**b**); the cavities are elongate and define the dip of the upper foreslope strata. *c.* Internal sediments overlain by botryoidal cements (**b**); the remaining pore-space is filled by calcite spar. *d.* Dip of foreslope defined by aligned fusilinids (*Polydiexodina*). McKittrick Canyon. Hammer 30cm long, lens cap 6cm, scale bar in centimetres, or pencil for scale.

fig. 2.18

fig. 2.19 *a.* Dolomitisation apparently following bedding in upper foreslope grainstone, and producing a 'nodular' appearance and pinkish grey colour. *b.* Some dolomitised 'nodules' appear to be reworked. *c.* A calcite-replaced sponge cross-cuts the boundary between dolomitised and non-dolomitised rocks, indicating that the 'nodules' are a result of diagenetic rather than sedimentary processes. McKittrick Canyon. Hammer 30cm long, or finger-tip for scale.

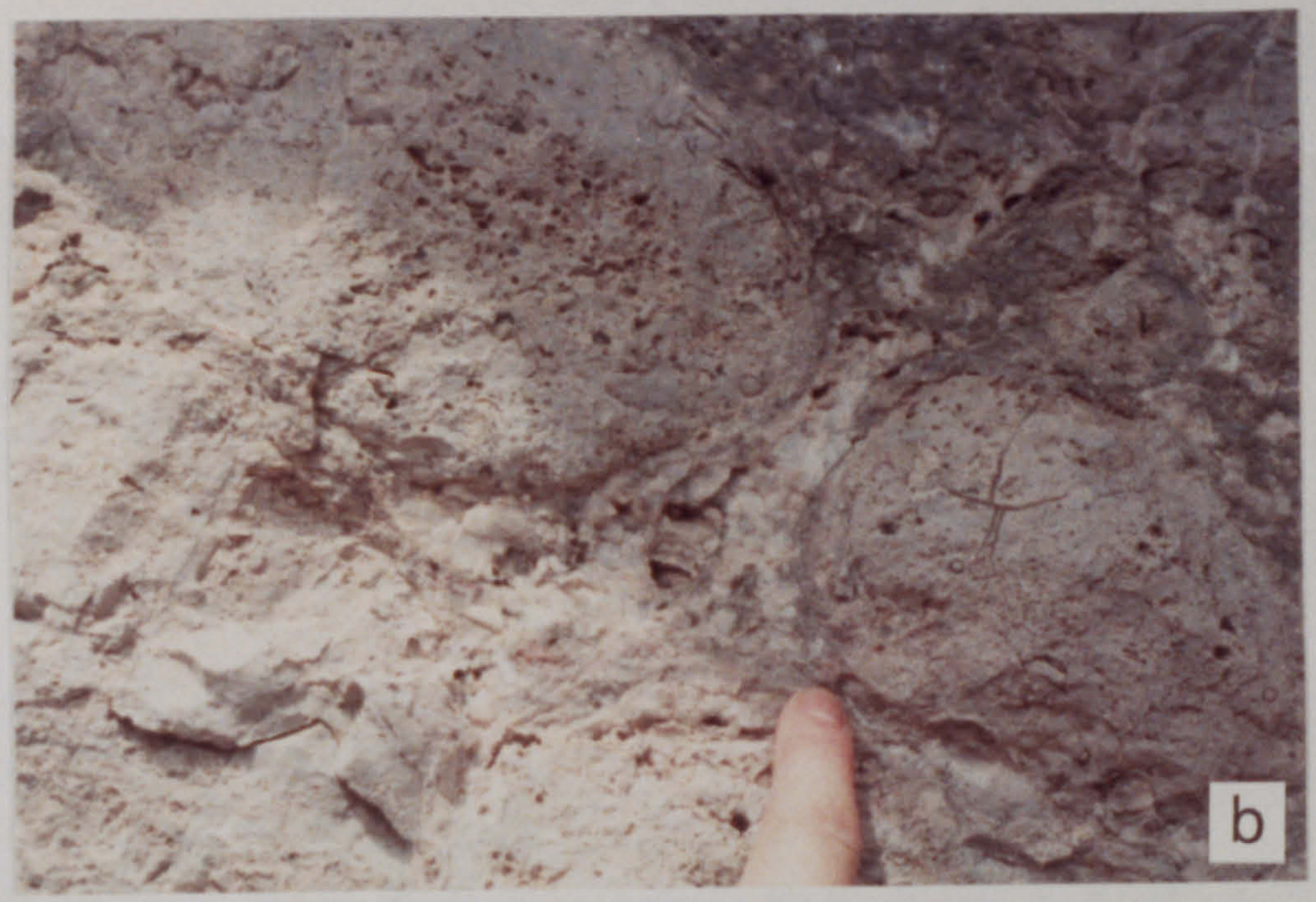

fig. 2.19

fig. 2.20 *a.* Horizontal fill of carbonate grains filling a fracture (f) which cross-cuts dolomitised, dipping foreslope beds. *b.* lithoclasts and sponges surrounded by calcite spar, in breccia matrix of upper foreslope flow unit. *c.* Siltstone smothering sponges (s) and forming geopetal structures (g) in upper foreslope strata. Sponges and other skeletal material has been pervasively dolomitised and all voids are filled by calcite spar. Pencil 15cm long or lens cap 6 cm for scale. *d.* Photomicrograph (plane polarised light) of the matrix of the siltstone which forms geopetals in the upper foreslope facies. It mainly comprises angular, sub-rounded quartz grains, with a dolomite matrix. Scale bar 1mm. Upper foreslope facies, McKittrick Canyon.

fig. 2.20

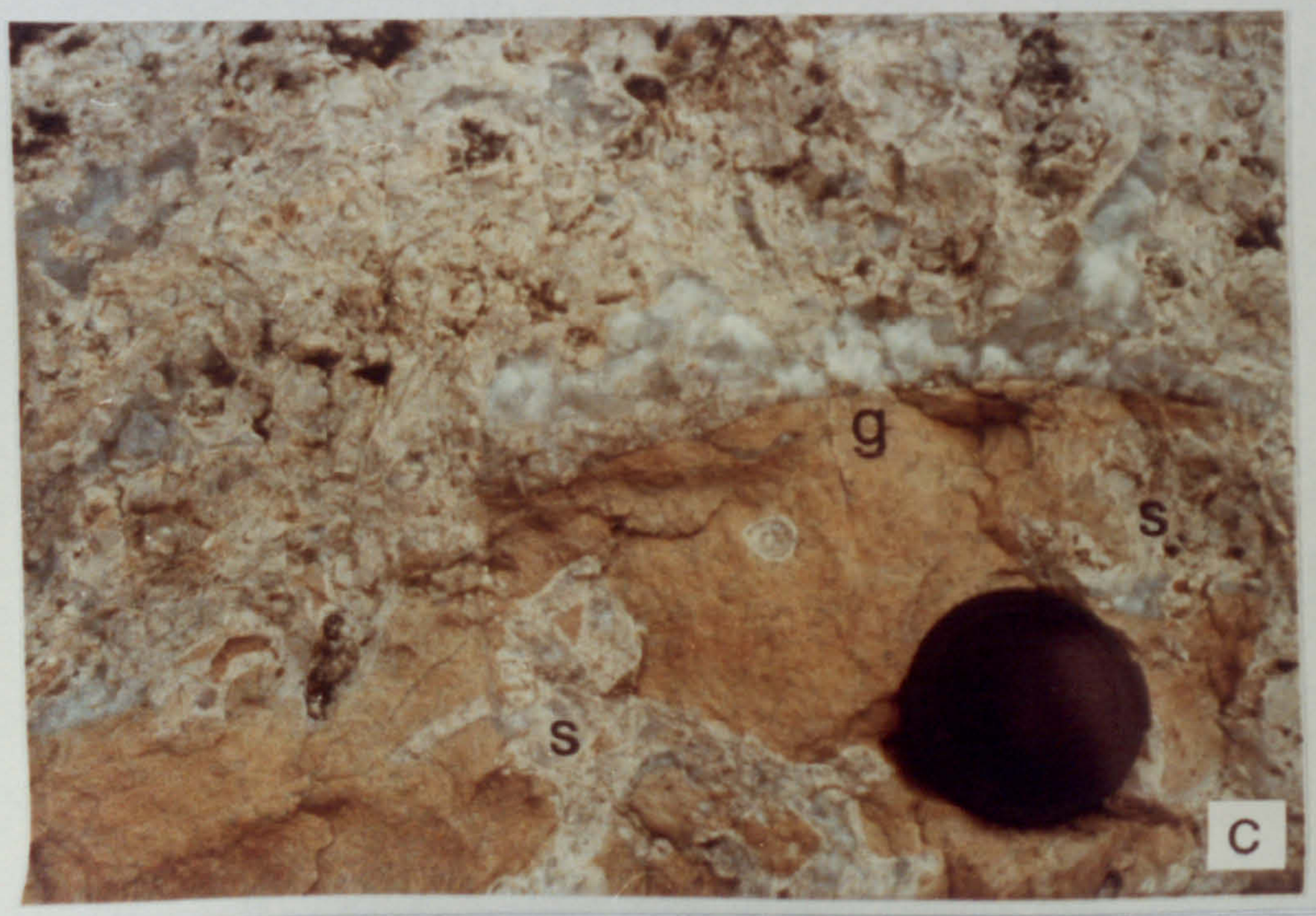

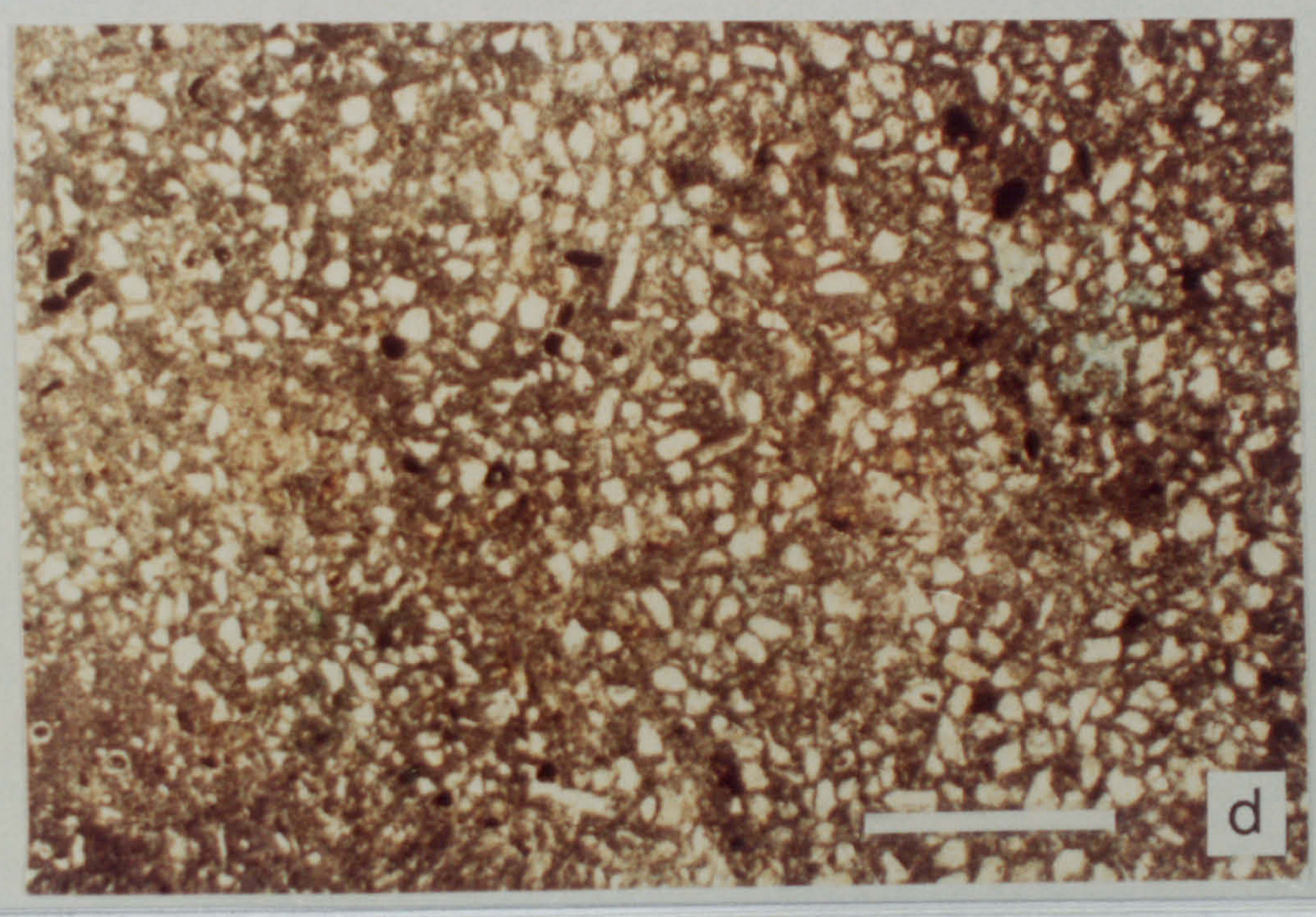

Location: McKittrick Canyon 'reef trail'

Formation: Capitan limestone mid-foreslope facies

Age: Upper Capitan

height	sample	lithology	structures sed.	structures diag.	grain size m	grain size w	grain size p	grain size g	grain size b	particles	%	components cements	%	dolomite%	colour	description	interpretations
27																breccia matrix	
26																dominantly reef boulders	reef collapse large scale flows
25																	
24																	
23																	
22																	
21																	
20												cc spar	20	pervasive 80			
19	MT43																
18	MT42													selective 60			
17	MT41																
16	MT40											cc spar		pervasive 70	very light grey	porous/chalky	
15																	
14																	
13	MT37 MT38														very pale	calcite-filled fractures	
12	MT39											cc spar		pervasive	orange	scoured channel base	channels large downslope flows
11	MT35 MT36														greyish pink	dolomitised mudstone clasts minor iron-staining	
10	MT44															calcite nodules, 2-4mm compacted reef boulders	
9																	
8	MT116																
7	MT115 MT45														light/ dark	travertine mottling/bioturbation	age unclear partial dolomitisation? deeper water
6	MT46														grey		
5																	
4																	
3																	
2	M26 MT117 MT118											cc spar		selective	pinkish	dip 28/218	
1	M25														grey	no large reef boulders well-bedded	
0	MT119																

fig. 2.21 Summary log of mid-foreslope facies, above and below the 'reef trail', McKittrick Canyon.

fig. 2.22 *a.* Well-bedded, mid-foreslope grain/wackestone strata, dipping at 28°. *b.* Scour surface (s) caused by grainstone (dolomitised) (d) cutting down into a unit composed of reef boulders (r). *c.* Close-up of dolomitised grainstone above scour surface, showing aligned mudstone clasts (m) and calcite spar-filled nodules. People, or lens cap 6cm, for scale. Mid foreslope facies; McKittrick Canyon.

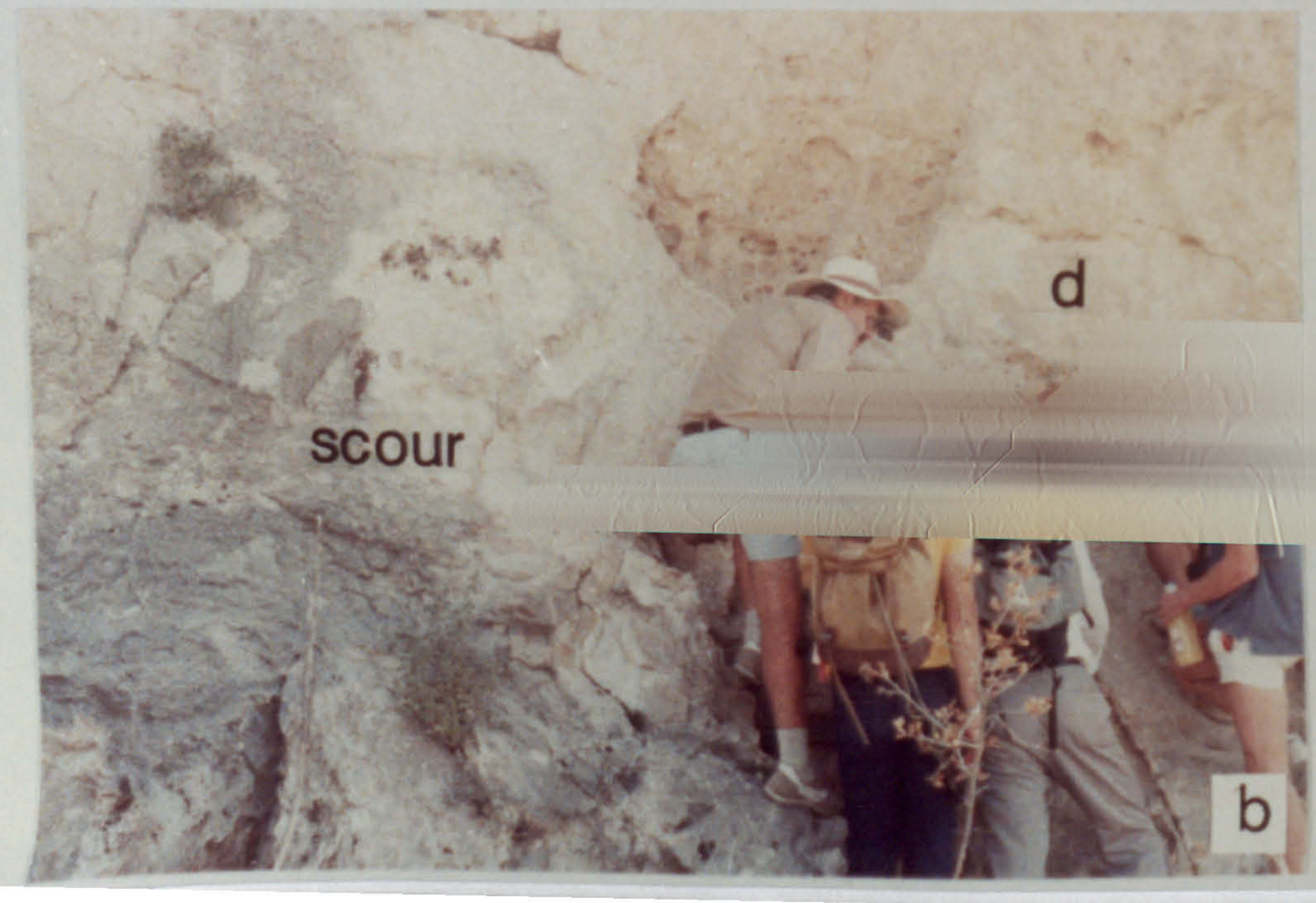

fig. 2.22

Mid-foreslope The mid-part of the foreslope (fig. 2.21) is composed of interbedded grainstones and wackestones interbedded with jumbled reef boundstone boulders which range in size from 'pebbles' to boulders about 5 metres across. Strata dip at around 28° (fig. 2.22 a). Grainstone units are more easy to trace than strata which contain large reef boulders. The composition of the grainstones in this part of the foreslope is similar to that of the grainstones in the upper part of the foreslope, although some ooids were found in some of the strata of the mid-foreslope and these have not been observed in *any* of the other facies. The reef boulders are also similar to those found elsewhere on the foreslope *i.e.*, up to 5m in diameter. These are generally compacted against each other and the intervening breccia matrix is squeezed and draped around the boulders. One large erosional scour surface is visible where a grainstone unit cuts down into strata composed mainly of reef boulders (fig. 2.22b). This grainstone contains mudstone clasts (fig. 2.22c) and both the grains and the mudstone clasts are pervasively dolomitised and contain many calcite-filled nodules.

There are many stylolite contacts throughout this part of the slope (fig. 2.23) and these are commonly iron-stained. The stylolites have several orientations, although they are most commonly sub-horizontal, and have amplitudes up to 10cm. Boundstone boulders are commonly separated by stylolites *i.e.*, no 'matrix' is present (fig. 2.23a). A particularly distinctive, extensively stylolitised, mottled mudstone horizon outcrops at 7-8m (fig. 2.23b). The mottled areas have diffuse margins; in thin section it can be seen that the mottling is due to varying degrees of dolomitisation, with the paler areas at outcrop being more heavily dolomitised than the darker areas. Reworked angular to sub-rounded clasts of the same lithology are found in some wackestones (fig. 2.22c) in the same part of the section, and are sufficiently abundant in some strata to constitute a breccia.

Travertine is common in this part of the section (fig. 2.23d). It is not readily apparent whether this travertine resulted from modern or past periods of drawdown in the foreslope. Thin section examination shows that the travertine is partially dolomitised (chapter 3).

lower foreslope The succession in the lower part of the slope comprises a combination of dark grey mudstones and wackestones interbedded with chaotic strata containing large, 2-5 metre diameter, rounded to sub-rounded reef boundstone boulders (fig. 2.24) in a breccia matrix. The reef boundstone boulders are similar to those found elsewhere on the slope, though in this region they are better exposed and appear to be more abundant. There are of two types of boulders: reef boundstone is the commonest *i.e.*, containing sponges, *Archaeolithoporella* and cements; the less common type is

composed of grainstone, which has distinctive 'smooth' weathering relative to the irregular weathered surface of the enclosing breccia matrix (fig. 2.25a). Reef boundstone boulders *are not* dolomitised although the grainstone boulders *are* dolomitised.

Where present, the mudstones are similar in lithology to those of the basin margin (section 2.4.4) and some of these mudstones have been reworked to form part of the matrix to units which contain boundstone boulders (fig. 2.25b,c) in the lower parts of the section. Generally, the matrix is a breccia composed of sub-angular to sub-rounded clasts ranging in size from millimetres to decimeters. The clasts are fragmented lithoclasts of reef and grainstone mixed with various skeletal grains and carbonate mud. This matrix is commonly pervasively dolomitised (fig. 2.26a), and calcite-filled nodules are common here. The distinction between pervasively dolomitised 'matrix' and non-dolomitised boundstone boulders is sharp and is readily apparent at outcrop by the difference in colour (fig. 2.26b).

Siliciclastic silt geopetal fabrics are present in some reef boulders (fig. 2.26 c); some are horizontal, and are composed of siliciclastic silt and mixed silt-and-carbonate grains, whilst others have other orientations. At least one silt geopetal which post-dates calcite spar is present (pers. comm., G. M. Harwood, 1989).

Interpretation

At the transition between the reef and the upper foreslope facies *in situ* reef and allochthonous reef boulders on the foreslope are difficult to distinguish. However, it appears that boulders of reef are not common in this part of the foreslope and that where boundstones occur, they are *in situ.* Most of the foreslope consists of gently dipping strata composed of sequences of grainstones, packstones and wackestones interbedded with units of breccia which contain reef boulders. Most of the dip of these strata is primary as demonstrated by topographic relationships visible at outcrop (fig. 1.9 and 2.16). However, some compaction of the foreslope strata must have occurred to generate dips of 50°, which are greater than the angle of repose, in the upper parts of the foreslope. Also, cavities in the upper foreslope facies dip basinward at about 10°; these may originally have been horizontal and their dip could be due to compaction. It is not clear how much compaction was syn-sedimentary and how much compaction was later, due to burial. However, dip in the upper slope is about 10° greater than the lower slope, stylolites are more common and have higher amplitudes in the mid-lower regions of the slope than in the upper parts of the foreslope, and the proportions of packstones to grainstones increases downslope. All these observations suggest that the reef, which was

fig. 2.23 *a.* Stylolite contacts separating reef boulders. *b.* Distinctive mottled mudstone, containing an articulated crinoid stem (c) and stylolite contacts. The mottling is due to variable dolomitisation, with the paler areas being more dolomitised. *c.* Reworked mudstone lithoclasts (arrowed) in a laminated, stylolitised wackestone. *d.* Banded travertine in cavity. McKittrick Canyon. Mid-foreslope facies. Lens cap 6cm.

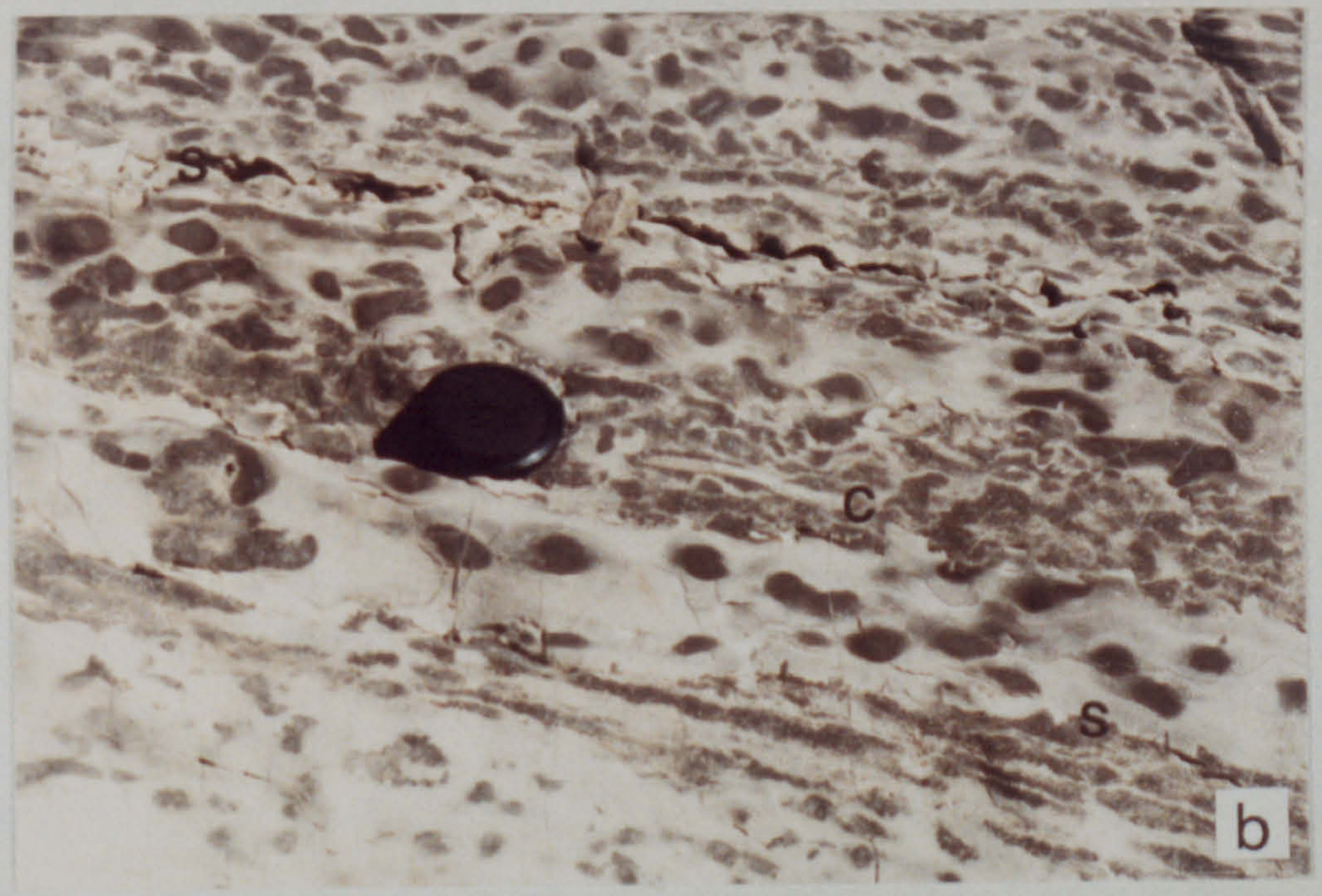

fig. 2.23

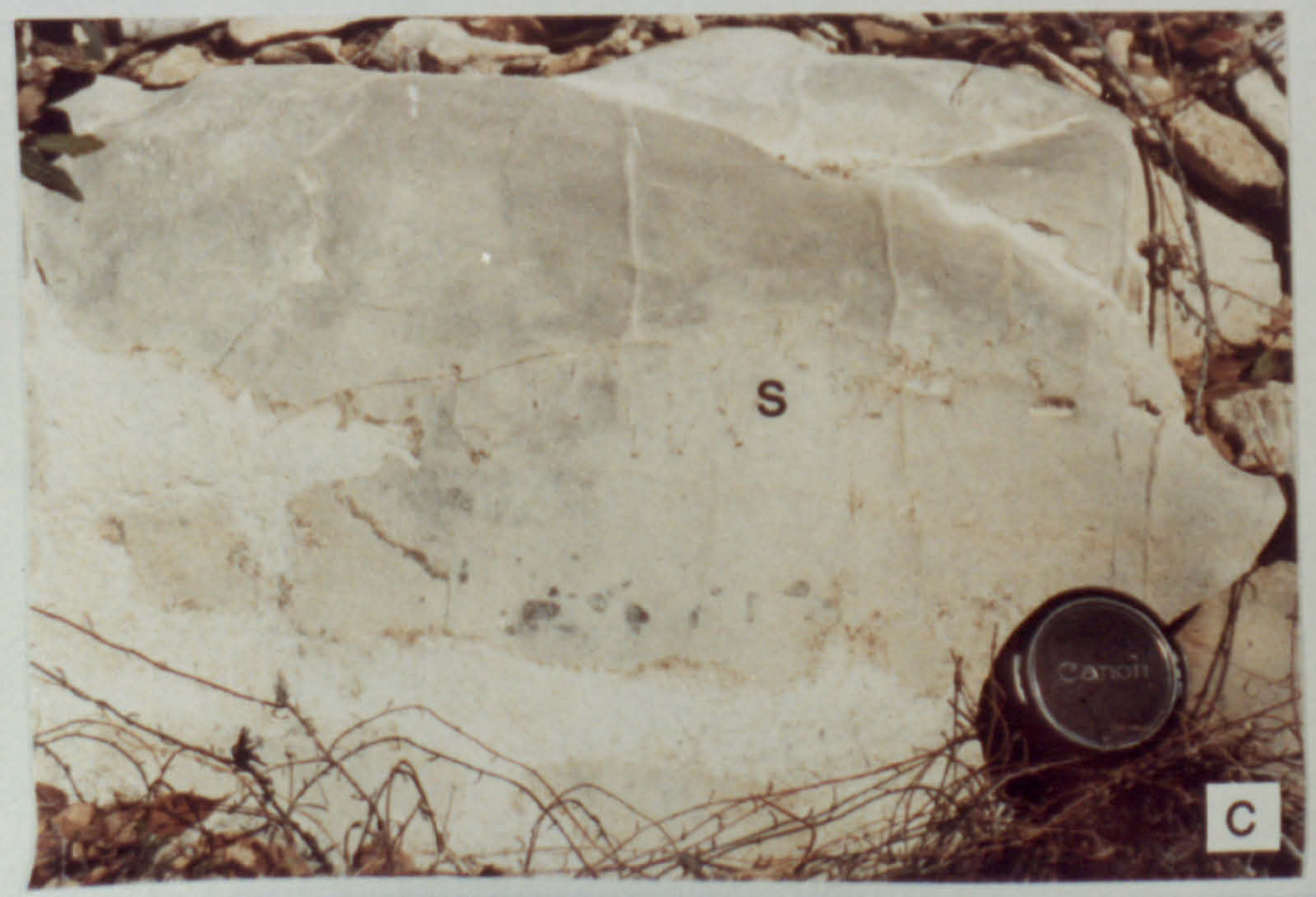

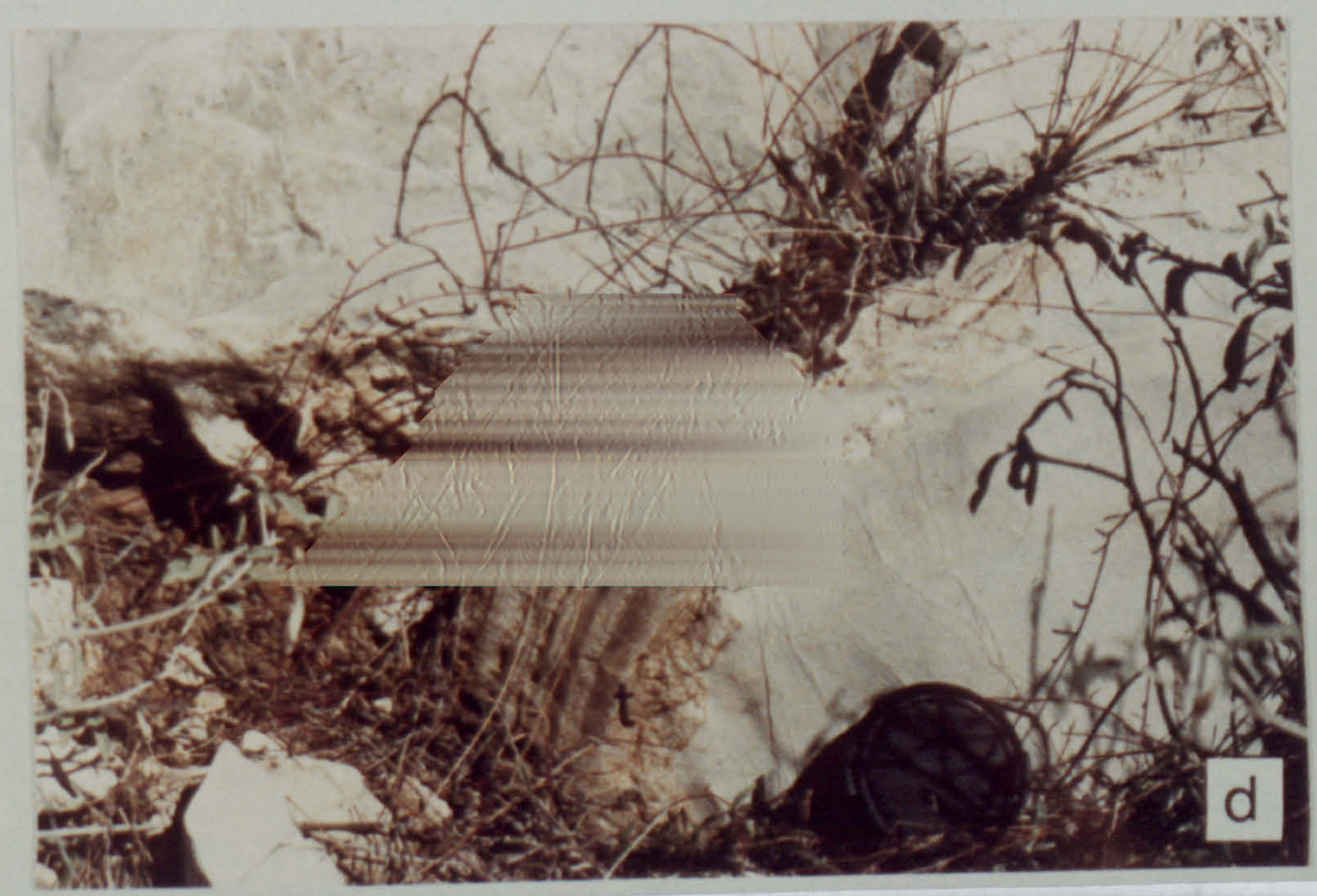

Location: McKittrick Canyon 'reef trail'

Formation: Capitan limestone lower foreslope facies

Age: Upper Capitan

height	sample	lithology	structures: sed.	structures: diag.	grain size: m	w	p	g	b	particles	%	components: cements	%	dolomite%	colour	description	interpretations
36										matrix		cc spar	15	pervasive in matrix	yellowish grey	compacted no bedding visible within flows, but flows are distinguishable	super-imposed distal foreslope debris flows
35																	
34										boulders				minor selective in boulders	light olive grey		
10m																	
24																	
23	M6									matrix							
22											50	k	5	pervasive	dusky yellow	calcite-filled nodules after anhydrite	replacive anhydrite
21											10	cc spar	30				
20										boulders	10						
											75	cc spar imc	10 15	minor	olive grey	mostly non-dolomitised grainstone	
19																geopetal silt in reef boulder	age of geopetal silt unclear
18	M5 M4																
17																	
16																	
15																	
14															dark grey		deeper water
13										mud						shells define compactional fabric parallel to bedding	extensive compaction
12																	
11															dark-medium grey	fewer inter-bedded reef boulders	
10																	
9																	
8																	
7															dark-medium grey	bioturbation	deeper water
6																	
5																	
4										mud		silica				bioclasts often silicified	
3																	
2																	
1																	
0																	

fig. 2.24 Summary log of lower foreslope facies, above the 'reef trail', McKittrick Canyon.

fig. 2.25 *a.* Large grainstone boulder with distinctive smooth weathering surface in lower foreslope. *b and c.* Breccia matrix containing reworked dark grey mudstone lithoclasts (m) and large reef boulders (**rb**). Clip board 30cm, lens cap 6cm. Lower foreslope facies, M^{c}Kittrick Canyon.

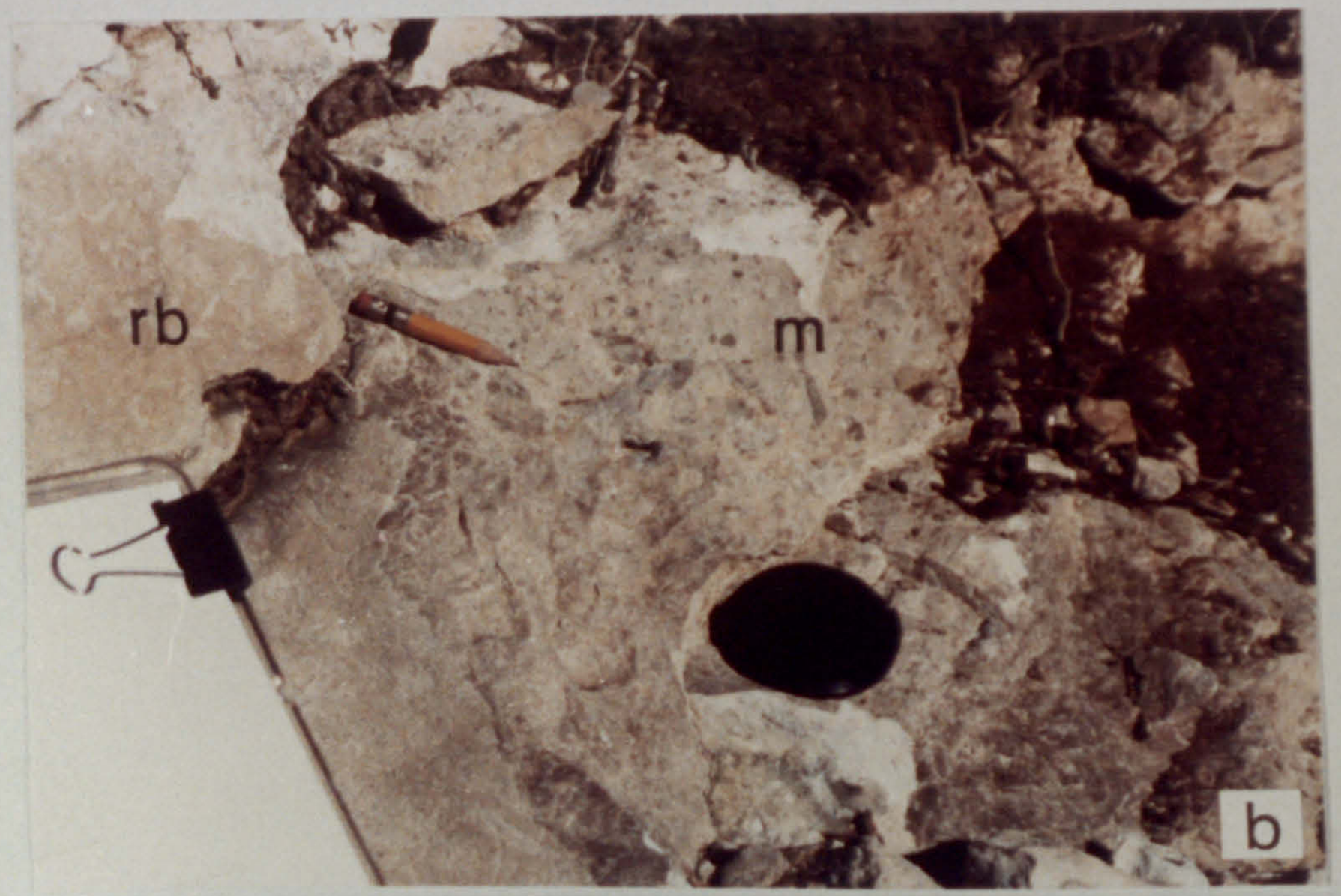

fig. 2.25

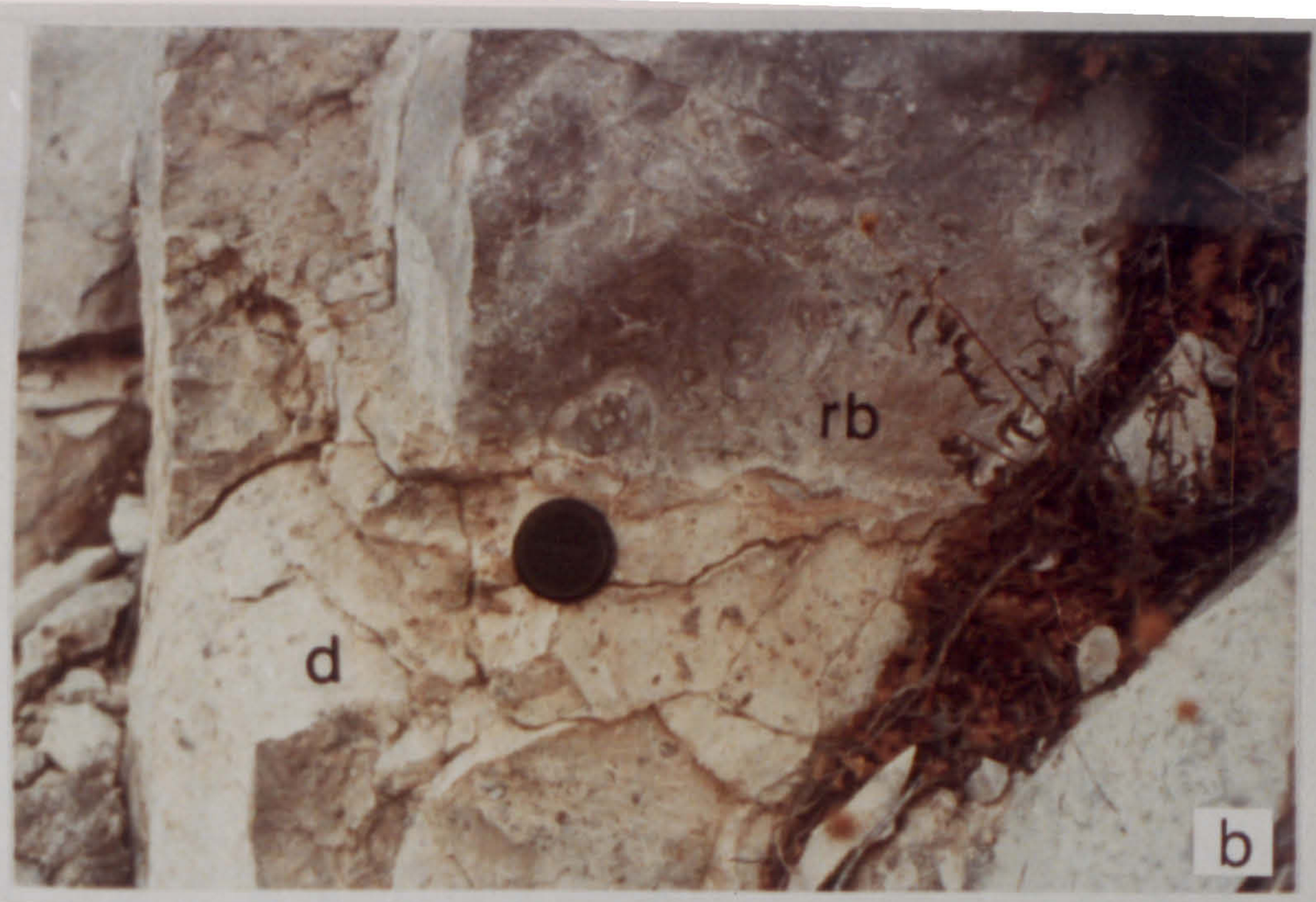

fig. 2.26

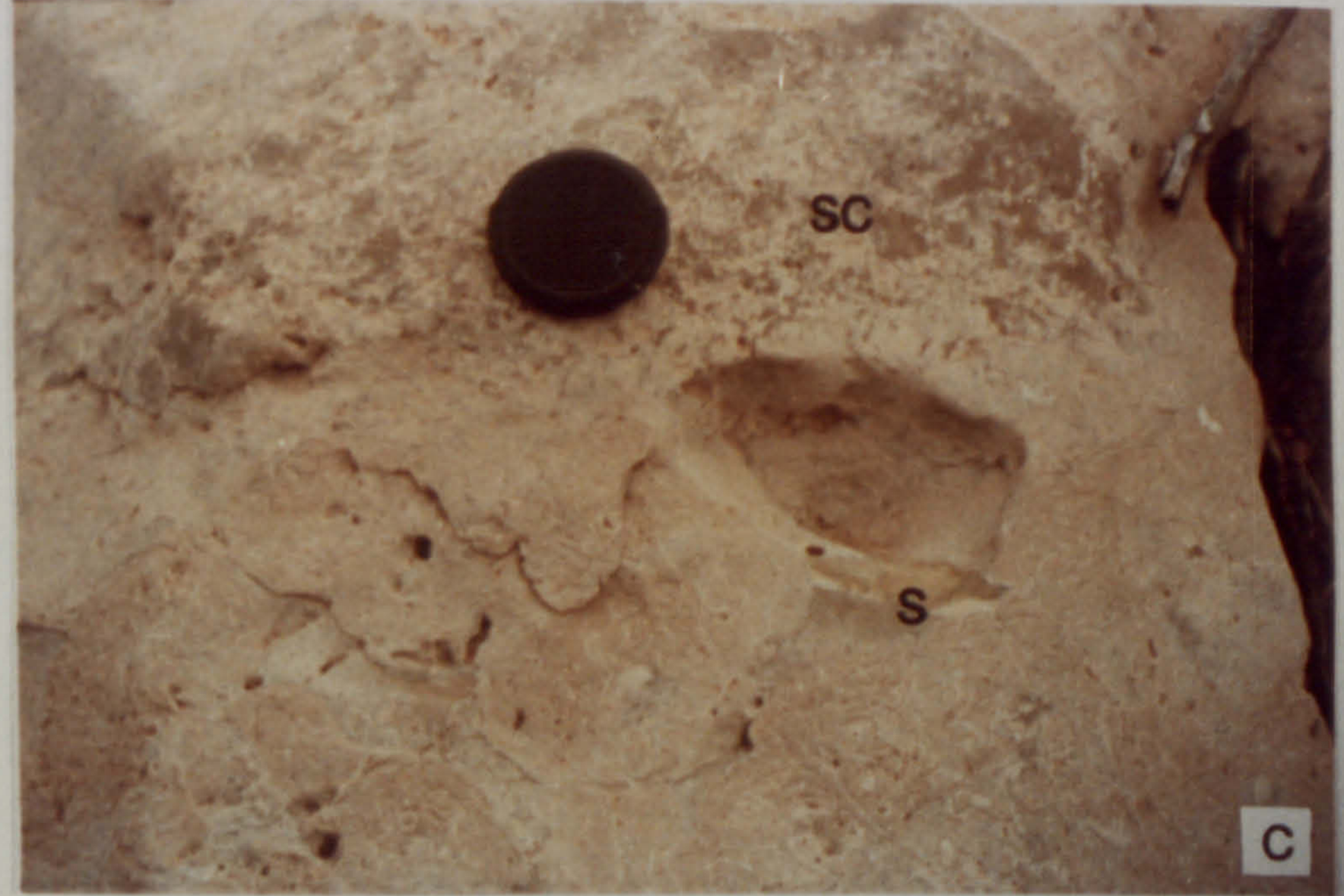

fig. 2.26 *a. and b.* Pervasively dolomitised (d) breccia matrix to debris flow containing non-dolomitised reef boundstone boulder (rb); the boundary between dolomitised and non-dolomitised rock is sharp and clearly visible from the colour difference. Calcite spar- filled nodules (c) are associated with the dolomitised matrix. *c.* Geopetal silts (s) and mixed siliciclastic/carbonate fill (sc) within reef boundstone boulder. McKittrick Canyon. Lens cap 6cm.

lithified early and formed a rigid mass, suffered little compaction and that the deposits of the foreslope *were* compacted. The larger amplitude of stylolites in the lower foreslope and the greater proportions of packstones to grainstones suggest that lower slope deposits underwent compaction for a longer duration than the upper slope deposits.

Lack of compactional features in the grainstones suggests that cementation was probably earlier in the upper slope deposits than in the lower slope deposits. The mudstone lithologies of the basin margin facies appear as reworked lithoclasts in the matrix to some flows; this indicates that these mudstones must have been at least partially lithified before they were reworked.

The similarity of grains found in strata on the foreslope facies with those found *in situ* in strata of the back reef facies, and the presence of reef boulders on the foreslope, indicate that the sediment deposited on the foreslope was sourced from the grainstone belt behind the reef and from the reef itself. All the grain types which occur in the deposits of the foreslope facies are also found in the reef and back reef facies. Organisms such as the fusulinid *Polydiexodina*, which forms a prominent bed on the upper foreslope, may have lived in the shallow waters of the back reef facies or above the reef. In either case it seems likely that the abundance of these organisms in this particular deposit represents a death assemblage, formed due to large stress being placed on the environment in which they lived *e.g.*, a storm. It is not clear how much reworking of upper foreslope deposits took place, but some is likely. The presence of lithified, rounded grainstone boulders at the base of the slope and grainstone intraclasts in the breccia matrix of many strata, confirms that reworking of upper foreslope deposits occurred, and that these upper foreslope deposits were lithified early. Fractures in upper slope deposits and the reef support the interpretation that cementation was early. Fracturing of these deposits may have caused lithified blocks to become completely separated and allowed these boulders to fall down the foreslope. The proportion of reef boulders to grainy deposits appears to increase downslope; the majority of upper slope strata are grainstones and wackestones whereas the majority of lowerslope strata are breccia containing large boulders. This apparent differentiation may be a reflection of the foreslope that the 'reef trail' traverses, because the upper foreslope is of Mid Capitan age and the lower foreslope is of Upper Capitan age. Another explanation for the relative abundance of large boulders in the lower foreslope, is that a large proportion of the smaller grains and mud that were deposited in this facies, was displaced by the processes of compaction which strongly affected the lower foreslope facies.

Scoured surfaces and the cross-cutting relationships of some strata suggest that deposition of some strata was as a result of high-energy flows. The strata above a

well-exposed scour surface are grainstones overlain by reef boulders. This relationship suggests that some large-scale, episodic flows may have caused the deposition of the thicker, well-bedded grainstone units and the graded grainstone units, with the reef boulders being supported by the grainstone. These high energy flows probably resulted from down-slope movements generated by instability of the foreslope deposits, due to the relatively steep primary dip of the foreslope. Breccia and rounded reef boulders might have formed by gradual downslope creep of foreslope sediments. Continuous deposition of lesser amounts of grainy debris and mud was probably interspersed with these large scale flows.

It is ambiguous as to whether the horizontal geopetal fabrics are pre- or post-redeposition because it is possible that a boulder already containing geopetal silts could have been re-deposited the 'right' way up, or that the silt formed the geopetal fabric *after* the boulder had been re-deposited on the foreslope. The presence of geopetal fabrics which are not horizontal suggests that at least some of the geopetal fabrics were already present in lithified reef boulders prior to re-deposition. However some siliciclastic silt was deposited contemporaneous with the carbonates of the foreslope. The evidence for this comes from the interbedded siltstone and carbonate units. A large influx of silt filled cavities in between sponges and other skeletal debris on the fore reef forming some geopetal fabrics before cements had time to precipitate over these skeletal components, and the remaining silt formed a 2 metre-thick unit. The deposition of at least some of the geopetal silts *after* the precipitation of the calcite spar (chapter 3), indicates that *these* silts were deposited relatively recently.

The dark mudstones with bioturbation features in the mid-part of the foreslope imply deeper water and lower sedimentation rates *i.e.*, more stable conditions than is represented by the majority of the foreslope deposits. This may be attributed to a rise in sea level which would make this part of the lower foreslope facies equivalent to the basin margin facies. The variable dolomitisation may be a purely diagenetic feature or may have been controlled by primary features of the rock such as bioturbation. The presence of an articulated crinoid stem enclosed within one of the mottled areas (fig. 2.23b) suggests that a diagenetic process may have been the primary control, rather than bioturbation. L.C. Babcock (1977) interpreted the mottling as being the result of bioturbation, and correlated this mottled zone with a bioturbated zone traceable in the basin facies. This is perhaps an over-simplification, as many other mottled horizons occur in similar mudstones (L.C. Babcock, 1977). The incorporation of mudstone clasts, in the matrix to flows which contain boundstone boulders, suggests that partial-lithification of these mudstones occurred early enough for down-slope processes to rework this mudstone and form clasts.

A prominent feature of the foreslope facies in particular, is the volume of calcite spar present. This occludes all void spaces left after the precipitation of earlier cements as well as cementing fractures and filling nodules. This calcite spar is associated with the presence of dolomitised carbonates. Calcite spar also fills all void space in the reef, and in the back reef facies where it fills pores and fractures which have castellated margins (fig. 2.7d). These relationships are discussed in chapter 3.

2.4.4 Basin margin facies

The strata exposed in the low cliffs at the mouth of McKittrick Canyon are of Lamar age (Tyrrell, 1969) and are packstones, wackestones and mudstones (fig. 2.27). Bedding is well defined, on a centi-decimetre scale, and is accentuated by stylolites. The stylolites are sub-horizontal and low amplitude (usually less than 2cm). The wackestones and packstones contain silicified skeletal fragments (echinoids plates, brachiopod shells, horn corals, foraminifers and ostracodes; fig. 2.28a) and also contain siliciclastic silt grains. The lower part of the section consists of a sequence of finely bedded dark grey mudstones which contains few skeletal fragments; these are organic rich and have a noticeable smell of hydrocarbons when fractured with a hammer. The mudstones are bioturbated and this results in a mottled appearance which has been enhanced by stylolites. The mudstones (0-20m) are siliceous, homogenous and are commonly jointed. The mudstones are part of fining upward sequences (fig. 2.28).

Breccia units composed of sub-angular, reworked mudstone lithoclasts in a muddy matrix are interspersed with the wackestones, packstones and mudstones (fig. 2.28c). These mudstone lithoclasts are a similar lithology to the mudstone clasts which are present in parts of the lower foreslope facies. Other breccia units occur which have quite a different appearance; these appear to have been fractured *in situ*, by fractures (fig. 2.29a,b) which are cemented by calcite and contain some dickite (chapter 3). These fractures strike at 205°, subparallel with the reef escarpment and this is the same strike as the large fracture system at the margin of the back reef and reef facies (section 2.4.1).

There is a disconformity towards the top (26m) of the low Lamar cliff at the base of the 'reef trail' (fig. 2.30 a). The difference in dip of beds above and below the disconformity is small, and is more a difference of strike than of dip. The disconformity observed in this outdrop is also visible on the south-western side of the mouth of McKittrick Canyon. What appears to be an enormous block of foreslope (note dip) rests on basin margin facies mudstones on the roadside at the entrance to the carpark at the mouth of McKittrick Canyon (fig. 2.30b). This may be a large transported block, or

Location: McKittrick Canyon 'reef trail'

Formation: Lamar limestone basin margin facies

Age: Upper Capitan

height	sample	lithology	structures: sed.	structures: diag.	grain size: m	grain size: w	grain size: p	grain size: g	grain size: b	components: particles	components: %	components: cements	components: %	components: dolomite%	colour	description	interpretations
34																uniform sequence of well-bedded grey siliceous limestones organic rich	
33																	
32																	
31																	
30																	
29	M27									mud	90				medium/ dark grey	debris flow/turbidite	
28	M3															fractures strike at 204 degrees	distal slope facies
27																calcite-filled fractures	
26																downlap surface with slump fold associated	hiatus in sedimentation? sea level fluctuation?
25	MT22																
24																	
23																	
22																fractures trend 204 degrees	
21																smells of hydrocarbons when fractured in situ breccia	brecciation caused by movement of fluids
20	MT21											calcite dickite?	10				
19																mottling due to bioturbation	
18																	distal slope facies periodic turbidites
17																	
16																	
15															dark grey	weathered surface orange siliceous	
14	MT20										5	silica					
13																	
12																	
11																	
10																	
9																	
8	M2									mica silt mud	20 5 70	silica			dark grey	silicified bioclastic fragments	
7																	
6																	
5																	
4	M1											dickite				dickite in fractures	
3																	
2																slump fold	downslope movement of partially lithified sediment
1															dark grey	breccia flow thins downslope	
0																	

fig. 2.27 Summary log of basin margin facies, lower 'reef trail', McKittrick Canyon.

fig. 2.28 *a.* Photomicrograph of compacted wacke/packstone containing shell fragments **(s)**, echinoid fragments **(e)** and forams **(f)** with early cement fringes **(c)** in micrite matrix. Scale bar 1mm. *b.* Graded bed containing silicified skeletal fragments at the base. *c.* Breccia unit of sub-angular, sub-rounded mudstone lithoclasts in a wackestone matrix. Basin margin facies, McKittrick Canyon. Lens cap 6cm.

fig. 2.28

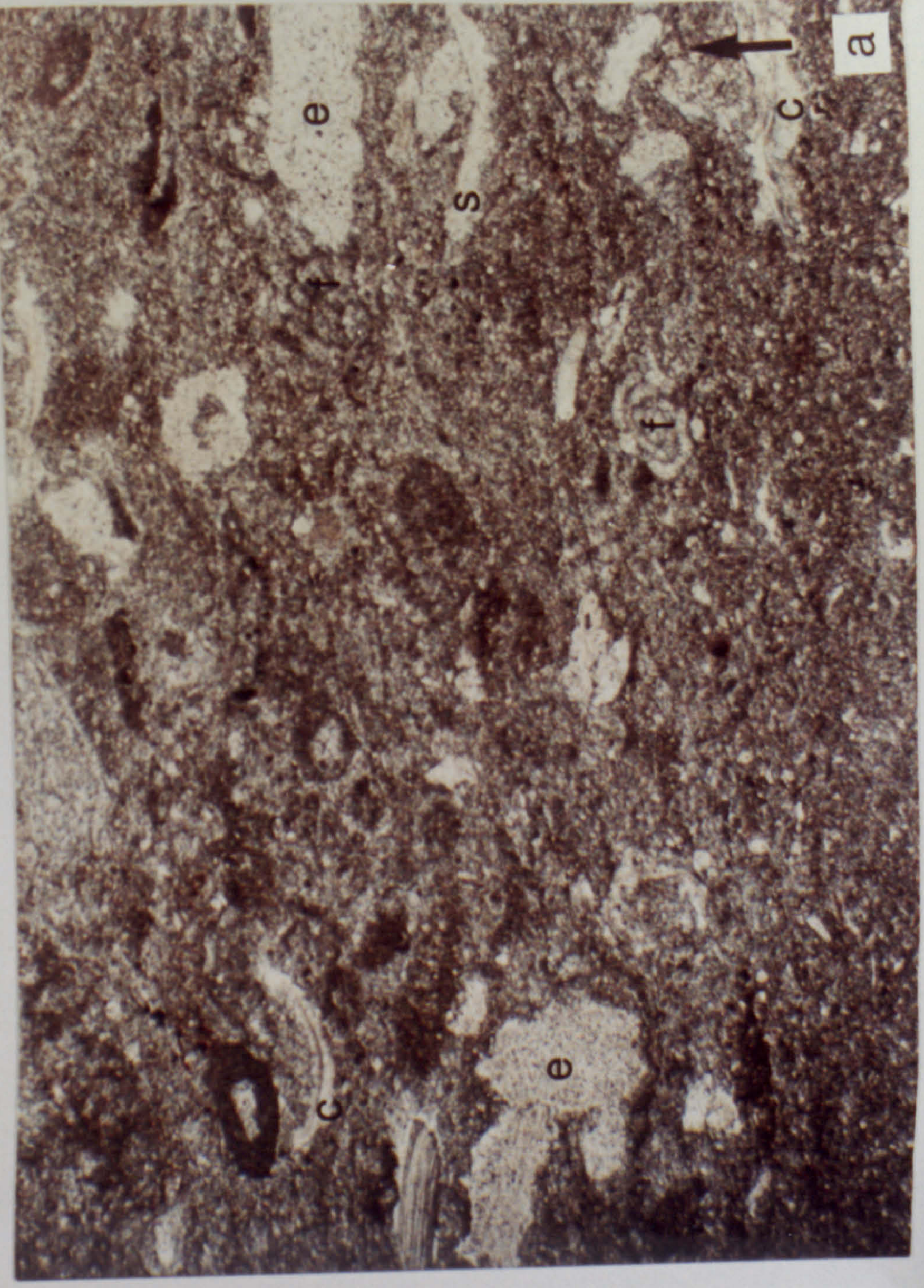

fig. 2.29 *a.* Breccia composed of mudstone clasts in mudstone matrix. *b.* Brecciated mudstone; fractures have strike of 205° and are filled with calcite and minor amounts of possible dickite. Basin margin facies, McKittrick Canyon. Hammer 30 cm long; compass 6cm diameter.

fig. 2.29

fig. 2.30 *a.* Well bedded grey mudstones which form a low cliff near to the 'reef trail' at the mouth to McKittrick Canyon. A disconformable surface is present 2 metres below the top of this outcrop. *b.* Large block (b) of dipping foreslope strata overlying well bedded grey mudstones. *c.* Slump fold in well bedded mudstones at disconformity surface. Basin margin facies, McKittrick Canyon. Scale bar 1 metre.

fig. 2.30

alternatively represent the intertonguing of the basin margin facies with lower foreslope facies. Slump features (fig. 2.30c) are associated with the disconformity in the Lamar cliff on the 'reef trail'.

Interpretation

The majority of strata in this facies are mudstones-wackestones which dip at around 5° and represent the distal parts of flows generated in the reef-upper slope area, mixed with continuous background sedimentation of a carbonate mud. Downslope movements generated slump folds and reworked mudstone clasts forming the breccias and possibly moving large blocks downslope. The bioturbated mudstones in the basin margin facies might be correlated (fig. 2.16) as they are in the same stratigraphic position within the sequence.

The disconformity may represent a rise in sea level causing downlap of proximal lower slope facies strata onto basin margin facies mudstones. A rise in sea level might also explain the occurrence of the mottled mudstones in the mid-part of the foreslope facies.

2.4.5 Basin facies

Strata in this facies were not examined at the same level of detail as the strata of the Capitan shelf margin which outcrop in McKittrick Canyon, because these basinal strata were peripheral to the main emphasis of this study.

Lamar limestone The Lamar limestone is the basinal equivalent of the Upper Capitan strata of the shelf margin (Tyrrell, 1969). A 3 metre section of Lamar limestone in an old road cut on US 62/180 was examined (fig. 2.31). The lowest beds are mottled and bioturbated (these have been correlated with the distinctive similar horizon in McKittrick Canyon (fig. 2.23b) by L.C. Babcock (1974)). The remaining sequence is well bedded, laminated, cherty, graded wacke-mudstones, containing sparse skeletal fragments and becomes more laminated and fissile towards the top. A slump fold with angular hinges is visible at 1.5m up the section (fig. 2.32a). Moulds of acicular radiating replacive evaporite minerals are present on some bedding plane surfaces (fig 2.32 b).

Interpretation Sediment input from the shelf edge at this locality 8 kilometres basinward of it, was minimal, except for thin turbidite units. Most sedimentation was

Location: Old road cut US 62/180 Formation: Lamar limestone basin facies Age: Upper Capitan

height	sample	lithology	structures sed.	structures diag.	grain size m	w	p	g	b	components particles	%	cements	%	dolomite%	colour	description	interpretations
3m										fine silt	90	clays?			grey-black	well-jointed, micritic uniform limestone	sedimentation by slow settling of lime mud
2.5m																	
2m																	
1.5m																slump fold, angular hinges	partial lithification downslope movement
1m			Z												pale orange/ grey	acicular evaporite moluds on bedding planes	post-compaction and lithification
.5m	L1		Z														
0			Z												light-dark grey	colour alternation due to weathering	

fig. 2.31 Summary log of a 3 m section of basinal facies Lamar limestone, exposed in an old road cut, US 62/180. Vertical scale 4cm = 1m.

fig. 2.32 *a.* Slump fold in basinal Lamar limestone. Lens cap 6cm. *b.* Lath-shaped moulds, after replacive evaporite crystals, on bedding planes. Pen for scale. *c and d.* Massive sandstones and siltstones in stacked channel lenses which cut down into darker siltstones; person for scale or 2cm = 2m. Brushy Canyon sandstone. Basinal facies, in roadcuts on US 62/180.

fig. 2.32

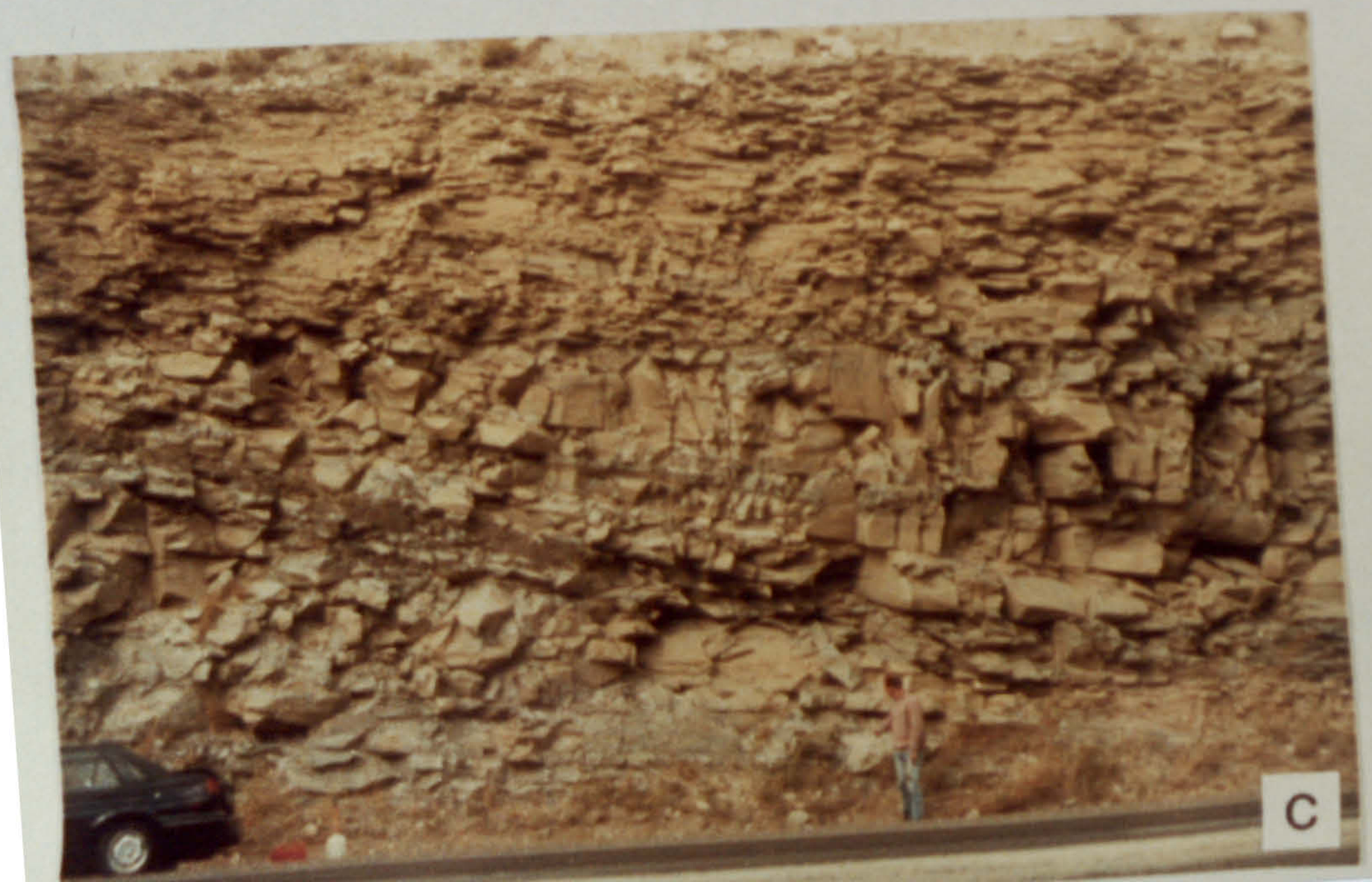

probably from continuous 'rain' of pelagic mud. L.C. Babcock (1974) studied this lithology in some detail and found crinoids, brachiopods, bivalves, siliceous sponges, holothurians, ostracodes, foraminifers, conodonts, radiolaria and ammonoids dispersed within the mudstone, particularly in the bioturbated beds. These fossils are not abundant, but do indicate that the water column was stable and sufficiently oxygenated for some life forms to inhabit the sea floor in this facies. The slump fold indicates that some downslope movement occurred periodically; the angular fold hinges suggest that the sediment was partly lithified rather than completely plastic.

The mottled, bioturbated beds have been correlated with the distinctive similar horizon in McKittrick Canyon (fig. 2.23b) by L.C. Babcock (1974), (section 2.4.3).

Brushy Canyon/Cherry Canyon sandstones These strata was not examined in detail because they are older than the section which forms the focus of this study (fig1.6). However, a set of samples was collected in the basinal sandstones of the Cherry Canyon sandstone and the Brushy Canyon sandstone, respectively. These 'sandstones' are in fact mixed siltstones and fine sandstones in which organic laminae are common. In both formations the strata are massive (figs. 2.32 c,d and 2.33 a) and comprise stacked lenticular deposits (fig. 2.32 d). Cross-bedding and other sedimentary structures are rare; this may be a reflection of uniformity of grain size. However ripple laminations (fig. 2.33 b) are visible on some exposures.

Interpretation A great deal of research has been done on the siltstones and sandstones of the Delaware Basin and there is still discussion about the mode of deposition. The stacked lenticular deposits (fig. 2.32 d) have been interpreted as channel deposits (Williamson, 1979) laid down in sub-parallel channels, 1/2 to 6 km wide, leaving deposits 5-35 metres thick. Newell *et al.* (1953), Hull (1957), Silver and Todd (1969) and Meissner (1972) interpreted the Brushy Canyon Formation as turbidity current deposits. Harms (1968) first suggested the importance of tractive, bottom-hugging fluid density currents, where the primary control on the density was *salinity* rather than *sediment load*, and this idea was developed by Williamson (1979) and Harms and Williamson (1988). They (*op. cit.*) rejected the sediment-turbidity current mechanism because of the lack of proximal-distal sorting and uniform sediment thicknesses. However, these siltstones may well have been derived from a pre-sorted source *e.g.*, aeolian deposits of the shelf. Studies of the siltstones and sandstones of the shelf indicate that these rocks are well-sorted, homogenous and of small grain size (Mazzullo *et al.*, 1985). Fischer and Sarnthien (1988) propose that the bulk of the silts were transported by aeolian processes but were water deposited, by analogy with

recent Atlantic deposits derived from the Sahara, and invoke aeolian dune systems on the shelf sorting silts and sands. These pre-sorted silts and sands could then have been delivered to the basin by turbidity currents.

The transport mechanism has still not been unequivocally resolved but the aeolian pre-sorting model (Fischer and Sarnthien, 1988) adequately explains the features of the Delaware Basin siliciclastic deposits. The density stratified basin model (Harms and Williamson, 1988) does not *conflict* with the pre-sorting model, but is not necessary to explain the features of the Delaware Basin siliciclastic deposits.

2.5 Discussion and conclusions

2.5.1 Shelf profile and sedimentary setting

The overall setting was one with a partially emergent grainstone belt, composed of skeletal and peloidal grainstones and packstones, a few hundred metres landward of the reef. An overview of the depositional environments and their main characteristics are summarised in figs. 7 and 8 of chapter 1. Skeletal diversity decreased and the environment became more restricted in a shelfward direction. This, coupled with a high evaporation rate, led to increased salinity in a lagoonal setting (Mazzullo and Hedrick, 1985). The pisolite/teepee belt was further shelfward (1.3.3). Neese and Schwartz (1977) concluded from their study of the Capitan shelf margin that the facies belts parallel to the shelf edge interdigitated and were persistent along strike. However, their relative width varied through time, and some were absent at some times. The question of lateral variability was further addressed by Pray (1989) who concluded that major facies are persistent along the rim of the Delaware Basin, although variablity has been observed (King, 1948; Garber *et. al.*, 1989) between facies of the area around the Carlsbad Embayment and the remainder of the Guadalupe Mountains. He also noted that there is evidence for appreciable lateral variability along the margins of the Delaware Basin, involving factors such as water circulation, sediment production and input, and local salinity. There are certainly major differences today in lithological composition *i.e.*, presence of dolomite and evaporite minerals, and this probably reflects original lateral variability at the time of deposition. However, there is no major evidence that the sedimentary features of the shelf margin from McKittrick Canyon reported in *this* study are in any way atypical.

Strata closest to the reef dip basinward at between 10° and 12°. About 200 metres shelfward the dip is only 5° -7° (fig. 2.3 a). Once the 5° tectonic tilt of the

Guadalupe Mountain block has been taken into consideration, it appears that the majority of strata of the back reef were deposited horizontally. The slightly steeper dip of back-reef strata towards the reef (the so-called "fall-in" beds of Lloyd Pray) could be a primary depositional feature or due to the subsequent compaction of foreslope talus and consequent movement of the reef. This has been investigated by several authors, of whom Pray and Esteban (1977), Yurewicz (1976, 1977) and Hurley (1978, 1979) interpreted most of this dip as depositional, whilst Smith (1974) felt that the dip was attributable to subsidence. It seems likely that the dip of the "fall-in" beds is due to a complex combination of contemporaneous depositional and compactional processes. The presence of dipping cavities in the reef and upper foreslope facies suggest that a 10° dip is due to post-depositional compaction.

2.5.2 Sediment production and supply

In a continental, equatorial, arid environment, such as existed during the formation of the Capitan Reef Complex, the position of relative sea-level would have controlled the rate of carbonate sediment production, as well as affecting water circulation and exposure of the shelf to aeolian processes. The position of relative sea-level thus would directly influence the shelf margin profile and its development through time. Almost all of the strata which comprise the Capitan formation are carbonates. This indicates that water depths were such as to allow the production of large volumes of carbonate sediment. Skeletal and peloidal grains and carbonate mud were generated by direct precipitation and by indirect precipiation by organisms. Most carbonate sediment was produced at the seaward margin of the shelf, in the lagoon and shallow waters above and landward of the reef (fig. 1.8). In this area of the back reef facies the water was shallow and agitated and this caused the development of coated grains and cross-bedding features. Basinward of the grainstone belt, adjacent to the break of slope, the reef facies developed. The deposits of the foreslope comprise talus derived from the reef and back reef facies and also some reworking of foreslope deposits. Foreslope sedimentation was more or less continuous, with spillage of grainy deposits down the upper and mid parts of the foreslope interspersed with flows containing large boulders of reef and upper foreslope rocks. These spalled-off from lithified portions of the reef and upper foreslope strata. These flows probably dislodged other foreslope deposits, and reworked partially lithified and lithified rocks and any organisms living on the foreslope, and caused further flows, some of which formed the graded wackestone units of the basin margin facies. Downslope movement in the basin margin and basin facies is also demonstrated by the presence of slump folds and reworked mudstone

lithoclasts. The angularity of the fold hinges suggests that the sediment was partially lithified. Downslope movement of sediment was inevitable, considering the depositional profile of the foreslope facies which must have had a primary dip of more than 20°. Major slump features currently develop on slopes with a dip of < 1° *e.g.*, in the Mississippi fan.

Some features in the immediate back reef facies suggest that this facies was periodically exposed and this would have exposed the shelf to aeolian processes. These features include the development of teepees, algal laminae and selective dolomitisation. However, there is no evidence that the immediate back reef facies facies was exposed for long periods of time. The large volumes of grainstones, which dominate the lithologies of the back reef strata, are interbedded with siltstones which were deposited subaqueously. These siltstones display sharp lower contacts with carbonate units whilst upper contacts are gradational. Few sedimentary structures are generally visible, with the exception of some cross-bedding features. The siltstones of the shelf at their most basinward outcrop in McKittrick Canyon are well-sorted, sub-angular, sub-rounded, matrix supported and often mixed with marine skeletal debris. Although the silt could have been pre-sorted, *e.g.*, by aeolian processes, these features indicate that these siltstones were at least reworked by marine waters, even if they were originally deposited in shallow or subaerial conditions associated with sea-level lowstand. Notably, the silts of the shelf, foreslope and basin are almost identical in composition. The siltstones found in the forereef were derived from the shelf, probably by aqueous flow. The siltstone unit which occurs on the foreslope may have been deposited during a sea-level lowstand or rise. The dispersed siliciclastic grains found in slope and basin margin carbonates, were probably windblown.

Several kilometres landward of the reef facies erosion surfaces are common between carbonate units and sandstones (Neese and Schwartz, 1977). Further landward the facies became even more restricted, emergent and evaporitic, with the development of stromatolites, mudstones, wackestones, possible caliche crusts (Sarg, 1977) and thick beds of anhydrite/gypsum and halite interbedded with apparently homogenous sandstones. These sandstones have remnant textures resulting from haloturbation (pers. comm., G.M. Harwood and A.C. Kendall, 1989) indicating arid, sabkha-type conditions. This evaporitic facies extends many tens of kilometers across the northwestern shelf as well as over the whole of the Permian Basin region. The study of the evaporitic facies is hampered by the ambiguity of how much of the section has been lost or distorted due to the dissolution of evaporites.

There are two current schools of thought presenting models for the environments of deposition for the shelf siliciclastics and relative sea-level fluctuations have been

used to explain the distribution of alternating sequences of carbonate and siliciclastic strata on the shelf and in the basin by numerous workers. Pray (1977), Sarg (1977), Neese and Schwartz (1977), Hurley (1978) and Candelaria (1985) favoured a submarine environment and envisaged their deposition during highstands. This model fails to explain the by-passing of the shelf edge by the majority of siliciclastics, the lack of fauna and bioturbation features, and offers no explanation for the increase in carbonate production (aggradation and progradation of the shelf margin) associated with major siliciclastic deposition in the basin (Garber *et al.*, 1989). Kendall (1969), Silver and Todd (1969), Meissner (1972), Smith (1974), Mazzullo and Hedrick (1985) and Borer and Harris (1989) favoured deposition on a subaerially exposed shelf, by a combination of aeolian and fluvial processes on emergent flats during sea-level lowstands. This model explains the sharp basal contact with the underlying carbonate strata below the sands, which would then have been a deflation surface. It is also possible to envisage lagoonal areas where waters of high salinity could have developed by evaporation, allowing the concentration of brines capable of causing the haloturbation features noted by Harwood and Kendall (pers. comm., 1989) and depositing the sequences of evaporites present on the distal parts of the shelf. The fine-grained, homogeneous nature of the sands, and the lack of biogenic structures and fossils that might be expected to be present if the sands were deposited in a fully submarine environment could also be explained by aeolian processes (Mazzullo and Hedrick, 1985), although homogeneity is not diagnostic of aeolian deposits. During these lowstands, sands could have been delivered to the basin by aeolian processes, by-passing the shelf margin. Carbonate production and accumulation of the reef and foreslope facies would have been enhanced during these periods when waters were shallow, thus causing the greater progradation rates reported by Garber *et al.* (1989). Subsequent sea-level rise would cause these sands to be trapped on the shelf, rework the upper parts and intermix carbonate debris as carbonate production resumed in the developing shallows, and perhaps account for some deposition of siliciclastics on the foreslope.

Downslope movement of carbonate sediment was the dominant process responsible for the aggradation/progradation of the foreslope facies, with sedimentation of pelagic mud becoming increasingly important basinward, where the section is condensed. It seems probable that there should be a direct relationship between the rate of carbonate production on the reef and upper foreslope (sea-level related), and the generation of reef-block-dominated talus as opposed to grainstone dominated talus on the foreslope. Recent studies by Garber *et al.* (1989) have demonstrated a relationship between the progradation and aggradation of the Capitan shelf margin (fig. 1.7) and the

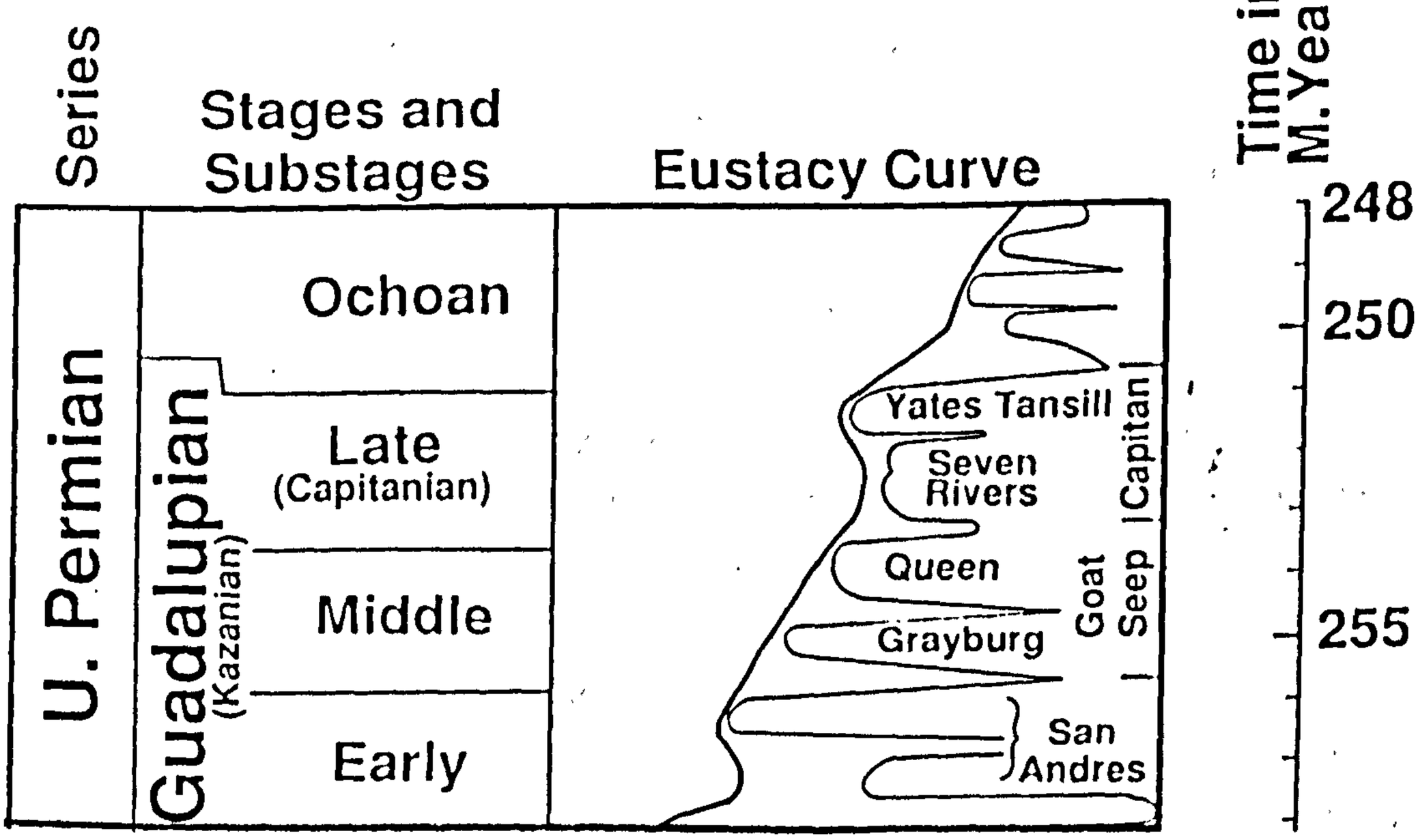

fig. 2.34 The relationship between sea-level fluctuations (Ross and Ross, 1987) and sediment deposition in the Guadalupian (Garber *et al.*, 1989).

sea-level curve (fig. 2.34) proposed by Ross and Ross (1987). Minor sea-level fluctuations superimposed on this curve would probably be sufficient to expose the shelf during lowstands, and to cause a dramatic increase of carbonate production during highstands.

Other evidence of sea-level fluctuation is seen in the sections at McKittrick Canyon. A disconformity is recognised in the basin margin facies which is associated with the development of (bioturbated) basin margin-type lithologies higher up the foreslope than would have been expected under 'normal' sea-level conditions. These features represent a highstand. If this horizon could be correlated with similar horizons further basinward, as suggested by L.C. Babcock (1977), then it should be possible to trace this minor sequence boundary within the Lamar limestone Formation.

Reef boulders are apparently more abundant above the disconformity an grainstones are more abundant below the disconformity. If this is actually the case then tectonic/eustatic changes may have been responsible for the creation of the disconformity and the downslope movement of boulders rather than grainstones. This would corroborate the observations of Garber *et al.* (1989) who developed a model from subsurface and outcrop observations which suggests that the development of the Capitan shelf margin was mainly aggradational in Upper Capitan times. A more rapid vertical accretion of the reef facies would explain the production of large reef boulders which fell down onto the foreslope.

It is clear from studying the outcrops of the Capitan shelf margin at McKittrick Canyon that the sedimentology of these facies are inextricably linked with one another, and that the development and nature of the strata were controlled by the position of relative sea level. Further work could be done to determine the relationships of the different types of talus deposits with the siliciclastics of the shelf and their interbedded carbonate strata. This could be done by detailed mapping of the strata which outcrop at the mouth of McKittrick Canyon. If these relationships were more clearly understood then variations could be correlated with minor fluctuations of sea-level. Multi-variate analysis of, for example, the bioclastic fragments which were incorporated within the foreslope strata could prove a useful tool in understanding the relationships between conditions on the shelf and reef, which are closely related to sea level, and the development of the foreslope strata.

Chapter 3: Diagenesis

'The best of artists hath no thought to show which the rough stone in its superfluous shell doth not include; to break the marble spell is all the hand that serves the brain can do.' Michaelangelo Buonarroti.

3.1 Introduction

This chapter documents the diagenetic events evident from petrographic study, and in particular records the significance of calcium sulphate in the diagenesis of the Capitan shelf margin. The relative timing of diagenetic 'events' and their distribution through the facies, is established. Diagenetic studies of the Capitan shelf margin as a whole are rare (Schmidt, 1977; Garber *et al.*, 1989). Studies have tended to concentrate on particular diagenetic features, visible at outcrop, in the Guadalupe Mountains (*e.g.*, Mazzullo and Cys, 1977; Given and Lohmann, 1985, 1986) or on a particular facies belt, (*e.g.*, Sarg, 1981; Mruk, 1985; Scholle and Melim,1988). The recent work based mainly on subsurface data, by Garber *et al.* (1989) has advanced this state of affairs considerably. However, outcrops in the Guadalupe Mountains still raise many questions which are waiting to be answered.

3.2 Methods

The petrographic relationships were studied by microscopic examination of polished thin sections, stained acetate peels and polished slabs and by observing the cathodoluminescence of polished thin sections. Details of these methods are given in appendix 3.1. An electron microprobe was used (Edinburgh University Geology department) to analyse the composition of the carbonate minerals, as well as other elements present in other minerals, and full analyses are given in appendix 3.2 along with detection limits. Tables of electron microprobe data within the text give Ca and Mg values as mole% carbonate. Other elements are given as weight% oxides (appendix 3.2). Only values which are higher than the detection limits are given in these tables (the abbreviation 'nd' is used to indicate non-detection).

3.3 Diagenesis

3.3.1 Early marine diagenesis

Algae Micrite envelopes around grains and *Archaeolithoporella* laminae (J.A. Babcock, 1977) are of algal/microbial origin and developed contemporaneous with reef growth. Micrite envelopes appear as dark brown rims, often several tens of microns thick, and occur around all grains and skeletal fragments in the reef, upper foreslope and back reef. Under cathodoluminescence they are dull red, and electron microprobe analysis reveals that they are mostly dolomite (table 3.1). *Archaeolithoporella* laminations are isopachous and coat skeletal fragments such as sponges and are also intergrown with marine cements, particularly botryoidal aragonite (fig. 3.1; Mazzullo and Cys, 1977). In thin section, the *Archaeolithoporella* laminae appear dark brown, microcrystalline and luminesce a dull red (fig. 3.1b). Electron microprobe analysis (table 3.1) indicates that it has a calcitic composition, although the dull red luminescence and $MgCO_3$ content suggest the presence of microdolomite inclusions. *Archaeolithoporella* laminae are found *in situ* in the reef and upper foreslope facies and in allochthonous blocks in the foreslope facies (fig. 3.5).

Botryoidal acicular cements The first generation of cement commonly forms large botryoids (fig. 2.12a and fig. 3.1) which fill primary voids in the reef and, to a lesser extent, in the upper foreslope. This cement has also been found lining fractures in the reef at outcrops at the mouths of Walnut and Dark Canyons (J.A. Babcock, 1977). It is also present in many allochthonous blocks on the foreslope. The acicular fabric is defined by traces of inclusions and crystal boundaries which define long slender crystals which are sub-parallel and fan out distally (fig. 3.1). The ends of these crystals usually have a rectangular appearance and this is characteristic of aragonitic crystal form. The acicular texture is probably preserved due to the microcrystalline texture of the *Archaeolithoporella* on the surface of the botryoids allowing the formation of moulds. The acicular crystal habit, rectangular terminations, abundant inclusions, botryoidal growth and association with algae all suggest an original aragonite mineralogy (Mazzullo and Cys,1977,1978 and1979; Mazzullo, 1980).

The former aragonite botryoids are commonly preserved as two types of syntaxial calcite. Inclusion rich areas of neomorphic calcite spar preserve the acicular, botryoidal texture and syntaxial, inclusion free calcite spar (spar Ic) has no preservation of original texture (fig. 3.1a). The inclusion rich areas luminescence a

description	no. analyses	sample	CaCO3 (mol.%)	MgCO3 (mol.%)	SO3 (wt.%)	Al2O3 (wt.%)	SiO2 (wt.%)	FeO (wt.%)	Na2O (wt.%)
microcrystalline	3	MT30	91.06-100	5.44-11.45		.2-.25			
matrix	1	MT60	83.09-100	.34-.86					
	1	M22	10.92	4.31	12.35	0.46	2.38		
bioclast	3	MT30	50.95-58.00	45.54-52.01	.17-.67	.18-.62			
	3	MT74I	56.12-57.14	51.9-52.67	nd-.44	.17-.21			
	9	MT60	51.46-71.77	26.56-48.24	nd-.53	.15-.19			
	1	MT102b	54.60	40.30		9.28	0.37		
	4	MT117	57.30-59.1	52.42-54.52					
micrite	3	M22	42.08-51.47	39.82-44.65		.5-.89	.17-.23	.27-.43	
envelopes	3	MT74I	56.75-58.12	51.59-53.08		.17-.29	nd-.41		
	2	MT74ii	100.00	.095-2.54		nd-.14	nd-.14		
Archaeolithoporella	2	MT33	95.89-97.49	.62-.70		.06-.27			
botryoidal (former) aragonite	10	MT33	96.68-98.88	.66-1.71	nd-.19	nd-1.67			
spar Ic	5	MT33	96.93-100	.62-.82					
isopachous	3	MT74I	94.93-100	.72-3.29					
marine cement	3	MT74ii	89.45-100	.46-.9		nd-5.14	nd-.12		nd-.15
	35	MT30	88.53-100	.39-18.24	nd-.59	nd-.51	nd-.45	nd-.47	nd-.13
	3	MT60	100.00	.29-.49	(N.B. SO3 and FeO not identif led in the same analyses				
spar Ia	3	MT74I	100.00	.67-.77					
(overgrowth)	12	MT30	96.14-100	.23-1.23		nd-.47			
spar Ib	3	MT74I	86.98-100	.25-.96					

table 3.1 Electron microprobe analyses of early marine diagenetic phases and spar I

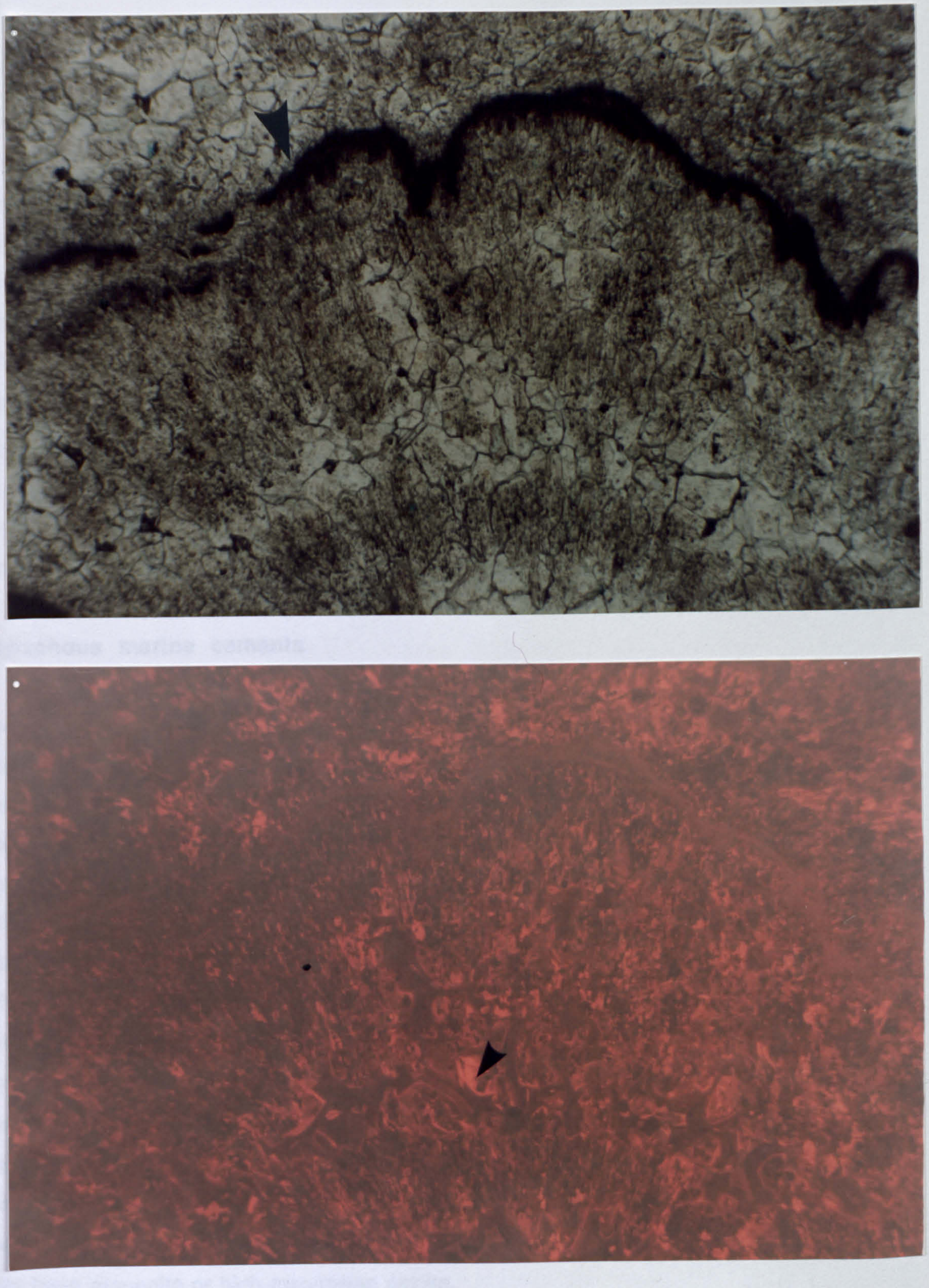

fig. 3.1a,b Plane polarised light and cathodoluminescence photomicrograph pair of former aragonite botryoid coated by an isopachous layer of *Archaeolithoporella* (arrowed). The relict acicular fabric is clearly visible, defined by numerous brown inclusions. Inclusion free calcite spar (arrowed) has concentric, parallel zones, indicating precipitation into pore space following partial dissolution of inclusion rich areas. Sample MT33; lower foreslope facies, 'reef trail', McKittrick Canyon. Scale: 25mm = 500μm.

dull red. The inclusions luminesce a bright red and this suggests that many of the inclusions are micro-dolomites. Electron microprobe analyses (table 3.1) show significant $MgCO_3$, Al and Si in the inclusion rich spar and indicate the presence of clays as inclusions. The $MgCO_3$ value of up to 1.71 mol.% indicates that either dolomite inclusions are also present in this calcite spar or that the Mg is incorporated into the calcite lattice. The clear calcite spar has parallel, concentric zones under cathodoluminescence indicating that a period of dissolution preceeded the precipitation of this calcite spar into pore space. Zones are on a 10μm scale, with the first zone having moderate orange luminescence and subsequent zones being less bright and the last zones non-luminescent. Electron microprobe analyses of spar Ic (table 3.1) show that it contains only traces of $MgCO_3$ (up to 0.82 mol.%) and that no other elememts were detected. Either dolomite inclusions are present in this calcite spar or the Mg is incorporated into the calcite lattice. This calcite spar (spar Ic) is found in former-aragonite botryoids which are *in situ* and in allochthonous blocks of the upper and lower foreslope.

Isopachous marine cements

Radial fibrous cements These cements usually form the first generation of cement lining primary voids in the reef back reef and upper foreslope (fig. 3.5). They are often found within ostracode chambers and fringing skeletal fragments. Where botryoidal aragonite and isopachous cement occur together, the isopachous cements are the later generation. The first layer is relatively inclusion free and 50-100 μm thick, with a radial acicular habit, indicating competitive growth from numerous nucleation points (fig. 3.2), and giving the cement fringe slightly sweeping extinction. This cement is non-luminescent, and apparently does not contain microdolomite inclusions. However, electron microprobe analyses (table 3.1) show the amount of $MgCO_3$ to vary between 0.29 and 3.29 mol%. These cements are also found fringing skeletal fragments in rocks from the basin margin facies (fig. 3.3) and the cement is often partially removed due to pressure solution. This is another indication that precipitation of this cement was both early and marine *i.e.*, was precipitated around grains prior to re-working and deposition lower down the foreslope. The acicular habit suggests that the original mineralogy may have been aragonite or high-magnesian calcite.

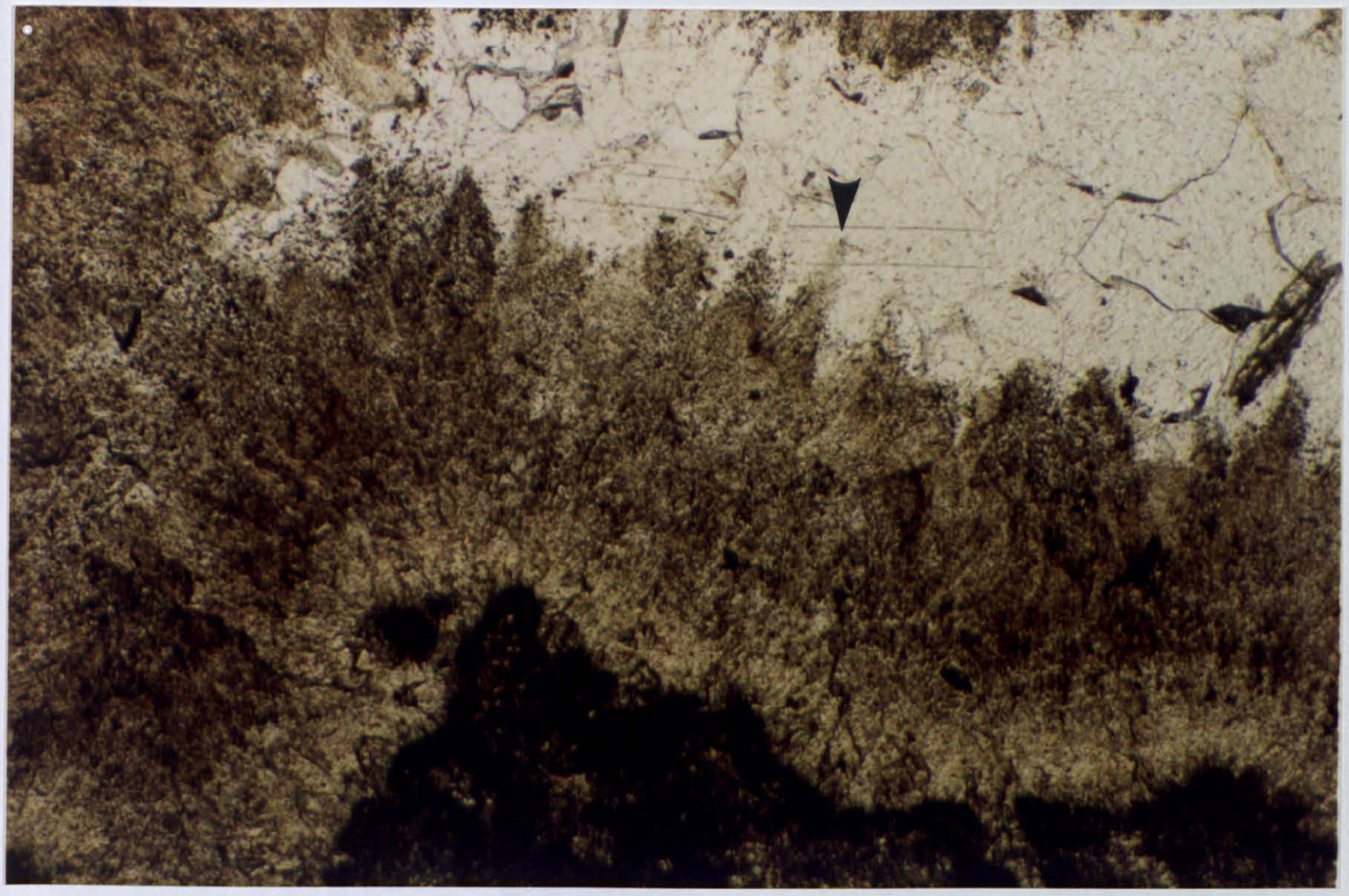

fig. 3.2 Plane polarised light photomicrograph showing radial, acicular calcite marine cement which is relatively inclusion free, and subsequent, inclusion rich columnar marine cements with scalenohedral terminations (arrowed). The remainder of the pore is filled by syntaxial calcite spar (spar Ia and Ib). Sample MC3; upper foreslope facies, 'reef trail', McKittrick Canyon. Scale: 25mm = 500µm.

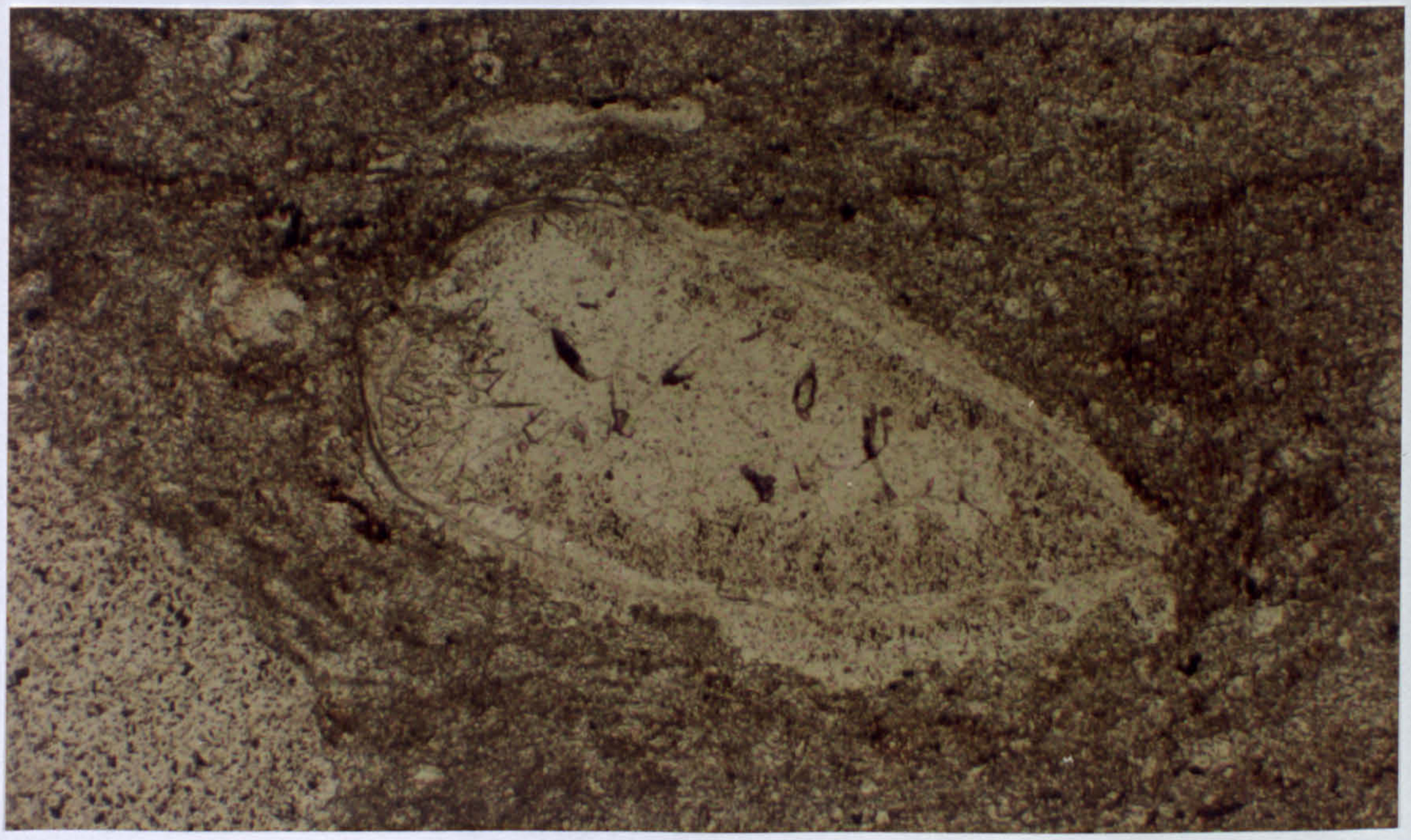

fig. 3.3 Plane polarised light photomicrograph of marine cements on an articulated shell. The marine cements have been partially removed due to pressure solution. Sample M2; basin margin facies, 'reef trail', McKittrick Canyon. Scale: 25mm = 250µm.

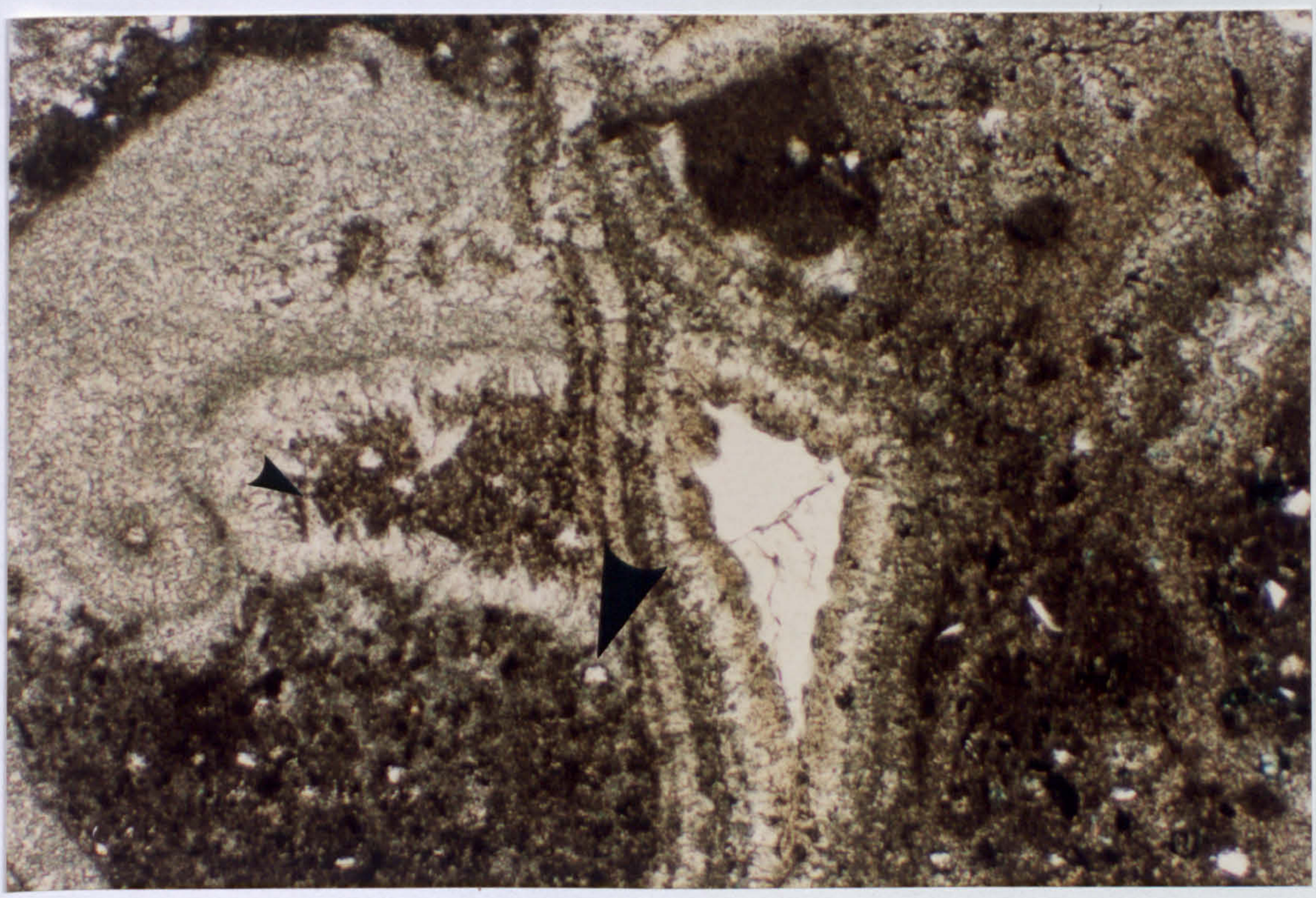

fig. 3.4 Plane polarised light photomicrograph of marine cements lining pores and fractures. Internal sediment, both carbonate and silt grains (arrowed), preserved the scalenohedral terminations (arrowed) of one generation of marine cement, before this pore was cross-cut by a fracture. This fracture is lined by several generations of marine cement. The remaining pore space is now filled by calcite spar IIc. Sample M13A; back reef facies, 'reef trail', McKittrick Canyon. Scale: 25mm = 500μm.

Columnar cements These cements usually form the majority of the volume of isopachous cements. There may be several layers, up to 10 mm thick in total in a particular cavity. These cements line primary pores, usually succeeding a layer of radial acicular cement, and also line fractures (fig. 3.4). The first layers are usually relatively inclusion poor and the density of inclusions increases towards the middle of the pore. This density of inclusions imparts a brown colour to the cement in thin section and at outcrop. Crystal margins are often outlined by inclusions rather than by any obvious crystal surface (fig. 3.2), especially towards the middle of a pore, where the inclusions define scalenohedral terminations. Crystal terminations are also defined where geopetal sediment filled a pore, creating a mould of microcrystalline calcite around them (fig. 3.4). These cements have a dull red speckled luminescence interpreted to be dolomite inclusions. Electron microprobe analyses (table 3.1, samples MT30 and MT60) indicate that $MgCO_3$, SO_3, Al_2O_3, SiO2, FeO and Na_2O are present in notable quantities (*N.B.*, the SO_3 and FeO values are *not* from the same analyses). The $MgCO_3$ value suggests that many of the inclusions are dolomite; the presence of the other elements indicates that minor iron minerals, clays and possibly calcium sulphate are present as inclusions. The iron minerals are not sulphides, because the SO_3 and FeO values are *not* from the same analyses, and the iron is more likely to be incorporated in an oxide. The SO_3 value could indicate the presence of calcium sulphate or could be contamination from the epoxy resin used in the preparation of the thin section. (*N.B.*, electron microprobe analysis of the 'Permabond' resin, used in the preparation of the thin sections, could give a SO_3 value of less than around 1%; pers. comm., from the manufacturer of 'Permabond'.)

Summary of early marine diagenesis

Several generations of isopachous cements are present in rocks of the back reef, reef and foreslope. These cements are evidently marine because they are inter-layered with geopetal sediment and they line early fractures (fig. 2.6a). There are two types of isopachous cements, radial acicular and columnar. Individual layers have uniform thickness although the thickness of different layers may vary. Their morphology, habit, microdolomite inclusions (Lohmann and Meyers, 1977) and similarity to modern marine cements (James *et al.*, 1976; James and Ginsburg, 1979) indicates that they were probably precipitated as high-magnesian calcite. Other evidence of early marine diagenesis is plentiful; micrite envelopes around grains and bioclasts,

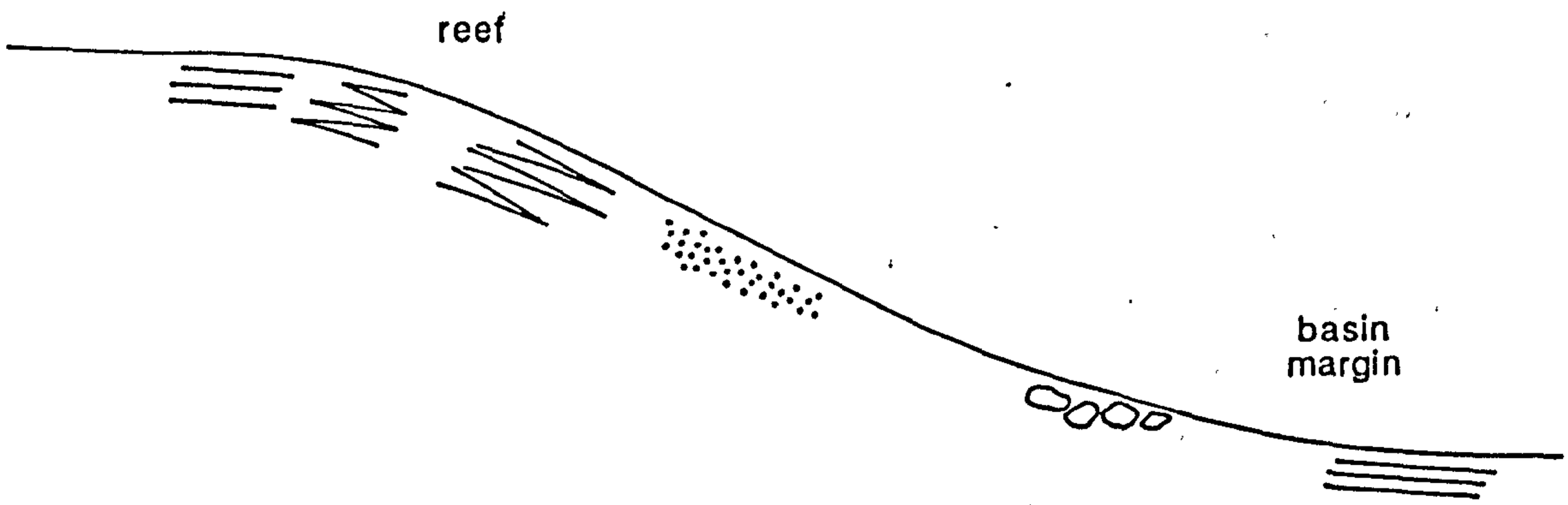

micrite envelopes ——— derived - - - - - - - - - -

algal encrustation ——— derived - - - - - - - - - -

botryoidal aragonite ——— derived - - - - - - - - - -

isopachous marine cements ——— - - - - - -

compaction - - ———————————————

fig. 3.5 Summary diagram of the facies distribution of early marine diagenetic phases.

Archaeolithoporella interlaminated with botryoidal agaronite, and the morphology and habit of isopachous cements accompanied by internal sediment, demonstrate algal/microbial activity concomitant with marine cementation and sedimentation. Calcification by modern red algae from temperate and tropical waters results in the formation of aragonitic botryoids and layers; similarities between these modern forms and late Palaeozoic forms (such as phylloid algae (fig. 2.15a), suggest that they may be related (James *et al.*,1988). The association of micritic laminae, interpreted to be *Archaeolithoporella* (Babcock, 1977) , with botryoids of former aragonite (Mazzullo and Cys, 1977) supports this suggestion. The abundance of micrite envelopes, as well as the presence of *Archaeolithoporella* and phylloid algae, and the lack of framework building organisms such as the corals of the modern reefs, all indicate the importance of algae and microbial processes in the formation and lithification of the Mid-Capitan Reef.

The inclusion rich isopachous cements are similar in morphology to many high-magnesian calcite marine cements forming in modern environments (James *et al.*, 1976; James and Ginsburg, 1979). Mruk (1986, 1989) interprets the inclusion rich prismatic cements as having formed in a mixed marine/meteoric diagenetic environment on the basis of texture, microdolomite inclusions and the lack of interlayered sediment and the absence of these cements in growth framework pores. These last two observations are at variance with the observations of *this* study where marine internal sediment can clearly be seen to interlayer with these cements and to line primary voids.

Cemented grainstones and boundstones, in the reef and upper foreslope facies, are cross-cut by fractures which contain marine internal sediments and isopachous marine cements (2.4). The lack of compaction in these grainstones, the volume of marine cements and the presence of fractures indicate that cementation by aragonite and high-magnesian calcite took place in the marine environment, concomitant with fracturing and sedimentation, and resulted in the formation of lithified reef rock.

3.3.2 Evidence for the former presence of calcium sulphate

There is direct petrographic evidence which indicates the former presence of *replacive* anhydrite in the strata of the Capitan shelf margin. The lack of compactional features in grainstones which no longer contain isopachous marine cements, the presence of pore-filling anhydrite in the subsurface strata of the Capitan shelf margin (Garber *et al.*, 1989), and palaeogeographic considerations, yield substantial *circumstantial* evidence for the former presence of *pore-filing* anhydrite.

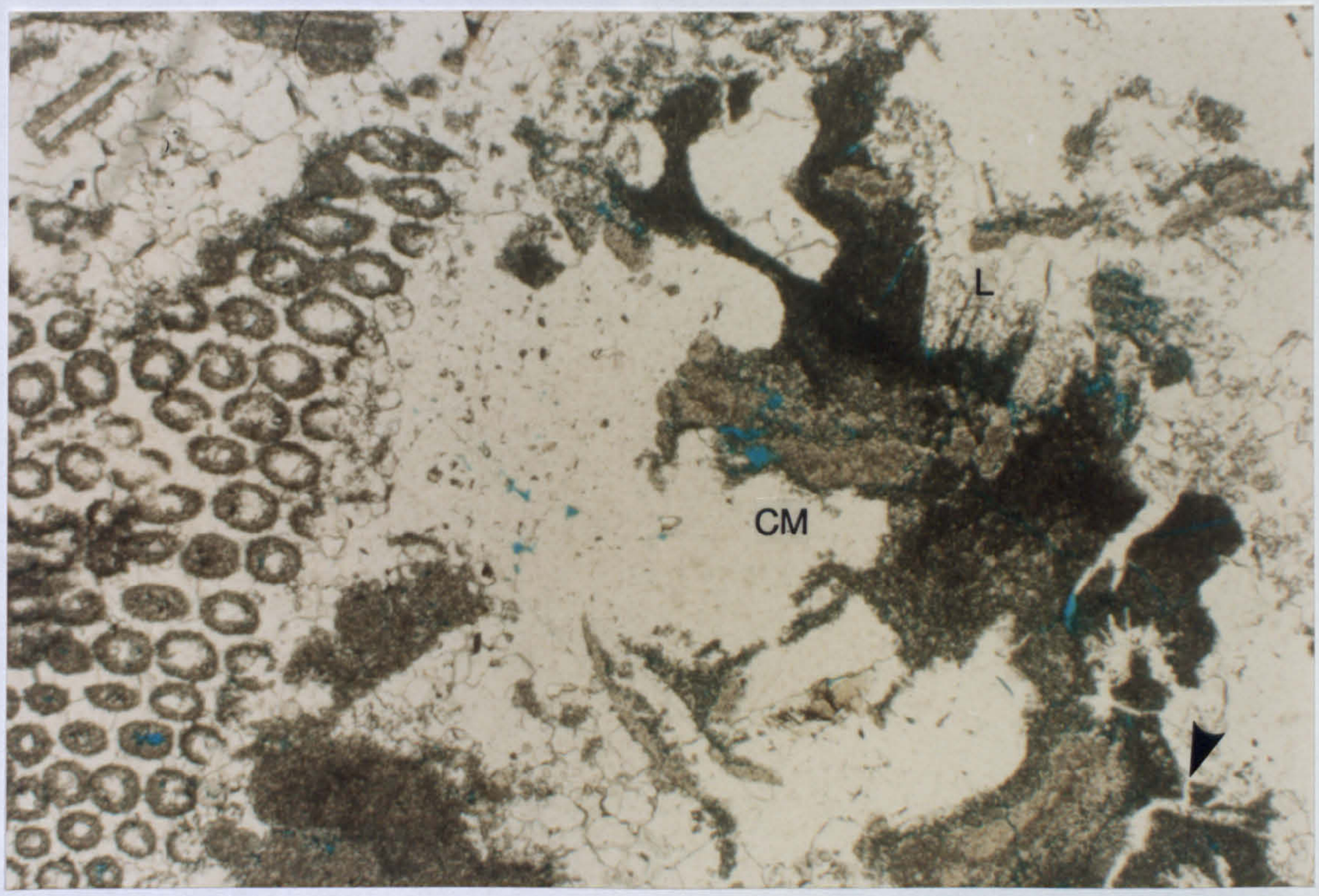

fig. 3.6 Plane polarised light photomicrograph of lath shapes (**L**), castellated margins (**CM**) and lack of collapse and compactional features which testify to the former presence of replacive and pore-filling anhydrite. Calcite spars IIb and IIc fill areas after replacive anhydrite, including fractures (arrowed). All the matrix is pervasively dolomitised. Sample MT117; upper foreslope facies, 'reef trail', McKittrick Canyon. Scale: 25mm = 1mm.

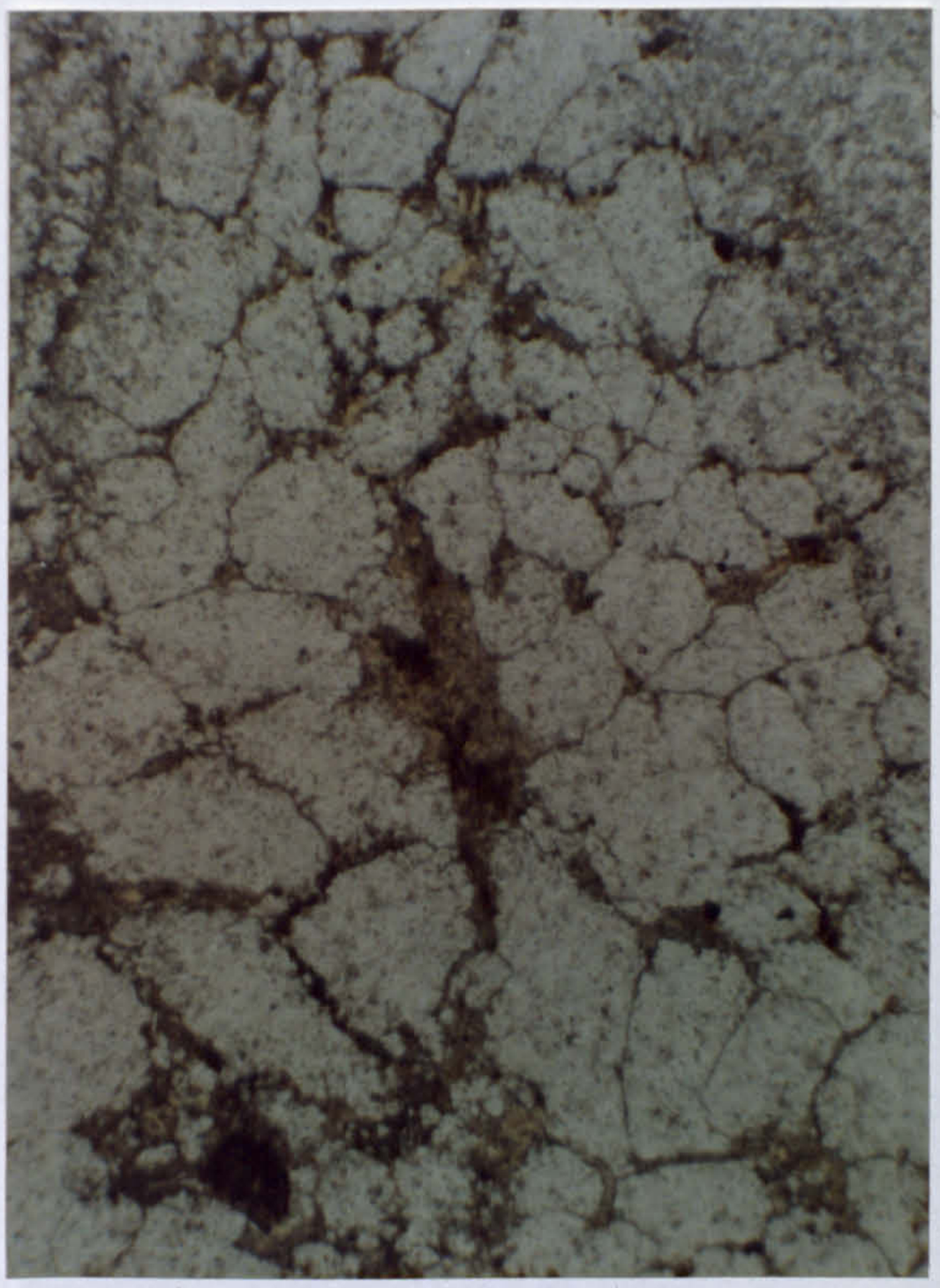

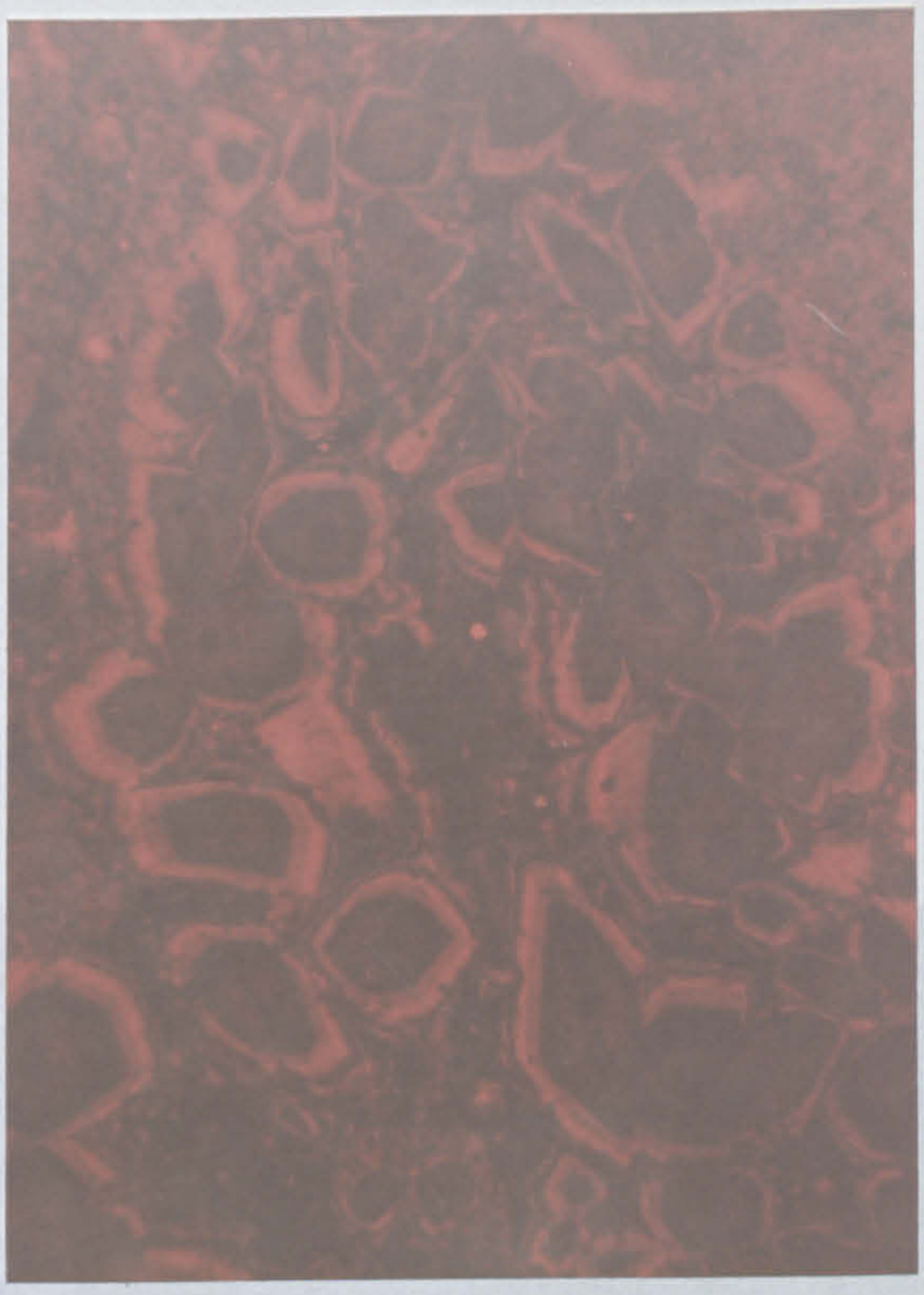

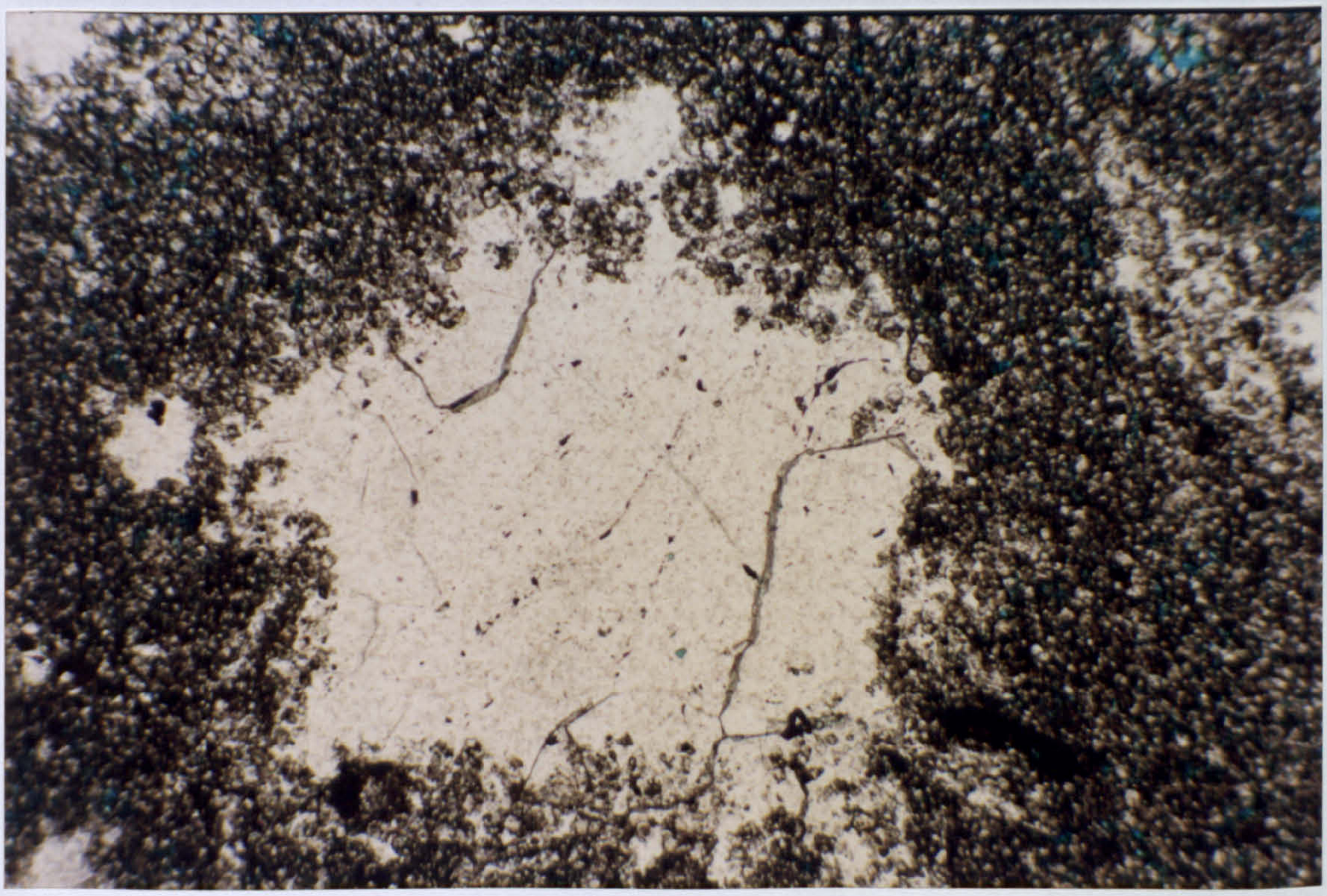

fig. 3.7a,b Plane polarised light and cathodoluminescence photomicrograph pair of coalesced nodules of replacive anhydrite (now calcite spar II) separated by thin partings of dolomite. The concentric zoning pattern in the calcite and the lack of geopetal fabrics of dolomite crystals, suggests that replacement of the anhydrite took place by solution and precipitation along a thin film, rather than following total anhydrite dissolution. Sample MT39. c. Plane polarised light photomicrograph of replacive anhydrite nodule, with lath-shaped protrusions into the matrix, (now calcite spars IIa and IIb) in pervasively dolomitised (fabric destructive) matrix. Sample MT38; lower foreslope facies, 'reef trail', McKittrick Canyon. Scale: 25mm = 500μm.

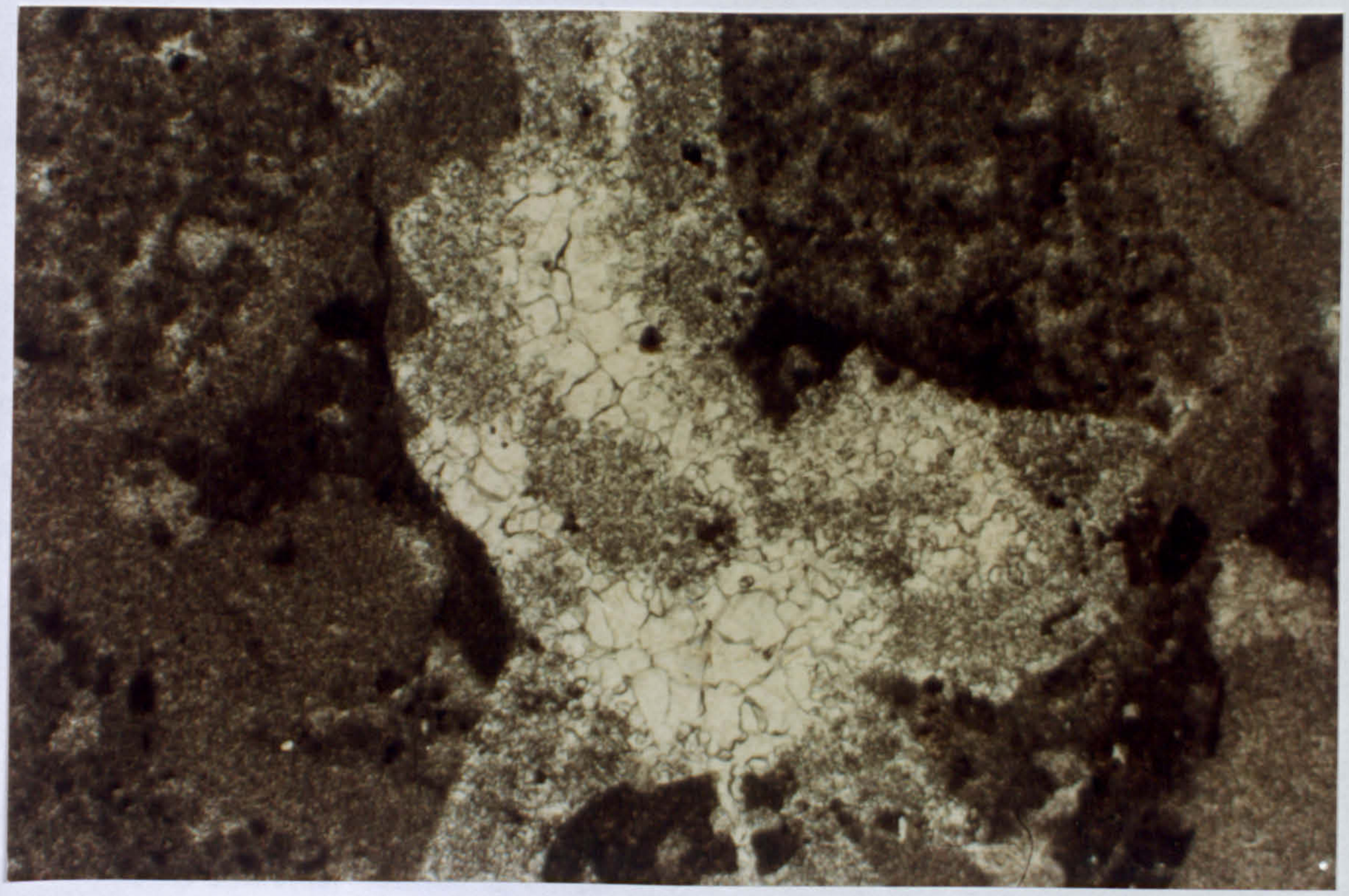

fig. 3.8 Plane polarised light photomicrograph of calcite spar (spar Id) nucleating on microcrystalline dolomite in a fracture formerly filled by replacive anhydrite (castellated margin). Sample MT74; back reef facies, 'reef trail', McKittrick Canyon. Scale: 25mm = 1mm.

Replacive anhydrite

Lath shapes with square terminations and castellated margins (fig. 3.6) are characteristic of replacive anhydrite textures (G.M. Harwood, pers. comm., 1986). These features have been observed in thin sections of rocks from the back reef and upper and lower foreslope facies, but not in the reef at all. In all cases the anhydrite is no longer present and calcite spar fills the moulds. Calcite-filled nodules after replacive anhydrite are common in pervasively dolomitised units of the lower foreslope (fig. 3.7) where the rock fabric has also been destroyed. These nodules range in size from millimetres to several centimetres, are roughly spherical and lath shapes protrude outwards from their margins and penetrate the rock matrix (fig. 3.7c). Replacive laths of former anhydrite also protrude from the margins to original pores (fig. 3.6) and fractures (fig. 3.8). Where laths protrude from the margins to original pores, most traces of the former presence of marine cements are removed and the rocks are pervasively dolomitised.

Replacive anhydrite textures are found in rocks of the foreslope and back reef facies but not in the reef facies (fig. 3.9). Replacive nodules of former anhydrite are only present in pervasively dolomitised rocks in the lower foreslope facies. Laths which protrude from the margins of primary pores and fractures are most common in dolomitised rocks from the upper foreslope and back reef facies but are also present in rocks from the lower foreslope facies.

Pore-filling calcium sulphate

Petrographic and field observation reveals a lack of geopetal and compactional fabrics in rocks of the foreslope facies, even in those rocks which no longer retain many traces of marine cements. Calcite spar appears to have taken the place of the marine cements and also to have filled any primary pore space remaining after the precipitaiton of these marine cements. Furthermore, these strata are invariably pervasively dolomitised and many of the primary components of the original limestone are still identifiable *e.g.*, skeletal fragments and isopachous cements (where present). The open structure of the dolostones *i.e.*, lack of compactional features (fig. 3.6), indicates that these spar-filled areas were occluded before significant burial. Furthermore, the presence of dolomite rhombs 'floating' in the calcite spar and the presence of solid inclusions in calcite spars which fill moulds after replacive sulphate, suggest retention of features associated with the formation of calcite after gypsum/anhydrite (3.3.4). This implies that the areas which are now occluded by calcite spar were originally

Replacive anhydrite

Lath shapes with square terminations and castellated margins (fig. 3.6) are characteristic of replacive anhydrite textures (G.M. Harwood, pers. comm., 1986). These features have been observed in thin sections of rocks from the back reef and upper and lower foreslope facies, but not in the reef at all. In all cases the anhydrite is no longer present and calcite spar fills the moulds. Calcite-filled nodules after replacive anhydrite are common in pervasively dolomitised units of the lower foreslope (fig. 3.7) where the rock fabric has also been destroyed. These nodules range in size from millimetres to several centimetres, are roughly spherical and lath shapes protrude outwards from their margins and penetrate the rock matrix (fig. 3.7c). Replacive laths of former anhydrite also protrude from the margins to original pores (fig. 3.6) and fractures (fig. 3.8). Where laths protrude from the margins to original pores, most traces of the former presence of marine cements are removed and the rocks are pervasively dolomitised.

Replacive anhydrite textures are found in rocks of the foreslope and back reef facies but not in the reef facies (fig. 3.9). Replacive nodules of former anhydrite are only present in pervasively dolomitised rocks in the lower foreslope facies. Laths which protrude from the margins of primary pores and fractures are most common in dolomitised rocks from the upper foreslope and back reef facies but are also present in rocks from the lower foreslope facies.

Pore-filling calcium sulphate

Petrographic and field observation reveals a lack of geopetal and compactional fabrics in rocks of the foreslope facies, even in those rocks which no longer retain many traces of marine cements. Calcite spar appears to have taken the place of the marine cements and also to have filled any primary pore space remaining after the precipitaiton of these marine cements. Furthermore, these strata are invariably pervasively dolomitised and many of the primary components of the original limestone are still identifiable *e.g.*, skeletal fragments and isopachous cements (where present). The open structure of the dolostones *i.e.*, lack of compactional features (fig. 3.6), indicates that these spar-filled areas were occluded before significant burial. Furthermore, the presence of dolomite rhombs 'floating' in the calcite spar and the presence of solid inclusions in calcite spars which fill moulds after replacive sulphate, suggest retention of features associated with the formation of calcite after gypsum/anhydrite (3.3.4). This implies that the areas which are now occluded by calcite spar were originally

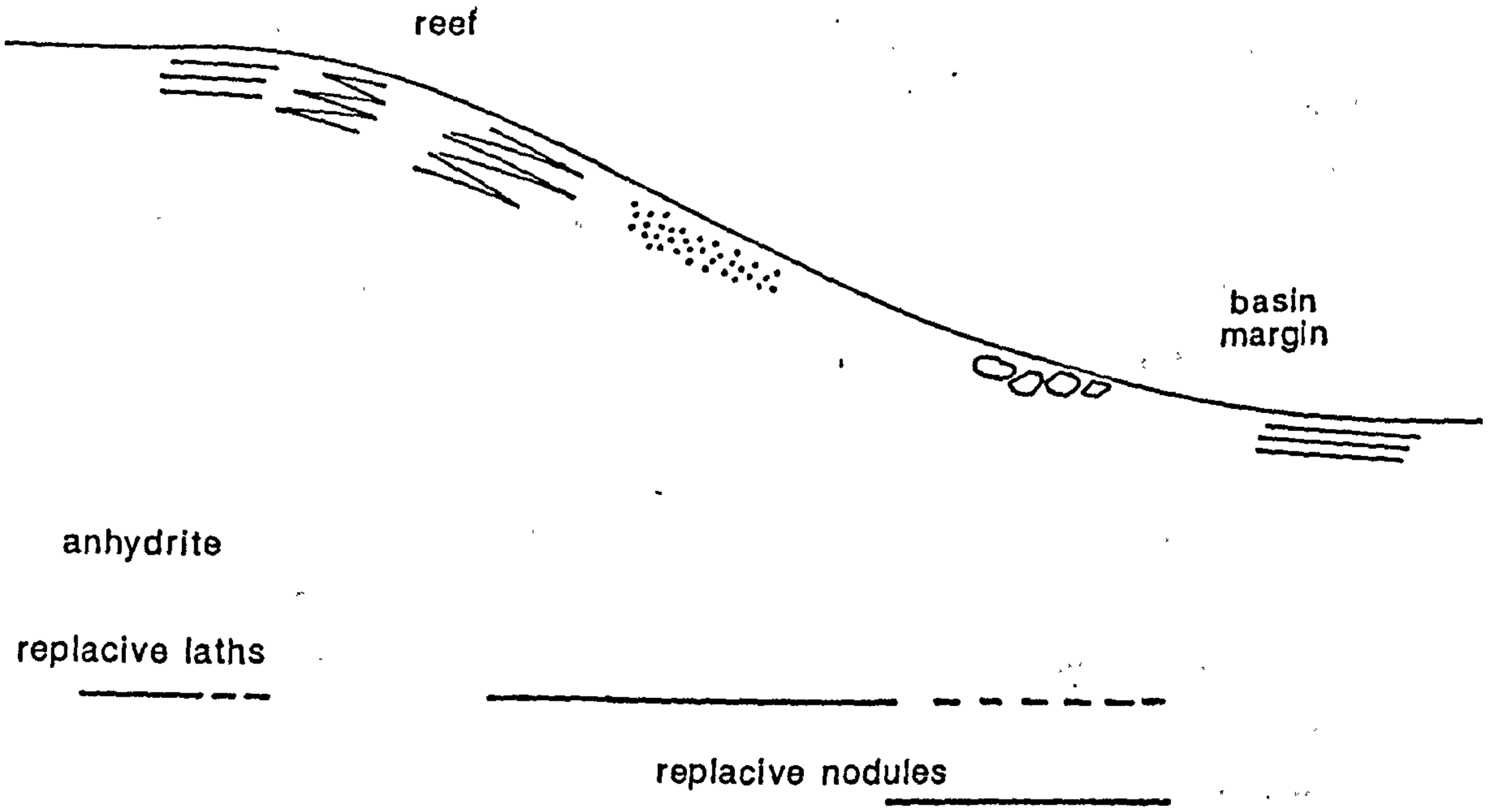

fig. 3.9 Summary diagram of the facies distribution of replacive anhydrite.

occluded by calcium sulphate.

Following the demise of the Capitan reef in Upper Permian times, the Delaware Basin was entirely filled with the Castile Formation and the Salado Formation was then deposited over the entire region. Both of these Formations are composed largely of evaporites. Evaporite deposition over a large area (that which is now the western United States) continued long into the Triassic. Therefore, it is difficult to conceive that the narrow belt of carbonates which comprised the Capitan Shelf Margin would have escaped contact with evaporite-associated brines following the demise of the Capitan Reef and during subsequent burial of the Capitan shelf margin. However, the time at which such contact would have occurred are not constrained by this stratigraphic/palaeogeographic relationship.

Much of the Capitan Shelf Margin in the subsurface is currently plugged by anhydrite, and some gypsum and magnesite is also present (Garber *et al.*, 1989). These evaporite minerals have the same associations as the calcite spar present in the rocks of *this* study *i.e.*, occlude all primary pore space left after the precipitation of marine cements. This is strong circumstantial evidence that the calcite spar observed in *this* study has taken the place of evaporite minerals (3.3.4)

Origin of the calcium sulphate

The origin and timing of calcium sulphate emplacement are important considerations. A better understanding of both the source and the timing of calcium sulphate emplacement will be gained if the hydrologic system active during the Upper Guadalupian is understood. The fluids from which the anhydrite precipitated must have been evaporatively concentrated brines. Given the equatorial position, the arid climate and known stratigraphy of the western margin of the Delaware Basin, several origins for these brines are possible. The brines which caused the emplacement of anhydrite in the Capitan shelf margin may have been derived penecontemporanously from: i. the shelf, where intense evaporation was producing sequences of evaporites throughout the Upper Guadalupian; ii. the Delaware Basin, which was filled-up by the evaporitic Castile Formation, or iii. from overlying sequences of evaporites such as the Salado Formation during burial.

Topographic relations show that the Delaware Basin is now, and always has been, approximately 600m deep from the shelf margin to the basin floor (fig.1.9). The Castile Formation (which comprises several hundreds of feet of anhydrite-calcite couplets interbedded with some halite) has recently been reinterpreted as having precipitated from shallow waters, which were 10's of metres deep at most and probably

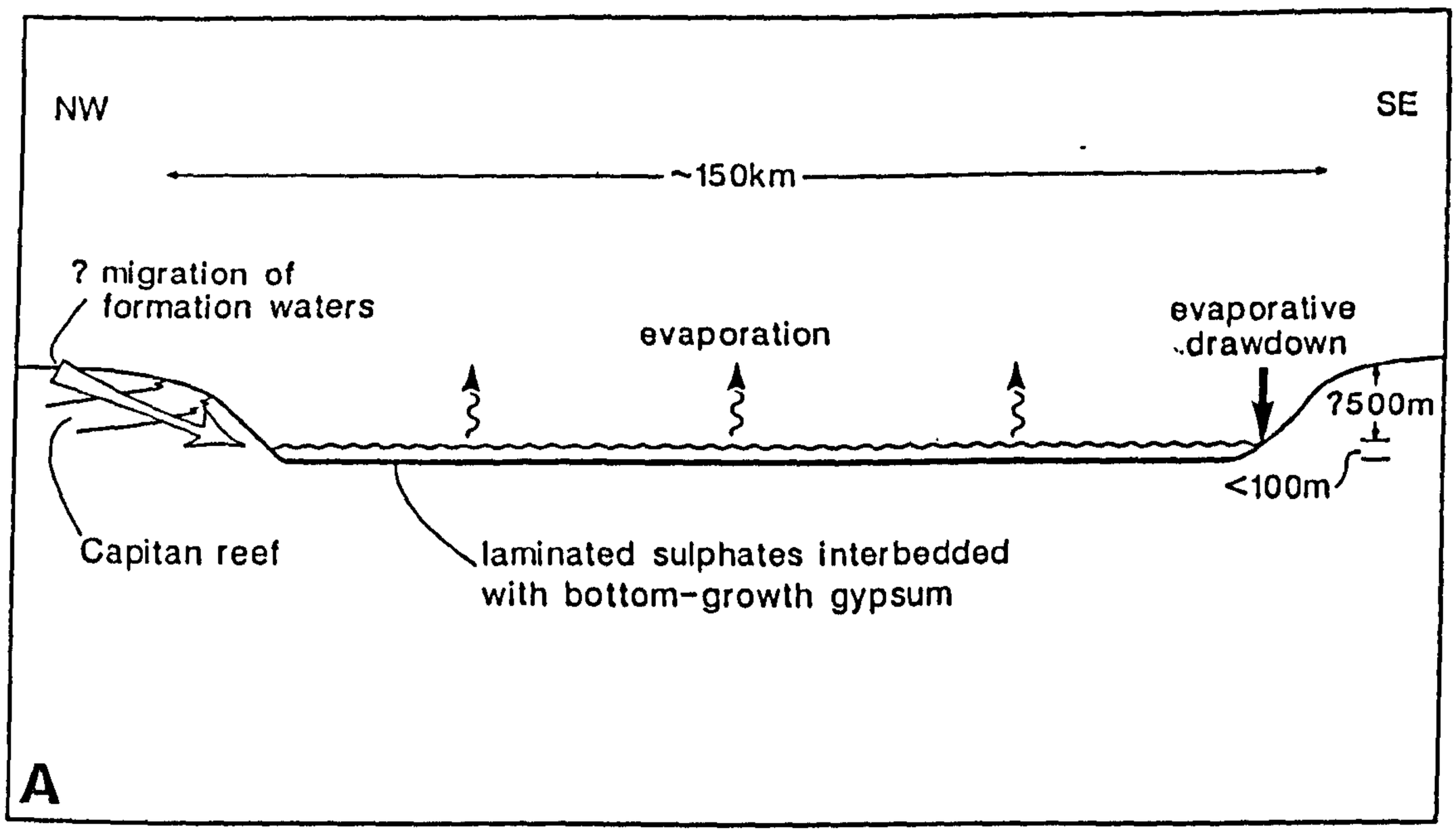

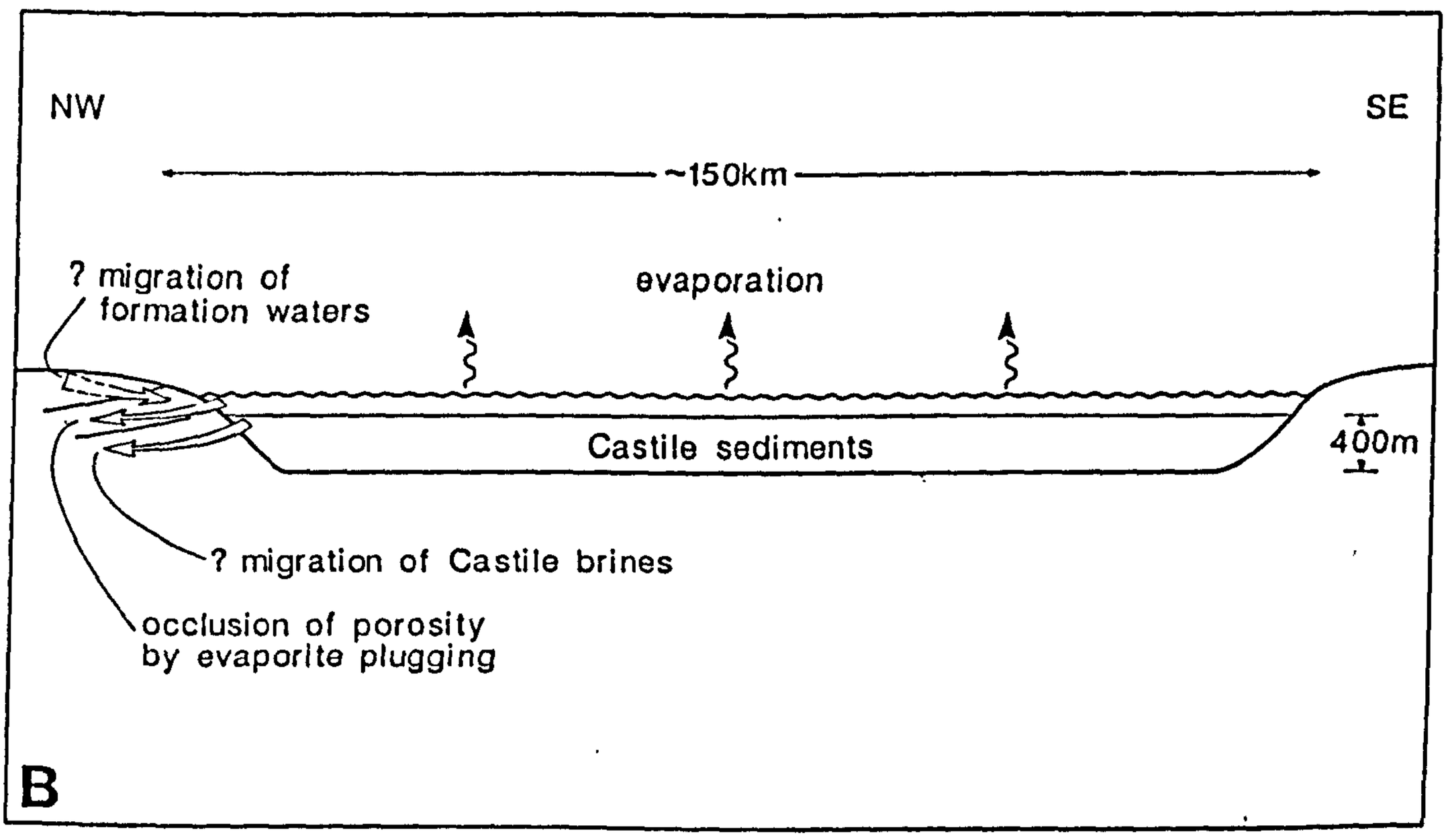

fig. 3.10 Model for the formation of most of the Castile Formation (Kendall and Harwood, 1989) showing: A. possible formation water flow into the basin *via* shelf marginal carbonates during initial desiccation of the basin; and, B. *refluxing of brines* through the marginal carbonates after the deposition of most of the Castile Formation, causing the dolomitisation of, and the occlusion of porosity and replacement of, carbonates in these marginal strata.

much less, on the basis of evaporite mineral solubility data and observations on field and subsurface material (Kendall and Harwood, 1989 and in press). Shallow brine depths on the floor of the basin imply that the Delaware Basin must have been largely desiccated. This implies that the surrounding shelf margin was exposed. The topographic difference of 600m or so, between the shelf and the basin floor implies that groundwater would have flowed in a shelf-to-basin direction (fig. 3.10a). Intense evaporation was already producing evaporite sequences on the shelf, even before the desiccation of the Delaware Basin and any rainfall onto the shelf would have been evaporatively concentrated to some extent, as well as being mixed with brines already present on the shelf. Consequently, during the period when the Delaware Basin was desiccated, evaporatively concentrated brines would have moved in a basinward direction through the Capitan shelf margin. During the period when the Delaware Basin was being gradually filled up with the Castile Formation there would also have been some percolation of brines from the Castile Formation back into the adjacent shelf margin (fig. 3.10b).

Gypsum is the stable polymorph in surface and near-surface environments and gypsum dehydrates to anhydrite on burial and hydrates to anhydrite again on uplift. The depths at which these transformations occur are not well known and widely different estimates have been made *e.g.*, 500-650m on burial and 300-170m on uplift (Murray, 1964) and 30-40m on burial (Lee and Harwood, in press). The presence of replacive anhydrite in the Capitan Shelf Margin at McKittrick Canyon is demonstrated by the diagnostic lath shapes and castellated margins between calcite spar-filled areas and pervasively dolomitised rock matrix. However, there is no unequivocal evidence that any anhydrite was initially precipitated as gypsum and dehydrated to anhydrite on burial. Although movement of brines through the Capitan shelf margin probably precipitated some gypsum in some primary porosity, the majority of primary porosity was occluded by anhydrite. The continued through-put of brines due to the 'deposition' of the Castile Formation caused further crystallisation of anhydrite in sufficient volumes to replace carbonates in parts of the Capitan shelf margin.

No anhydrite or gypsum was identified during petrographic examination of thin sections from the Capitan shelf margin at McKittrick Canyon. However, calcite spars are interpreted to have taken the place of anhydrite and some gypsum and now occlude all porosity which remained after the precipitation of marine cements and also fill fractures. The petrographic evidence for this, and formation of these calcite spars are discussed in section 3.3.4.

3.3.3 Dolomites and dolomitisation

Fabric selective dolomitisation

The separation of dolomite into 'types' has been done on the basis of petrographic observation of habit and occurrence. Fabric selective and non-fabric-selective dolomite are apparent and dolomitisation can be pervasive whether there is any preservation of the primary features of the rock or whether the original fabric of the rock has been completely oblitorated. Some rocks of the back reef and foreslope facies, and the reef facies to a lesser extent, are dolomitised although fabric-destructive dolomitisation is only present in the lower foreslope facies.

Dolomitised microcrystalline calcite This dolomite is finely crystalline and forms equidimensional, small rounded crystals rather than rhombs. Crystal sizes range from 5μm to 20μm and crystal faces are not easily visible. The dolomite has a brown appearance in thin section and has a dull red appearance under cathodoluminescence. The colour in thin section is related to inclusion density and electron microprobe analyses (table 3.2) indicate the presence of sulphur, aluminium, silicon and sodium, presumably present as inclusions within the dolomite. The dolomite itself has a range of compositions and the proportions of $CaCO_3$ to $MgCO_3$ varies both within a sample and between samples. In some cases the $CaCO_3$ and $MgCO_3$ values are lower than expected and the values for sulphur, aluminium and silicon are notably high. The sulphur values are may be due to contamination from accidental analysis of the epoxy resin used in the preparation of thin sections (3.3.1) or may reflect the presence of small calcium sulphate inclusions either within or in between the dolomite crystals. The sulphur values cannot be explained by the analysis of iron sulphides because iron is not detected. The presence of aluminium and silicon indicates the presence of clays. The presence of sodium is more difficult to explain but it may be incorporated within clays or possibly feldspar.

Selective dolomitisation of grains, peloids and micrite is ubiquitous in the back reef and foreslope strata, including the matrix of siltstone units. In a few areas of the back reef and in much of the reef, dolomitisation is limited (fig. 3.19). In the lower foreslope facies, where dolomitisation is often pervasive and fabric destructive, dolomitised grains are sometimes still distinguishable from pervasively dolomitised matrix by having larger, better-developed dolomite crystals. This development of these dolomite crystals suggests that the grains were dolomitised early, and that this early

description	no. analyses	sample	CaCO3 (mol.%)	MgCO3 (mol.%)	SO3 (wt.%)	Al2O3 (wt.%)	SiO2 (wt.%)	FeO (wt.%)	Na2O (wt.%)	TiO2 (wt.%)	K2O (wt.%)
within ostracodes	6	MT60	58.31-68.1	30.87-51.18		0.14-1.53			nd-0.13		
isopachous	3	M22	55.9-56.3	53.52-54.16							
marine cement	7	MT102b	49.95-59.15	40.36-69.99	nd-0.55	nd-3.33	nd-0.81				
	14	MT74i	20.12-56.62	10.61-53.41	nd-10.04	0.11-10.38	nd-1.13		0.13-0.72		
microcrystalline	7	M6i	50.87-57.92	51.31-52.58		nd-0.17					
matrix	1	MT19	57.42	54.2							
	4	MT39	58.2-72.83	35.79-53.01		nd-0.25	nd-0.4				
		MT74i	55.88-57.29	50.22-54.38	nd-0.79	nd-1.49			nd-0.15		
pervasive rhombs	3	MT39	29.42-52.34	22.77-45.62	nd-4.74	2.27-4.02	3.46-6.03	0.33-0.38	nd-0.11		0.39-0.75
	2	MT39i	11.75-37.41	12.47-30.05	0.52-6.11	3.5-21.89	1.83-36.35	0.13-2.85	nd-0.23	nd-0.82	nd-4.63
overgrowths	4	M6i	52.07-56.66	51.3-56.23							
after magnesite?	2	MT117	51.59-61.48	36.92-44.86	0.13-0.26	0.16-0.30					

table 3.2 Electron microprobe analyses of dolomite types

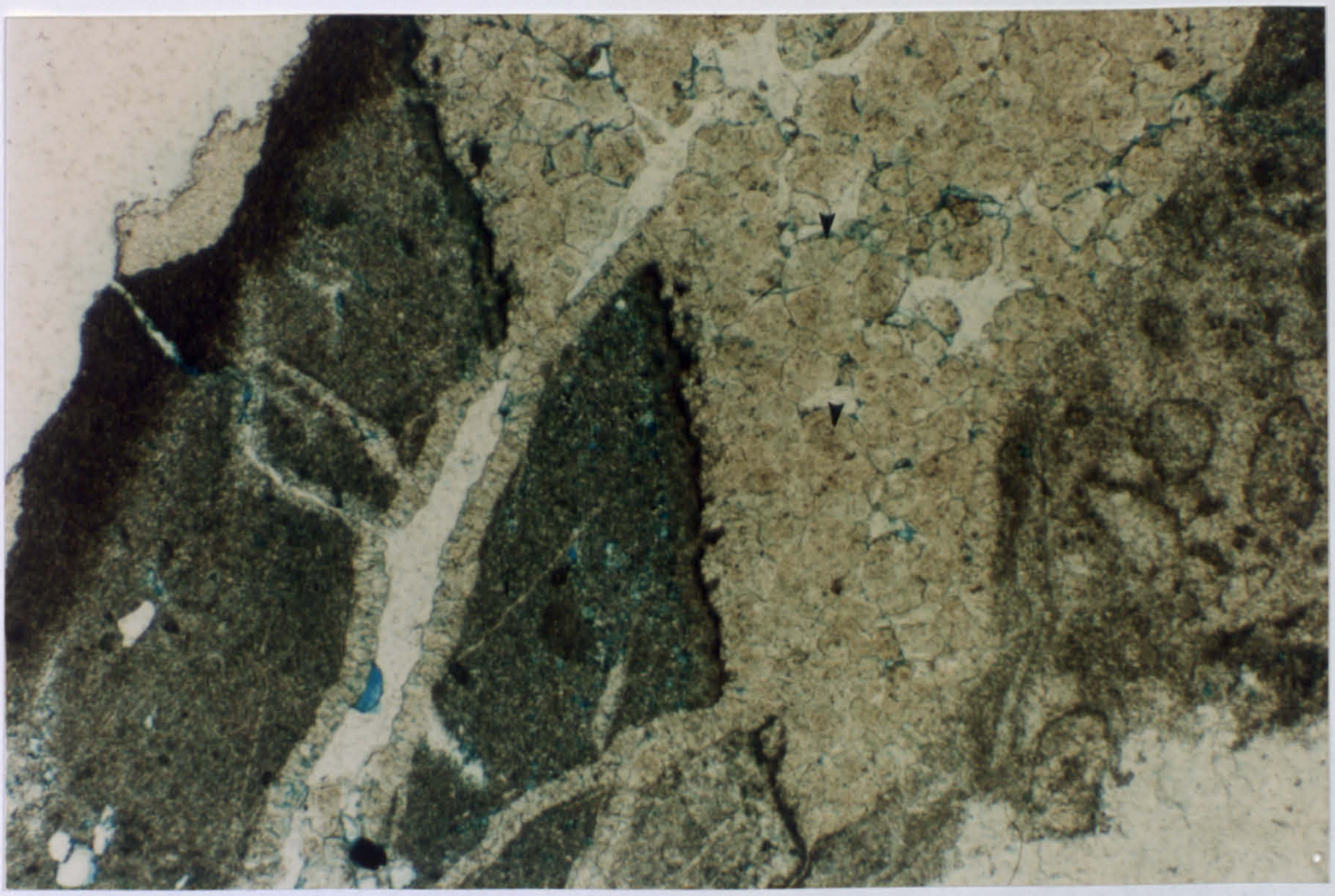

fig. 3.11 Plane polarised light photomicrograph of isopachous marine cement, coating fractures and in pore space, which has been dolomitised by inclusion rich, brown dolomite. The dolomite has radial extinction in cross polarised light, and a spherulitic appearance (arrowed). Sample MT71; upper foreslope facies, 'reef trail', McKittrick Canyon. Scale: 25mm = 500μm.

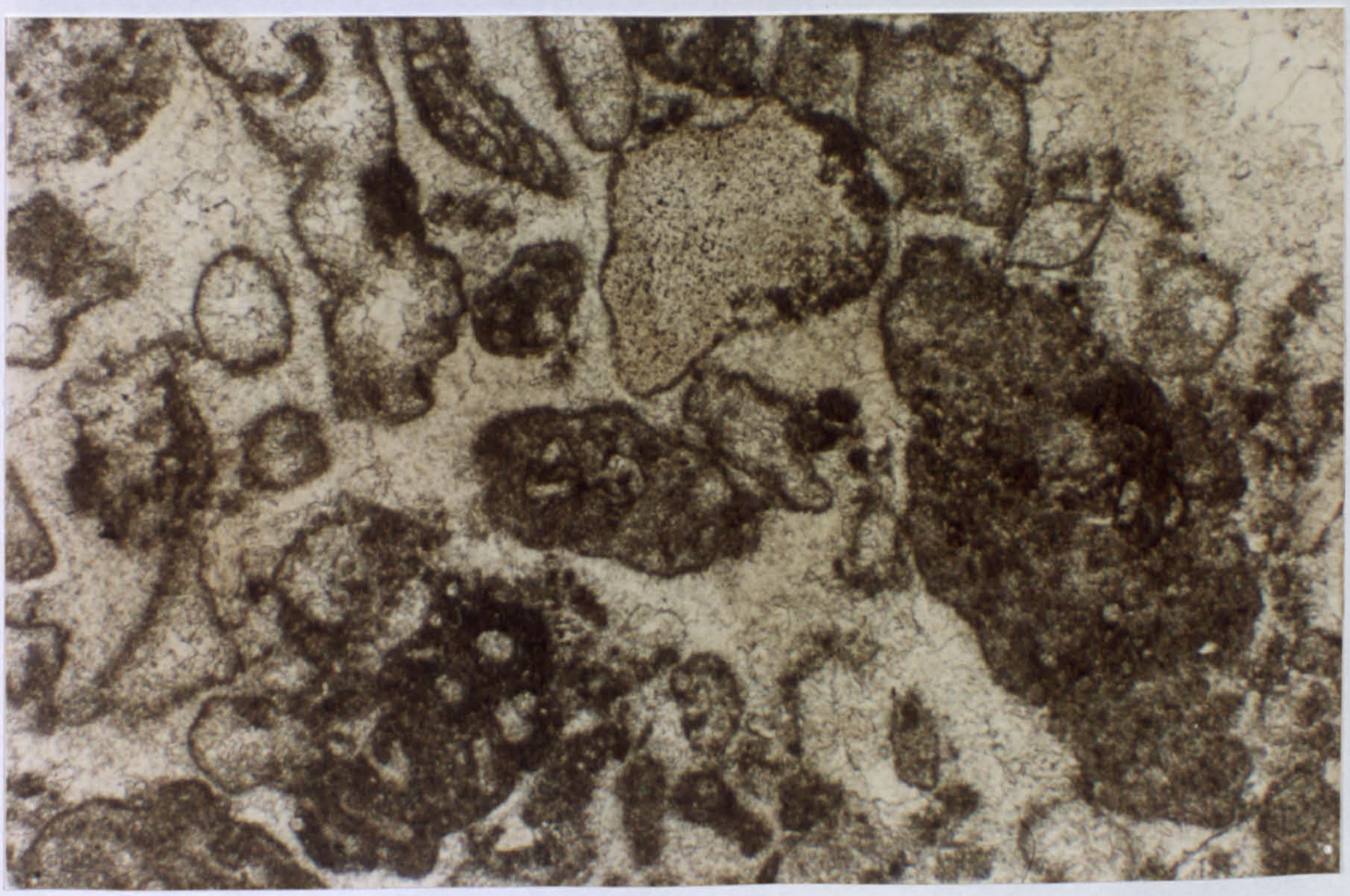

fig. 3.12 Plane polarised light photomicrograph of the complete occlusion of porosity by marine cements, and the lack of dolomitisation. Sample M21; upper foreslope facies, 'reef trail', McKittrick Canyon. Scale: 25mm = 500μm.

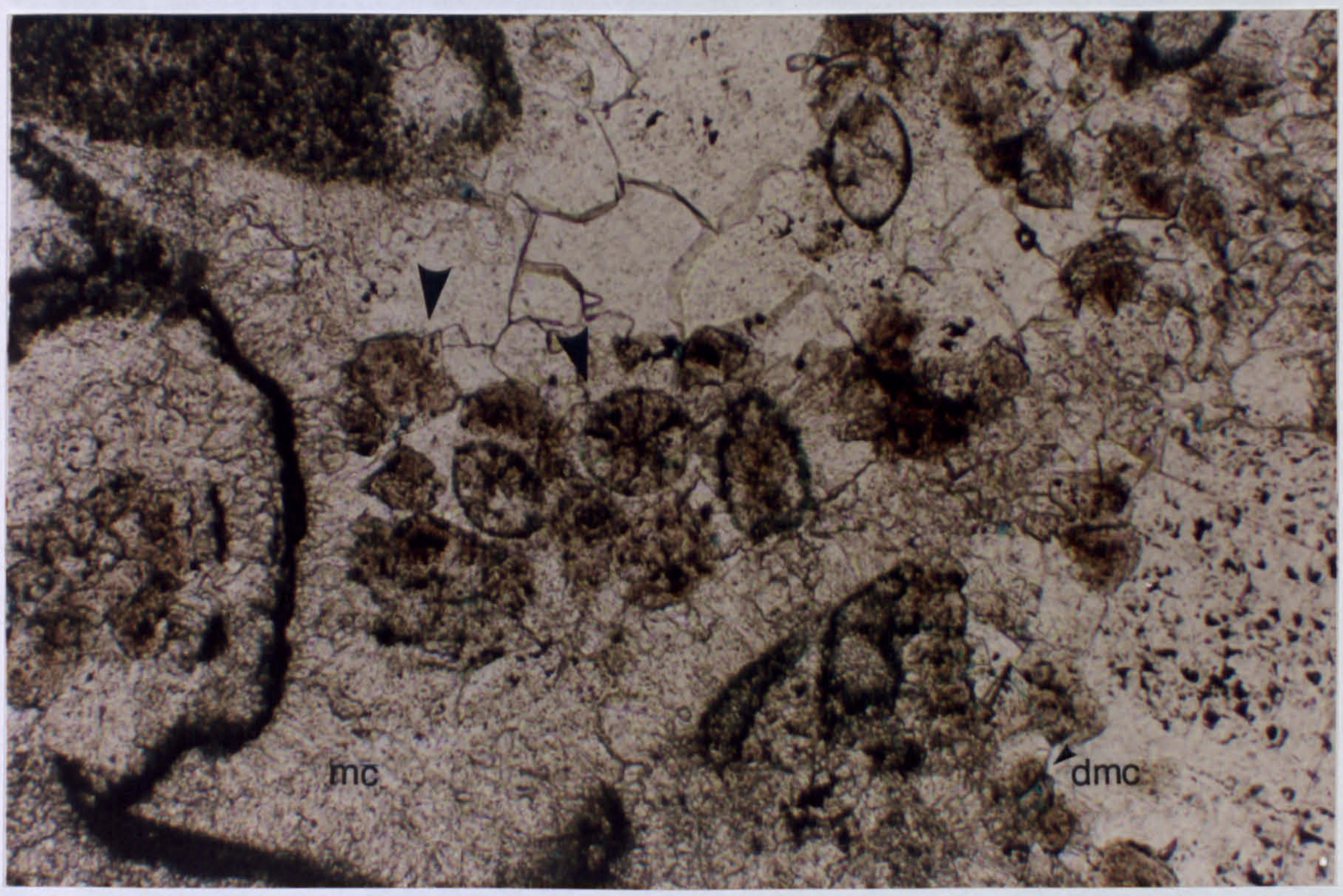

fig. 3.13 Plane polarised light photomicrograph of single dolomite crystals enclosing ostracodes (arrowed). This dolomite shows an extinction cross in cross polarised light and is a *replacement* of early marine cement. Marine cement (**mc**) coats some surfaces; this is dolmitised (**dmc**) in places (arrowed). Spar Ia, Ib and IIc fill the remainder of the pore space. Sample MT60; upper foreslope facies, 'reef trail', McKittrick Canyon. Scale: 25mm = 250μm.

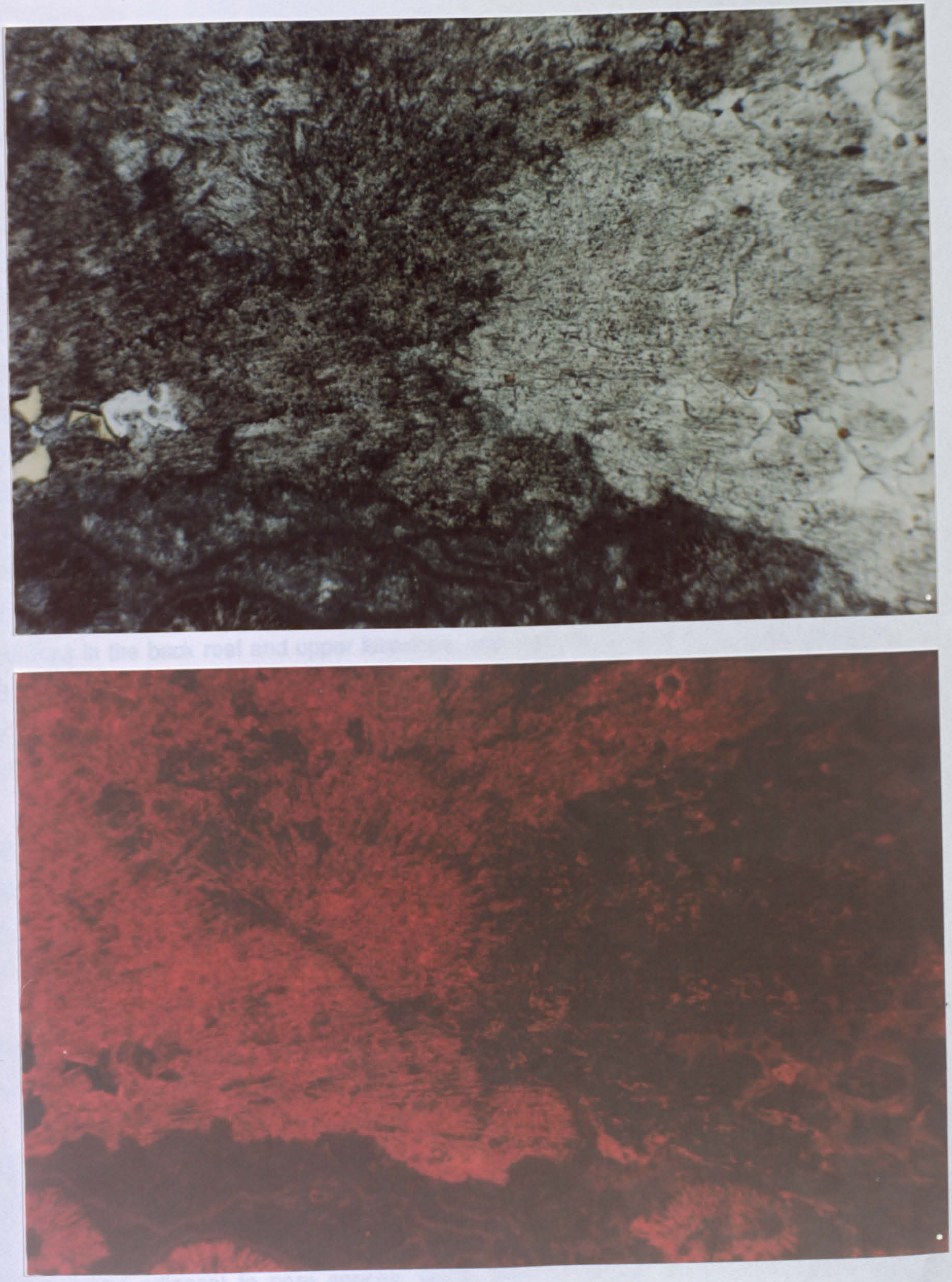

fig. 3.14a,b Plane polarised light and cathodoluminescence photomicrograph pair of dolomitised former aragonite botryoids. Radial, acicular fabric is just discernable in the dolomitised areas. The inclusion rich areas appear to be preferentially dolomitised, and have dull red luminescence. Dolomite rhombs are only present adjacent to pore space. Sample MT98; reef facies, 'reef trail', McKittrick Canyon. Scale: 25mm = 500μm.

dolomite was enhanced by a second phase of dolomitisation. This second period of dolomitisation probably also dolomitised the rock matrix.

Dolomitised isopachous marine cements Dolomitised isopachous marine cements commonly line pore spaces and fractures (fig. 3.11) where the present pore-fill is calcite spar. Often only the last generation of isopachous marine cement is dolomitised. The dolomitised marine cements are invariably inclusion rich, with the inclusions forming a dark core to the crystals. The crystals are generally somewhat rounded and some have an almost spherulitic appearance, with sweeping, undulose extinction in cross-polarised light. In some cases, ostracode shells are visible enclosed within individual dolomite crystals (fig. 3.13). Some of these dolomitised radially-divergent cements show an extinction cross in cross-polarised light. The crystals range in size from 50 μm to 100 μm. The habit, inclusion density, extinction pattern and presence of ostracodes inside some dolomite crystals, all suggest that this dolomite formed by the dolomitisation of a pre-existing cement composed of radially divergent crystals. Clear dolomite overgrowths are commonly seeded onto these dolomitised marine cements. Under cathodoluminescence the dolomite has dull red luminescence and the intensity of the luminescence appears to be related to the inclusion density. There are some instances in the back reef and upper foreslope, and many instances in the reef, where the primary porosity was completely occluded by marine cements (fig. 3.12). In these cases, the marine cements are not dolomitised and even dolomitisation of microcrystalline calcite is more limited.

Electron microprobe analyses (table 3.2) reveal that the composition of the dolomite varies both within samples and between samples. Significant amounts of sulphur, aluminium, silicon and sodium are also detected. This indicates the presence of clays and calcium sulphate as inclusions and in these respects the dolomitised marine cements are similar in composition to the dolomitised microcrystalline calcite.

Isopachous marine cements are most commonly dolomitised in the upper foreslope facies and dolomitisation appears to be more limited in the back reef , reef and lower foreslope facies (fig. 3.19).

Dolomitised botryoidal former-aragonite marine cement Some botryoids are partially preserved as inclusion rich dolomite rather than calcite (fig. 3.14) and some of the original fibrous texture is normally preserved. Dolomite rhombs can only be distinguished adjacent to pore spaces, which may be calcite filled, within the former aragonite botryoids. This dolomite pre-dates the zoned calcite spar present in pore-spaces in these former-aragonite botryoids and has slightly undulose extinction

and luminesces a dull red. Inclusion density and degree of dolomitisation appear to be related. Dolomitised botryoids have only been recorded in parts of the reef and upper foreslope facies (fig. 3.19) and only occur where calcite spar is also present.

Fabric destructive dolomitisation

Dolomite rhombs Fabric destructive dolomitisation is also pervasive. The dolomite crystals are euhedral and are 30-40μm in diameter (fig. 3.15). Replacive anhydrite nodules, which are now filled by calcite spar, are intimately associated with this dolomite (fig. 2.26a and b and fig. 3.7). Electron microprobe analyses (table 3.2, samples MT39 and MT39i) indicate the presence of sulphur, aluminium, silicon, iron, sodium, titanium and potassium presumably present as inclusions within the dolomite. The dolomite itself has a range of compositions and the proportions of $CaCO_3$ to $MgCO_3$ varies both within a sample and between samples and the $CaCO_3$ and $MgCO_3$ values are lower than expected. The values for sulphur, aluminium and silicon are correspondingly relatively high. The sulphur values are too high to be due to contamination from accidental analysis of the epoxy resin used in the preparation of thin sections (3.3.1) and probably reflect the presence of small calcium sulphate inclusions either within or in between the dolomite crystals. These sulphur values cannot be explained by the analysis of iron sulphides because high sulphur and iron values do *not* occur within the same analyses. The presence of aluminium and silicon indicates the presence of clays. The presence of iron and titanium, which do not occur with sulphur, suggest that small quantities of iron oxide(s) are present, or alternatively that iron may be incorporated within the dolomite lattice. The presence of sodium and potassium are more difficult to explain but may be incorporated within clays or possibly feldspar. It occurs mainly in the lower foreslope facies (fig. 3.19)

Dolomite overgrowths These are euhedral and inclusion free and form overgrowths (fig. 3.15 and fig. 3.16) on earlier dolomite crystals *i.e.*, dolomitised marine cements, micrite and dolomite rhombs. They have uniform extinction and bright red luminescence. These overgrowths are on average 10μm thick and are prominent adjacent to calcite-filled pores and do not appear to have replaced pre-existing cements or particles. Electron microprobe analyses (table 3.2) indicate that the dolomite of the overgrowths is almost stoichiometric. Overgrowths are most abundant in the lower foreslope facies in fabric-destructive, pervasive dolomites (fig. 3.19). In this facies

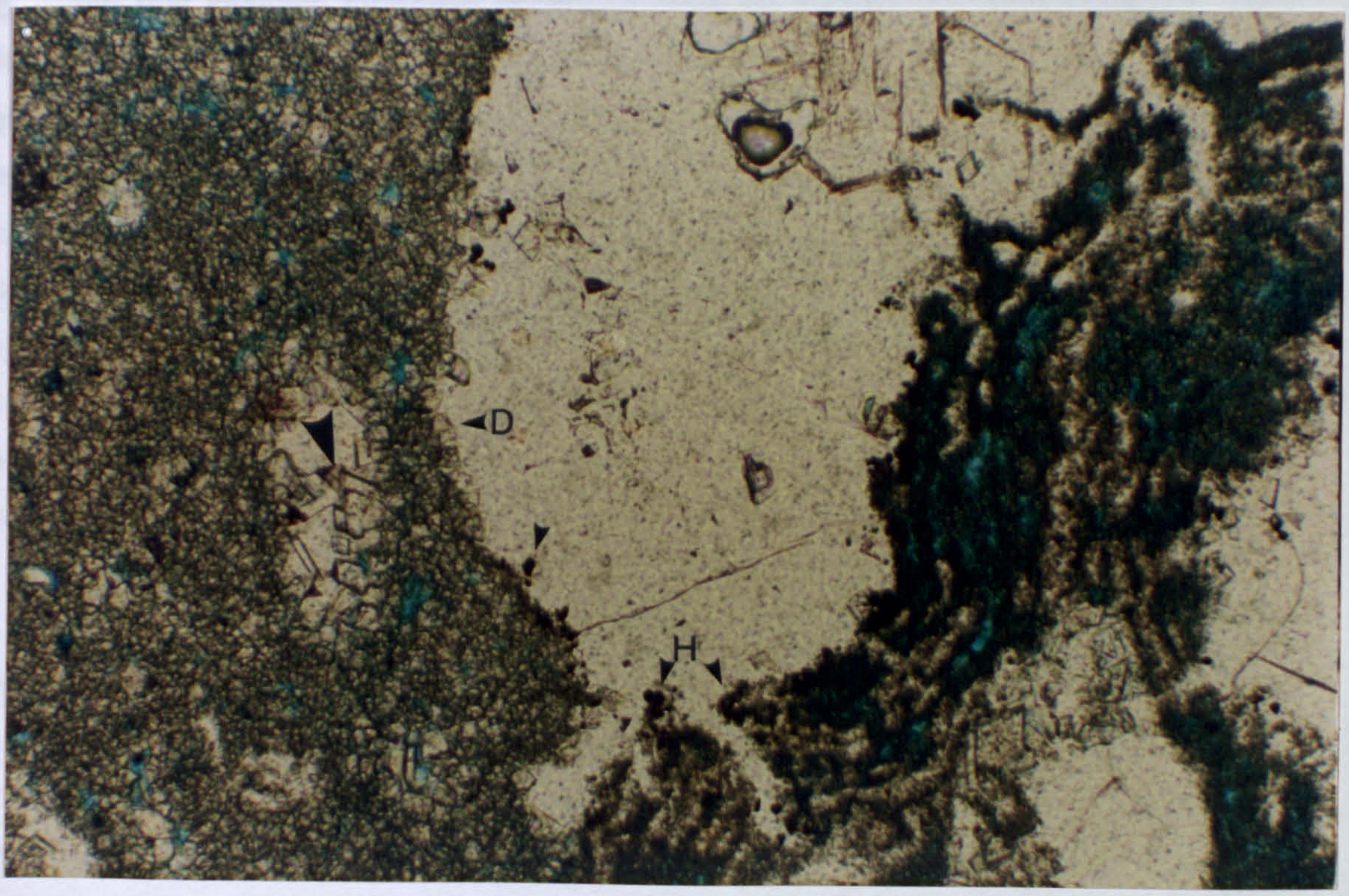

fig. 3.15a,b Plane polarised light photomicrograph of dolomitised matrix (**D**), dolomite overgrowths (arrowed) and calcite spar IIc. The dolomitisation of the matrix is prevasive and fabric destructive. Haematite (**H**) (arrowed) is associated with the margin of the spar-filled area. Sample MT19; lower foreslope facies, 'reef trail', McKittrick Canyon. Scale: 25mm = 250μm.

they are associated with small (10-15μm) euhedral dolomite rhombs which appear to float in calcite spar (fig. 3.15). The dolomite overgrowths and these dolomite rhombs have similar luminescence colours and are likely to be the same generation.

Other occurrences of dolomite Small dolomite rhombs also occur at the margins of calcite spar-filled pores in the lower foreslope facies (fig. 3.17 and fig. 3.18). This dolomite is different to the matrix dolomite as it forms distinct, small (10μm) brown rhombs, and is associated with minor amounts of clays and some iron oxide staining. The dolomite-rich regions cannot be geopetal silts resulting from dissolution of a host phase, as they do not show any consistent orientation. Where it occurs in the same pore as authigenic kaolinite, the two are virtually mutually exclusive (fig. 3.18). However, one or two kaolinite crystals can occasionally be found in amongst this dolomite, suggesting that kaolinite formation continued after the formation of this dolomite. The dolomite appears to be 'floating' in calcite spar and the margin of this dolomite-rich region is indented and castellated. This implies that some mineral/substance was present prior to the emplacement of anhydrite in the remaining pore space. This mineral may have been gypsum that was replaced by anhydrite. Alternatively, it may have been magnesite. Garber *et al.* (1988 and 1989) report magnesite and anhydrite in the same pore from a core in the Capitan shelf margin. Where magnesite and anhydrite are both present, the magnesite lines the pore. Subsequent dissolution of magnesite would provide a source of Mg^{++} ions for formation of this dolomite. Dolomite associated with magnesite is also reported in Mid Miocene of Egypt (Pierre and Rouchy, 1988).

Dolomitisation

Two categories of dolomite are present; fabric-selective and fabric-destructive. Both types are pervasive in certain places. In each case the dolomite has different habit, occurrence and petrographic characteristics. Textures are well preserved where the dolomitisation is fabric selective and the internal structure and outline of grains, bioclasts and cements are usually still recognisable. Pervasive, fabric-selective dolomitisation is usually associated with calcite spars which fill original, intergranular pore spaces and fractures. These calcite spars form between 30% and 80% of the rock volume. Pervasive, fabric-destructive dolomitisation is accompanied by the creation of intercrystalline porosity of between 5% and 10% (visual estimate), whereas no significant porosity development is associated with fabric selective dolomitisation. Some

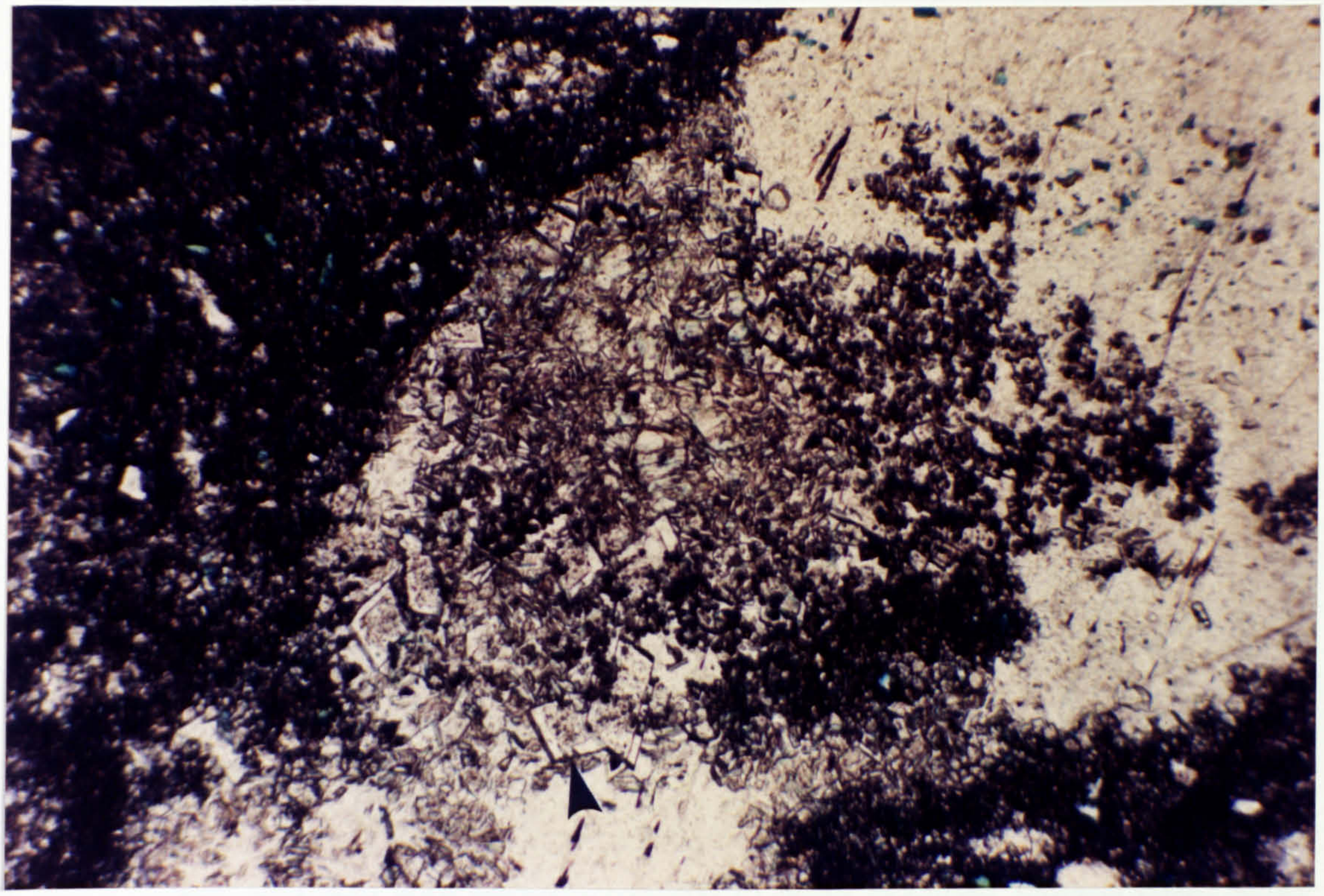

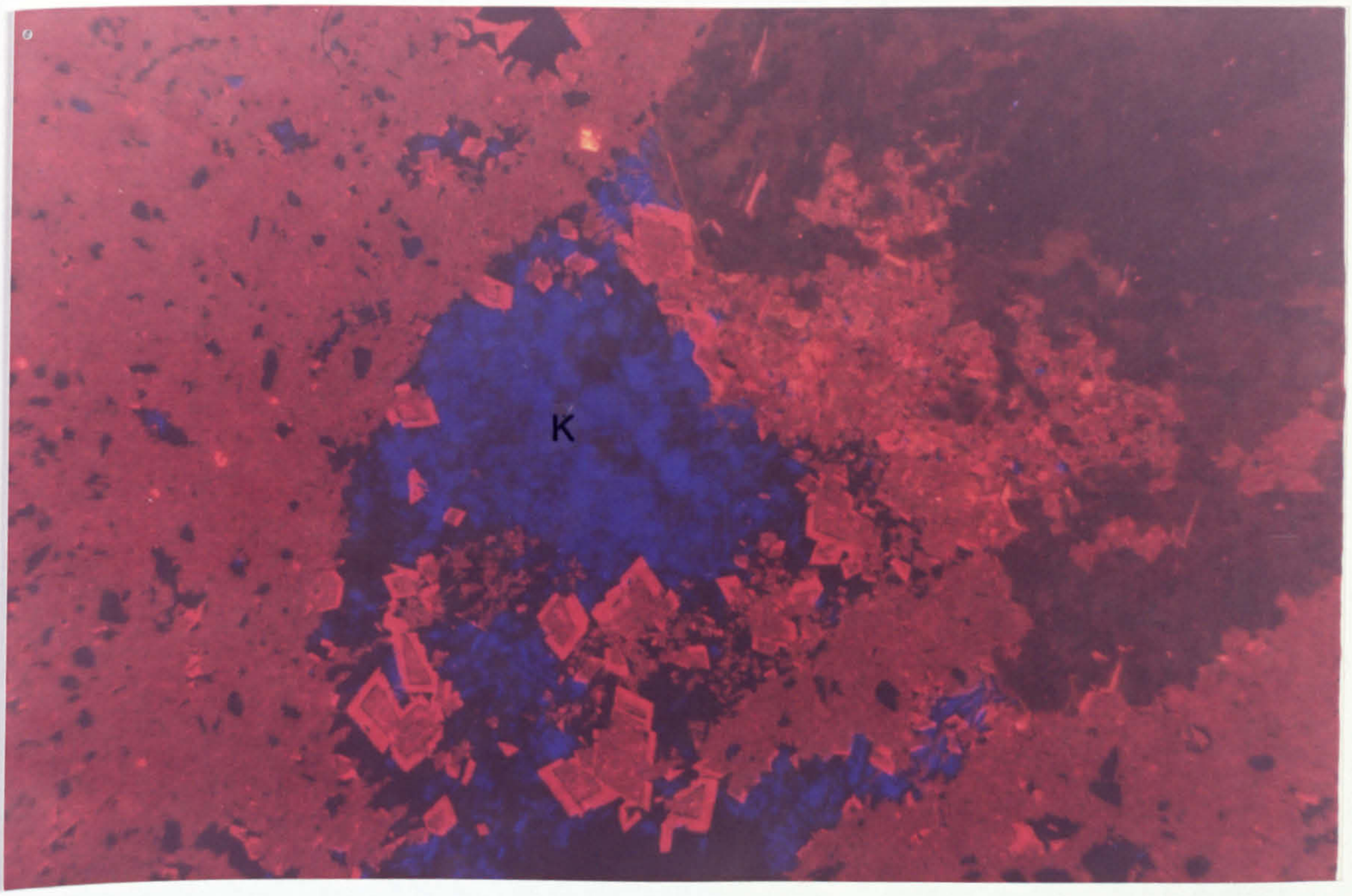

fig. 3.16a,b Plane polarised light and cathodoluminescence photomicrograph pair showing the bright red luminescence of the dolomite overgrowths (arrowed) and the blue luminescence of authigenic kaolinite (**K**). The overgrowths are pitted by the kaolinite indicating either that kaolinite and the overgrowths were contemporaneous, or that minor dissolution preceeded kaolinite precipitation. Kaolinite and dolomite are enclosed within non-luminescent calcite spar III. Sample MT19; lower foreslope facies, 'reef trail', McKittrick Canyon. Scale: 25mm = 500μm.

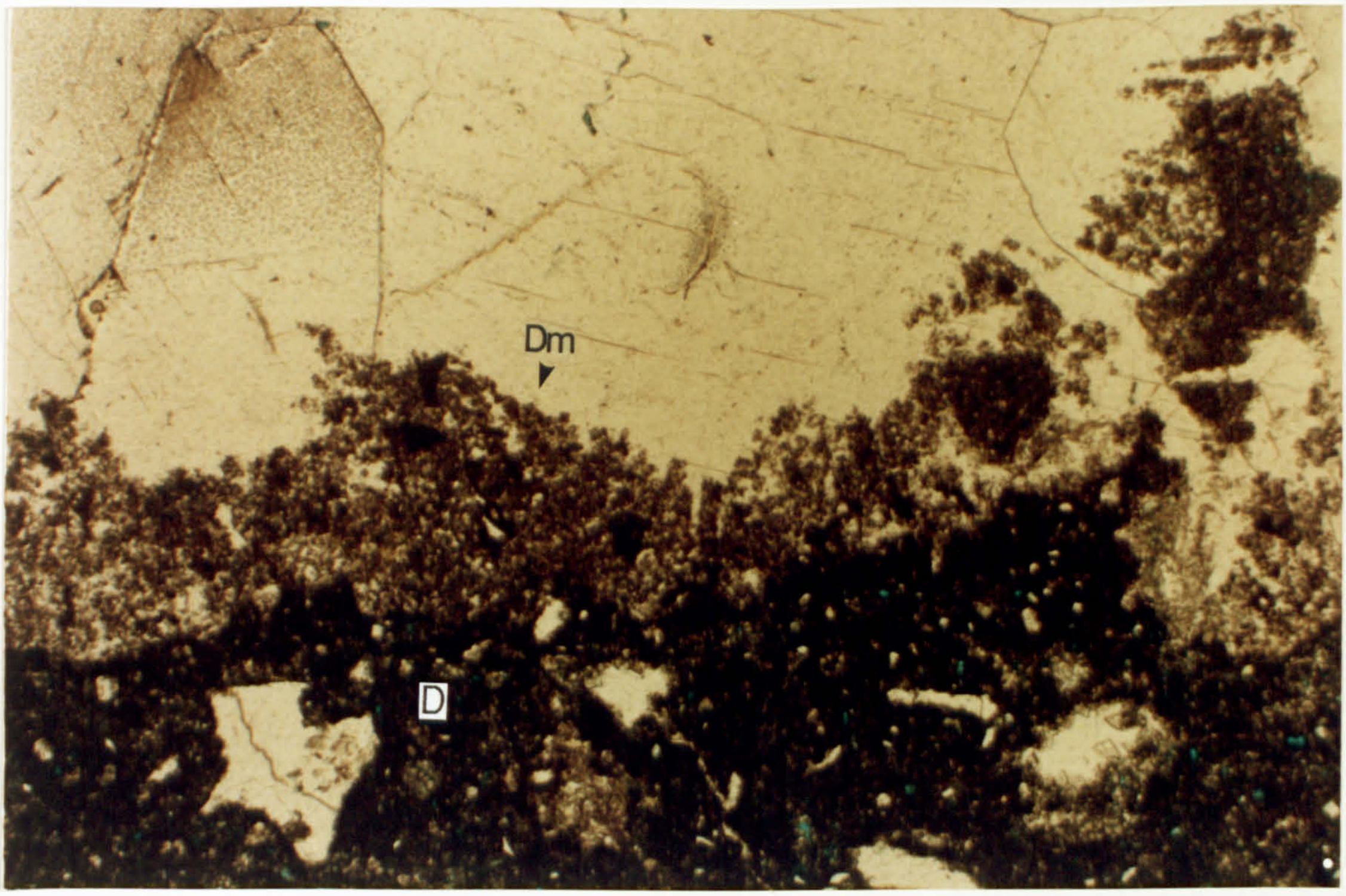

fig. 3.17 Plane polarised light photomicrograph of small dolomite rhombs (**Dm**) lining a pore. The remainder of the pore is filled by calcite spar IIc, after replacive anhydrite. The castellated margin between the calcite and dolomite indicates that the anhydrite replaced a mineral (magnesite?, now (Dm)). Calcite spar fills all porosity in the dolomite matrix (**D**). Sample MT19; lower foreslope facies, 'reef trail', McKittrick Canyon. Scale: 25mm = 500μm.

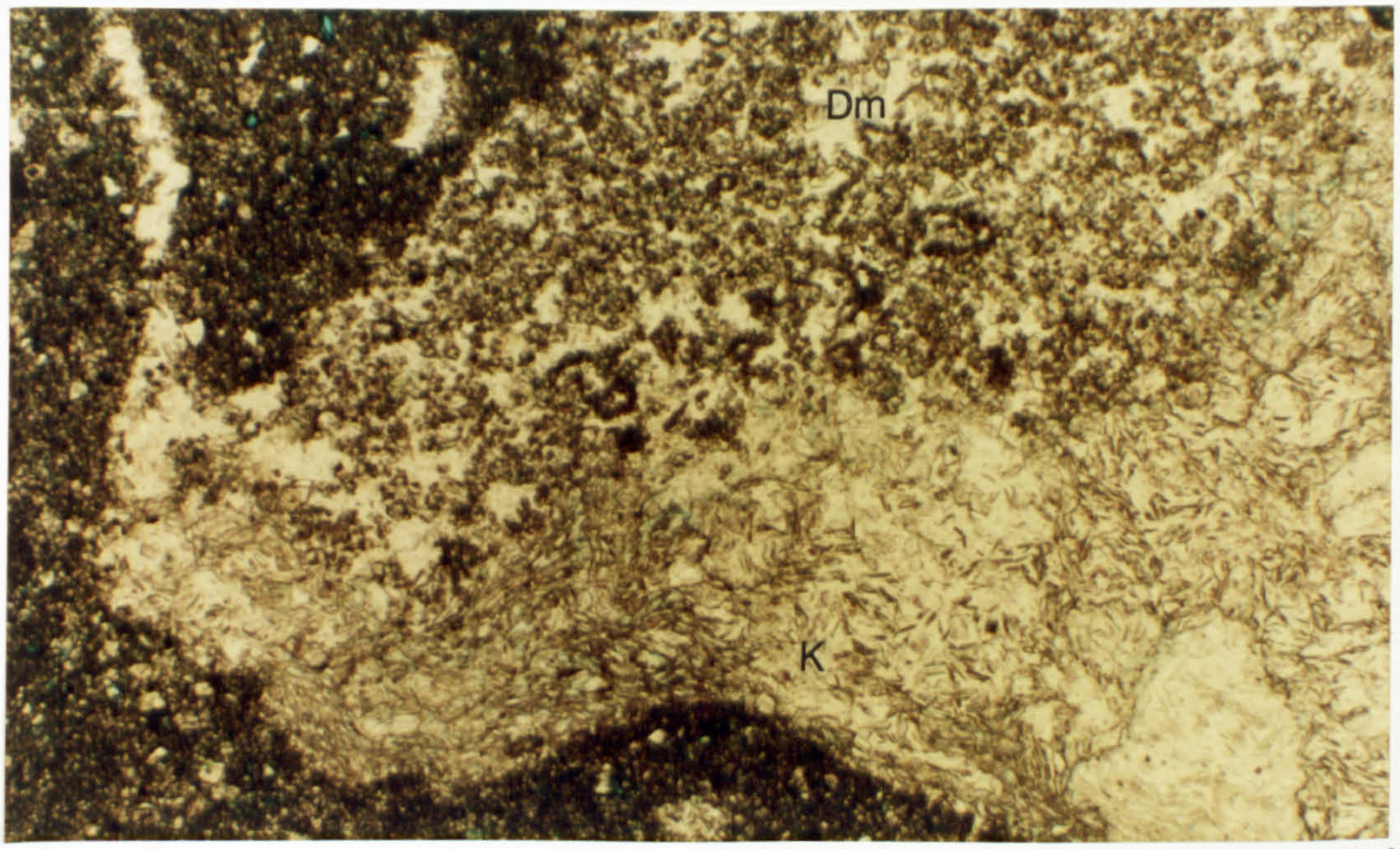

fig. 3.18 Plane polarised light photomicrograph of small dolomite rhombs (after magnesite?, now (Dm)) in the same pore as kaolinite (**K**). The two phases are mutually exclusive. The kaolinite has a fabric (arrowed) which parallels the pore margin. Kaolinite and dolomite are enclosed in spar III. The rock matrix is pervasively dolomitised with no fabric preservation. Sample MT19; lower foreslope facies, 'reef trail', McKittrick Canyon. Scale: 25mm = 500μm.

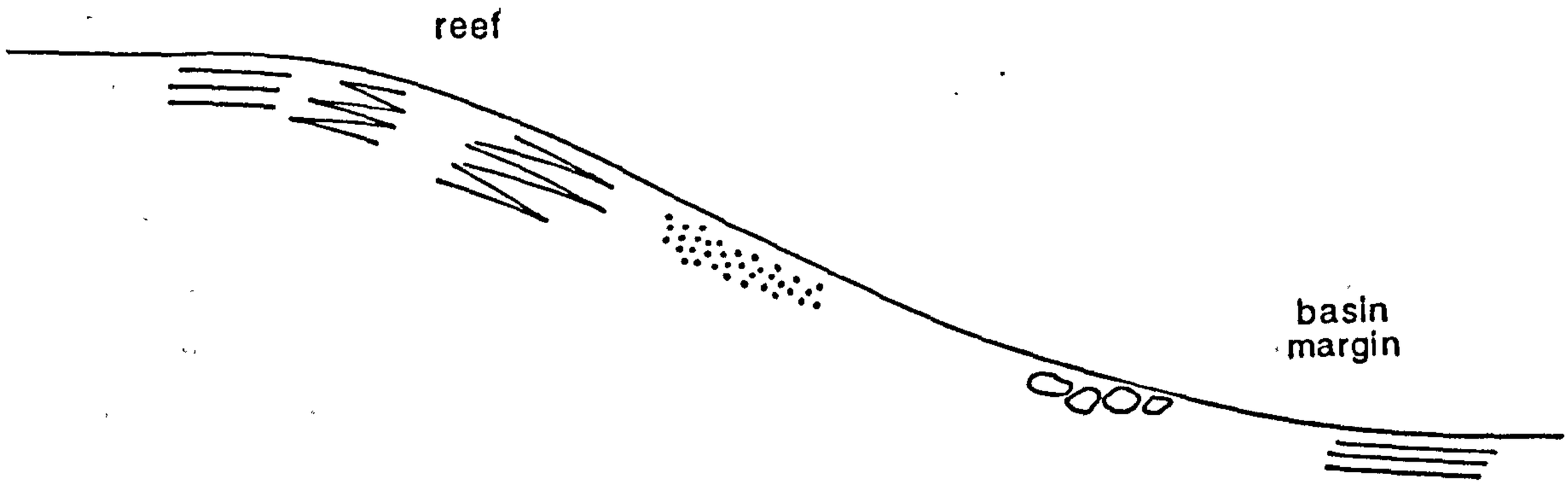

fabric selective

micrite

isopachous cements

botryoidal aragonite

fabric destructive

overgrowths

after magnesite ?

fig. 3.19 Summary diagram of the facies distribution of dolomite types.

traces of the original rock fabric remain in the case of fabric destructive dolomitisation; calcite spar is only present in mouldic porosity after dissolution of replacive sulphate nodules (3.3.4), and as intercrystalline cement. The texture and habit of dolomites is related to different dolomitisation processes, as well as differences in the nature of the original substrate.

The facies distribution of these different dolomite types varies (fig. 3.19). Selective dolomitisation of microcrystalline calcite and marine cements is prevalent in the upper foreslope, and occurs to a lesser extent in the back reef facies and the lower foreslope facies. Dolomitisation is minor in the reef facies. Pervasive, fabric destructive dolomitisation is prevalent in the lower foreslope facies and is less common in the upper foreslope and back reef facies. The dolomite which occurs within calcite spars, possibly after magnesite, only occurs in the lower foreslope facies.

Dolomitisation of peloids and grains and micrite preceeded the dolomitisation of the rock matrix. Evidence for this relative timing comes from petrographic evidence of the enhancement of dolomitised former-micrite envelopes in shelf-derived grains of the lower foreslope facies. and from the observations of contemporaneous dolomitisation of equivalent Holocene sedimentary sequences (*e.g.*, Alderman and Skinner, 1957 and Shinn *et al.*, 1964). The Mg^{++} ions for initial dolomitisation were probably derived from sea water and dolomitisation was probably driven by 'evaporative pumping' (Hsu and Siegenthaler, 1969). Throughflow of evaporatively concentrated brines and the inversion of high-magnesian to low-magnesian calcite, caused the majority of the dolomitisation *i.e.*, the selective dolomitisation of marine cements and dolomitisation of the matrix. The formation of rhombic dolomite, particularly abundant in the lower foreslope facies, was cogenetic with formation of replacive sulphate nodules in this facies.

In the past few years geochemical studies have established that, under natural conditions, high salinities and high Mg/Ca ratios are not pre-requisites for dolomitisation (*e.g.*, Hanshaw et al., 1971) as long as the rate of groundwater flow is high enough to supply Mg ions and remove Ca ions. Also in the last few years it became the trend for studies to concentrate on the fluids that allegedly 'caused' dolomitisation. One of the most favoured models involved the mixing zone. This model relied upon the mixing of groundwater and hypersaline water which produced solutions capable of dolomitisation at low concentrations and at low Mg/Ca ratios (Badiozamani, 1973; Folk and Land, 1975). Mruk (1985) interprets the dolomite as *not* having formed from hypersaline fluids on the basis of their isotopic compositions (table 3.3). Mruk (*op. cit.*) infers a single dolomitising 'event' in a mixing zone between marine and meteoric waters as the environment of formation of the dolomite, and goes on to interpret the

diagenetic phases visible in terms of sea level fluctuations (high stands and low stands). Comparison with other data (Hardie, 1987; Garber *et al.*, 1989; and others) suggests that these isotopic compositions do, in fact, support the interpretation that these dolomites precipitated from hypersaline fluids (table 3.3).

However, it is not necessary to seek any special conditions to explain the dolomitisation of the strata of the Capitan shelf margin althogh many other models have been developed (Chilingar *et al.*, 1979; Hardie, 1987; Zenger *et al*, 1980). Observations in this study clearly show the crucial role of calcium sulphate in the diagenesis of the Capitan shelf margin (section 3.3.2). The movement of evaporatively concentrated brines from the shelf towards the Delaware Basin during the deposition of the Castile formation seems to be the likely source of potentially dolomitising fluids (Kendall and Harwood, 1989). Brines would have travelled via the large primary voids in the reef (now filled by calcite spar) and through fractures (fig. 2.4 b,c,d) and down into the strata of the foreslope. It is likely that more permeable strata, such as the siltstones and grainstones of the foreslope, acted as preferential 'conduits' for brine movement down-dip. The lack of dolomitisation in the reef facies is probably explained by lack of permeability due to prior cementation by marine cements. Preferential cementation of certain *strata* of the back reef facies, and consequent lack of dolomitisation, is not as easily explained. Lithology possibly controlled the movement of brines *i.e.*, flow rates may have been greater within strata such as the siltstones.

The precipitation of gypsum would have raised the Mg:Ca ratio of pore waters, encouraging dolomitisation (precipitation of calcium sulphate removes Ca^{++} ions from solution). This would have encouraged the precipitation of further calcium sulphate and promotes dolomitisation due to the relative availability of Mg^{++} ions. This process is well documented on modern sabkhas, but less well so in the burial environment (see Hardie, 1987 for discussion). It has been suggested that the presence of sulphate ions inhibits the formation of dolomite (Baker and Kastner, 1981). Closer examination of their experimental data (Hardie, 1987) shows that this is only likely to be the case for unusually high temperatures, and therefore does not apply in most natural systems. A model has been put forward by Melim and Scholle (1989) which also invokes dolomitisation by shelf-derived brines, interpreted to have entered the foreslope via 'solution enlarged vertical fractures and karstic features' in an otherwise 'tightly cemented and impermeable' reef during Ochoan times. No solution enlarged fractures or karstic features of this age have been identified in the present study.

This model is a modification of the model proposed by Adams and Rhodes (1960) who suggested that dolomitisation was driven by high evaporation rates for water in a restricted lagoon. Dense hypersaline brines, enriched in Mg ++ as a result of

Author(s)	mineral	isotopic composition
Mruk (1985)	marine cement	$\partial^{18}O$ = -3.0 to -7.7‰
		$\partial^{13}C$ = +7.3 to -3.1‰
	spar I	$\partial^{18}O$ = -8.5‰
		$\partial^{13}C$ = -0.6 to -4.9‰
	spar II	$\partial^{18}O$ = -11.5 to -13.9‰
		$\partial^{13}C$ = +0.6‰
	spar III	$\partial^{18}O$ = -15.1 to -16.6‰
		$\partial^{13}C$ = -0.4 to -2.6‰
Given and Lohmann (1986)	marine cement	$\partial^{18}O$ = -2.5‰ (extrapolated)
		$\partial^{13}C$ = +5.3‰ (extrapolated)
	spar I	$\partial^{18}O$ = -8.2‰ (average)
		$\partial^{13}C$ = -5.5 to -1.0%
	spar II	$\partial^{18}O$ = -12.3‰ (average)
		$\partial^{13}C$ = 0.0‰ (average)
Garber *et al.* (1989)	calcite spar	$\partial^{18}O$ = -2.0 to -6.0‰
		$\partial^{13}C$ = +1.5 to +3.5‰
	(Fe)calcite spar	$\partial^{18}O$ = -1.0 to -5.0‰
		$\partial^{13}C$ = +4.0 to +5.5‰
Mruk (1985)	dolomite	$\partial^{18}O$ = +1.0‰ (average)
		$\partial^{13}C$ = +5.5‰ (average)
Garber *et al.* (1989)	dolomite	$\partial^{18}O$ = -2.6 to +3‰
		$\partial^{13}C$ = +4.5 to +8.0‰
	magnesite	$\partial^{18}O$= -1.9 to +1.6‰ (+1.04‰ av.)
		$\partial^{13}C$ = +5.7 to +7.5‰ (+6.84‰ av.)

Table 3.3 Summary table of isotopic analyses of calcite spars, dolomite and magnesite of other workers.

precipitation of gypsum in this lagoon, were responsible for dolomitisation. These dense brines were envisaged to flow along the base of this lagoon until they reached a more permeable zone, at which point, these brines refluxed through this zone, thus causing dolomitisation. Seepage through such a zone displaced connate water and provided a source of Mg^{++} ions at the same time.

The Adams and Rhodes model (1960) model was originally developed in the Capitan shelf margin, but one problem was that the rate of the process was not appropriate to account for the amount of dolomitisation seen in the Capitan shelf margin, given the time available (Bathurst, 1971). This criticism cannot be raised at the model proposed herein because evaporatively concentrated, sulphate-laden brines affected the Capitan shelf margin during the development of the Castile Formation until the dissolution of anhydrite on uplift during the Tertiary *i.e.*, from the times of early burial through to maximum burial in the late-Cretaceous.

One potential problem for the model proposed is the apparent lack of calcitised dolomite. Schmidt (1977) reports calcitised dolomite, but does not give a petrographic description or compositional analysis. In a carbonate aquifer containing calcite, dolomite and gypsum, groundwaters evolve to the point where they are supersaturated with respect to Ca^{++} and carbonate but are undersaturated with respect to Mg^{++}. This results in the dissolution of dolomite and the precipitation of calcite (Lee and Harwood, in press; Hanshaw and Back, 1979). This model relies on the relative availability of Ca^{++} and Mg^{++} ions. The lack of calcitised dolomite may be explained by the release of Mg^{++} ions due to concomitant dissolution of magnesite and anhydrite, either from the shelf (particularly the overlying Salado Formation) or from within the foreslope.

Shale dewatering during compaction of basinal sediments has been reported as a likely cause of dolomitisation for limestones marginal to a basin (*e.g.*, Machel, 1986). These dolomites are characterised by high boron content and high content of radiogenic strontium. Although shales (*sensu stricto*) are not present in the Delaware Basin, geochemical analysis for B and Sr in the dolomites needs to be done in order to ascertain whether dewatering of the siliciclastic-dominated sediments of the Delaware Basin and the migration of fluids up-dip, contributed to formation of dolomite in the Capitan shelf margin. If this was a possible source for some of the dolomitising fluids, more dolomite would be expected in the lower foreslope facies. This is in fact the case, but may just as readily be explained by compactional dewatering of the Castile Formation and the reflux of Castile-derived brines into the strata of the Capitan shelf margin following the desiccation of the Delaware Basin.

3.3.4 Calcite spars

The calcite spars identified in this study have been distinguished on their *petrographic* characteristics in plane- and cross-polarised light and under cathodoluminescence. This classification is based on intrinsic characteristics and is thus different to the interpretive classifications of Mruk (1985) and Given and Lohmann (1985, 1986). These calcite spars have been labelled numerically (I, II and III) according to their relative timing. Where there is no evidence for putting these spars into a relative sequence, the spars have been labelled alphabetically (a,b,c and d). The various names given to these calcite spars, in this study and by previous workers, are summarised in table 3.4.

Patterns of luminescence and zoning are useful in determining similarities and differences betweeen calcite spars. It is well established that Fe and Mn content are major controls on the cathodoluminescence of calcite spars . The incorporation of Fe and Mn into the calcite lattice is controlled primarily by the availability of ions and by Eh although different redox conditions can give rise to the same luminescence characteristics (fig.3.20). Consequently, the relationship between cathodoluminescence and redox conditions is ambiguous unless other solid phases such as iron sulphides or iron oxides/hydroxides occur in association with the calcite. The pH of the pore fluid also has an effect but this is relatively minor.

Recently published data on the roles of Fe and Mn in the cathodoluminescence of calcites indicated that intensity is directly related to Mn concentrations at constant Fe/Mn ratios and for narrow ranges of Fe contents (Hemming *et al.*, 1989). Absolute concentrations of Fe and Mn also affect luminescence intensity, and Fe does not appear to extinguish Mn-activated luminescence up to at least 10,000ppm Fe. Other rare earth elements do not appear to play a role in the luminescence of calcite.

Mn(ppm)	Fe(ppm)	luminescence
>100	moderate amounts	luminesces
150-650	none detected	moderate
>700	none detected	bright

(data from Hemming *et al.*, 1989)

Author	calcite spar classification							
Darke (1989 this work)	Ia	Ib early	Ic	Id telogenetic (meteoric)	IIa	IIb	IIc late	III
Schmidt (1977)	'Spar I' mesogenetic (early)		'Spar II' mesogenetic		'Spar III' telogenetic (early)			
Mruk (1985, 1989)	'Spar I' eogenetic (meteoric)		'Spar II' ?		'Spar III' telogenetic ?			
Given and Lohmann (1985, 1986)	'Spar I' eogenetic (meteoric)		'Spar II' early mesogenetic (meteoric)					

Table 3.4 Summary table of calcite spar names, and their interpreted origins, given in previous studies and in this study.

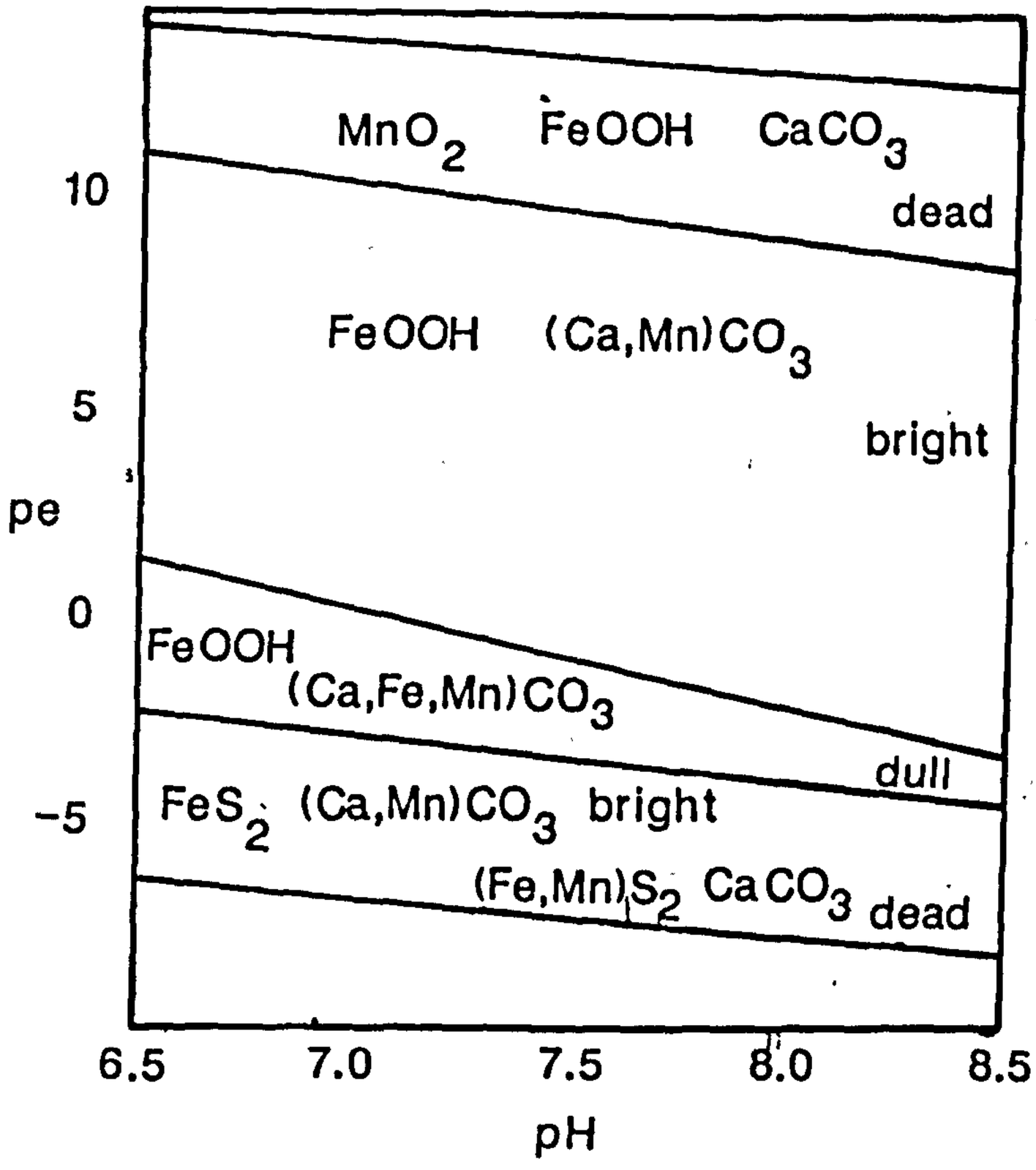

fig. 3.20 Predicted mineral assemblages, calcite composition and calcite cathodoluminescence as function of Eh and pH (Frank *et al.*, 1982).

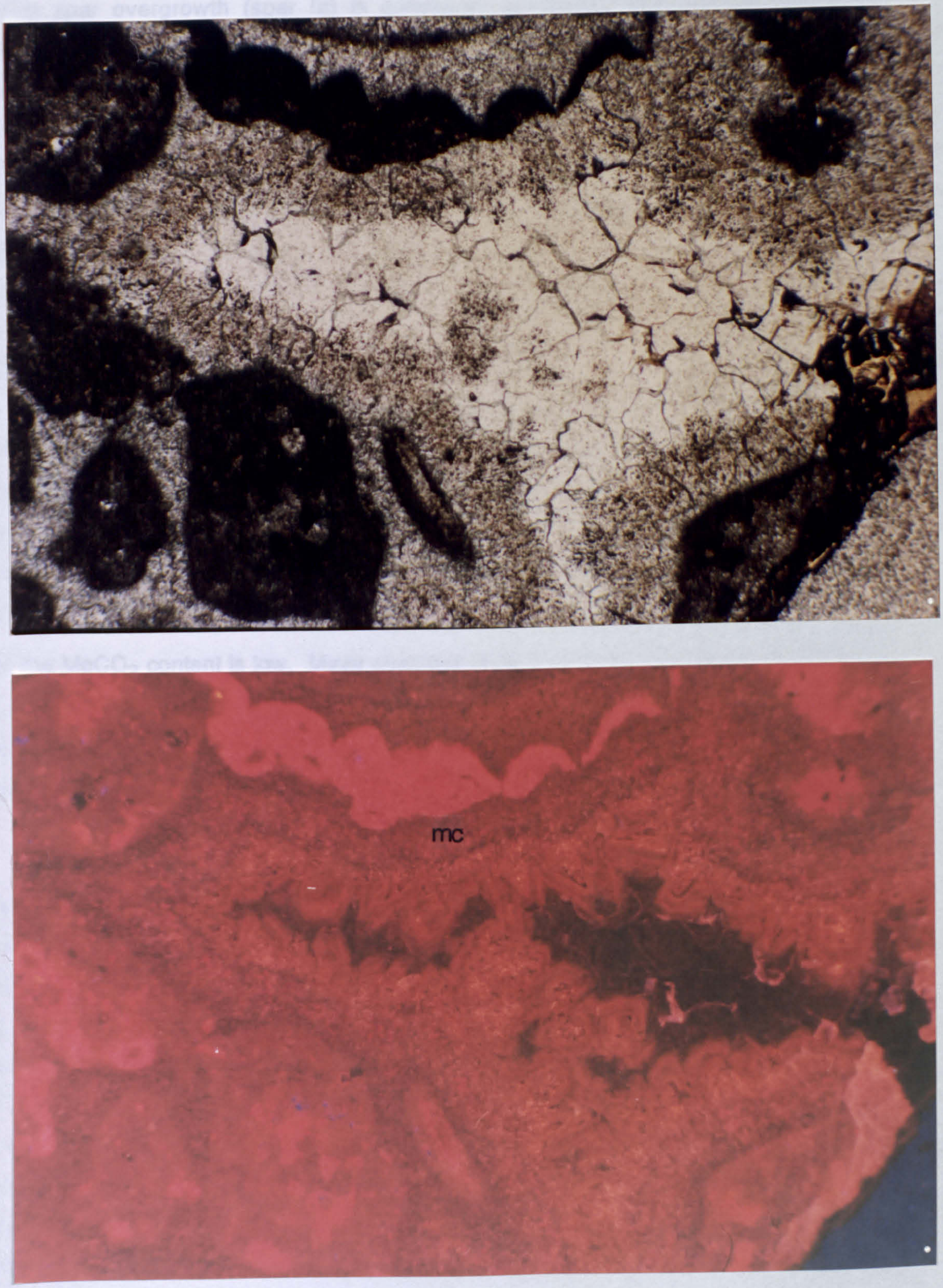

fig. 3.21a,b Plane polarised light and cathodoluminescence photomicrograph pair of calcite overgrowth (spar Ia) on prismatic marine cement (**mc**). The overgrowth has scalenohedral habit defined by luminescence zones. The middle of the pore is occluded by spar IIb. Sample MT74; back reef facies, 'reef trail', McKittrick Canyon. Scale: 25mm = 500μm.

Calcite spar I

Calcite spar overgrowth on early marine cements (spar Ia and Ib) A clear calcite spar overgrowth (spar Ia) is commonly associated with the last isopachous cement in some pores (fig. 3.21). The overgrowths are small, relatively inclusion-free crystals and syntaxial on the underlying marine cement. This overgrowth has scalenohedral form and dull-bright narrow parallel, concentric zones under cathodoluminescence indicating growth into pore space (fig. 3.21). There are usually about 5 thin bright zones (total thickness 50-100μm) which are followed by several dull zones, each of a few microns thickness (total thickness 100-150μm). The brightness of these zones diminishes towards the centre of the pore and the last zone is non-luminescent. There is no sign of dissolution of the underlying marine cements prior to the precipitation of the calcite spar overgrowth. These scalenohedral crystals do not completely occlude the pore space. The remaining pore space is occluded by similar crystals which are 100-600μm in size and have parallel, concentric zones. Luminescence intensity decreases towards the middle of the pore. *This* spar is interpreted as being the same generation as the scalenohedral overgrowth and is referred to as spar Ib to avoid confusion. These spars have been analysed using an electron microprobe (table 3.1). These analyses show that the $CaCO_3$ and $MgCO_3$ values vary and that the $MgCO_3$ content is low. Minor quantites of Al, Tl and Sr were also detected in spar Ia, and these probably indicate the presence of inclusions. Spar Ia and Ib are present in the back reef, reef and foreslope facies (fig. 3.30) but are not volumetrically significant.

Calcite spar associated with former aragonite botryoids (spar Ic), and spar Id Calcite spar in former-aragonite botryoids occurs as euhedral, relatively inclusion-free crystals, 100-600μm in diameter (fig. 3.1). These crystals have parallel, concentric zones which indicates that they were precipitated into pore space *i.e.*, that dissolution took place prior to the precipitation of this spar. Intensity of luminescence decreases towards the middle of the pore space. In these respects there is no petrographic difference between this spar and spar Ib. Electron microprobe analysis of spar Ic (table 3.1) indicates that this spar is low-magnesian calcite. By definition, this spar only occurs in botryoids after former aragonite *i.e.*, *in situ* in the reef and upper foreslope and in allocthonous blocks of the lower foreslope (fig. 3.30). Another calcite spar (Id) with different occurrence but similar petrographic characteristics is found only in the back reef facies in areas after calcium sulphate (as identified by

castellated margins). These calcite crystals are small (20μm-350μm) and are characterised by zoned orange luminescence, the intensity of which decreases towards the middle of the pore.

Other calcite spars (spars IIa, IIb, IIc and III)

The calcite spars not hitherto described, form the bulk of those present in the Capitan shelf margin in McKittrick Canyon. There are several types which are distinguished primarily by their distinctive luminescence zones, and also using other criteria such as inclusion density and crystal morphology. These spars occur in primary and secondary pore space *e.g.*, framework voids in the reef, and also in fractures (*e.g.*, fig. 2. 13 and fig. 2.14).

Calcite spar IIa This calcite spar is moderately luminescent, but does not display either sector or parallel zoning (*c.f.*,spar IIb and IIc). Instead it has a meshed, blotchy appearance (fig. 3.22). It is not common, and only occurs in areas where moulds of replacive anhydrite are also present. These features suggest that this calcite may be calcitised anhydrite that formed without the wholesale dissolution of anhydrite. The meshed, blotchy appearance may represent the felted texture of an anhydrite precursor (fig. 3.22c). Electron microprobe analyses are given in table 3.5. This calcite spar predates spar IIb and spar IIc and has only been observed in samples from the foreslope facies (fig. 3.30 and table 3.5).

Calcite spar IIb This calcite spar forms euhedral crystals >500μm in diameter. It has bright-moderate orange luminescence, and parallel zones. The zones are numerous, and each one is usually only a few microns thick. This spar nucleates over spar Ia, where this is present (fig. 3.23), and otherwise directly onto the pore margin. This spar is found in the lower foreslope facies in primary voids (after sulphate) and in moulds after replacive nodular anhydrite. It is also found in fractures and after replacive anhydrite in the back reef and foreslope facies (fig. 3.30).

Calcite spar IIc This calcite spar forms large, poikilotopic crystals, commonly several centimetres in diameter. These crystals occlude the majority of pore space and fractures formed due to calcium sulphate dissolution. It has bright-moderate luminescence and is commonly sector zoned, as well as having parallel zones (fig. 3.24). Where spar IIb is not present, spar IIc precipitates directly onto the dolomite which

description	no. analyses	sample	CaCO3 (mol.%)	MgCO3 (mol.%)	SO3 (wt.%)	Al2O3 (wt.%)	SiO2 (wt.%)	FeO (wt.%)	Na2O (wt.%)
spar IIa	2	MT19	57.36-57.99	0.21-0.27		nd-0.23		nd-0.81	
spar IIb	20	MT19	98.08-100	0.93-1.37					
	20	M22	100	0.16-1.51					
	8	M6i	86.57-100	0.21-1.65					
	8	MT39	99.3-100	0.18-1.99		nd-0.31	nd-0.44		
	5	MT102b	99.3-100	1.24-1.58					
spar IIc	7	MT117	100	0.24-1.36					
(inclusion rich)	107	MT60	84.28-100	0.58-18.38	nd-0.44	2.85-10.02	nd-0.13	nd-0.82	nd-0.18
(inclusion free)	68	MT60	96.64-100	0.34-1.94		nd-0.38			
	25	MT30	84.15-100	0.26-1.56		nd-0.14			
	30	MT74i	98.88-100	0.2-1.10					
spar III	24	MT74i	99.25-100	0-1.37	nd-0.19			nd-0.53	

table 3.5 Electron microprobe analyses of calcite spar II and III

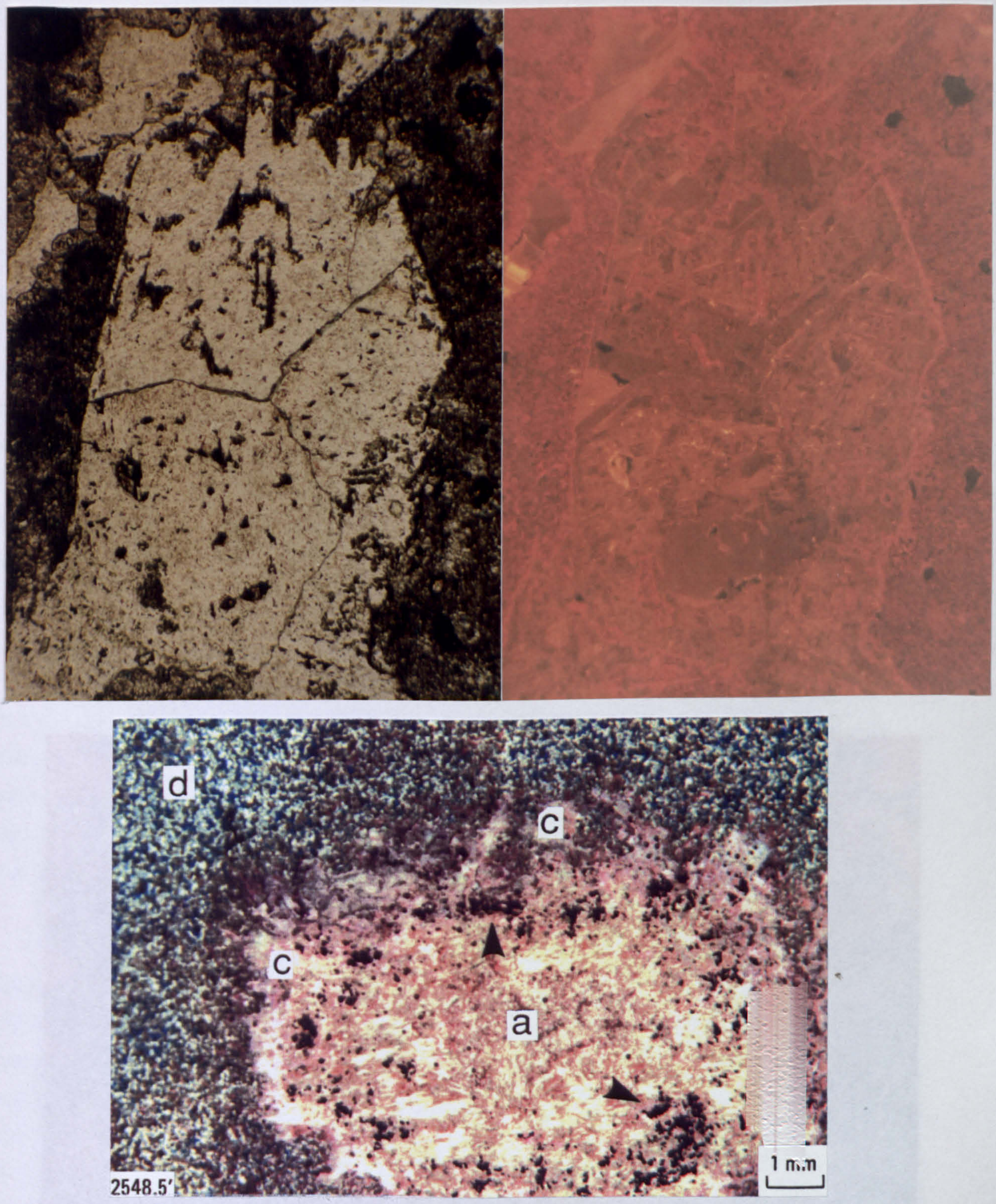

fig. 3.22a,b Plane polarised light and cathodoluminescence photomicrograph pair showing the distinctive luminescence pattern of calcite spar IIa, after replacive anhydrite (lath shapes and planar margins) and inclusions in the calcite. The calcite spar has moderate orange luminescence and a meshed appearance; this is interpreted as being replacive of anhydrite. Spar IIa is followed by spar IIb. The matrix and marine cements are pervasively dolomitised, with some preservation of texture. Sample M22; upper foreslope facies, 'reef trail', M^{c}Kittrick Canyon. Scale: 25mm = 500μm. c. photomicrograph of partly calcitised (c) replacive anhydrite (a) with castellated margin; pyrite oxidising to haematite marks the boundary between the anhydrite and the calcite. The matrix is fabric-destructive dolomite. From Chevron core, PDB-04; courtesy of Mitch Harris and George Grover, Chevron.

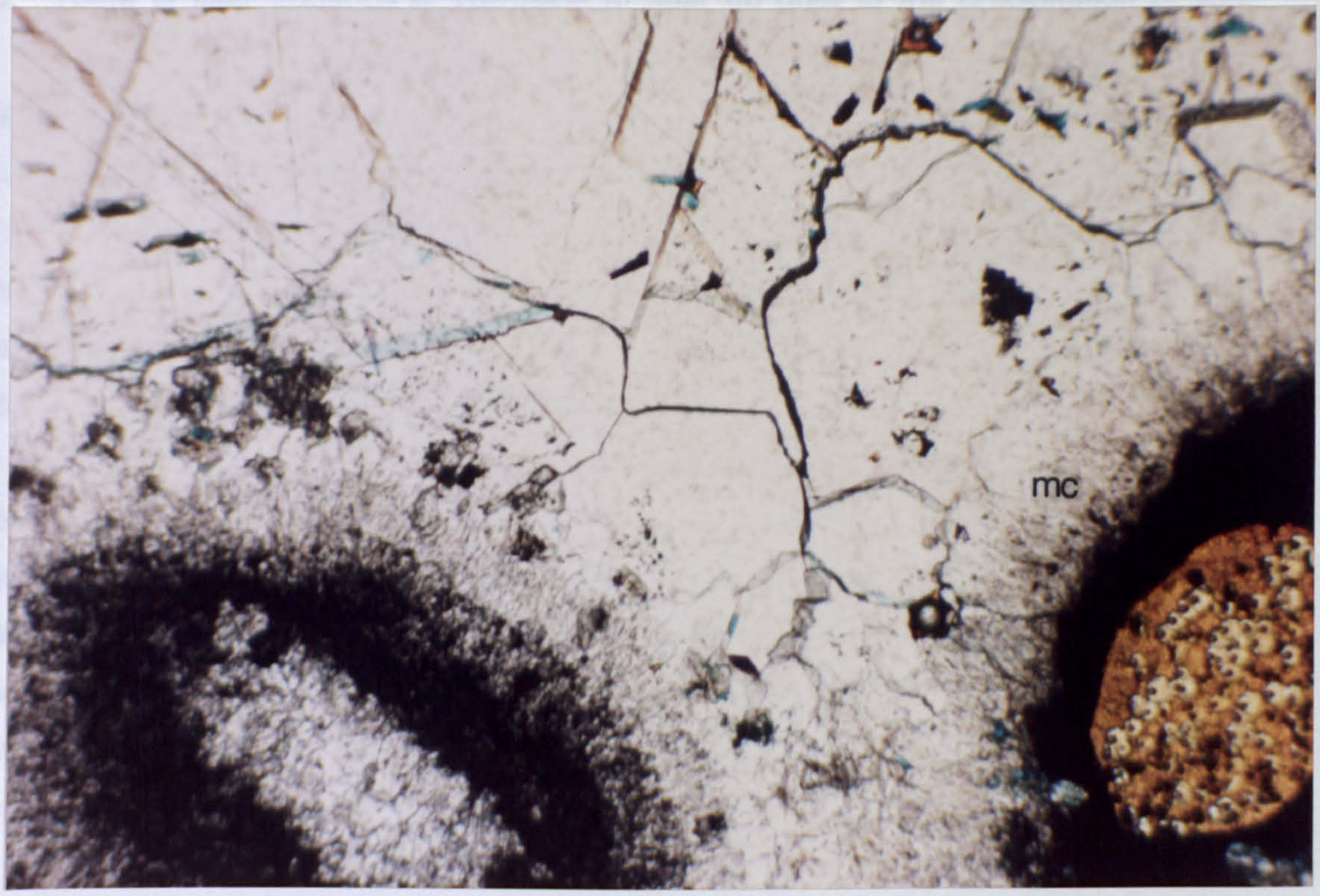

fig. 3.23a,b Plane polarised light and cathodoluminescence photomicrograph pair showing sequence of spar Ia (nucleated onto marine cement)(**mc**). Spar IIb has larger crystals and zones and nucleates onto spar Ia. Spar IIc has the largest crystals and zones and fills remaining pore space. Spars IIb and IIc were corroded (arrowed) prior to the precipitation of spar III into the resultant pore space. Sample MT33; lower foreslope facies, 'reef trail', McKittrick Canyon. Scale: 25mm = 500μm.

lines pores. In the lower foreslope in particular, kaolinite is sometimes included within calcite spar IIc. This indicates that kaolinite formation preceeded precipitation of this spar. There is also evidence of corrosion of spar IIb prior to the precipitation of spar IIc. This is consistent with acidic conditions prevailing during the precipitation of kaolinite (section 3.3.5, and fig. 3.16). Calcite spar IIc often contains abundant solid inclusions. Electron microprobe analysis shows high Si, Al and S; high iron values and sulphur values are not detected in the same analyses which suggests that the iron is etither present as iron oxides or is incorporated within the calcite lattice. This also suggests that the inclusions are clays, dolomite and calcium sulphate. These inclusions are not randomly distributed, but define the margins of areas of inclusion free calcite (figs. 3.25 and 3.26). These areas have straight sides and define square shapes in places. One possible explanation for the difference between inclusion-rich and inclusion-free calcite spars is that calcite spar IIc post-dates two different anhydrite types. Machel (1986) reports felted anhydrite (an irregularly felted mass of small crystals 10-500 μm) and large porphyrotopic crystals, from the Devonian Nisku buildups of Alberta. Some of these have square terminations which protrude into the surrounding dolostone, Machel (*op. cit.*) suggests that the anhydrite with felted texture was originally precipitated as gypsum, and was transformed to its present texture on burial, whereas the other anhydrite types precipitated directly as anhydrite in the subsurface. Alternatively, the inclusion rich calcite could have directly replaced gypsum, and the inclusion free calcite could have replaced anhydrite which itself replaced gypsum. Spar IIc is common in the back reef, reef and upper foreslope facies and occurs to a lesser extent in the lower foreslope facies (fig. 3.30).

Calcite spar III This is the latest calcite spar visible, and represents the last diagenetic event other than minor present-day dissolution. This cement forms large poikilotopic crystals, several tens of millimetres in diameter. It is characterised by being non-luminescent (fig. 3.24 and fig. 3.27), apart from a few (usually two) thin bright orange zones < 10μm thick. There are up to eleven thin bright zones in this spar from some parts of the upper foreslope (fig. 3.27). These zones clearly show that spar III is distinct from spar IIc because small crystals, nucleated onto spar IIc are visible. There is no evidence of dissolution of spar IIc prior to the precipitation of spar III. Electron microprobe analyses (table 3.5) indicate that this spar is composed of low-magnesian calcite. Sulphur and iron are detected but not in the same analyses. Spar III is common in the reef and upper foreslope facies, and is also present in the back reef and lower foreslope facies (fig. 3.30).

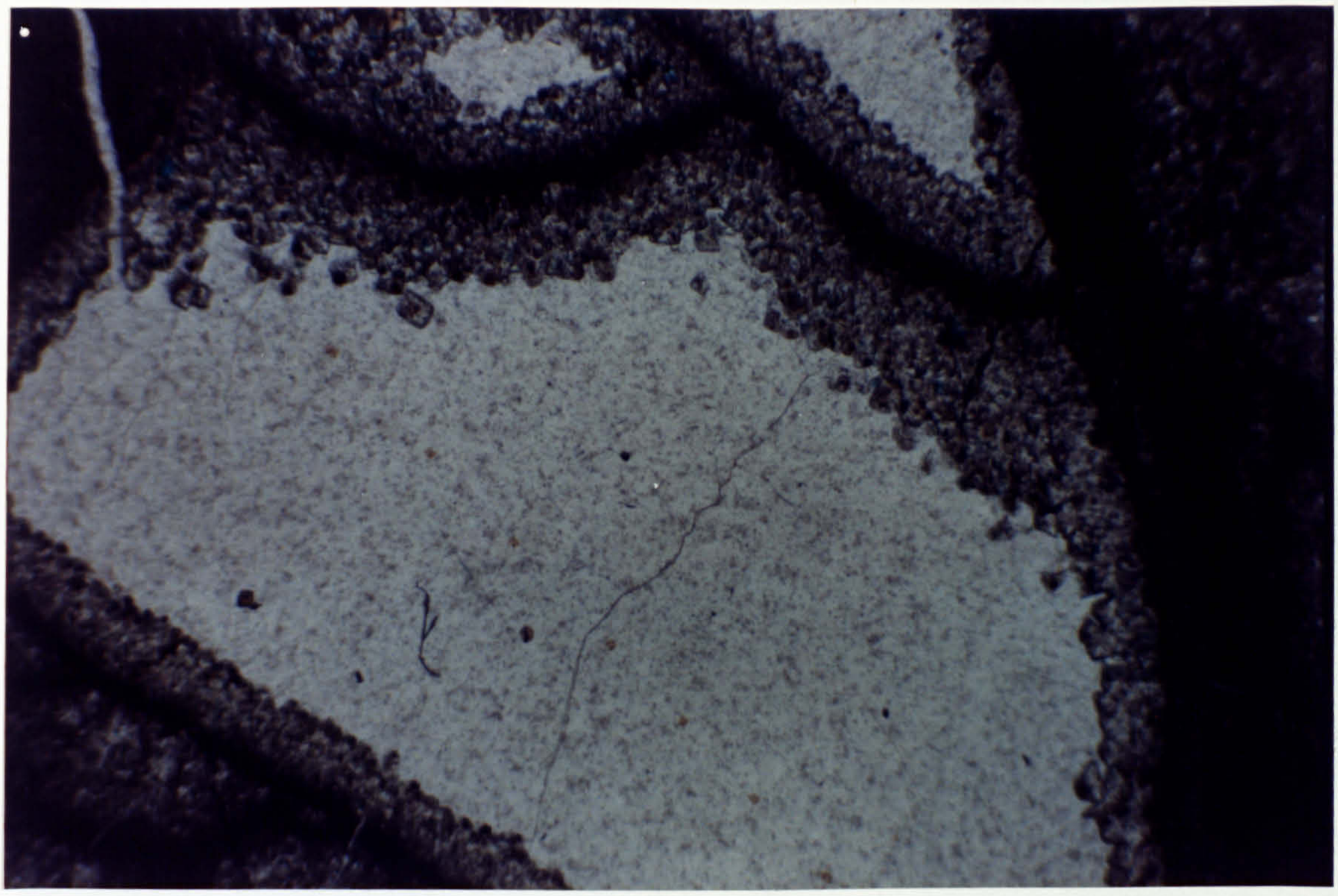

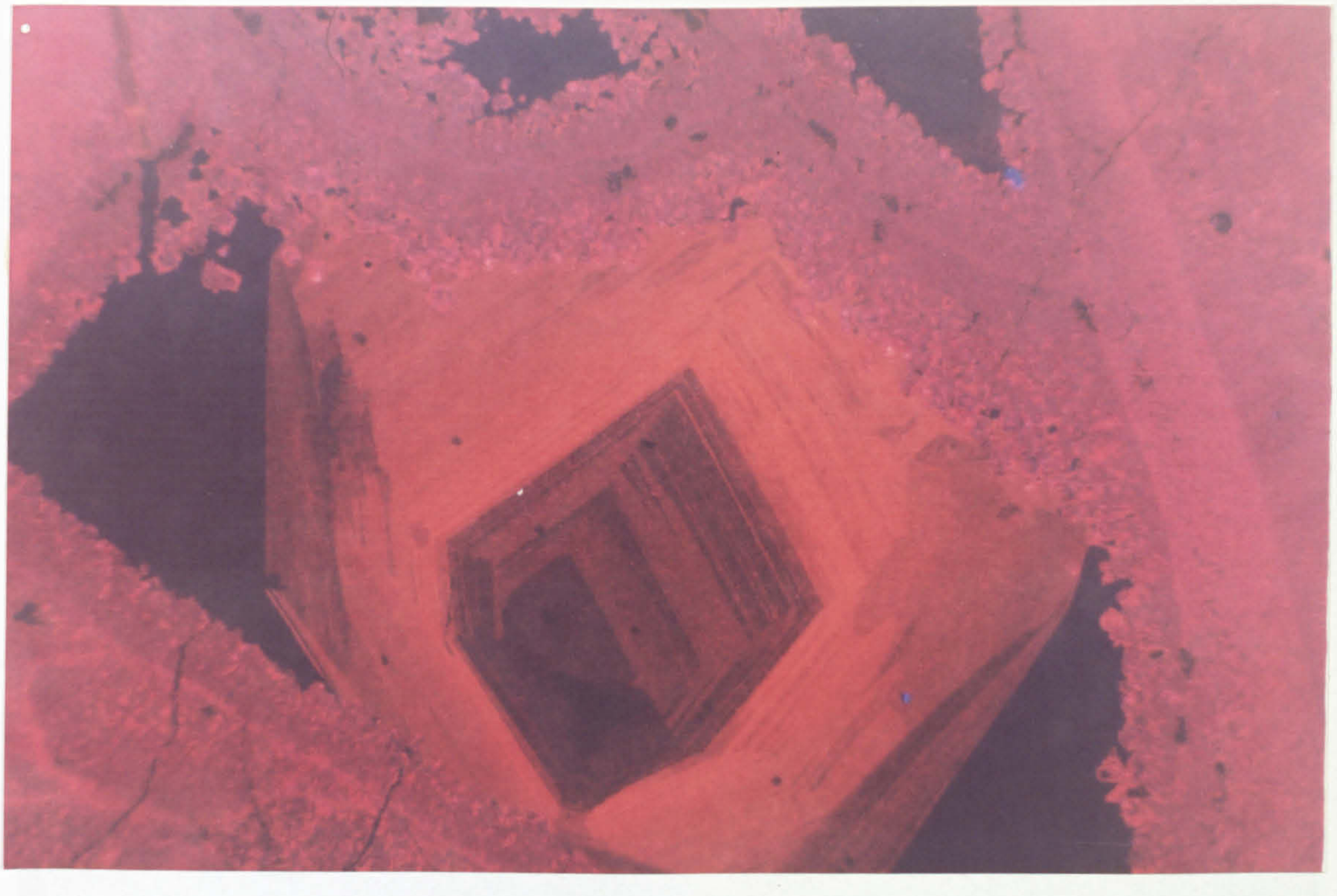

fig. 3.24a,b Plane polarised light and cathodoluminescence photomicrograph pair showing the characteristic sector and parallel zoning of calcite spar IIc, in this case precipitated into the chamber of a sponge (?). The walls of the sponge are lined with dolomitised marine cement; dolomite overgrowths (bright luminescence) occur adjacent to the calcite spar. The chambers of this sponge were filled with calcium sulphate prior to burial. Non-luminescent calcite spar III is syntaxial on spar IIc, and fills all remaining voids. Sample MT74; back reef facies, 'reef trail', McKittrick Canyon. Scale: 25mm = 500μm.

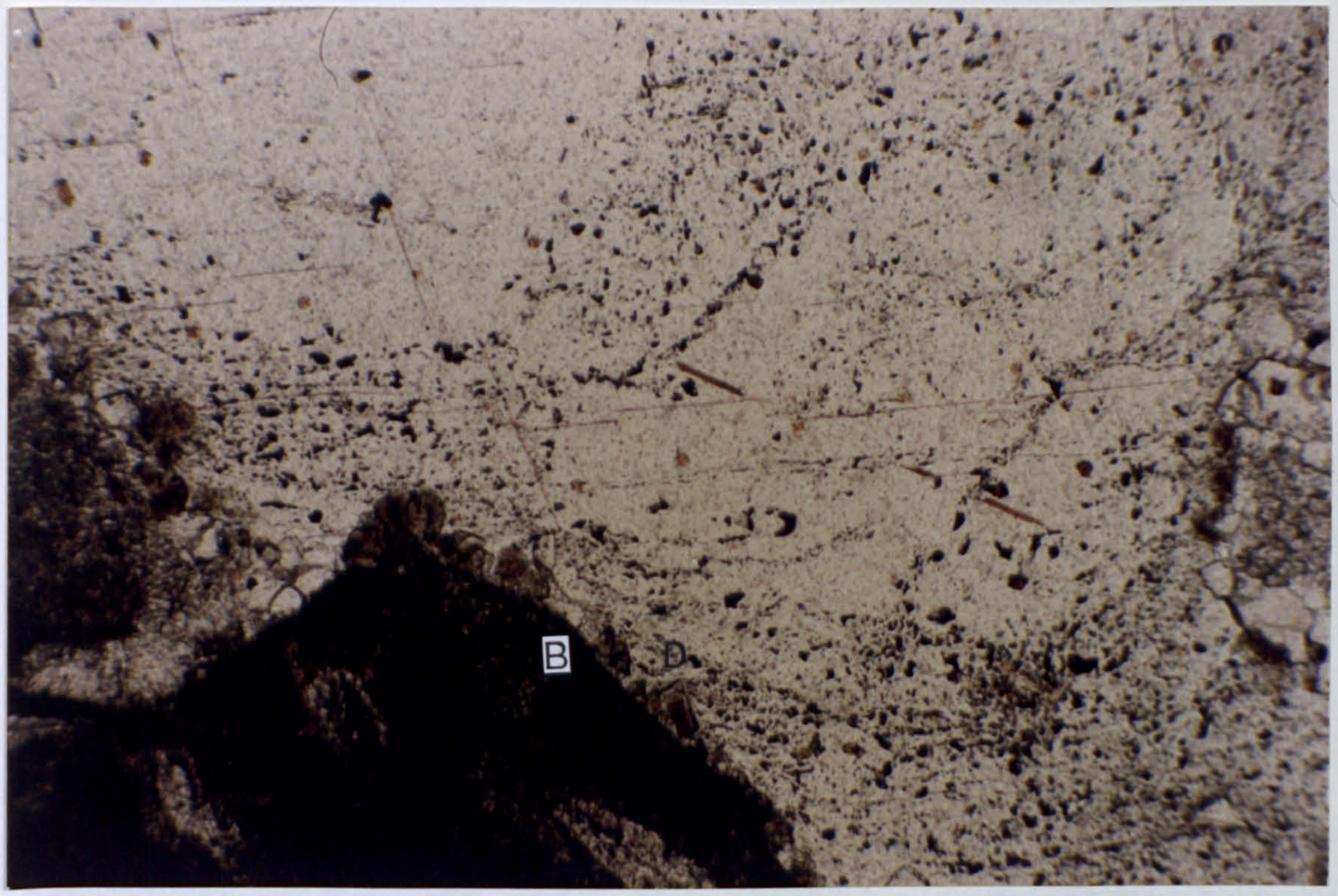

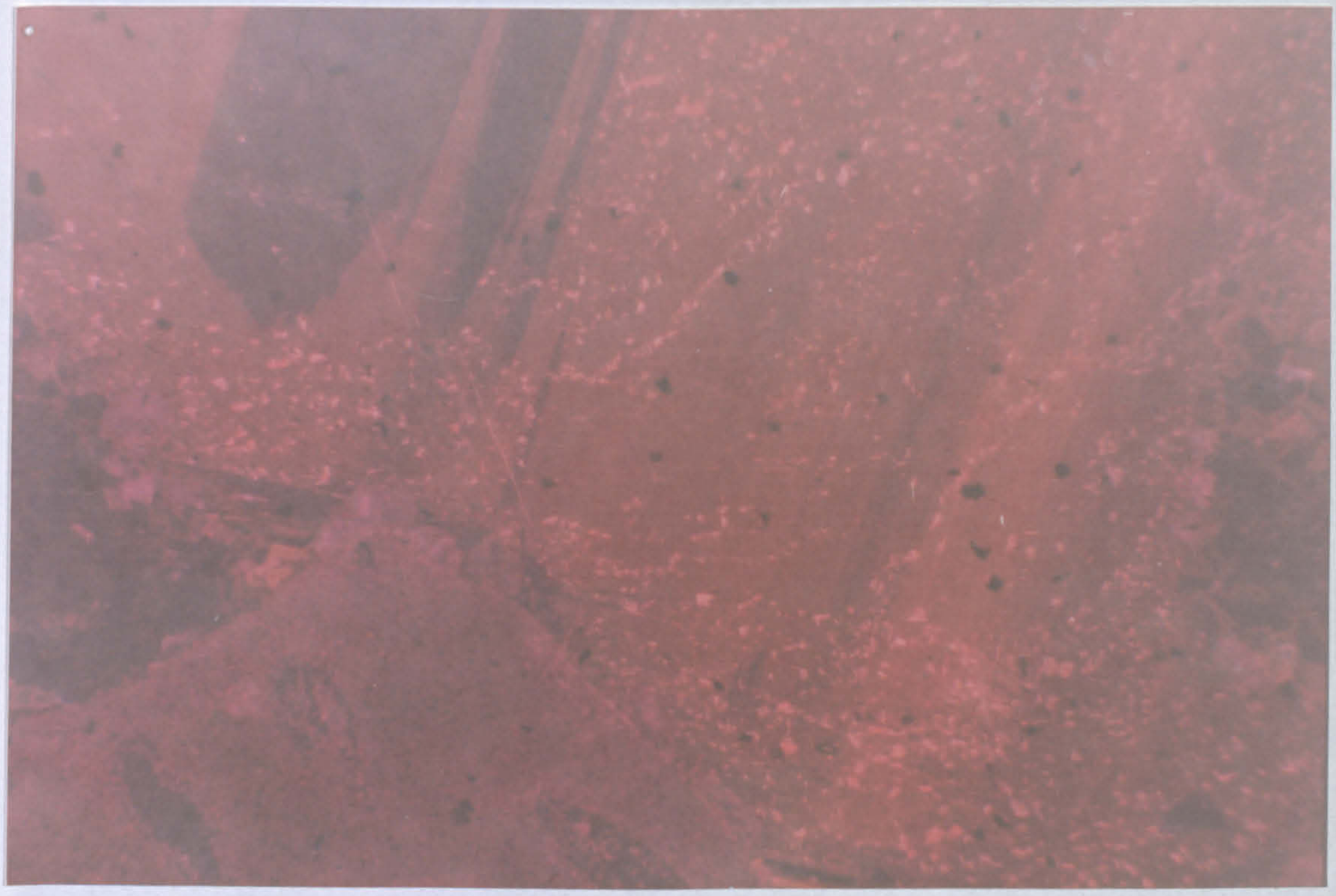

fig. 3.25a,b Plane polarised light and cathodoluminescence photomicrograph pair of spar IIc, showing areas containing solid inclusions defining square shapes and planar boundaries with the inclusion free spar. Luminescence zones cross-cut the inclusion rich and inclusion free areas. Many inclusions have red luminescence. The inclusion pattern may indicate repalcement of gypsum by anhydrite prior to replacement of both phases by calcite spar IIc. Dolomite rhombs (**D**) have nucleated on the margins of a bioclast (**B**) adjacent to the calcite spar. Sample MT60; upper foreslope facies, 'reef trail', McKittrick Canyon. Scale: 25mm = 500μm.

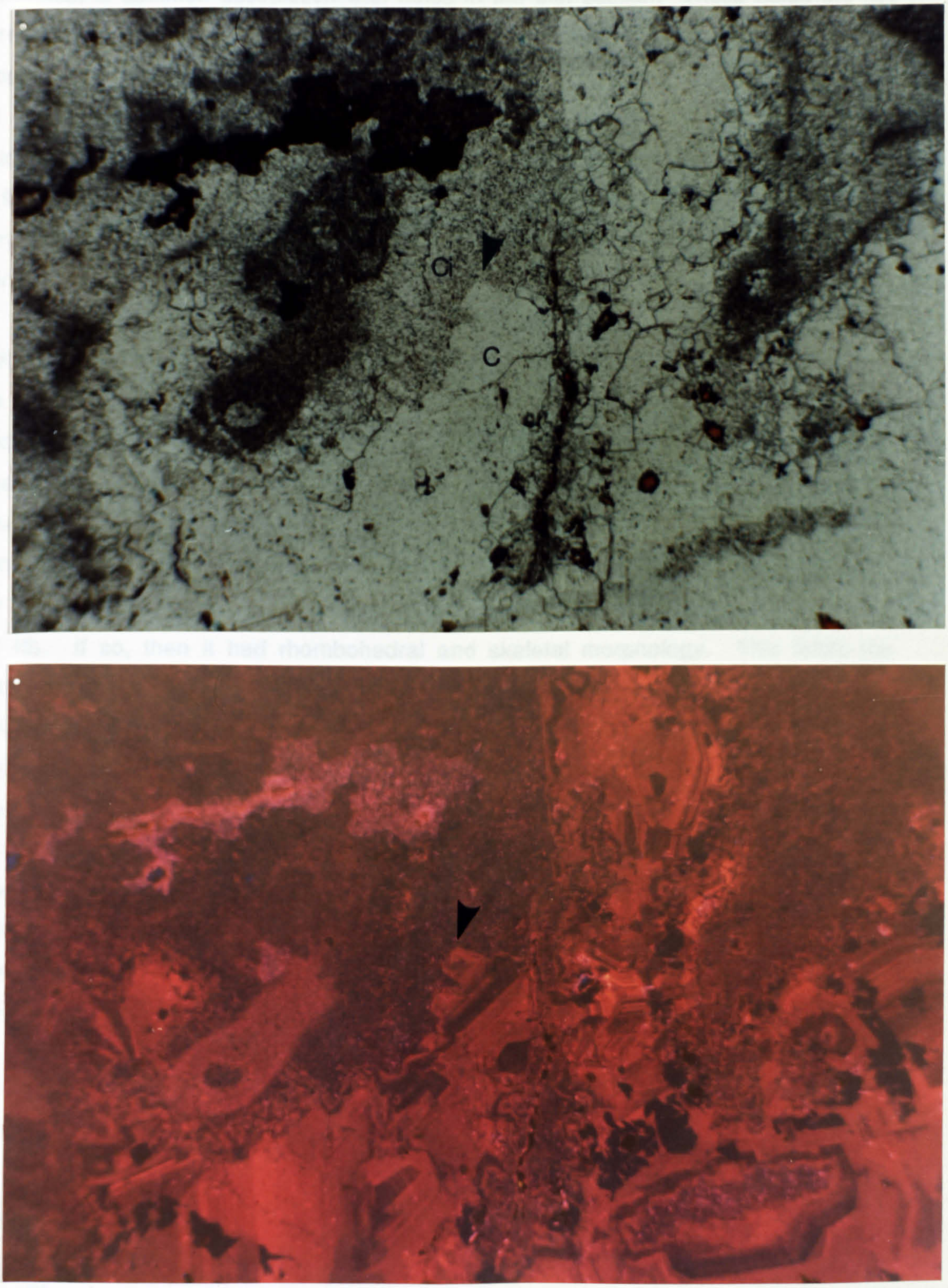

fig. 3.26a,b Plane polarised light and cathodoluminescence photomicrograph pair showing castellated margin (arrowed) between inclusion rich calcite spar (**Ci**) and inclusion free calcite (**C**), indicating replacement by anhydrite of an inclusion rich phase (gypsum?) prior to the precipitation of calcite spar IIc. Sample M11; upper foreslope facies, 'reef trail', McKittrick Canyon. Scale: 25mm = 500μm.

Other features in calcite spars Calcite spar IIc, and occasionally spar IIb, show a cross-cutting relationship with distinctive patches of non-luminescent spar (calcite spar III; figs. 3.28 and 3.29). These areas are characterised by having: i. planar boundaries; ii. common association with holes in the thin section. These holes are not impregnated (implying that either the holes formed as a result of the section making process, or that the impregnating epoxy did not reach these pores); iii. being angular and often having rhombic appearance. This rhombic morphology is apparently not related to the present calcite spar *i.e.*, to cleavage or growth zones, in many cases; iv. not following compositional zones (which would imply dissolution) in calcite spar IIc, in many cases; v. only occurring in the calcite spar with large crystals and bright luminescence *i.e.*, spar IIb and IIc.

It is difficult to determine whether these areas formed due to i. dissolution of calcite, or ii. dissolution of a rhombic mineral (mineral 'x') which was present in the pore space prior to the precipitation of calcite spar II, or possibly a combination of both i. and ii. The evidence is inconclusive in each case. Given that case i. is correct, and that these areas are entirely due to dissolution of spar II, then it is difficult to explain the planar, non-pitted boundaries, and the lack of structural control *i.e.*, cleavage or compositional zones, in spar II. Alternatively, a mineral 'x' may have been present in pore space prior to the precipitation of spar IIc, but concomitant with precipitation of spar IIb. If so, then it had rhombohedral and skeletal morphology. This limits the choices to the carbonate group (*i.e.*, calcite, dolomite or magnesite (Dana, 1892; Deer *et al.*, 1966) as the most likely). It seems somewhat unlikely that such a scenario could have existed, because precipitation of this mineral must have post-dated dissolution of anhydrite. The other alternative is that primary magnesite may have been intergrown with anhydrite. However there is no direct evidence to support this conjecture, although Garber *et al.* (1989) have reported magnesite in association with anhydrite in the subsurface. Consequently, it semms more likely that these features are due to dissolution of calcite spars IIb and IIc, even though the morphology of these features is not satisfactorily explained.

These corrosion features have only been seen in rocks from the foreslope facies, and appear to be more prevalent in the lower foreslope facies (fig. 3.30). This suggests that the corrosive fluids were concentrated in this facies.

Origin of the calcite spars

The decrease of luminescence intensity towards the middle of a pore space reflects the chemical evolution of water within that pore. Zones indicate fluctuations of

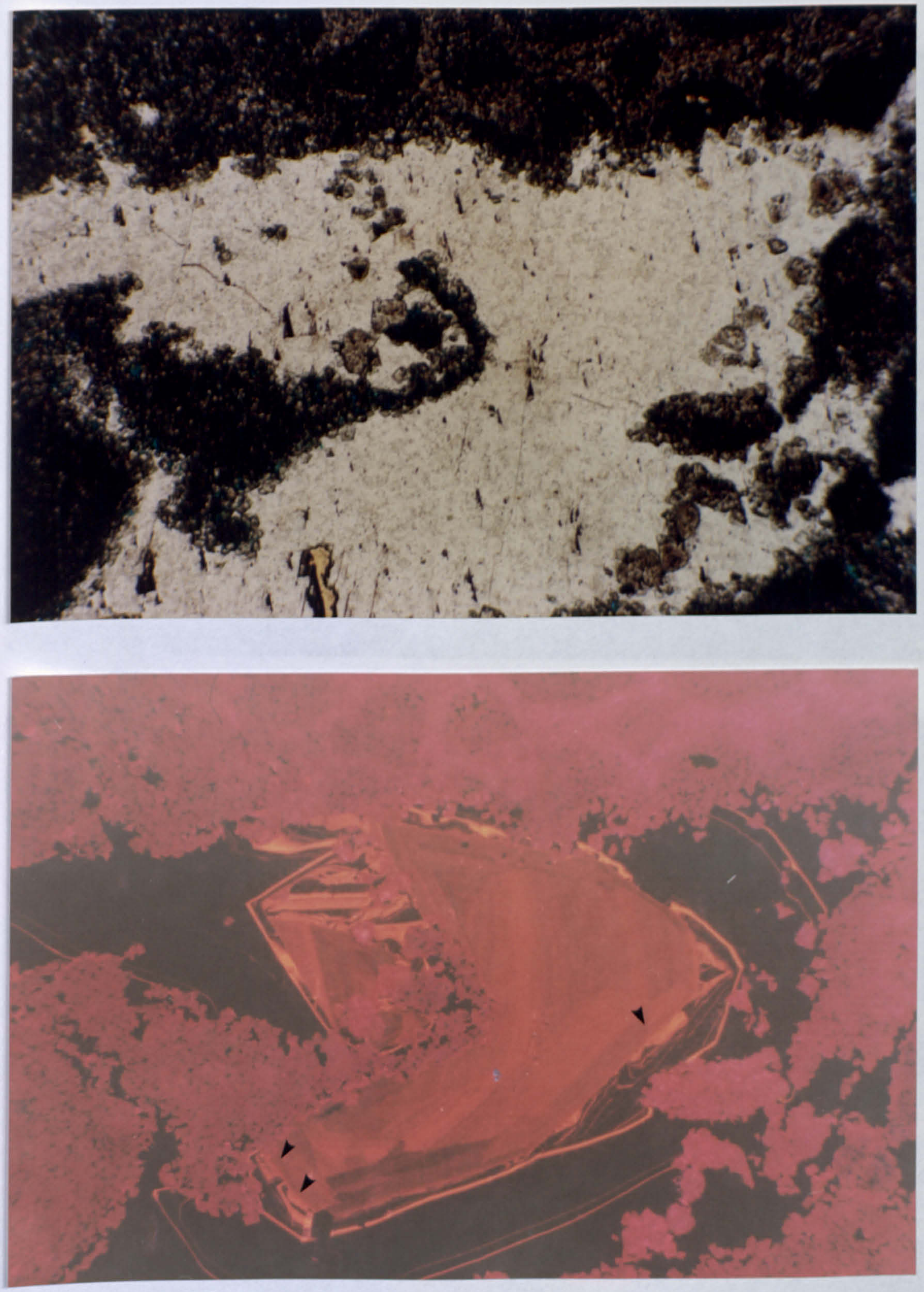

fig. 3.27a,b Plane polarised light and cathodoluminescence photomicrograph pair of bright zones in calcite spar III which show that spar III nucleated in several places (arrowed) on the surface of calcite spar IIc crystals and thus represents a separate diagenetic event. The surrounding rock is pervasively dolomitised with some fabric preservation. Sample MT62; upper foreslope facies, 'reef trail', McKittrick Canyon. Scale: 25mm = 500μm.

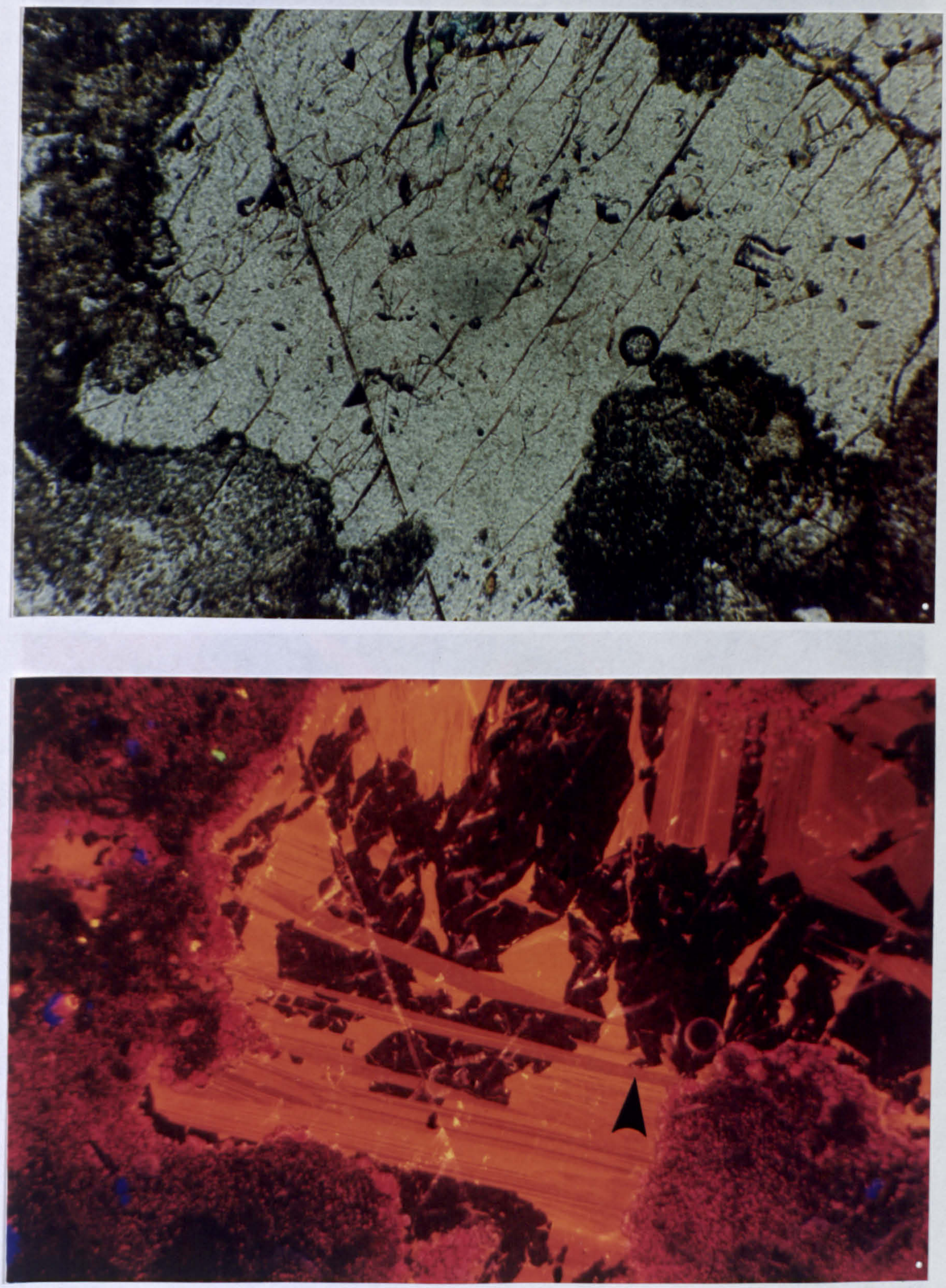

fig. 3.28a,b Plane polarised light and cathodoluminescence photomicrograph pair of spar III filling areas of dissolution in calcite spar IIc. The dissolved areas appear to be constrained by compositional zones in spar IIc in some places but not in others (arrowed). Sample M23; upper foreslope facies, 'reef trail', McKittrick Canyon. Scale: 25mm = 500μm.

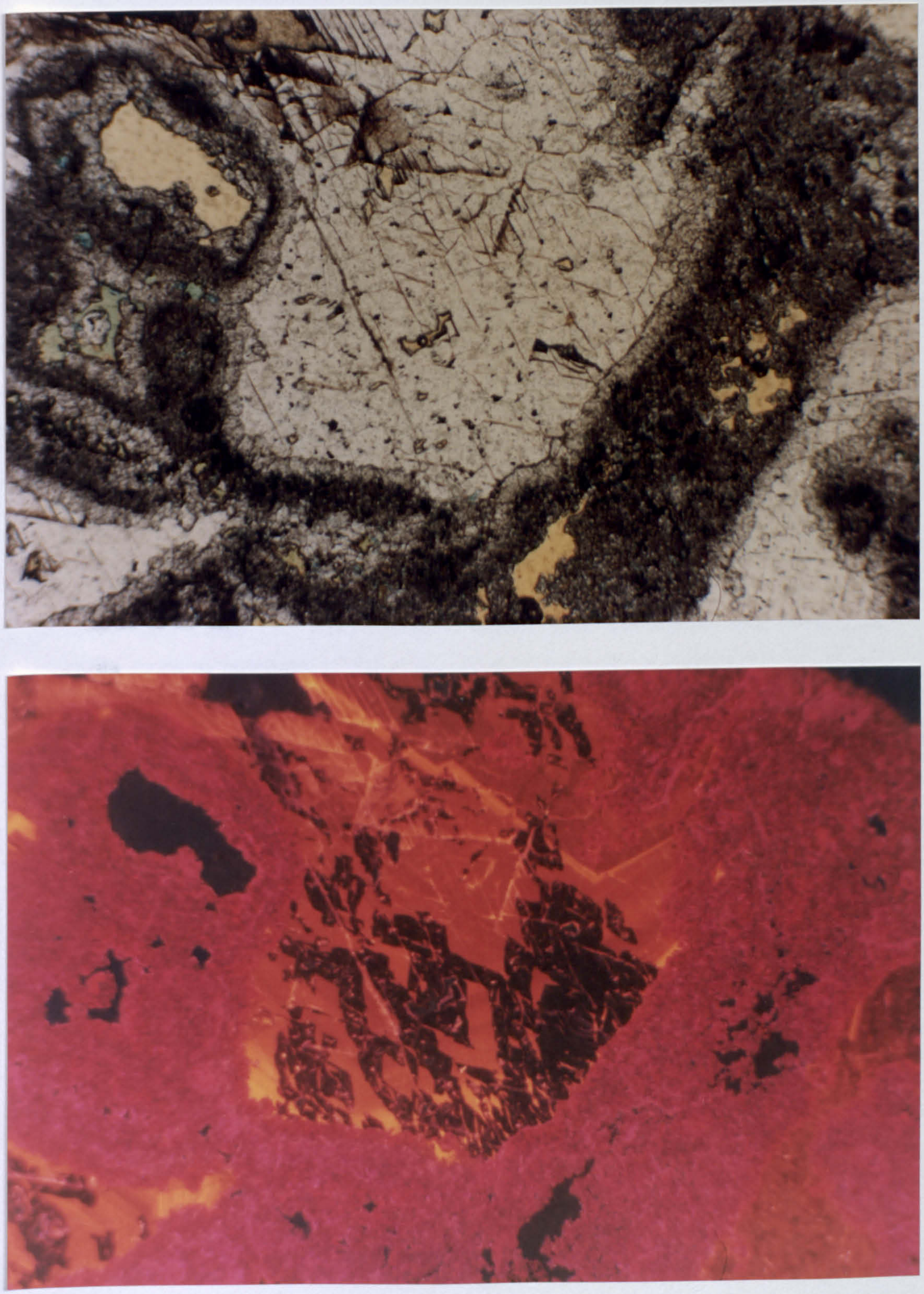

fig. 3.29a,b Plane polarised light and cathodoluminescence photomicrograph pair showing rhombic outlines to areas formed by dissolution of calcite spar IIc, and which are now filled by calcite spar III. The rhombic outlines are not parallel to the cleavage of spar IIc. The rock is pervasively dolomitised with fabric preservation of isopachous marine cement. Sample M10; upper foreslope, 'reef trail', McKittrick Canyon. Scale: 25mm = 500μm.

redox conditions, as well as amounts of Fe and Mn in the pore waters. These are related to the flow rate through the pore system. Progressive decrease in luminescence intensity characterises spar Ia, Ib, Ic and Id. There are other similarities between the luminescence patterns of the calcite overgrowth (spar Ib), the calcite spar which precipitated in solution-enlarged pores in former aragonitic botryoids (spar Ic), and the spar which precipitated in areas after sulphate dissolution (spar Id). These similarities include crystal size and lack of inclusions. This suggests a similar origin for these calcite spars. The calcite overgrowth on early marine cements (spar Ia and Ib) occurs in the reef, back reef and upper foreslope strata, and in transported blocks on the lower foreslope (fig. 3.30). The calcite spar in pores in the aragonite botryoids (spar Ic) occurs in the reef, upper foreslope and in transported blocks of the lower foreslope (fig.3.30). The calcite spar with small crystals (spar Id), in pore space after sulphate dissolution, occurs in the back reef (fig.3.30). There are two alternative interpretations for the timing of precipitation of clear calcite spar as overgrowths on early marine cements and in pore spaces. Either, precipitation of calcite spar took place prior to the emplacement of blocks on the lower foreslope, in which case dissolution occurred prior to the emplacement of the blocks on the foreslope, or precipitation took place at some later stage *i.e.*, from meteoric water, after dissolution and removal of pore-occluding calcium sulphate.

Given and Lohmann (1985 and 1986) studied of the isotopic composition of the inclusion rich calcite spar which replaces former aragonite botryoids, and the clear calcite spar which fills dissolutional pores in these botryoids. They interpreted two seperate diagenetic events on the basis of isotope values. Implicit in their work is the assumption that the transformation from metastable marine cement to stable calcite spar is reflected in the isotopic signatures *i.e.*, that no other fluid was involved. The constancy of the isotopic signatures suggests that this assumption is valid. However, their subsequent interpretations of the luminescent calcite spar are open to discussion, as there are several inconsistencies in their argument, and several discrepancies between their observations (*op. cit.*) and those presented in this study. These factors place a large question mark over their interpretation. They (*op. cit.*) state that the luminescent calcite is aligned along the original intercrystalline boundaries of the marine cement fibres, and interpret this as indicating that neomorphism of the aragonite was contemporaneous with the precipitation of the luminescent calcite spar. Nowhere has this texture been recognised in the present study. On the contrary, there is much evidence that the luminescent calcite spar precipitated into pore space following a period of dissolution. Furthermore, they (*op. cit.*) infer that the emplacement of the luminescent calcite occurred during the neomorphism of the aragonite to calcite (*i.e.*,

whilst the bulk of the botryoid was still aragonite) and at the same time state that the isotopic compositions of these two separate calcite spars are significantly different (*i.e.*, the luminescent calcite spar is isotopically enriched, and that the non-luminescent, inclusion rich calcite spar is isotopically depleted). This is a fundamental inconsistency in their own argument (*op. cit.*). If neomorphism and precipitation of calcite spar occurred as part of the same diagenetic event then both calcite spars should have the same isotopic signature.

Other inconsistencies include: i. the calcite spar precipitated in dissolutional pore spaces in botryoids in the upper part of the slope is defined (*op. cit.*) on the basis of its isotopic composition as 'spar I' (their terminology). By this definition, 'spar I' (their terminology) is not present in lower parts of the foreslope. This interpreted distribution then forms the basis for their later interences on the meteoric diagenesis of the Capitan Shelf Margin. This is an entirely circular argument. ii. They (*op. cit.*) interpret the isotopic compositions of clear calcite spars (*i.e.*, spar I $\partial^{18}O$ = -8.2‰, and spar II $\partial^{18}O$ = -12.3‰, their terminology) to indicate meteoric diagenesis in the Upper Capitan and Ochoan due to exposure of the shelf by sea level change (spar I, their terminology) and later, by desiccation of the Delaware Basin (spar II, their terminology). The work of Mruk (1985) essentially agrees with these interpretations. However, any meteoric waters at these times, especially during the Ochoan, would almost certainly have been in contact with evaporatively concentrated brines of the back reef facies in which case an isotopically enriched oxygen signature would be expected.

The closed system for neomorphism of aragonite to calcite, indicated by constancy of isotopic composition (Given and Lohmann, 1985, 1986), is equally well explained by early diagenesis on the following lines: i. neomorphism of the entire botryoid to calcite, with fabric retention; ii. dissolution; iii. precipitation of calcite spar (Ib), or another phase such as gypsum, causing occlusion of the pore space. If the pore space *was* occluded by gypsum, then precipitation of calcite spar Ib did not take place until Tertiary times, following uplift and dissolution of all calcium sulphate. The meteoric signature of this calcite spar (Given and Lohmann, 1985, 1986), uncontaminated by evaporatively concentrated waters, supports this latter idea. It is also corroborated, unknowingly, by Mazzullo and Cys (1977) who made the suggestion (amidst other suggestions) that the neomorphism of the aragonite to calcite could have taken place in a shallow subsurface environment perhaps in contact with waters enriched in sulphate, in order to explain the morphology, the relatively low Sr content and the lack of vadose dissolutional and cement features of the calcitised aragonite botryoids. Thus, I suggest that these data may be better interpreted as indicating a period of meteoric diagenesis which post-dates the effects of evaporatively concentrated brines *i.e.*, of Tertiary age.

Spar IIa, IIb and IIc (my terminology) are characterised by bright-moderate luminescence. Reducing conditions are implied for Spar IIa, which is interpreted as calcitised anhydrite. Spar IIa precipitated before spars IIb and IIc. No iron minerals are visibly associated with spar IIa or IIb, although calcite spar IIc and III are visibly associated with haematite (fig. 3.31). The haematite is likely to have formed from the oxidation of pyrite which formed during the reduction of calcium sulphate. The oxidation of pyrite to haematite requires oxidising conditions, and suggests that calcite spar IIc and III were precipitated from pore waters which were oxidising. The lack of Fe incorporated into the lattice, as determined from electron microprobe analysis, supports this interpretation. There is no reason to suppose that there was any significant difference between the waters from which spars IIc and III were precipitated as there is no sign of corrosion of spar IIc prior to the precipitation of spar III. Although not conclusive, it seems reasonable to suppose that the pore waters from which spars IIc and III were precipitated were oxidising, as there is no evidence to the contrary. Spar IIa was precipitated from pore waters which were reducing due to concomitant sulphate reduction (Anderson and Garven, 1987). A change in pore water composition between precipitation of spar IIb and IIc, is indicated by corrosion of spar IIb and the formation of kaolinite. There is no reason to invoke a change in pore water composition between spar IIa and spar IIb *i.e.*, spar IIb is interpreted as having precipitated under reducing conditions. Corrosion and kaolinite formation was related to acidic conditions, possibly occurring due to the cessation of sulphate reduction. This may be related to an increased rate of meteoric water influx.

Similarities between textures of calcitised evaporites of Mid Miocene age in Egypt (Pierre and Rouchy, 1988) and spar IIa include large poikilotopic calcite crystals which contain abundant solid inclusions and sparry calcite mosiacs associated with fine limestone partings. Machel (1986) reports several morphologies for replacive anhydrite in the subsurface in Devonian Nisku buildups of Alberta. Many of the features he describes are similar to those observed in calcite spars in the Capitan Shelf Margin in this study *e.g.*, equidimensional to elongate replacive crystals, which form subhedral mosaics.

There have been several previous studies which included study of these calcite spars, and these have all concentrated on the foreslope facies in McKittrick Canyon (Mruk, 1985; Given and Lohmann, 1985, 1986). The interpretations of Mruk (*op. cit.*) and Given and Lohmann (*op. cit.*) based on petrographic and isoptopic evidence, are that these calcite spars formed as a result of diagenesis involving a deep, meteoric lens, interpreted as Upper Guadalupian in age *i.e.*, generated during sea level fluctuations (Mruk, *op. cit.*) and exposure of the shelf (Given and Lohmann, *op. cit.*).

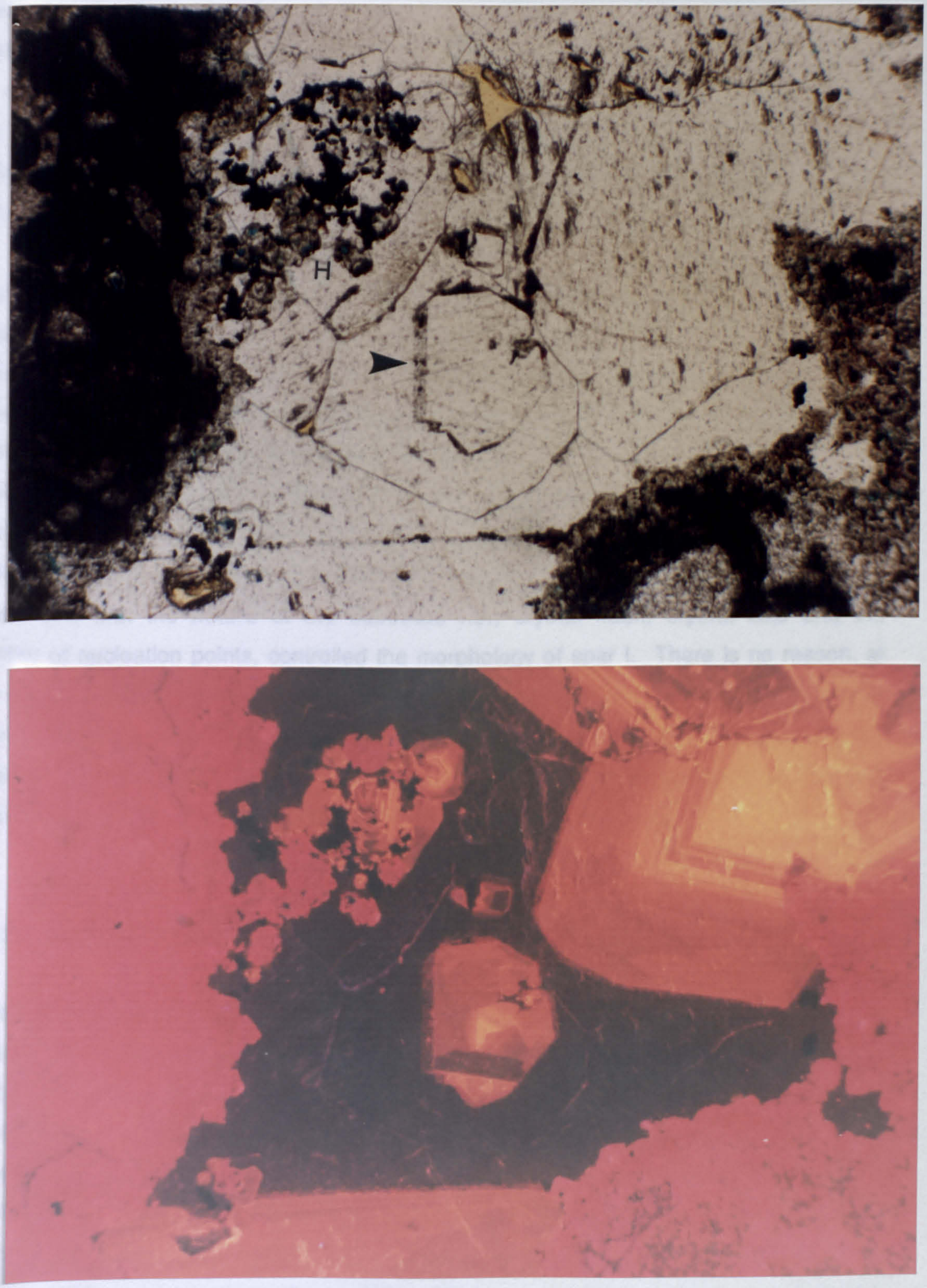

fig. 3.31a,b Plane polarised light and cathodoluminescence photomicrograph pair of haematite (H) in calcite spar IIc and at the crystal boundary (arrowed) between spar IIc and spar III, indicating that spars IIc and III precipitated under oxidising conditions. The pore is lined by dolomitised isopachous marine cement. The haematite formed from oxidation of authigenic iron sulphides which formed as a by-product of sulphate reduction. Oxidation to haematite took place during precipitation of spar IIc. Sample MT120; upper foreslope facies,'reef trail', McKittrick Canyon. Scale: 25mm = 500µm.

Calcitised evaporites have been reported in the foreslope facies of the Guadalupe Mountains on the basis of comparison with subsurface cores from the northern and eastern margins of the Delaware basin (Scholle and Melim, 1988). The texture of spar IIa corroborates this (fig. 3.22). However, the presence of parallel, concentric zones in the vast majority of calcite spars (spar Ia,b,c,d and spar IIb and c, and spar III), indicates that precipitation of calcite spar into pore space was the dominant process, rather than calcitisation of the evaporites.

I propose that the calcite spars, defined as spar I (a,b,c,d) and spar II (b,c) and spar III in this study, precipitated during and after the removal of calcium sulphate by dissolution. Dissolution was due to the input of meteoric water during uplift of the Guadalupe Mountains (fig. 1.5). Petrographic evidence enables distinction of the separate diagenetic events which caused precipitation of calcite spars IIa, IIb, IIc and III in that order. This is not the case for spars Ia, Ib, Ic and Id. These spars are distinguished on occurrence and to some extent morphology, and a diagenetic sequence cannot be established. Yet, all these spars have similar crystal sizes and luminescence patterns. The simplest explanation is that all spar I resulted from a single diagenetic event, and that the nature of the substrate *i.e.*, crystal habit, crystal size and the number of nucleation points, controlled the morphology of spar I. There is no reason, at this stage, to distinguish these spars and to infer that they represent separate diagenetic events. It is possible that detailed chemical analysis may separate these spars into different categories. However, such analysis would prove difficult to perform accurately, because of the small scale of these spars and their zones.

3.3.5 Silicate phases

Authigenic kaolinite Kaolinite is present in all facies, with the exception of the reef (table 3.6). It fills mouldic pores, mainly after bioclastic fragments (fig. 3.16 and fig. 3.32), as well as fractures and pores left after the dissolution of anhydrite. The kaolinite forms well-developed, large euhedral plates or books up to 100μm in size. These have pseudo-hexagonal form, are colourless in plane polarized light, have grey birefringence colours and luminesce a bright blue colour (fig. 3.16). Porosity (identified by blue-stained epoxy), minor amounts of goethite needles and iron staining are commonly associated with the kaolinite. These are probably related to present day weathering processes. Kaolinite is commonly found in association with calcite spar, where it may appear to float in the spar, or it may occupy one end of a pore and spar occupies the other part (fig. 3.32). Calcite spar of two phases is associated with the

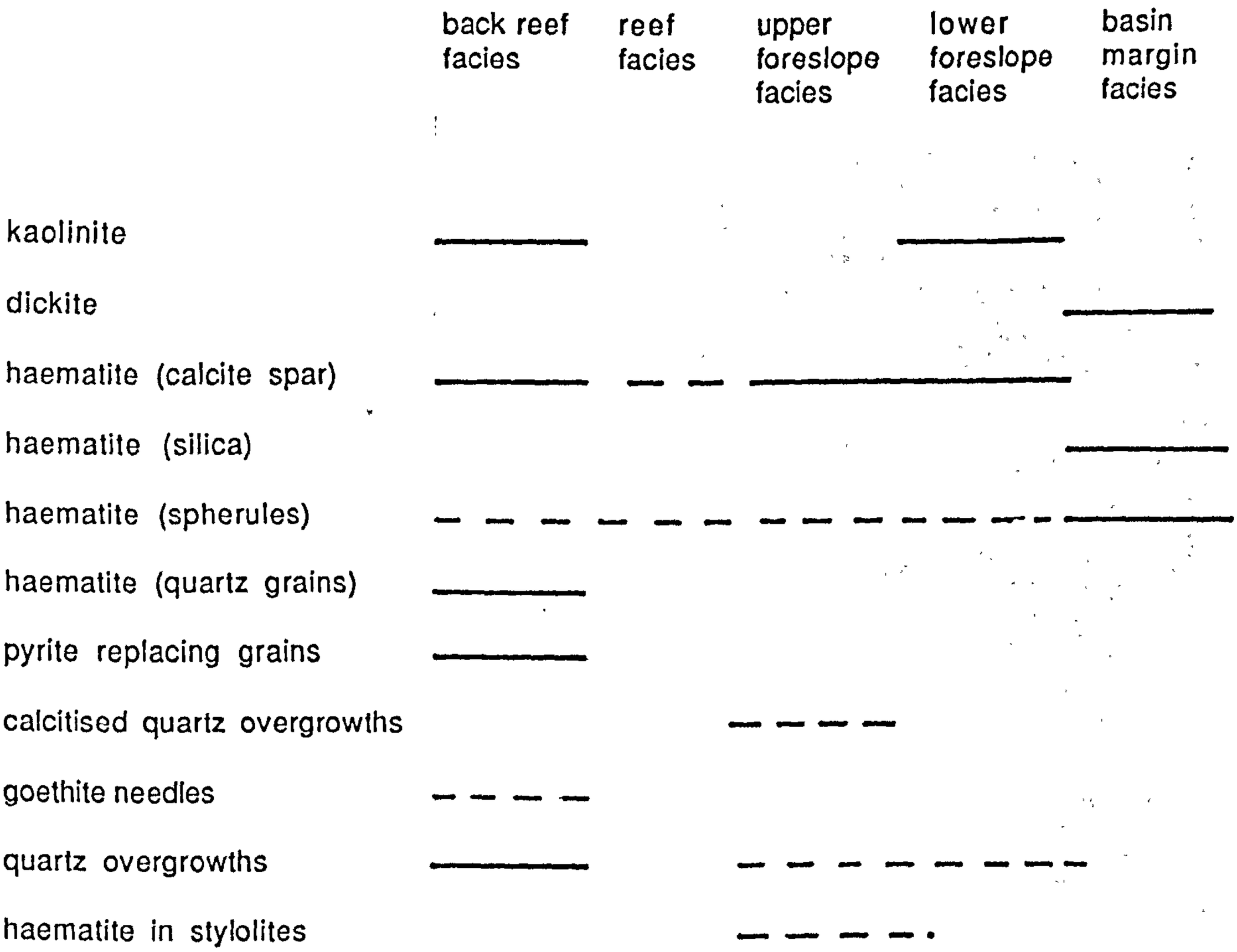

table 3.6 Facies distribution of silicate phases and iron minerals

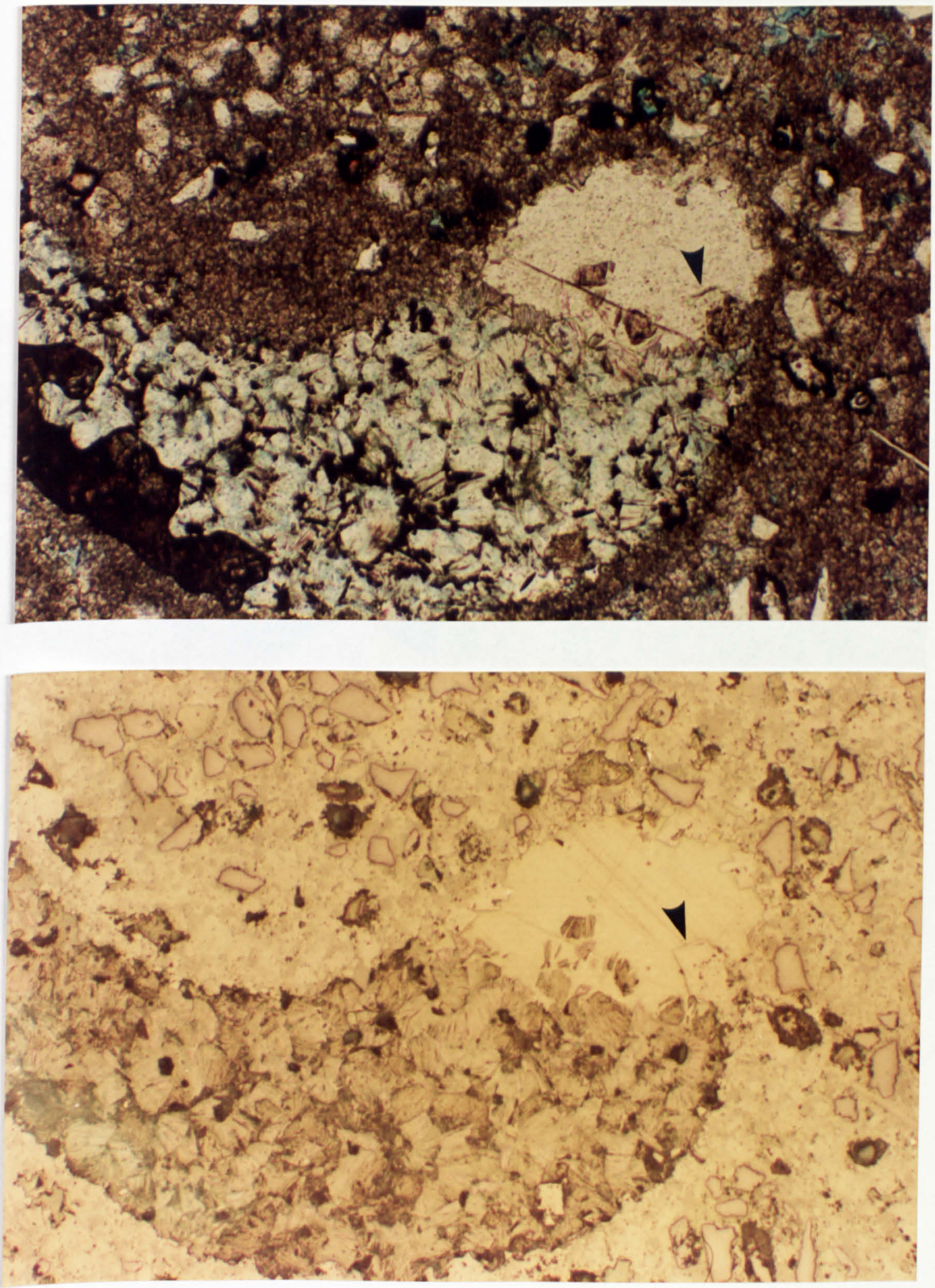

fig. 3.32a,b Plane polarised light and reflected light photomicrograph pair showing pore-filling kaolinite books and calcite (spar IIc) in siltstone. Dolomite overgrowths (arrowed) grew into pore prior to, or concomitant with, the precipitation of kaolinite. Kaolinite formation preceeded calcite precipitation. Sample M14; back reef facies, 'reef trail', McKittrick Canyon. Scale: 25mm = 125µm.

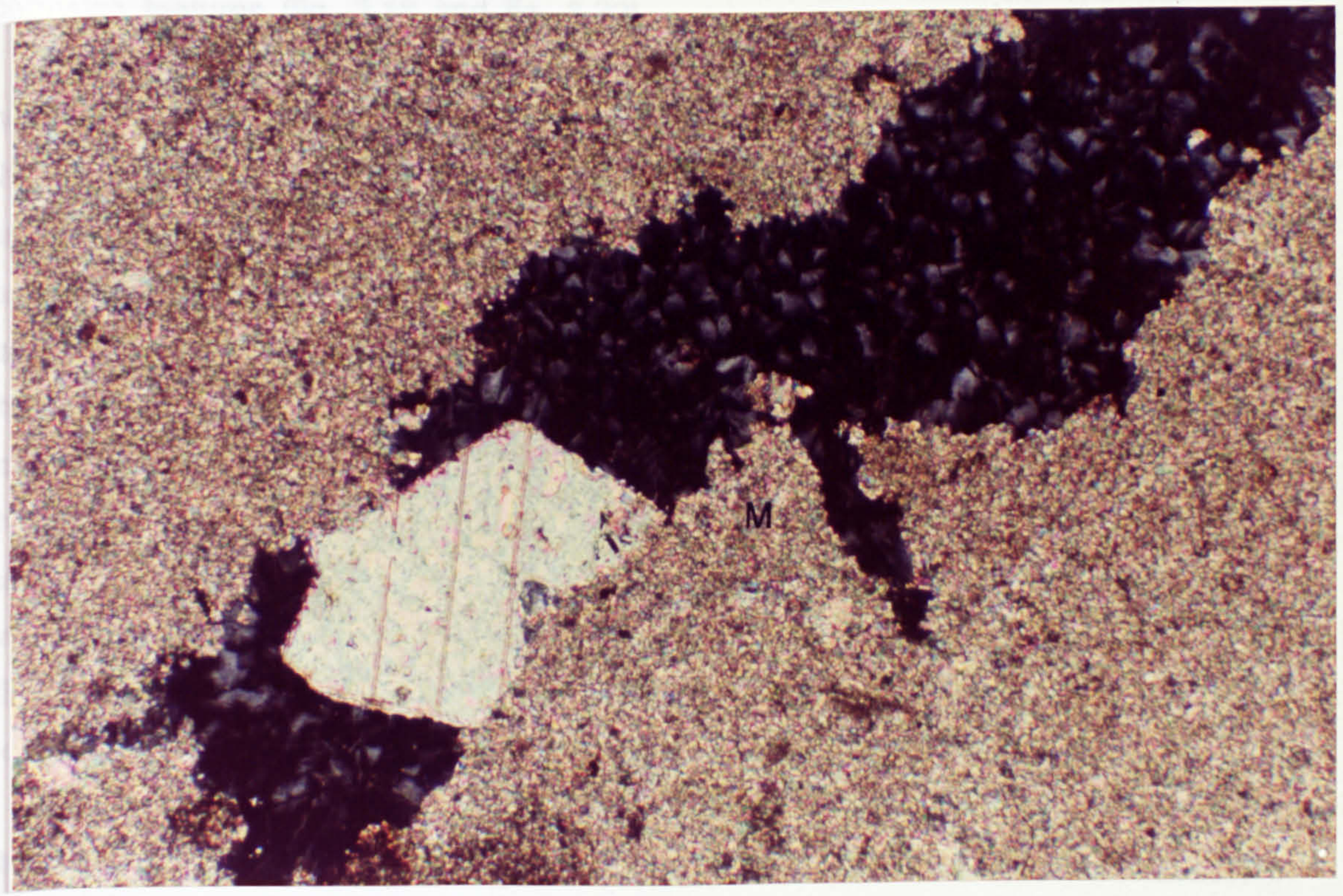

fig. 3.33 Cross polarised light photomicrograph of dickite books filling a fracture in micrite (**M**). The dickite post-dates the calcite spar (spar IIb) which has corroded margins. Sample MC34; basin margin facies, 'reef trail', McKittrick Canyon.

kaolinite; zoned, brightly luminescing calcite (spar IIc) and non-luminescing calcite (spar III; fig. 3.16). Where calcite encloses the kaolinite (spar IIc), the kaolinite is usually in the form of single platelets, whereas in the pore-filling habit, the kaolinite forms books. There is a greater density of kaolinite in spar III. The zones of the calcite are not disrupted by the kaolinite crystals and in most cases it appears that the kaolinite either pre-dates the calcite spar, or that the two phases are synchronous. Kaolinite formation probably predated the precipitation of spar IIc; this is suggested by the corrosion of spar IIb and the fact that kaolinite formation requires acid conditions. Kaolinite formation may also be related to the movement of hydrocarbons. Kaolinite books post-date the euhedral dolomite overgrowths on dolomite rhombs, as indicated by corrosion features (fig. 3.16 and fig. 3.32).

In the basin margin facies dickite is found in fractures (fig. 3.33). Dickite has not been unequivocally identified, but the habit of these crystals is slightly different to the pore-filling kaolinite of the foreslope and back-reef facies in that i. the crystals are smaller (up to 40 μm) and ii. the crystals invariably form a tight interlocking patchwork of well-developed books. These features are characteristic of dickite (Deer *et al.*, 1966). Calcite spar IIc fills the remainder of the fracture. The fractures in which this mineral is found in the basin margin facies have a trend of 205°. This is identical to the trend of fractures in the upper reef/back-reef, and sub-parallel to the trend of the shelf margin. Dickite is also found in association with calcite spar in two other areas around the Delaware basin: in the Glass mountains (fig. 1.4) dickite is found associated with a Tertiary igneous intrusion in Bird Mine; and in the Apache mountains (fig. 1.4) dickite is found associated with sphalerite and calcite spar in Buck Zinc Mine (pers. comm., C. Hill, 1989).

Quartz Authigenic silica is found in three main habits; i. as nodular masses; ii. replacing bioclasts; and iii. as quartz overgrowths. In all its manifestations it is a minor phase.

Replacive silica (table 3.6) In the basin margin facies some shell fragments, particularly brachiopods (fig. 3.34), are partially replaced by silica. Replacive nodules of silica also occur but are rare. These are elliptical masses (fig. 3.35), up to several centimetres in size, which replace the surrounding carbonate. The silica has a yellowish appearance in plane polarized light, and stands out particularly well in reflected light. This silica is commonly associated with crystalline haematite (fig. 3.34 and fig. 3.35).

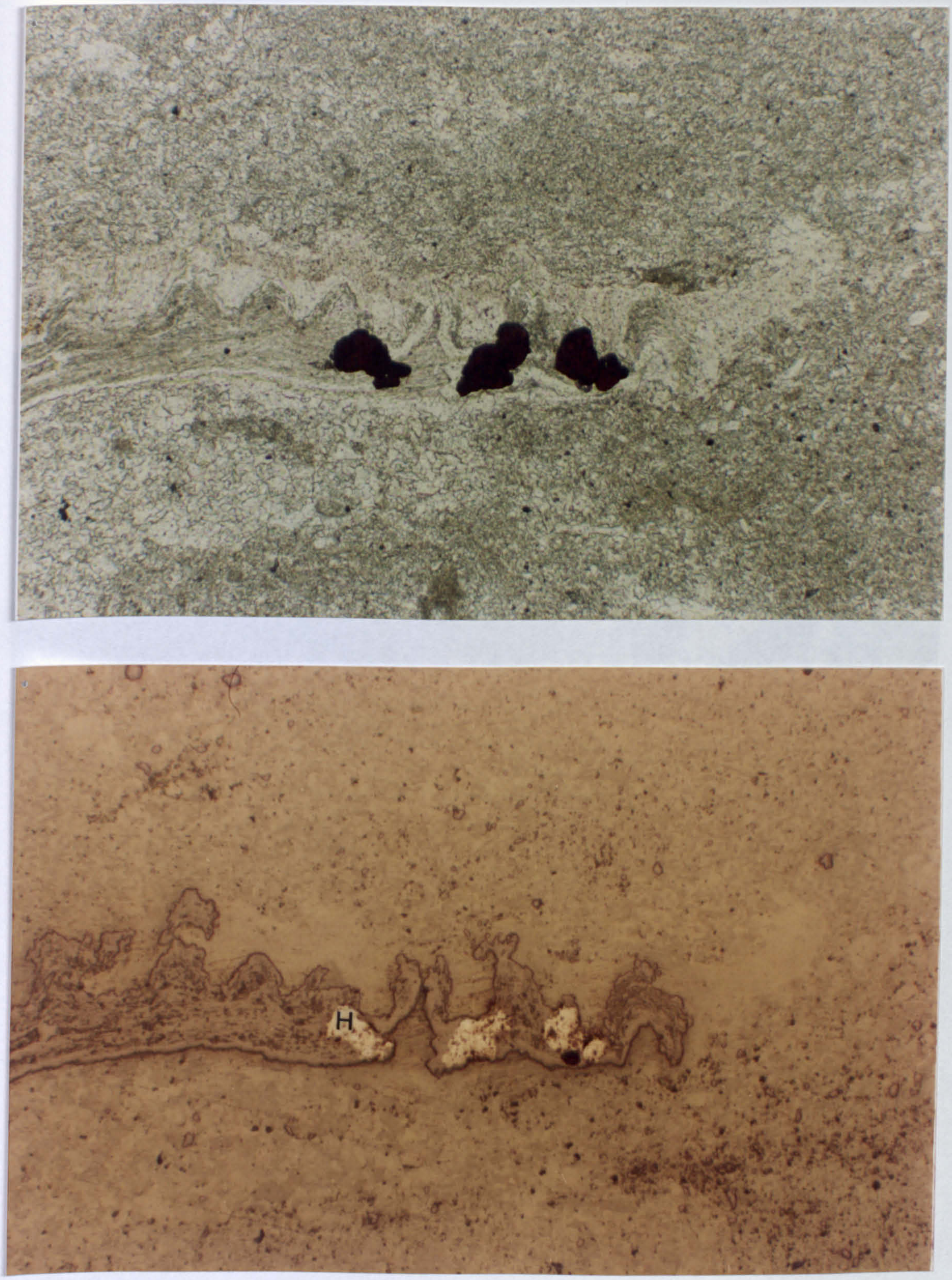

fig. 3.34a,b Plane polarised light and reflected light photomicrograph pair of haematite crystals (H) associated with a silicified brachiopod in micrite. The silicified areas are clearly visible in reflected light. Sample M3; basin margin facies, 'reef trail', McKittrick Canyon. Scale: 25mm = 250μm.

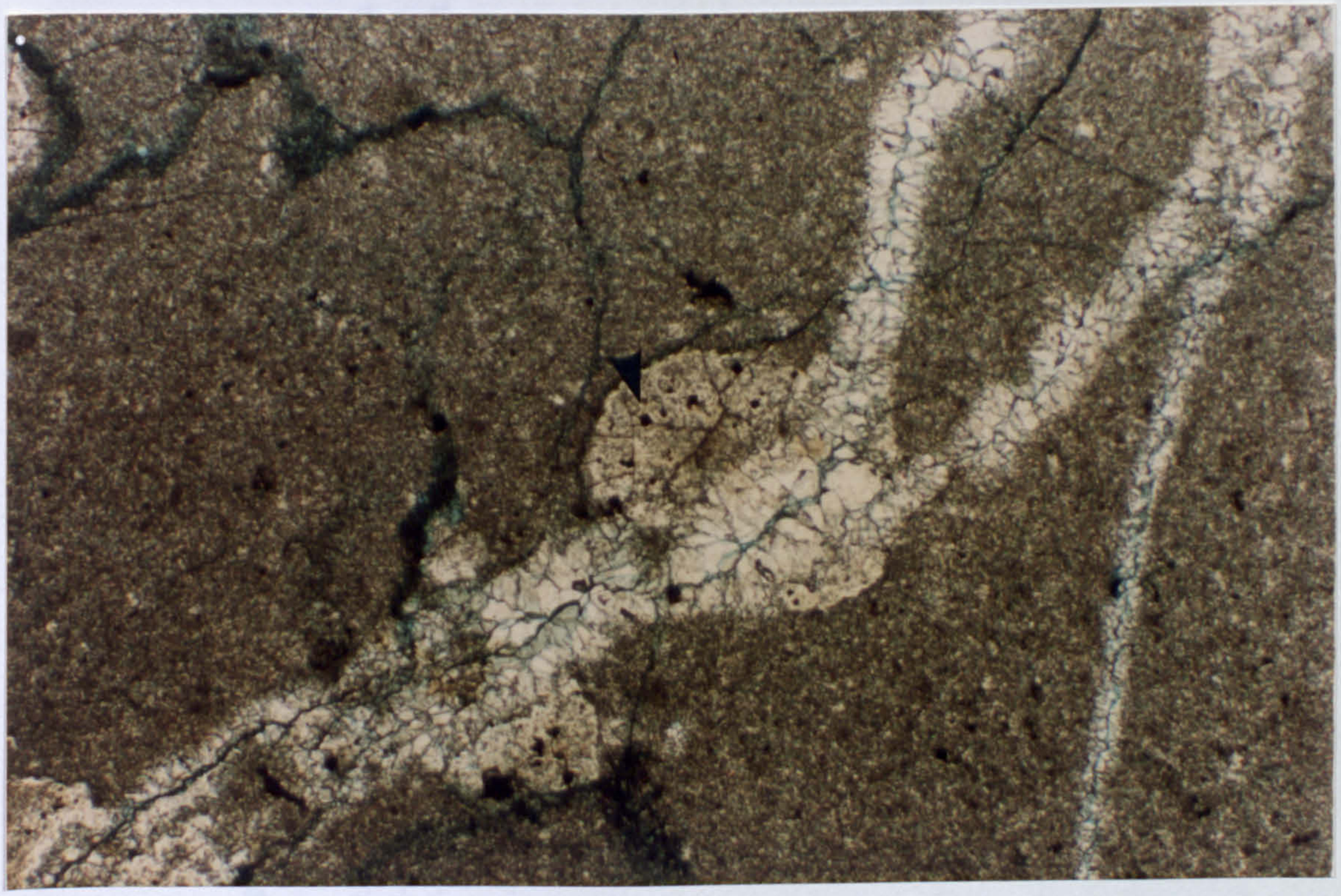

fig. 3.35 Plane polarised light photomicrograph of nodules of silica (containing haematite (arrowed)) replacing micrite. The nodules have been cross-cut by calcite-filled fractures. Sample MT22; basin margin facies, 'reef trail', McKittrick Canyon. Scale: 25mm = 500μm.

description	no. analyses	sample	CaO (wt.%)	MgO (wt.%)	SO3 (wt.%)	Al2O3 (wt.%)	SiO2 (wt.%)	FeO (wt.%)	Na2O (wt.%)	TiO2 (wt.%)	K2O (wt.%)	MnO (wt.%)
haematite	1	M22	1.85	0.25		1.25	2.32	71.19				
	5	MT19	0.57-0.75	0.64-1.01	nd-0.19	0.33-0.63	2.84-3.61	72.33-73.76	0.11-0.17			
	5	M6i	0.44-12.58	0.55-2.54		0.64-0.51	nd-3.04	56.02-70.61				
	3	MT74i	0.57-0.62	0.54-0.94		0.60-0.79	3.42-3.73	70.85-73-94				nd-0.22
feldspar	3	MT39	nd-6.54	1.05-4.83		26.95-33.03	37.48-48.46	2.23-3	0.59-0.80	0.3-0.38	6.10-7.71	

table 3.7 Electron microprobe analyses of haematite and feldspar

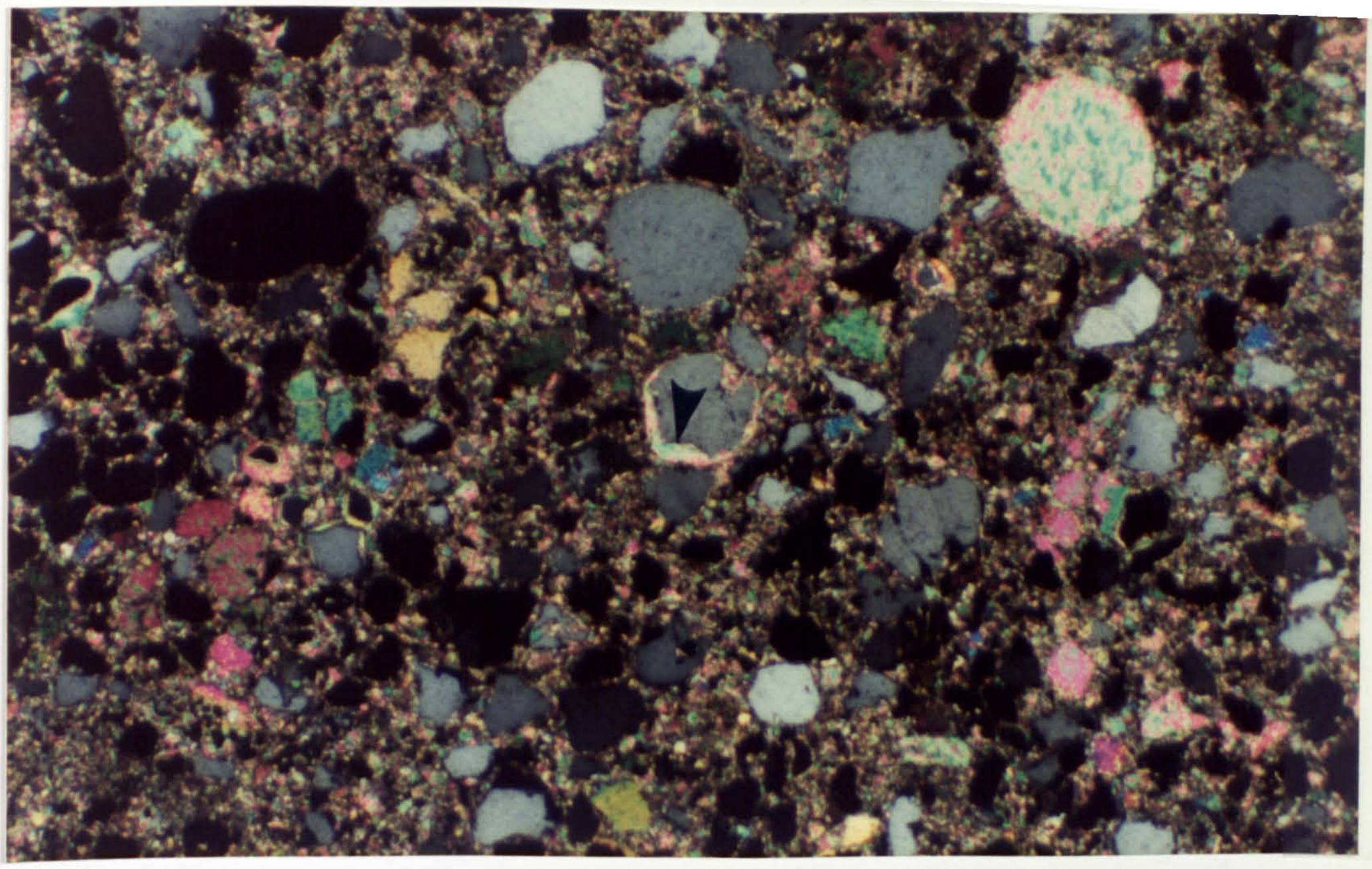

fig. 3.36 Cross polarised light photomicrograph of calcitised quartz overgrowth cements (arrowed). The overgrowths are rounded which suggests formation of the overgrowths prior to reworking of the silt grains. Sample M23; back reef facies, 'reef trail', McKittrick Canyon. Scale: 25mm = 125µm.

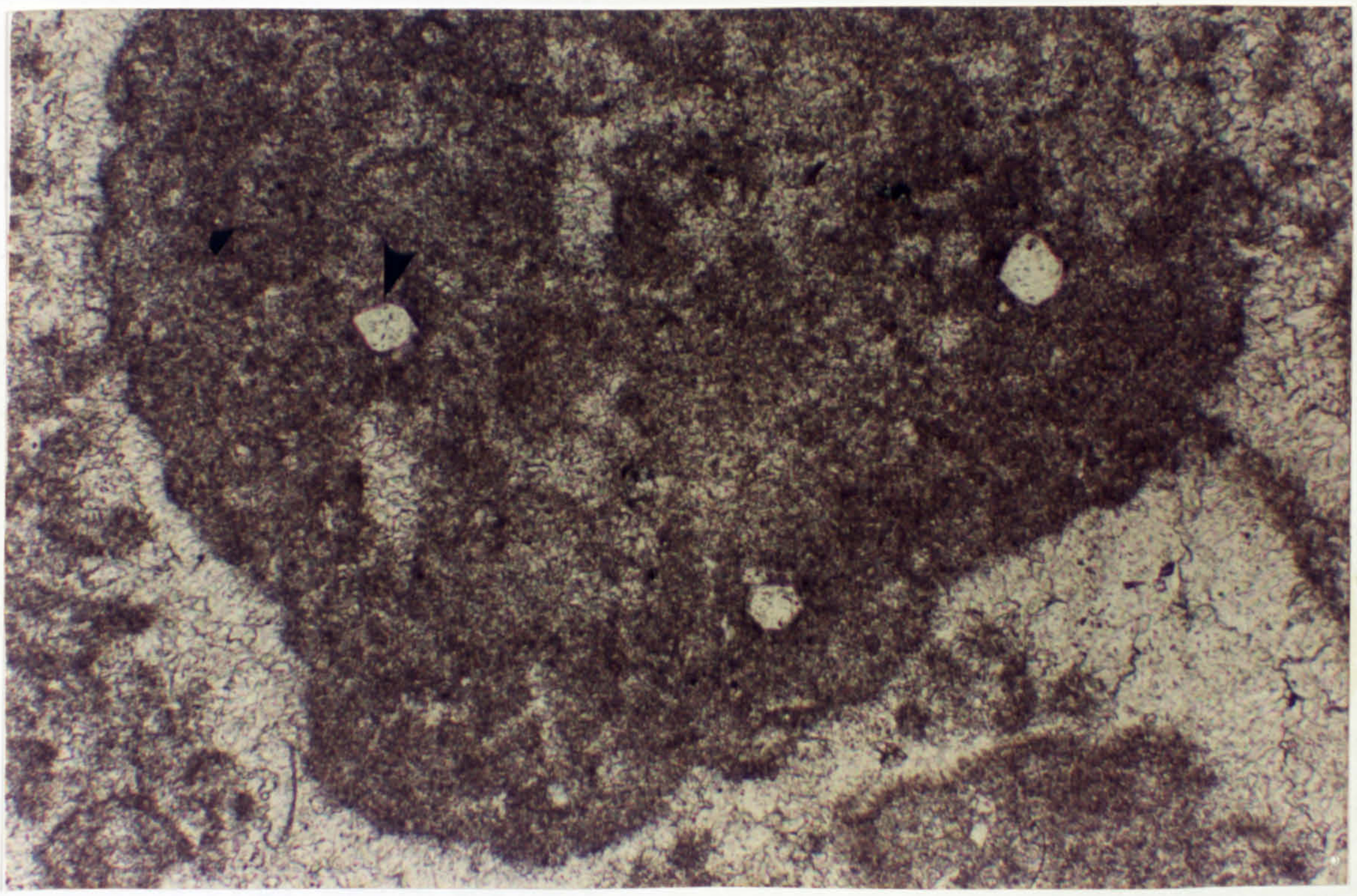

fig. 3.37 Plane polarised light photomicrograph of authigenic, euhedral quartz overgrowth cements (arrowed) on silt grains enclosed within a carbonate lithoclast. Sample M13; back reef facies, 'reef trail', McKittrick Canyon. Scale: 25mm = 125µm.

Quartz overgrowths (table 3.6) Some detrital quartz grains have quartz overgrowth cements. Quartz overgrowths appear to have developed at different times; i. pre- and ii. post-deposition of the grains. Pre-depositional overgrowths are often replaced by calcite (fig. 3.36). They are separated from the underlying detrital grain by a thin layer of clays (and carbonate). The overgrowth itself usually has rounded appearance , rather than being hexagonal in form, and appears to have been abraded, suggesting transport (G. Harwood, pers. comm., 1989). These grains are found in the siltstones of the foreslope facies and are commonly calcitised. Post-depositional overgrowths are equidimensional, pseudo-hexagonal in form and have plane crystal faces (fig.3.37). They occur most commonly on detrital quartz grains which are incorporated into micritic lithoclasts in dolomitised grainstones of the back-reef facies. They are not common in siltstone units.

Authigenic feldspar This is a rare and minor phase and would not have been identified without electron microprobe analysis (table 3.7). The feldspar occurs as small lath shapes a few microns in size, and is associated with pervasive dolomitisation in the lower foreslope.

Origins of silicate phases

The replacive silica is restricted to the basin margin facies and it is associated with haematite. Schmitt and Boyd (1981) report silicification of invertebrate skeletal material from strata of Permian age from Wyoming. They recognise 5 patterns of silicification and suggest that these could be used as a frame of reference for other studies. Two of the silicification patterns (pattern IV; subhedral to euhedral megaquartz and discoid masses of chalcedony, in the form of beekite discs arranged concentrically, and pattern V; subhedral megaquartz aligned parallel to the skeletal boundary, with the silicified portion commonly enclosing skeletal carbonate) are found in the basin margin facies (Lamar limestone). They (*op. cit.*) suggest that type IV may have formed by direct precipitation into pore space, due to the absence of fabric retention, and the large size of silica euhedra, and that type V formed from the direct replacement of a preceeding fabric. Interestingly, this type (V) has been found to replace sulphate minerals (Folk and Pittman, 1971, and Siedlecka, 1972) as well as aragonitic and calcitic fossils (*e.g.*, Jacka, 1974).

Sponge spicules have been cited by several workers as a probable source for diagenetic silica (*e.g.*, Schmitt and Boyd, 1981; Jacka, 1974; L.C. Babcock, 1977).

These are composed of amorphous silica which is significantly more soluble than quartz and dissolves readily (see Schmitt and Boyd, 1981, their fig. 16).

McBride (1987) suggests that silica cement and kaolinite may both be derived from the alteration of feldspar according to the following equations

$2KAlSi_3O_8 + 2H^+ + H_2O \rightarrow Al_2Si_2O_5(OH)_4 + 4SiO_2 + 2K^+$

$4(Na_5\ Ca_5)Al_{1.5}Si_{2.5}O_8 + 3H_2O + 6H^+ \rightarrow 3Al_2Si_2O_5(OH_4) + 4SiO_2 + 2Na^{+}{}^{+} + 2Ca^{++}$

Both require acidic conditions.

It is not necessarily the case that the quartz overgrowths found in the back reef and foreslope facies and the replacive quartz found in the basin margin facies have the same origin. The spatial distributions suggest that they have different origins. The quartz overgrowths derived silica primarily from the dissolution of feldspar (and possibly clay minerals coating siliciclastic grains as 'desert varnish') concomitant with the formation of authigenic kaolinite. The quartz which selectively replaced skeletal material in the basin margin was probably derived fron the dissolution of siliceous sponge spicules (L.C Babcock, 1977).

3.3.6 Iron minerals

Iron sulphides Thin sections were examined for the presence of iron sulphides, particularly pyrite and pyrrhotite. Although these minerals have different optical properties in reflected light (pyrite is cubic and pyrrhotite is hexagonal or monoclinic) resolution of the mineralogy of *minute* framboids can be difficult. However, some iron sulphides have been identified petrographically, and occur replacing grains in siltstone units, and as minute framboids in basin and basin margin facies rocks. Pyrite/pyrrhotite have been interpreted as being present from magnetic studies (chapter 5).

Haematite

Haematite occurs in several habits and associations (table 3.6); i. in calcite spar as minute spherules (fig. 3.39) and well-developed crystals, up to 500μm in diameter; ii. in detrital quartz grains as minute equidimensional crystals <10μm in diameter); iii. in silicified shell fragments (fig. 3.34) and siliceous nodules (fig. 3.35) as euhedral crystals (up to 500μm in diameter) in the basin margin facies only; iv. along stylolites; v. associated with pore-space due to modern weathering where it has acicular

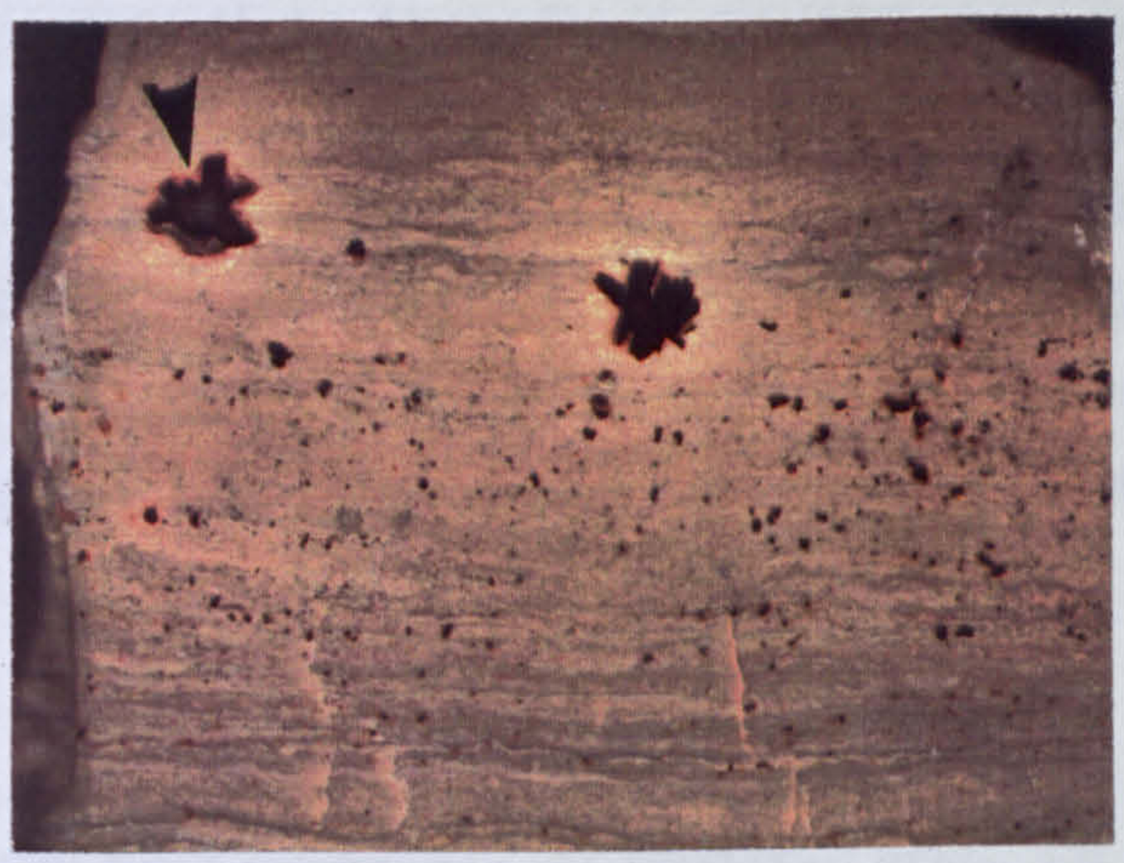

fig. 3.38 Replacive iron sulphide (arrowed) after replacive anhydrite laths in dolomitised laminated algal wackestone. Most of the iron sulphide has oxidised to haematite. Back reef facies (Queen fmn.), scale bar in cm; courtesy of Rick Sarg.

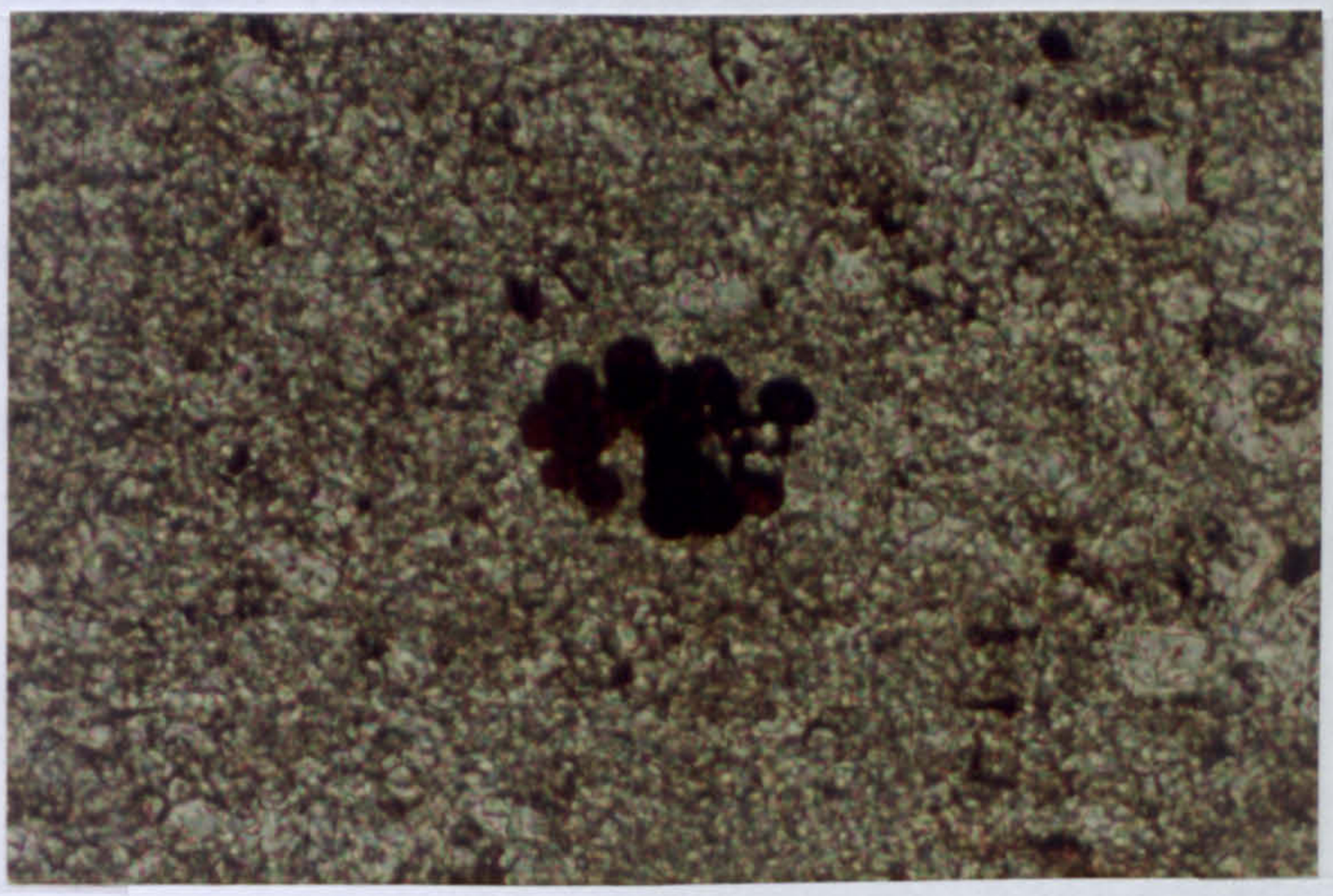

fig. 3.39 Plane polarised light photomicrograph of spheroidal haematite, oxidised from framboidal pyrite, in micrite. Sample M2; basin margin facies, 'reef trail', M^{c}Kittrick Canyon. Scale: 22mm = 50μm.

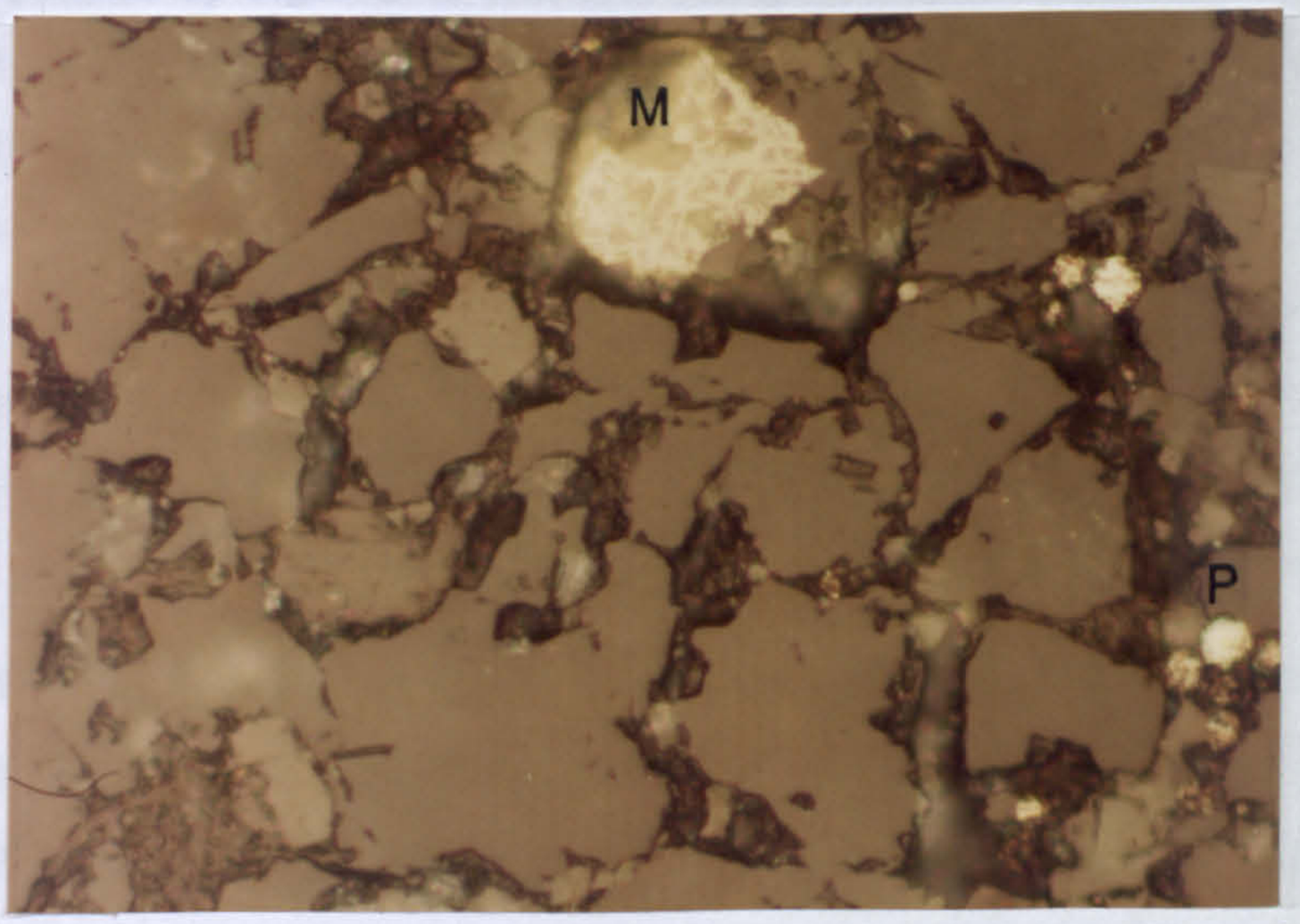

fig. 3.40 Reflected light photomicrograph of detrital magnetite (**M**), showing exsolution lamellae of ilmenite, in Brushy Canyon siltstone. Framboidal pyrite (**P**), showing partial oxidation to haematite, is also present. Brushy Canyon siltstone; basin facies, road-cut on highway US 62/180. Scale: 22mm = 50μm.

morphology. The morphology of the haematite is not resolvable where it occurs along stylolites. Electron microprobe analysis (table 3.7) reveals that Si and Al are present in small quantities in the haematite, suggesting the presence of clay inclusions. Kaolinite inclusions up to 30μm in size are present in large (centimetre) haematite crystals from samples from the back reef facies in the Yates Formation (fig. 3.38). Haematite has also been interpreted as being present from magnetic studies.

Magnetite

Magnetite has only been unambiguously identified, using petrographic studies, in Brushy Canyon sandstone, where it is found as detrital grains (table 3.6). These appear to show exsolution lamellae of ilmenite (fig. 3.40), which are characteristic of magnetite of igneous origin. Alternatively, this texture could be due to maghemitisation of magnetite (pers. comm., J.R. Cann, 1990). There are many cases, particularly in basinal carbonates such as the Lamar limestone, which contain tiny opaque spherules. These may be magnetite or iron sulphide. Further study, for instance using SEM or XRD analysis on isolated spherules would be necessary to resolve their mineralogy. Magnetite has been identified from magnetic studies.

Origins of Iron minerals

Diagenetic processes can affect a sedimentary sequence from the time of deposition until the present day. The reactions which take place depend upon the availability of particular ions and on the redox and pH conditions. Many diagenetic reactions are mediated by organisms and also many biological reactions take place in the diagenetic realm and different iron minerals will form as a consequence (table 3.8).

Pyrite formation by bacterial sulphate reduction and oxidation of sedimentary organic matter is a common process in normal marine sediments below the sediment/water interface, where conditions are anoxic (Berner, 1984), because of the ubiquity of organic matter and the availability of sea water sulphate. The pyrite formed in this way commonly has a framboidal form. Aerobic organisms and haematite cannot tolerate traces of H_2S without death of the organisms and conversion to sulphide respectively, and *vice versa.* Also H_2S and O_2 cannot co-exist in solution (Berner, 1981). These two points form the basis for the classification of sedimentary environments proposed by Berner (1981). Iron reduction is not directly coupled to

sulphide formation. Depending on Eh-pH relations, reduction of iron(II) may produce other authigenic minerals such as siderite, (Fe CO_3), and vivianite ($Fe(PO_4)_2 \cdot 8H_2O$), as well as pyrite, depending on the availability of the anion species; (Bell *et al.*, 1987). Because siderite is rapidly destroyed by oxidation it can be inferred that weathering due to uplift and exposure would cause oxidation to magnetite or maghemite which then decays over time to haematite.

Iron (and other metal) sulphides such as pyrrhotite, marcasite and pyrite are by-products of the reduction of anhydrite/gypsum. HCO_3^-, H_2S and sulphide minerals are the products of the reactions involved. If there is a source of iron available then iron sulphides, such as pyrrhotite, marcasite and pyrite will form. This iron sulphide can pseudomorph the anhydrite (fig. 3.38; and pers. comm., G. Harwood; Machel, in press). Framboidal pyrite has also been reported as forming as a result of bacterial sulphate reduction (Machel, in press). Reduction of anhydrite may occur *via* two processes *i.e.*, bacterial or thermo-chemical, but the reaction products are the same in both cases. However, the geochemical characteristics, such as sulphur and carbon isotope fractionation and the composition of the associated organic compounds left after sulphate reduction, are different (Machel, 1989). Bacterial sulphate reduction operates up to 85°C and requires reducing conditions and the presence of organic compounds for the bacteria to survive. The temperatures at which thermo-chemical sulphate reduction operates are not well known, but are estimated to be between 100°C and 135°C (Machel, 1989).

It is likely that the large euhedral crystals of haematite associated with silicification of skeletal material have a different origin from the spheroidal and small crystals of haematite which occur within calcite spar. Brachiopods and crinoids replaced by quartzine and haematite have been reported in silty wackestones from Nebraska and Utah (Loope and Watkins, 1989). Their conclusion was that the iron was originally concentrated in the skeletal material as scattered pyrite framboids and euhedra resulting from early anaerobic decay of skeletal organic matter. Subsequent oxidation of sulphide to haematite caused locally acidic conditions allowing migration of iron through the quartz. Buffering of these solutions by surrounding carbonate caused preferential accumulation of iron oxide at the perimeters of the silicified zones. The associations they describe (*op. cit.*) are identical to those observed in the basin margin facies in this study, and their interpretation may be equally valid.

The haematite which occurs in calcite spars has different origin to that which accompanies silicification. The haematite in calcite spar formed from the oxidation of authigenic pyrite/pyrrhotite after the dissolution of calcium sulphate and concomitant

pyrite formation. Framboidal haematite probably formed from the oxidation of early diagenetic sulphides, which had formed during early diagenesis by bacterial sulphate reduction. The timing of haematite formation relative to precipitation of calcite spars is uncertain from petrographic studies, but appears to be contemporaneous. Palaeomagnetic results shed more light on the timing (chapter 5 and 6).

Detrital magnetite could have been derived from weathering and transport of continental igneous rocks (Lovlie *et al.*, 1971) in which case the magnetite derived would be titanium-rich and would have formed by crystallisation from a melt. Magnetite has been identified petrographically from the Brushy Canyon siltstone in the basin facies, and this magnetite exhibits exsolution lamellae of ilmenite (fig. 3.40) which indicates that it formed by crystallisation from a melt. However, magnetite has not been *unequivocally* identified from any other rocks in this study (but see chapter 5).

The occurrence in a salt marsh environment of a bacterium which contained within its cell wall several ultra-fine-grained magnetite crystals (Blakemore, 1975) indicated another possible source of magnetite. Since that discovery, many other workers have reported and investigated the occcurrence of these magnetotactic bacteria in a varitey of sedimentary environments (table 3.8). However, the environmental factors controlling their distributions are still not well known (Blakemore, 1975; Frankel *et al.*, 1979 and Stolz *et al.*, 1986). Bacteria which synthesised extracellular magnetite under anaerobic conditions (Lovley *et al.*, 1987) and interest and research into the occurrence of biogenic magnetite is growing (Chang *et al.*, 1987, McCabe *et al.*, 1983, Horton *et al.*, 1984 and Blakemore *et al.*, 1985). The characteristics of biogenically produced magnetic minerals are now becoming known and can be compared with the characteristics of detrital and authigenic minerals (table 3.8b). Magnetite also occurs as a metabolic *by-product*. The mechanism for the production of magnetite involves the reduction of ferric oxyhydroxides and/or oxidation of dissolved ferrous iron from the underlying iron reduction zone as energy sources for the oxidation of organic matter. Some of this biogenically mediated, early diagenetic magnetite itself provides energy for iron reducing organisms which live deeper in the sediment column; (Karlin and Levi, 1983 and Karlin *et al.*,1987). Results from a sediment core from the East Pacific Rise, suggest that fine-grained magnetite is precipitating at the top of the iron reduction zone *i.e.*, about 20 cm deep within the sediment (Karlin *et al.*, 1987). This observation is consistent with microbially mediated extracellular magnetite production (Lovely *et al.*,1987). Downcore porewater and sulphur analyses show a marked decrease in porewater sulphate and an increase in pyrite and metastable monosulphides. This suggests that organic matter, magnetites and other iron oxides become progressively reduced and subsequently sulphidised and pyritised with depth. The smallest magnetic

grains (*i.e.*, the single domain) are the first to be altered and this causes downcore coarsening of the magnetic fraction, and a decrease in the remanence and other magnetic properties with depth.

Carbonates which contain hydrocarbons or bitumen may contain associated magnetite (McCabe *et al.*, 1985; McCabe *et al.*,1987; Benthien and Elmore, 1987). Several possibilities exist as to the origin of these minerals. Bitumen is commonly derived from the microbial degradation of liquid crude oil and it has been suggested, (Elmore, 1988; McCabe *et al.*,1987), that the magnetite results from microbial activity though no direct evidence has been found. However the discovery of a dissimilatory iron-reducing anaerobic bacterium which produces magnetite as a metabolic by-product (Lovley 1987), and the discovery that this bacterium can oxidise an aromatic hydrocarbon anaerobically (Lovley 1989), makes this proposed association more plausible. Other alternatives are the oxidation of iron sulphides such as framboidal pyrite or the reduction of precursor oxides, or the release of iron from iron-rich carbonate phases as a result of diagenetic changes (McCabe *et al.*, 1987).

In the oxic environment, pyrite will oxidise to haematite according to the equation: $FeS_2(s) + 15/4\ O_2(aq) + H_2O(l) \rightarrow Fe(OH)_3(s) + 2\ H_2SO_4(aq)$ *i.e.*, this is an acid generating reaction. In nature this reaction is not simple; the ultimate driving force is the availability of atmospheric oxygen, derived from recharge of meteoric waters, but the rate determining step may not involve oxygen at all. Also, iron hydroxides may well form as well as, or instead of, haematite (Nordstrom, 1982).

The iron necessary for iron mineralisation has three possible sources; i. from exsolution of iron during calcitisation of ferroan dolomite, or from recrystallisation of ferroan calcite; ii. from basinally derived fluids; iii. from iron associated with desert varnish and clays on silt grains. No ferroan carbonate phases have been identified in this study, although minor amounts are reported in Garber *et al.* (1989). This is therefore unlikely to be a significant source of iron. If the iron was derived from basinal fluids, much greater amounts of iron minerals and a variety of other minerals might have been expected to be present. This is therefore not a likely source of iron. Iron staining, interpreted to be desert varnish, is associated with sands of the back reef facies (Borer and Harris, 1989). Remobilisation of this iron during flushing of the Capitan shelf margin by meteoric waters during uplift, is considered to be a likely source for the iron incorporated in iron minerals.

occurence/associations	mineral	habit	reference
weathering of continental rock and oceanic basalts	Ti-magnetite	elongate inclusions within silicate minerals;framboidal; octahedral;spherules;angular. Ti content 2-25%; Curie temp. 150-400C	Lovlie et al., 1971 Morgan et al., 1981 Fishman et al., 1989 Petersen et al., 1986
cosmic dust	Ti-magnetite	micro-spherules 0.1mm	Worm et al., 1987
chiton teeth	magnetite	Curie temp. 570-600C	Kirschvink et al., 1979
magnetotactic algae	magnetite	intracellular	Torres de Aranjo 1986
magnetotactic bacteria (aerobic)	magnetite	intracellular;commonly in chains;hexagonal;teardrop shapes;narrow SD size range Ti<0.5%	Frankel et al., 1979 Karlin et al., 1987 Blakemore et al., 1985
anaerobic bacteria	magnetite	extracellular;broad size range <0.05um;sometimes <SD size	Lovley et al., 1987,1989 Bazylinski 1988 Lowenstam 1981
hydrocarbons; solid bitumen Mississippian	magnetite	spherical aggregates,hollow cores	McCabe et al., 1987
hydrocarbons; bitumen Silurian, Wabash Fmn.	magnetite		McCabe et al., 1985
hydrocarbons; fenestral dolomites	magnetite	15um spheres	Benthien et al., 1987
Permian, Phosphoria Fmn.	haematite	plates<10um	
hydrocarbons; gilsonite	magnetite	spheres	Elmore et al., 1987
Permian speleothems	haematite		
Cement Oil Field	pyrrhotite		Reynolds 1985
calcitisation of ferroan dolomite	haematite	1mm plates	Elmore 1985
shallow water carbonates,Taum Sauk limestone (U.Cambrian), Kindblade Fmn (Ordovician)	goethite	rosettes,needles 1-3um	Frank 1981
	haematite	thin red plates 0.7-1.0um	
MVT; sulphide mineralised carbonates,Bonneterre Fmn (U. Camb)	magnetite	spherical crystal aggregates	Wisniowiecki et al., 1983
	pyrrhotite	non-magnetic	McCabe et al., 1983
pseudomorphs after pyrite; liesgang bands, Arbuckle Grp.	haematite	cubes	Cochran et al., 1987
fenestral dolomites, Phosphoria Fmn.(Permian)	haematite	cubes	Benthien et al., 1987
Jura (Jurassic)	goethite	cubes	Johnson et al., 1984
reef limestone, Canning Basin	haematite	cyanobacterial influence??	Hurley et al., 1987
	magnetite		
	goethite	diagenetic??	
dolomitised Leadville carbonates (Mississippian)	magnetite	spheroidal	Horton et al., 1984
basinal,pyritic,organic limestone Craven Basin (Carboniferous)	magnetite	10-20um	Turner 1975
	haematite		
dolomitised,silicified limestone	magnetite	volcanic origin??	Addison et al., 1975
Pendleside Limestone (Carbonif.)	haematite		
	pyrrhotite		
blue limestones, Jura Mts. (Lias)	magnetite		Johnson et al., 1984

fig. 3.8a Summary table of magnetic mineral occurrences in carbonate rocks
table

mineral	environment	habit	reference
magnetite	soils (UK)	*ultra-fine grained*; grains 0.1-0.01um; octahedral, hexagonal.	Maher et al., 1988
magnetite	deep sea sediments	SD and pSD grains; hexagonal prisms,sub-rounded and tear-drop shapes.	Kirschvink et al., 1984
ferrihydrite magnetite	marine and fresh-water sediments	chiton teeth; grains 0.1um.	Kirschvink et al., 1979
ferrihydrite magnetite	bogs, lakes, open-marine	SD, pure	Karlin et al., 1987
magnetite	*estuarine*, salt-marsh	anaerobic magnetotactic bacterium	Bazylinski et al., 1988
magnetite	freshwater	*aerobic magnetotactic* bacterium	Blakemore et al., 1985
magnetite	river sediments (Potomac River)	non-magnetotactic, anaerobic bacterium	Lovley et al., 1987
magnetite	Sugerloaf Key,Florida	ultra-fine grained, bacterial	Chang et al., 1987
magnetite	freshwater	SD	Towe et al., 1981 Matsuda et al., 1983 Mann et al., 1984
magnetite	freshwater marsh	aerobic magnetotactic bacterium	Balkwill et al., 1979 Mann et al., 1984
magnetite	deep sea (DSDP 79)	SD	Kirschvink et al., 1984
magnetite	marine sediments Santa Barbara Basin	several morphologies	Stolz et al., 1986 Chang et al., 1987
magnetite	sewage pond		Kirschvink 1980
magnetite	salt marsh, Cape Cod	chains ,magnetotactic bacteria	Blakemore 1975
magnetite	freshwater swamp	aerobic, magnetotactic bacteria	Frankel et al., 1979
magnetite	salt marsh, fresh water rivers and ponds,thermal springs, caverns	magnetotactic bacteria	Blakemore et al., 1981

table 3.8b Occurrence of magnetite in modern sedimentary environments

3.4 Paragenetic sequence

The paragenetic sequence for the Capitan shelf margin is illustrated in fig 3.41 and further discussed in chapter 6. Diagenesis in the marine environment lithified grainstones and boundstones before significant burial and exposure of the shelf during desiccation of the Delaware basin. Marine cementation primarily affected the back reef, reef and upper foreslope facies, whilst significant compaction was affecting the lower foreslope, basin margin and basin facies. Large volumes of botryoidal aragonite developed in the reef facies in particular. Grainstones were cemented by isopachous, high-magnesian calcite marine cements following the formation of micrite envelopes around virtually all grains. Isopachous marine cements are thickest in rocks closest to the reef and become thinner further from the reef. In the lower foreslope isopachous cements are thin and relatively rare. this is partly due to the paucity of grainstones in this facies. Early fractures and voids were filled with geopetals, of both siliciclastic and carbonate grains and lined with isopachous high-magnesian calcite marine cements.

Selective dolomitisation of grains and micrite occurred early, probably before significant burial. The Mg source for the dolomitisation was probably sea water with additional Mg from the inversion of high-magnesian to low-magnesian calcite.

Some rocks show no evidence of marine cementation, particularly in the back reef facies. However, samples of these rocks show no signs of compaction, all are dolomitised, all have calcite spars where marine cements would be expected, and all show direct evidence of replacive anhydrite. In these samples either early cementation by gypsum prevented compaction, or, marine cements were subsequently replaced by gypsum/anhydrite during early burial, following exposure of the shelf. The presence of marine cements in adjacent rocks suggests that the latter scenario is more likely. Nevertheless, this raises the question of how some marine cements were replaced by sulphate whilst others were not. Minor dissolution of some bioclasts and former-aragonite botryoids, followed by dolomitisation, accompanied gypsum precipitation during exposure of the shelf due to the initial stages of drawdown associated with the desiccation of the Delaware Basin. Gypsum formed a passive fill in all porosity and fractures. Further dolomitisation accompanied the drawdown of evaporatively concentrated brines and continued during burial of the Capitan shelf margin by evaporite sequences (Castile and Salado Formations). Remaining primary porosity in the reef, upper foreslope and lower foreslope facies were plugged by gypsum during early burial.

On deeper burial anhydrite replaced some carbonate (and possibly calcitised the reworked quartz overgrowth cements). The relative paucity of replacive anhydrite textures is probably due to the fact that most of these sediments were already dolomitised by this time. Dolomite overgrowth formation may have accompanied the dehydration of gypsum, due to the release of intracrystalline water from the gypsum. This could be tested by looking at the $\partial^{18}O$ isotope composition of the overgrowth.

The Capitan shelf margin remained plugged with anhydrite until uplift began in the late Cretaceous/early Tertiary. Dissolution of the majority of calcium sulphate by inflowing meteoric waters accompanied uplift. Formation of well-developed crystals of authigenic kaolinite followed complete dissolution of calcium sulphate. The timing of the quartz overgrowths is uncertain, but probably accompanied kaolinite formation. The presence of geopetals of dolomite and kaolinite (in the back reef facies only), fracturing and the absence of calcite spar IIa suggests that dissolution of calcium sulphate was total in the back reef facies. This required acidic and possibly reducing conditions. Pyrite formed as a by-product of minor sulphate reduction, probably due to the action of sulphate-reducing bacteria, introduced in meteoric waters, concomitant with minor calcitisation of evaporites.

The majority of calcite spar was precipitated after sulphate dissolution. A phase of dissolution followed precipitation of calcite spar IIc. This dissolution was associated with further kaolinite precipitation under acidic conditions. Dickite in fractures in the basin margin facies suggest that this fluid may have been hot *i.e.*, derived from the basin; this is corroborated by the assoication of dickite with sphalerite and igneous intrusions elsewhere around the Delaware basin (pers. comm., C. Hill, 1989). Calcite spars Ib, IIc and III are all associated with small amounts of haematite. The haematite formed from the oxidation of authigenic pyrite during continuing influx of oxidising meteoric waters.

3.5 Conclusions and further work

There is sparse direct evidence of subaerial exposure in the Capitan. Vadose cements and dissolutional features are largely absent. However, Garber *et al.* (1989) report meniscus and pendant cements in pisoids of the back reef facies (Garber *et al.*, 1989, their fig. 61 A) and Melim and Scholle (1989) report a suabaerial exposure surface in the Capitan in Rattlesnake Canyon. However, the latter has been discredited upon further examination (pers. comm., N. Hurley, R. Sarg, D. Mruk, D.A. Yurewicz and A.C. Kendall, 1989). In any case, meteoric waters in any hydrologic system involving

exposure of the Capitan Shelf Margin in Upper Permian times, would almost certainly be evaporatively concentrated (Schmidt, 1977) and/or combined with previously evaporated brines of the shelf. Therefore the chemical composition of this modified water would not have been the same as that usually associated with meteoric water. Thus, diagenetic interpretations involving 'normal' meteoric water must post-date the influence of evaporite-laden brines, either from direct evaporation or from the dissolution of evaporite sequences.

Dolomitisation was early and proceeded as a result of the development of the hydrologic system which accompanied the desiccation of the Delaware Basin during upper Capitan and Castile times. Pervasive dolomitisation can be ascribed to two main processes; i. drawdown of evaporatively concentrated brines from the shelf, and ii. back-filling of porosity in the Capitan Shelf Margin by sulphate-laden fluids during the filling of the Delaware Basin by the Castile Formation.

Calcitisation of evaporites, concomitant with bacterial or thermochemical sulphate reduction and minor sulphide formation, was of minor diagenetic significance.

Calcite spars are of Tertiary age and formed mainly in voids created after the dissolution of sulphate, following the uplift of the Guadalupe Mountains and the development of a meteoric groundwater system. Oxidation of diagenetic iron sulphides to haematite accompanied precipitation of these calcite spars.

It is perplexing that the Capitan Shelf Margin is not completely and pervasively dolomitised. This may be attributed to a combination of two main factors i. insuficient time and ii. early occlusion of most porosity by marine cements and then sulphates which caused significant reduction in permeability. The lack of volumetrically significant magnesite may also partly explain the lack of dolomite relative to other parts of the Capitan shelf margin. Magnesite has been reported in volumetrically significant anounts by Garber *et al.* (1989) in other parts of the shelf margin.

The main diagenetic phases have been identified and placed in a paragenetic sequence which best fits my observations and other available data. In order to further constrain my petrographic observations and test the diagenetic model, it would be helpful to do some geochemical studies, including carbon, oxygen and sulphur isotopes to help elucidate the chemistry of the pore waters responsible for dolomitisation, sulphate dissolution/replacement, and calcite cementation. It should be pointed out that isotopes of the shelf evaporites and the basin-fill evaporites should have similar values if this model is correct, as they have similar origins (A.C. Kendall, pers. comm., 1988). It may be that the distinction between calcitised evaporites (not *proven* in this study) and calcite spar formed after the dissolution of evaporites (abundant) may be made on the basis of their isotopic compositions. Further geochemical analysis may also help to

correlate the cathodoluminescence patterns of these calcite spars. Oxygen isotope composition of dolomite overgrowths might reflect their origin *i.e.*, from the water exsolved during dehydration of gypsum to anhydrite. Studies of inclusions in the dolomites and calcites could also be used to help further constrain the chemistry of the pore waters from which they precipitated.

Chapter 4: Magnetic fabric

4.1 Introduction

In this chapter the magnetic fabric *i.e.*, the anisotropy of susceptibility, of samples from a variety of facies and lithologies is discussed. Samples were measured on a Minisup and a 'Kappa' bridge, and some samples which had been heated to 650°C were also measured. These results and results from measurements of anisotropy of isothermal remanent magnetism are presented in this chapter.

4.1.1 Susceptibility

When an external magnetic field is applied to a substance this field will interact with the substance which acquires a magnetic moment in one of three ways. The ease with which this moment is acquired is called the magnetic susceptibility. Susceptibility is an intrinsic crystal property and, in many substances, its magnitude depends upon the direction in which it is measured, in which case it is anisotropic and the anisotropy is defined by the three principal susceptibilities, K_{max}, K_{int} and K_{min} (fig. 4.1). Magnetic susceptibility is a ratio of induced magnetisation to magnetic field intensity (Collinson, 1983). Susceptibility values are given in SI units x 10^{-6} for data generated on the Kappa bridge, and in volume units x $10^{-6}GOe^{-1}$ for data generated on the Minisup throughout this chapter (Appendix 4.2).

There are three types of susceptibility behaviour and these are defined in terms of the 'response' to an applied field. When an external field is applied to *diamagnetic* substances, it exerts a force on each orbiting electron in the substance and causes this moment to precess. The net result of this is to create a magnetic moment which tends to oppose the applied field; thus diamagnetic susceptiblity is *negative*. Calcite, dolomite and quartz are diamagnetic. When an external field is applied to substances which have incomplete electron shells, net spin dipole moments are produced, and these tend to align with the applied field producing a *positive* increase in magnetism. This is *paramagnetic* behaviour. Ions of the transition elements, especially Mn^{2+}, Fe^{2+} and Fe^{3+}, are the ions most commonly responsible for paramagnetic behaviour in natural minerals, because the two outermost electron shells are incomplete in these ions. Common paramagnetic minerals include clays and micas. *Ferromagnetic* substances have large, *positive*

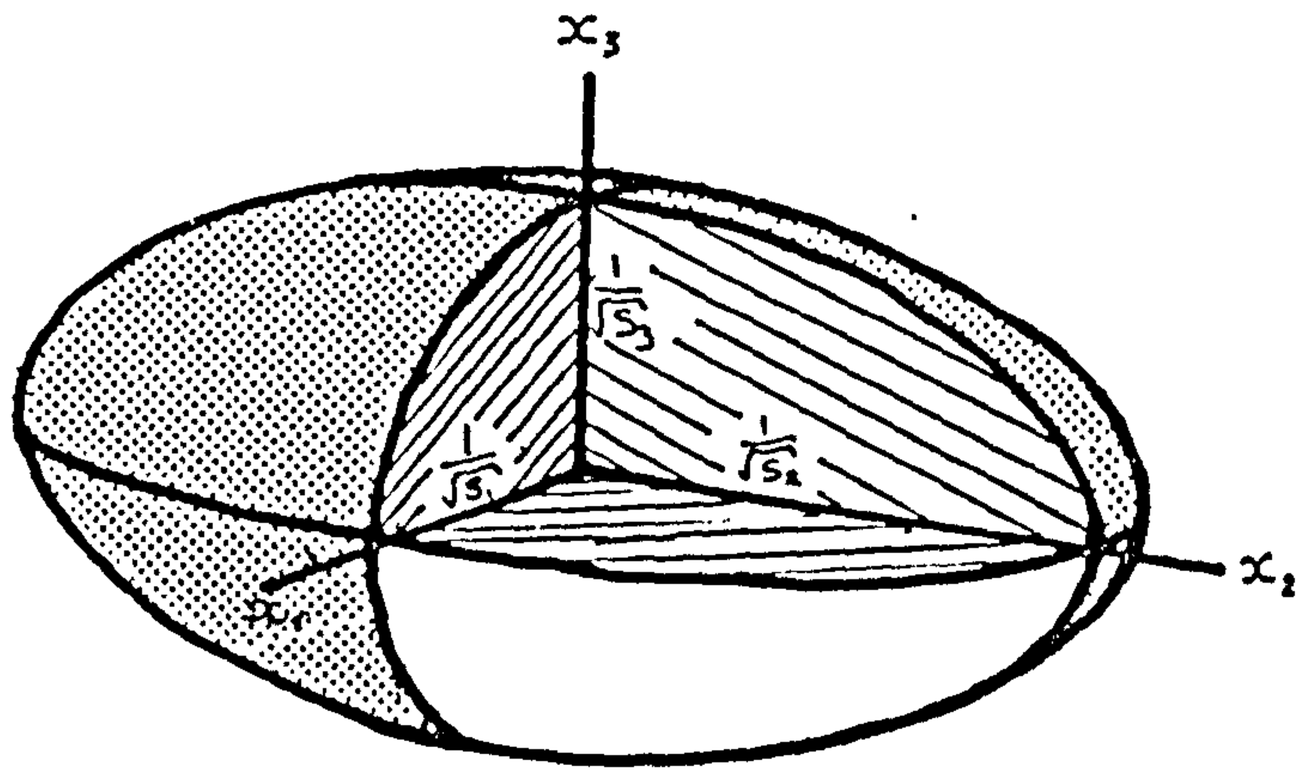

fig. 4.1 Ellipsoid used to represent anisotropy. For anisotropy of susceptibility *i.e.*, magnetic fabric, the principal components (S_1, S_2 and S_3) define the susceptibility ellipsoid and the lengths of the axes are inversely proportional to the square root of the values of the principal components.

susceptibility and this dominates any dia- or paramagnetic effects. Ferromagnetic behaviour is caused by interactions between the electrons of several adjacent atoms. There are several types of ferromagnetism and this is due to the complexity of ways in which spin dipole moments can be arranged. When electron orbits overlap and the coupling between them is parallel and additive, this is ferromagnetic behaviour (*s.s*). When electron orbits overlap and the coupling between them is antiparallel but the opposing directions are not exactly equal, then this is *ferrimagnetic* behaviour. In *anti-ferromagnetic* substances these opposing directions are exactly balanced but the magnetic moments are not exactly anti-parallel and a this results in a small magnetisation in a direction bisecting the two dipole directions. However, the term ferromagnetic (*s.l.*) is used throughout this thesis to describe these various types of behaviour.

4.1.2 Magnetic fabric

Magnetic fabric is defined as the anisotropy of susceptibility and is used as a measure of the preferred orientation of components present in a rock sample. Anisotropy is usually represented in terms of an ellipsoid (fig. 4.1; Nye, 1969). Anisotropy of bulk susceptibility is a measurement of the net contribution from dia-, para- and ferro-magnetic components, as well as the different shapes, sizes and proportions of these components *i.e.*, it is a combination of the contributions of fundamental anisotropy of crystal structure and non-spherical particle shape of the dia-, para- and ferro-magnetic components present. For this reason it is important to understand the nature of the contribution from each type of component before attempting to distinguish them.

Some minerals have an intrinsic crystalline anisotropy (table 4.1) but non-spherical particle shape is the dominant cause of anisotropy of susceptibility in rocks. This is because external processes such as flow or compaction can affect the grain orientation in a rock. The shape of grains is affected by the crystal structure of the mineral *e.g.*, magnetite grains are usually equidimensional, haematite grains are commonly platy and micas and other phyllosilicates are usually platy (table 4.1). Therefore, processes which cause an alignment of particles give rise to a magnetic fabric which is due to both the preferential alignment of particles *and* to the intrinsic anisotropy of these particles. It is usual that particles in a sedimentary rocks are non-spherical. For crystalline anisotropy to affect magnetic fabric, there has to be a

behaviour	*mineral*	*anisotropy (SI units x10^{-8})*	*reference*
diamagnetic	**calcite**	K_{max}/K_{min} = 1.13 K_{max} = -1.38 K_{min} = -1.24	Owens *et al.*, 1976
	dolomite	as above	Rochette, 1988
	quartz	almost isotropic	Hrouda, 1986
paramagnetic	**Fe-calcite**	K_{max} parallel to c axis	Rochette, 1987
	siderite	large anisotropy, K_{max}/K_{min} = 4.2 K_{max} parallel to c axis	Jacobs, 1963
	Fe-phyllo-silicates	anisotropic, K_{max}/K_{min} = 1.1 to 1.37 K_{min} parallel to c axis *i.e.*, perpendicular to sheet plane	Foex, 1957 Ballet *et al.*, 1983
ferromagnetic	**goethite**	anisotropic, K_{max}/K_{min} = 1.28	Hedley, 1971
	haematite	anisotropic, K_{max} parallel to long axis or within the basal plane	Rochette, 1988 Neél *et al.*, 1952
	pyrrhotite	anisotropic, as haematite	Rochette, 1988
	magnetite	SD grains isotropic MD grains anisotropic as haematite	Rochette, 1988
other	**pyrite**	isotropic, weak positive susceptibility, independent of temperature, not dia- para- or ferro-magnetic.	Serres, 1953

table 4.1 Summary table of anisotropy, due to a combination of crystalline anisotropy and shape anisotropy, of the minerals which are commonly found in sedimentary rocks.

preferential alignment of the crystallographic axes of particles, such as occurs due to intense metamorphism.

Given that most magnetic fabrics are due to a preferred alignment of non-spherical grains of magnetic minerals, the magnetic fabric can theoretically be used to investigate processes that cause this preferential alignment *e.g.*, current flow or compaction. Laboratory studies by Rees (1965) showed that where sediments are deposited from still water, uniformly over a horizontal plane, the fabric produced has K_{max} and K_{int} parallel to the plane of depositon and K_{min} normal to it. For sediment transport studies, K_{max} is used to estimate the preferred long axis orientation of grains (Rees, 1965) and lies perpendicular to the direction of maximum compression; the K_{min} axis is thought of as being normal to the foliation plane which contains both K_{min} and K_{int} and is therefore oblate and parallel to the axis of maximum compression. Thus, for a set of samples exhibiting a flat depositional fabric, K_{min} should be close to vertical (Hamilton and Rees, 1970, Hailwood and Folami, 1984). This would also be the case where *compaction* perpendicular to the bedding direction had occurred *i.e.*, in an otherwise undisturbed sedimentary sequence.

Magnetic fabric is variously described by different authors using the declination and inclination of K_{max}, K_{int} and K_{min} directions in varying combinations. These include:

a. the mean susceptibility, $K_{mean} = K_{max} + K_{int} + K_{min} /3$;

b. eccentricity, E=F/L (if E<1 the ellipsoid is prolate, if E>1, the ellipsoid is oblate);

c. percentage anisotropy, $K_{max}- K_{min}/ K_{int}$ (Hamilton and Rees, 1970);

d. lineation, $L= K_{max} / K_{int}$ (Collinson, 1983) or $K_{max} - K_{int}/ K_{mean}$ (Khan, 1962);

e. foliation, $F= K_{int}/ K_{min}$ (Collinson, 1983) or $K_{int} - K_{min}/ K_{mean}$ (Khan, 1962);

f. the anisotropy factor or planarity, $P = K_{max}/ K_{min}$ (Collinson, 1983);

g. the 'q' factor= $K_{max} - K_{int}/ (K_{max} + K_{int})-2 K_{min}$ which relates the strength of the lineation to the foliation, and where $0.06 < q < 0.69$ for undisturbed sediments (Hamilton and Rees, 1970).

Only the simplest expressions have been used in this study I.e., lineation, foliation and anisotropy factor (Collinson, 1983); the 'q' factor (Hamilton and Rees, 1970) has also been calculated in some instances.

mineral	susceptibility ($x10^{-8}$ SI units)
quartz	-1.6
calcite	-1.3
siderite	487
ankerite	-0.48
anhydrite/gypsum	-1.5
magnesite	-1.4
pyrrhotite	125 - 628,400 (157,000)
ilmenite	3,140 - 377,000 (188,000)
haematite	50 - 3,800 (680)
magnetite	125,7000 - 2,010,900 (620,000)
maghemite	300,000
goethite	80 - 280
pyrite	5 - 530 (160)
kaolinite	-4.2
Illite	15
montmorillonite	6
biotite	229 - 333
muscovite	30 - 200
pyroxenes	180 - 325
amphiboles	49 - 320
garnets	148 -860
water	-0.9

table 4.2 Susceptibility values for the common constituents of sedimentary rocks illustrating the range of values. Ranges are given where known and the 'mode' is given in brackets. Compiled from Piper (1987) and Collinson (1983).

If any original *i.e.*, 'primary', fabric is identifiable, then this can be measured and contrasted with other (secondary) measured fabrics. These 'primary' and 'secondary' fabrics have been successfully identified as 'primary' depositional and 'secondary' diagenetic fabrics by Addison *et.al.* (1985).

If the *magnetic* minerals in a rock are aligned then this can affect the natural remanent magnetism direction of a rock and cause it to deviate from the ambient direction of Earth's magnetic field at the time of acquisition. This is because the remanence will tend to be acquired along the 'easy' direction (*i.e.*, axis of maximum susceptibility) of a particle rather than parallel with the direction of the applied field (Stacey, 1960; Uyeda *et al.*,1963 and Irving and Park,1973). This would apply in the case of the acquisition of a chemical remanent magnetism or thermo-remanent magnetism due to burial (chapter 5).

4.2 Methods

4.2.1 Measurement of susceptibility

Measurements were made on a Minisup (Newcastle University) and on a 'Kappa' Bridge (Norwegian Geological Survey) and only brief details are given here. Further details of the equipment used for the measurement of magnetic fabric and the measurement of bulk susceptibility are given in Collinson (1983). Bulk (axial) susceptibility was measured on a Minisup by introducing a sample along the axis of one of two coils, which have previously been balanced so that there is no flux linkage between them, and applying a small field (<1mT) to the sample. The magnetisation induced by this is measured along the axis of the sample (by calibration of the voltage change in the coil) and is therefore commonly referred to as the axial susceptibility. Anisotropy of susceptibility was also measured on a Minisup by introducing the sample into two perpendicular coils which have been balanced so that there is no flux linkage between them, and *rotating* the sample. The exciting coils produce an alternating field of 0.7mT and the pick up coils are set within these (*N.B.*, an isotropic sample would not affect the flux linkage between the coils). The sample is measured in three perpendicular orientations and this data is Fourier analysed generating a tensor described by nine components, with reference to the fiducial mark on the sample (fig. 1.11). This tensor was then transformed to its principal axes (Nye, 1969), where the principal components define the susceptibility ellipsoid and the lengths of the axes of the

ellipsoid are proportional to 1 over the square root of the values of the principal components (fig. 4.1).

In order to get an estimate of the repeatability of the bulk susceptibility measurements, two samples were measured 20 times on the Minisup (appendix 4.1). These results show that these measurements are repeatable, whether bulk susceptibility is positive or negative, *i.e.* whether bulk susceptibility is dominated by diamagnetic or paramagnetic minerals. In both cases the standard deviation was less than 0.03. Addison (1982) carried out a study of noise levels and concluded that in general, the longer the time that the sample was spun, the lower the noise level. A noise level of less than $5x10^{-8}$ could be obtained (Addison, 1982), theoretically allowing susceptibility difference of $5x10^{-7}$ to be measured.

A small selection of samples was measured on a 'Kappa' Bridge (by Trond Torsvik, at the Norwegian Geological Survey, Bergen) for comparison with data from the Minisup, because the 'Kappa' Bridge is the most sensitive equipment available for the masurement of susceptibility. Details of this equipment are available in Collinson (1983).

4.2.2 Determination of low field isothermal remanent magnetism anisotropy

After calibration of a Digico magnetometer (Collinson, 1983) samples were demagnetised by tumbling in an alternating magnetic field at 90mT peak field for about two minutes. Any natural remanent magnetism remaining was measured along the x, y and z directions of the sample (fig. 1.11). The sample was then given an isothermal remanent magnetism of 400mT along the x axis of the sample, and the isothermal remanent magnetism acquired was measured. The sample was then demagnetised again and then given the same isothermal remanent magnetism along the y axis. The process was repeated for the z axis of the sample. The natural remanent magnetism remaining after the initial demagetisation was then subtracted from these isothermal remanent magnetism values in order to calculate the isothermal remanent magnetism magnitudes along the x, y and z sample directions. This gives a tensor with M_{11}, M_{22} and M_{33} being the principal components (Nye, 1969), and these values indicate the field acquired along the x, y and z axes (*N.B.*, for an isotropic sample, the values M_{11}, M_{22} and M_{33} would be equal).

4.3 Anisotropy of susceptibility

The susceptibility of the majority of samples was measured on the Minisup because this equipment was available in the geophysics department at the University of Newcastle-upon-Tyne. A small number of samples were measured on a 'Kappa' Bridge (at the Norwegian Geological Survey) in order to get a comparison with data generated on the Minisup. The sensitivity of this equipment is greater than that of the Minisup and it was hoped that the data would be less noisy.

4.3.1 Data from the Minisup (table 4.3)

The declination and inclination of the principal susceptibilities were determined and repeatedly measured in order that average values could be determined. Between 3 and 5 repeat measurements of magnetic fabric were made of samples from a wide range of lithologies and facies, including grainstones, wackestones and boundstones from the back reef and reef facies (table 4.3; units x 10^{-6}GOe^{-1}; see appendix 4.2). Without exception, the declination and inclination of the three principal susceptibility directions were not repeatable, with A95 values never less than 10° and usually greater than 40°. This was the case for repeat measurements of individual samples and between samples from the same site *e.g.*, DC1,DC3, DC4, DC5 and DC6 (table 4.3). In all these cases axial susceptibility was negative, indicating that the susceptibility of the samples was dominated by diamagnetic minerals *i.e.*, calcite and dolomite.

These results indicate that these rocks have no *measurable* magnetic fabric. This is due to the fact that either these samples *possess* no magnetic fabric, or that the susceptibility values of these samples were below the limits of accurate detection of the instrument. A further complication is introduced by the fact that the samples used in the study of magnetic fabric were hand-samples subsequently drilled in the laboratory and it is possible that the hand-samples were not sufficiently accurately orientated in the field, considering the low suceptibility values, and that errors were thus introduced.

Some further measurements were made of different lithologies *e.g.*, sandstones and limestones of the basin facies (appendix 4.2) in order to ascertain whether lithologies other than grainstones, wackestones and boundstones, possessed a measurable magnetic fabric. These data show that the majority of measurements of K_{max}, K_{int} and K_{min} were not repeatable, although measurements of certain samples did give similar repeat results, and the quality of the data improved for samples which had a positive

sample	measurement		Kmax	Kint	Kmin	Kmean
DC1.1.1	1	D	31	136.6	265.2	-0.98
Isopachous		I	26.6	28.3	49.3	
marine	2	D	8	105.3	276.2	
cements		I	3.7	62.9	26.8	
back reef	3	D	159.9	252	68.9	
facies		I	1.5	55.6	34.3	
	summary	D	49.2	151.5	293.8	
		I	23.4	64.1	64.7	
		N	3	3	3	
		A95	90	78.9	90	

sample	measurement		Kmax	Kint	Kmin	Kmean
DC1.2.1	1	D	166.2	268.9	59.8	-0.73
Isopachous		I	15	39.6	46.5	
marine	2	D	200	51.9	291.4	
cements		I	11.6	76.5	6.9	
back reef	3	D	32	142.5	277.3	
facies		I	24.4	37.8	42.4	
	summary	D	160.8	191.9	307.1	
		I	37.3	77.1	48.8	
		N	3	3	3	
		A95	90	90	90	

sample	measurement		Kmax	Kint	Kmin	Kmean
DC1.2.2	1	D	321.9	114.8	209.2	-1.08
Isopachous		I	64.9	22.7	10.4	
marine	2	D	114	313.4	205.4	
cements		I	15	74.2	5.1	
back reef	3	D	58.4	152.1	213.7	
facies		I	17.7	11.8	68.6	
	4	D	11.3	179.7	149.9	
		I	9.7	8.3	77	
	5	D	37.3	128.6	226.9	
		I	22.4	3.6	67.3	
	summary	D	45.6	149.3	213.3	
		I	33.4	44.8	49.7	
		N	5	5	5	
		A95	53.5	90	42.1	

sample	measurement		Kmax	Kint	Kmin	Kmean
DC1.3.1	1	D	346.2	248.9	78.5	-0.97
Isopachous		I	4.1	60.4	29.3	
marine	2	D	324.2	207.2	72.1	
cements		I	24	45.4	34.9	
back reef	3	D	322.7	166	56	
facies		I	21.4	66.8	8.4	
	summary	D	331.4	210.1	68.2	
		I	16.8	61.3	24.5	
		N	3	3	3	
		A95	25.9	35.1	27.4	

table 4.3 Summary table of repeat measurements of the declination and inclination (in degrees) of the principal susceptibility directions (susceptibility anisotropy) for samples measured on the Minisup. Data summaries are field corrected. The mean susceptibility is also given. Samples are from the back reef and reef facies in Dark Canyon (DC). D = declination; I = inclination; K = principal susceptibilities (volume units x 10^{-6}GOe^{-1}; see appendix 4.2). N is the number of repeat measurements.

sample	measurement		Kmax	Kint	Kmin	Kmean
DC1.5.1	1	D	321.1	119.9	214.1	-1.18
isopachous		I	62.8	25.7	8.6	
marine	2	D	219.5	117.7	27	
cements		I	76.1	3	13.5	
back reef	3	D	322.7	56.3	185.2	
facies		I	15	12.9	69.9	
	4	D	359.8	92	192.2	
		I	25	4.9	64.4	
	5	D	304.1	37.5	161.4	
		I	16.1	11.4	70	
	summary	D	322.6	84.8	186.9	
		I	43.2	13.6	71.7	
		N	5	5	5	
		A95	40.4	37.9	63.7	

sample	measurement		Kmax	Kint	Kmin	Kmean
DC1.6.1	1	D	348.5	253.5	121	-0.62
isopachous		I	16.3	16.3	66.5	
marine	2	D	356.4	265.3	112.3	
cements		I	5.3	10.8	77.8	
back reef	3	D	48.7	308.2	178.6	
facies		I	23.1	22.9	56.3	
	summary	D	9.8	274.7	146.8	
		I	16.5	18	69.8	
		N	3	3	3	
		A95	53.1	44.8	27.5	

sample	measurement		Kmax	Kint	Kmin	Kmean
DC2.8.1	1	D	43.4	143.4	276.7	-0.5
wackestone		I	21.2	24.2	56.9	
back reef	2	D	178.3	283.6	67.3	
facies		I	19	37.7	46.1	
	3	D	151.8	244.4	351	
		I	21.4	6.7	67.5	
	4	D	152.3	57.2	280	
		I	15.2	17.9	66.3	
	5	D	174.7	67.1	276.8	
		I	15.2	48.2	37.7	
	summary	D	150.5	124.4	307.3	
		I	25.3	80.8	70.3	
		N	5	5	5	
		A95	52.8	90	36.2	

sample	measurement		Kmax	Kint	Kmin	Kmean
DC3.1.1	1	D	97.9	217.6	344.2	-0.61
grainstone		I	30	40.5	34.9	
back reef	2	D	201.6	89.9	335.8	
facies		I	38.6	24.9	41.3	
	3	D	193.6	71.2	328.8	
		I	53.4	21.8	27.9	
	summary	D	163.2	102.8	336	
		I	52.3	46.8	34.9	
		N	3	3	3	
		A95	78.8	90	14.2	

table 4.3 (continued)

sample	measurement		Kmax	Kint	Kmin	Kmean
DC3.2.1	1	D	314.6	149.1	50.8	-1
grainstone		I	40.1	49	7.3	
back reef	2	D	354.6	129.4	229.7	
facies		I	56.5	25.1	20.8	
	3	D	236.4	329.8	81.7	
		I	20.7	8.8	67.3	
	4	D	242.3	184.4	123.6	
		I	20.3	7.2	52.4	
	5	D	234.3	339.3	134.6	
		I	12.3	50.1	37.3	
	summary	D	261.7	161.4	118.4	
		I	38.3	72.3	58.5	
		N	5	5	5	
		A95	47.8	90	65.2	

sample	measurement		Kmax	Kint	Kmin	Kmean
DC3.3.1	1	D	101.8	199.6	316.2	-0.6
grainstone		I	26.5	15.2	58.8	
back reef	2	D	162.3	66.5	331.4	
facies		I	47	5.5	42.6	
	3	D	148.9	52.1	316.5	
		I	48.1	6.2	41.3	
	summary	D	134.5	85.9	321.9	
		I	43.8	18.7	47.8	
		N	3	3	3	
		A95	44	90	17.6	

sample	measurement		Kmax	Kint	Kmin	Kmean
DC3.4.1	1	D	90	200.7	327	-0.79
grainstone		I	29.6	31.8	43.8	
back reef	2	D	250.8	155.4	347	
facies		I	5.8	42.1	47.4	
	3	D	76.7	171.5	340.4	
		I	5.3	42.4	47.2	
	summary	D	96.3	176.9	338.1	
		I	37.3	40.4	46.4	
		N	3	3	3	
		A95	90	29.6	11.4	

sample	measurement		Kmax	Kint	Kmin	Kmean
DC3.5.1	1	D	219.5	324.9	95.4	-0.71
grainstone		I	25.7	29.1	49.4	
back reef	2	D	12.2	103	248.4	
facies		I	5.6	8.5	79.8	
	3	D	210	301.6	21.6	
		I	4.3	109.6	68	
	summary	D	235.8	341.3	106.8	
		I	30.2	44.1	71.9	
		N	3	3	3	
		A95	90	90	40.1	

table 4.3 (continued)

sample	measurement		Kmax	Kint	Kmin	Kmean
DC4.1.1	1	D	280.9	129.6	30.3	-1.01
wackestone		I	53.3	33.1	13.8	
back reef	2	D	191.4	348.6	84.1	
facies		I	59.5	28.4	9.8	
	3	D	77.3	181.8	301.1	
		I	31.2	22.5	49.8	
	4	D	107.5	11	267.9	
		I	34.3	9.2	54.1	
	5	D	150.9	356	258.4	
		I	22.7	45.5	35.6	
	summary	D	132.1	47.8	336.9	
		I	59.2	58.4	65.3	
		N	5	5	5	
		A95	54.2	88.1	81.8	

sample	measurement		Kmax	Kint	Kmin	Kmean
DC4.2.1	1	D	175.3	84.8	265.6	-0.75
wackestone		I	0.5	51.3	38.6	
back reef	2	D	174.2	315.5	80.5	
facies		I	16.2	69.8	12	
	3	D	356.3	132.3	261.7	
		I	16.4	67.8	14.5	
	summary	D	173.3	85.8	267.1	
		I	29.6	76	54.5	
		N	3	3	3	
		A95	90	49.4	90	

sample	measurement		Kmax	Kint	Kmin	Kmean
DC4.3.1	1	D	285.3	182.7	74.8	-0.27
wackestone		I	38	15.7	47.7	
back reef	2	D	292.2	170.3	58	
facies		I	42.1	30.4	32.9	
	3	D	51.7	166.6	312.3	
		I	16.4	56.3	28.8	
	4	D	95.9	354.8	233.5	
		I	27.9	20.3	54.4	
	5	D	54.2	167.7	306.1	
		I	22.1	44.6	37.3	
	summary	D	31.4	172	343.4	
		I	53.3	51.2	66.4	
		N	5	5	5	
		A95	74.8	61.4	59.3	

sample	measurement		Kmax	Kint	Kmin	Kmean
DC4.4.1	1	D	322.8	147.8	54.4	-1.01
wackestone		I	33	57	2.2	
back reef	2	D	329.1	182.9	73.2	
facies		I	37.9	47.1	17.4	
	3	D	342	225	89.8	
		I	23.8	45.6	34.8	
	summary	D	331.6	188.3	71.3	
		I	31.8	54.1	18.7	
		N	3	3	3	
		A95	17	38.8	36.7	

table 4.3 (continued)

sample	measurement		Kmax	Kint	Kmin	Kmean
DC4.5.1	1	D	76.5	190.1	302	-0.82
wackestone		I	40.8	24.9	39	
back reef	2	D	160.7	58.5	320.5	
facies		I	50.3	10	38.1	
	3	D	116.5	18	277.1	
		I	40.9	9.7	47.5	
	summary	D	115.2	60.4	301.1	
		I	49.2	33.9	42.9	
		N	3	3	3	
		A95	47.3	90	26	

sample	measurement		Kmax	Kint	Kmin	Kmean
DC4.6.1	1	D	251.5	18.4	121.1	-1
wackestone		I	52.9	24.3	26.1	
back reef	2	D	265.5	153.8	61.4	
facies		I	66.3	5.7	22.9	
	3	D	285.7	38.2	141.7	
		I	48.9	18.3	35.3	
	summary	D	266.2	61.5	107.6	
		I	57	28.8	32.8	
		N	3	3	3	
		A95	21.7	90	62.2	

sample	measurement		Kmax	Kint	Kmin	Kmean
DC5.1.1	1	D	4	237.5	96.1	-0.71
boundstone		I	1	18.8	71.6	
reef facies	2	D	120	210.3	302.7	
		I	16.6	0.9	73.3	
	3	D	290	199.1	28.8	
		I	2.7	17.1	72.6	
	4	D	141.8	236.5	24.4	
		I	12	21.2	65.2	
	5	D	159.3	253.9	11.6	
		I	20.9	11.8	65.6	
	summary	D	131.1	234.4	21.9	
		I	37.7	15.6	74.9	
		N	5	5	5	
		A95	90	30.6	15.3	

sample	measurement		Kmax	Kint	Kmin	Kmean
DC5.2.1	1	D	271.1	4.6	95.9	-0.98
boundstone		I	58	2	31.8	
reef facies	2	D	179.9	299.1	47.9	
		I	45.1	25.8	33.6	
	3	D	183.6	279.9	63.8	
		I	14.6	22.8	62.4	
	4	D	51.4	142	272.7	
		I	6	5.4	81.9	
	5	D	103.9	194.8	293.8	
		I	17.4	3	72.3	
summary		D	138.7	262.8	61.1	
		I	52.6	38.4	66.9	
		N	5	5	5	
		A95	83.6	90	36.6	

table 4.3 (continued)

sample	measurement		Kmax	Kint	Kmin	Kmean
DC6.1.1	1	D	4.3	271.6	118	-0.94
boundstone		I	8.2	17.9	70	
reef facies	2	D	22.2	113.8	262.9	
		I	7.2	12.6	75.3	
	3	D	56.8	154.8	301.8	
		I	14.8	28	57.7	
	summary	D	27.3	164.8	282.6	
		I	10.8	39.5	81.4	
		N	3	3	3	
		A95	42.3	90	43.2	

sample	measurement		Kmax	Kint	Kmin	Kmean
DC6.2.1	1	D	131.8	228.2	36.3	-0.58
boundstone		I	6.1	46.2	43	
reef facies	2	D	264.4	171.1	53.9	
		I	18.2	9.9	69.1	
	3	D	333.1	226.4	66	
		I	7	66.5	22.2	
	summary	D	281.1	200.9	53.1	
		I	39	44.7	45.5	
		N	3	3	3	
		A95	90	64.8	41.8	

sample	measurement		Kmax	Kint	Kmin	Kmean
DC6.3.1	1	D	195.1	285.3	19.4	-0.53
boundstone		I	9.4	0.7	80.7	
reef facies	2	D	80.3	173.3	340.9	
		I	5.3	29.3	60.1	
	3	D	72.7	173.64	321.7	
		I	15.7	33.9	51.8	
	summary	D	106.8	108.3	336	
		I	17	33.1	65.3	
		N	3	3	3	
		A95	90	90	27.5	

table 4.3 (continued)

bulk susceptibility. However, the data obtained from measurements on the Minisup were considered generally poor-quality and therefore not reliable and rejected from further study. Consequently, some measurements were made on a 'Kappa' Bridge (4.3.2) and some measurements were also made of samples which had been heated to 650°C (4.3.3), for comparison.

4.3.2 Data from the 'Kappa' Bridge (table 4.4)

The sensitivity of the 'Kappa' Bridge is greater than that of the Minisup (pers. comm., D.H. Tarling, 1986) and it was hoped that the data from *this* instrument would be less noisy. A small number of samples (table 4.4) were measured on a 'Kappa' Bridge (by Trond Torsvik at the Norwegian Geological Survey) in order to get a comparison with data generated on the Minisup. These results have not been corrected for sampling orientation. Unfortunately, no repeat measurements were made, so it is not possible to assess the repeatability of these data.

These results suggest that all the samples are slightly anisotropic (table 4.4; SI units x 10^{-6}) with the ratios of linearity, foliation and planarity around 1.005 in most cases *i.e.*, no samples displayed *large* anisotropy and magnetic fabric was generally weak. However, once the size of the errors has been taken into account, none of the ratios of L, F or P are significantly different from 1 *i.e.*, these samples show no *measureable* anisotropy.

Further work is recommended, using repeat measurements, in order to establish the repeatability of data generated on the 'Kappa' bridge, and this should be related to the sedimentology and structure of the sedimentary rocks from which the samples were taken *i.e.*, detailed field observations must be made.

4.3.3 Thermal 'enhancement' of magnetic fabrics (table 4.5)

The anisotropy of susceptibility was measured (using a Minisup) of samples which had been heated to 650°C. This was done in order to investigate whether fabric was enhanced after heating (Perarnau and Tarling, 1985; table 4.5; volume units x $10^{-6}GOe^{-1}$; see appendix 4.2). The samples selected for this treatment were those which showed signs of having a 'primary' magnetic fabric or a petrographic fabric, and which had a high initial susceptibility, relative to other samples in this study. These included dark, micritic limestones from the basin margin and basin facies and sandstones

table 4.4 Summary table of measurements of the declination and inclination (in degrees) of the principal susceptibility directions (susceptibility anisotropy) for samples measured on the Kappa bridge. These data are not field corrected, and the appropriate field corrections are given. Samples are from the back reef and reef facies in Dark Canyon (DC) and the 'scenic loop' (SL; Carlsbad Caverns National Park); shelf facies from Rocky Arroyo (RA); basinal facies sandstones and limestones from sites on the highway US62/180 (RL); back reef, reef and foreslope and basin margin facies from the 'reef trail' of McKittrick Canyon (MC). D = declination; I = inclination; K = principal susceptibilities (SI units x 10^{-6}). L = linearity ($L = K_{max}/K_{int}$); F = foliation ($F = K_{int}/K_{min}$); P = planarity ($P = K_{max}/K_{min}$).

			normalised	principal	susceptibilities	
sample			Kmax	Kint	Kmin	Kmean
RL1.G			1.0709	1.02	0.9091	13.4
Bone		error	0.003	0.003	0.003	
Spring						
Limestone						
basin facies	principal	D	87	301	188	
	directions	I	32	53	17	
	sample					
	orientation	156/78				
				error		
		L	1.05	0.049		
		F	1.122	0.115		
		P	1.178	0.164		

			normalised	principal	susceptibilities	
sample			Kmax	Kint	Kmin	Kmean
RL2.A.2			1.0156	1.0147	0.9697	39.73
Brushy		error	0.001	0.001	0.001	
Canyon						
Sandstone						
basin	principal	D	90	0	180	
facies	directions	I	0	0	89	
	sample					
	orientation	049/06				
				error		
		L	1.001	0.001		
		F	1.046	0.045		
		P	1.047	0.046		

			normalised	principal	susceptibilities	
sample			Kmax	Kint	Kmin	Kmean
RL4.C.1.3			1.0099	1.0087	0.9813	64.4
Cherry		error	0.0003	0.0003	0.0003	
Canyon						
Sandstone						
basin	principal	D	174	344	82	
facies	directions	I	28	62	4	
	sample					
	orientation	323/87				
				error		
		L	1.001	0.001		
		F	1.028	0.028		
		P	1.029	0.029		

table 4.4 (continued)

			normalised	principal	susceptibilities	
sample			Kmax	Kint	Kmin	Kmean
RL6.10.1			1.006	1.0027	0.9913	58.86
Rader		error	0.0007	0.0007	0.0007	
Slide						
sandstone						
basin	principal	D	235	359	89	
facies	directions	I	85	3	4	
	sample					
	orientation	137/76				
				error		
		L	1.003	0.003		
		F	1.012	0.011		
		P	1.015	0.015		

			normalised	principal	susceptibilities	
sample			Kmax	Kint	Kmin	Kmean
RL6.M.2			1.0078	1.004	0.9883	19.82
Rader		error	0.0008	0.0008	0.0008	
Slide						
turbidite						
basin	principal	D	181	341	90	
facies	directions	I	15	74	5	
	sample					
	orientation	018/17				
				error		
		L	1.004	0.004		
		F	1.016	0.016		
		P	1.02	0.02		

			normalised	principal	susceptibilities	
sample			Kmax	Kint	Kmin	Kmean
RL8.A.1			-0.9979	-1	-1.0021	-9.08
Castile		error	0.0025	0.0025	0.0025	
Formation						
basin						
facies	principal	D	180	90	0	
	directions	I	45	0	45	
	sample					
	orientation	192/67				
				error		
		L	1.002	0.002		
		F	1.002	0.002		
		P	1.004	0.004		

			normalised	principal	susceptibilities	
sample			Kmax	Kint	Kmin	Kmean
RA1.4			1.073	1.0038	0.9589	1.11
dolomite		error	0.0211	0.0211	0.0211	
Azotea						
Fmn.						
shelf	principal	D	338	78	217	
facies	directions	I	19	27	56	
	sample					
	orientation	311/84				
				error		
		L	1.033	0.033		
		F	1.047	0.046		
		P	1.082	0.079		

table 4.4 (continued)

			normalised principal susceptibilities			
sample			Kmax	Kint	Kmin	Kmean
RA2.C			1.0022	1.0002	0.9976	49.43
Shattuck		error	0.0005	0.0005	0.0005	
sandstone						
shelf						
facies	principal	D	268	174	358	
	directions	I	0	86	4	
	sample					
	orientation	123/85				
				error		
		L	1.002	0.002		
		F	1.003	0.003		
		P	1.005	0.005		

			normalised principal susceptibilities			
sample			Kmax	Kint	Kmin	Kmean
RA3.D			1.0131	1.0046	0.9823	4.22
dedolomite		error	0.0054	0.0054	0.0054	
Shattuck						
sandstone						
shelf	principal	D	270	0	90	
facies	directions	I	13	0	77	
	sample					
	orientation	084/86				
				error		
		L	1.008	0.008		
		F	1.023	0.022		
		P	0.022	0.031		

			normalised principal susceptibilities			
sample			Kmax	Kint	Kmin	Kmean
DC1.B.2			-0.9914	-0.9987	-1.0099	-9.48
Isopachous		error	0.001	0.001	0.001	
marine						
cements						
back reef	principal	D	71	311	199	
facies	directions	I	42	29	34	
	sample					
	orientation	336/53				
				error		
		L	1.011	0.011		
		F	1.007	0.007		
		P	1.019	0.019		

			normalised principal susceptibilities			
sample			Kmax	Kint	Kmin	Kmean
SL1.h.1			-0.9947	-0.9985	-1.0068	-5.27
Yates		error	0.0064	0.0064	0.0064	
Formation						
teepee						
back reef	principal	D	250	60	153	
facies	directions	I	60	30	4	
	sample					
	orientation	065/51				
				error		
		L	1.008	0.008		
		F	1.004	0.004		
		P	1.012	0.012		

table 4.4 (continued)

sample			normalised principal susceptibilities Kmax	Kint	Kmin	Kmean
SL2.E			-0.9867	-1.004	-1.0093	-4.52
Yates		error	0.0037	0.0037	0.0037	
Formation						
pisolite						
back reef	principal	D	283	189	18	
facies	directions	I	5	38	52	
	sample					
	orientation	082/45				
				error		
		L	1.005	0.005		
		F	1.018	0.017		
		P	1.023	0.023		

sample			normalised principal susceptibilities Kmax	Kint	Kmin	Kmean
MC10.1			-0.9928	-1.001	-1.0063	-9.2
grainstone		error	0.0021	0.0021	0.0021	
reef facies						
	principal	D	82	190	338	
	directions	I	16	46	40	
	sample					
	orientation	271/24				
				error		
		L	1.005	0.005		
		F	1.008	0.008		
		P	1.014	0.013		

sample			normalised principal susceptibilities Kmax	Kint	Kmin	Kmean
MC15.2			-0.9845	-1.0015	-1.014	-9.02
boundstone		error	0.0039	0.0039	0.0039	
reef facies						
	principal	D	269	123	1	
	directions	I	15	72	10	
	sample					
	orientation	331/81				
				error		
		L	1.012	0.012		
		F	1.017	0.017		
		P	1.03	0.03		

sample			normalised principal susceptibilities Kmax	Kint	Kmin	Kmean
MC17.1.1			-0.9976	-0.9998	-1.0026	-8.94
grainstone		error	0.0023	0.0023	0.0023	
upper						
foreslope						
facies	principal	D	35	248	131	
	directions	I	23	63	13	
	sample					
	orientation	315/33				
				error		
		L	1.003	0.003		
		F	1.002	0.002		
		P	1.005	0.005		

table 4.4 (continued)

			normalised principal susceptibilities			
sample			Kmax	Kint	Kmin	Kmean
MC22.2			-0.9971	-1.0003	-1.0025	-8.98
boundstone		error	0.0026	0.0026	0.0026	
boulder						
in						
foreslope		D	347	144	236	
facies		I	72	17	7	
	principal					
	directions	042/48				
	sample			error		
	orientation	L	1.002	0.002		
		F	1.003	0.003		
		P	1.005	0.005		

			normalised principal susceptibilities			
sample			Kmax	Kint	Kmin	Kmean
MC32.1			-0.9942	-0.9972	-1.0086	-4.49
Lamar		error	0.0038	0.0038	0.0038	
limestone						
basin						
margin		D	45	147	258	
facies		I	35	17	50	
	principal					
	directions	052/11				
	sample			error		
	orientation	L	1.011	0.011		
		F	1.003	0.003		
		P	1.014	0.014		

			normalised principal susceptibilities			
sample			Kmax	Kint	Kmin	Kmean
MC36.A.1			1.0503	0.9862	0.9635	1.42
Lamar		error	0.0207	0.0207	0.0207	
limestone						
basin						
margin		D	81	192	346	
facies		I	11	62	26	
	principal					
	directions	058/35				
	sample			error		
	orientation	L	1.065	0.063		
		F	1.024	0.023		
		P	1.09	0.086		

table 4.4 (continued)

from the basin and shelf facies *I.e., not* including carbonate rocks from the back reef, reef and foreslope facies of the Capitan shelf margin.

Site MC31 is from the basin margin facies in McKittrick Canyon. Two samples from this site were heated and three and two repeat measurements were made respectively (table 4.5). The principal susceptibility axes are well-defined with *A95* being less than 3° for all three axes. Both samples gave the same directions. K_{max} lies in the horizontal plane; K_{int} is inclined at around 25° and K_{min} is inclined at around 65°. This suggests that the fabric results from primary depositional or compactional processes (4.1.2). The axial susceptibility after heating was measured at 79.55 (volume units x $10^{-6}GOe^{-1}$; see appendix 4.2) in the first sample and 69.71 (volume units x $10^{-6}GOe^{-1}$; see appendix 4.2) in the second sample. These are high values compared to the rest of the sample collection. The initial value of axial susceptibility was not measured for this sample, but sample MC34 is from the same facies and had an initial susceptibility of -0.5 (volume units x $10^{-6}GOe^{-1}$; see appendix 4.2) and possessed no measurable fabric (Appendix 4.2). The large susceptibility increase indicates the growth of a phase with high susceptibility (table 4.2) such as magnetite or maghemite (table 5.3).

Sample RA2.2.1 was taken from a site in the Shattuck sandstone in the distal back reef facies in Rocky Arroyo. Four repeat measurements were made and the principal susceptibility axes are undefined. The axial susceptibility was 3.02 (volume units x $10^{-6}GOe^{-1}$; see appendix 4.2) prior to heating and 7.71 (volume units x $10^{-6}GOe^{-1}$; see appendix 4.2) after heating, which indicates growth of new magnetic phases due to heating. The low susceptibility value, and the colour change from yellow to orange, suggests the growth of haematite from goethite (table 4.2). The anisotropy of this sample was also measured on the 'Kappa' bridge prior to heating (table 4.4) but no magnetic fabric was detected. Heating caused an increase in bulk susceptibility due to new mineral growth.

Sample MC16.3.2 is a grainstone and was taken from the upper foreslope facies in McKittrick Canyon. The axial susceptibility after heating was 1.0 (volume units x $10^{-6}GOe^{-1}$; see appendix 4.2). Three repeat measurements of the fabric were made, and the principal susceptibility axes were found to be undefined with *A95* greater than 30° in all cases. The magnetic fabric prior to heating was not measured for *this* sample, although similar samples from site MC17 and site MC18 were measured on the 'Kappa' bridge and Minisup respectively (table 4.4 and 4.3) and neither sample showed any magnetic fabric. The initial susceptibility was about -1 (volume units x $10^{-6}GOe^{-1}$;

table 4.5 Summary table of repeat measurements of the declination and inclination (in degrees) of principal susceptibilities (susceptibility anisotropy) for samples heated to 650°C and measured on the Minisup. These data are field corrected. Samples are from the shelf facies from Rocky Arroyo (RA); basinal facies sandstones and limestones from sites on the highway US62/180 (RL); and basin margin facies from the 'reef trail' of McKittrick Canyon (MC). D = declination; I = inclination; K = principal susceptibilities (volume units x 10^{-6}GOe^{-1}; see appendix 4.2). L = linearity ($L=K_{max}/K_{Int}$); F = foliation ($F = K_{int}/K_{min}$); P = planarity ($P = K_{max}/K_{min}$).

sample	measurement		Kmax	KInt	Kmin	Kmean	mean
MC31.1.1	1	D	271.3	176.4	24.4	79.55	before
Lamar		I	11	23.7	63.5		heating
limestone	2	D	272	177.1	28.6		unknown
basin		I	12	22	64.5		
margin facies	3	D	269.3	175.3	20.3		
		I	9.4	22.8	65		
	summary	D	40.8	309.2	139.8		
	(field	I	3.8	23.1	66.5		
	corrected)	N	3	3	3		
		A95	2.9	1.8	3		
		standard deviation					
	L = 1.0057	0.0012					
	F = 1.0088	0.0021					
	P = 1.0145	0.0021					
	q = 0.049	0.0333					

sample	measurement		Kmax	KInt	Kmin	Kmean	mean
MC31.3.1	1	D	93.9	180.7	17.3	69.71	before
Lamar		I	-6.5	25.5	63.5		heating
limestone	2	D	266.7	172.5	18.9		unknown
basin		I	9.9	22.5	65.1		
margin facies							
	summary	D	309.7	309.7	133.3		
	(field	I	25.5	24.3	65.6		
	corrected)	N	2	2	2		
		A95					
		standard deviation					
	L = 1.0044	0.0014					
	F = 1.0149	0.002					
	P = 1.0193	0.0014					
	q = .2602	0.013					

table 4.5 (continued)

sample	measurement		Kmax	Kint	Kmin	Kmean	mean
RA2.2.1	1	D	-140.3	239.9	138.3	7.71	before
Shattuck		I	-40	48.1	10.1		heating
sandstone	2	D	-164.5	258.2	155.6		3.02
shelf facies		I	-51.7	19.8	31.1		
	3	D	-137.1	204.9	128		
		I	-31	57.7	-8.1		
	4	D	-56.3	112.6	120.7		
		I	-2.7	-21.2	68.5		
	summary	D	335.9	88.6	181		
	(field	I	41.1	43.5	45.7		
	corrected)	N	4	4	4		
		A95	27.4	90	43		

	standard deviation
L =	-
F =	-
P =	-
q =	-

sample	measurement		Kmax	Kint	Kmin	Kmean	mean
MC16.3.2	1	D	110.5	22.1	347.6	1	before
grainstone		I	7.7	-11.6	75.9		heating
upper foreslope	2	D	96.1	357.2	257.5		unknown
facies		I	42.9	9.4	45.4		
	3	D	110.9	18.9	232.2		
		I	11	26.4	56.5		
	summary	D	105.6	354.4	253.7		
	(field	I	52.3	12.2	33.8		
	corrected)	N	3	3	3		
		A95	30.3	35.9	42.7		

	standard deviation
L =	-
F =	-
P =	-
q =	-

sample	measurement		Kmax	Kint	Kmin	Kmean	mean
RL1.4.1	1	D	92.6	140.6	190.9	7.72	before
Bone Spring		I	21.2	-59.8	20.3		heating
limestone	2	D	81.4	285	184.4		0.73
basin facies		I	46.4	41	11.9		
	3	D	-97.4	328	174.3		
		I	-6.2	75.3	13.1		
	summary	D	176.8	104.4	348.6		
	(field	I	20.8	15.6	83.5		
	corrected)	N	3	3	3		
		A95	90	90	14.3		

	standard deviation
L = 1.0095	0.0032
F = 1.0131	0.0049
P = 1.0228	0.0024
q = 0.0567	0.2434

table 4.5 (continued)

sample	measurement		Kmax	Kint	Kmin	Kmean	mean
RL2.3.4.1	1	D	190.9	348.3	84.2	15.41	before
Brushy Canyon		I	58.1	29.8	10.1		heating
sandstone	2	D	28.5	298.8	118.5		2.38
basin facies		I	-0.1	79.2	10.7		
	3	D	36.5	44	127.9		
		I	-25.1	64.6	-2.9		
	summary	D	239.3	179.6	21.3		
	(field	I	42.8	20.2	63.5		
	corrected)	N	3	3	3		
		A95	90	53.1	38.2		

	standard deviation
L = 1.0043	0.0021
F = 1.0059	0.0027
P = 1.0102	0.0043
q = 0.5493	0.0327

sample	measurement		Kmax	Kint	Kmin	Kmean	mean
RL3.6.1	1	D	-101.3	304.9	170.3	40.36	before
Cherry Canyon		I	-9.2	76.7	9.4		heating
sandstone	2	D	263.3	39.7	172		2.34
basin facies		I	8.8	77.8	8.2		
	3	D	271.6	-107.2	173.6		
		I	40.1	-48.2	9.4		
	summary	D	60.6	109	255.1		
	(field	I	8.7	7.3	81.2		
	corrected)	N	3	3	3		
		A95	40.9	90	2.7		

	standard deviation
L = 1.0012	0.0017
F = 1.0153	0.0024
P = 1.0166	0.0017
q = 0.0816	0.0626

sample	measurement		Kmax	Kint	Kmin	Kmean	mean
RL4.3.6.1	1	D	175.3	348.4	85.2	20.27	before
Cherry Canyon		I	6.2	83.7	0.7		heating
sandstone	2	D	357	184.7	87.1		2.49
basin facies		I	84.2	84.2	0.7		
	3	D	175.4	175.6	85.4		
		I	-21.3	68.6	0.1		
	summary	D	165	226.2	354.4		
	(field	I	5.5	2.9	85.2		
	corrected)	N	3	3	3		
		A95	90	21.2	1.7		

	standard deviation
L = 1.0048	0.0024
F = 1.1427	0.0032
P = 1.1481	0.0012
q = 0.0375	0.0139

table 4.5 (continued)

sample	measurement		Kmax	Kint	Kmin	Kmean	mean
RL5.1.1	1	D	292.2	70.6	176.1	4.65	before
Hegler		I	47.8	34	21.6		heating
limestone	2	D	55.4	270.5	173.7		1.99
basin facies		I	60.9	24.4	14.7		
	3	D	72	296.1	182		
		I	37.8	42.7	23.7		
	summary	D	118.1	81	264		
	(field	I	7.6	6.2	82.6		
	corrected)	N	3	3	3		
		A95	80.7	90	9.4		

	standard deviation
L = 1.0130	0.0027
F = 1.0373	0.0042
P = 1.0508	0.0038
q = 0.3062	0.0541

sample	measurement		Kmax	Kint	Kmin	Kmean	mean
RL6.12.3.1	1	D	136.9	44.9	257.3	37.02	before
sandstone		I	8.1	13.5	74.1		heating
Rader Slide	2	D	351	82.6	229.4		unknown
basin facies		I	7.4	11.7	76		
	3	D	345.4	76.1	215.8		
		I	5.8	6.9	80.9		
	summary	D	191.1	248.3	70.9		
	(field	I	18.1	18.5	70.3		
	corrected)	N	3	3	3		
		A95	90	31.3	8.9		

	standard deviation
L = 1.0016	0.0017
F = 1.0089	0.0017
P = 1.0105	0.0021
q = 0.1638	0.0581

sample	measurement		Kmax	Kint	Kmin	Kmean	mean
RL6.13.2.3	1	D	10.5	181.7	92.4	31.55	before
turbidite		I	73.6	16.1	-2.3		heating
Rader Slide	2	D	347.6	10.1	99.9		1.69
basin facies		I	83.7	-5.8	2.3		
	3	D	349.8	4	93.6		
		I	79.6	-9.9	2.4		
	summary	D	299.1	20.5	131.7		
	(field	I	12.7	11.8	76.7		
	corrected)	N	3	3	3		
		A95	8.6	90	7.4		

	standard deviation
L = 1.0097	0.0017
F = 1.0246	0.0027
P = 1.0345	0.0032
q = 0.3373	0.0174

table 4.5 (continued)

see appendix 4.2). This indicates the formation of small amounts of some phases with higher susceptibility (table 4.2).

Sample RL1.4.1 was collected from the Bone Spring Limestone (basin facies). Three repeat measurements were made and K_{min} was found to be the only principal susceptibility axis that was well-defined with an *A95* of 14.3°. This axis is almost vertical. This is consistent with a depositional/compactional fabric (4.1.2). The axial susceptibility increased by an order of magnitude, from 0.73 to 7.73 (volume units x $10^{-6}GOe^{-1}$; see appendix 4.2) on heating to 650°C. Two repeat measurements were made of this sample (on the Minisup) prior to heating (appendix 4.2) but no fabric was detected. Thus it is not possible to tell whether the fabric in this case has been *enhanced* on heating, although the susceptibility values are greater and thus easier to measure. A sample from this site was also measured on the 'Kappa' bridge (table 4.4) prior to heating but no fabric was detected. The low susceptibility values suggest the presence of haematite (table 4.2).

Sample RL2.3.4.1was taken from the Brushy Canyon sandstone (basin facies) at the base of a large channel. Three repeat measurements were made. However a magnetic fabric is not defined with *A95* being greater than 38° in all cases, even though the axial susceptibility increased from 2.38 to 15.41 (volume units x $10^{-6}GOe^{-1}$; see appendix 4.2) on heating. No clear fabric was detected on the Minisup prior to heating (sample RL2.4.1, appendix 4.2).

Sample RL3.6.1 was taken from the Cherry Canyon sandstone (basin facies). Three repeat measurements were made but only K_{min} is well-defined with an *A95* of 2.7°. K_{min} is inclined at 81.2° *i.e.* is almost vertical. This is consistent with a depositional/compactional fabric (4.1.2). Axial susceptibility increased from 2.34 to 40.36 (volume units x $10^{-6}GOe^{-1}$; see appendix 4.2) on heating. This large increase suggests the growth of a high-susceptibility mineral such as magnetite or maghemite due to the heating process. The fabric was measured om the Minisup prior to heating (appendix 4.2) and K_{min} appears to be repeatable for 2 measurements. However, the directions defined before and after heating differ significantly, by >90° of declination and 60° of inclination. It is therefore not accurate to conclude that the fabric has been *enhanced,* despite the large increase of susceptibility on heating. The differences in directions of data before and after heating may, in part, be a reflection of the different instrumentation used to make these measurements (4.3.1).

Sample RL4.3.6.1 was taken from a fine-grained sandstone in the upper part of the Cherry Canyon sandstone (basin facies). Three repeat measurements were made and

mineral	saturation magnetisation	coercivity of remanence	saturation magnetisation
magnetite	92 Am^2kg^{-1}	10-50 mT	50-150 mT
haematite	0.2-0.4 Am^2kg^{-1}	0.1-0.5 T	
maghemite	80-85 Am^2kg^{-1}		
pyrrhotite	1-20 Am^2kg^{-1}		

table 4.6 Summary table of saturation magnetisation and coercivity of remanence for magnetite, haematite, maghemite and pyrrhotite, where known (Collinson, 1983 and Piper, 1987).

K_{min} is well- defined with *A95* of 1.7° and K_{int} has *A95* of 21.2°. K_{min} is vertical and K_{int} is sub- horizontal. This is consistent with a depositional/compactional fabric (4.1.2). The axial susceptibility increased substantially from 2.49 to 20.27 (volume units x $10^{-6}GOe^{-1}$; see appendix 4.2) on heating. This sample had a magnetic fabric prior to heating and measurements were made on the Minisup (appendix 4.2) and also on the 'Kappa' bridge (table 4.4). The Miniosup results show that K_{min} is vertical and K_{max} and K_{int} are sub- horizontal. This sample is therefore a clear example of fabric enhancement due to heating. No fabric was detected using the Kappa bridge.

Sample RL5.1.1 was taken from the Hegler limestone in the Cherry Canyon sandstone formation (basin facies). Three repeat measurements were made. Only K_{min} is well-defined with *A95* of 9.4° and it is sub-vertical. The axial susceptibility increased from 1.99 to 4.65 (volume units x $10^{-6}GOe^{-1}$; see appendix 4.2) on heating; this is a relatively small change in comparison to the other samples. The magnetic fabric of another sample from this site was measured prior to heating (sample RL5.4.1, appendix 4.2) and, although these repeat measurements were similar to one another, the data is not of sufficiently good quality to be reliable.

Sample RL6.12.3.1 was taken from the unweathered, grey sandstone matrix of the Rader 'slide' (basin facies). Three repeat measurements were made. K_{min} is the only principal axis that is well-defined with *A95* of 8.9°. This has a high inclination of 70.3°. This is consistent with a depositional/compactional fabric (4.1.2). The axial susceptibility increased from around 1.5 to 37.02 (volume units x $10^{-6}GOe^{-1}$; see appendix 4.2) on heating, suggesting the formation of magnetite or maghemite (table 4.2). The magnetic fabric of a similar sample was measured prior to heating (sample RL6.8.2, appendix 4.2). The repeat measurements on the Minisup were similar, and K_{max} and K_{int} dip at around 45° and K_{min} is sub-horizontal. These directions, defined before and after heating, differ significantly and it is therefore not accurate to conclude that the fabric has been *enhanced*, despite the large increase of susceptibility on heating. The differences in directions of data before and after heating may, in part, be a reflection of the different magnitudes of the susceptibilities and may also be due to the fact that different samples were measured.

Sample RL6.13.2.3 was taken from the first turbidite overlying the Rader 'slide' (basin facies). Three repeat measurements were made and K_{max} and K_{min} were well-defined with *A95's* of 8.6° and 7.4° respectively. K_{max} is inclined at 12° and K_{min}

is inclined at 77°. This is consistent with a depositional/compactional fabric (4.1.2). The axial susceptibility increased from 1.69 to 31.55 (volume units x 10^{-6}GOe^{-1}; see appendix 4.2)) on heating, indicating significant growth of new phases due to heating. Some fabric was detected prior to heating (sample RL6.13.1.3, appendix 4.2) although the directions, defined before and after heating, differ significantly and it is therefore not accurate to conclude that the fabric has been *enhanced*, despite the large increase of susceptibility on heating. The differences in directions of data before and after heating may, in part, be a reflection of the different magnitudes of the susceptibilities.

Conclusions In all cases the axial susceptibility increased after heating to 650°C. Changes in susceptibility accompanying mineralogical changes are discussed in section 5.3.1 (table 5.3). The only visible fabric, in all samples, is a depositional/compactional fabric. Such a fabric is indicated by anisotropy of susceptibility in samples from sites MC31, RL1, RL3, RL4, RL5 and RL6, *after* heating, but not before. However, an *enhancement* of fabric was only detected in sample RL4 which is sandstone from the Cherry Canyon Formation. For the remaining samples no *enhancement* was detected, mainly because there was no *measurable* fabric prior to heating.

Samples from sites MC31(basin margin facies, Lamar limestone), RL3 (basin facies, Cherry Canyon sandstone), RL5 (basin facies, Hegler limestone) and RL6 (basin facies, turbidite, Rader 'slide') did possess some trace of initial fabric prior to heating, but the directions after heating were significantly different. Therefore, the relationship between the directions, before and after heating, is not easy to interpret, and may even be spurious. Generally speaking, fabric was easier to measure *after* heating because of the increase in susceptibility. However, several samples showed no fabric before or after heating (sites MC16, grainstone; and RL2, Brushy Canyon sandstone) and are therefore considered to be isotropic.

4.4 Anisotropy of Isothermal remanent magnetism (table 4.7)

Samples from a variety of lithologies and facies were given an isothermal remanent magnetism (IRM) in order to investigate any anisotropy in the *magnetic* minerals present (Stephenson *et al.*, 1986). Different magnetic minerals have different propertes, and their different coercivities (table 4.6) can be used in their identification (Collinson, 1983; Stephenson *et al.*, 1986). Samples were taken from a transect through the facies exposed at the mouth of McKittrick Canyon including back

unheated samples

sample	facies	IRM x	IRM y	IRM z	norm.IRM z	norm.IRM y	norm.IRM z
MC2.2.2	backreef	3.33	3.47	3.21	1.037	1.081	1
MC7.1.1	backreef	0.67	-0.47	0.09	-1.425	1	-0.1915
MC11.1.1	reef	5.41	4.9	5.15	1.104	1	1.051
MC16.1.1	upper foreslope	0.72	1.27	1	1	1.764	1.389
MC23.1.1	upper foreslope	0.57	0.7	0.74	1	1.228	1.298
MC27.1.2	upper foreslope	0.8	1.6	1.6	1	2	2
MC30.4.1	lower foreslope	4.9	5.2	5	1	1.061	1.02
MC31.2.2	basin margin	39	38	38.4	1.026	1	1.01
MC32.5.1	basin margin	6	6	6	1	1	1
MC34.4.1	basin margin	19	19.4	18.9	1.005	1.026	1
MC35.3.1	basin margin	5.6	6	6.8	1	1.071	1.214
RL1.6.2	basin	31.5	33.4	33.6	1	1.06	1.067
samples heated to 650 C							
MC11.4.1	reef	228	218	219	1.046	1	1.005
MC16.3.2	upper foreslope	362	350	364.5	1.034	1	1.041
MC31.1.1	basin margin	796	800	790	1.007	1.013	1
MC36.2.1	basin margin	2807	2810.5	2670	1.051	1.053	1
RL1.4.1	basin	2901	2998	2962	1	1.033	1.021
RL2.1.1	basin	332.5	338.5	307.5	1.081	1.101	1
RL3.6.1	basin	3099	3148	3152	1	1.016	1.017
RL4.3.6.1	basin	1153.5	1188.5	1185	1	1.03	1.027
RL6.12.3.1	basin	980.5	979	943	1.039	1.038	1
RL6.13.5.2	basin	1997.5	2064	2076	1	1.033	1.039
RL7.2.2	basin	1507	1502	1528	1.003	1	1.017
RA4.4.2	back reef	222	224	220	1.009	1.018	1
SL2.7.1	back reef	407.5	413.5	406	1.004	1.018	1

table 4.7 Summary table of anisotropy of isothermal remanent magnetism (IRM) acquisition for unheated and heated samples. Samples were initially demagnetised by tumbling in a field of 90mT and then given an IRM of 400mT in the x, y and z sample *directions, respectively. Units x 10^{-4} Am^{-1}.*

reef, reef, upper and lower foreslope and basin margin facies. Measurements were made of untreated samples and of some samples that had been heated to 650°C, in order to investigate chemical changes due to heating.

4.4.1 Unheated samples

All samples except MC32.5.1 (Lamar limestone, basin margin facies) are anisotropic and show a range of isothermal remanent magnetism intensities (table 4.7). Samples of Lamar and Bone Spring limestones have the highest isothermal remanent magnetism intensities. These are organic rich micritic limestones. The remaining samples have much lower intensities suggesting that minerals with lower coercivities, such as haematite, goethite or pyrrhotite, rather than magnetite (table 4.6) are present, or that these samples contain significantly smaller quantities of magnetic phases, or both.

The variation in the initial isothermal remanent magnetism of the Lamar limestone samples (samples MC31, MC32, MC34, Mc35) reflects the variation in the magnetic phases present. Magnetite has a significantly lower coercivity than haematite, goethite or pyrrhotite and thus will dominate the isothermal remanent magnetism. However, haematite and pyrrhotite are inherently anisotropic (table 4.1) whereas magnetite tends towards isotropy. This suggests that magnetite may be the main carrier in the samples from sites MC31, MC32 and MC34 with minor contributions from a strongly anisotropic phase; the sample from site RL1 behaves in a similar way. Haematite or pyrrhotite is likely to be the main carrier in samples from site MC35 which have a strong anisotropy and low initial natural remanent magnetism value.

Samples from sites MC7, MC11, MC16, MC23 and MC27 have quite a strong anisotropy but low initial isothermal remanent magnetism values. This suggests that no magnetite is present, and that haematite of pyrrhotite is the main isothermal remanent magnetism carrier. The values of isothermal remanent magnetism after heating preclude the presence of pyrrhotite as these values are low and if pyrrhotite had been present then magnetite would have formed. The low isothermal remanent magnetism values of samples from sites MC2 and MC30 are more isotropic. This may be due to low quantities of magnetic phases being present and also to a combination of magnetite and a low coercivity mineral.

4.4.2 Samples heated to 650°C

Samples from sites MC11, MC16, MC31, RL2, RA4 and SL2 have isothermal remanent magnetism intensities at least an order of magnitude lower than those from samples from the remaining sites. This suggests that the new phase developed is a low coercivity phase such as haematite (table 4.6), and that the magnetic phase developed in the samples with higher isothermal remanent magnetism intensities is magnetite or maghemite. Comparison of isothermal remanent magnetism magnitudes before heating with those after heating for samples M11, M16, M31 and RL1 are informative as low initial values seem to correlate with low final values, and high initial values correlate with high final values. This suggests that haematite, goethite or pyrrhotite is present in the samples with low isothermal remanent magnetism, and that magnetite is being formed due to the heating process in the samples with higher isothermal remanent magnetism intensities. The high values which indicate the presence of magnetite also hint at the initial presence of pyrite in these samples. Pyrite would not contribute to the initial isothermal remanent magnetism of a sample, but would oxidise to magnetite on heating (table 5.3). Samples from site MC31 are interesting as this has the highest initial isothermal remanent magnetism value, but has a final value intermediate between the highest and lowest isothermal remanent magnetism values. This could indicate that the sample contined no pyrite which could subsequently be altered to magnetite, or that a large part of the initial isothermal remanent magnetism value was due to haematite, which disguises the presence of magnetite.

Conclusions The investigation of isothermal remanent magnetism anisotropy is in many ways more informative in 'weak' rocks than the investigation of anisotropy of susceptibility. This is because i. the isothermal remanent magnetism method investigates only the ferromagnetic minerals present and ignores the 'matrix' minerals; ii. intensities are higher which brings the measurements well above the noise level of the instrumentation; and iii. some information on the magnetic phases present and thus the potential natural remanent magnetism carriers is generated.

It would be worthwhile further investigating the isothermal remanent magnetism ellipsoids by calculating the principal axes and relating these to any primary geological features. It would also be instructive to compare the anisotropy of the isothermal remanent magnetism ellipsoid with the anisotropy of the susceptibility, in order to obtain some measure of the contribution to bulk magnetic fabric of the 'matrix' versus the ferromagnetic minerals.

There is anisotropy of isothermal remanent magnetism in almost all samples. whether untreated or whether heated to 650°C. However, the *degree* of anisotropy does not appear to be enhanced by the heating process and the consequent generation of new magnetic phases.

4.5 Discussion

Data from measurements on the Minisup was found to be not repeatable and therefore unreliable. This is probably due to the susceptibility values of the rocks studied being below the detection limits of this instrument. Ellwood (1984) reports that although torsion fibre magnetometers are more time consuming to use than spinners, they are significantly better than a Minisup, because a spurious second harmonic remanence signal is generated in spinners, which adds significantly to the noise of the instrument. Ellwood (1984) also reported that the precision with which susceptibility anisotropy measurements can be made, is a function of the axial ratios of susceptibility, and not a function of the susceptibility magnitudes. It was observed that when K_{max}/K_{min} or K_{int}/K_{min} are less than or equal to 1.003 then the replicate precision is poor. When these axial ratios are greater than or equal to 1.005, then the replicate precision is excellent. He thus proposes an empirical method for the rejection of anisotropy of susceptibility data that are not sufficiently anisotropic for reliable measurement. Data from the Kappa bridge showed that no significant anisotropy was measured. The sensitivity and precision of equipment available for the measurement of anisotropy of susceptibility is often such that the agreement between results obtained on different instruments is poor (Collinson, 1983).

In all cases the axial susceptibility of samples increased after heating to 650°C. Changes in susceptibility accompanying mineralogical changes are diccussed in section 5.3.1 (table 5.3). The only visible fabric, in all samples, is a depositional/compactional fabric. Such a fabric was indicated by anisotropy of susceptibility in some samples (from sites MC31, RL1, RL3, RL4, RL5 and RL6), *after* heating, but not before. However, an *enhancement* of fabric was detected in two samples (sample RL4, which is sandstone from the Cherry Canyon Formation and in samples from site RA2, Shattuck sandstone) For the remaining samples no *enhancement* was detected, mainly because there was no *measurable* fabric prior to heating. Generally speaking, fabric was easier to measure *after* heating because of the increase in susceptibility. However, several

samples showed no fabric before or after heating (sites MC16, grainstone; and RL2, Brushy Canyon sandstone) and are therefore considered to be isotropic.

There is anisotropy of isothermal remanent magnetism acquisition in almost all samples. whether untreated or whether heated to 650°C. However, the *degree* of anisotropy does not appear to be enhanced by the heating process and the consequent generation of new magnetic phases. The investigation of isothermal remanent magnetism anisotropy is in many ways more informative in 'weak' rocks than the investigation of anisotropy of susceptibility. This is because i. the isothermal remanent magnetism method investigates only the ferromagnetic minerals present and ignores the 'matrix' minerals; ii. intensities are higher which brings the measurements well above the noise level of the instrumentation; and iii. some information on the magnetic phases present and thus the potential natural remanent magnetism carriers is generated.

Measurements of the magnetic fabric of some samples after heating showed that some samples possessed a fabric *after* heating, which was not easily measured, or not present, *prior* to heating. Perarnau and Tarling (1985) did some fabric studies on weakly anisotropic rocks and discovered that their fabric was enhanced after heating to 650°C. Thermally induced fabrics appeared to enhance what little 'primary' fabric was present and susceptibility changes were attributed to magnetite formation from illite or vermiculite clays. The results from this preliminary study indicate that bulk susceptibility increased in every sample due to thermally induced chemical/mineralolgical changes (table 5.3). However, it would be inaccurate to say that the 'primary' fabric had been *enhanced*, because no 'primary' fabric was reliably measured. If repeatable measurements of 'primary' fabric could be obtained then thermally-induced chemical/mineralolgical changes in magnetic fabric could be informative and easier to measure because of the increase in susceptibility. However, the processes involved in thermally induced chemical/mineralolgical changes are not well understood, and more research need to be carried out on these aspects before using results of thermally-induced magnetic fabric to interpret 'primary' magnetic fabrics.

Various problems are associated with the measurement and interpretation of magnetic fabric. There is the potential problem of contamination from the drill barrel; this could affect susceptibility measurements, but not natural remanent magnetism measurements, as the drill barrel is made of non-magnetic brass. Sample shape can affect the anisotropy by the spurious effects of non-spherical sample shape on the sensor-flux linkage and by the contribution to anisotropy from using a non-spherical sample. Addison (1982) and Rathore (1975) report modifications to equipment necessary, and recommend a shape ratio of 0.86±0.02 for the length:diameter ratio,

such that the shape difference from a spherical sample is almost negligible. This ratio was used for all samples in this study, and therefore the contribution to noise from sample shape should be negligible.

Any fabric interpretation in limestones is likely to be problematic because of the range of grain morphologies and sizes and domain states of the ferromagnetic component, combined with the effects of the negative diamagnetic contribution from calcite.

The presence of a small quantity of ferromagnetic grains *e.g.*, magnetite or haematite, can dominate the effects of the matrix *i.e.*, the paramagnetic and diamagnetic components. This is because the susceptibility of ferromagnetic grains is large and positive, whilst that of paramagnetic and diamagnetic grains is small and positive/negative (table 4.2; Owens and Bamford, 1976). Because of the dominance of the effects of the ferromagnetic minerals, the magnetic fabric has commonly been assumed to be *entirely* due to the contribution from ferromagnetic minerals and the contribution to anisotropy of susceptibility of the rock *matrix* has commonly been considered insignificant and/or ignored. This is not a valid assumption, because the matrix minerals themselves can have significant anisotropy (table 4.1; Rochette, 1987) and therefore the contribution to anisotropy of susceptibility of the rock *matrix* should be distinguished from anisotropy of susceptibility due to the ferromagnetic component, if possible. The anisotropy of the ferromagnetic component alone is informative because it is easier to quantify than anisotropy of bulk susceptibility and is therefore easier to interpret. The anisotropy of the ferromagnetic component alone was investigated by measuring the anisotropy of isothermal remanence acquisition (Stephenson *et. al.*, 1986) and some minor anisotropy was detected.

A similar method has been devised by McCabe *et al.* (1985), which involves giving the sample an anhysteretic remanence and measuring the anisotropy of the anhysteretic remanence, AAR. After comparison with anisotropy of magnetic susceptibility data, they concluded that the anisotropy of the anhysteretic remanence method was preferable when bulk susceptibility is low. The anisotropy of anhysteretic remanence method is especially good where magnetite is present as it has low coercivity and will thus acquire a remanence easily. Haematite and goethite have higher coercivities than can be practically applied, using this method, and thus these minerals contribute minimally to the anisotropy of the anhysteretic remanence. Domain size also affects the degree to which an anhysteretic remanence can be acquired. Anhysteretic remanence is carried preferentially by stable single domain or pseudo-single domain grains and effects of super-paramagnetic or multi-domain grains are minimal. Another advantage of the anisotropy of the anhysteretic remanence method is that a cryogenic

magnetometer can be used, and the precision and sensitivity is therefore greater than that from the measurement of susceptibility.

Calcite (and other carbonate minerals) are the only diamagnetic minerals with a significant anisotropy (table 4.1). Owens and Rutter (1978) succeeded in measuring a fabric in pure Carrara marble in which there was a net alignment of crystallographic axes due to the effects of laboratory compaction. A fabric will only be present if the crystallographic axes are aligned, which will not be the case under most natural circumstances. However the relative contributions from the diamagnetic, paramagnetic and ferromagnetic components are important to determine. McCabe *et al.* (1985) report that a limestone containing 10ppm magnetite has a net susceptibility of zero, as the contributions to the susceptibility are equal and opposite. This appears to be the case in most of the samples measured in this study. Such a case presents a problem for the measurement of a magnetic fabric, and has been largely ignored by past studies probably because *a.* the ferromagnetic component is easier to measure and *b.* because of the lack of appropriate instruments.

The only direct way of measuring the contribution of the matrix component is to use high fields which saturate the ferromagnetic minerals whilst leaving the matrix minerals unaffected. Experimental details of this method are given in Rochette (1988).

Furthermore, it is rather simplistic to assume that current flow is the only factor that will *significantly* affect the orientation of particles within a sedimentary rock (4.1.2). Other important factors include processes acting at or immediately following the time of deposition , as well as diagenetic processes.

Depositional/post-depositional processes Gravity affects the orintation of particles, especially where deposition is on a slope. Griffiths *et al.* (1960) showed that DRM is influenced by fluid and gravitational forces acting on settling particles. Obviously there is some overlap of processes and terminology here. Noel (1983) studied undisturbed, magnetite-containing cave silts, which had undergone minimum compaction, and took account of these various 'errors' to interpret a depositional fabric and the natural remanent magnetism directions. The rolling of particles systematically shallows the remanence (Rees, 1961). This is known as the 'inclination error'. The rolling of particles due to current flow on a slope is known as the 'rotation error' (Noel, 1983) and the angular difference between the natural remanent magnetism direction in a sediment deposited in still water on a horizontal surface, and that produced in the same conditions on a slope, is known as the 'bedding error' (King, 1955; Rees, 1966).

Collision with other particles, grain size, the flocculation of clay-sized phyllosilicates and resistance to fluid flow will also affect the orientation of particles.

Bioturbation, by sediment ingestion, habitation, cementation and resuspension, is likely to affect the orientation of particles within a sediment. Hounslow (1987) studied the anisotropy of susceptibility of bioturbated and non-bioturbated sandstones and found a fabric in both sets of samples which he interpreted to be due to wave or current processes, thus implying that thorough bioturbation did not disturb the 'primary' depositional fabric. He also interpreted that some of the fabric was caused by the reorientation of phyllosilicates (chlorite and micas) during the early stages of compaction. The 'q' factor (4.1.2) has been used to identify 'undisturbed' sediments *i.e.*, those which possess 'primary' features, and is defined as $0.06 < q < 0.69$ (Hamilton and Rees, 1970). Ellwood (1984) did some experimental work on a modern beach on which he sprinkled magnetite particles, and interpreted the results as showing that bioturbation did not affect the magnetic fabric and actually *enhanced* the 'primary' fabric. These interpretations disagree with that of Lowrie and Hirt (1987) and myself, who feel that it is unlikely that any significant remnant of an original sedimentary fabric will survive intense bioturbation; the implication being that this fabric is being misinterpreted as of sedimentary origin. However, these interpretations also question the validity of the assumption that the 'q' factor can be used to identify 'primary' fabrics in sedimentary rocks which, by implication, have *not* been bioturbated, and also questions the assumption that bioturbation always results in a 'secondary' fabric. This suggests that the processes involved in the acquisition of so-called 'primary' and 'secondary' magnetic fabrics are not adequately understood. However, it might be expected that intense bioturbation would allow the reorientation of magnetic particles with the Earth's field direction, or that this fabric was caused by early compaction.

Earth's magnetic field exerts a force on magnetic grains. Magnetic fabric is dominated by the contributions from magnetic minerals which have high susceptibilities. Studies by Turner (1975), Hamilton (1979) and Noel (1983) on natural rocks, have not satisfactorily demonstrated that there is a geomagnetic control on fabric, although experimental studies by Rees (1961) measured a deflection of K_{max} towards the Earth's field direction. This force has been shown to be negligible, except for particles which are smaller than a pore-space, in comparison to the forces exerted by gravity and fluid flow (Hamilton, 1967).

Diagenetic processes Processes such as compaction causing passive rotation of particles and causing mineral transformations and recrystallisation and the growth of new phases

during diagenesis may alter the magnetic fabric of a sedimentary rock. Rochette (1988) states that compaction plays a major role in the development of fabric in fine-grained marine sediments, but adds the cautionary note that the interpretation of compactional fabric in limestones is particularly problematic because limestone compacts by mass-transfer or pressure-solution processes rather than grain rotation. McCabe *et al.* (1985) detected a foliation developed by overburden compaction and pressure solution of a Palaeozoic limestone, which was carried by diagenetic magnetite. The CRM carried by this magnetite was thus constrained by the timing of the development of this magnetic fabric. Rochette (1988) goes as far as to state that compactional processes play the major role in causing fabric in marine sedimentary rocks and that other post-depositional processes such as bioturbation and the growth of authigenic phases, and the effects of Earth's magnetic field are not satisfactory explanations to account for magnetic fabric.

4.6 Conclusions and further work

Orientated hand samples were not sufficiently accurate with respect to their orientation for accurate fabric analysis *i.e.*, errors were too large. Furthermore, sedimentological and structural features must be accurately described in detail, in order to be able to interpret magnetic fabric results. Three samples was not a large enough sample to get a satisfactory estimate of the mean. In future, samples should be orientated as accurately as possible in the field *i.e.*, using a portable drilling device (1.4).

Data from measurements on the Minisup was found to be not repeatable and therefore unreliable. This is probably due to the susceptibility values of the rocks studied being below the detection limits of this instrument. Axial susceptibility measurements *were* repeatable even when anisotropy measurements *were not*.

No significant anisotropy was detected in most samples when the 'Kappa' bridge was used.

Heating samples to 650°C caused susceptibility increases, commonly of an order of magnitude, and fabric was easier to measure as a consequence. In all cases the axial susceptibility increased after heating to 650°C. A fabric was indicated by anisotropy of susceptibility in some samples (from sites MC31, RL1, RL3, RL4, RL5 and RL6), *after* heating, but not before. However, an *enhancement* of fabric was detected in two samples (sample RL4, which is sandstone from the Cherry Canyon Formation and in samples from site RA2, Shattuck sandstone). For the remaining samples no *enhancement* was

detected, mainly because there was no *measurable* fabric prior to heating. Generally speaking, fabric was easier to measure *after* heating because of the increase in susceptibility. However, several samples showed no fabric before or after heating (sites MC16, grainstone; and RL2, Brushy Canyon sandstone) and are therefore considered to be isotropic.

There is anisotropy of isothermal remanent magnetism in almost all samples. whether untreated or whether heated to 650°C. However, the *degree* of anisotropy does not appear to be enhanced by the heating process and the consequent generation of new magnetic phases. The investigation of isothermal remanent magnetism anisotropy is in many ways more informative in 'weak' rocks than the investigation of anisotropy of susceptibility. This is because i. the isothermal remanent magnetism method investigates only the ferromagnetic minerals present and ignores the 'matrix' minerals; ii. intensities are higher which brings the measurements well above the noise level of the instrumentation; and iii. some information on the magnetic phases present and thus the potential natural remanent magnetism carriers is generated. It would be worthwhile further investigating the isothermal remanent magnetism ellipsoids by calculating the principal axes and relating these to any primary geological features. It would also be instructive to compare the anisotropy of the isothermal remanent magnetism ellipsoid with the anisotropy of the susceptibility, in order to obtain some measure of the contribution to bulk magnetic fabric of the 'matrix' versus the ferromagnetic minerals.

Calcite crystals are anisotropic with K_{max} parallel to the crystallographic c axis and $K_{int} = K_{min}$ (Owens and Rutter, 1978). Therefore in order to detect a fabric in *pure* carbonates i. the calcite must be crystalline and ii. there must be a preferred orientation of crystallographic axes. In all carbonate rocks, the contribution to the magnetic fabric of the *diamagnetic* components *i.e.*, the calcite/dolomite *etc.*, must be considered as well as the contribution to magnetic fabric from the *ferromagnetic* component. High-field measurements of the contribution to susceptibility of the sample matrix (Rochette, 1987) would be done in conjunction with studies of the anisotropy of the magnetic minerals by studying the anisotropy of isothermal remanence acquisition (Stephenson *et al.*, 1986) and anisotropy of anhysteretic remanence acquisition (McCabe *et al*, 1985).

Chapter 5: Palaeomagnetism and magnetic characteristics

5.1 Introduction

The palaeomagnetic characteristics of a suite of samples taken from outcrops along the 'reef trail' in McKittrick Canyon and in roadcuts on US highway 62/180 (fig. 1.2) are reported in this chapter. It includes discussion of the minerals which carry the natural remanent magnetism (NRM), as well as discussion of magnetic vectors and their significance. It is important to emphasise that examination of the palaeomagnetic and magnetic characteristics of these samples was done prior to, and independent from petrographic observations. Knowledge of which magnetic minerals carry the remanence can constrain the diagenetic conditions which caused their formation and the timing of natural remanent magnetism acquisition. Factors which cause the deviation of actual natural remanent magnetism directions from expected directions are also discussed. Discussion of sedimentological and diagenetic influences on the timing of natural remanent magnetism acquisition is reserved for chapter 6.

In ferromagnetic substances a strong magnetisation or *remanence* is retained even when an applied field is removed. (*N.B.* for clarity, the term *ferromagnetism* will be used to describe ferro-, ferri-, and antiferro-magnetic behaviour, throughout this chapter; clarification of these terms is given in chapter 4). Ferromagnetic behaviour is dependent on temperature. The Curie temperature (T_C) is the temperature at which the interatomic distances critical for the retention of remanence to occur are exceeded. Above this temperature the mineral is no longer able to retain a remanence and behaves as a paramagnetic mineral. In anti-ferromagnetic substances this temperature is called the Neel Temperature (T_N).

The acquisition of natural remanent magnetism by rocks allows the study of the ancient geomagnetic field *i.e.*, palaeomagnetism, because magnetic minerals present in rocks are oriented in the direction of Earth's magnetic field at the time of their deposition or formation. A magnetisation that is acquired by rocks due to the cooling of magnetic minerals through the Curie temperature is called thermo-remanent magnetism (TRM). Where the particle has *not* been cooled through the Curie temperature, the remanence is called a partial thermo-remanent magnetism (pTRM). The temperature at which a thermal remanence direction is fixed into a mineral is called the blocking temperature (T_b). During burial of a sequence of rocks, temperatures may become high

enough to unblock the remanences carried by some grains, particularly small ones. On uplift and cooling, different remanences will become blocked into those grains. The magnetisation acquired by a magnetic mineral *precipitated during diagenesis* is known as chemical (or crystalline) remanent magnetism (CRM). The critical grain size at which a mineral *growing* in a magnetic field can develop a fixed remanence direction is referred to as the blocking volume. Magnetisation acquired during *deposition* of pre-existing magnetised grains, is known as depositional remanent magnetism (DRM); magnetisation acquired immediately *post-deposition* by re-orientation of pre-existing magnetised grains, is known as post-depositional remanent magnetism (pDRM). The age of the magnetism carried by rocks dates the timing of acquisition of the natural remanence at a specific point in geological time. Different magnetic minerals have different magnetic stabilities, and the ability of a magnetic mineral to retain a 'memory' of the Earth's magnetic field depends particularly upon the grain size of the magnetic mineral as well as the temperature at which the magnetisation direction became fixed into that mineral.

The characteristics of magnetic minerals in rocks depend upon the grain sizes of those minerals present in the rock. This is because magnetic grains are divided into small volumes of uniform magnetisation known as *domains*, and the domain state controls magnetic behaviour. In natural minerals domain sizes depend on impurities and defects in the crystal lattice and on grain size and grain shape. In magnetite they are 0.1-1.0μm, and in haematite they are 1-100μm in diameter. It is important to understand the domain state of the magnetic minerals in rocks because this can yield information on the grain size and thermal history of the magnetic minerals and hence their origin. A particle smaller than the size of a domain must be a *single domain* (SD). At a critical size a particle will have more then one domain; these are called *multi-domain* (multi-domain). Adjacent domains have different magnetisation directions. The larger the particle the more domains it can contain. Very large multi-domain grains can become easily demagnetised to have no overall magnetic moment; these are commonly referred to as 'soft' components. A single domain grain has uniform magnetisation across its entire volume which will not alter under natural cicumstances and is commonly referred to as a 'hard' component. (It can be removed by heating to above the Curie temperature.) Particles with few domains tend to behave in a similar way to single domain grains. They are referred to as pseudo-single domain (pSD). In very small single domain grains, thermal vibration energies of the crystal lattice may exceed the total magnetic energy which means that these grains only retain a magnetic moment for a few seconds or minutes - this is called super-paramagnetic behaviour.

Thus, in a sedimentary sequence which has been buried and undergone diagenesis, several different types of natural remanence may be present. These remanences may be carried by several different magnetic minerals, with a range of magnetic behaviour according to grain size. Consequently, the palaeomagnetism and magnetic characteristics of sedimentary rocks can be complex. Over geological time, some or all of the magnetisation locked into a magnetic grain will decay away. The time taken for this to occur is called the relaxation time. There is a relationship between grain size, blocking temperature and relaxation time for a particular mineral. The theoretical curves for magnetite and haematite have been established by Pullaiah *et al.* (1975) and these can be used to help establish the conditions of formation of these magnetic minerals. The temperatures to which a sequence of rocks has been subjected depends upon the burial/thermal history of the region. Hence, a study of magnetic characteristics can help elucidate the geological history of a sequence of rocks .

A basic assumption involved in all palaeomagnetic interpretations is that the average Earth's magnetic field can be modelled by an axially geocentric dipole (Tarling, 1983). By convention, the magnetic field direction is the one indicated by the North-seeking end of the magnetic needle which will point straight down at the north pole and straight up at the south pole. 'Normal' polarity is defined as occurring where magnetic north lies in the same hemisphere as geographical north. Palaeomagnetic study of rocks at various ages has enabled a record of the *polarity* of Earth's magnetic field to be determined through geological time; the so-called 'normal' and 'reversed' periods of time. From study of the *direction* of Earth's magnetic field in rocks of various ages, the movement of continental masses through time can be deduced by comparing the apparent position of the magnetic poles on one continent with the apparent position of the magnetic poles from other continents. The movement of the apparent positions of the magnetic poles with time is referred to as the apparent polar wander path (APWP); these are now available for most continents. Comparison of observed natural remanent magnetism directions with the polarity time-scale (Piper, 1987) and the apparent polar wander path established for the western United States (Irving and Irving, 1982), formed the basis for the dating of natural remanent magnetism in rocks in this study. Remanence directions from sample sites were compared directly with the apparent field direction wander path (fig. 5.1). The apparent field direction wander path for the study area was derived from the apparent polar wander path using the geometrical relationship between latitude, longitude and pole position. In order to compare site directions directly with palaeo-pole positions (*i.e.*, the apparent polar wander path) the virtual pole positions for each site were calculated (Piper, 1987).

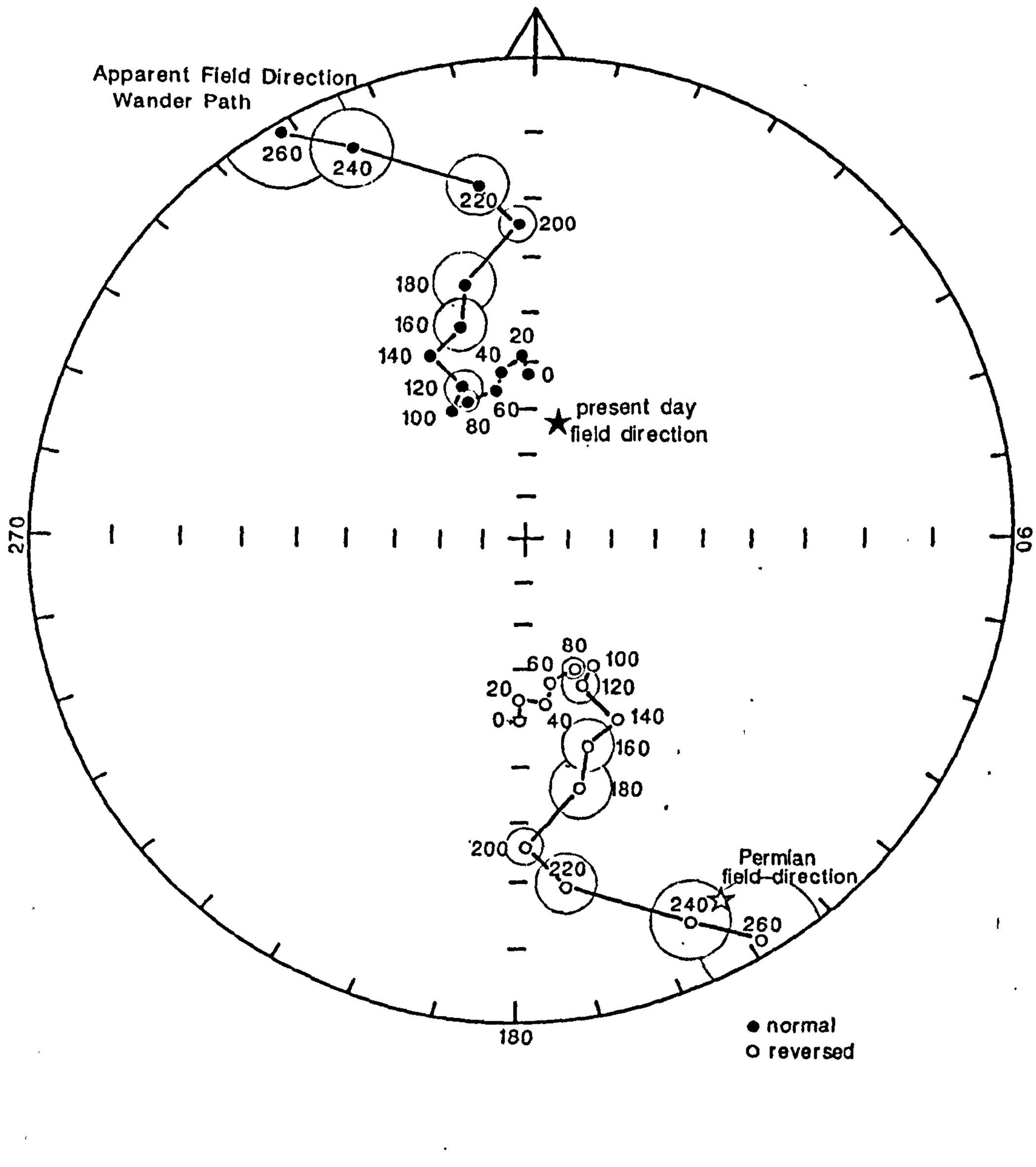

fig. 5.1 The apparent field direction wander path (AFDWP) used in this study. This was derived from the apparent polar wander path (Irving and Irving, 1982) for cratonic North America. Normal and reversed directions are shown; solid symbols indicate normal directions, open symbols indicate reversed directions.

5.2 Methods

In order to remove less magnetically stable components and to isolate the different remanences carried by the various minerals present, samples were progressively demagnetised. Demagnetisation involves subjecting samples to progressively greater amounts of energy in order to unblock the remanence by exceeding the magnetic energy required to retain a remanence direction. In this way a picture of the stability of the remanences of the magnetic particles in the sample (*i.e.* the blocking temperature spectra) can be developed. The majority of samples were demagnetised by heating to successively higher temperatures, cooling and then measuring the remanence after each cooling step (thermal demagnetisation). For comparison, two samples from 12 different sites were demagnetised using successively larger alternating magnetic fields (AF demagnetisation). The AF demagnetiser used was a Highmoor two-axis tumbling system operating at a signal frequency of 50Hz. Instrumental effects involved in AF demagnetisation were minimised by reversing the orientation of the sample in the sample holder, repeating the measurement and averaging the results (Johnson *et al.*, 1984). AF demagnetisation steps are summarised in table 5.1a. The heating steps used in thermal demagnetisation varied between sample sites and are summarised in table 5.1b.

The declination, inclination and intensity of natural remanent magnetism and bulk (axial) susceptibility, were measured using a cryogenic magnetometer and a low field susceptibility meter, respectively. One problem involved in thermal demagnetisation is the acquisiton of spurious remanences by very small particles. For this reason, care was taken to ensure that all aspects of the demagnetisation process were carried out in minimum magnetic field *i.e.*, as close to zero field as practically attainable. Details of all equipment used during the course of this study are given in Collinson (1983). All measurements were made at the Nuffield palaeomagnetic laboratory, Close House, University of Newcastle upon Tyne.

5.3 Data presentation

5.3.1 Magnetic mineralogy

Bulk susceptibility and intensity of natural remanent magnetism were used as indicators of the amount and grain size of para- and ferromagnetic minerals present in a sample. Changes of susceptibility with thermal demagnetisation indicate that chemical changes to the mineralogy of the sample are taking place. Changes in intensity of

site	samples	demagnetisation steps mT					
		5	10	20	30	40	50
M2	13.1,14.1	*	*	*	*	*	*
M3	15.1,16.1	*	*	*	*	*	*
M4	17.1,18.1	*	*	*	*	*	*
M6	17.1,18.1	*	*	*	*	*	*
M7	17.1,18.1	*	*	*	*	*	*
M9	15.1,16.1	*	*	*	*	*	*
M10	17.1,18.1	*	*	*	*	*	*
M13	16.1,18.1	*	*	*	*	*	*
M13A	6.1,11.1	*	*	*	*	*	*
M15	15.1,16.1	*	*	*	*	*	*
M16	17.1,18.1	*	*	*	*	*	*
M20	11.1,20.1	*	*	*	*	*	*

table 5.1a Steps used in AF demagnetisation

site	samples	Temperature steps C 20	110	170	210	260	320	390	430	480	530	590
M2	1.1,3.1,4.1,5.1	*	*	*	*	*	*	*	*			
M3	1.1,2.1,3.1,3.2	*	*	*	*	*	*	*	*	*	*	
M4	1.1,2.1,4.1,4.2	*	*	*	*	*	*	*	*	*	*	*
M6	1.1,2.1,3.1,6.1	*	*	*	*	*	*	*	*	*	*	*
M7	1.1,2.1,3.1,4.1	*	*	*	*	*	*	*	*			
M9	1.1,2.1,3.1,4.1	*	*	*	*	*	*	*	*	*		
M10	1.1,3.1,4.1,5.1	*	*	*	*	*	*	*	*	*	*	*
M13	2.1,3.1,5.2,6.1	*	*	*	*	*	*	*	*	*	*	
M13A	1.1,2.1,3.1,4.1	*	*	*	*	*	*	*	*	*	*	
M15	1.1,2.1,3.1,4.1	*	*	*	*	*	*	*	*	*		
M16	1.1,2.1,3.1,4.1	*	*	*	*							
M20	1.1,2.1,3.1,4.1	*	*	*	*	*	*	*	*	*	*	*
M21	1.1,2.1,3.1,4.1	*	*	*	*	*	*	*	*	*	*	
M23	1.1,2.1,3.1,4.1	*	*	*	*	*	*	*	*			
M25	1.1,2.1,4.1,5.1	*	*	*	*	*	*	*	*	*	*	
BC1	1.1,2.1,3.1,4.1	*	*	*	*	*	*	*				
CC1	1.1,1.3,2.2,3.3	*	*	*	*	*	*	*				

site	no. of samples remaining	Temperature steps C 20	100	150	200	250	300	350	400	450	500	550	600
M2	4	*		*	*	*	*	*	*				
M3	10	*	*	*	*	*	*	*	*	*			
M4	8	*	*	*	*	*	*	*	*	*	*	*	
M6	8	*			*		*		*	*	*	*	*
M7	9	*	*	*	*	*	*	*	*	*	*	*	*
M9	8	*		*	*	*	*	*	*	*	*	*	*
M10	10	*			*	*	*	*	*	*	*	*	*
M13	8	*		*	*	*	*	*	*	*			
M13A	10	*	*	*	*	*	*	*	*	*	*		
M15	10	*		*	*		*	*	*	*			
M16	0												
M20	8	*		*	*	*	*	*	*	*	*	*	
M21	7	*	*	*	*	*	*						
M23	12	*	*	*	*	*	*	*	*				
M25	9	*		*	*	*	*	*	*	*	*		
BC1	7	*		*	*	*	*	*					
CC1	15	*		*	*	*	*	*					

site	no. of samples demagnetised	Temperature steps C 20	100	150	190	240	280	330	380	430	480	530	585
M1	21 (all)	*	*	*	*	*	*	*	*	*	*	*	*
M5	10 (all)	*	*	*	*	*	*	*	*	*			
M8	12 (all)	*	*	*	*	*	*	*	*	*	*		
M11	10 (all)	*	*	*	*	*	*	*	*	*	*		
M12	12 (all)	*	*	*	*	*	*	*	*	*	*		
M14	18 (all)	*	*	*	*	*	*	*	*	*	*	*	*
M17	16 (all)	*	*	*	*	*	*	*	*	*	*		
M18	13 (all)	*	*	*	*	*	*	*	*	*	*		
M19	15 (all)	*	*	*	*	*	*	*	*	*	*	*	
M22	3 (all)	*	*	*	*	*	*	*	*	*	*	*	
J	1 (all)	*	*	*	*	*	*	*	*	*	*		
M24	14 (all)	*	*	*	*	*	*	*	*	*			
M26	23 (all)	*	*	*	*	*	*	*	*	*	*		
M27	17 (all)	*	*	*	*	*	*	*	*	*	*	*	*
L1	15 (all)	*	*	*	*	*	*	*	*	*	*		

table 5.1b Steps used in thermal demagnetisation

remanence similarly indicate the removal or acquisition of natural remanent magnetisations, and can also indicate destruction of remanence carriers due to mineralogical changes. These changes in susceptibility and intensity were used to establish, wherever possible, the blocking temperature (T_b) spectra of the magnetic phases and to establish which para- and ferromagnetic phases were present in each sample.

Susceptibility

The magnitude of the bulk susceptibility of a sample is a measurement of the net susceptibility of all the components present within a sample *i.e.*, the total contribution from dia- para- and ferromagnetic minerals. It can give information about the relative proportions of components present in a sample because different minerals have different initial susceptibilities (table 5.2). For instance, magnetite and maghemite have initial susceptibilities which are roughly an order of magnitude larger than those of haematite or goethite; hence if the same quantities of haematite and magnetite were present in two different samples, then the susceptibility of the magnetite-bearing sample would be much larger than that of the haematite-bearing sample. The susceptibility of pyrrhotite can vary considerably, but is still larger than the susceptibility of haematite. If pyrrhotite oxidises to magnetite on heating during thermal demagnetisation, then a large increase in susceptibility would be expected. Absolute quantification of such changes is impossible because it is not possible to account for the *negative* contribution from diamagnetic minerals separately from the *positive* contribution from para- and ferro-magnetic minerals.

Changes in the mineralogy of a sample, resulting from redox reactions and dehydration reactions due to heating in air in the thermal demagnetisation process, can be monitored by measuring susceptibility after each heating step. The mineralogical changes that occur depend upon the original composition of the rock sample, but commonly include the oxidation of iron sulphides *e.g.*, pyrite and pyrrhotite, to iron oxides and the dehydration of hydrous iron oxides *e.g.*, goethite, to iron oxides in carbonate rocks (table 5.3). Other mineralogical changes are also likely to occur, such as the destruction of paramagnetic minerals *e.g.*, clays, micas and ferroan carbonates and also the alteration of diamagnetic minerals *e.g.*, calcite and dolomite. Most of these mineralogical changes and associated changes in bulk susceptibility have not yet been documented in any detail. However, the magnitude and the temperatures at which these changes occur will depend upon several factors including: original composition of the

mineral	susceptibility (x10^{-8} SI units)
quartz	-1.6
calcite	-1.3
siderite	487
ankerite	-0.48
anhydrite/gypsum	-1.5
magnesite	-1.4
pyrrhotite	125 - 628,400 (157,000)
ilmenite	3,140 - 377,000 (188,000)
haematite	50 - 3,800 (680)
magnetite	125,7000 - 2,010,900 (620,000)
maghemite	300,000
goethite	80 - 280
pyrite	5 - 530 (160)
kaolinite	-4.2
Illite	15
montmorillonite	6
biotite	229 - 333
muscovite	30 - 200
pyroxenes	180 - 325
amphiboles	49 - 320
garnets	148 -860
water	-0.9

table 5.2 Susceptibility values for the common constituents of sedimentary rocks illustrating the range of values which enables estimation of the initial mineral content of samples and the monitoring of mineralological changes which take place during the thermal demagnetisation process. Ranges are given where known and the 'mode' is given in brackets. Compiled from Piper (1987) and Collinson (1983).

mineral	behaviour	domain size μm (approx.)	T(C)	mineralogy change on heating	susceptibility change
magnetite	ferrimagnetic	0.025-0.08	578	oxidises to haematite/maghemite	slight decrease
maghemite	ferrimagnetic	0.06	645	inverts to haematite,300-450C	decrease
haematite	anti-ferromagnetic	0.025-15.0	675	inverts to magnetite >550C	increase
goethite	anti-ferromagnetic		110-120	dehydrates to haematite 100-300C	decrease
lepidocrocite	anti-ferromagnetic		110-120	dehydrates to maghemite 220-270C	increase
pyrrhotite	anti-ferromagnetic	1.6-3.0	320	oxidises to magnetite	large increase
pyrite	paramagnetic			oxidises to magnetite 350-500C	large increase
siderite	paramagnetic			oxidises to magnetite >200C	increase

table 5.3 Mineralogical changes and associated susceptibility changes likely to occur on heating during thermal demagnetisation

sample; heating and cooling rate; grain size (*I.e.*, surface area); the presence of water; the presence of impurities in any mineral phases. Other factors which can affect susceptibility are, for example, a systematic increase of susceptibility with temperature up to the Curie Temperature of a particular mineral, and subsequent drop, known as the *Hopkinson effect* (Collinson, 1983). The shape of the resultant graph depends upon the range of particle and domain sizes; in large multi-domain grains, the peak is narrow and near the T_C. Thus, blocking temperature spectra and low field susceptibility as a function of temperature, are strongly indicative of the range of iron-bearing minerals present, but are not simple to interpret.

Intensity

Change of remanence intensity with progressive demagnetisation is useful for several reasons. Blocking temperature is an intrinsic property and is characteristic of each mineral. However, there may be a spectrum of blocking temperatures for a sample which contains a mixture of particles of varying size, composition and domain state. An estimate of blocking temperature is obtained during thermal demagnetisation where the natural remanent magnetism is progressively removed until a temperature is reached above which the remanence is unblocked. Some typical graphs of intensity changes with increasing temperature are given in fig. 5.2 and these illustrate the use of blocking temperature for the identification of the natural remanent magnetism carriers in a sample. In order to illustrate within-site variation, graphs of absolute intensity change *and* graphs of normalised intensity change with heating are presented. Variation in the intensity of remanences beween samples from the same site is proportional to the *amount* of magnetic mineral present in individual samples. Variations in the graphs of *normalised* intensity change indicate that there are differences between the magnetic mineralogical compositions of samples. Demagnetisation usually results in a reduction of remanence intensity, as magnetisations are progresively removed. However, intensity may rise if an anti-parallel remanence is removed. This is particularly common when a viscous component which has been recently acquired by a sample is removed in the first stages of demagnetisation.

5.3.2 Vectors

Demagnetisation data were processed using a computer programme and equal angle polar stereographic projections (fig. 5.3) and Zijderveld diagrams (Zijderveld,

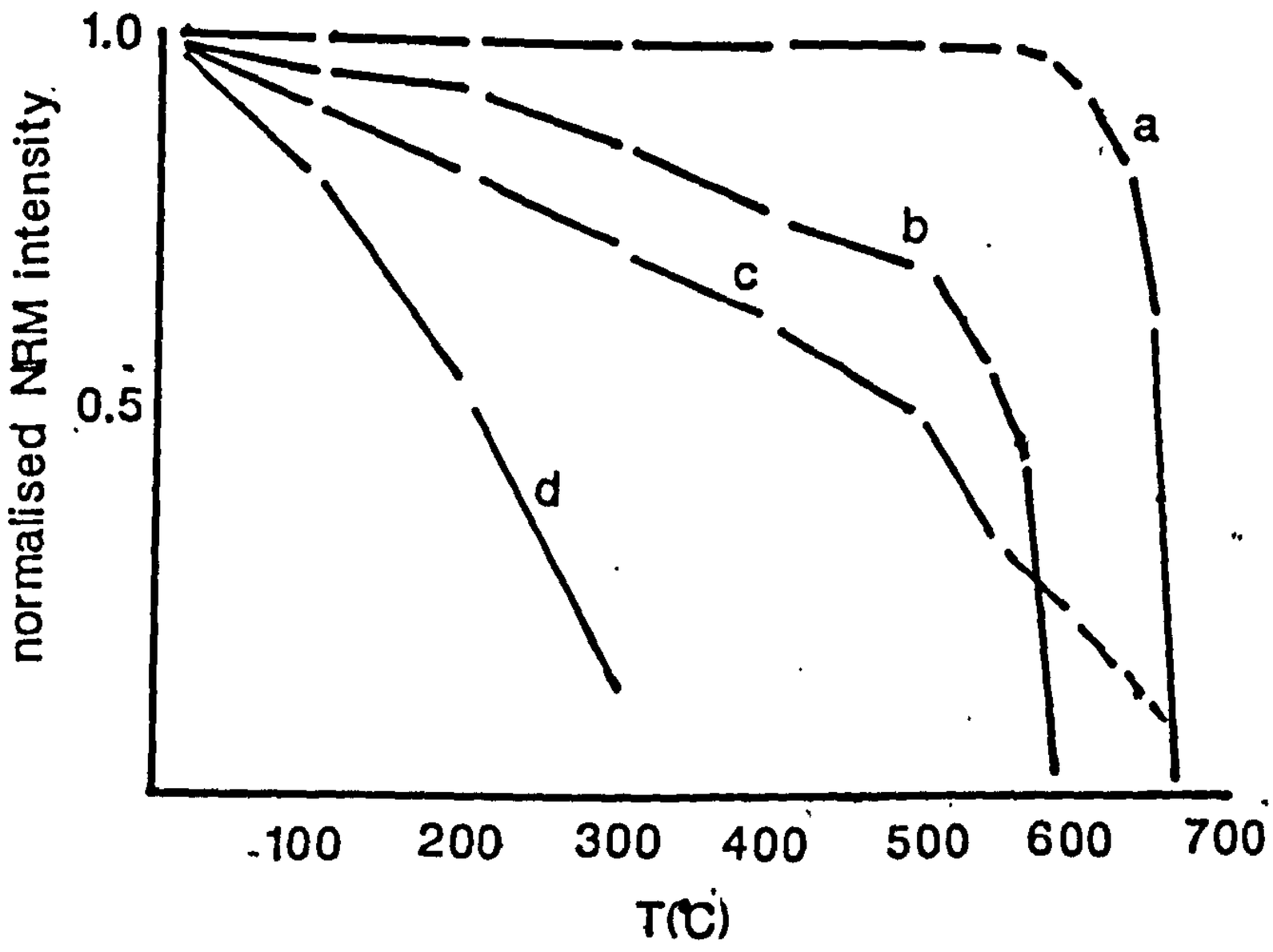

fig. 5.2 Summary diagram illustrating changes in normalised intensity of natural remanent magnetisation with increasing temperature during thermal demagnetisation for **a.** haematite; **b.** magnetite; **c.** haematite and magnetite and **d.** pyrrhotite (Piper, 1987).

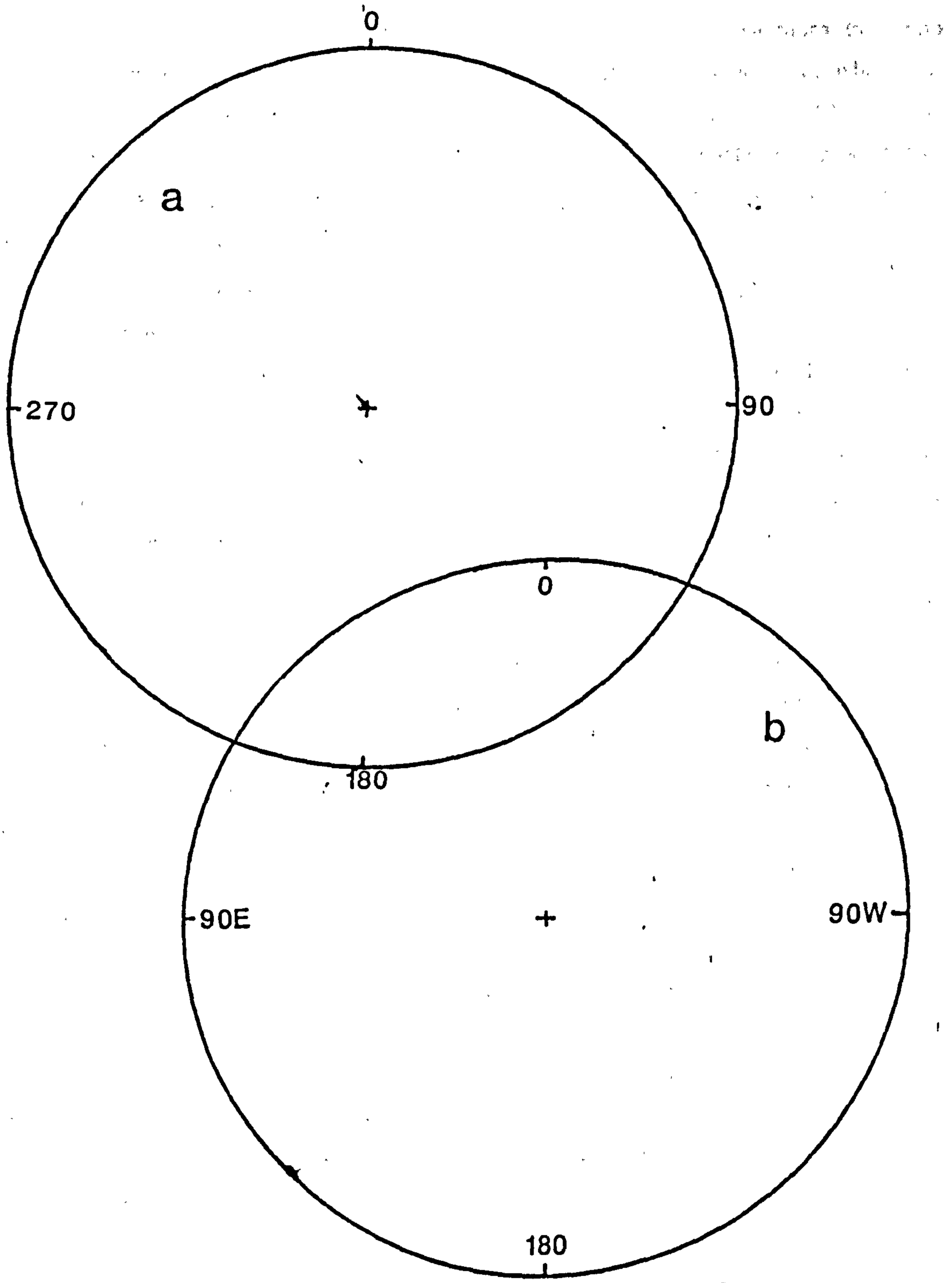

fig. 5.3 **a.** equal angle stereographic projection used for the presentation of sample directions and site mean directions. These are represented by declination and inclination. **b.** equal angle stereographic polar projection used for the presentation of virtual poles and the apparent polar wander path. These are represented by latitude (°N) and longitude (°E). By convention, positive (normal) inclinations are shown as full circles and negative (reversed) inclinations are shown as open circles.

1967) were plotted for every sample. Zijderveld diagrams were used to show changes in intensity and direction of vectors with progressive demagnetisation. These orthogonal plots were particularly useful in separating vectors in cases where more than one component contributes to the total natural remanent magnetism and in cases where the blocking temperature spectra of mineral phases overlap (Dunlop, 1979). The declination of the component being demagnetised is measured directly in the horizontal plane, eastwards from north. The inclination is derived from the apparent inclination (measured on the vertical plane) where: *tan* Inc = *tan* Inc_{app}/*cos* D. Estimates of precision were determined based on Fisherian statistics (Fisher, 1953). The magnetic stability of the remanence was determined with the aid of the *stability index* (SI) (Tarling and Symons, 1967) and *linearity* (Kirschvink, 1980). The stability index is based on the magnitude of directional changes and is independent of intensity. The lowest scatter of directions is found over the widest range of demagnetisation steps *I.e.*, for the highest value of *n*. A stable direction must be defined by at least 3 successive points. A SI of <1 is considered unstable; a SI of 1-2 is considered meta-stable; a SI of 2-5 is considered stable; and a SI of >5 is considered very stable (Tarling, 1983). Linearity was evaluated by using the *diagonal error* of a minimum of three consecutive maesurements. Linearity is based on intensity and directional changes and is calculated by fitting consecutive measurements into a linear box, the *diagonal angle* of which is then calculated. The lower the value of the diagonal angle, the more linear the vector over this series of demagnetisation steps (Kirschvink, 1980). A diagonal angle of 10° was taken as a maximum level of acceptability. These two analytical tools are complementary to some extent because the stability index is based on directional changes and linearity involves consideration of intensity and directional changes.

Analysis of demagnetisation data for individual samples

The principal natural remanent magnetism vectors for each sample were selected after computer analysis of stability and linearity, followed by a visual inspection of stereographic and Zijderveld projections for every sample (*N.B.*, a summary of the raw data for every site is available in the library of the University of Newcastle upon Tyne or from the author). The stability index and linearity parameters were tabulated against the highest value of *n* and the lowest value of *A95* (Tarling, 1983) for each sample. A stability index of > 1 and linearity values of <10° were used as rejection criteria. Data which were of low intensity and close to the detection levels of the magnetometer were included, but used with due caution. A summary of data for samples

which passed the rejection criteria is available, for every site, in appendix 5.1. The vectors so obtained from individual samples were then collated with those from other samples from the same site and these data used to calculate mean direction for each site, giving equal weight to each sample (Piper, 1987). A discussion of the observed data and its interpretation is given for each site.

5.4 Site descriptions

In this section, a summary of the magnetic results from each site are presented in conjunction with interpretations of these results. This format was chosen in preference to long-winded site-by-site description, in the interests of being brief and concise (*N.B.* there are 30 sites to consider). Summaries of analyses of site data are presented facies by facies. This spatial format was chosen because there was initially no reason to group sites together on the basis of their magnetic behaviour and because of a wish to keep description separate from interpretation as much as possible.

A summary of the magnetic behaviour displayed by individual sites is given with reference to one or two representative samples from each site. The demagnetisation data has been presented in several forms; sample directions from each site are illustrated on a summary stereogram (where directions are from samples demagnetised thermally, unless the direction is labelled 'AF' which refers to samples demagnetised using an alternating field) and by giving examples, where appropriate, of demagnetisation behaviour of particular samples. On these diagrams, heating steps are coded 0 to 9; if more steps were used then these are labelled alphabetically. The actual temperature steps used are given in table 5.1. On the orthogonal plots, projections of vectors onto the horizontal plane are denoted by digits; projections onto the vertical plane are denoted by digits accompanied by a letter V. Changes in intensity (absolute and normalised) and susceptibility with temperature are presented in graph form, with all data from each site summarised onto a single graph to enable assessment of within-site variations. A key refers to the sample numbers from each site. For clarity of the figures, units are not given on each graph axis. The units of natural remanent magnetism intensity are in $10^{-4}Am^{-1}$. Volume susceptibility is given in units x $10^{-6}GOe^{-1}$; see appendix 4.2) (Graphs of normalised susceptibility change with temperature are not used because of the confusion introduced by changes of sign). These graphs are presented in the same order and format for each site.

a.

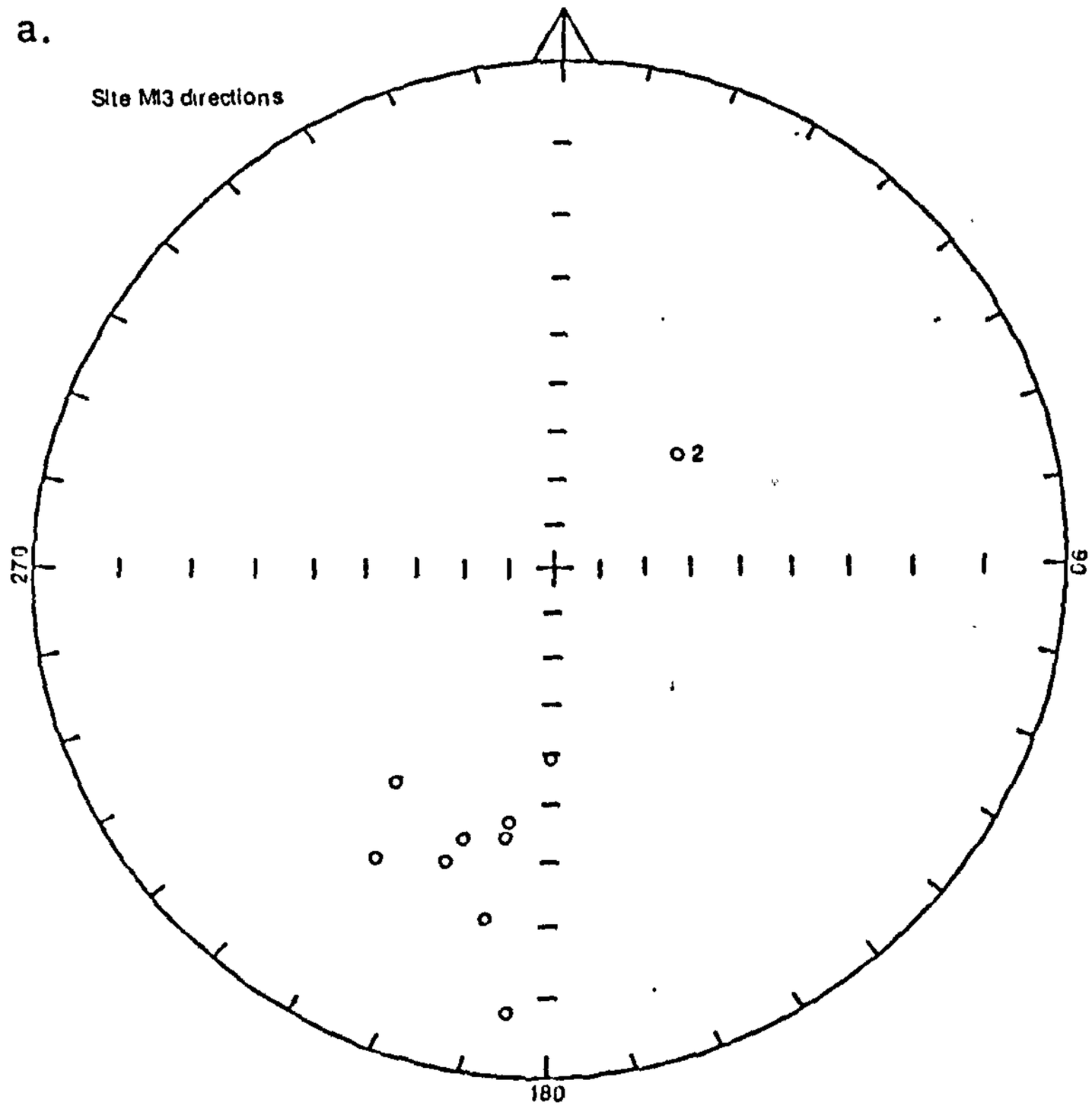

b.

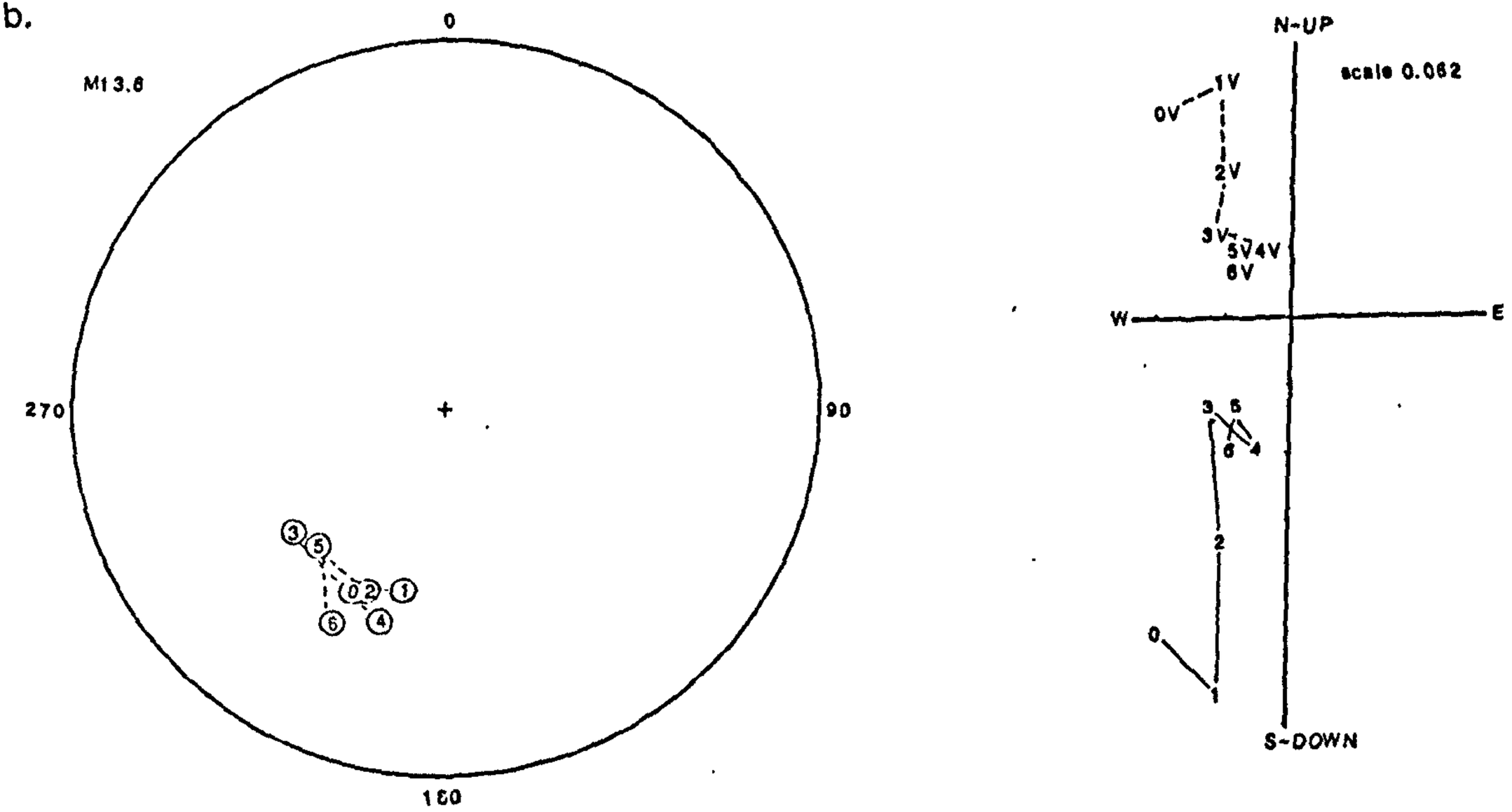

fig. 5.4 Summary of demagnetisation behaviour of samples from site M13. Natural remanent magnetism (NRM) intensity is given x $10^{-4}Am^{-1}$; susceptibility units x 10^{-6} GOe^{-1}
a. stereographic projection of stable sample directions; **b.** stereographic projection and accompanying orthogonal plot illustrating vector movement with progressive demagnetisation; **c.** NRM intensity change with increasing temperature illustrating variation of magnetic mineral content between samples; **d.** normalised NRM change with increasing temperature illustrating within-site variation; **e.** susceptibility variation with increasing temperature illustrating changes which occur due to mineralogical alteration.

c

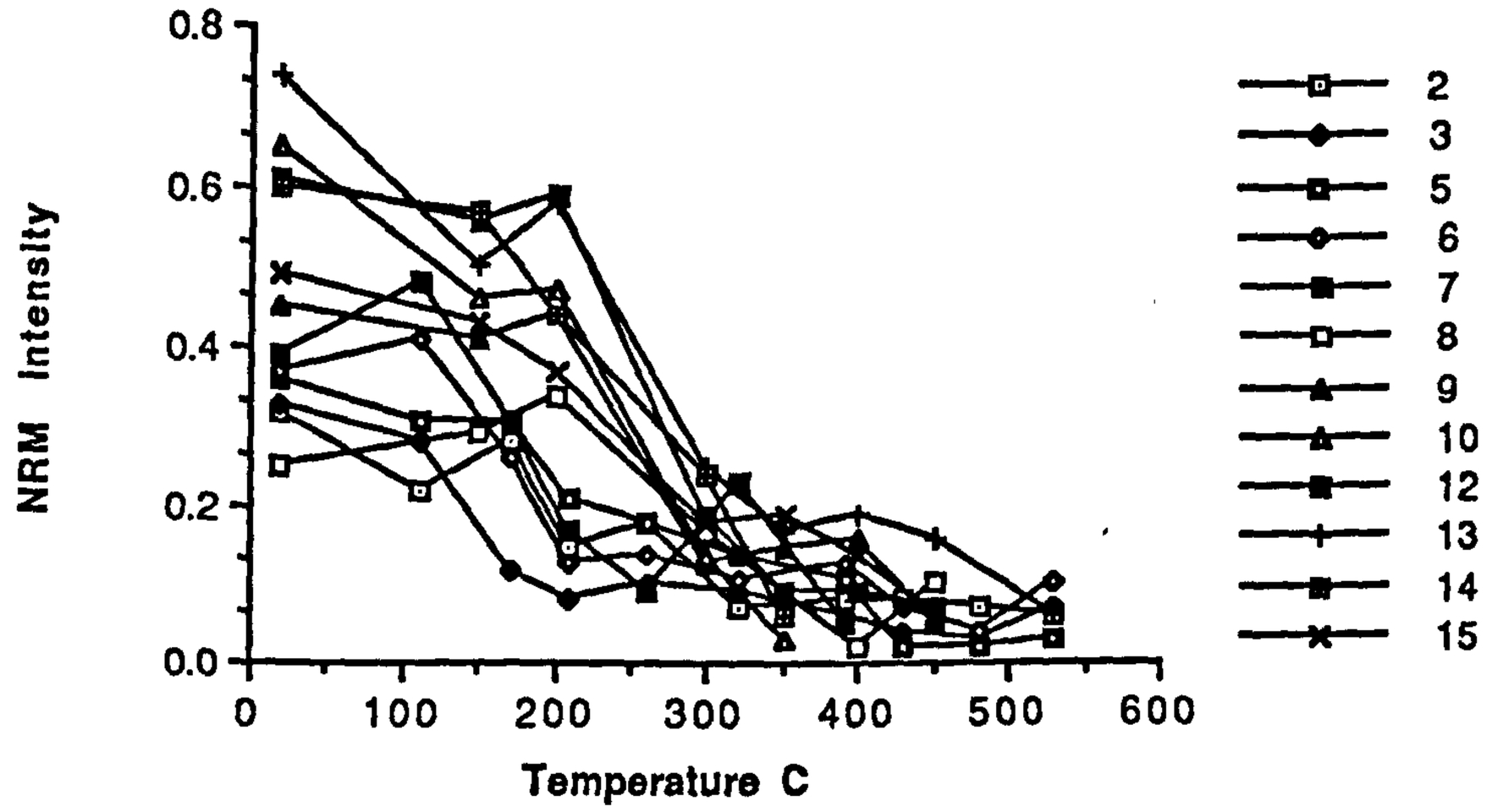
NRM Intensity
0.8
0.6
0.4
0.2
0.0
0
100
200
300
400
500
600
Temperature C
2
3
5
6
7
8
9
10
12
13
14
15

d

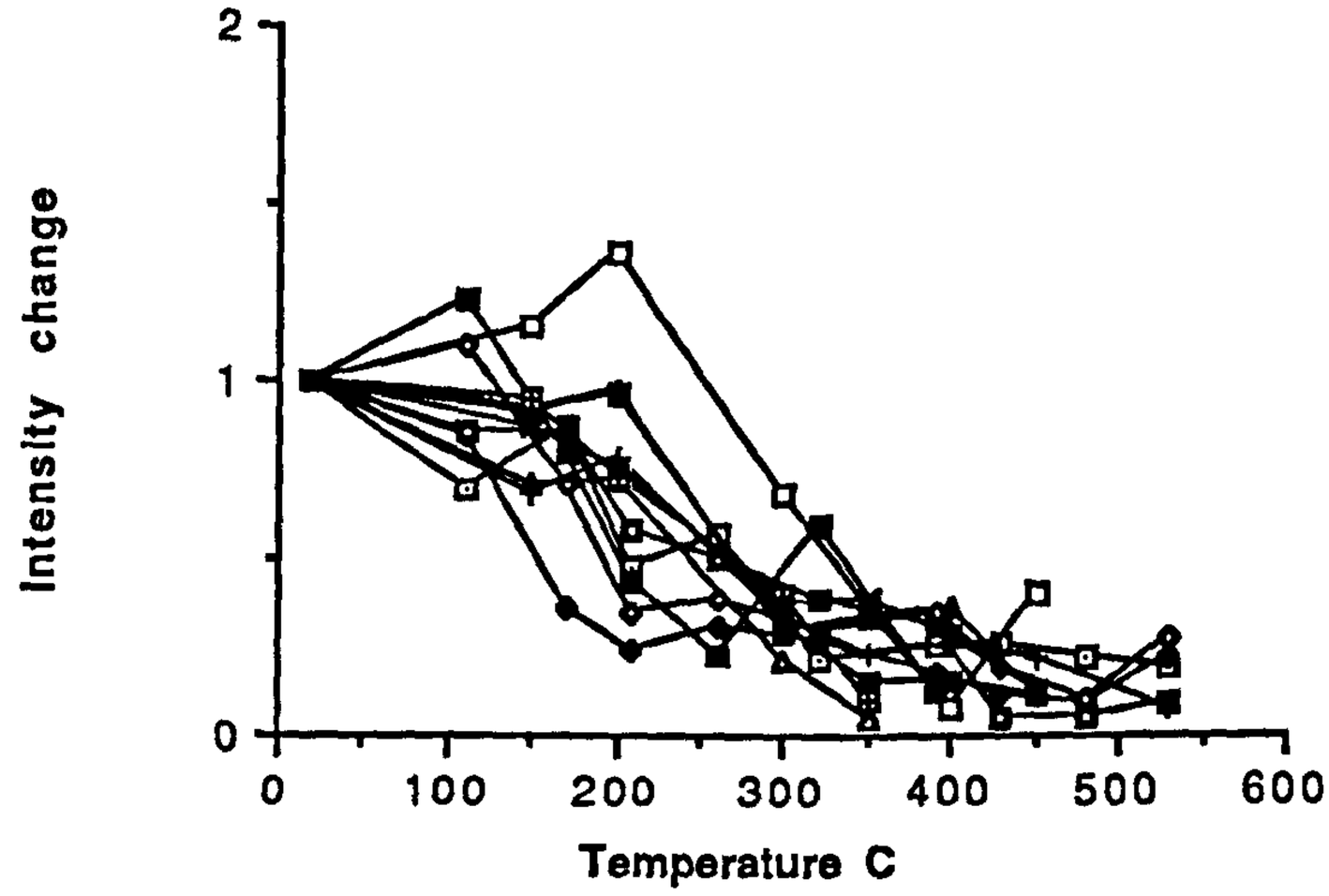
Intensity change
2
1
0
0
100
200
300
400
500
600
Temperature C

e

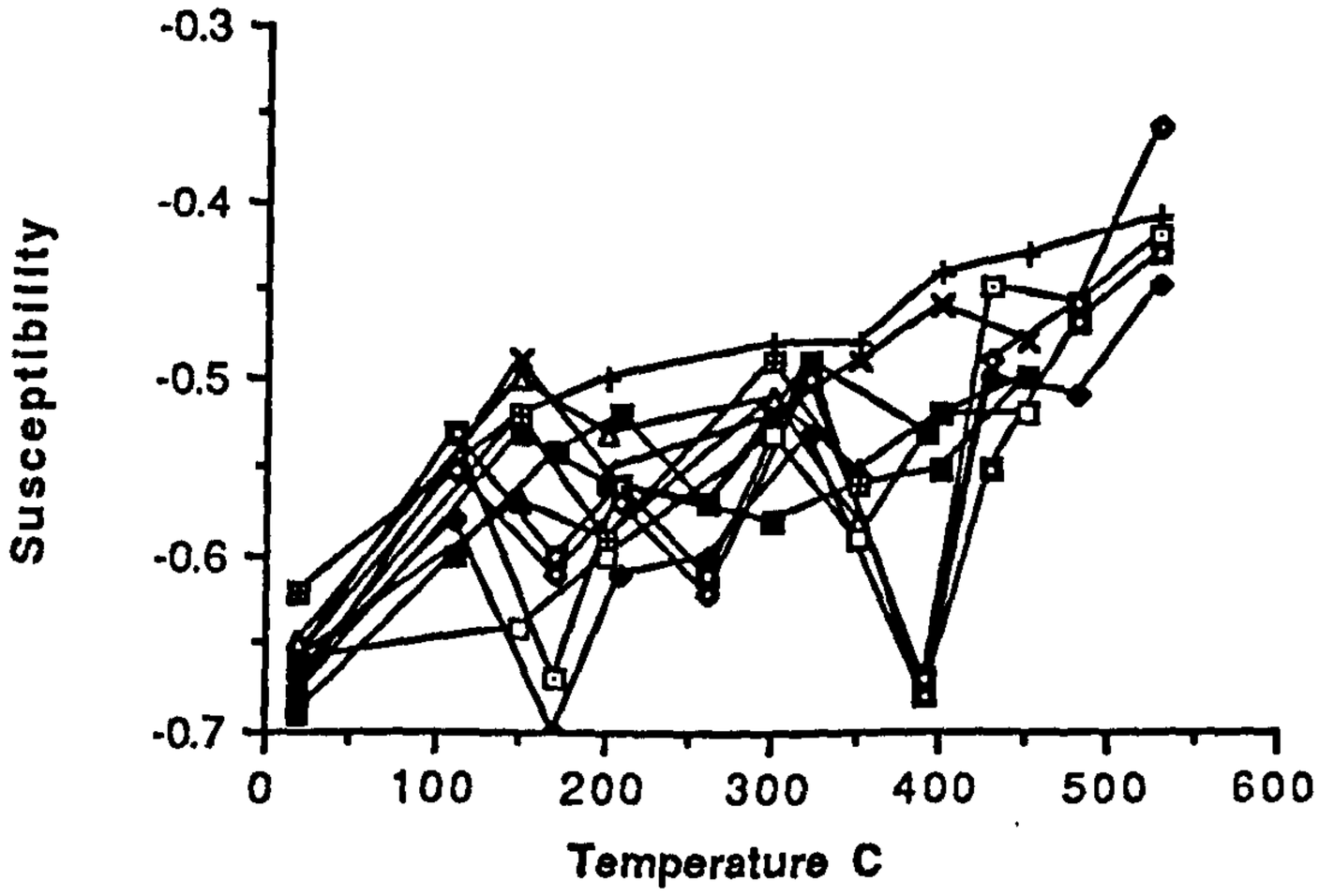
Susceptibility
-0.3
-0.4
-0.5
-0.6
-0.7
0
100
200
300
400
500
600
Temperature C

5.4.1 Back reef facies

A summary of the demagnetisation behaviour for sites from the back reef facies, and interpretations of vectors and magnetic mineralogy are as follows:

Site M13 (fig.5.4) Maximum initial intensity of 0.65 $x10^{-4}Am^{-1}$ and initial susceptibility of -0.62 (volume units x $10^{-6}GOe^{-1}$; see appendix 4.2) indicate that samples from this site contain low quantities of magnetic minerals. After the removal of an initial normal or reversed polarity component by 100°C, probably carried by goethite, the natural remanent magnetism steadily demagnetises to 320°C. Site directions are meta-stable, reversed polarity and form a cluster, the mean direction of which has the same inclination as the apparent field direction wander path at 185 Ma, but differs in declination by 25°. There is little variation in the direction of the vector at higher demagnetisation temperatures *i.e.*, effective demagnetisation is complete by around 320°C. This temperature of demagnetisation suggests that pyrrhotite is the magnetic carrier. However, there is no large increase in susceptibility after 320°C which would have been expected from the oxidation of pyrrhotite to haematite and therefore suggests that maghemite may be the remanence carrier. Susceptibility increases with progressive heating steps, suggesting the continued oxidation of hydroxides to haematite. This might also be the Hopkinson effect in haematite. Several samples show a significant decrease in susceptibility to 400°C; this is difficult to explain in terms of chemical changes and may reflect error in measurement. AF demagnetisation did not yield any stable directions.

Site 13A (fig. 5.5) Maximum initial natural remanent magnetism intensity of 3.97 $x10^{-4}Am^{-1}$ and susceptibility of 0.05 (volume units x $10^{-6}GOe^{-1}$; see appendix 4.2) indicate that samples from this site have a low, but significant magnetic mineral component. A range of magnetic mineral content between samples is indicated by the variety of initial natural remanent magnetism intensity values. However, samples demagnetise in a similar way, suggesting that they contain similar mineralogy. Resolution of the magnetic carrier is ambiguous because demagnetisation is complete by around 500°C which is not the T_C of any pure magnetic phase. Consequently, an impure mineral is implied which has a low T_b which could be magnetite or haematite, depending on the domain size. Site directions are stable and form a grouping of normal directions. These directions are spread between an inclination of around 30° to equatorial, and the directions isolated after AF and thermal demagnetisation are similar. The spread of

a.

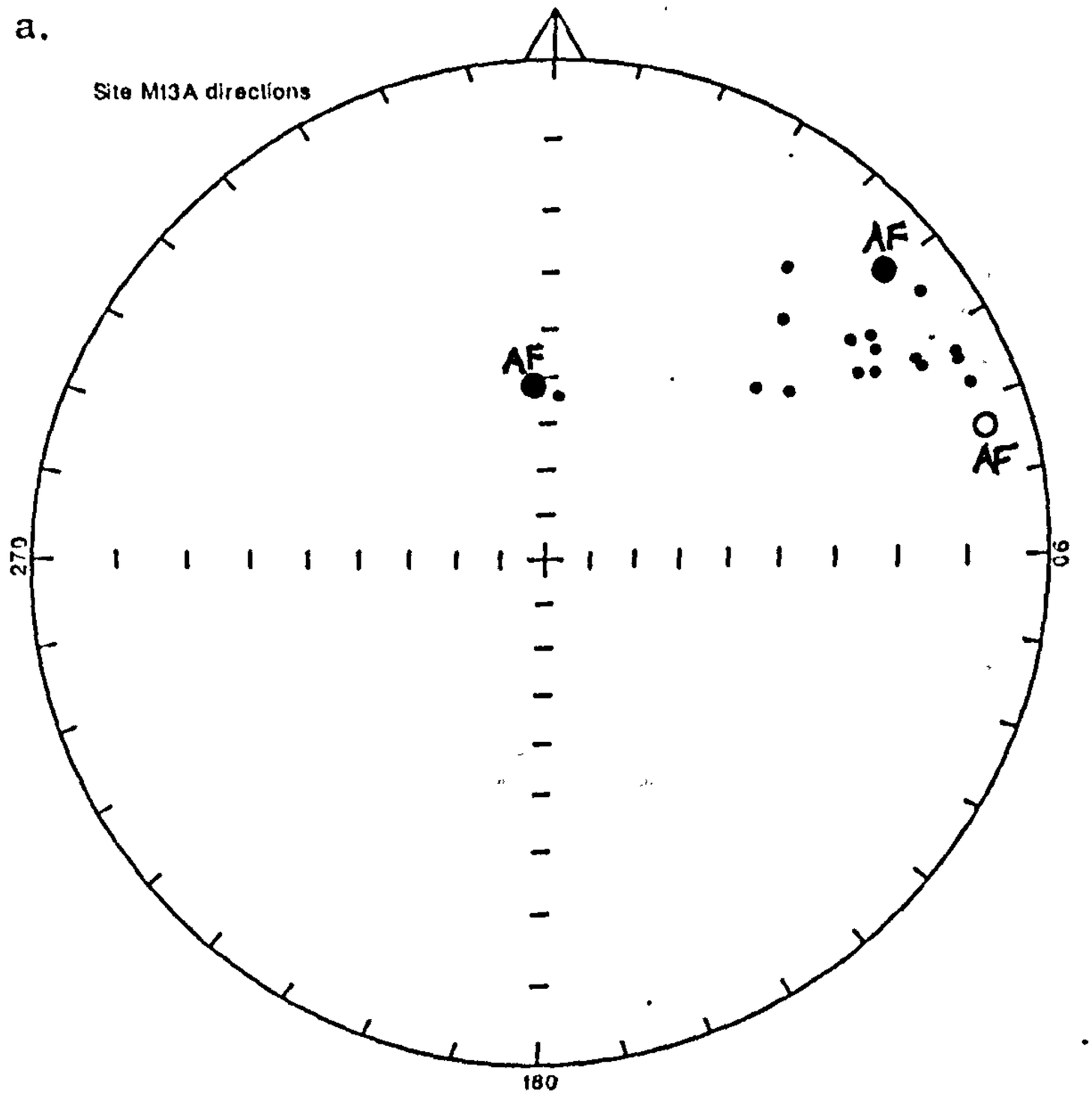

b.

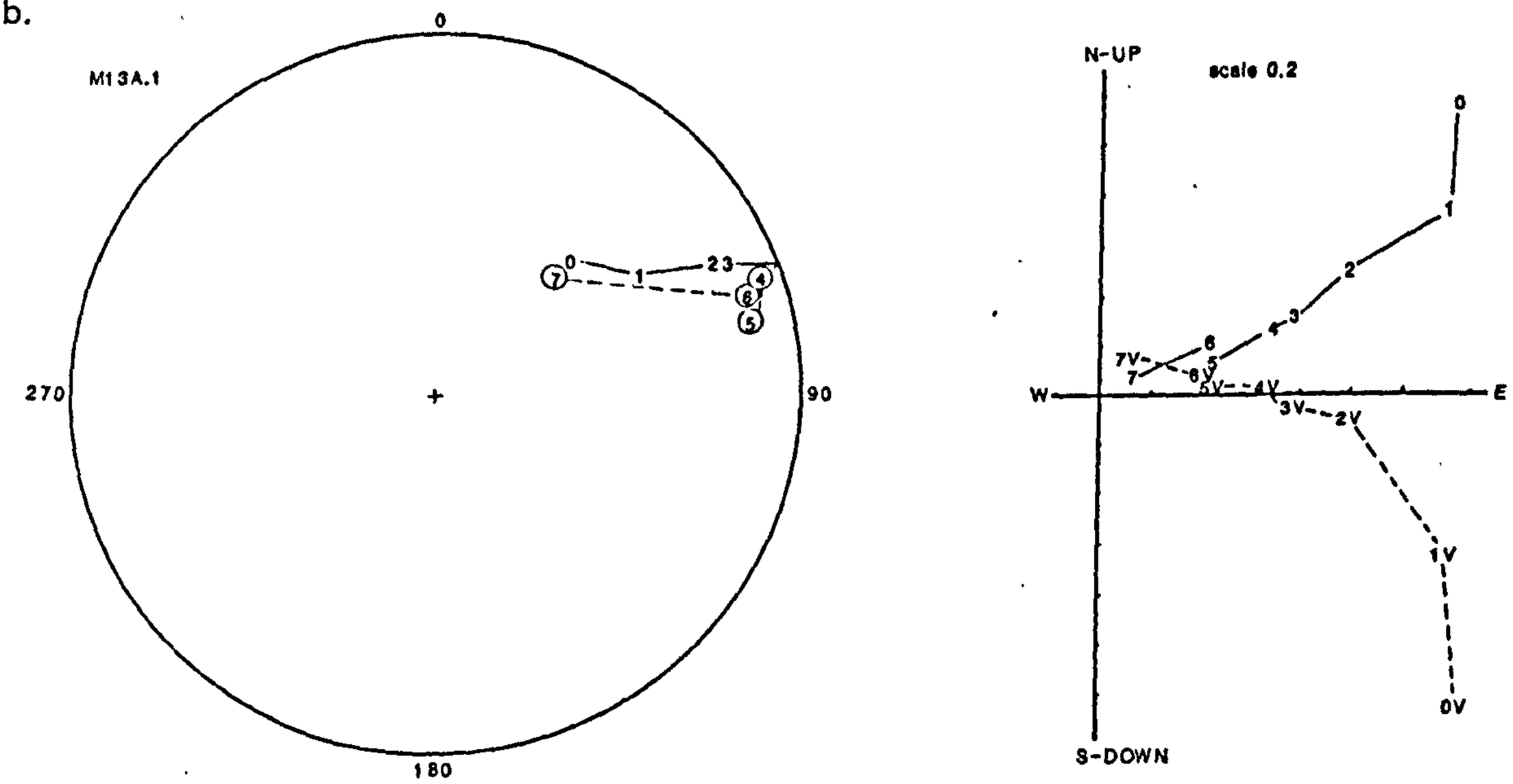

fig. 5.5 Summary of demagnetisation behaviour of samples from site M13A. Natural remanent magnetism (NRM) intensity is given x $10^{-4}Am^{-1}$; susceptibility units x 10^{-6} GOe^{-1}|
a. stereographic projection of stable sample directions; **b.** stereographic projection and accompanying orthogonal plot illustrating vector movement with progressive demagnetisation; **c.** NRM intensity change with increasing temperature illustrating variation of magnetic mineral content between samples; **d.** normalised NRM change with increasing temperature illustrating within-site variation; **e.** susceptibility variation with increasing temperature illustrating changes which occur due to mineralogical alteration.

c

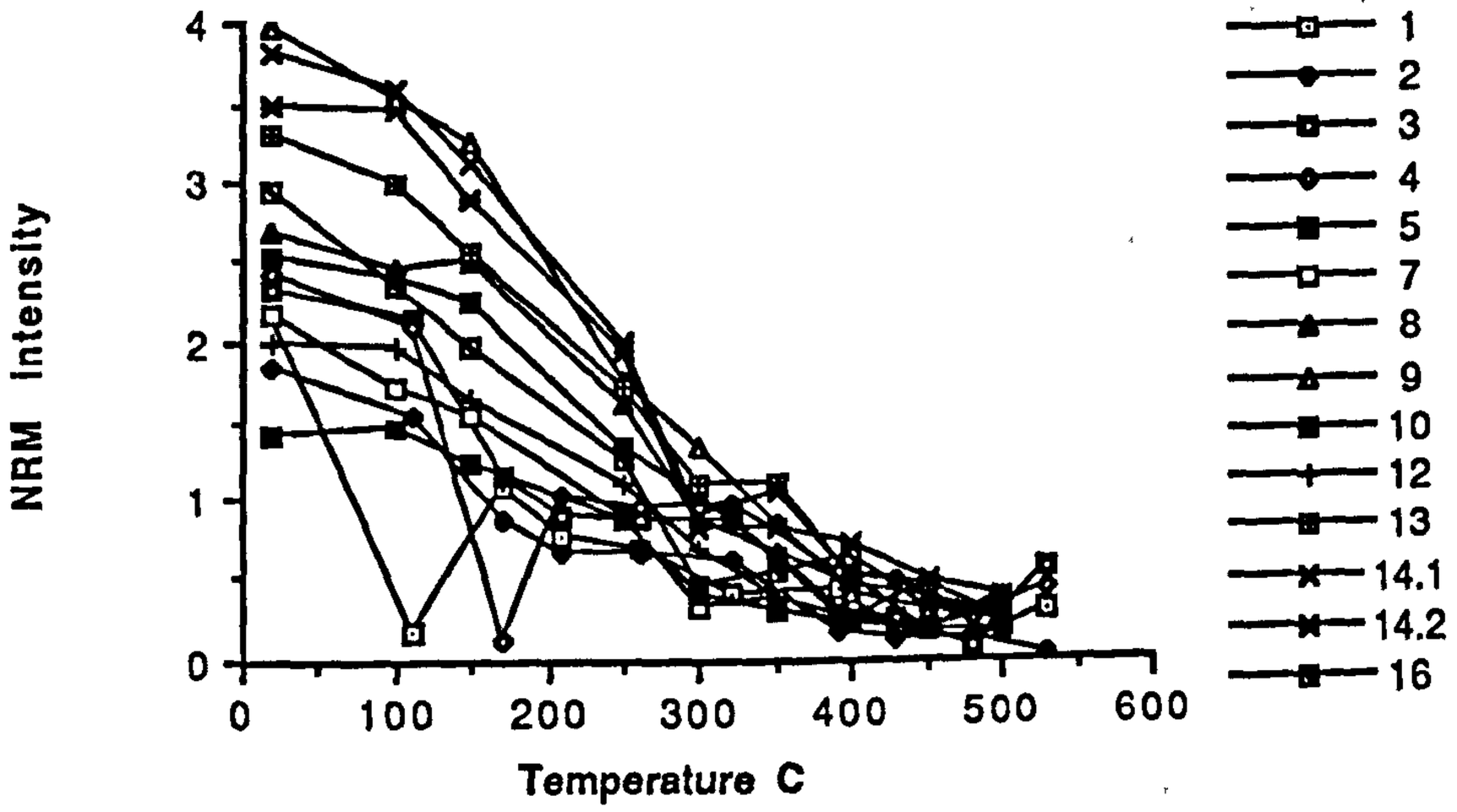
NRM Intensity
Temperature C
1
2
3
4
5
7
8
9
10
12
13
14.1
14.2
16

d

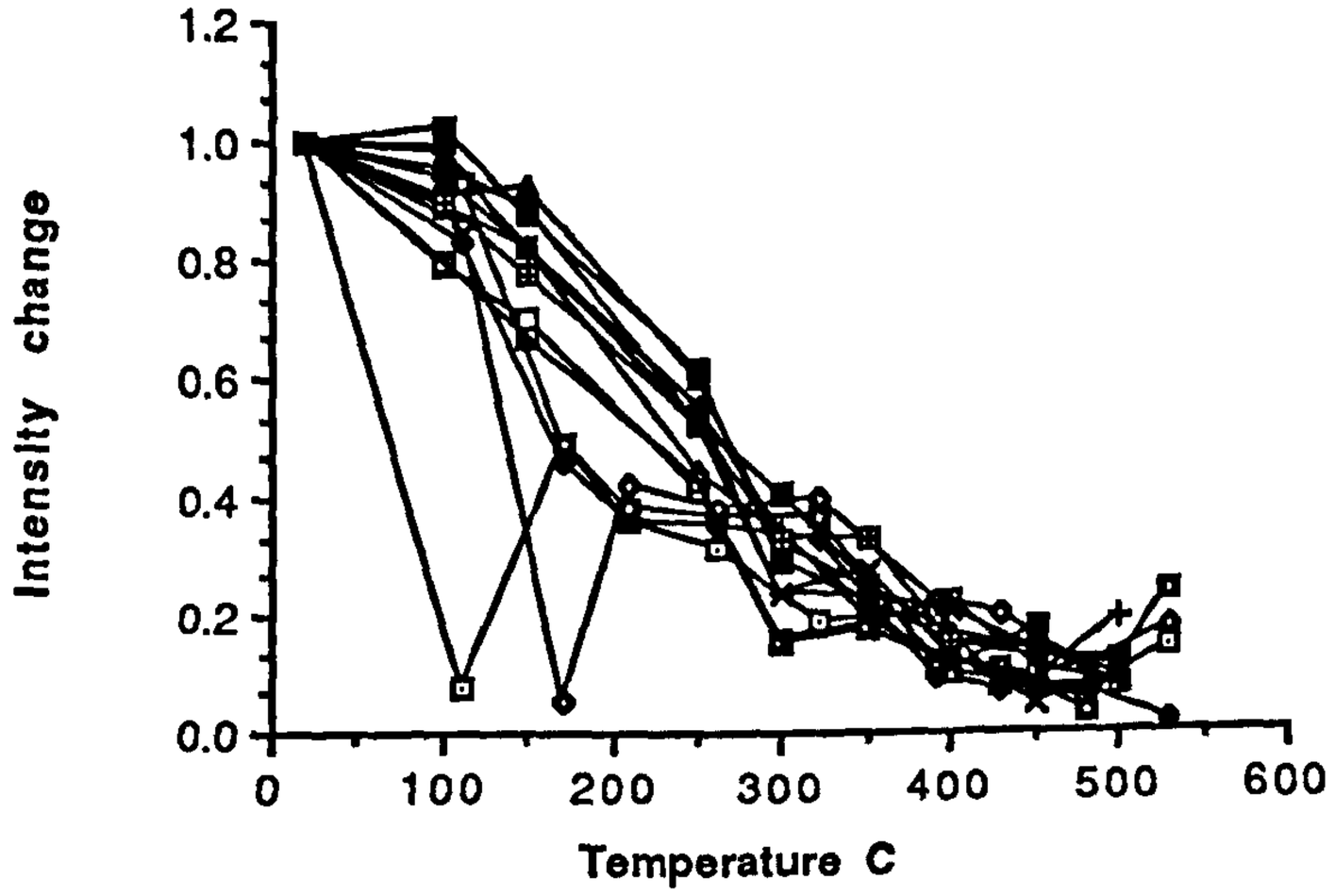
Intensity change
Temperature C

e

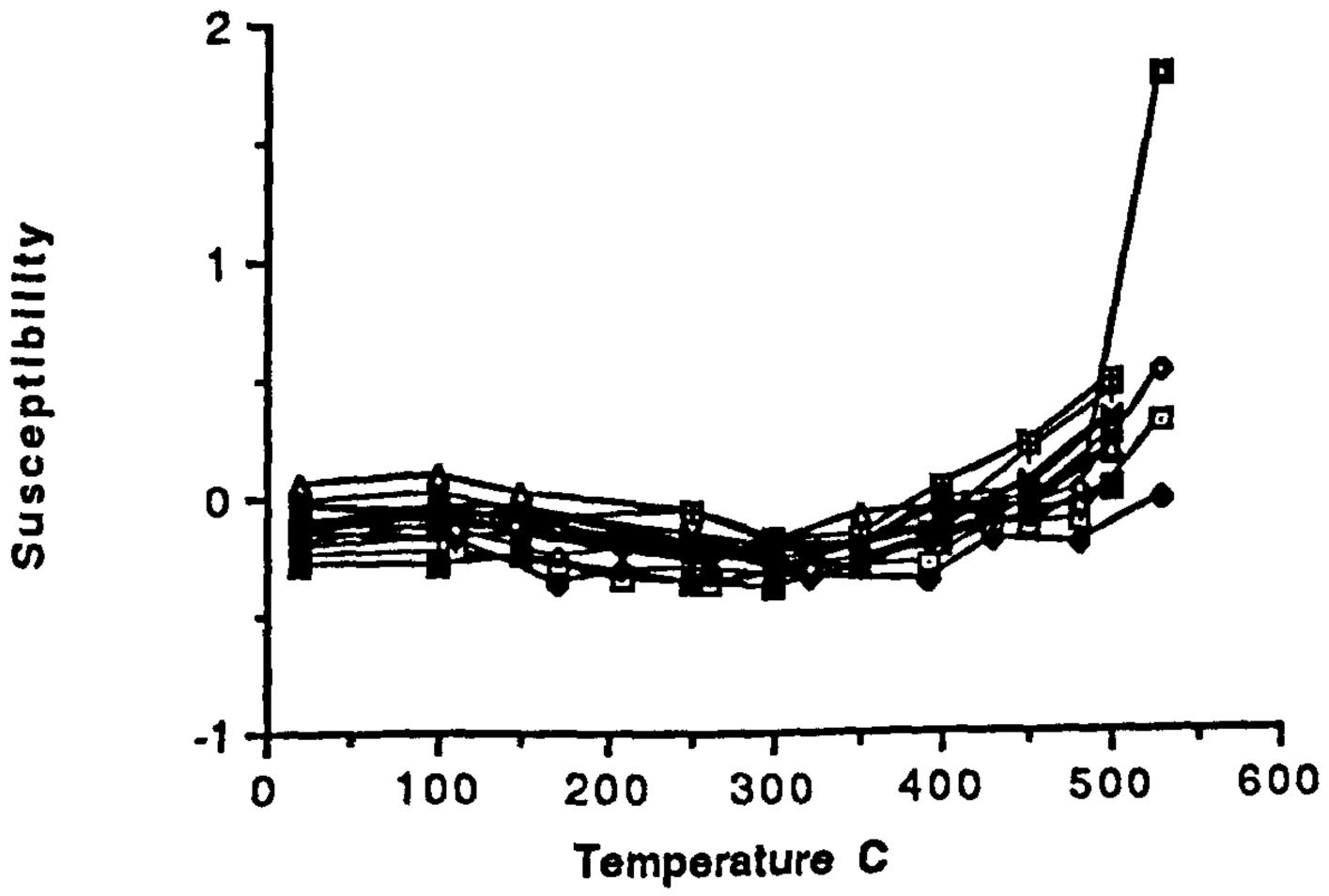
Susceptibility
Temperature C

directions is probably due to a mixture of two natural remanent magnetism components. A mix of normal and reversed polarity components with similar direction are clearly visible on the Zijderveld diagram. The vector moves progressively with increasing demagnetisation steps and becomes increasingly shallow in inclination, until it actually reverses polarity. Although the site mean direction is normal polarity and well defined, it does not lie on the apparent field direction wander path. Incomplete resolution of vectors may explain this. The within site variation may be explained by the mixing of different magnetic carriers which have different natural remanent magnetism directions. Directions are not easily interpretable as they do not lie on the apparent field direction wander path.

Site M14 (fig. 5.6) There is considerable variation in initial natural remanent magnetism intensity, although all values are high (up to 50.34 $x10^{-4}Am^{-1}$), indicating significant magnetic mineral content in samples from this site. However, the susceptibility values are almost identical (maximum of -0.02 volume units x $10^{-6}GOe^{-1}$; see appendix 4.2). This range of intensity values with uniform susceptibility, suggests wide variation in domain states or composition of the natural remanent magnetism carrier. The low susceptibility values suggest that the magnetic carrier is haematite. Site directions are very stable and clearly defined to 530°C, but range widely in direction and polarity. Demagnetisation paths are relatively straight, indicating single component magnetisations with each sample demagnetising uniformly in a constant direction and without changing polarity. This behaviour may be explained as resulting from lightening strike, with the variation in remanence intensity due to distance from the point of impact of the lightening bolt. Both intensity and susceptibility values show little change to 430°C. At this temperature, intensity decreases rapidly, and susceptibility starts to increase. Demagnetisation is complete by 530°C. This T_b range indicates a range of grain sizes and domain sizes within individual samples. Two types of vector can be distinguished; those which group together and have a well defined mean direction (samples 2,5,6,8,12,12.2) and those which have shallow inclination, *i.e.*, equatorial, reversed directions (samples 3,4,10,11,13,14,15,17,18,18.2,19). Neither of these groups of directions lie on the apparent field direction wander path, and they are therefore difficult to interpret. There is no obvious correlation between intensity of natural remanent magnetism and its direction.

Site M15 (fig. 5.7) Maximum initial natural remanent magnetism intensity of 1.51 x $10^{-4}Am^{-1}$ and susceptibility of -0.27 (volume units x $10^{-6}GOe^{-1}$; see appendix 4.2)

fig. 5.6 Summary of demagnetisation behaviour of samples from site M14. Natural remanent magnetism (NRM) intensity is given x $10^{-4}Am^{-1}$; susceptibility in units x 10^{-6} GOe^{-1}

a. stereographic projection of stable sample directions;

b. and **c.** stereographic projections and accompanying orthogonal plots illustrating vector movement with progressive demagnetisation for samples with different behaviour;

d. NRM intensity change with increasing temperature illustrating variation of magnetic mineral content between samples;

e. normalised NRM change with increasing temperature illustrating within-site variation;

f. susceptibility variation with increasing temperature illustrating changes which occur due to mineralogical alteration.

a.

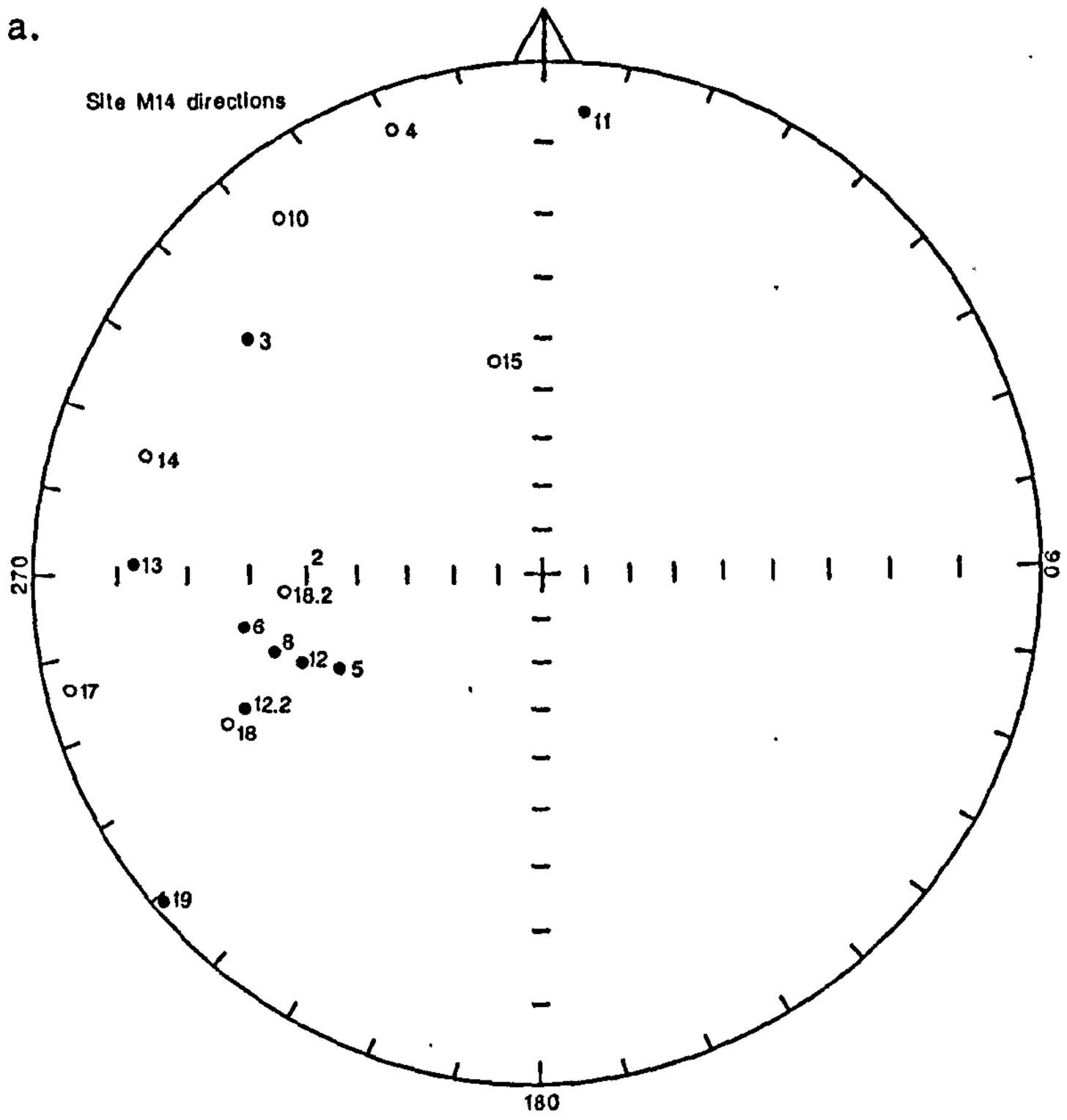
Site M14 directions
0
90
180
270
11
4
10
3
15
14
13
2
18.2
6
8
12
5
17
12.2
18
19

b.

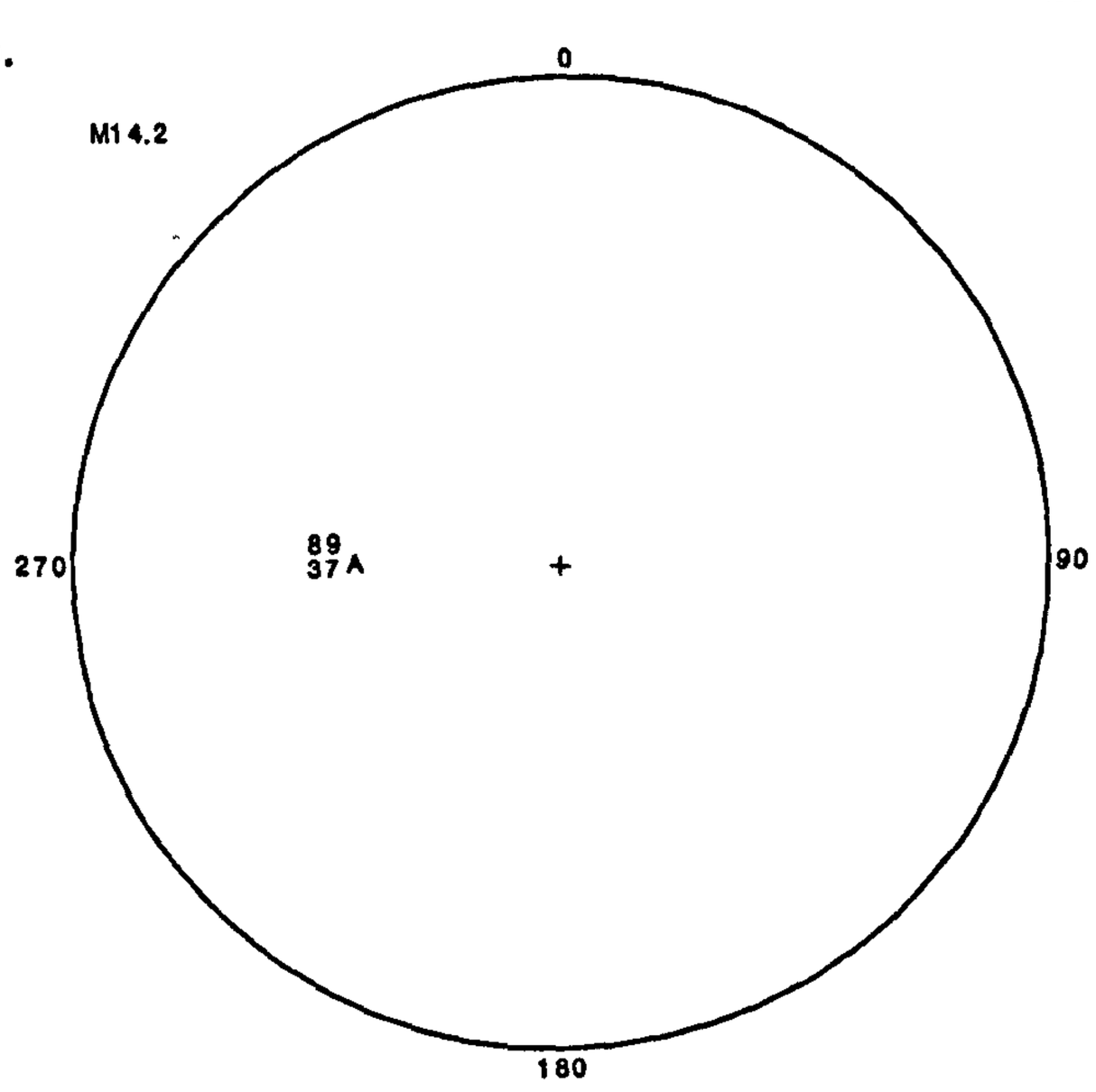
M14.2
0
90
180
270
89
37 A

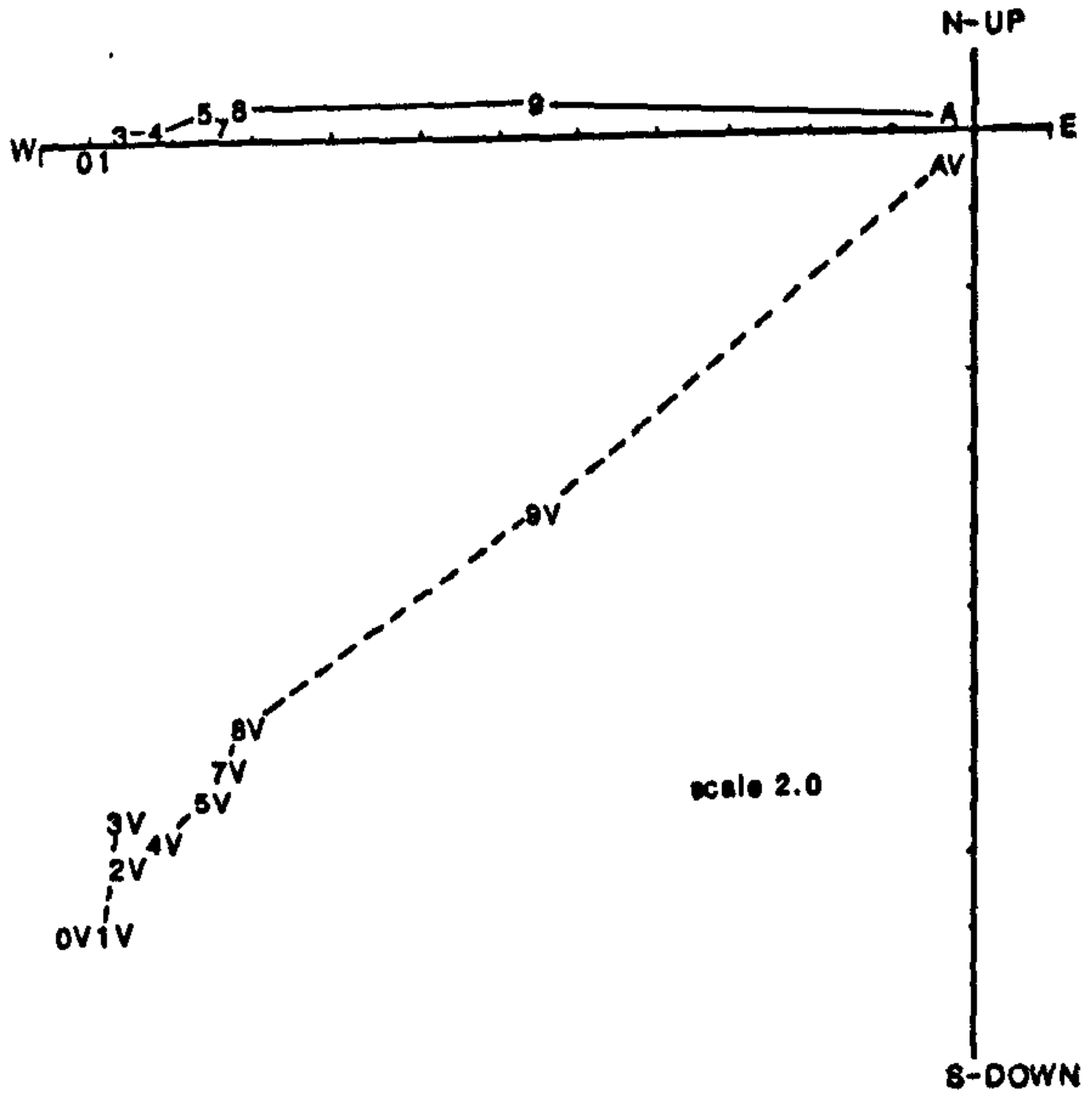
N-UP
W
E
S-DOWN
scale 2.0
0V
1V
2V
3V
4V
5V
7V
8V
9V
AV

C.

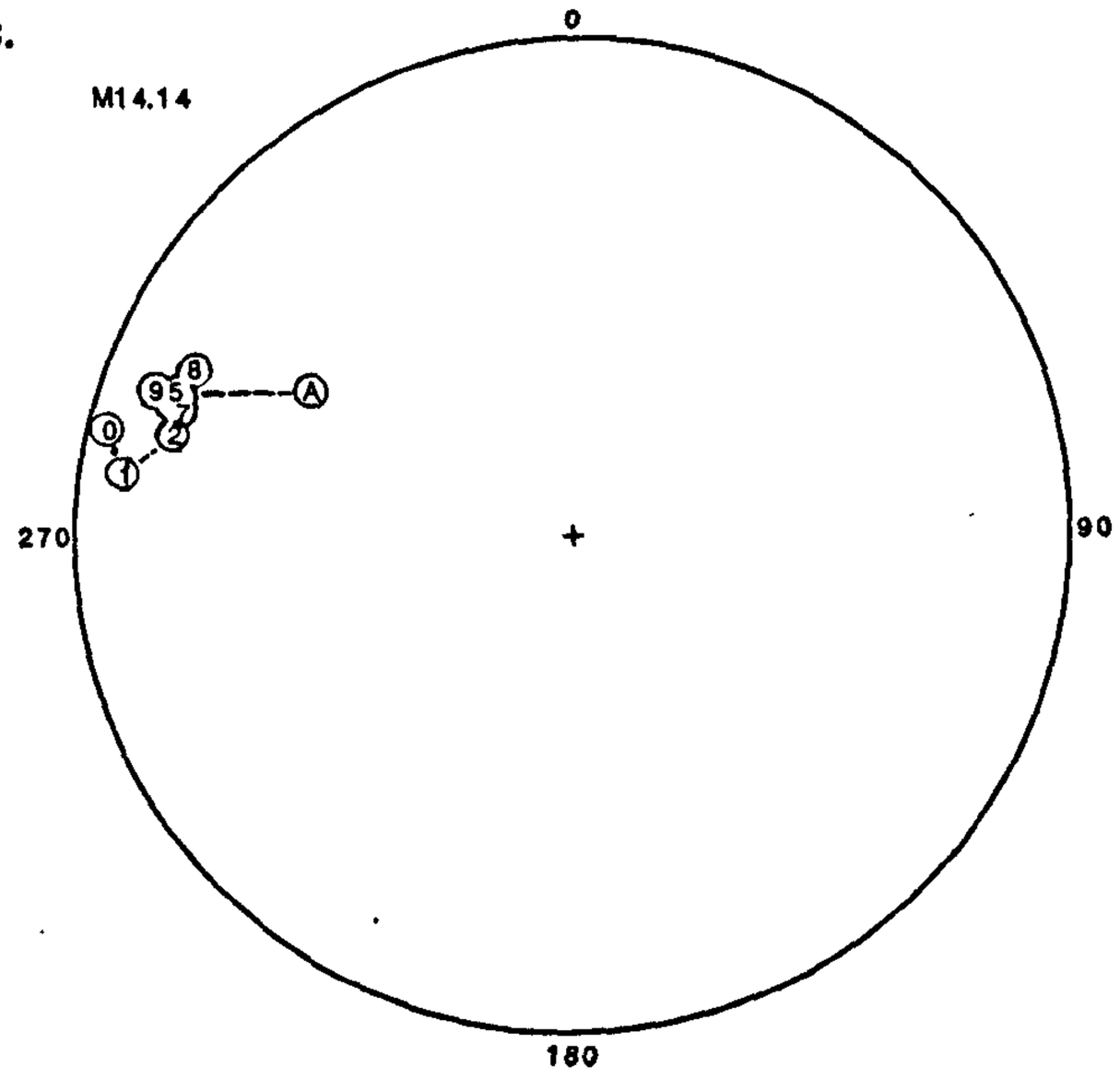
M14.14
0
90
180
270

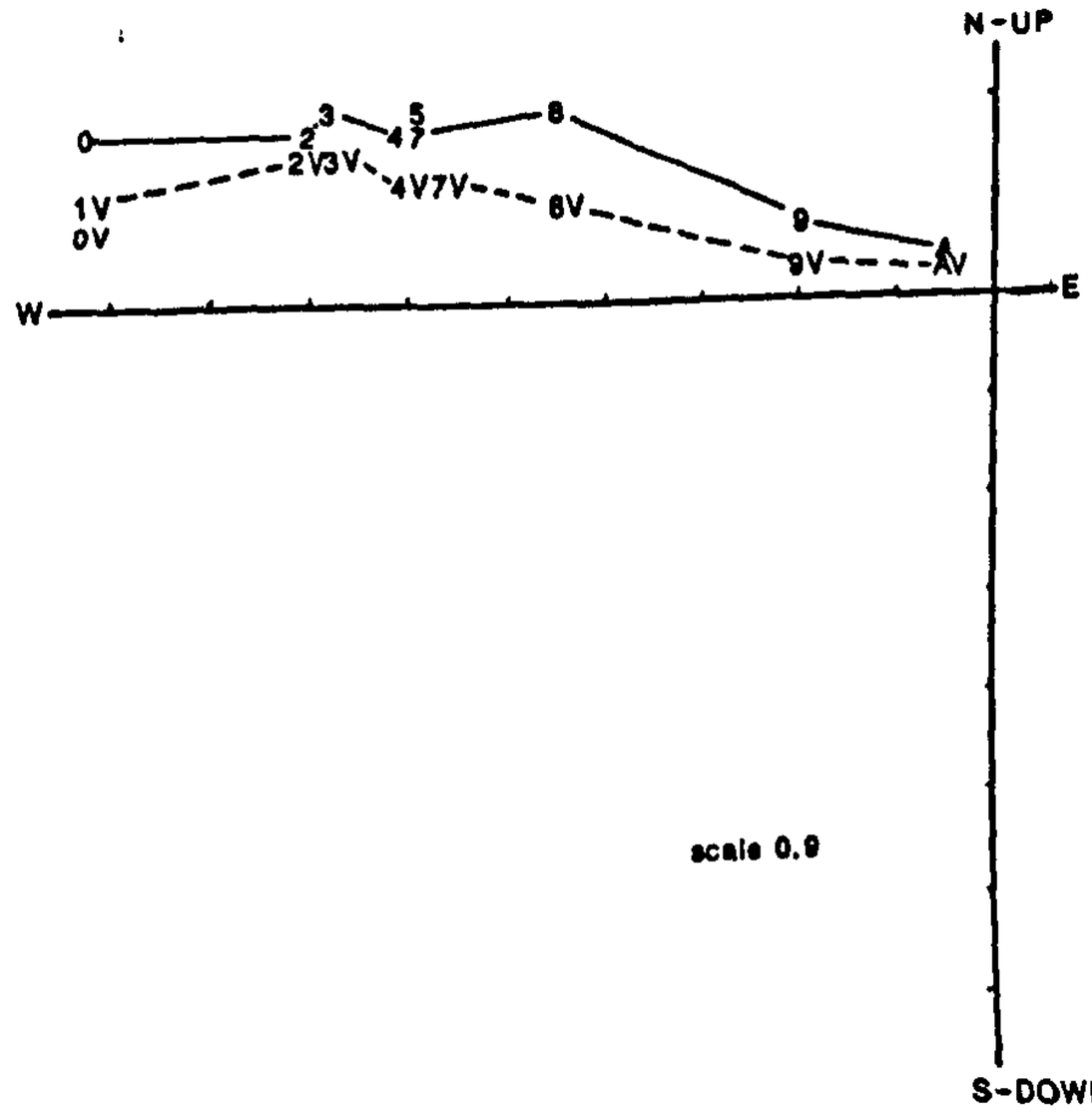
N-UP
W
E
S-DOWN
scale 0.9
0V
1V
2V
3V
4V
7V
8V
9V
AV

d

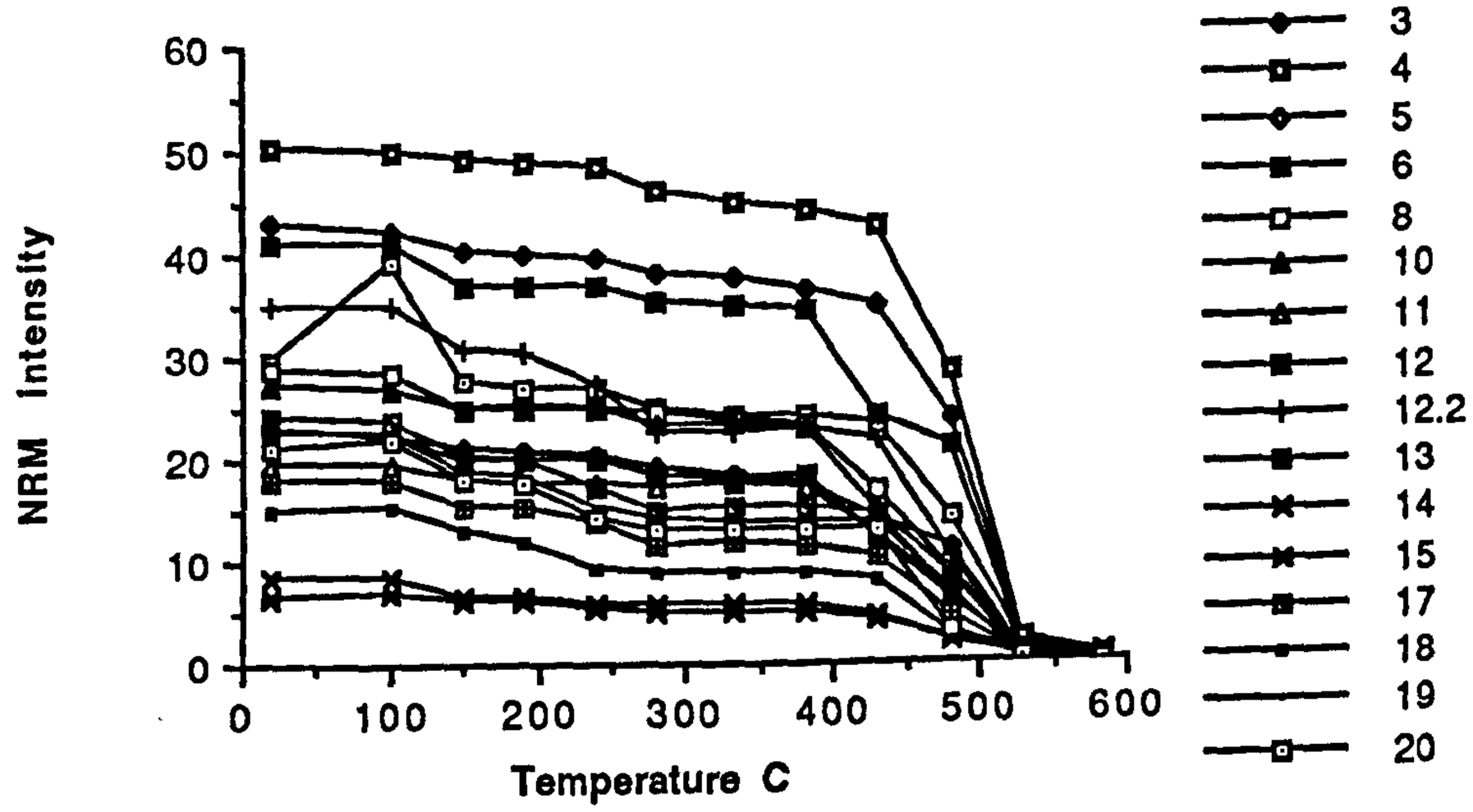
NRM Intensity
60
50
40
30
20
10
0
0
100
200
300
400
500
600
Temperature C
2
3
4
5
6
8
10
11
12
12.2
13
14
15
17
18
19
20

e

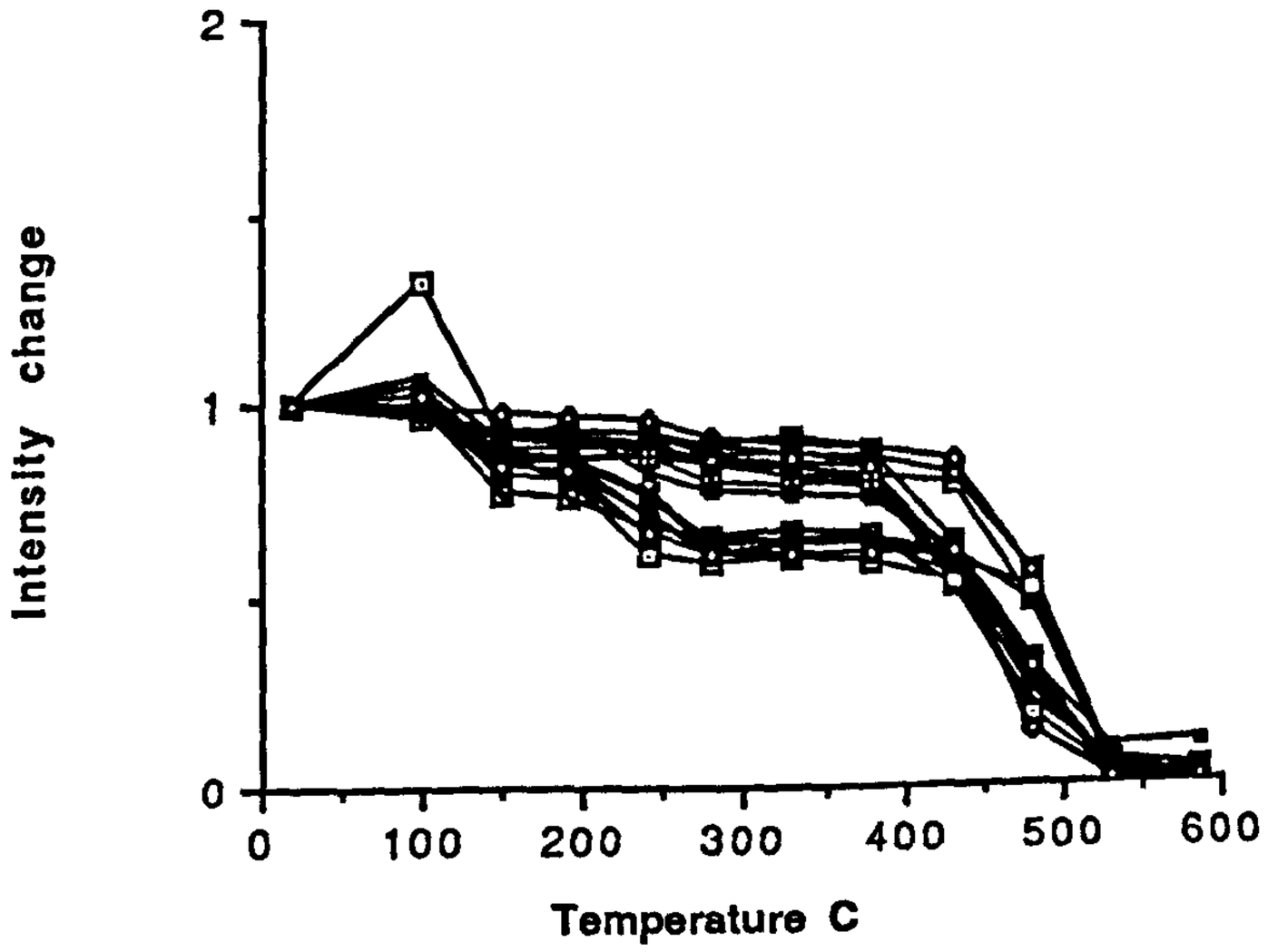
Intensity change
2
1
0
0
100
200
300
400
500
600
Temperature C

f

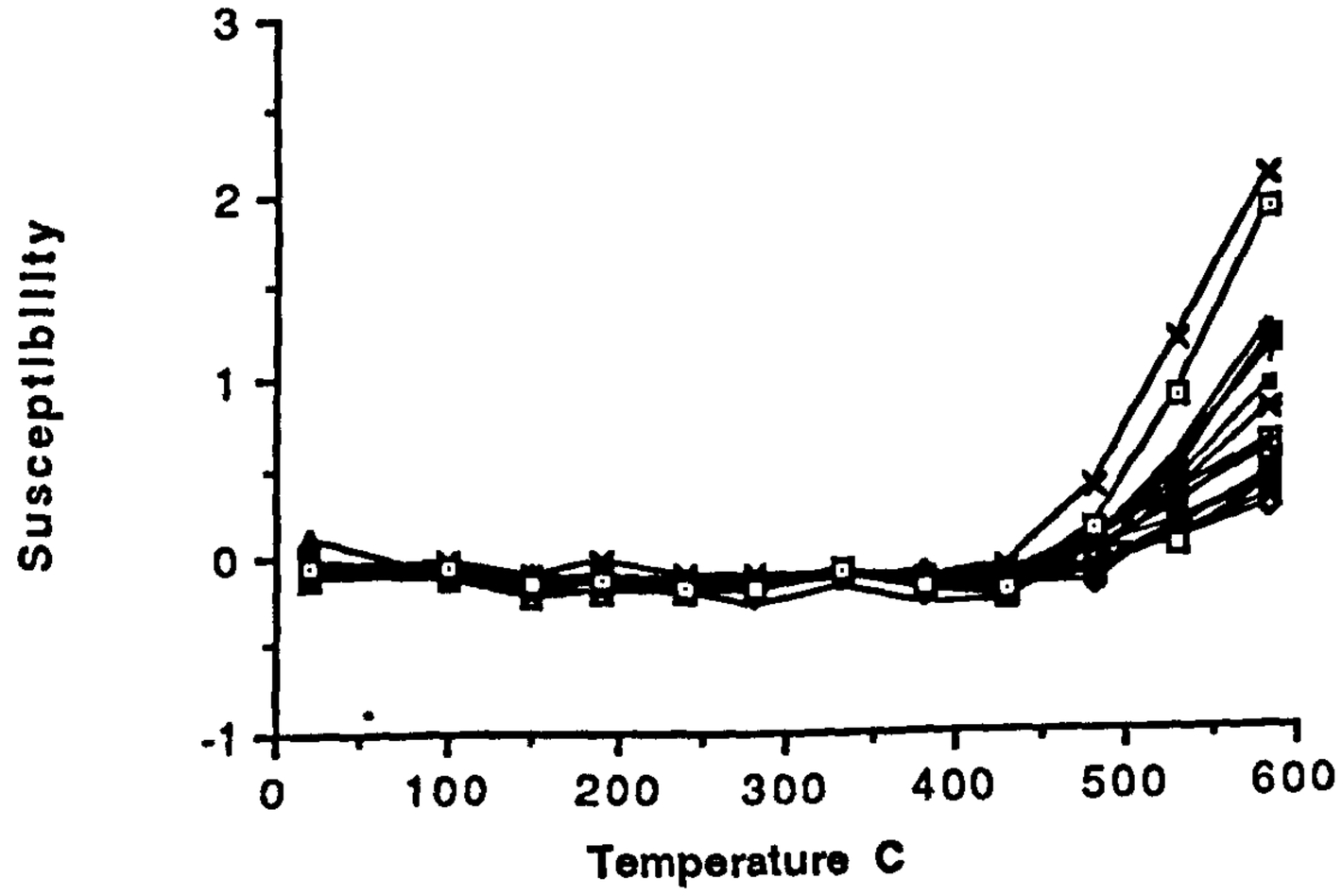
Susceptibility
3
2
1
0
-1
0
100
200
300
400
500
600
Temperature C

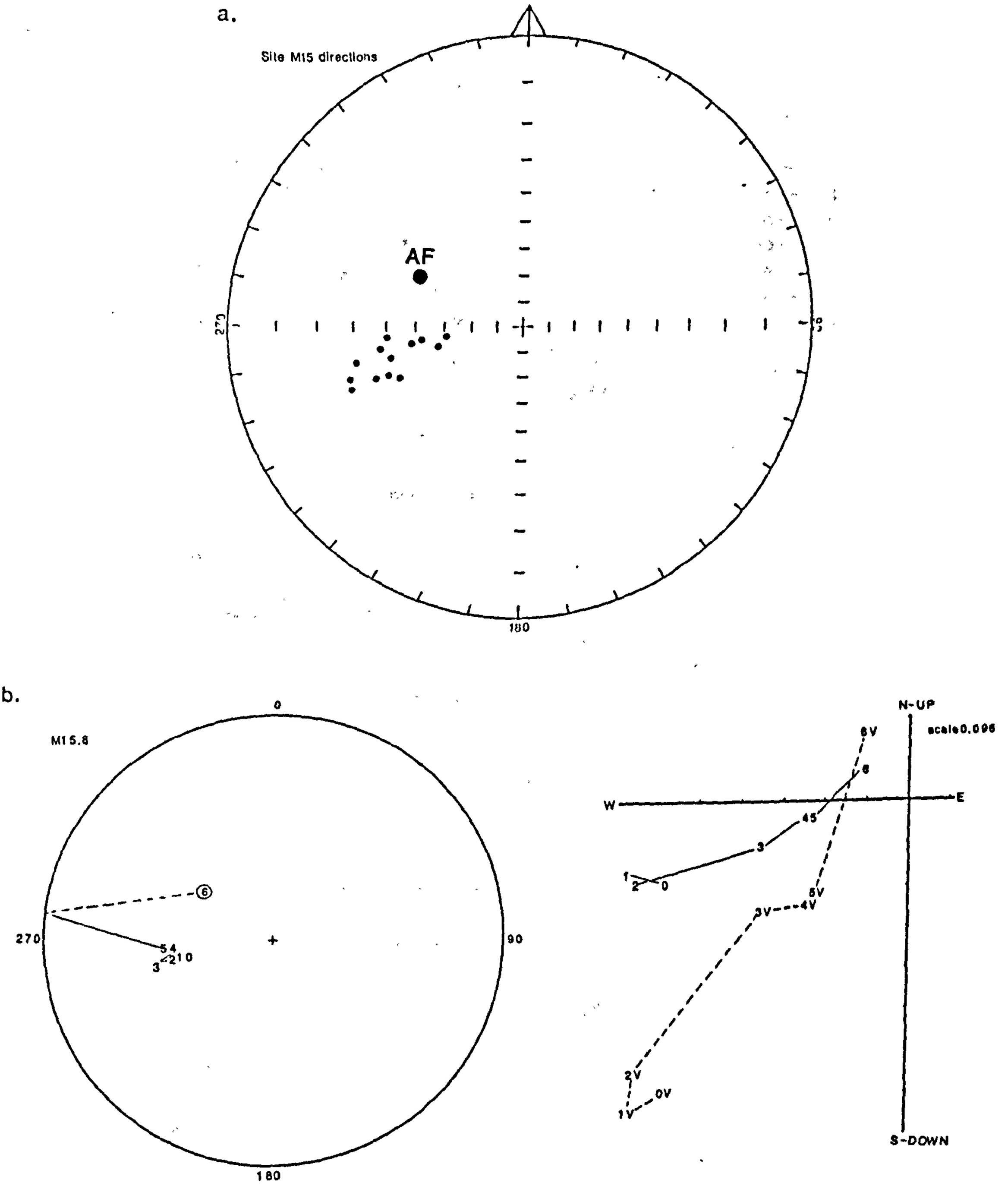

fig. 5.7 Summary of demagnetisation behaviour of samples from site M15. Natural remanent magnetism (NRM) intensity is given x $10^{-4}Am^{-1}$; susceptibility units x 10^{-6} GOe^{-1}
a. stereographic projection of stable sample directions; **b.** stereographic projection and accompanying orthogonal plot illustrating vector movement with progressive demagnetisation; **c.** NRM intensity change with increasing temperature illustrating variation of magnetic mineral content between samples; **d.** normalised NRM change with increasing temperature illustrating within-site variation; **e.** susceptibility variation with increasing temperature illustrating changes which occur due to mineralogical alteration.

c

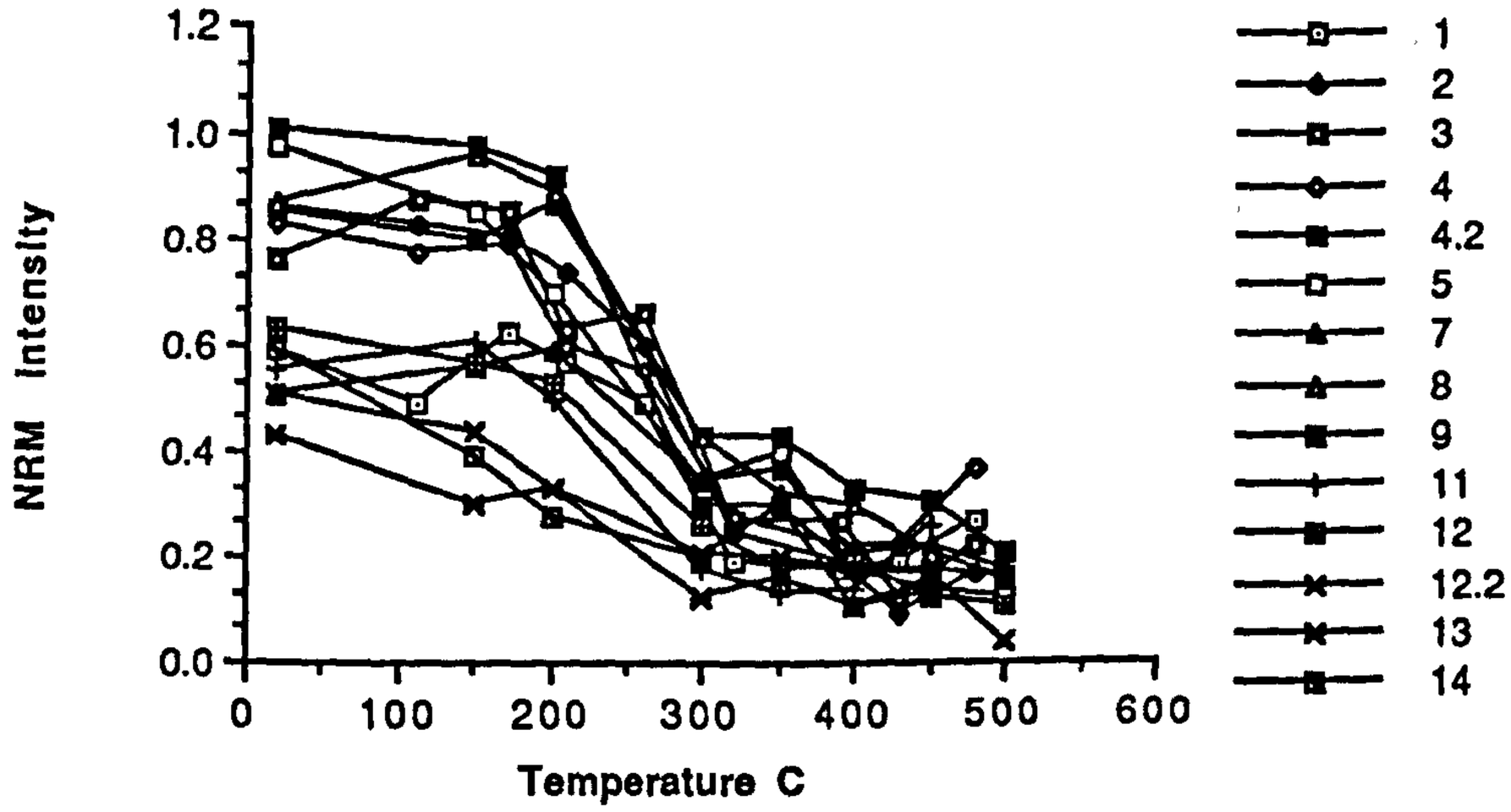
NRM Intensity
1.2
1.0
0.8
0.6
0.4
0.2
0.0
0
100
200
300
400
500
600
Temperature C
1
2
3
4
4.2
5
7
8
9
11
12
12.2
13
14

d

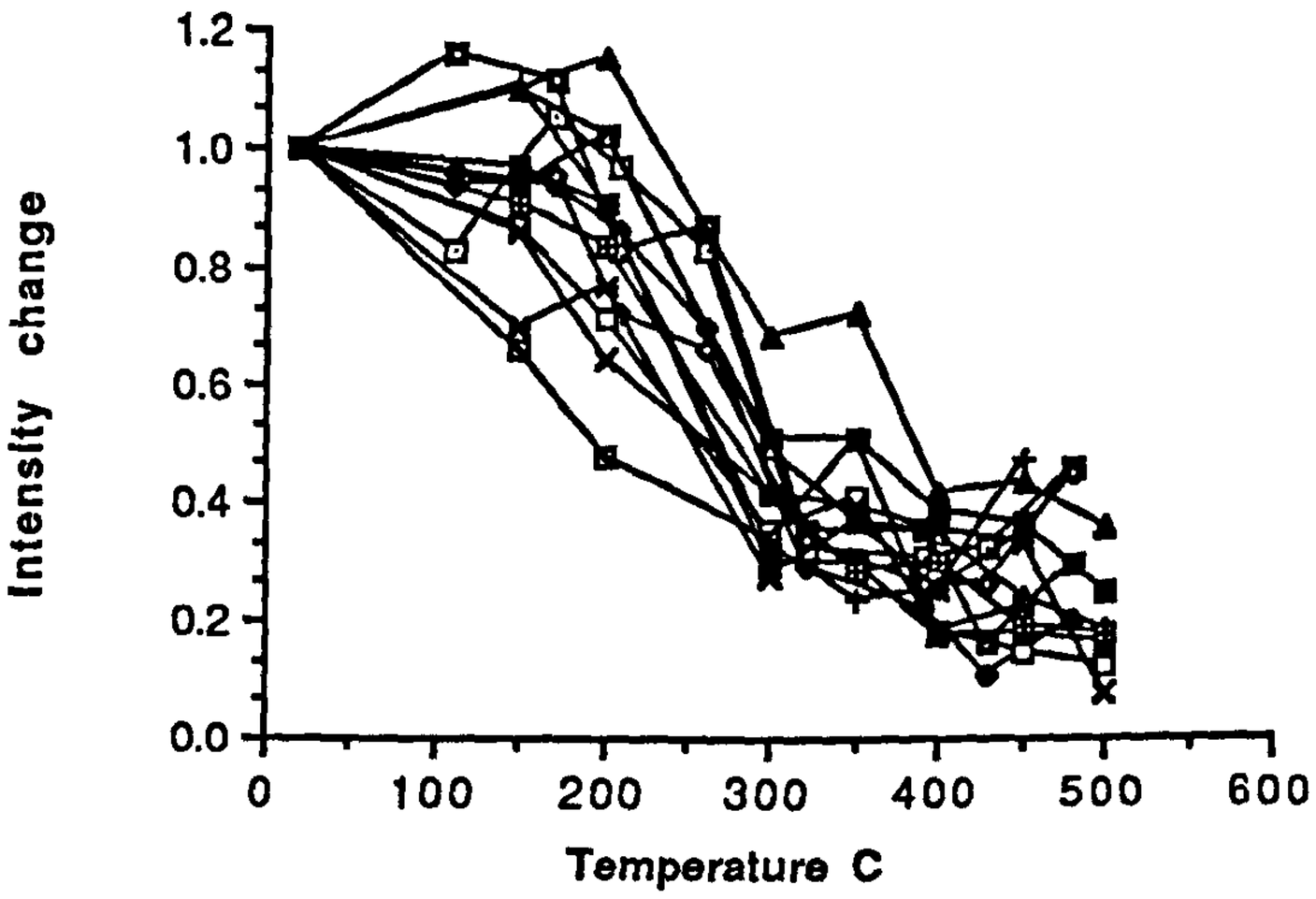
Intensity change
1.2
1.0
0.8
0.6
0.4
0.2
0.0
0
100
200
300
400
500
600
Temperature C

e

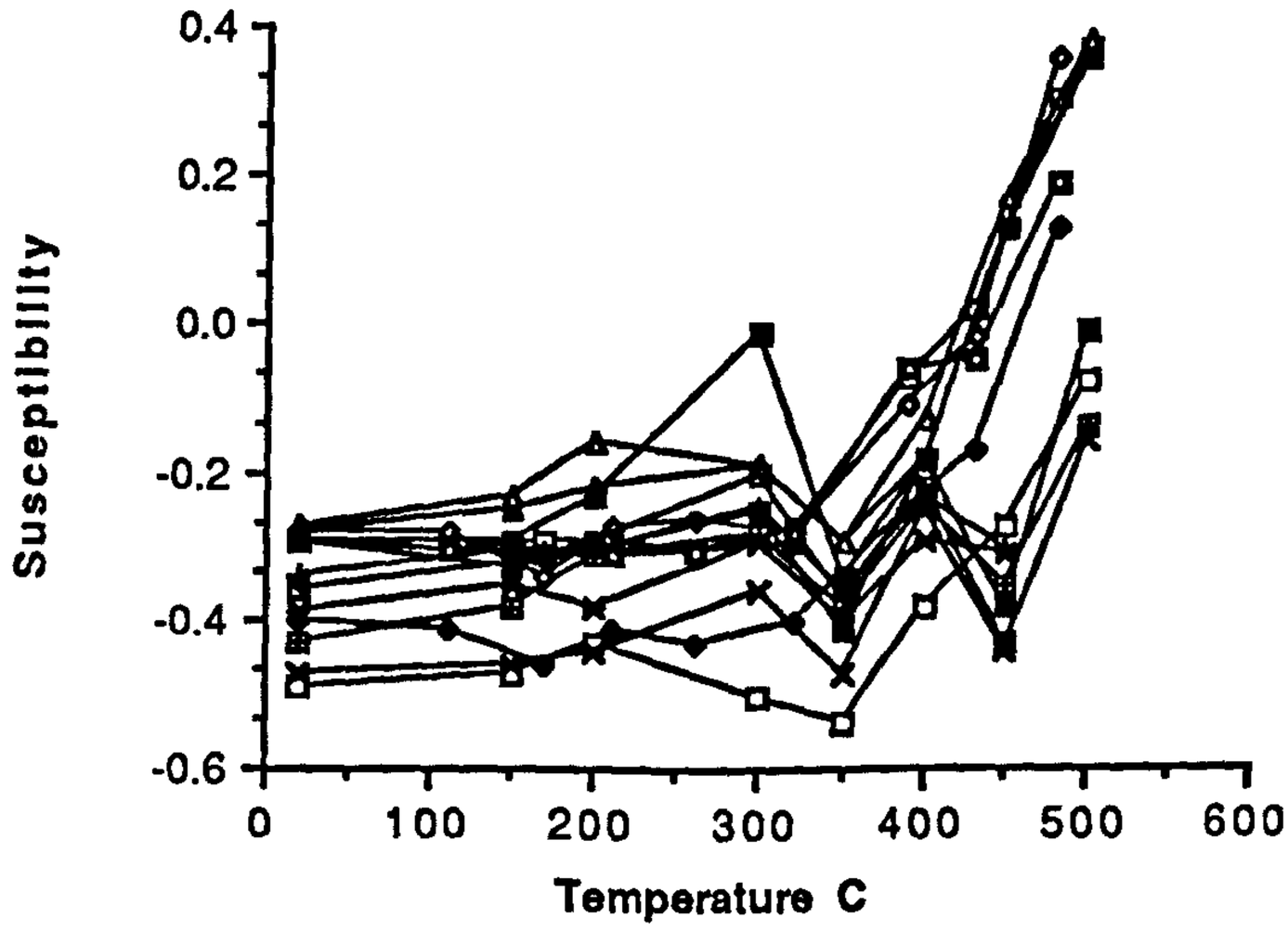
Susceptibility
0.4
0.2
0.0
-0.2
-0.4
-0.6
0
100
200
300
400
500
600
Temperature C

indicate that magnetic mineral content is relatively low, and suggest that the carrier of the natural remanent magnetism is goethite or haematite. After removal of a viscous reversed component carried by goethite (T_b = 100°C) the vector demagnetises steadily and is defined to 300°C. This low temperature, along with the intensity and suceptibility data, suggest that the magnetic carrier could be pyrrhotite or impure, multi-domain or pseudo-single domain haematite. It is unlikely to be pyrrhotite as there is no susceptibility increase at 320°C which is the temperature at which magnetite forms from the oxidation of pyrrhotite. Site directions are well grouped, stable and of normal polarity and the directions derived from both AF and thermal demagnetisation are similar. The mean direction is well defined but differs from the apparent field direction wander path by a declination of 90°. Samples from this site behave consistently in all respects and have a single natural remanent magnetism direction which has normal polarity but ambiguous direction.

Site M16 This site contained negligible quantities of magnetic minerals (maximum initial intensity of 0.21 x $10^{-4}Am^{-1}$ and initial susceptibility of -0.58 units x $10^{-6}GOe^{-1}$(see appendix 4.2) and yielded unstable directions from both AF and thermal demagnetisation.

Site M17 This site contained negligible quantities of magnetic minerals (maximum initial intensity of 0.32 x $10^{-4}Am^{-1}$ and initial susceptibility of -0.33 units x $10^{-6}GOe^{-1}$(see appendix 4.2) and yielded unstable directions.

Site M18 This site contained negligible quantities of magnetic minerals (maximum initial intensity of 0.317 x $10^{-4}Am^{-1}$ and initial susceptibility of -0.64 units x $10^{-6}GOe^{-1}$(see appendix 4.2) and yielded unstable directions.

Summary (table 5.4 and fig. 5.8)

i. 3 out of 7 sites contain negligible amounts of magnetic minerals;

ii. 4 out of 7 sites yield stable vectors, with *A95* of site mean directions <10° in each case;

iii. only one main component was identified from each site, although a viscous component was removed by around 150°C in many samples;

iv. There is relatively little within-site variation in demagnetisation behaviour for

site	stable proportion	N	site mean direction dec	inc	A95	pole(North) lat.	long.(E)	polarity
M13	10 of 12	9	195	-30.1	9.6	69.1	31	R
M13A	15 of 15	16	52.2	20.3	8.5			N
M14	18 of 18	6	253	35.9	8.9	3	11	N(R)
M15	14 of 14	14	255.9	41.8	10.2	2.	193.9	N
M16	0 of 4	4	-	-	-	-	-	-
M17	0 of 16	16	-	-	-	-	-	-
M18	0 of 13	13	-	-	-	-	-	-

	intensity (max.)	susc. (max.)	blocking temperature C	magnetic minerals	interpreted age
M13	0.65	-0.62	110, 320	G,P,M/H	190my
M13A	3.97	0.05	110, 500	G,P,M/H	ambiguous
M14	50.34	-0.02	110, 500	G,M/H	ambiguous
M15	1.51	-0.27	110, 300	G,P,M/H	ambiguous
M16	0.21	-0.58	-	-	-
M17	0.32	-0.33	-	-	-
M18	0.17	-0.64	-	-	-

table 5.4 Summary of mean directions and other data for sites in the back reef facies

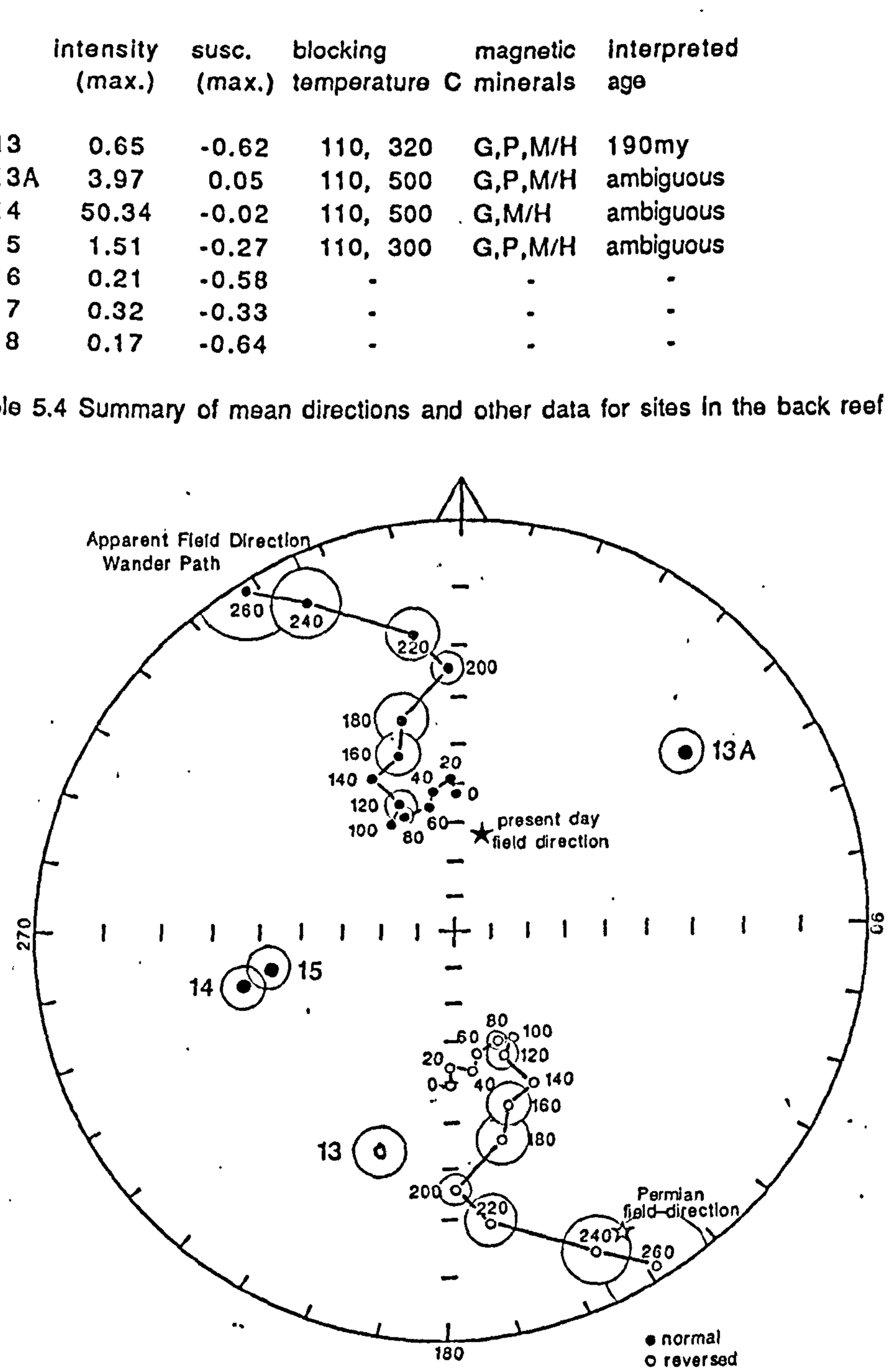

fig. 5.8 Stereographic projection of mean directions for sites in the back reef facies

site M13, site M13A and site M15. Site M14 displays a range of behaviour, and of vector directions;

v. three site mean directions are normal polarity (sites M13A, M14 and M15), site M13 is reversed polarity;

vi. the natural remanent magnetism carrier is pyrrhotite or maghemite in site M13, haematite in site M14, ambiguous in site M13A, goethite or haematite in site M15. Impure, or multi-domain or pseudo-single domain magnetic phases are indicated by blocking temperature spectra which are significantly lower than the Curie temperatures for pure magnetic phases, in many cases;

vii. the age of natural remanent magnetism in site M13 is interpreted to be 200 Ma old. This is a reversed direction;

viii. the age of natural remanent magnetism acquisition in sites M13A, M14 and M15 do not lie on the apparent field direction wander path and are difficult to interpret in these terms;

ix. Sites M14 and M15 have similar site mean directions, probably resulting from lightening strike.

5.4.2 Reef facies

A summary of the demagnetisation behaviour for sites from the reef facies, and interpretations of vectors and magnetic mineralogy are as follows:

Site M12 (fig. 5.9) Maximum initial natural remanent magnetism intensity of 0.82 x $10^{-4}Am^{-1}$ and susceptibility of -0.52 (volume units x $10^{-6}GOe^{-1}$; see appendix 4.2) indicate that the magnetic mineral content is very low. All samples show an initial increase or decrease in natural remanent magnetism intensity to around 150°C, which indicates the presence of viscous remanent magnetism, probably carried by goethite. Two dominant vector directions are displayed by some samples from this site; I. a normal polarity, vertical component with low T_b (100°C) which demagnetises steadily at higher temperatures removing a vector with shallow inclination and reversed direction which trends towards the apparent field direction wander path at 200 Ma (*e.g.*, sample 12.11); and ii. normal polarity vectors which demagnetise steadily after the initial removal of a viscous component (*e.g.*, sample 12.13); this is demagnetised by around 300°C. This vector is clearly defined but does not lie near to the apparent field direction wander path, though the inclination is similar to the 100 Ma direction,

fig. 5.9 Summary of demagnetisation behaviour of samples from site M12. Natural remanent magnetism (NRM) intensity is given x $10^{-4}Am^{-1}$; susceptibility in units x 10^{-6} GOe^{-1}

a. stereographic projection of stable sample directions;

b. and **c.** stereographic projections and accompanying orthogonal plots illustrating vector movement with progressive demagnetisation for samples with different behaviour;

d. NRM intensity change with increasing temperature illustrating variation of magnetic mineral content between samples;

e. normalised NRM change with increasing temperature illustrating within-site variation;

f. susceptibility variation with increasing temperature illustrating changes which occur due to mineralogical alteration.

a.

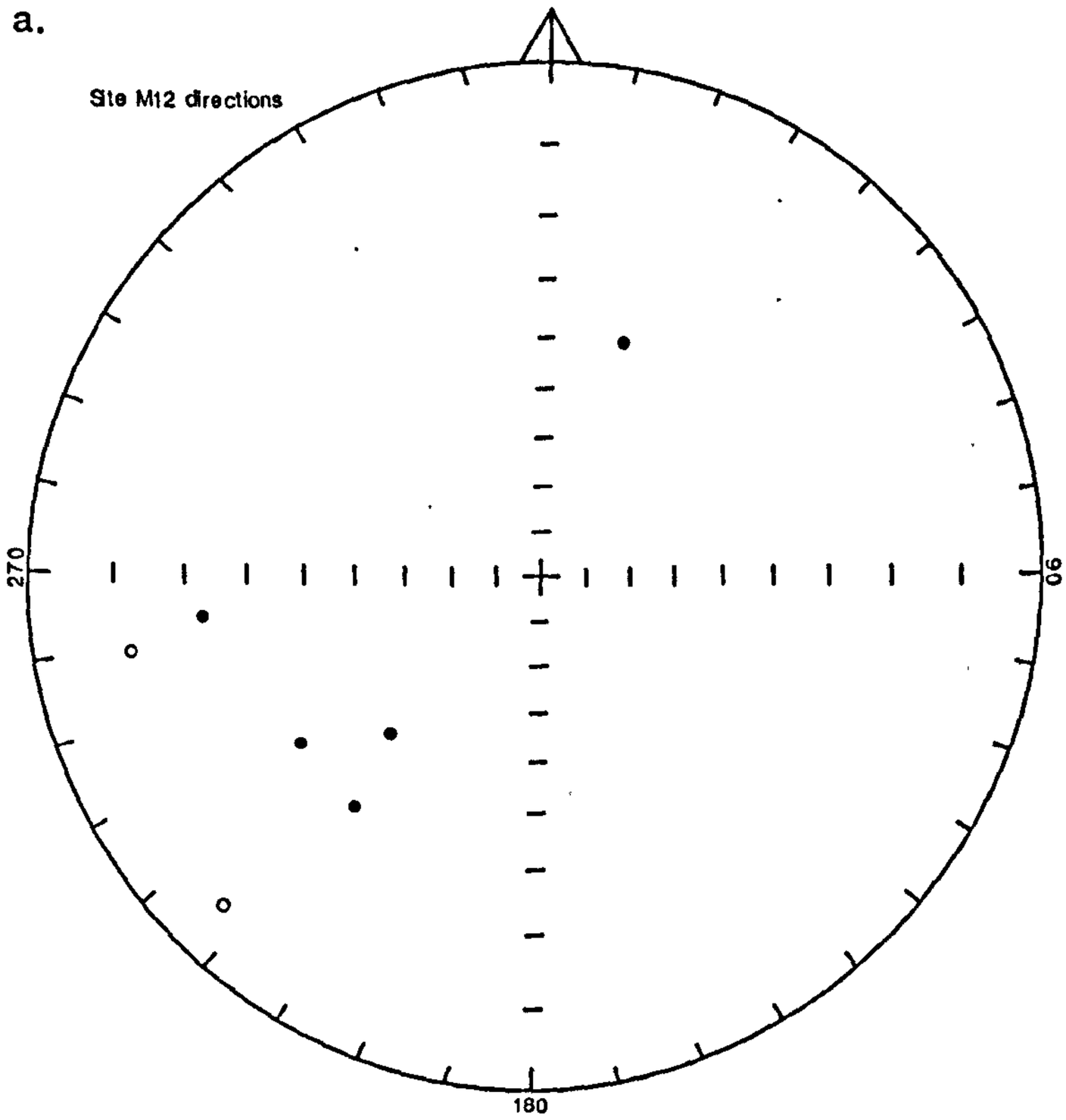
Site M12 directions
270
90
180

b.

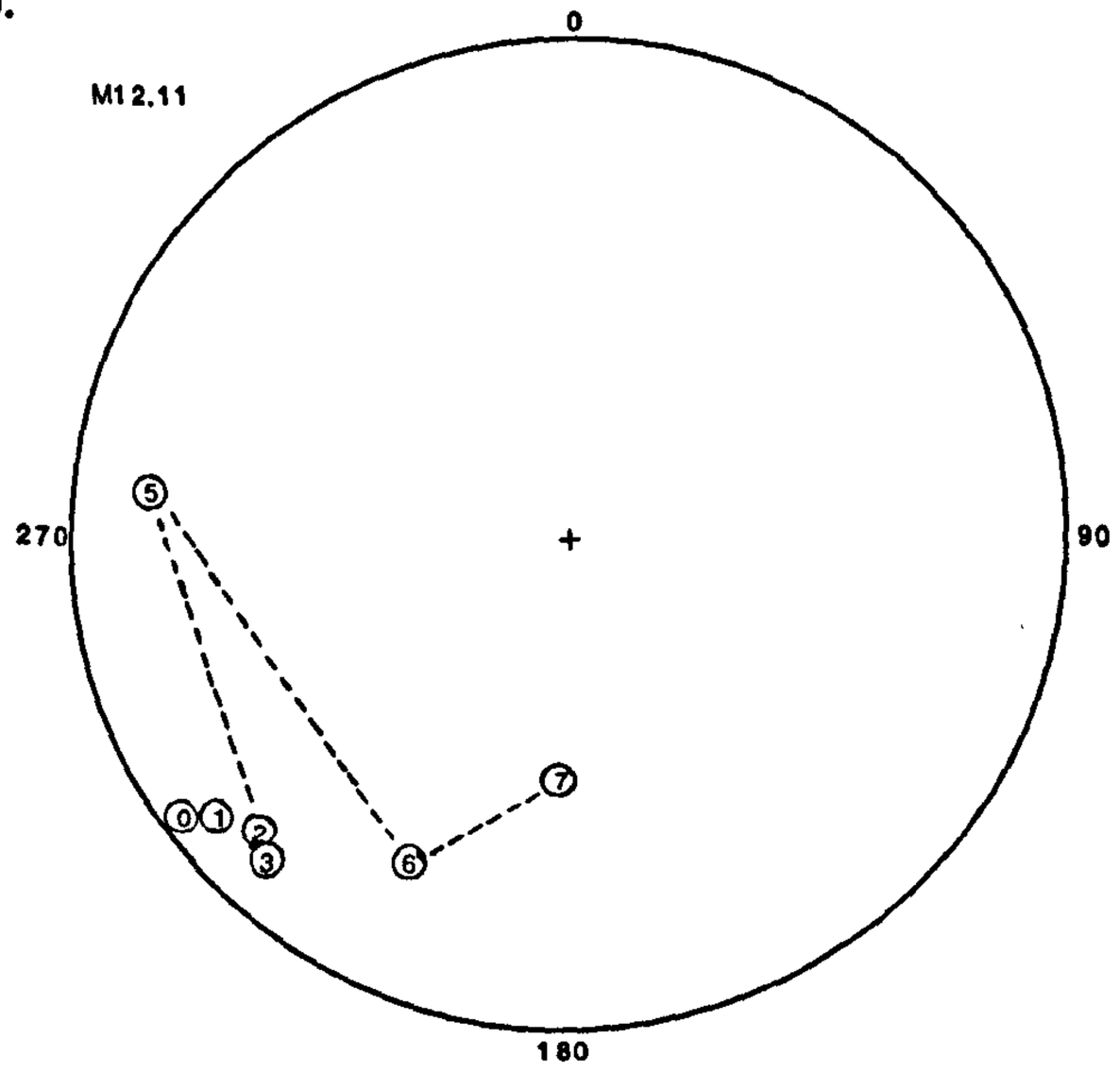
M12.11
0
270
90
180
5
0
1
2
3
6
7

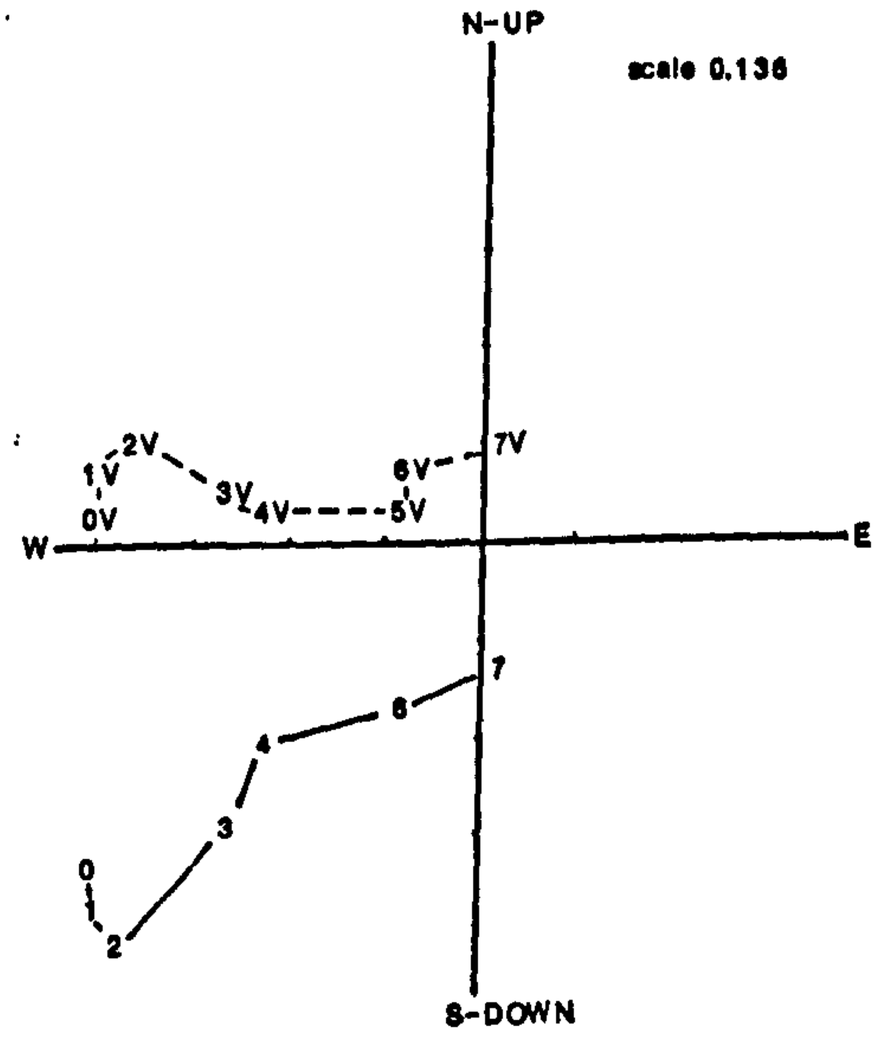
N-UP
scale 0.136
W
E
0V
1V
2V
3V
4V
5V
6V
7V
0
1
2
3
4
6
7
S-DOWN

C.

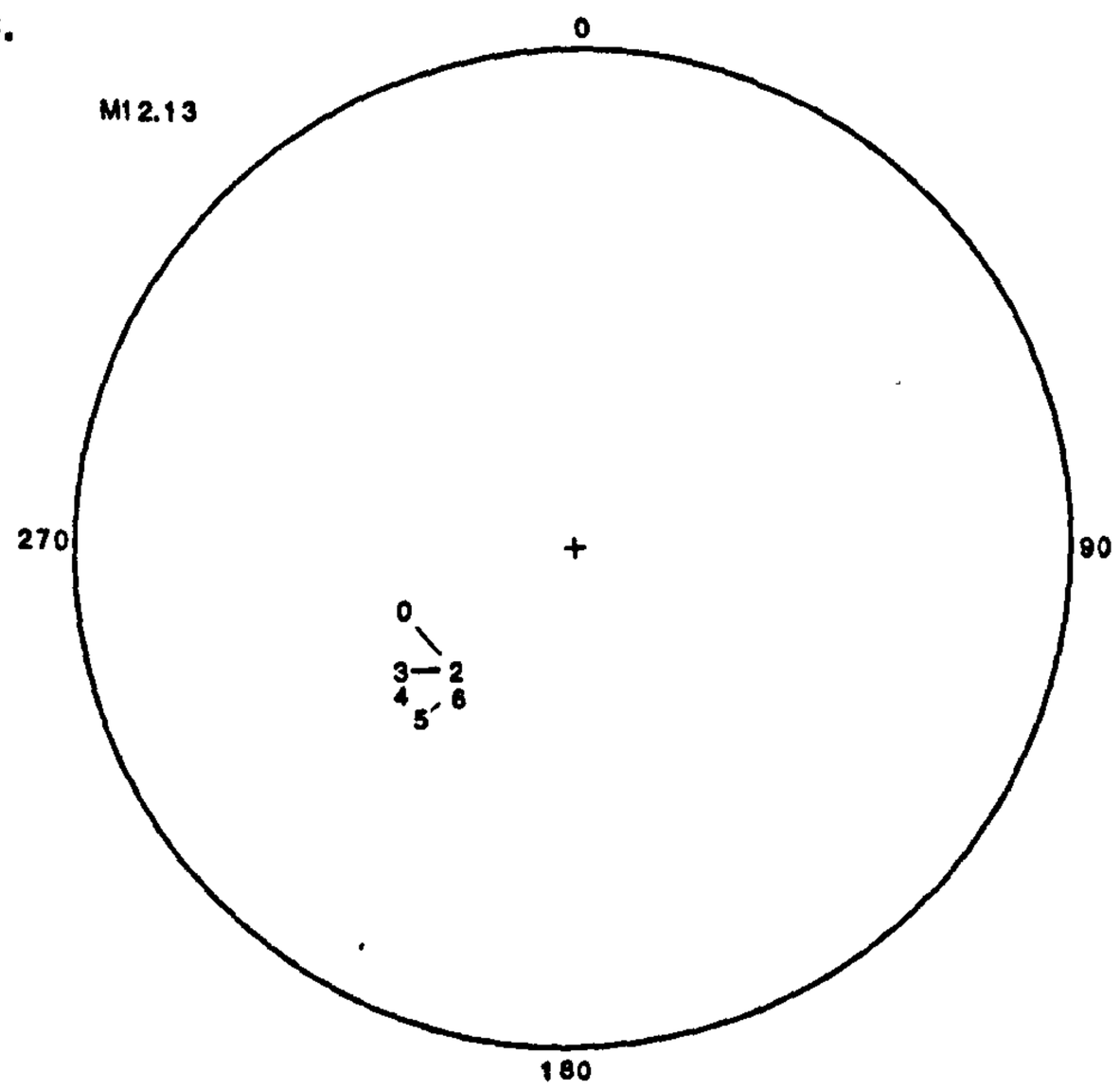
M12.13
0
270
90
180
0
3
2
4
5
6

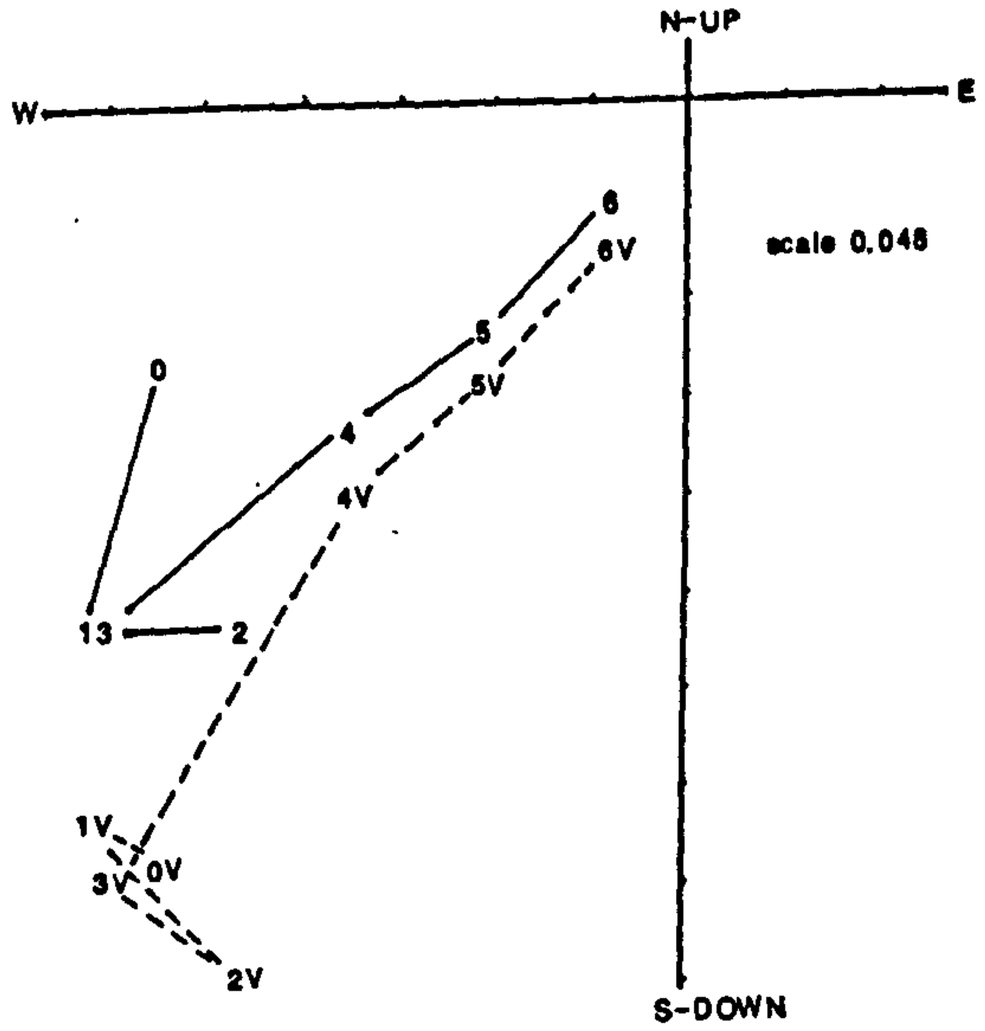
N-UP
scale 0.048
W
E
0
1V
2V
3
4
4V
5
5V
6
6V
13
2
S-DOWN

d

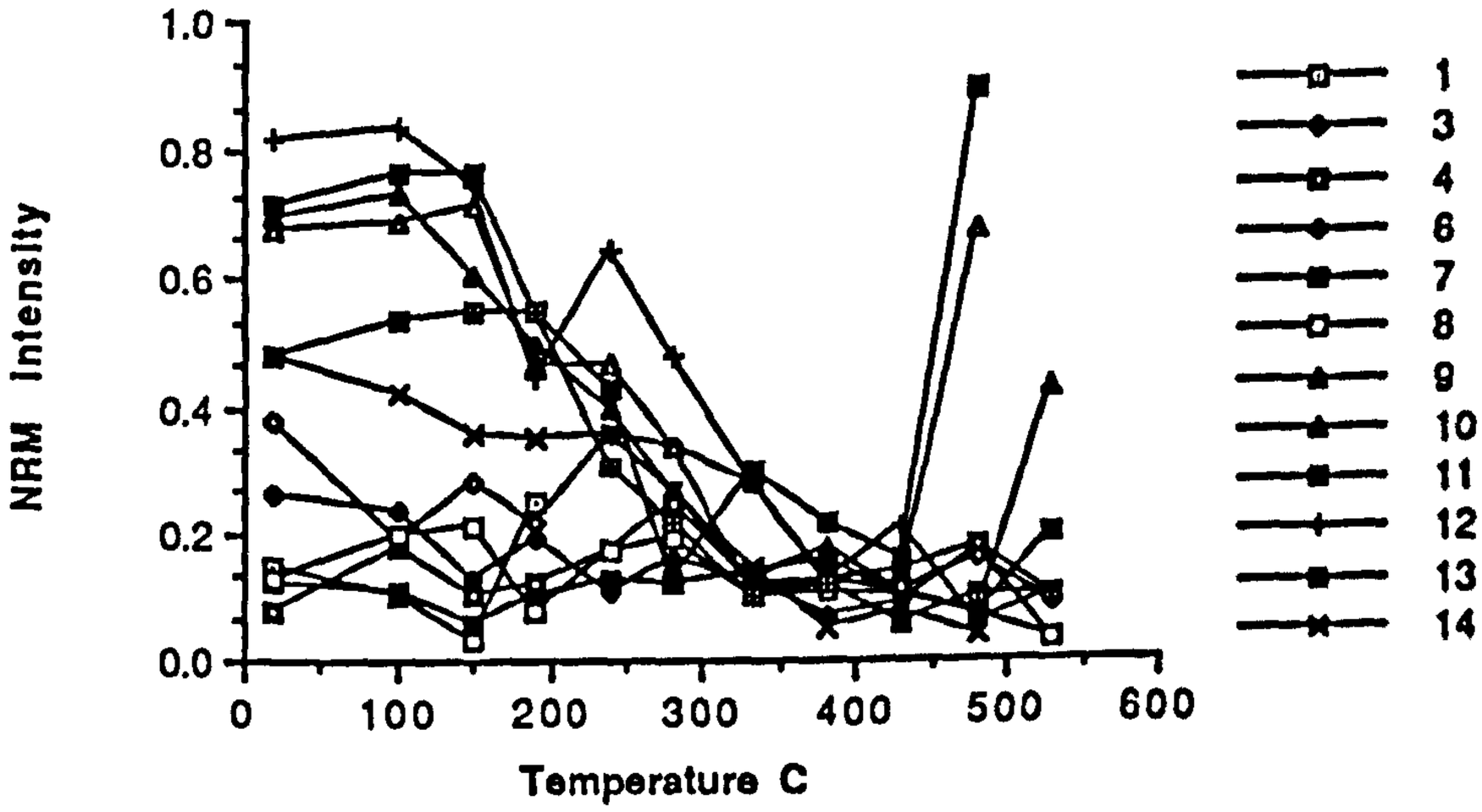
NRM Intensity
1.0
0.8
0.6
0.4
0.2
0.0
0
100
200
300
400
500
600
Temperature C
1
3
4
6
7
8
9
10
11
12
13
14

e

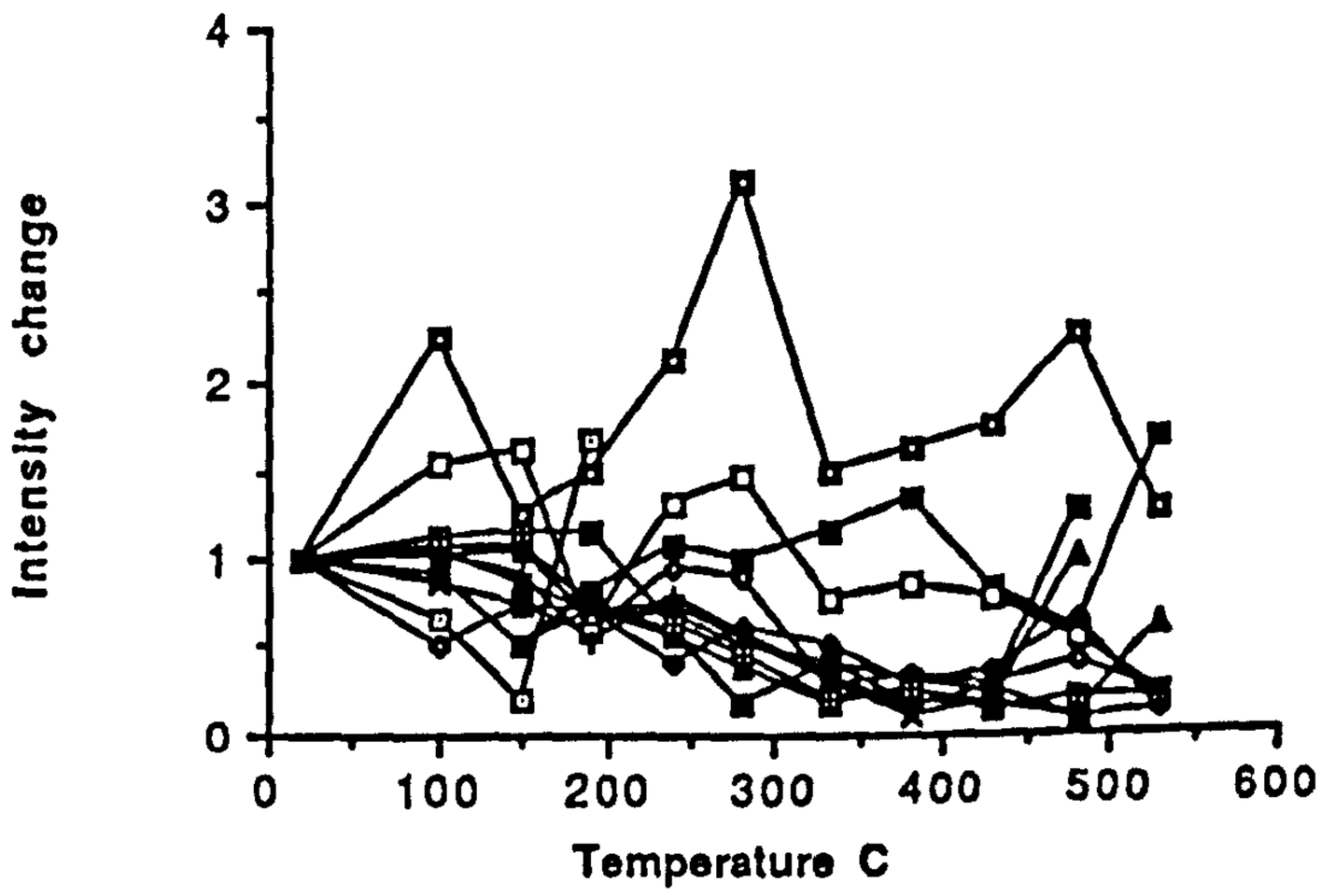
Intensity change
4
3
2
1
0
0
100
200
300
400
500
600
Temperature C

f

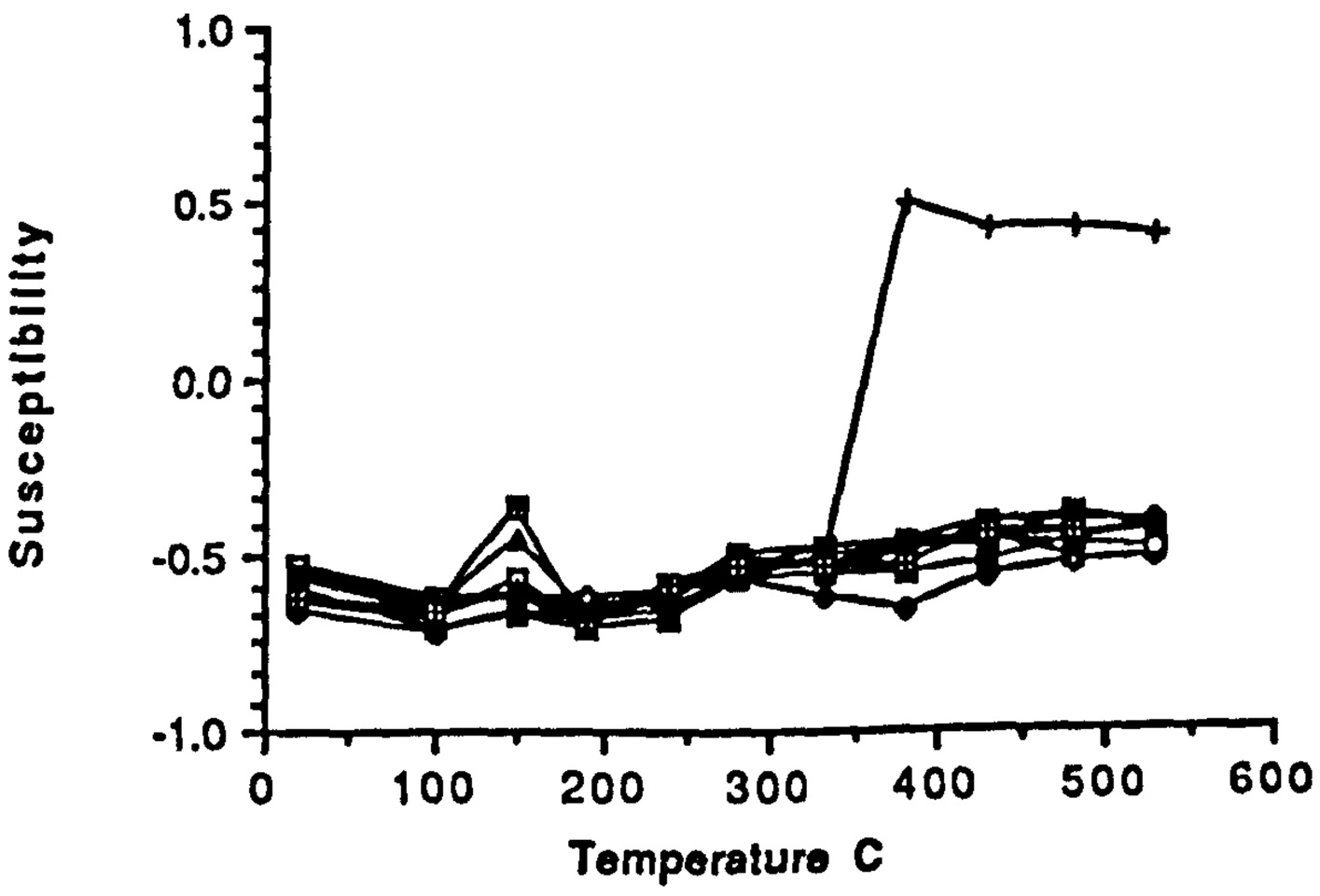
Susceptibility
1.0
0.5
0.0
-0.5
-1.0
0
100
200
300
400
500
600
Temperature C

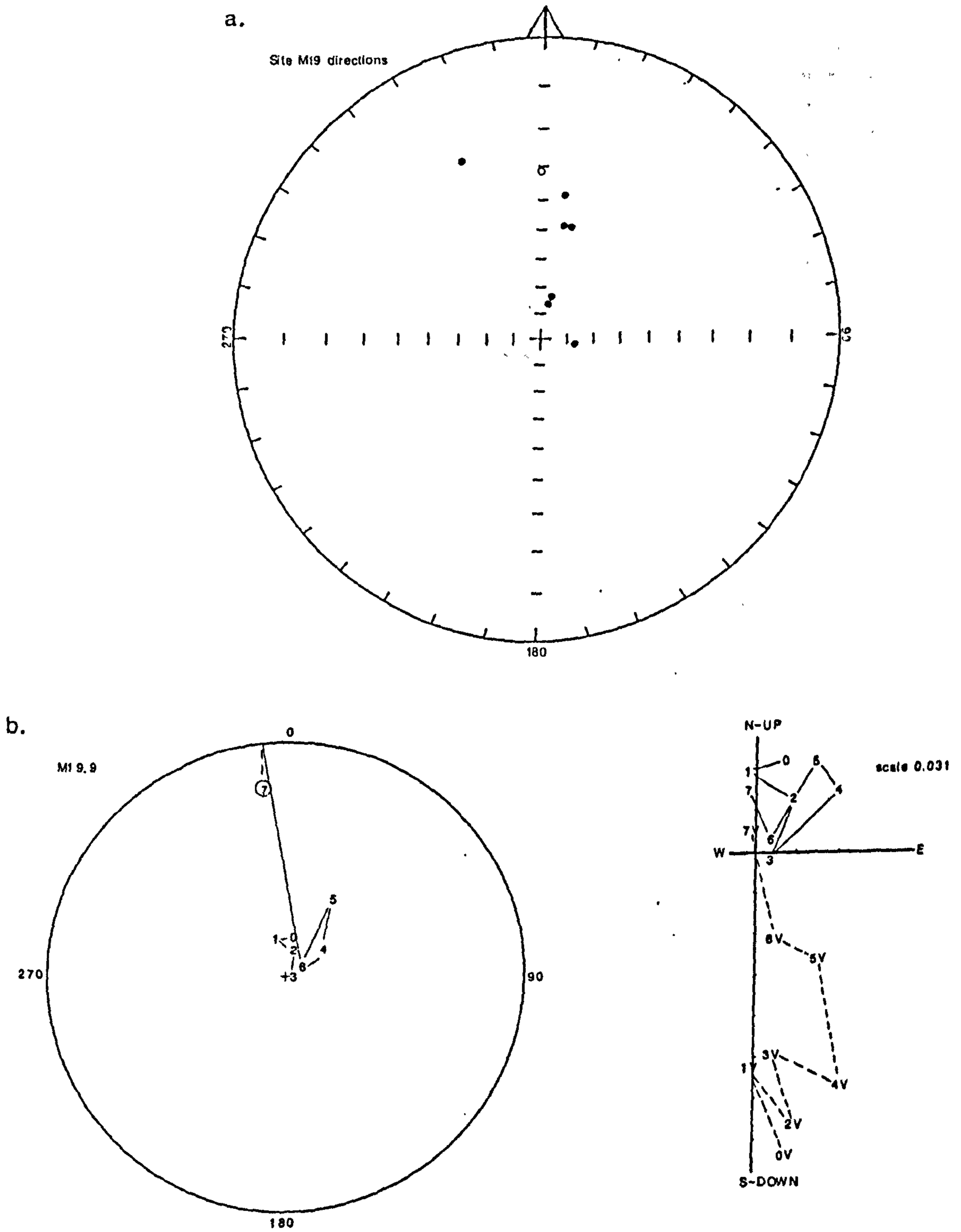

fig. 5.10 Summary of demagnetisation behaviour of samples from site M19. Natural remanent magnetism (NRM) intensity is given x $10^{-4}Am^{-1}$; susceptibility units x 10^{-6} GOe^{-1}
a. stereographic projection of stable sample directions; **b.** stereographic projection and accompanying orthogonal plot illustrating vector movement with progressive demagnetisation; **c.** NRM intensity change with increasing temperature illustrating variation of magnetic mineral content between samples; **d.** normalised NRM change with increasing temperature illustrating within-site variation; **e.** susceptibility variation with increasing temperature illustrating changes which occur due to mineralogical alteration.

c

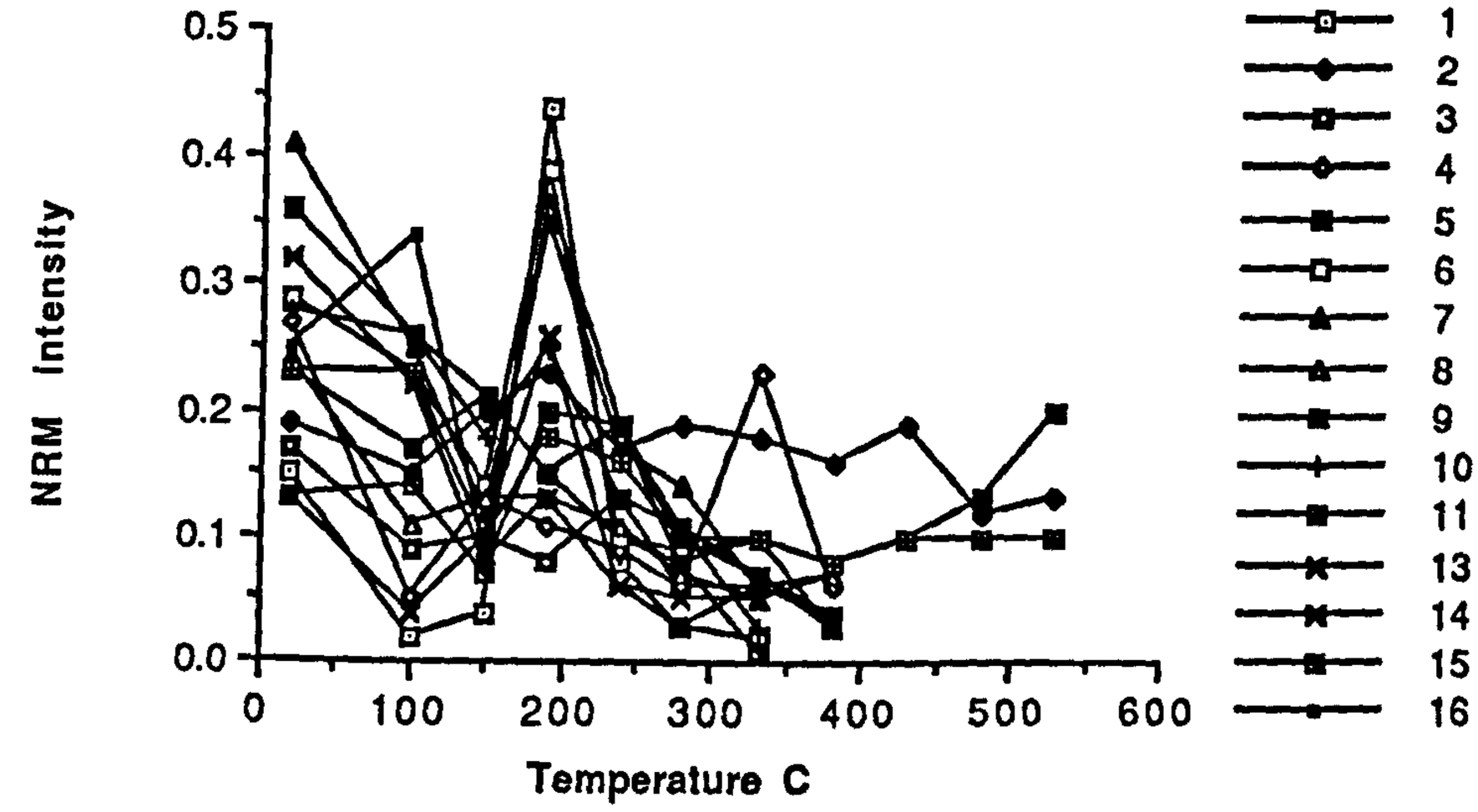
NRM Intensity
0.5
0.4
0.3
0.2
0.1
0.0
0
100
200
300
400
500
600
Temperature C
1
2
3
4
5
6
7
8
9
10
11
13
14
15
16

d

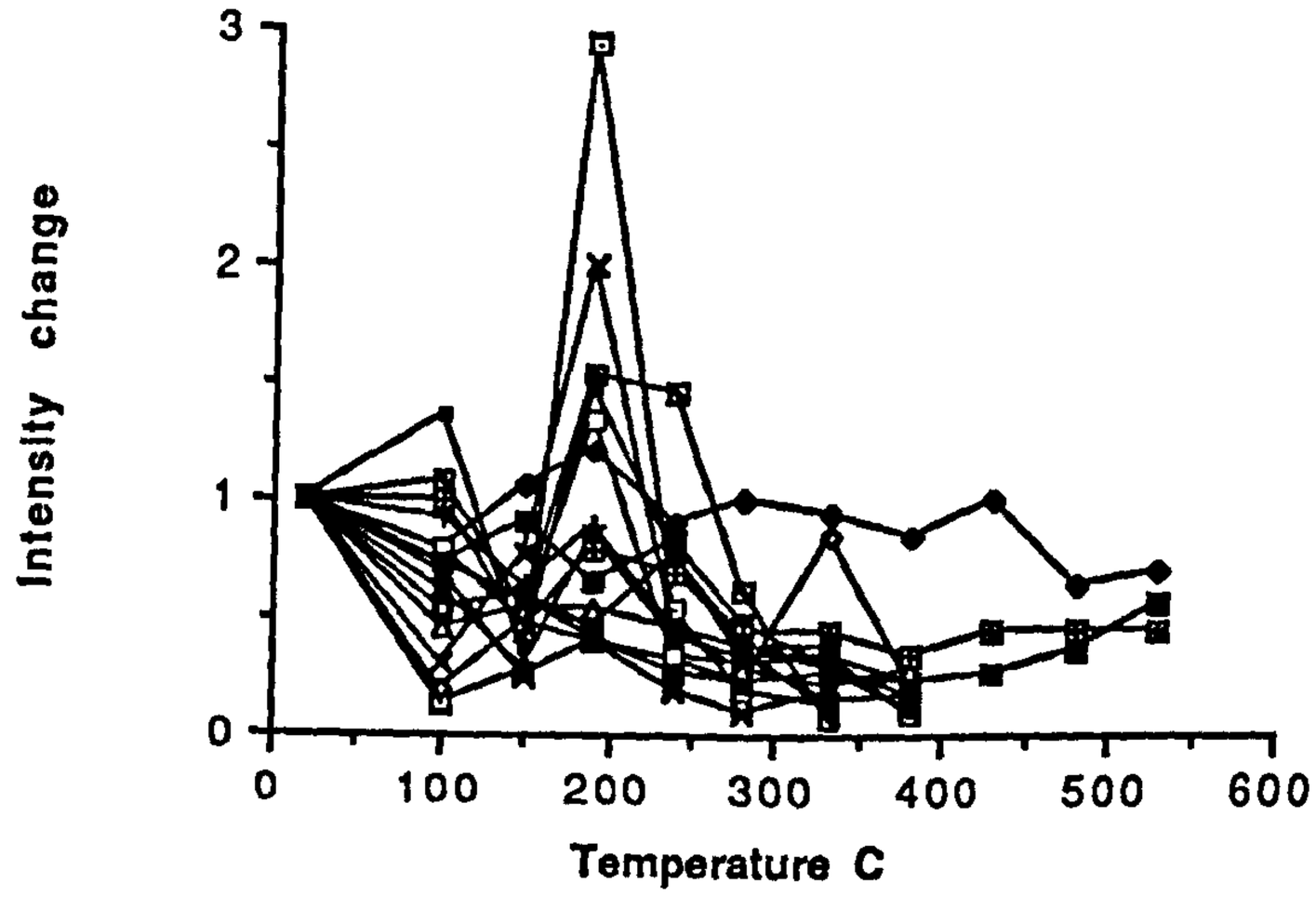
Intensity change
3
2
1
0
0
100
200
300
400
500
600
Temperature C

e

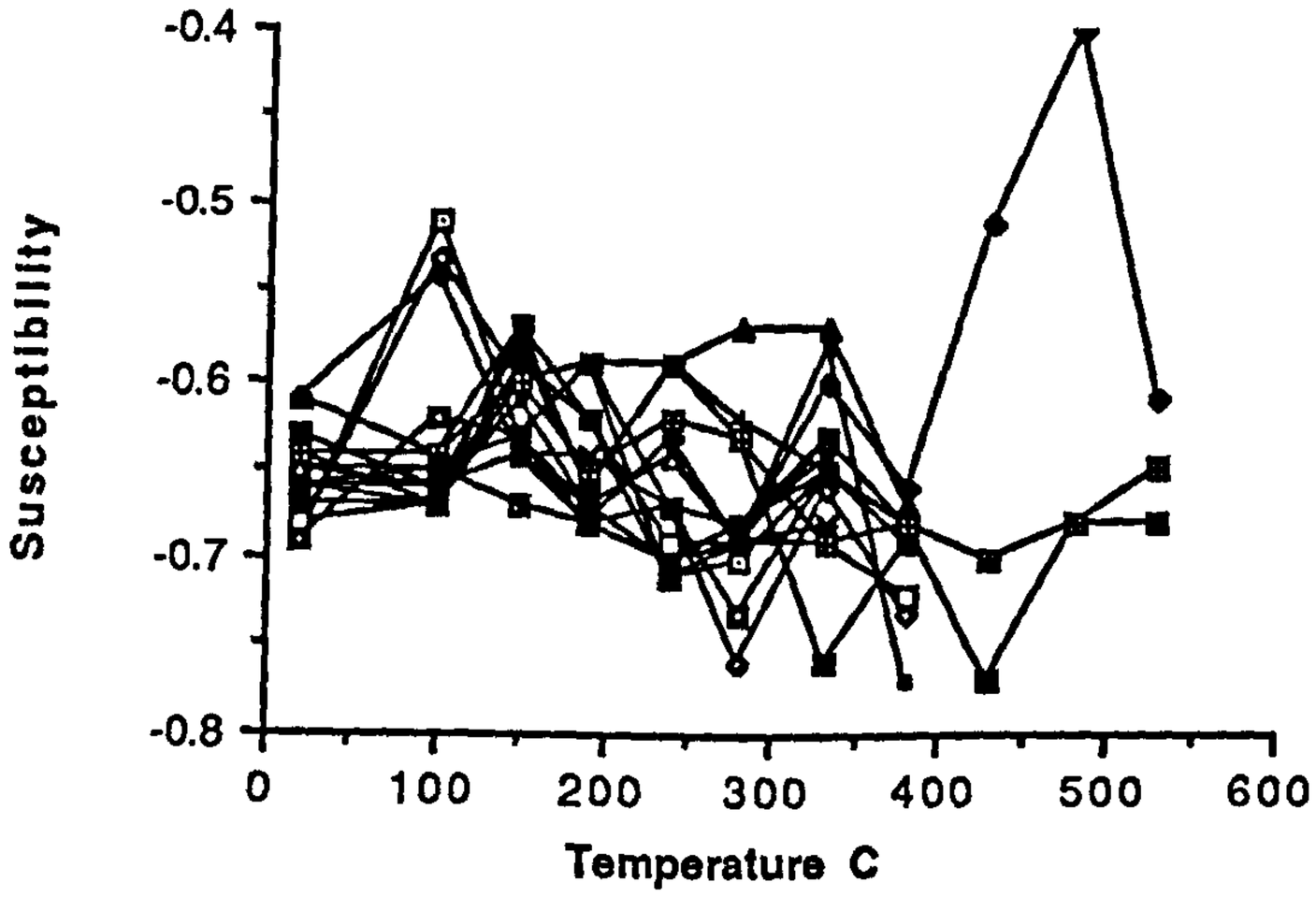
Susceptibility
-0.4
-0.5
-0.6
-0.7
-0.8
0
100
200
300
400
500
600
Temperature C

site	stable proportion	N	site mean direction dec	inc	A95	pole(North) lat.	long.(E)	polarity
M12	-	-	-	-	-	-	-	N(R)
M19	-	-	-	-	-	-	-	N

site	intensity (max.)	susc. (max.)	blocking temperature C	magnetic minerals	interpreted age
M12	0.82	-0.52	150, 300	G	Tertiary?
M19	0.36	-0.61	100, 240	G	Tertiary?

table 5.5 Summary of directional data for sites in the reef facies

the declination differs by more than 90°. Data has low intensity and stability and is thus interpreted with caution.

Site M19 (fig. 5.10) Maximum initial natural remanent magnetism intensity of 0.36 x $10^{-4}Am^{-1}$ and susceptibility of -0.61 (volume units x $10^{-6}GOe^{-1}$; see appendix 4.2) indicate that the magnetic mineral content is very low. Consequently, site directions are unstable. However, all observed directions have normal polarity and high inclinations. Movement of vectors with progressive demagnetisation is not surprisingly variable. This either reflects spurious noise or shows a mix of normal and reversed polarity directions which are removed by around 240°C. This suggests that the natural remanent magnetism might be recent. Goethite is the likely remanence carrier. The magnetic mineral content is so low that directions are not well defined, although a Tertiary/present day vector is suggested with a mix of normal and reversed components. Data has low intensity and stability and is thus interpreted with caution.

Summary (table 5.5)

i. both sites analysed have low natural remanent magnetism intensity and low susceptibility indicating very low magnetic mineral content;
ii. mean natural remanent magnetism directions were not isolated from either site due to low vector stability. However, certain samples yield directions which are meta-stable and represent a viscous natural remanent magnetism; and certain groupings of vectors are apparent within these two sites, despite their low stability;
iii. most vectors are normal polarity with medium-high inclinations, although some reversed polarity, low inclination vectors were isolated;
iv. goethite is the likely natural remanent magnetism carrier; pyrrhotite is possibly a remanence carrier in a few samples;
v. the age of natural remanent magnetism acquisition is cautiously interpreted as Tertiary/Recent.

5.4.3 Upper foreslope facies

A summary of the demagnetisation behaviour for sites from the upper foreslope facies, and interpretations of vectors and magnetic mineralogy are as follows:

Site M8 (fig. 5.11) Maximum initial natural remanent magnetism intensity of 0.79 x $10^{-4}Am^{-1}$ and susceptibility of -0.60 (volume units x $10^{-6}GOe^{-1}$; see appendix 4.2)

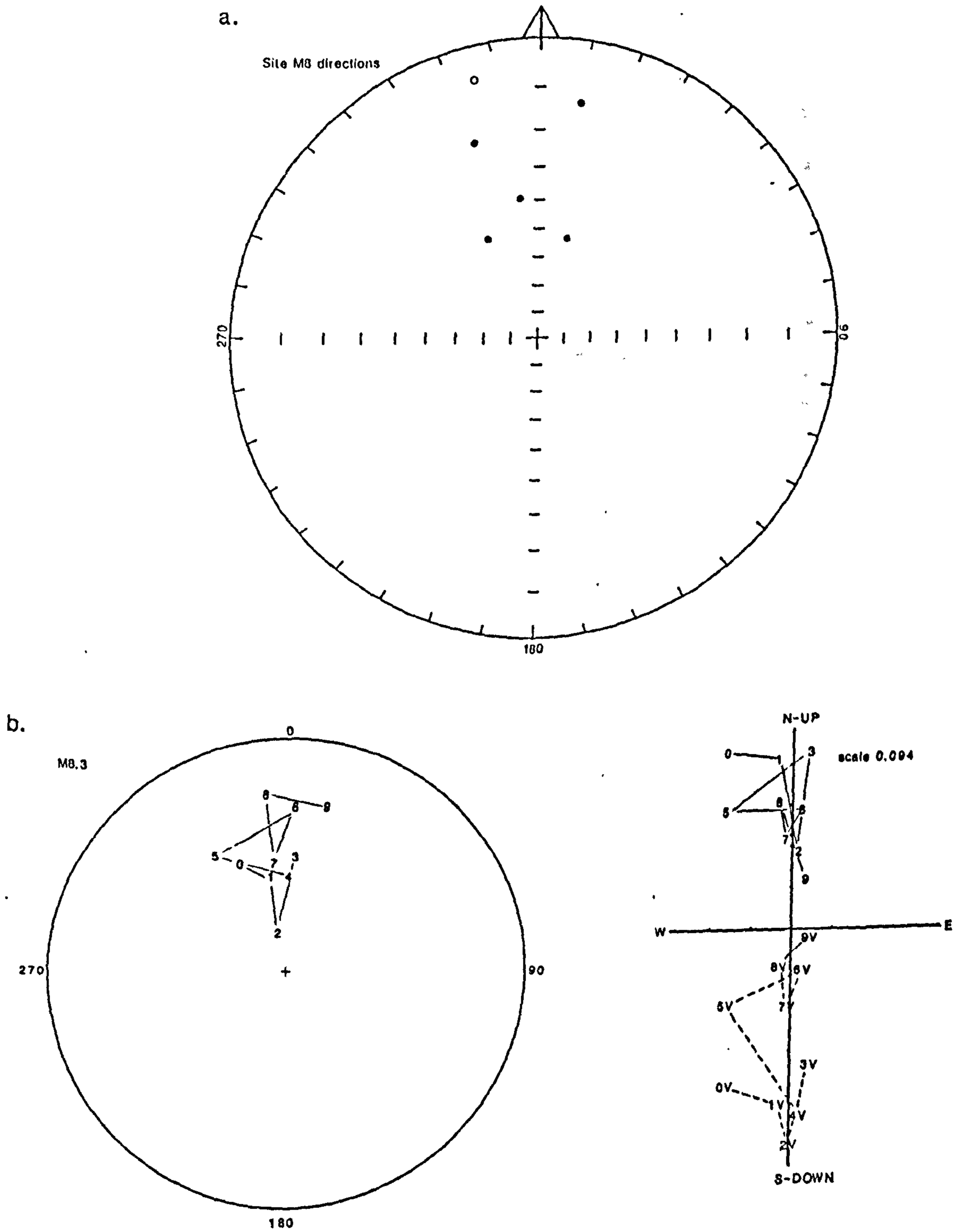

fig. 5.11 Summary of demagnetisation behaviour of samples from site M8. Natural remanent magnetism (NRM) intensity is given x $10^{-4}Am^{-1}$; susceptibility units x 10^{-6} GOe^{-1}
a. stereographic projection of stable sample directions; **b.** stereographic projection and accompanying orthogonal plot illustrating vector movement with progressive demagnetisation; **c.** NRM intensity change with increasing temperature illustrating variation of magnetic mineral content between samples; **d.** normalised NRM change with increasing temperature illustrating within-site variation; **e.** susceptibility variation with increasing temperature illustrating changes which occur due to mineralogical alteration.

c

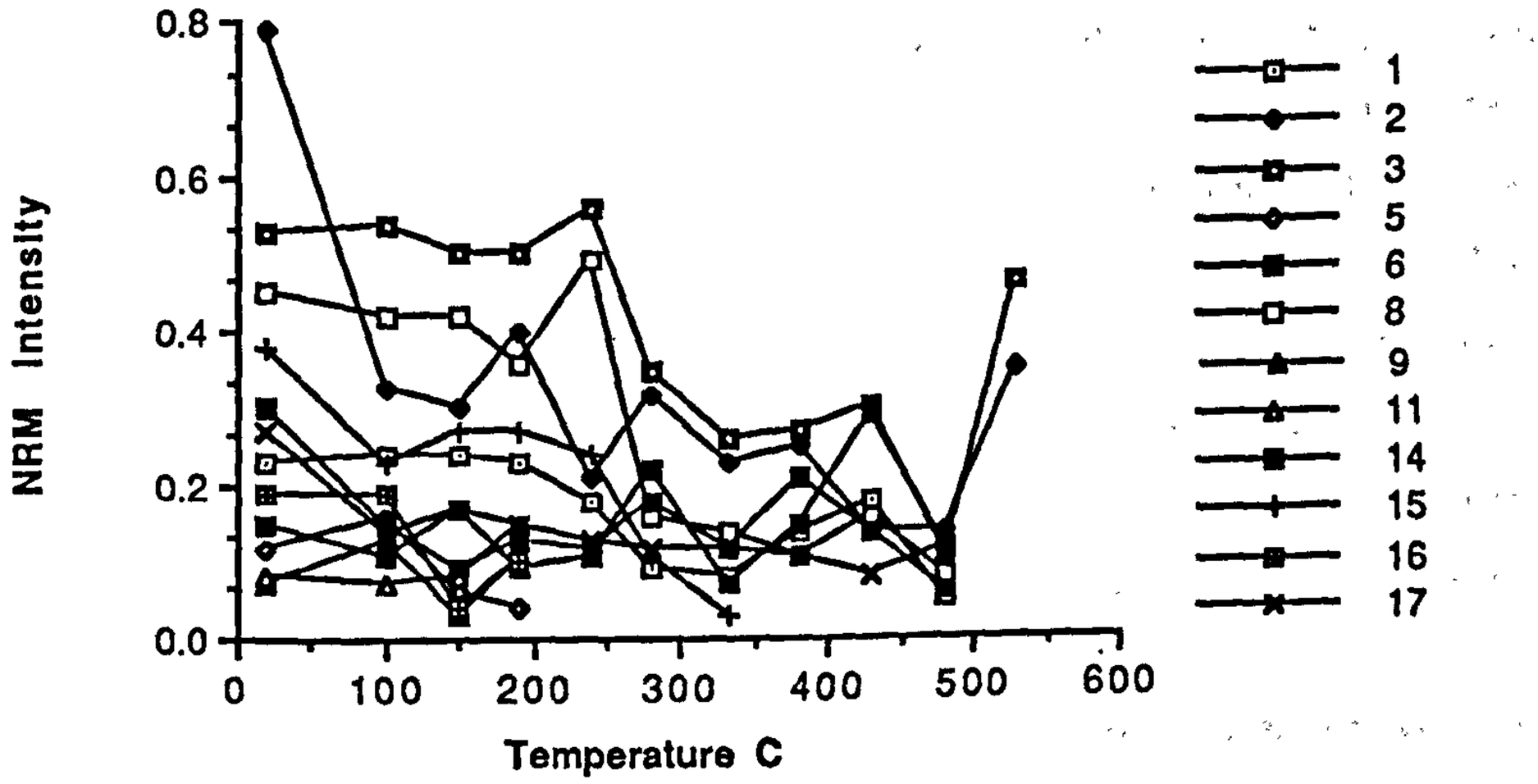
NRM Intensity
0.8
0.6
0.4
0.2
0.0
0
100
200
300
400
500
600
Temperature C
1
2
3
5
6
8
9
11
14
15
16
17

d

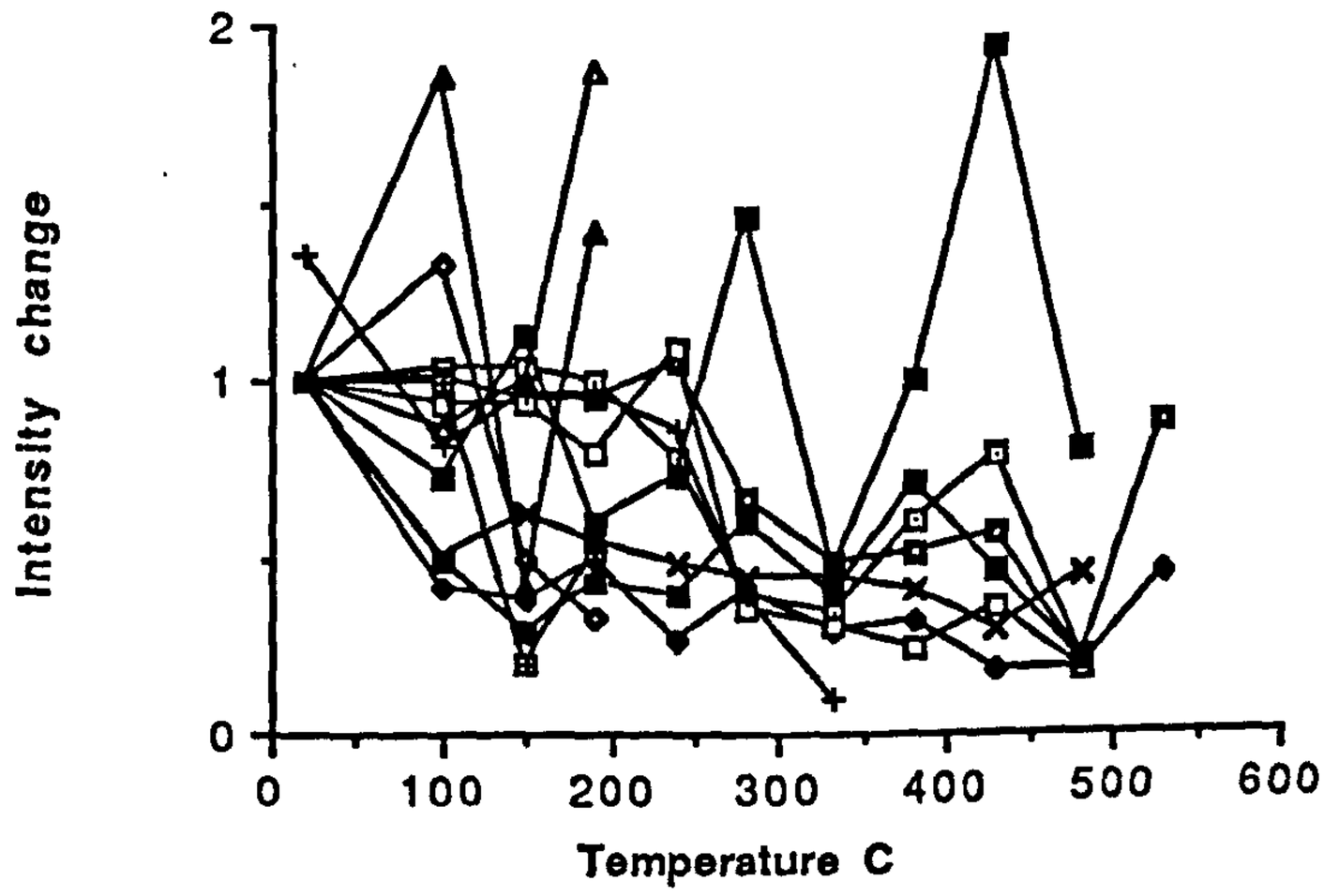
Intensity change
2
1
0
0
100
200
300
400
500
600
Temperature C

e

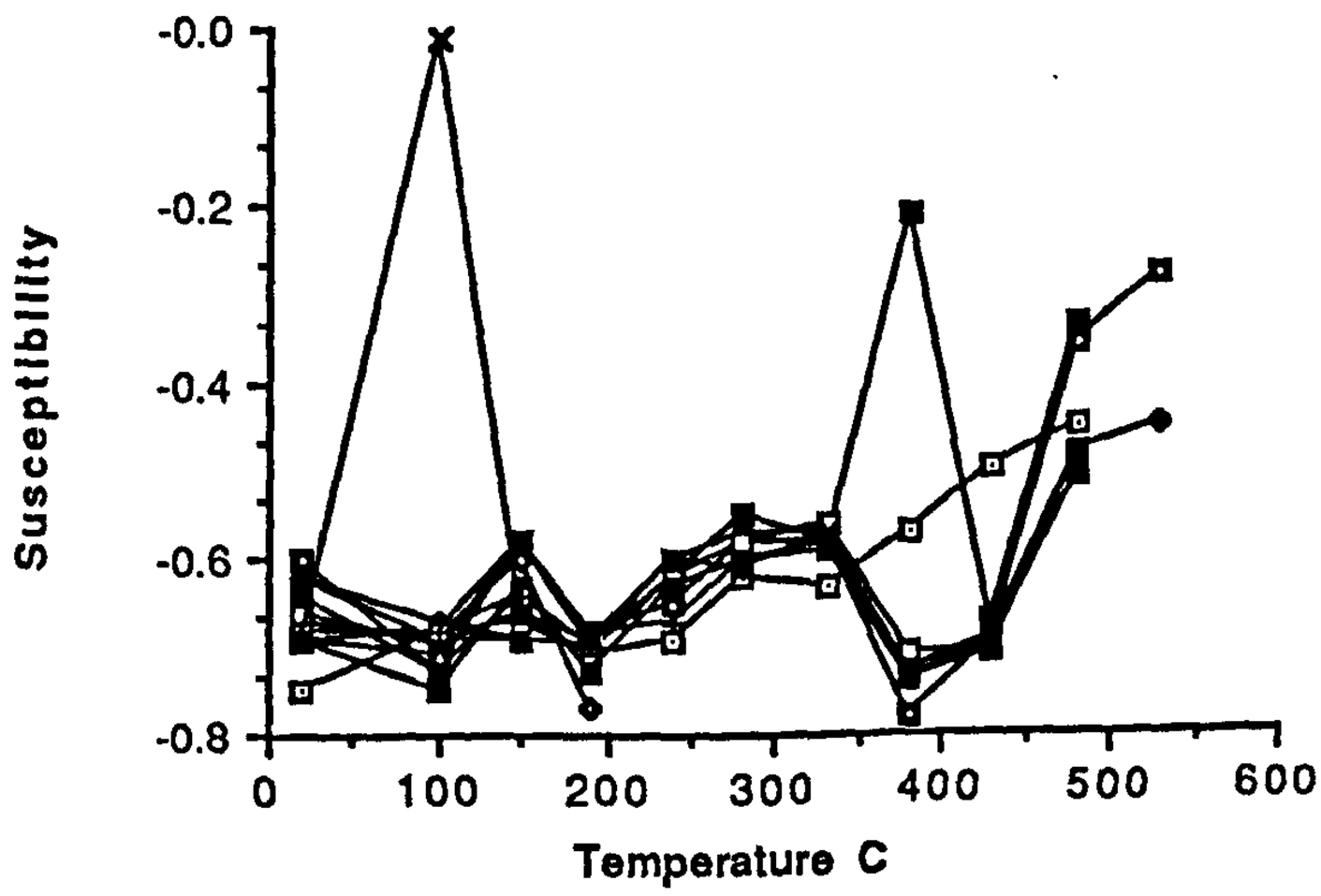
Susceptibility
-0.0
-0.2
-0.4
-0.6
-0.8
0
100
200
300
400
500
600
Temperature C

indicate that the magnetic mineral content is very low. Despite the low susceptibility displayed in this site, there is little within site scatter. The initial natural remanent magnetism intensities are more variable, with several samples not containing any magnetic minerals at all. The vectors are only metastable. The continual movement of the natural remanent magnetism vector with progressive demagnetisation suggest that two components may be involved, despite the low intensity of natural remanent magnetism. This is confirmed by the orthogonal plot, which illustrates that at least two components are involved and that vector movement is erratic. The two components have similar direction but differ in inclination with the lower T_b component having higher inclination. Intensity and susceptibility data also indicate that two phases might be present because there is an intensity drop to around 320°C and a consequent susceptibility increase above 380°C. This could indicate that pyrrhotite carries the low temperature natural remanent magnetism. The decrease of intensity from 380°C to 480°C could indicate the demagnetisation of impure haematite; this may be carrying the higher temperature natural remanent magnetism. Although site directions are metastable and quite scattered, they form a grouping, the mean of which has a *A95* = 19.8°, normal polarity and lies on the apparent field direction wander path at 190 Ma. This date is tentatively placed, considering the *A95* value and the low stability of the directions.

Site M9 (fig. 5.12) The maximum intial value of intensity of natural remanent magnetism is 16.84 x $10^{-4}Am^{-1}$, and the maximum initial susceptibility is 0.17 (volume units x $10^{-6}GOe^{-1}$; see appendix 4.2). These values indicate that haematite is present, and in significant quantities relative to most samples in this study. There is a considerable scatter of initial intensity values between samples from this site. However, normalised intensity change and change of susceptibility with progressive demagnetisation indicate that these differences reflect the quantity of magnetic minerals present, rather than differences in mineralogy. Inflection points in the graphs of intensity and susceptibility change at around 350°C and 550°C suggest the demagnetisation of natural remanent magnetism carried by pyrrhotite and either magnetite or impure haematite. The increase in susceptibility above 350°C indicates oxidation of pyrrhotite to haematite. Site directions are quite scattered but two groupings are still apparent. Samples from most sites have a well-defined demagnetisation path, and define a near-vertical, normal polarity vector, and this includes AF demagnetised samples. It may be that this vector represents a combination of a normal and a reversed Tertiary component, as the mean direction plots intermediate

fig. 5.12 Summary of demagnetisation behaviour of samples from site M9. Natural remanent magnetism (NRM) intensity is given x $10^{-4}Am^{-1}$; susceptibility in units x 10^{-6} GOe^{-1}

a. stereographic projection of stable sample directions;

b. and **c.** stereographic projections and accompanying orthogonal plots illustrating vector movement with progressive demagnetisation for samples with different behaviour;

d. NRM intensity change with increasing temperature illustrating variation of magnetic mineral content between samples;

e. normalised NRM change with increasing temperature illustrating within-site variation;

f. susceptibility variation with increasing temperature illustrating changes which occur due to mineralogical alteration.

a.

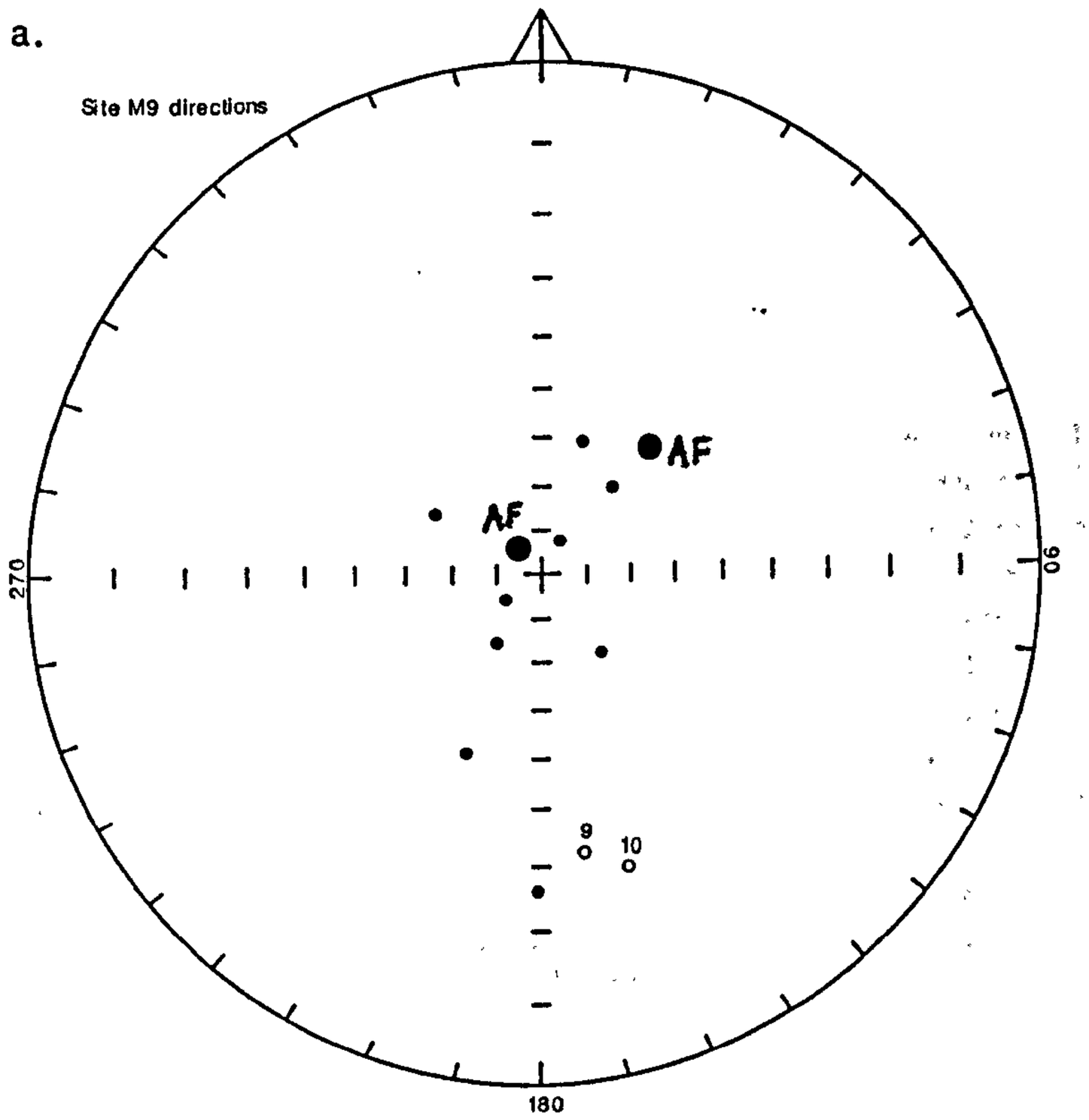
Site M9 directions
AF
AF
270
90
180
9
10

b.

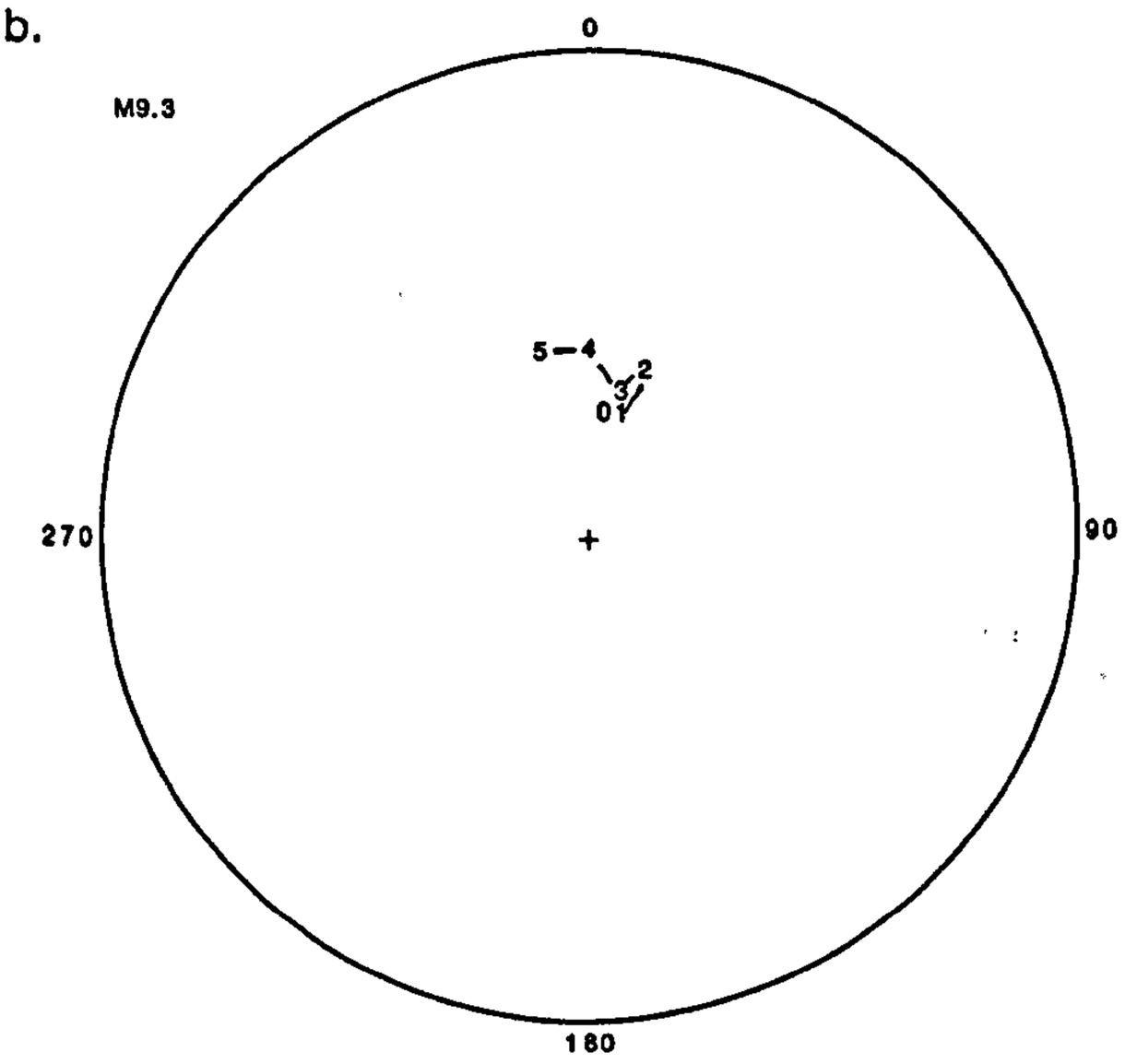
M9.3
0
5—4
3
2
0
1
270
90
180

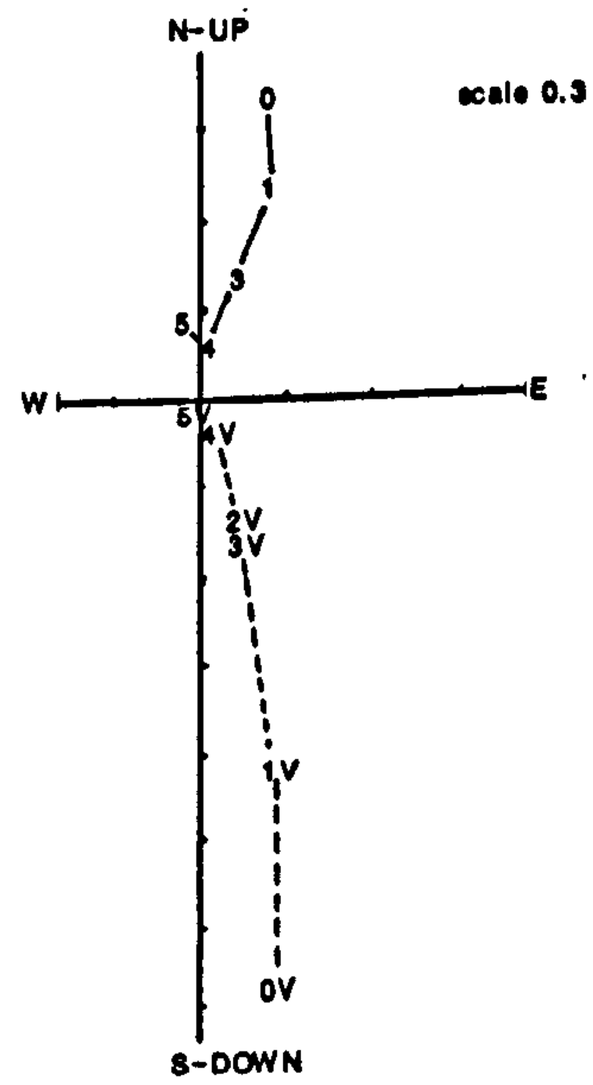
N-UP
scale 0.3
0
1
3
5
4
W
E
5
4V
2V
3V
1V
0V
S-DOWN

C.

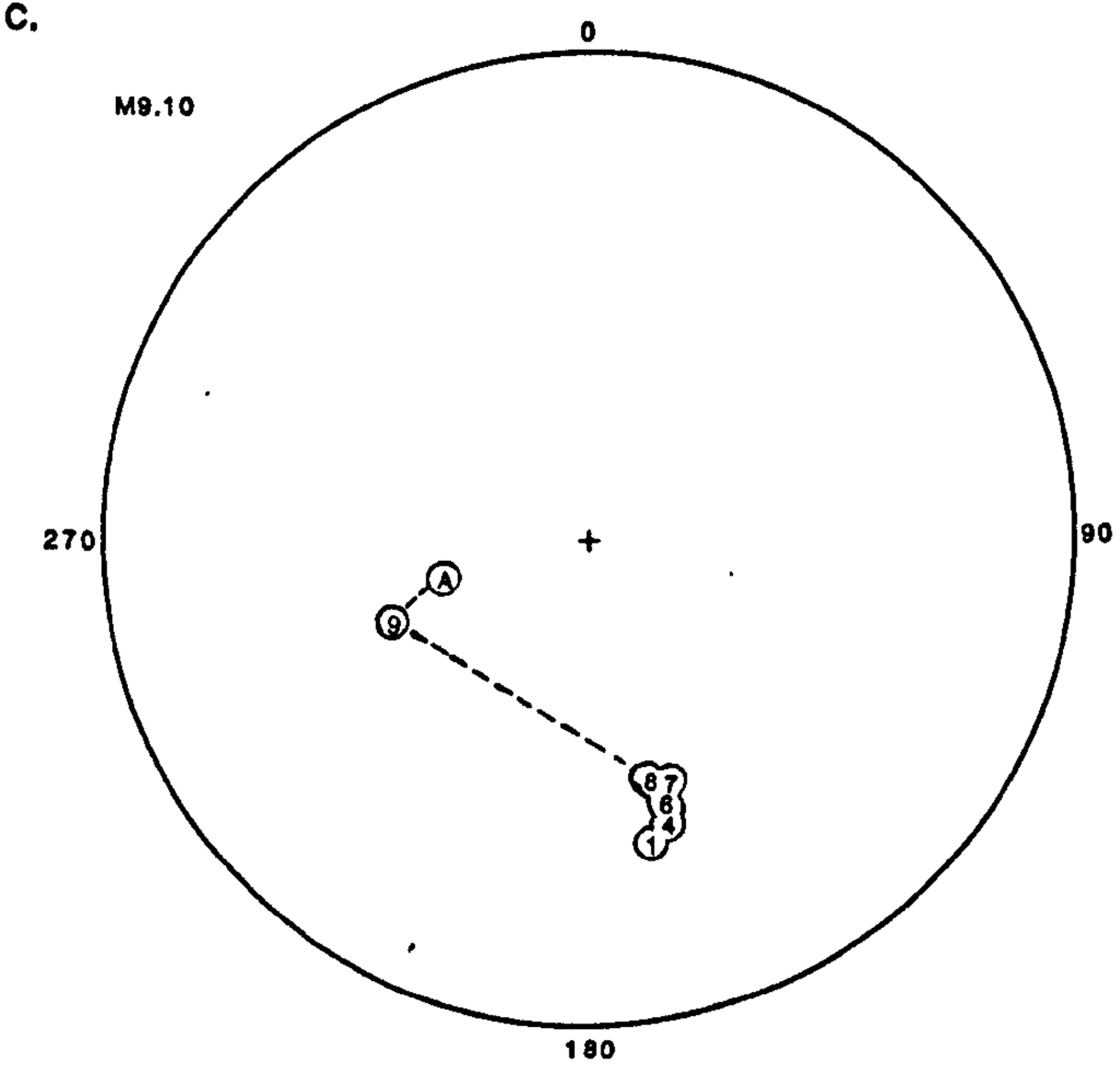
M9.10
0
270
90
180
A
9
8
7
6
4
1

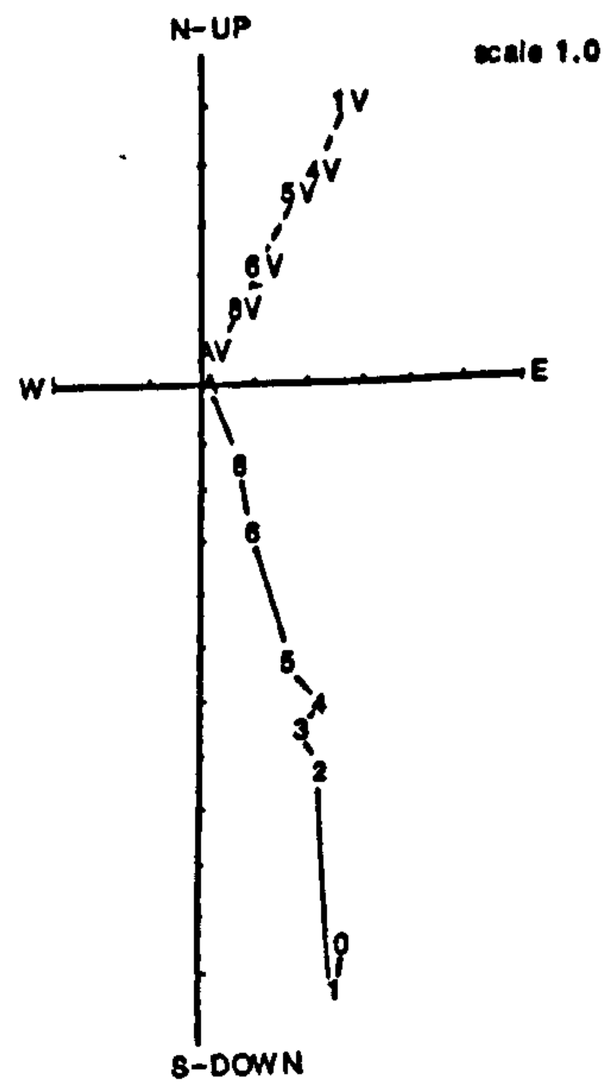
N-UP
scale 1.0
1V
5V
4V
6V
8V
4V
W
E
8
6
5
4
3
2
0
1
S-DOWN

d

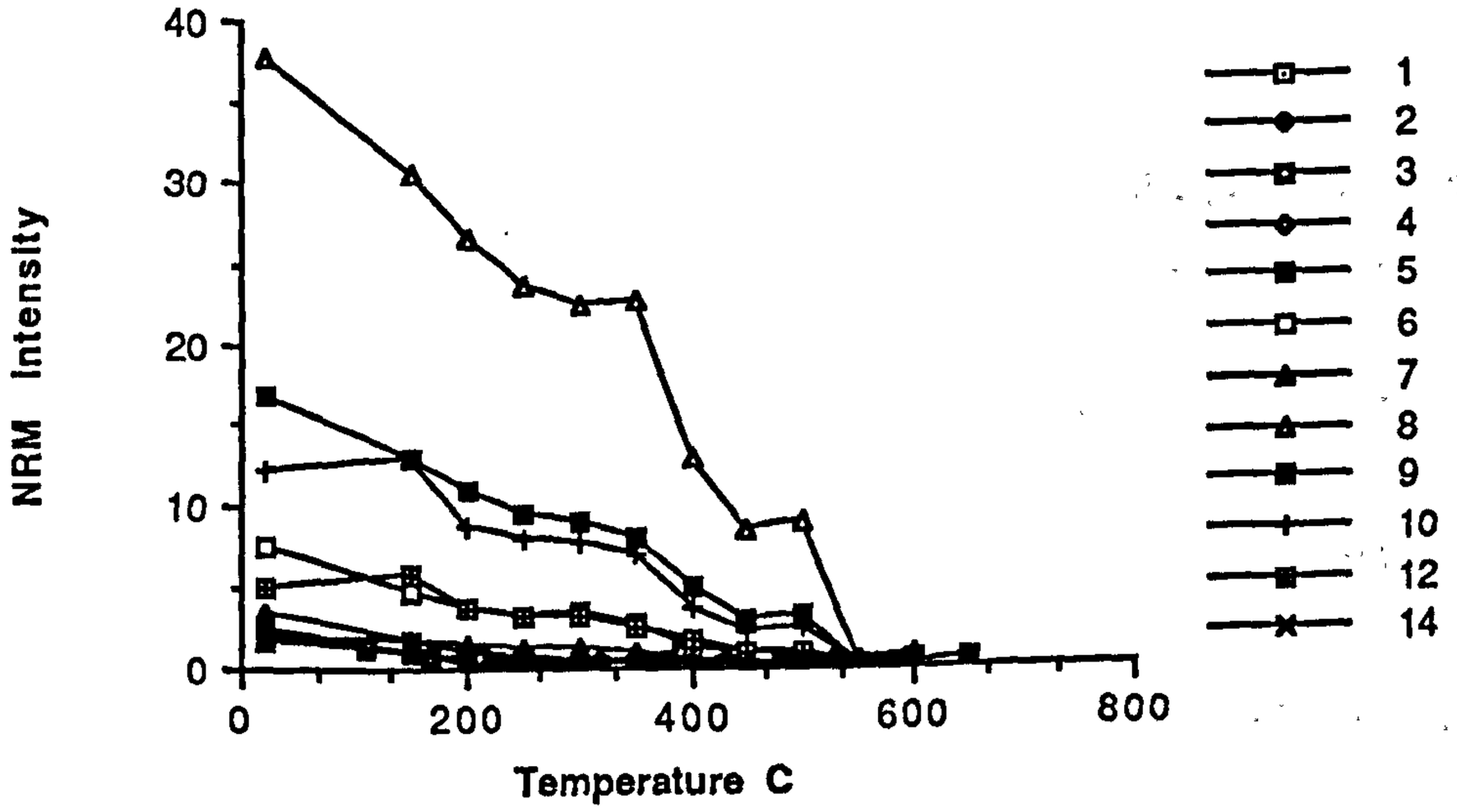
NRM Intensity
40
30
20
10
0
0
200
400
600
800
Temperature C
1
2
3
4
5
6
7
8
9
10
12
14

e

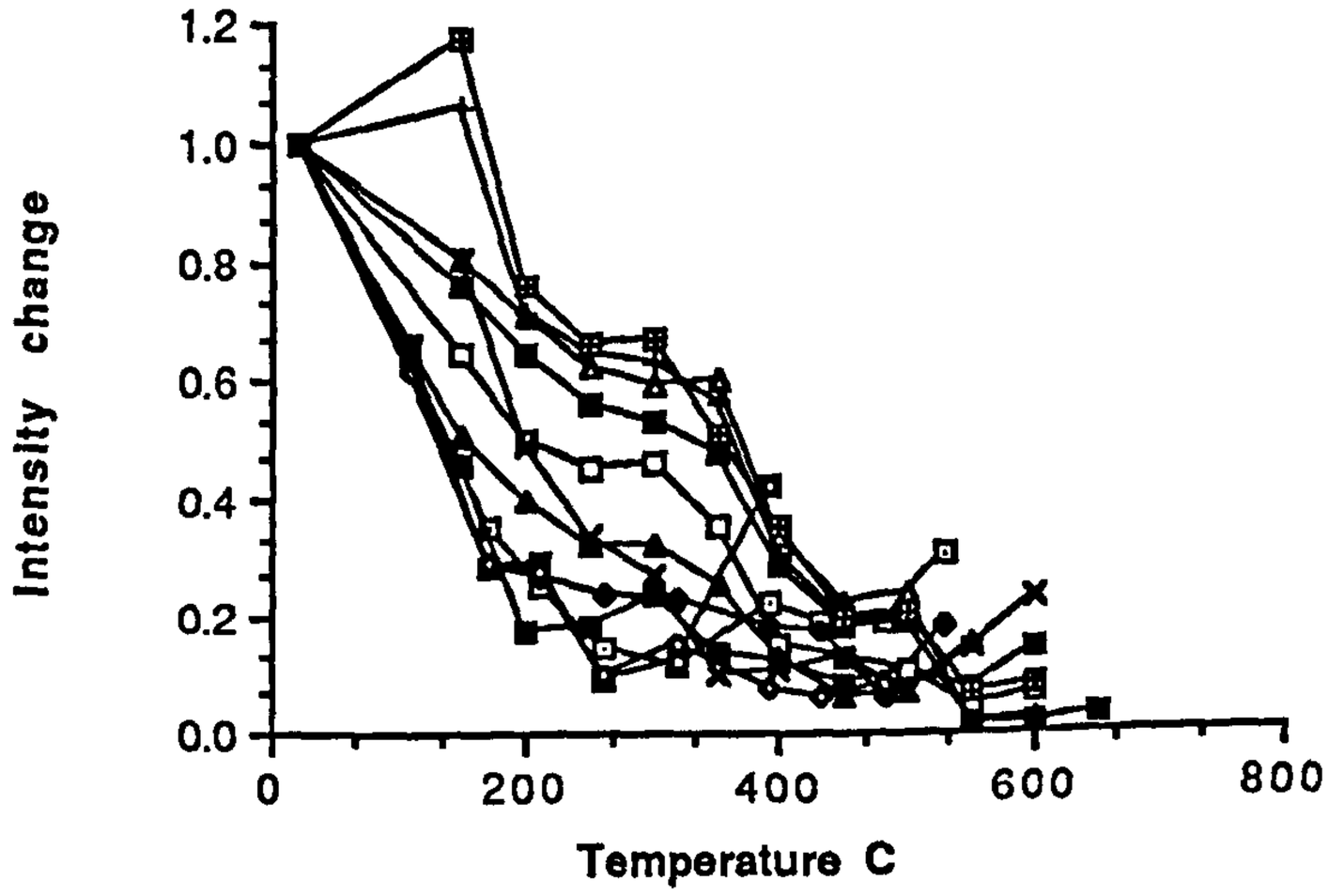
Intensity change
1.2
1.0
0.8
0.6
0.4
0.2
0.0
0
200
400
600
800
Temperature C

f

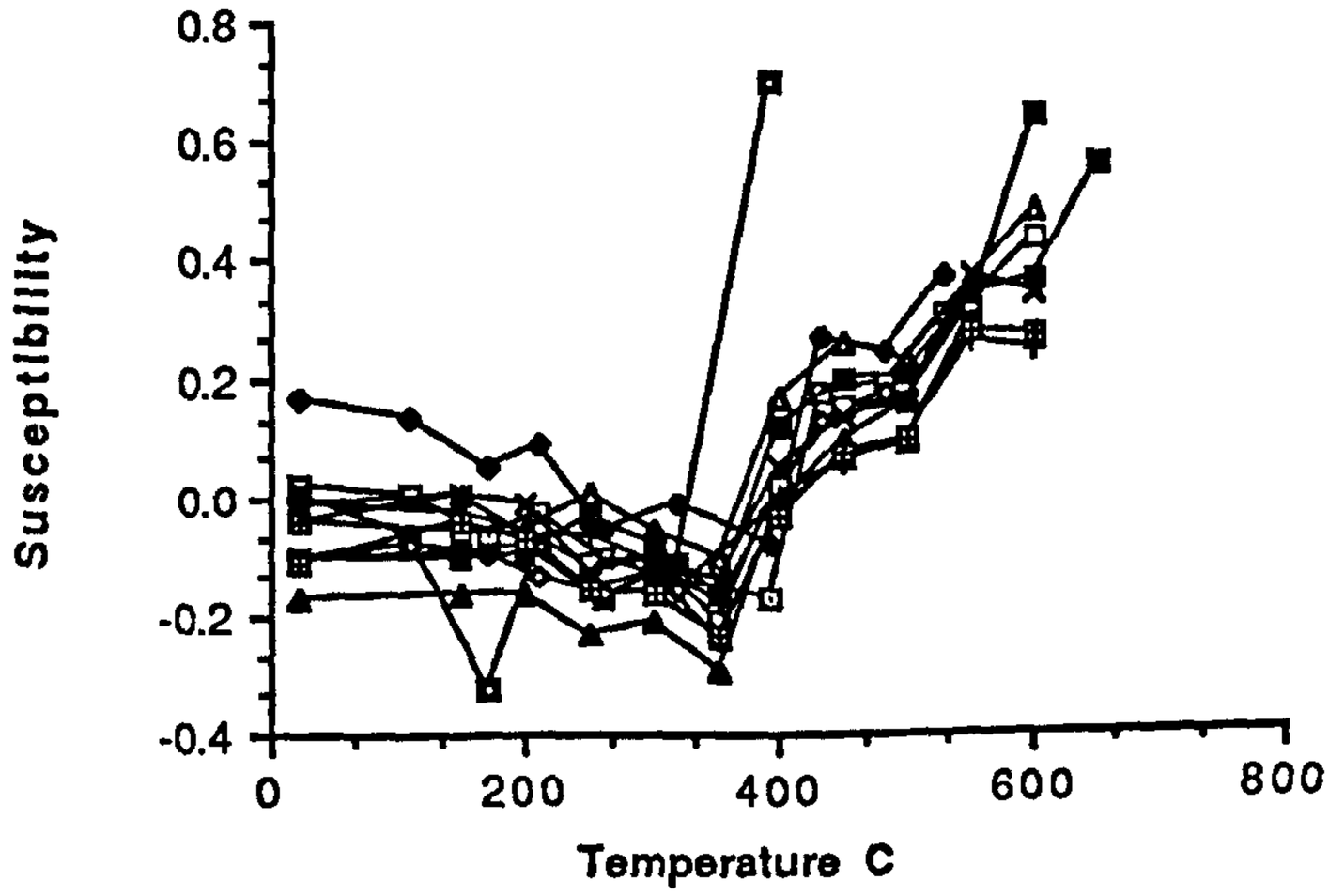
Susceptibility
0.8
0.6
0.4
0.2
0.0
-0.2
-0.4
0
200
400
600
800
Temperature C

fig. 5.13 Summary of demagnetisation behaviour of samples from site M10. Natural remanent magnetism (NRM) intensity is given x $10^{-4}Am^{-1}$; susceptibility in units x 10^{-6} GOe^{-1}

a. stereographic projection of stable sample directions;

b. and **c.** stereographic projections and accompanying orthogonal plots illustrating vector movement with progressive demagnetisation for samples with different behaviour;

d. NRM intensity change with increasing temperature illustrating variation of magnetic mineral content between samples;

e. normalised NRM change with increasing temperature illustrating within-site variation;

f. susceptibility variation with increasing temperature illustrating changes which occur due to mineralogical alteration.

a.

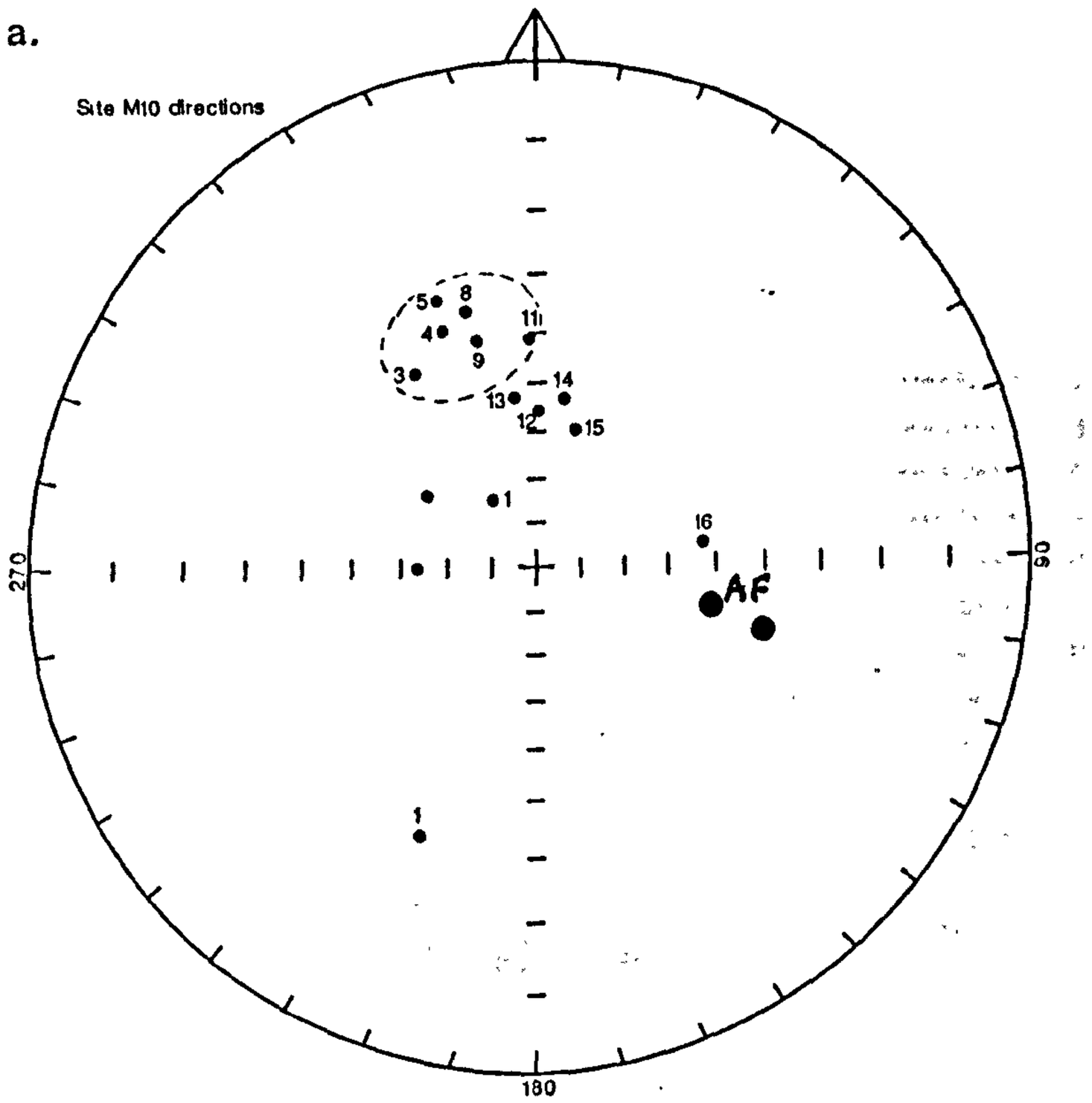
Site M10 directions
270
90
180
AF

b.

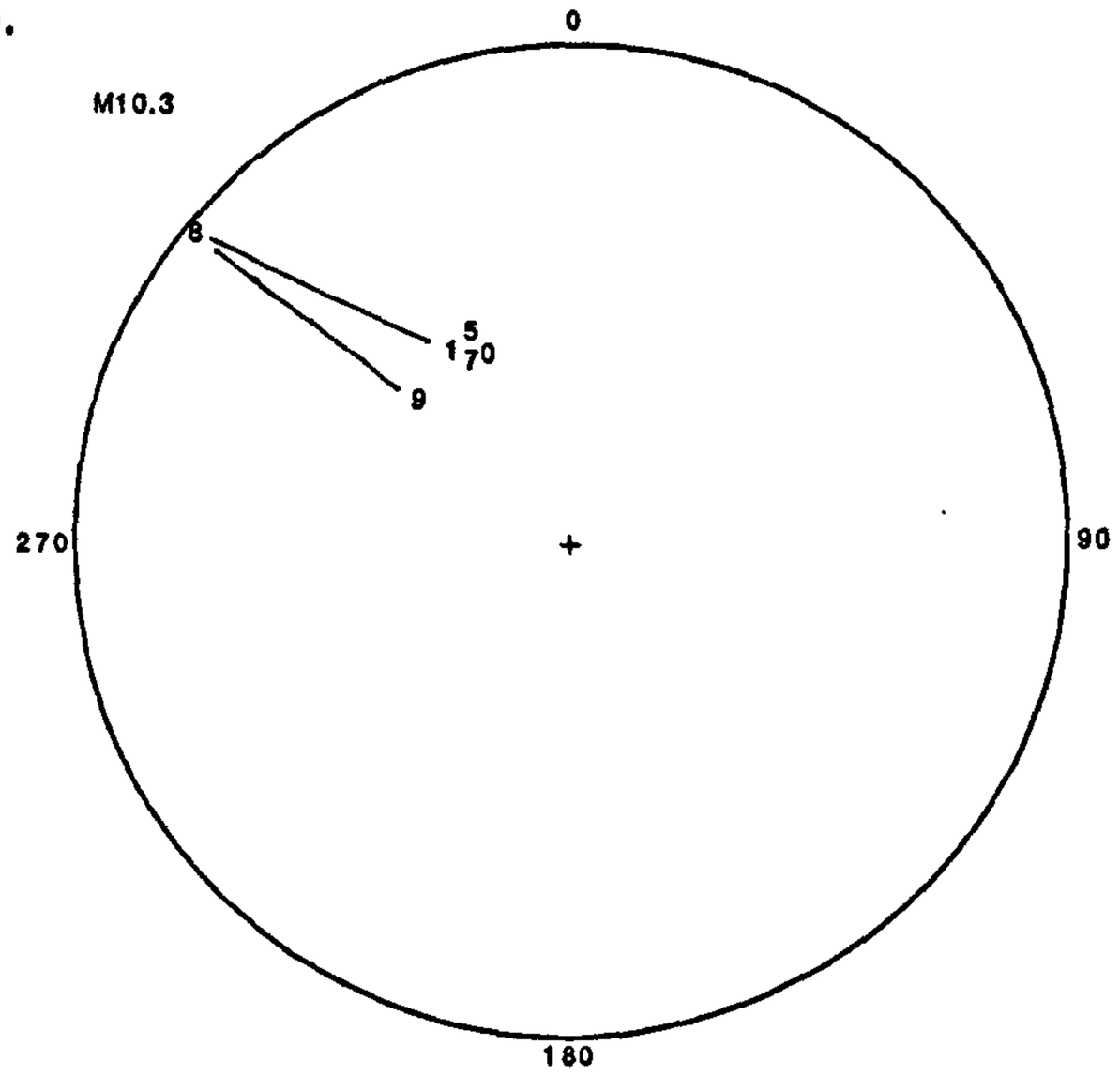
M10.3
0
270
90
180

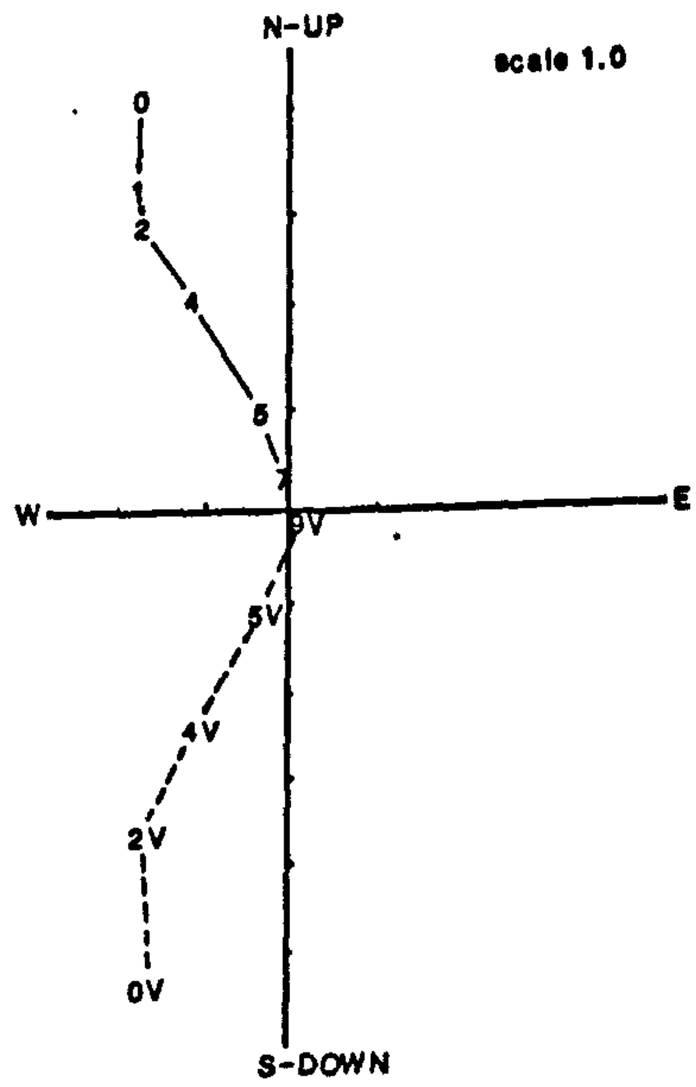
N-UP
scale 1.0
W
E
S-DOWN

C.

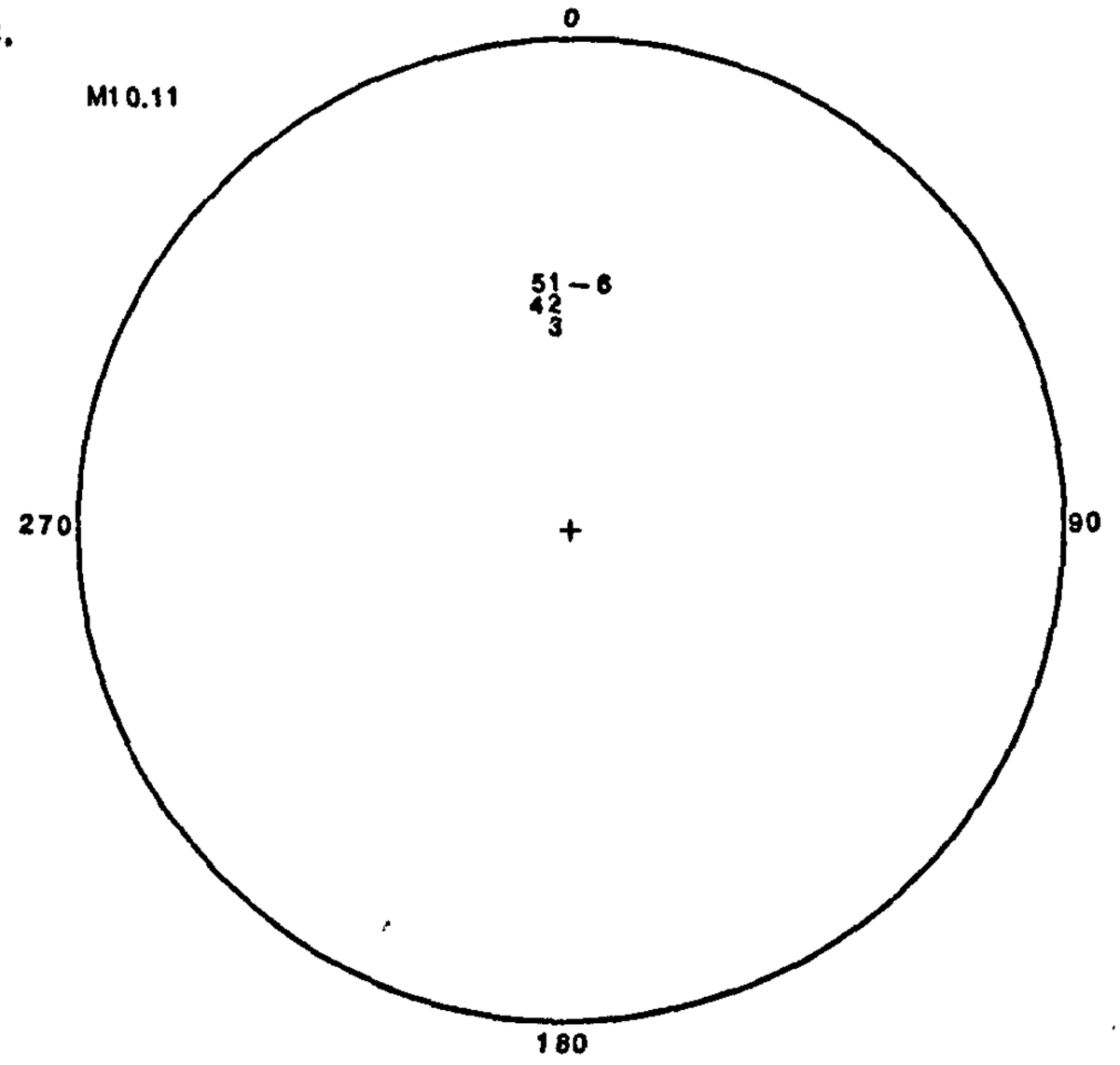
M10.11
0
270
90
180

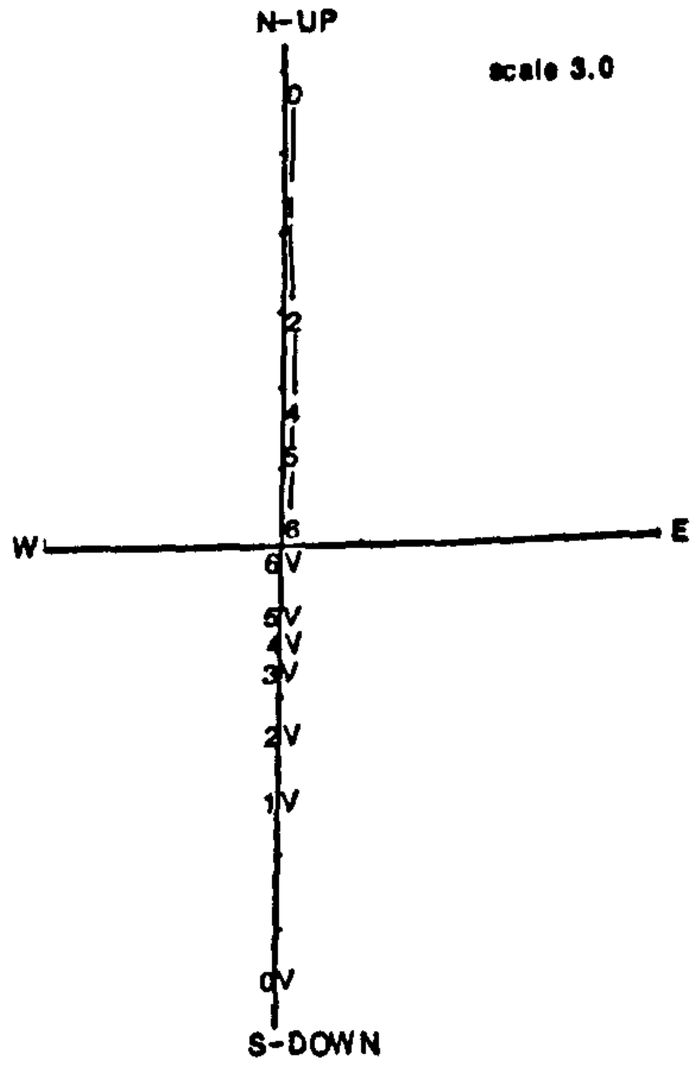
N-UP
scale 3.0
W
E
S-DOWN

d

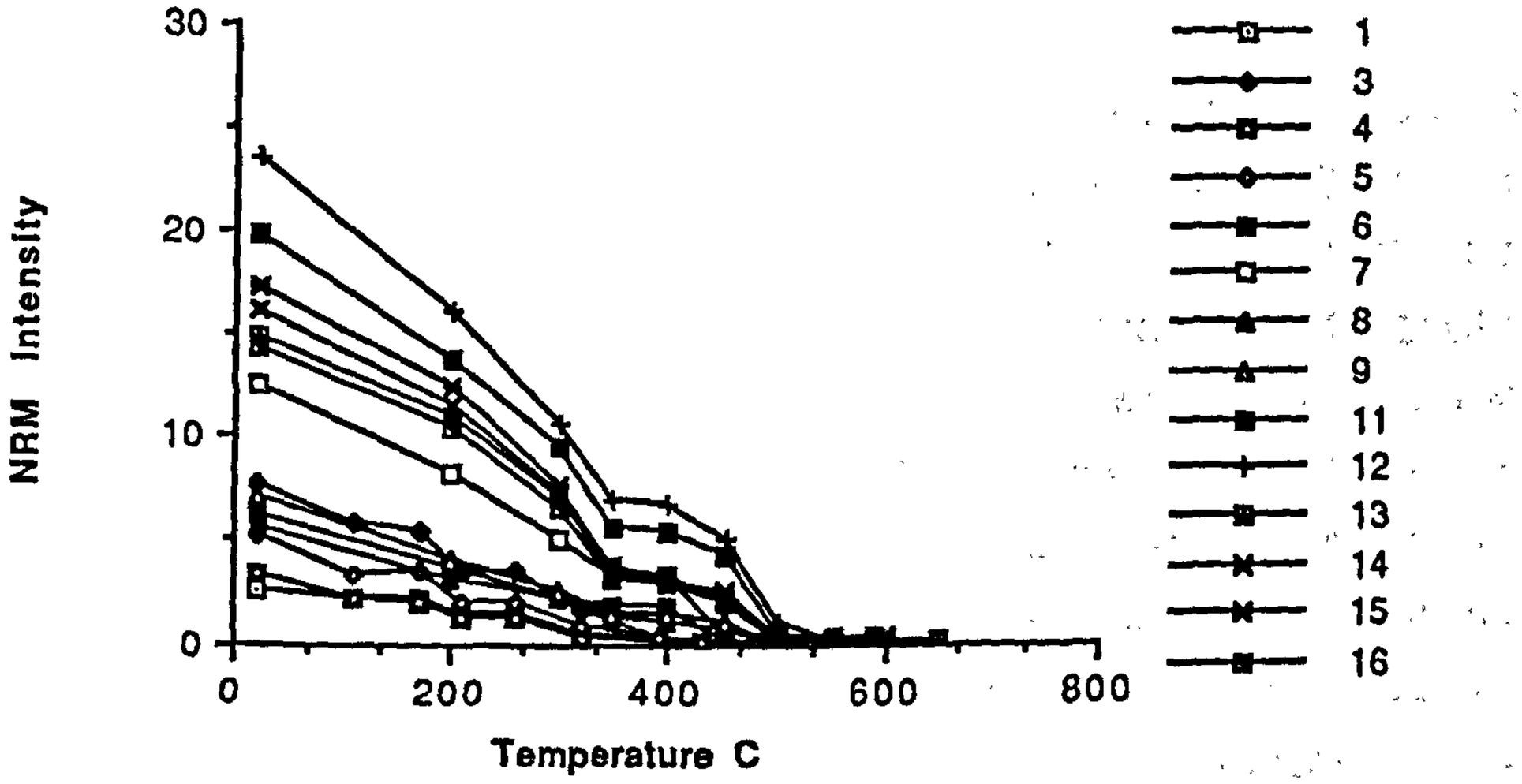
NRM Intensity
30
20
10
0
0
200
400
600
800
Temperature C
1
3
4
5
6
7
8
9
11
12
13
14
15
16

e

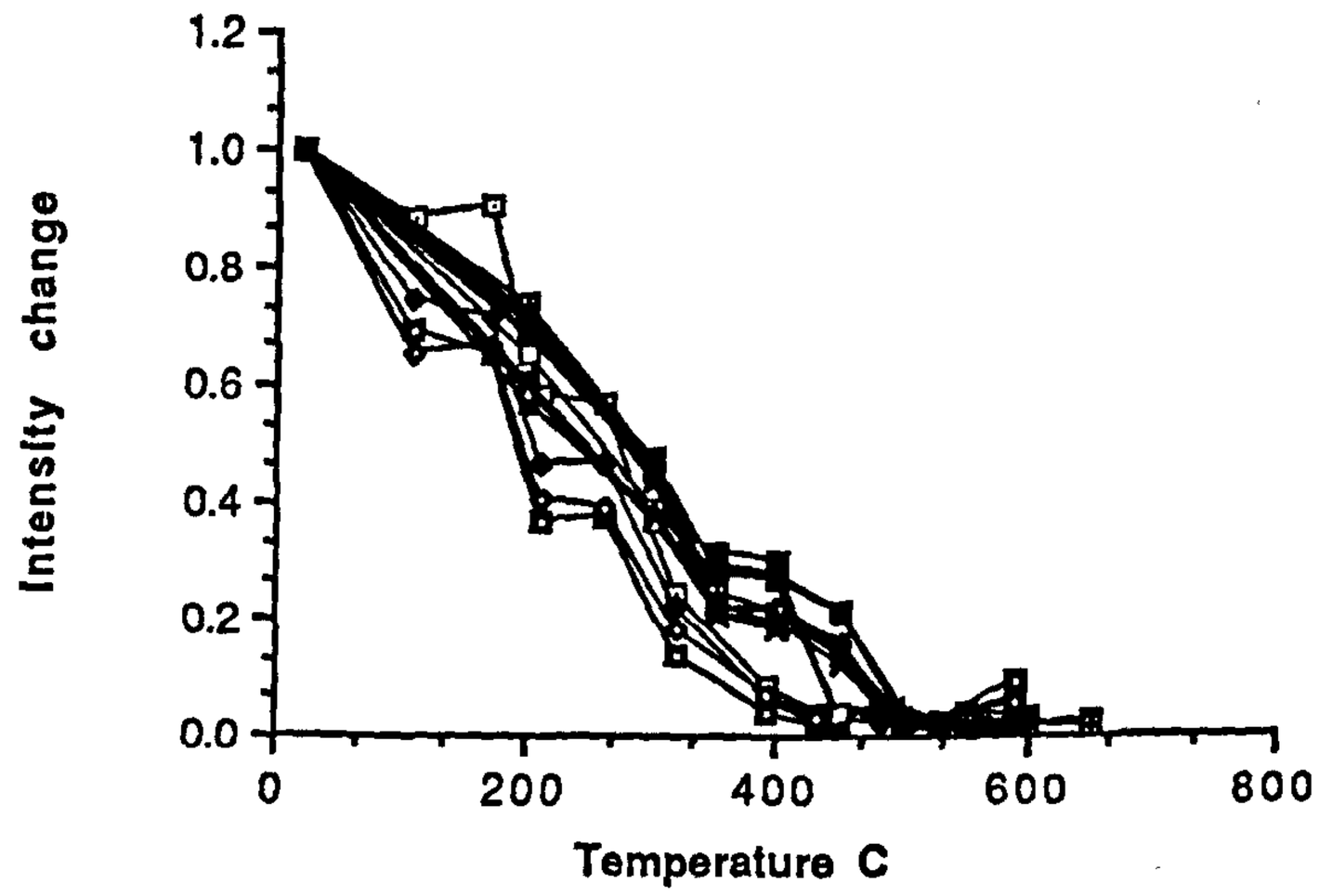
Intensity change
1.2
1.0
0.8
0.6
0.4
0.2
0.0
0
200
400
600
800
Temperature C

f

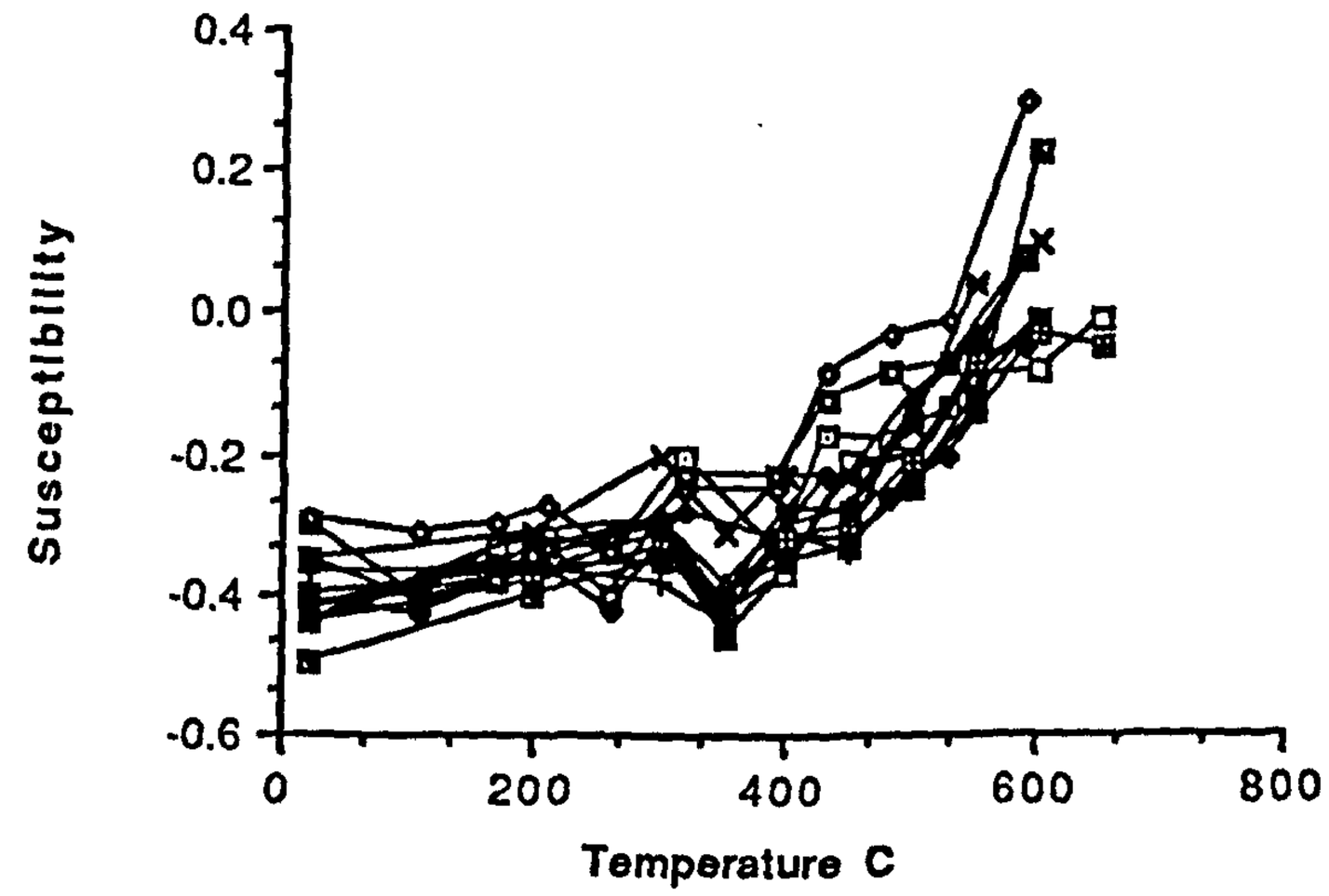
Susceptibility
0.4
0.2
0.0
-0.2
-0.4
-0.6
0
200
400
600
800
Temperature C

between a reversed and a normal Tertiary direction. Samples 9 and 10 have a stable, reversed mean direction which lies on the apparent field direction wander path at 190 Ma. Within site scatter may be caused by different natural remanent magnetism directions being carried by different minerals, although this is not reflected in the natural remanent magnetism intensity and susceptibility data.

Site M10 (fig. 5.13) The maximum initial natural remanent magnetism intensity of 23.58 x $10^{-4}Am^{-1}$ and susceptibility of -0.29 (volume units x $10^{-6}GOe^{-1}$; see appendix 4.2) indicate that the magnetic mineral content is relatively high, and that the magnetic mineral present is haematite. Two inflection points are apparent on the graphs of intensity and susceptibility change with progressive demagnetisation. These are at around 350°C and 500°C, suggesting that pyrrhotite and impure, multi-domain or pseudo-single domain magnetite/haematite are the main natural remanent magnetism carriers. Graphs of intensity change with progressive demagnetisation reveal two groupings of behaviour. This division is also reflected in site directions. Site directions are clearly defined, of normal polarity and stable/very stable. Some samples have a single natural remanent magnetism component and straight demagnetisation paths, whilst other have a curved demagnetisation path indicating that more than one natural remanent magnetism component is present. This mix of vectors explains the vector groupings. Group I. (samples 3, 4, 5, 8, 9, 11) has a mean direction which lies on the apparent field direction wander path at 155 Ma; group iia. (samples 12, 13, 14, 15) has a mean direction which lies on the apparent field direction wander path at 20 Ma - present day. The group iib. (samples 1, 6, 7) and group iic. (sample 16 and AF demgnetised smples) have mean directions which do not lie on the apparent field direction wander path, but the high inclinations suggest that the natural remanent magnetism may also be present- day. Group I. has lower intensities than group II. Within site variation is probably best explained by different proportions of magnetic carriers carrying different remanences of different ages being present in each sample *i.e.*, group I. contain a greater proportion of pyrrhotite to haematite, and *vice versa* for group ii. For this reason, dating the natural remanent magnetism is problematic. High intensity values and low susceptibility values suggest that the main magnetic carrier is haematite, although the samples which have highest intensities also appear to have pyrrhotite as an natural remanent magnetism carrier, as suggested from the inflection point at 350°C on graphs of intensity change with progressive demagnetisation. All vectors are normal polarity and range in age between 155+ Ma and 20 Ma - present day.

Site M11 (fig. 5.14) The maximum initial natural remanent magnetism intensity of $1.43 \times 10^{-4}Am^{-1}$ and susceptibility of -0.48 (volume units x $10^{-6}GOe^{-1}$; see appendix 4.2) indicate that the magnetic mineral content is low. The natural remanent magnetism intensity initially increases in some samples and decreases in other samples. This reflects the removal of viscous remanent magnetism which has reversed polarity in some samples and normal polarity in others. This viscous remanent magnetism is removed by 150°C implying that goethite is the carrier. The remainder of the natural remanent magnetism apears to be removed by around 350°C. This suggests that the main natural remanent magnetism carrier is pyrrhotite. Site directions are stable or meta-stable, high inclination and vary in declination. A single sample direction lies on the Tertiary part of the apparent field direction wander path; the remainder have similar inclinations but the declination differs from the apparent field direction wander path by around 110°. Vectors are a mixture between a high inclination, normal polarity direction and a low inclination reversed polarity direction. Incomplete resolution of the vectors, and low natural remanent magnetism intensity may explain the ambiguity of directions from this site.

Site M20 (fig. 5.15) The maximum initial natural remanent magnetism intensity of $4.36 \times 10^{-4}Am^{-1}$ and susceptibility of 0.02 (volume units x $10^{-6}GOe^{-1}$; see appendix 4.2) indicate that the magnetic mineral content is quite low. Graphs of normalised intensity change, and of susceptibility change, with progressive demagnetisation indicate that two categories of behaviour are displayed by this site. This is probably a reflection of different magnetic carriers being present. This division of behaviour is reflected in site directions, which are stable and fall into two groups. Group I. (samples 1 and 7) are normal polarity, and have higher initial natural remanent magnetism intensity and susceptibility. The erratic demagnetisation path on the stereogram suggests that more than one component is present, although only one main component is visible on the orthogonal plot. This has normal polarity an a declination of 260° and an inclination of 60°. This direction does not lie on the apparent field direction wander path. Group I. vectors could be carried by 'soft' multi-domain haematite which demagnetises easily. Alternatively, this natural remanent magnetism could be carried by pyrrhotite because the natural remanent magnetism is demagnetised by 300°C. However, no greater increase in susceptibility (due to the formation of magnetite from pyrrhotite) occurs above this temperature for these samples than occurs for the other group of samples. The normal polarity and high inclinations of these vectors is suggestive of a present day direction, although the declination differs from the apparent field direction wander path by 90°. This error may partly be a reflection of the small number of vectors (2) in

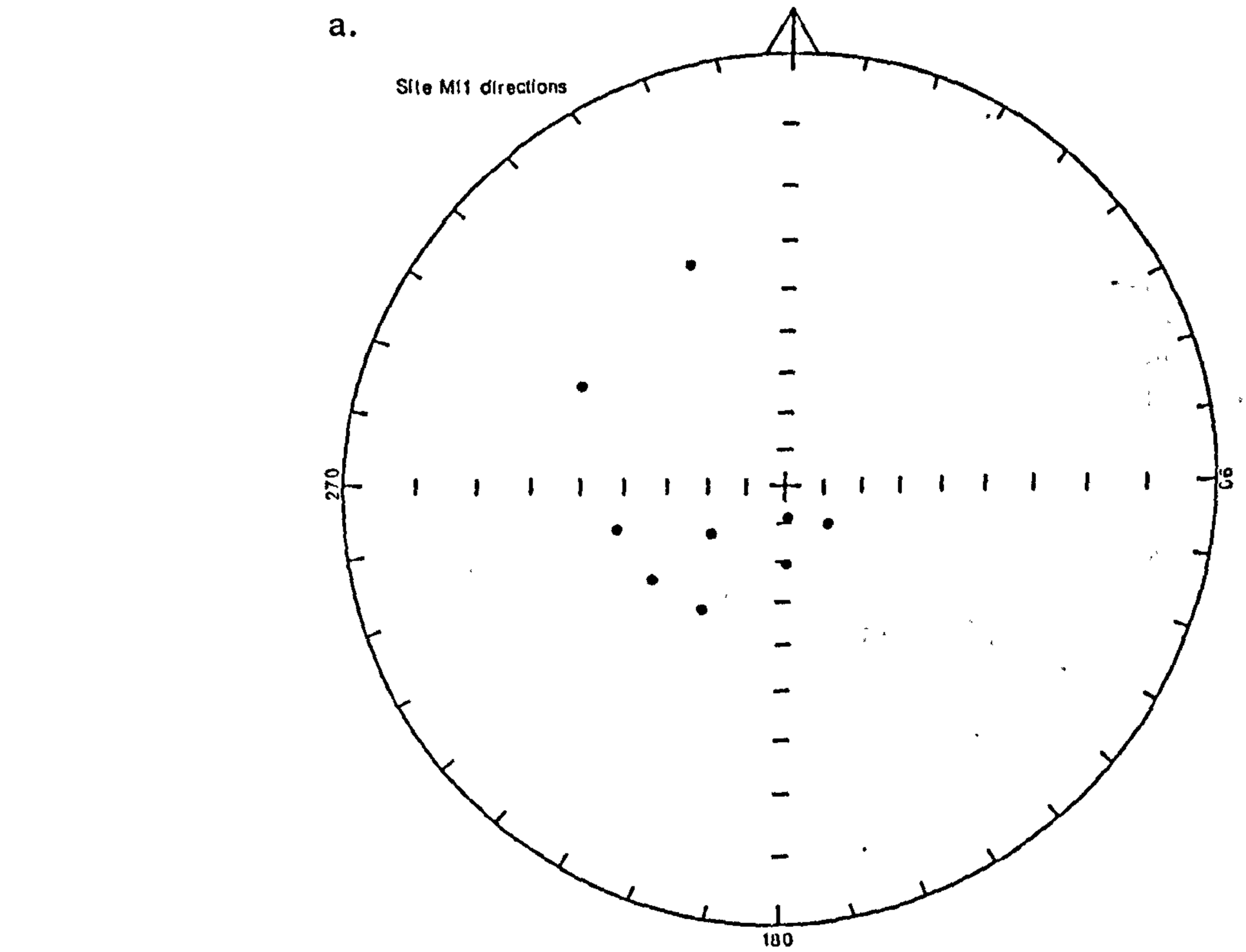

fig. 5.14 Summary of demagnetisation behaviour of samples from site M11. Natural remanent magnetism (NRM) intensity is given x $10^{-4}Am^{-1}$; susceptibility units x 10^{-6} GOe^{-1};
a. stereographic projection of stable sample directions; **b.** stereographic projection and accompanying orthogonal plot illustrating vector movement with progressive demagnetisation; **c.** NRM intensity change with increasing temperature illustrating variation of magnetic mineral content between samples; **d.** normalised NRM change with increasing temperature illustrating within-site variation; **e.** susceptibility variation with increasing temperature illustrating changes which occur due to mineralogical alteration.

c

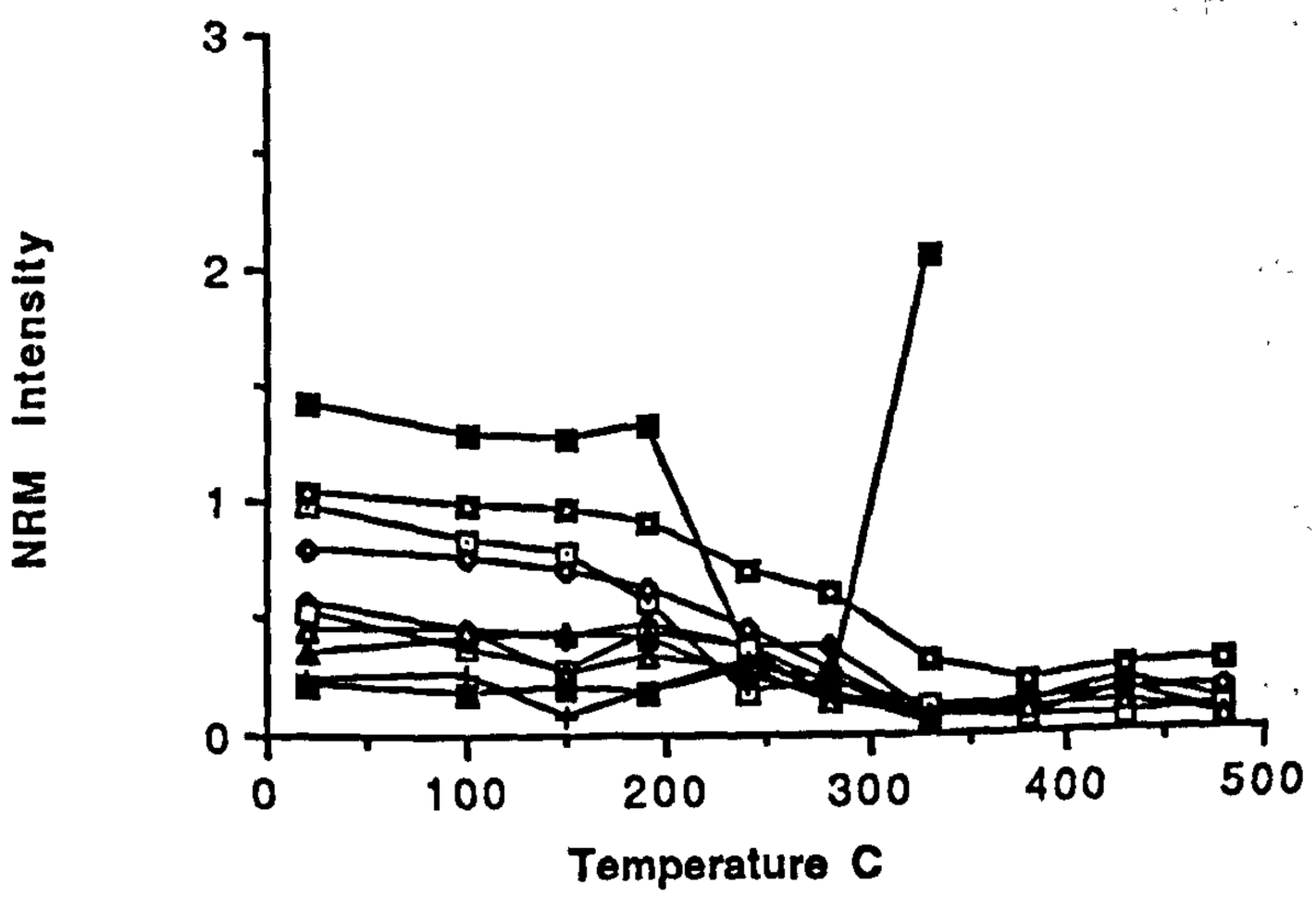
NRM Intensity
3
2
1
0
0
100
200
300
400
500
Temperature C
1
3
4
7
8
12
13
14
15
16

d

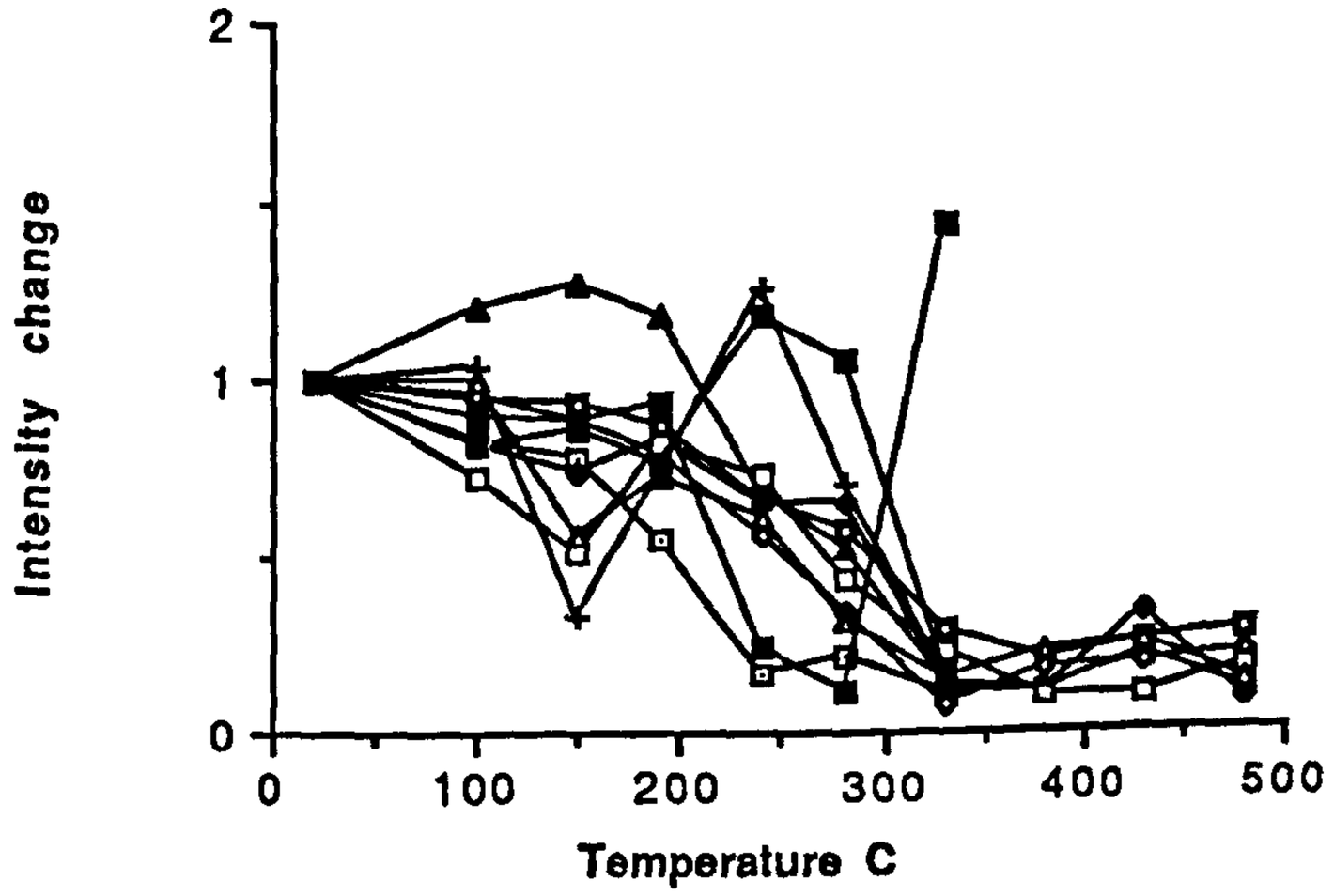
Intensity change
2
1
0
0
100
200
300
400
500
Temperature C

e

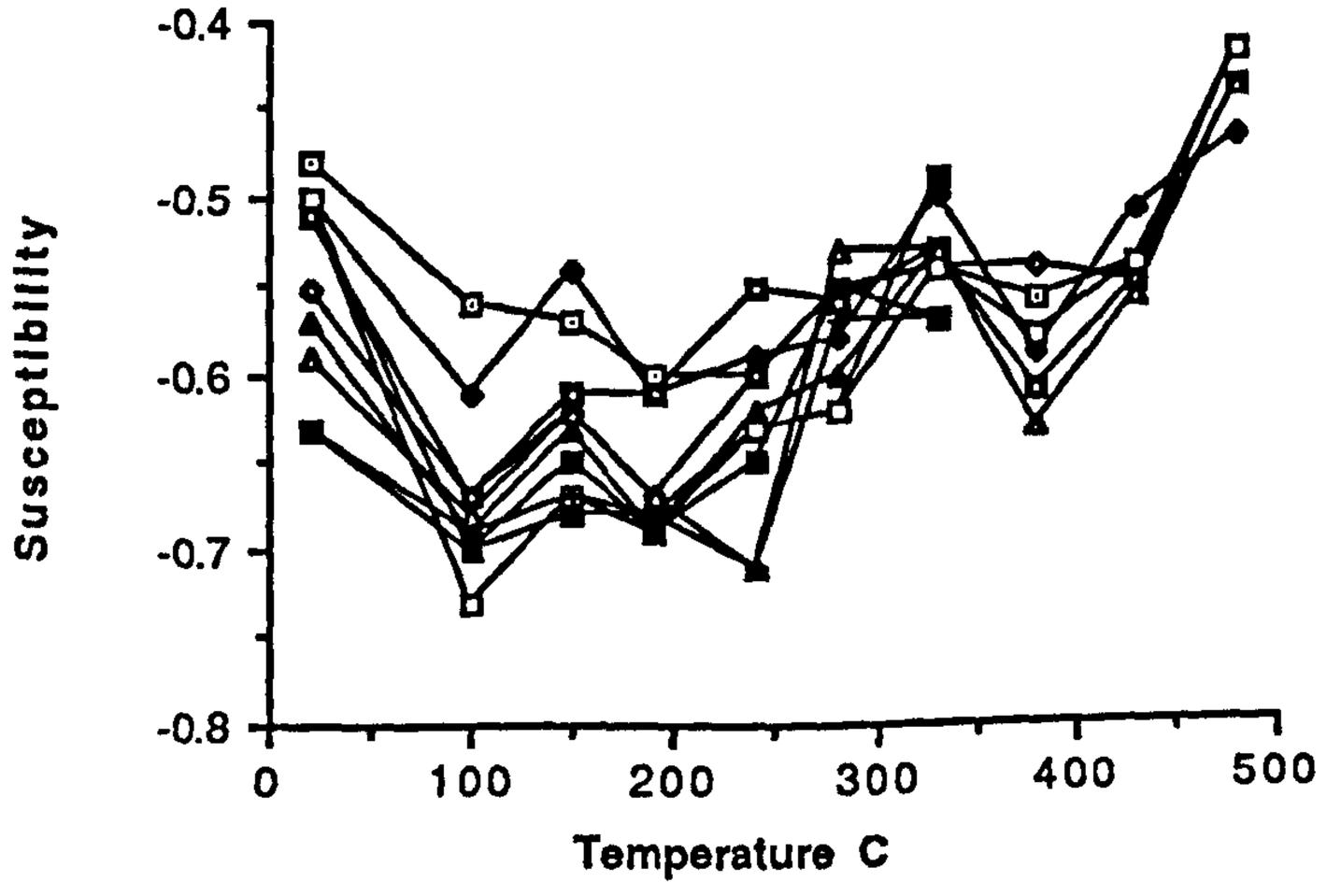
Susceptibility
-0.4
-0.5
-0.6
-0.7
-0.8
0
100
200
300
400
500
Temperature C

fig. 5.15 Summary of demagnetisation behaviour of samples from site M20. Natural remanent magnetism (NRM) intensity is given x $10^{-4}Am^{-1}$; susceptibility in units x 10^{-6} GOe^{-1}

a. stereographic projection of stable sample directions;

b. and **c.** stereographic projections and accompanying orthogonal plots illustrating vector movement with progressive demagnetisation for samples with different behaviour;

d. NRM intensity change with increasing temperature illustrating variation of magnetic mineral content between samples;

e. normalised NRM change with increasing temperature illustrating within-site variation;

f. susceptibility variation with increasing temperature illustrating changes which occur due to mineralogical alteration.

a.

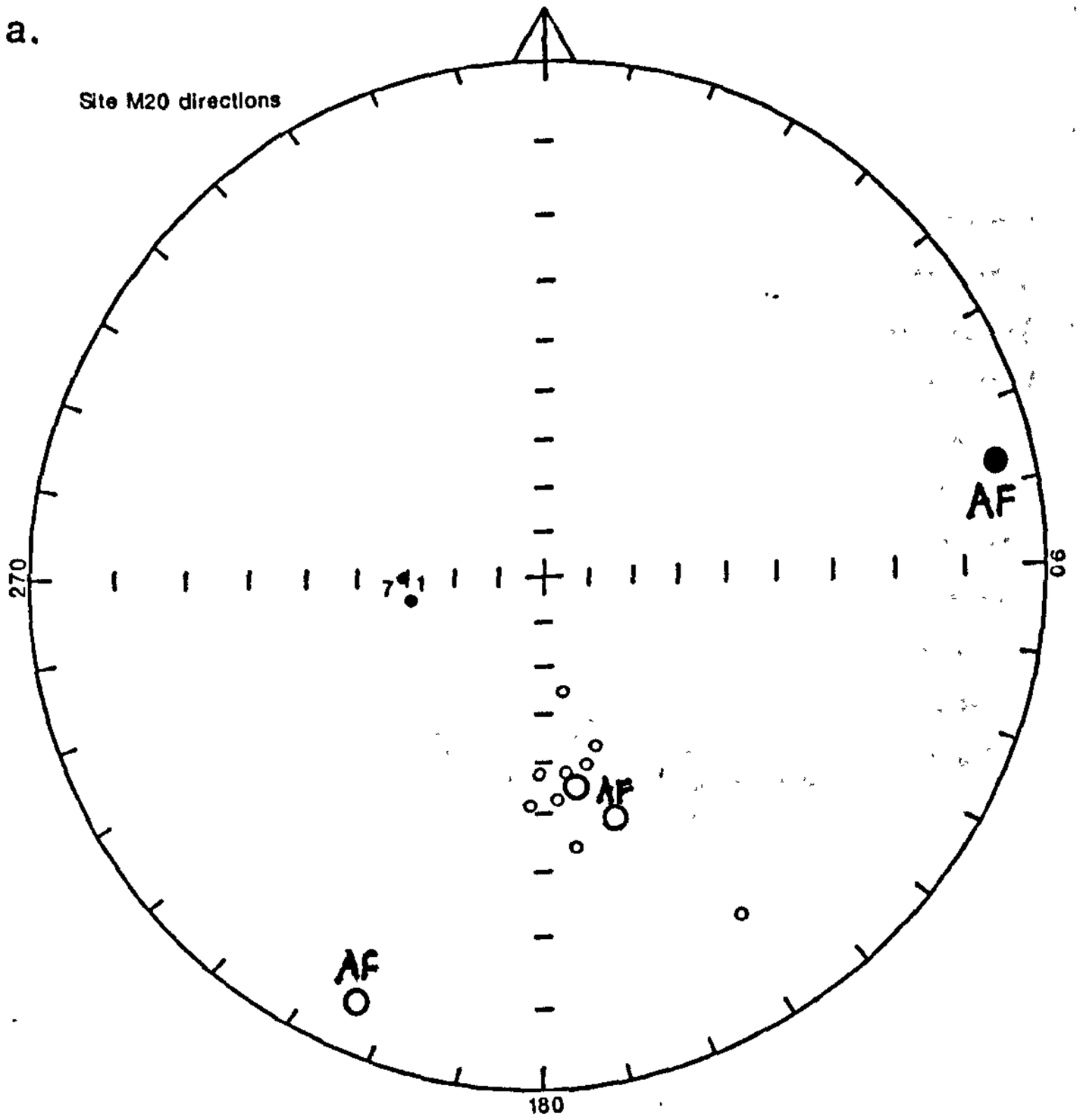
Site M20 directions
AF
270
90
180
AF
AF

b.

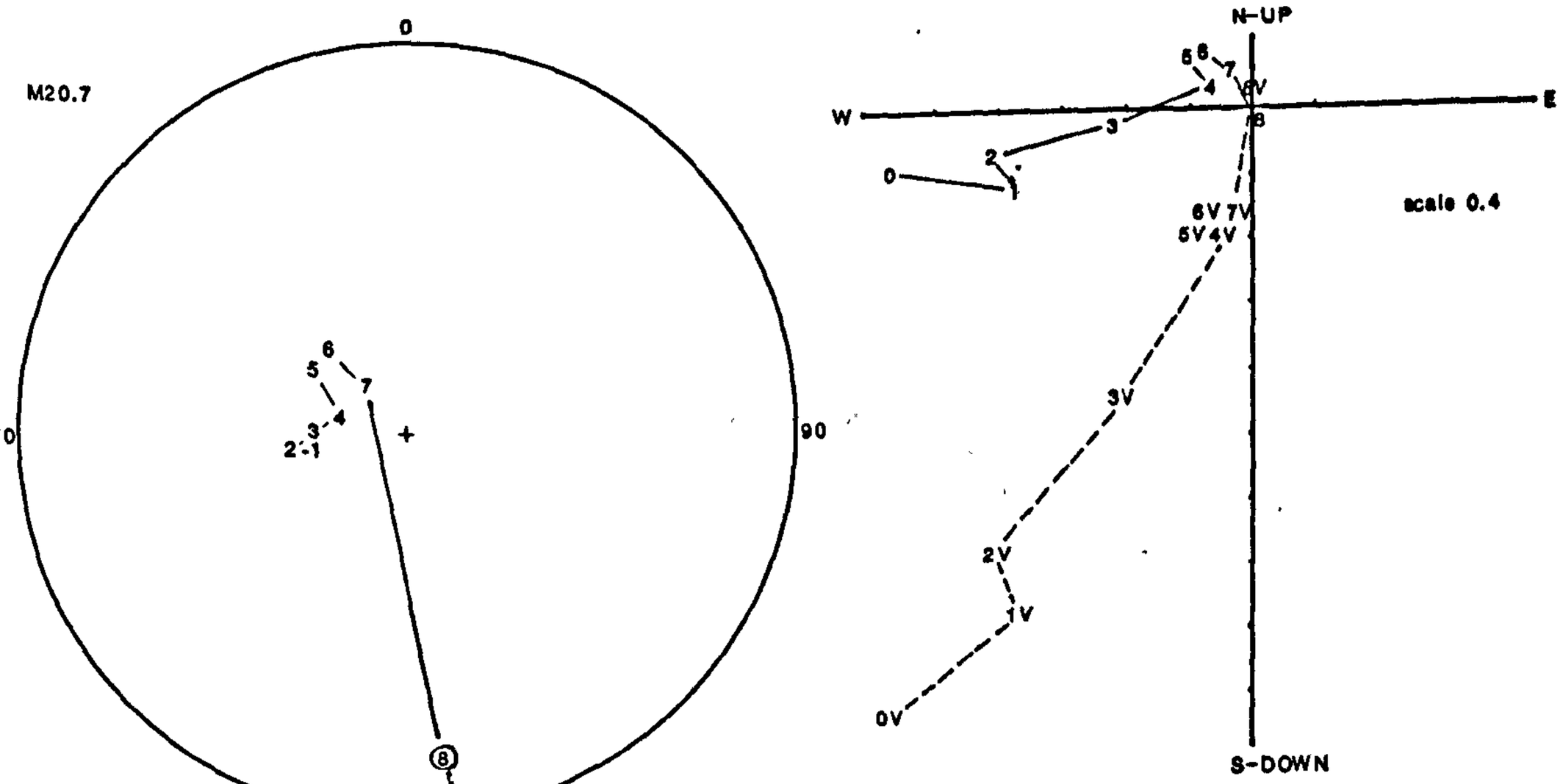
M20.7
0
90
180
270
N-UP
E
W
S-DOWN
scale 0.4

C.

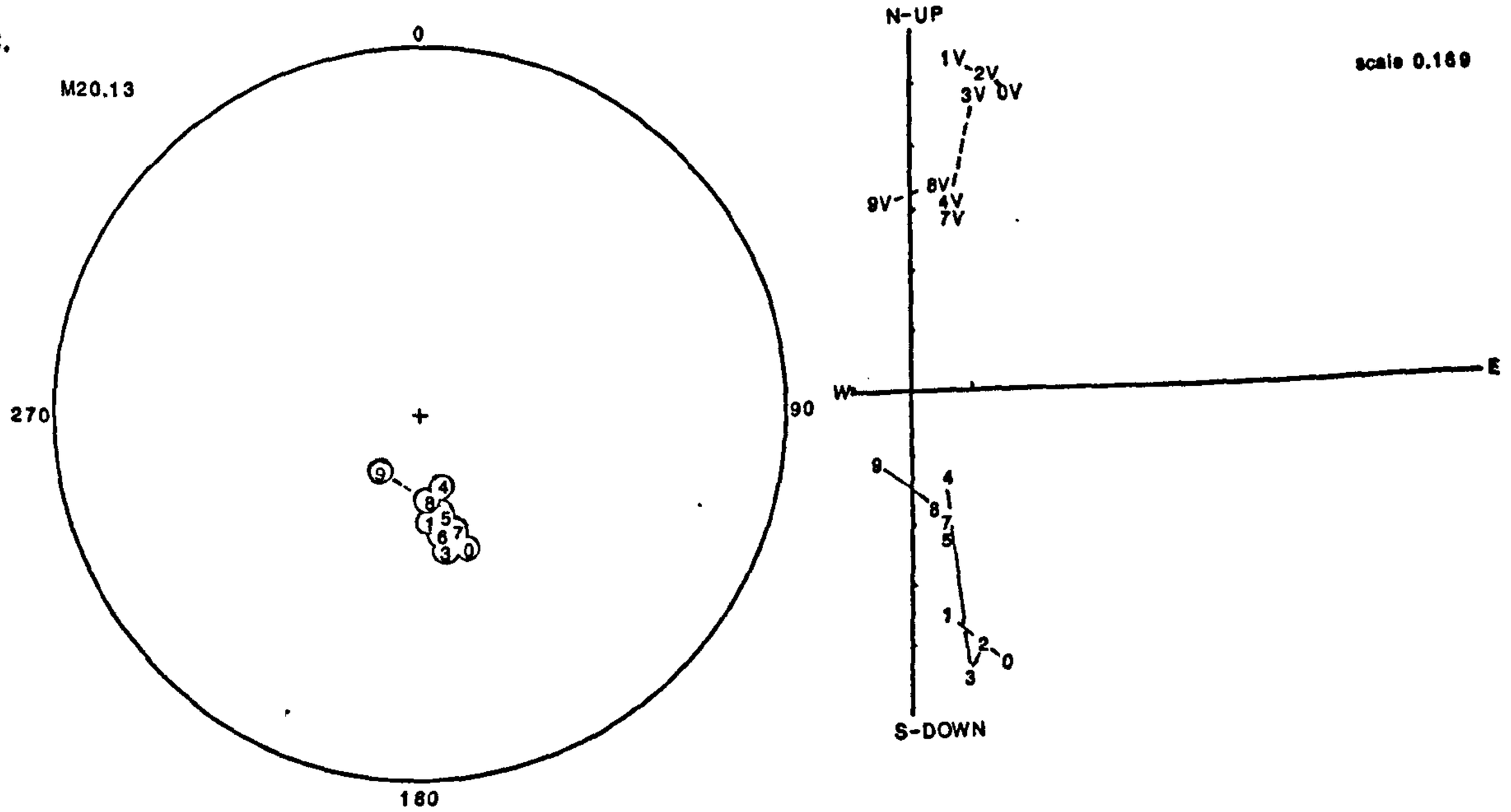
M20.13
0
90
180
270
N-UP
E
W
S-DOWN
scale 0.169

d

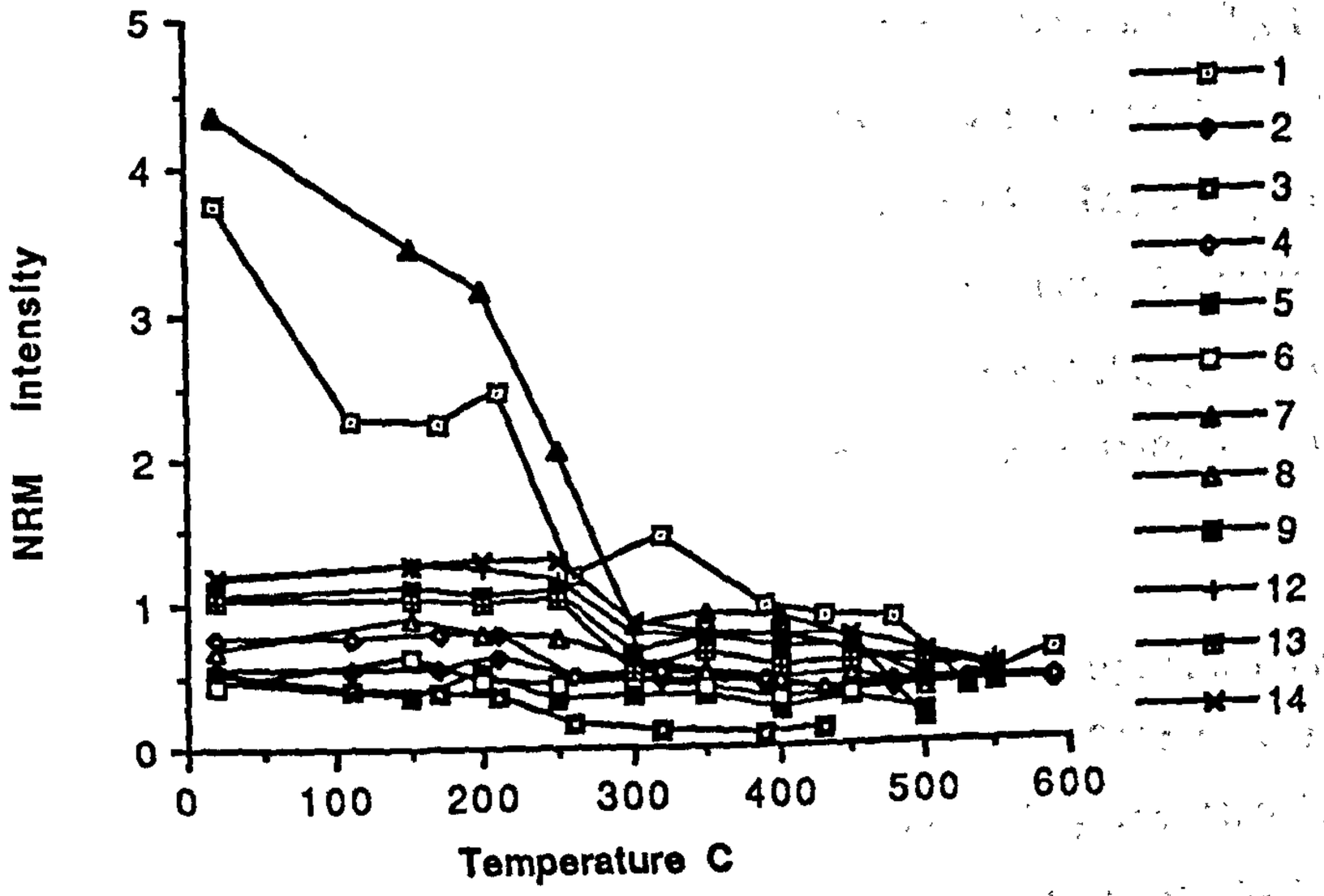
NRM Intensity
5
4
3
2
1
0
0
100
200
300
400
500
600
Temperature C
1
2
3
4
5
6
7
8
9
12
13
14

e

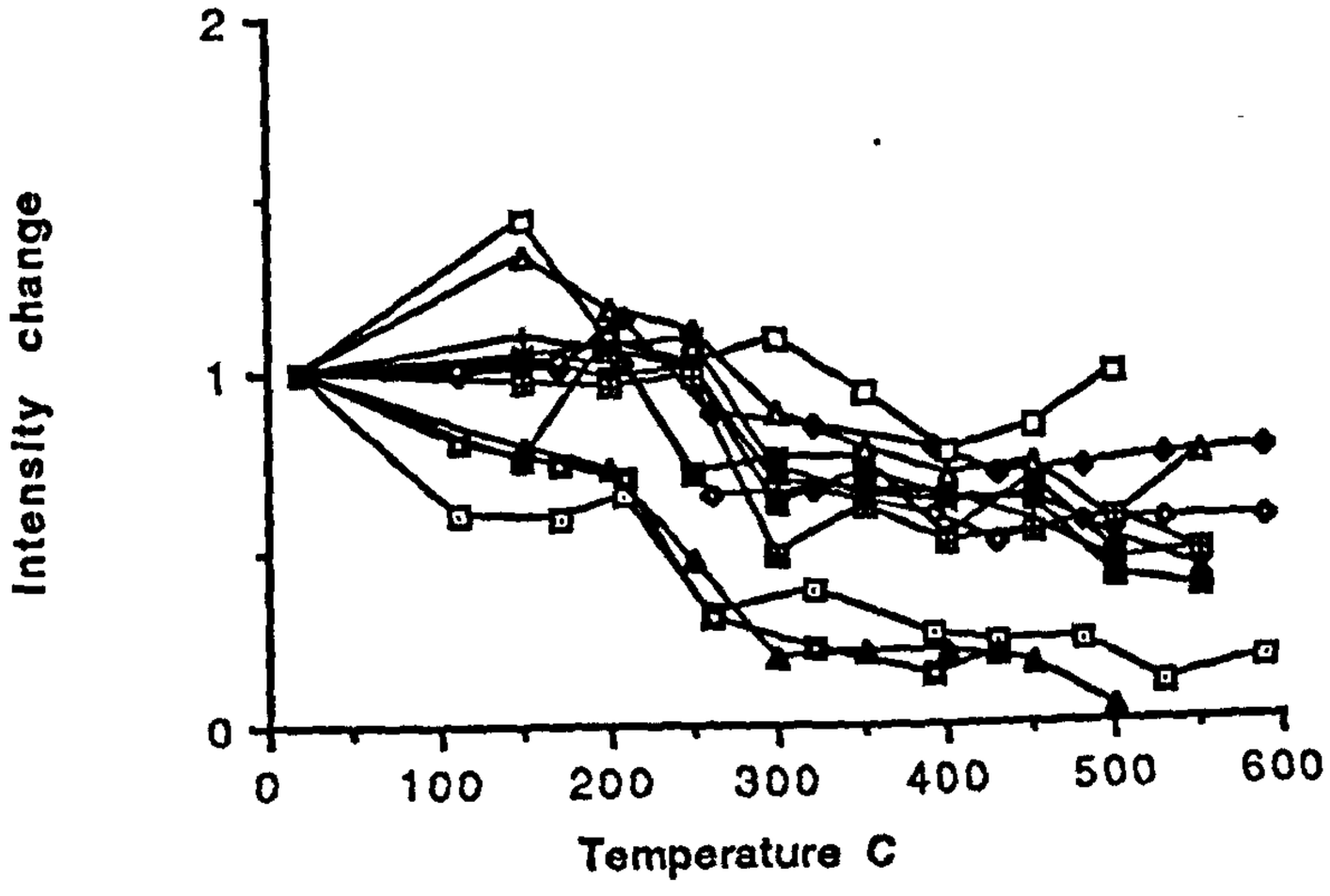
Intensity change
2
1
0
0
100
200
300
400
500
600
Temperature C

f

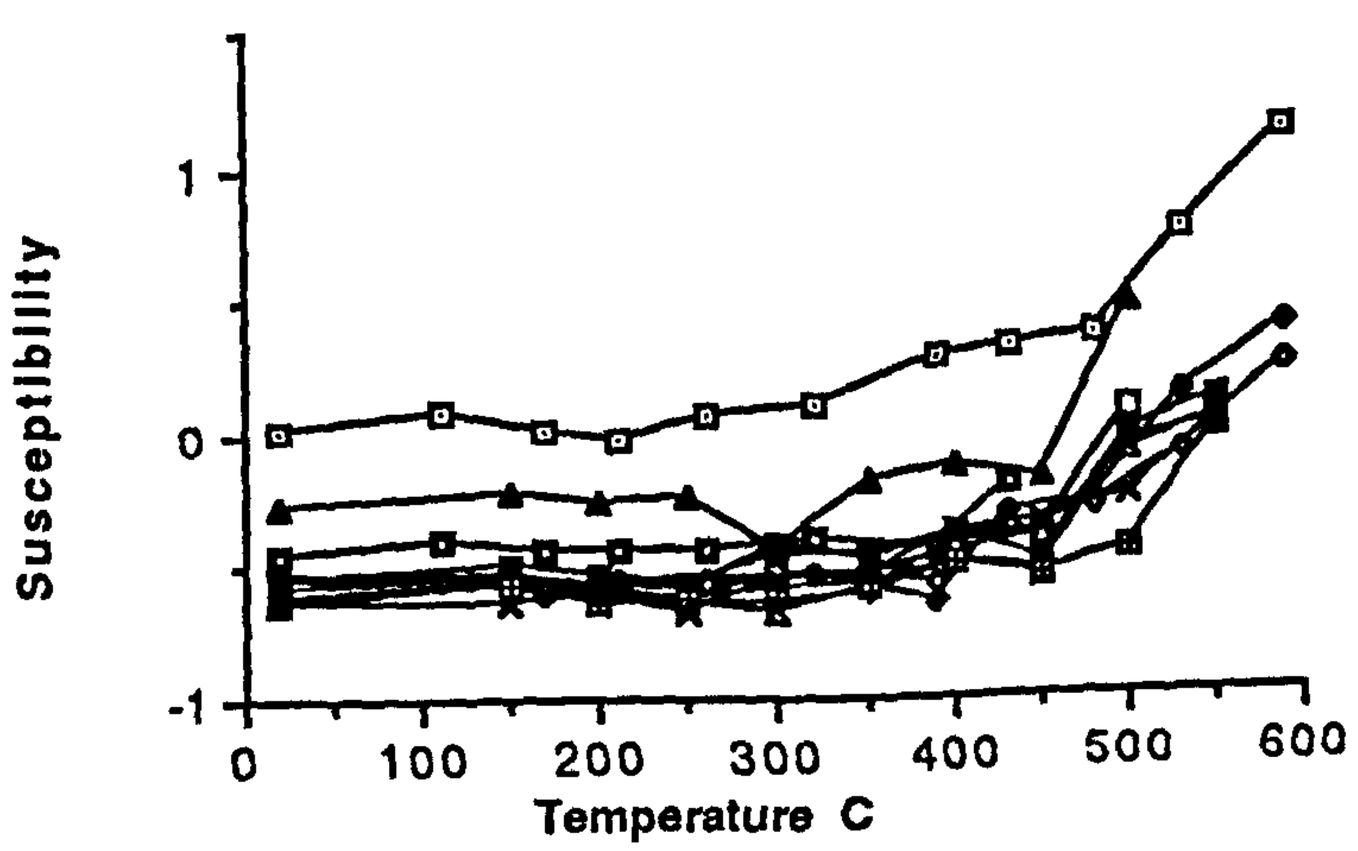
Susceptibility
1
0
-1
0
100
200
300
400
500
600
Temperature C

this group. Group ii. (remaining samples) have directions of lower natural remanent magnetism intensity and susceptibility and reversed polarity. Two components are distinguished on the orthogonal plots. The component with the lowest T_b (190°C) is shallow inclination, reversed with a declination of 135°; the component with higher T_b is also reversed, higher inclination, with a declination of 175°. This component is not totally demagnetised. The low T_b component is Tertiary. The higher T_b component lies on the apparent field direction wander path at 45 Ma. The small decrease in intensity, and incomplete demagnetisation with increasing temperature, suggests that group ii. vectors are carried by haematite.

Site M21 (fig. 5.16) The maximum initial natural remanent magnetism intensity of 0.82 x $10^{-4}Am^{-1}$ and susceptibility of -0.60 (volume units x $10^{-6}GOe^{-1}$; see appendix 4.2) indicate that the magnetic mineral content is very low. Only two samples (3 and 4)have meta-stable vector directions; the remainder of samples contain negligible amounts of magnetic minerals. The meta-stable vector directions are normal polarity and high inclination and have demagnetisation paths which are reasonably straight. The directions lie close to the Tertiary part of the apparent field direction wander path. However, definition is poor as the direction is only defined by two vectors. Inflection points in the graphs of natural remanent magnetism intensity and susceptibility at around 150°C and 390°C indicate that a viscous remanent magnetism is carried by goethite and another natural remanent magnetism is carried by another ambiguous magnetic phase.

Site M22 (fig. 5.17) Maximum initial natural remanent magnetism intensity of 0.92 x $10^{-4}Am^{-1}$ and susceptibility of -0.55 (volume units x $10^{-6}GOe^{-1}$; see appendix 4.2) indicate that the magnetic mineral content is very low. Site directions are meta-stable, poorly defined and noisy. They have normal polarity, high inclination and approximate to the present-day/Tertiary part of the apparent field direction wander path. Vectors move about with progressive demagnetisation and are only defined to 190°C. This suggests that goethite carries a viscous remanent magnetism. Above this temperature the data becomes noisy and susceptibility shows a marked increase.

Site M23 (fig. 5.18) Maximum initial natural remanent magnetism intensity of 8.01 x $10^{-4}Am^{-1}$ and susceptibility of 0.81 (volume units x $10^{-6}GOe^{-1}$; see appendix 4.2) indicate a reasonable magnetic mineral content. All natural remanent magnetism intensity is lost by 100°C, indicating that the main natural remanent magnetism carrier

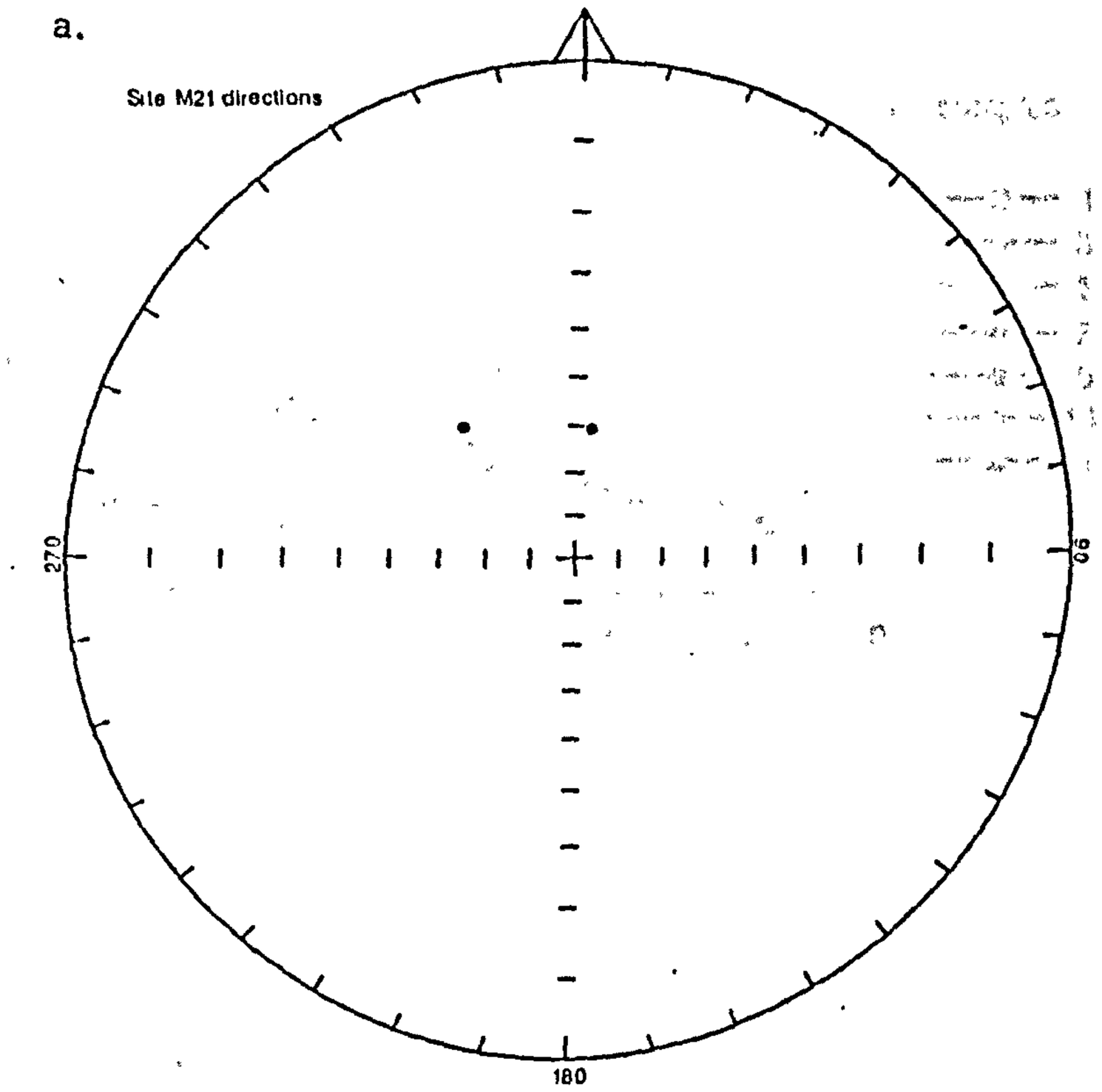

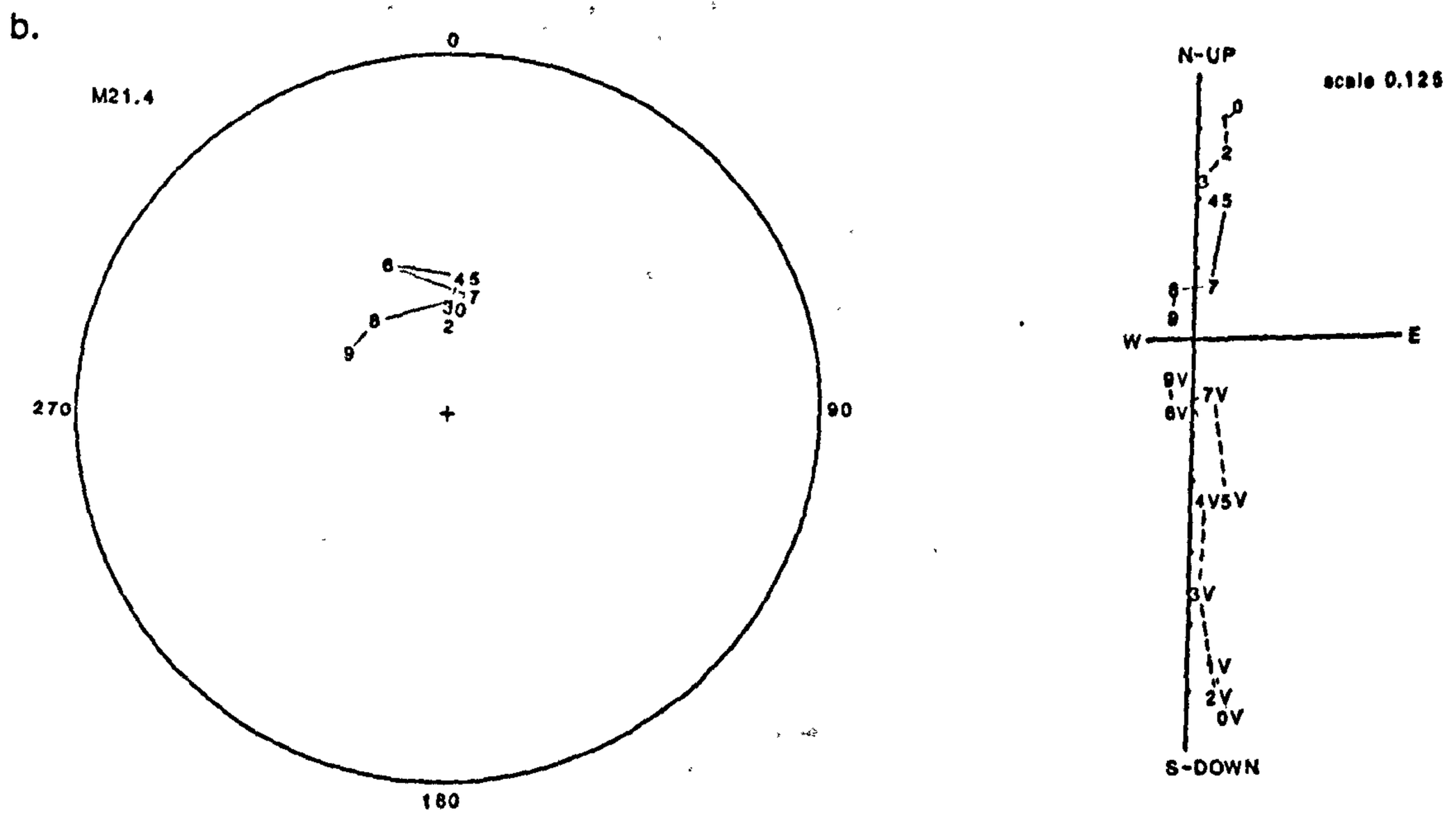

fig. 5.16 Summary of demagnetisation behaviour of samples from site M21. Natural remanent magnetism (NRM) intensity is given x $10^{-4}Am^{-1}$; susceptibility units x 10^{-6} GOe^{-1}
a. stereographic projection of stable sample directions; **b.** stereographic projection and accompanying orthogonal plot illustrating vector movement with progressive demagnetisation; **c.** NRM intensity change with increasing temperature illustrating variation of magnetic mineral content between samples; **d.** normalised NRM change with increasing temperature illustrating within-site variation; **e.** susceptibility variation with increasing temperature illustrating changes which occur due to mineralogical alteration.

c

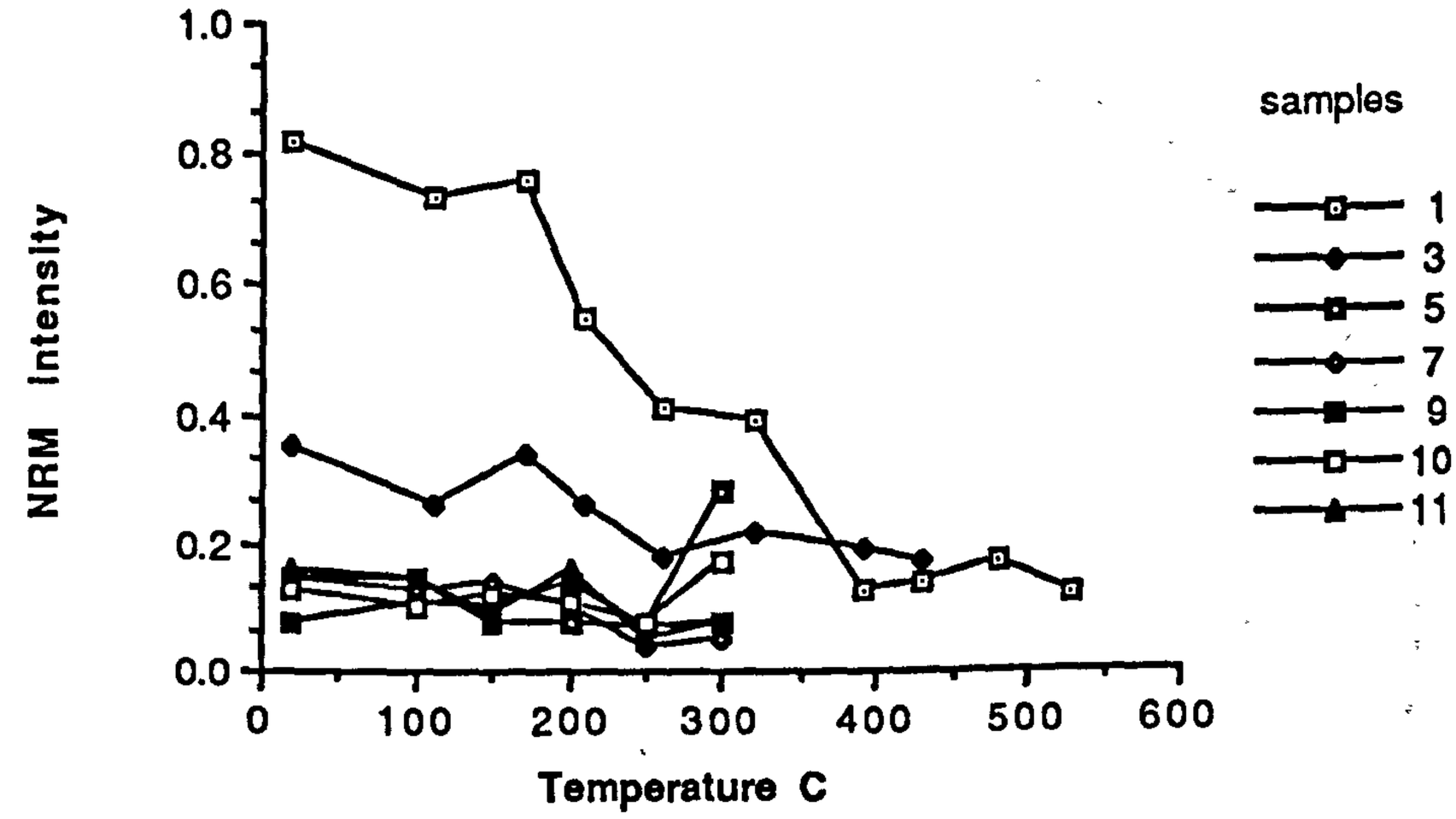
NRM intensity
1.0
0.8
0.6
0.4
0.2
0.0
0
100
200
300
400
500
600
Temperature C
samples
1
3
5
7
9
10
11

d

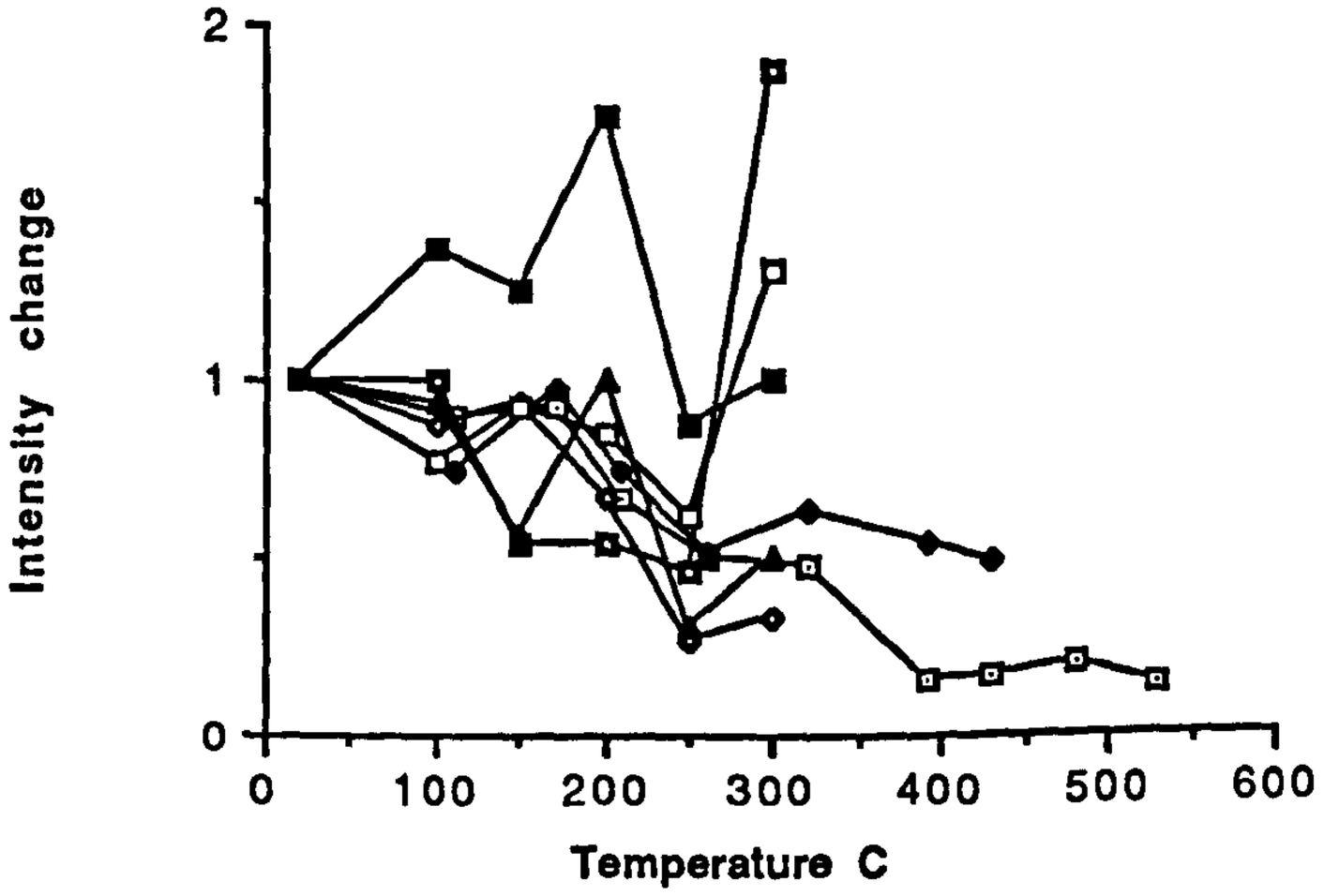
Intensity change
2
1
0
0
100
200
300
400
500
600
Temperature C

e

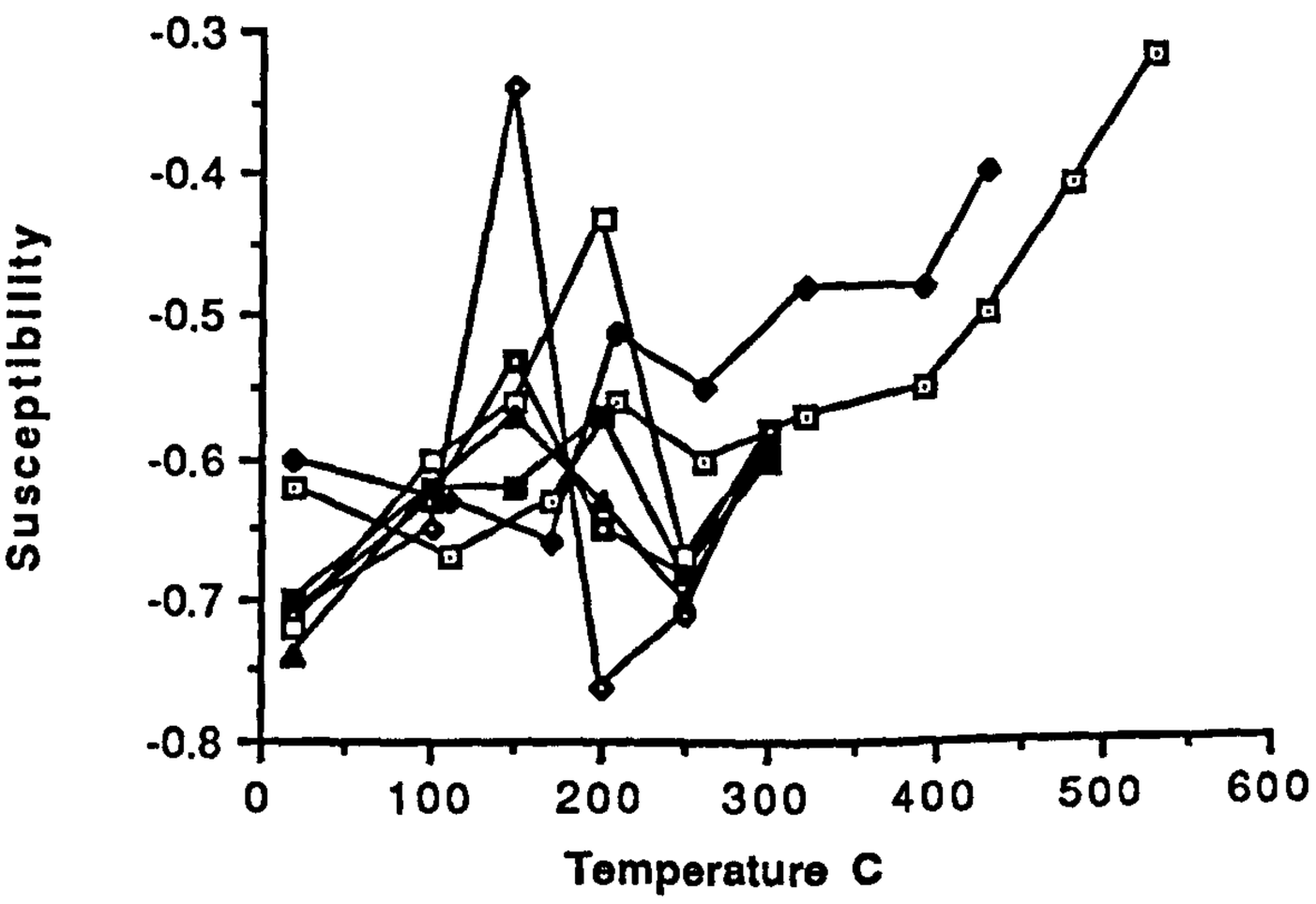
Susceptibility
-0.3
-0.4
-0.5
-0.6
-0.7
-0.8
0
100
200
300
400
500
600
Temperature C

a.

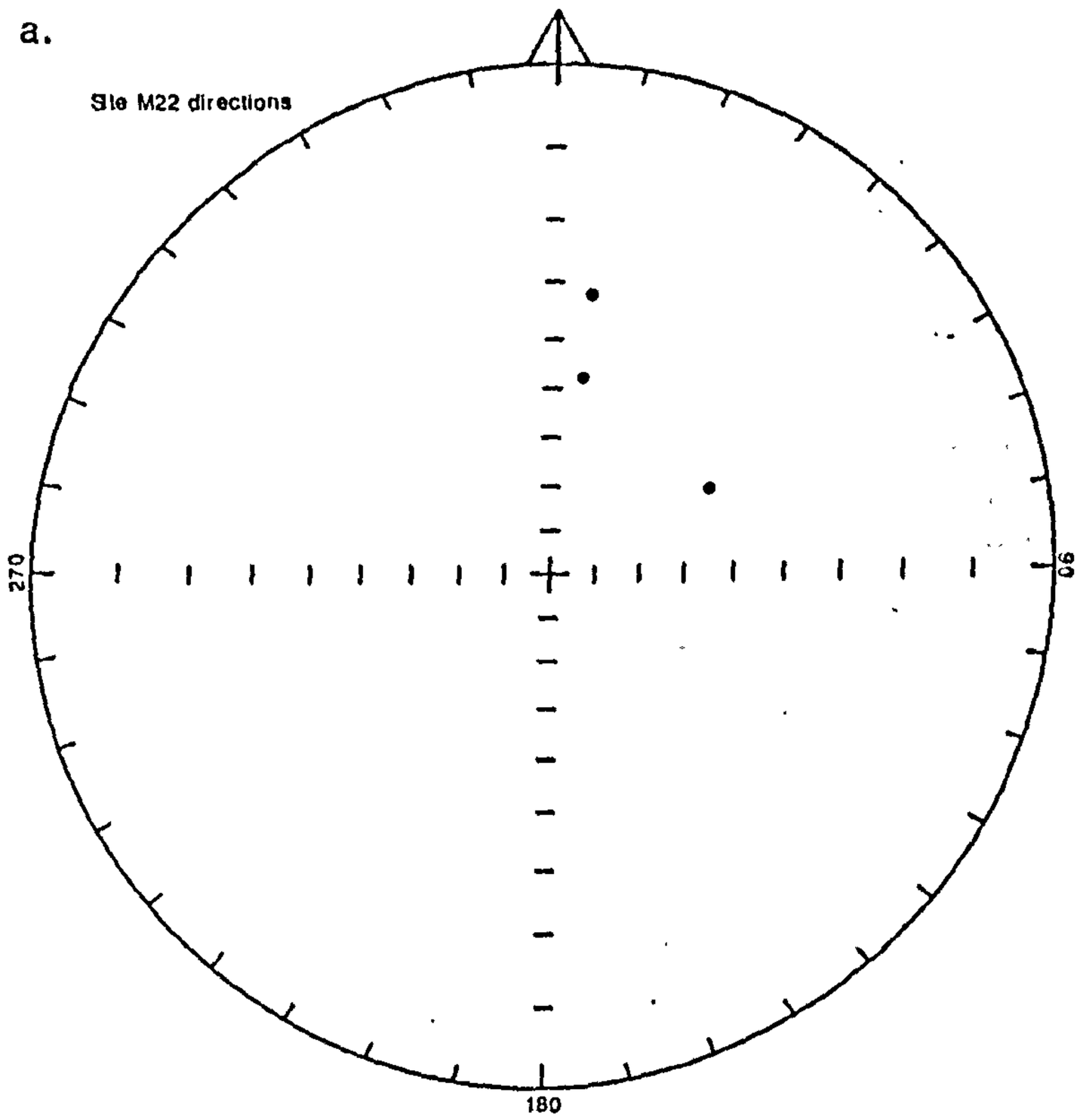

b.

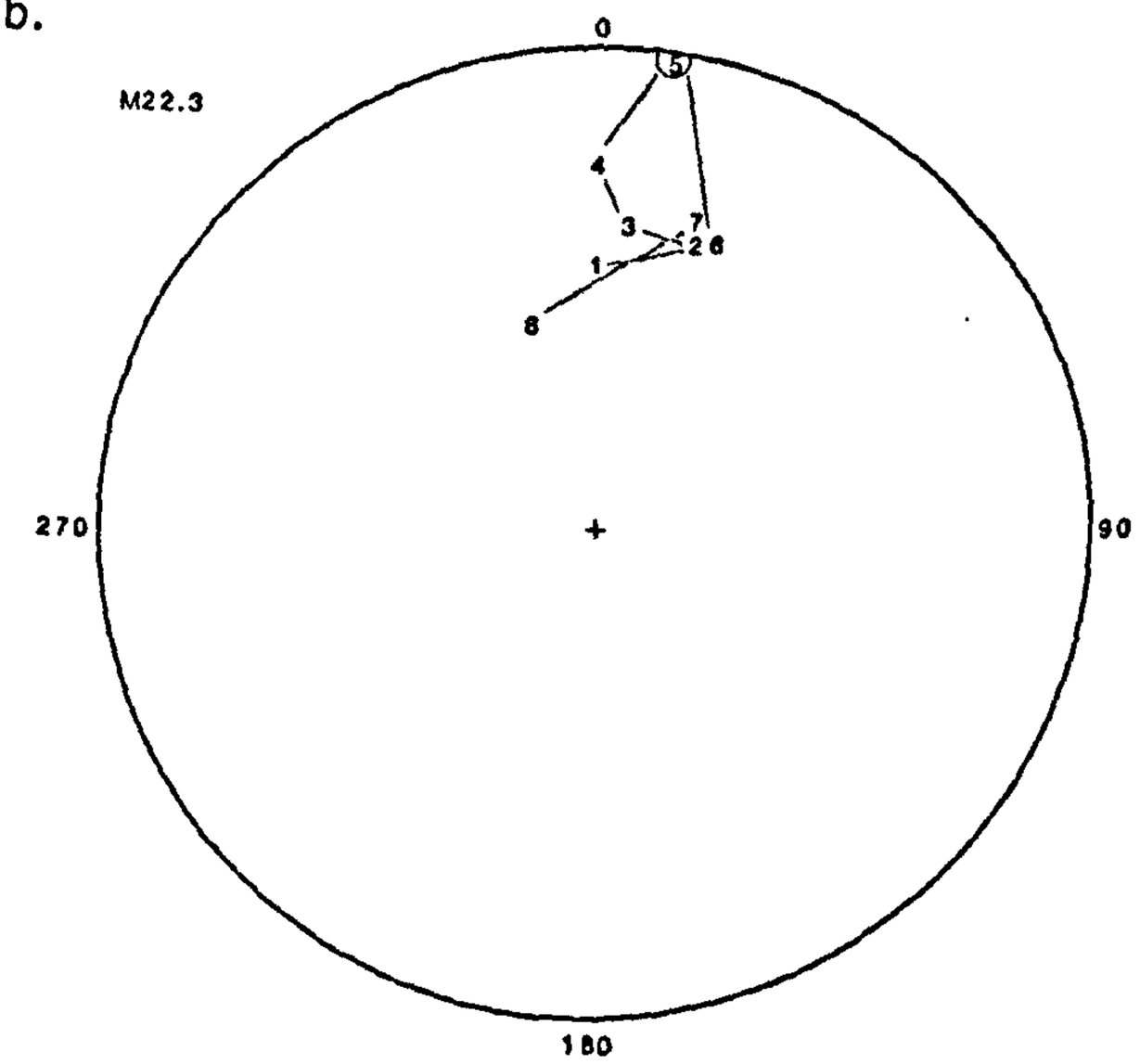

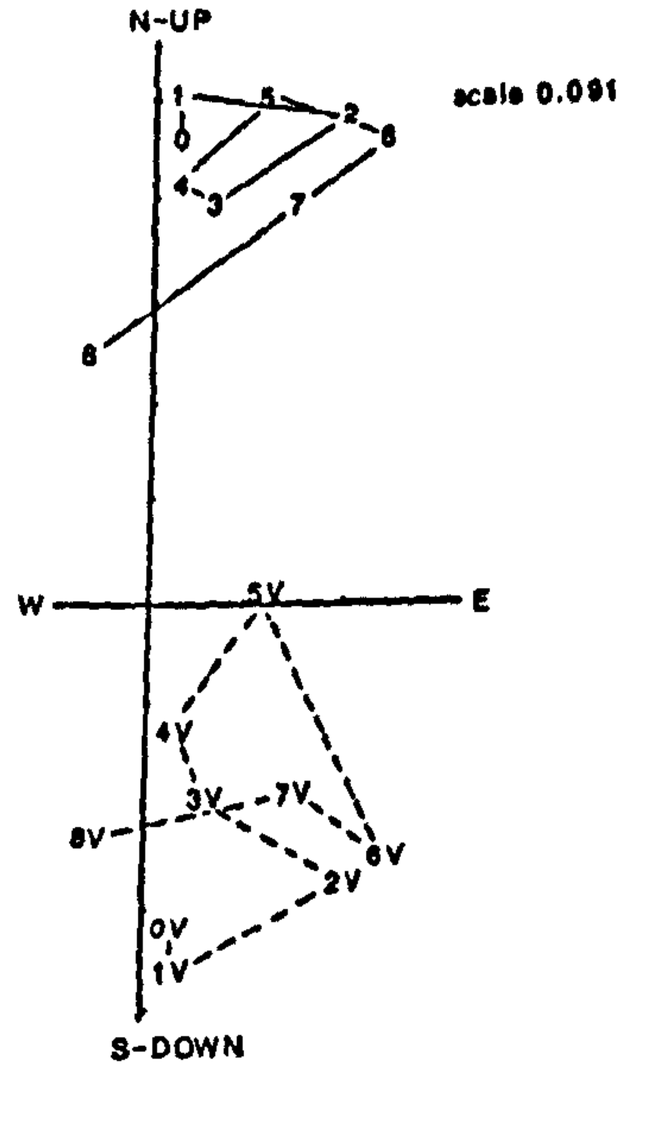

fig. 5.17 Summary of demagnetisation behaviour of samples from site M22. Natural remanent magnetism (NRM) intensity is given x $10^{-4}Am^{-1}$; susceptibility units x 10^{-6} GOe^{-1}.
a. stereographic projection of stable sample directions; **b.** stereographic projection and accompanying orthogonal plot illustrating vector movement with progressive demagnetisation; **c.** NRM intensity change with increasing temperature illustrating variation of magnetic mineral content between samples; **d.** normalised NRM change with increasing temperature illustrating within-site variation; **e.** susceptibility variation with increasing temperature illustrating changes which occur due to mineralogical alteration.

c

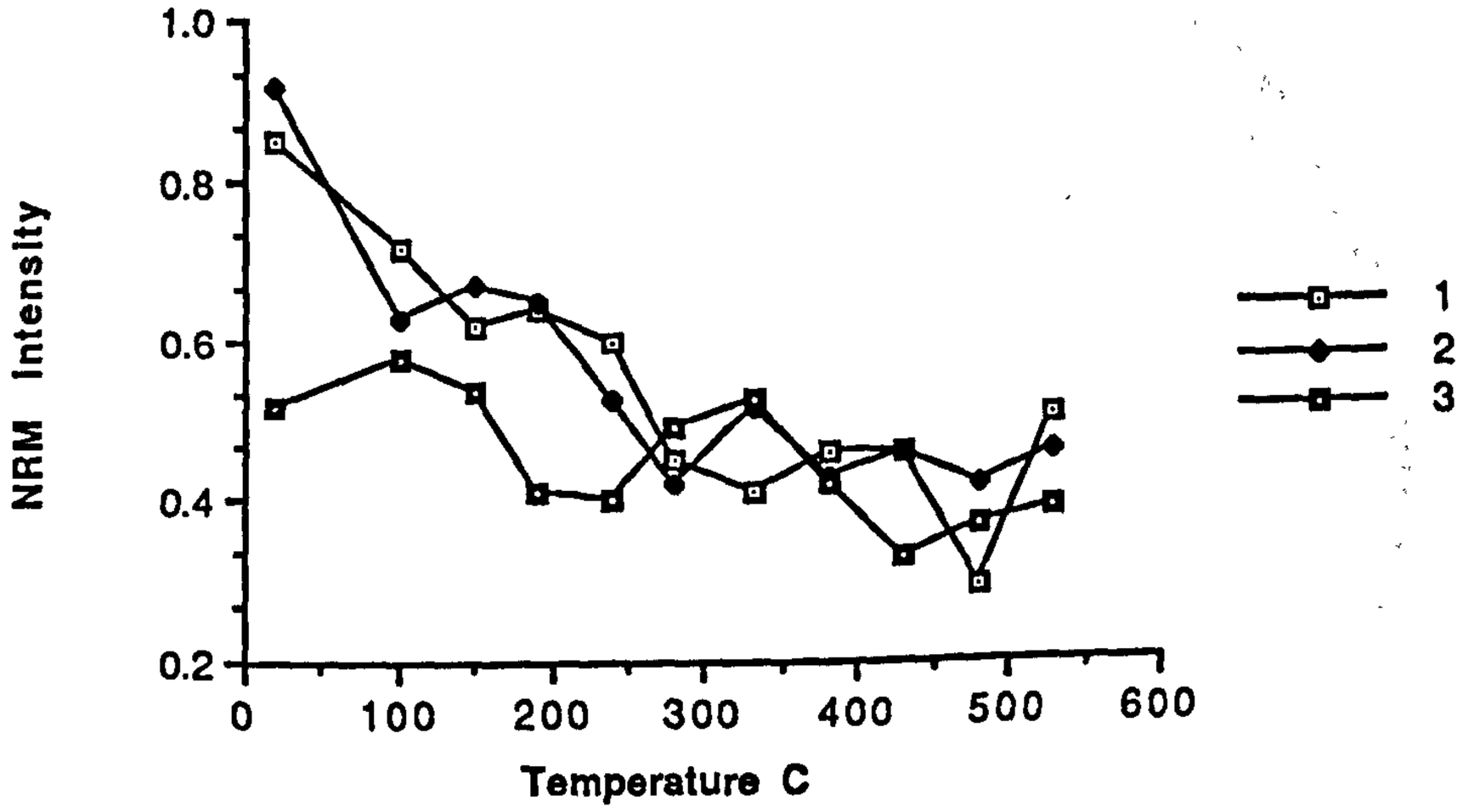
NRM Intensity
1.0
0.8
0.6
0.4
0.2
0
100
200
300
400
500
600
Temperature C
1
2
3

d

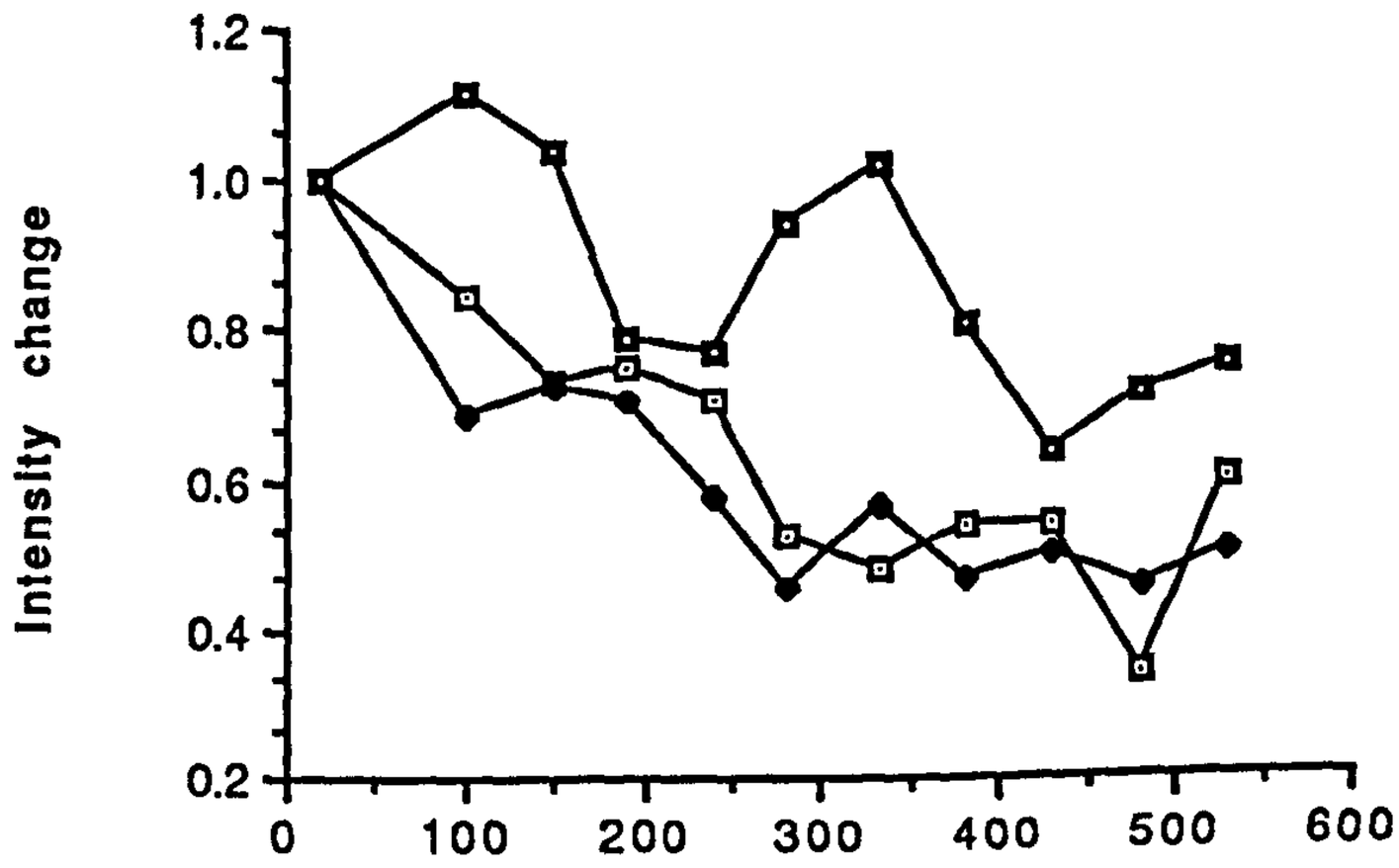
Intensity change
1.2
1.0
0.8
0.6
0.4
0.2
0
100
200
300
400
500
600
Temperature C

e

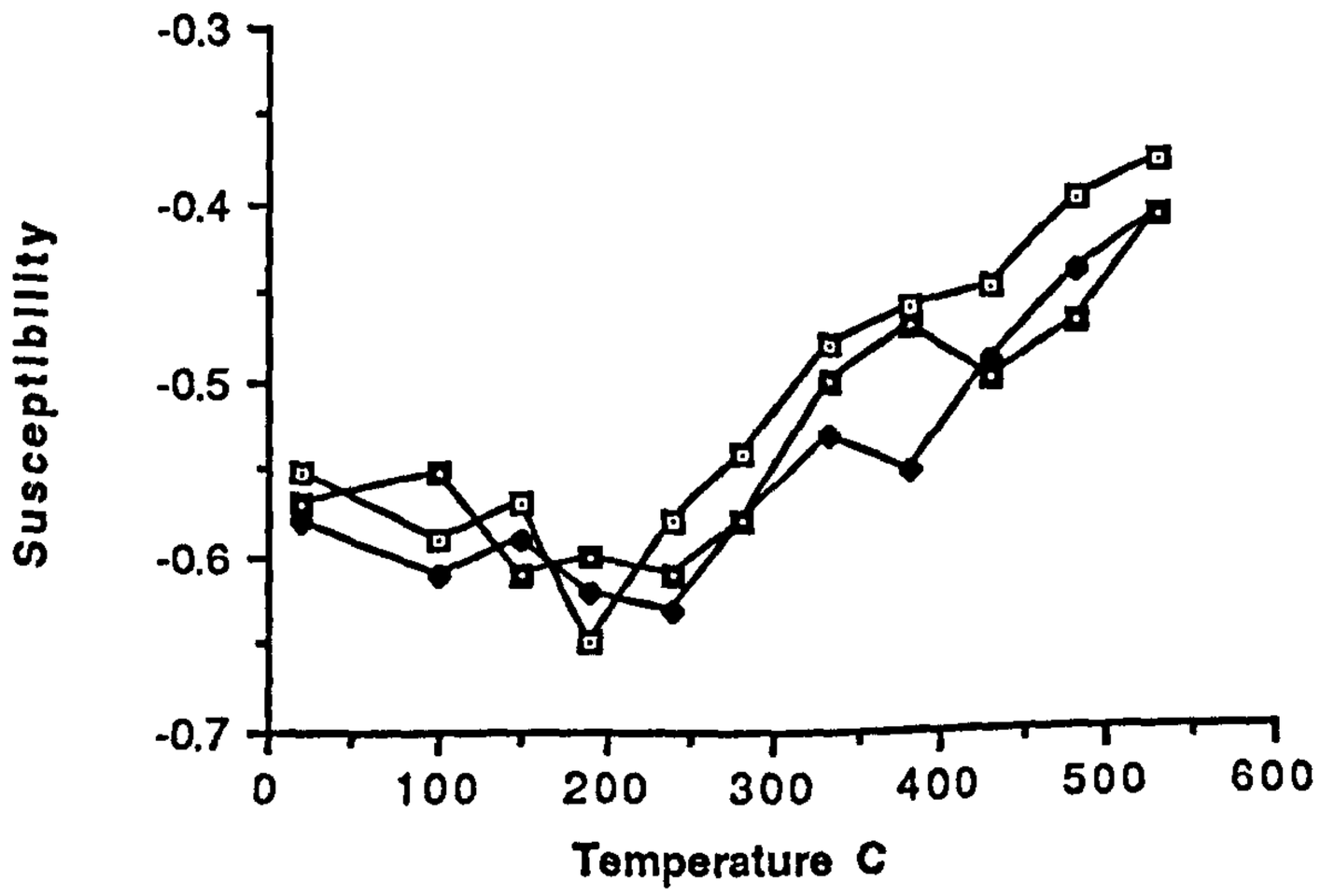
Susceptibility
-0.3
-0.4
-0.5
-0.6
-0.7
0
100
200
300
400
500
600
Temperature C

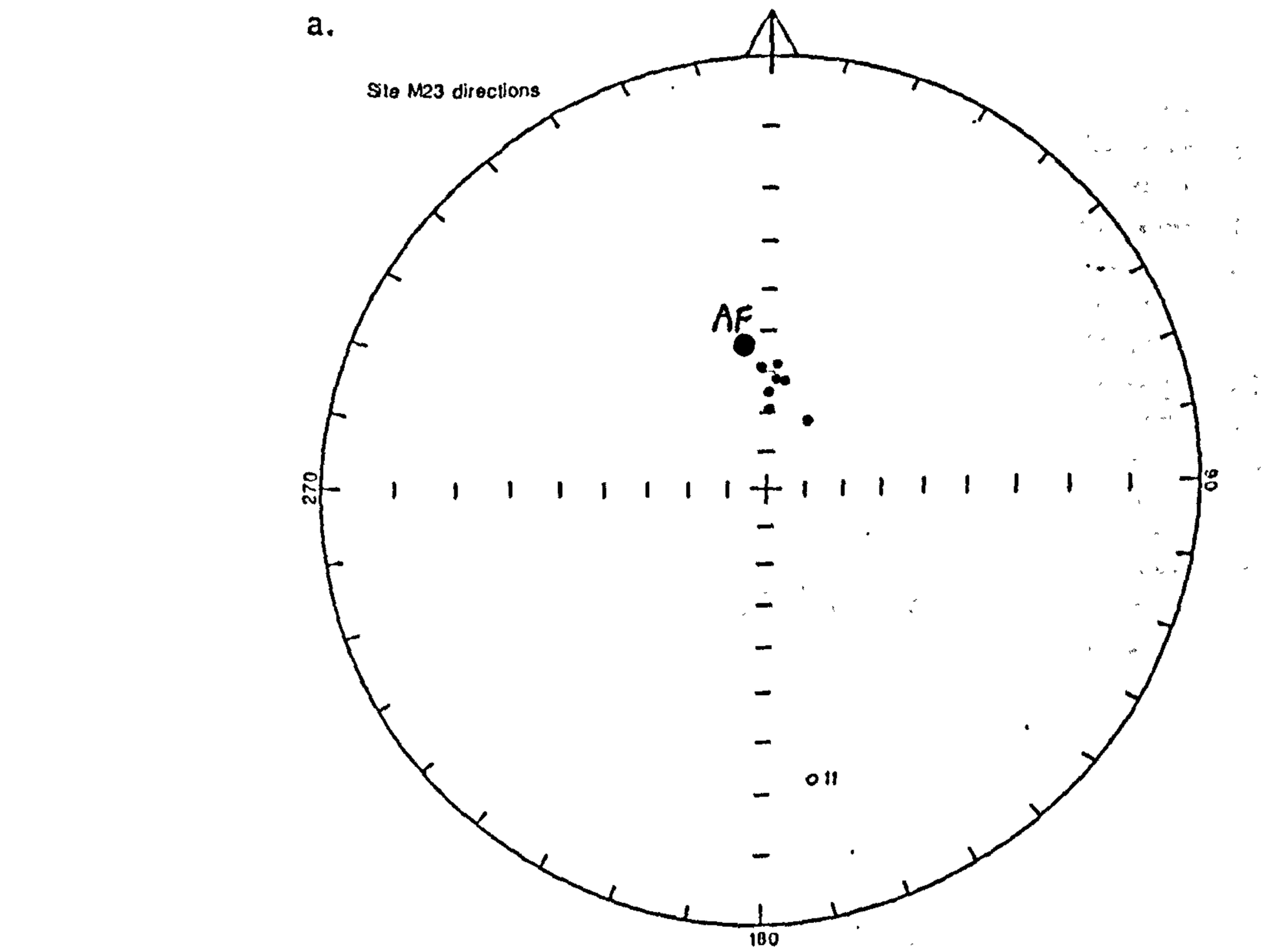

fig. 5.18 Summary of demagnetisation behaviour of samples from site M23. Natural remanent magnetism (NRM) intensity is given x $10^{-4}Am^{-1}$; susceptibility units x 10^{-6} GOe^{-1}
a. stereographic projection of stable sample directions; **b.** stereographic projection and accompanying orthogonal plot illustrating vector movement with progressive demagnetisation; **c.** NRM intensity change with increasing temperature illustrating variation of magnetic mineral content between samples; **d.** normalised NRM change with increasing temperature illustrating within-site variation; **e.** susceptibility variation with increasing temperature illustrating changes which occur due to mineralogical alteration.

c

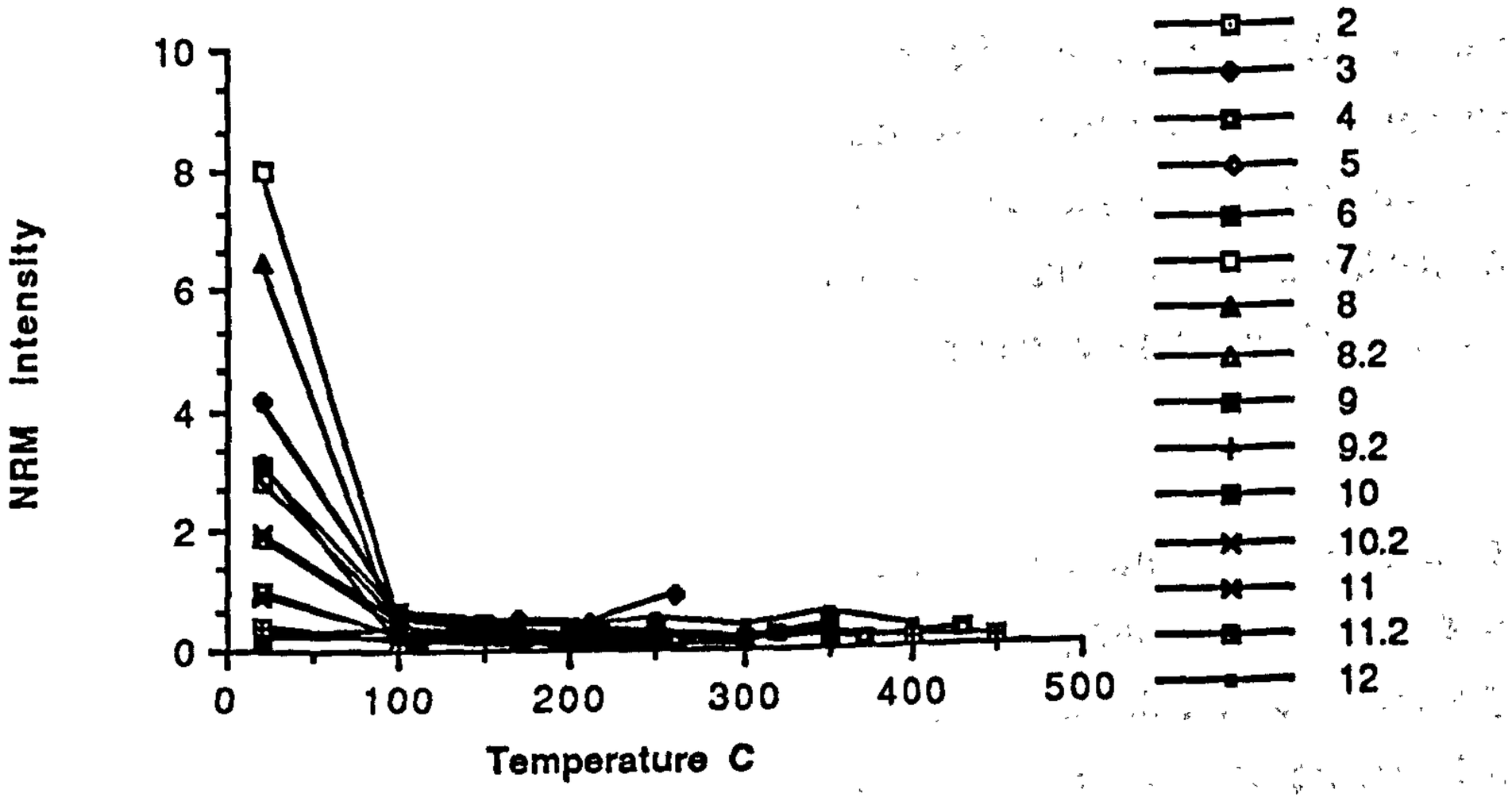
NRM Intensity
10
8
6
4
2
0
0
100
200
300
400
500
Temperature C
2
3
4
5
6
7
8
8.2
9
9.2
10
10.2
11
11.2
12

d

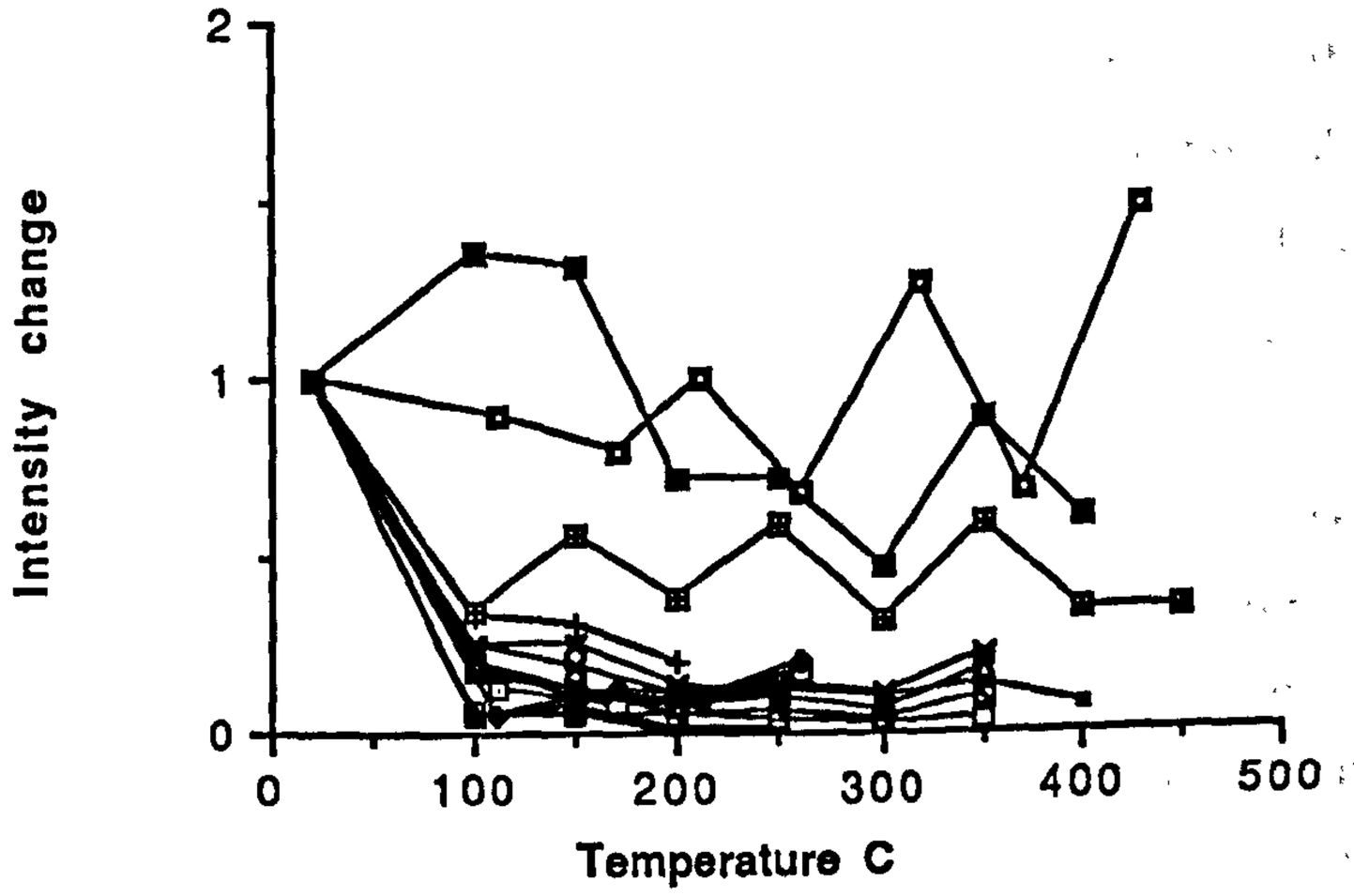
Intensity change
2
1
0
0
100
200
300
400
500
Temperature C

e

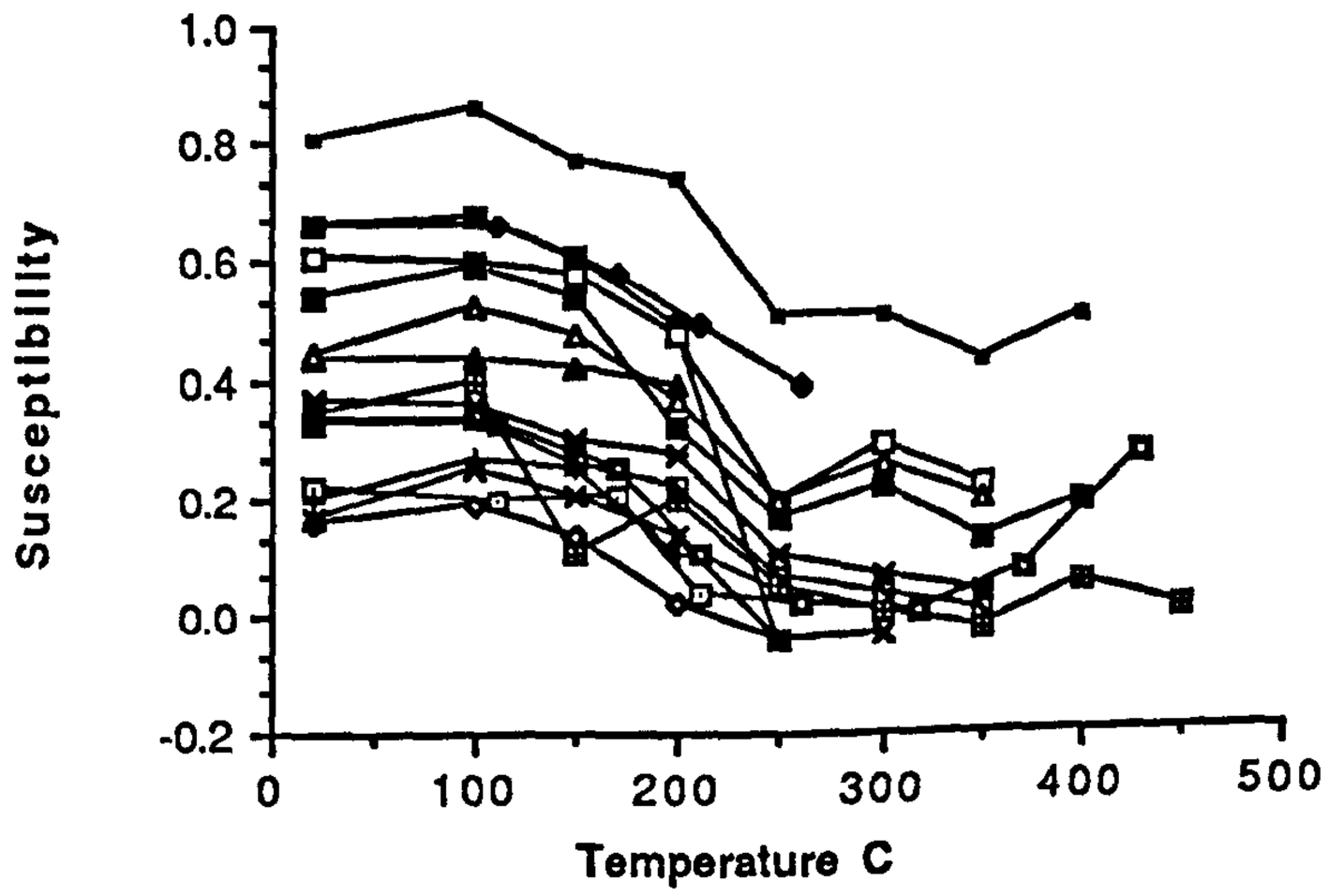
Susceptibility
1.0
0.8
0.6
0.4
0.2
0.0
-0.2
0
100
200
300
400
500
Temperature C

is goethite. All samples from this site have the same initial direction. The main vector direction is removed from 20°C to 100°C. The mean direction has normal polarity and lies on the apparent field direction wander path close to the present day field direction. The same direction is yielded from AF demagnetisation. Only one sample (sample 11) has a vector that is meta-stable above 100°C. This is rather poorly defined, reversed polarity and lies on the apparent field direction wander path at 210 Ma. There is little within site variation except for the initial values of intensity and susceptibility. Goethite carries a viscous natural remanent magnetism with present day direction. A second, poorly defined vector is also carried by goethite in one sample; this is reversed polrity and around 210 Ma old.

Site M24 (fig. 5.19) Maximum initial natural remanent magnetism intensity of 3.39 x $10^{-4}Am^{-1}$ and susceptibility of 0.56 x $10^{-6}GOe^{-1}$ (see appendix 4.2) indicate a reasonable magnetic mineral content. Similarities between samples of susceptibility and normalised natural remanent magnetism intensity changes with progressive demagnetisation indicate similar magnetic mineral content. Variation in natural remanent magnetism intensity reflects the different quantities of magnetic minerals present in different samples.Demagnetisation is complete by around 500°C Progressive demagnetisation indicates a vector with low T_b (150°C)and high inclination (dec 010) moving to a direction with lower inclination at higher temperatures. However, the vector directions at the higher temperatures are not defined by many steps, making interpretation of this vector difficult. Site directions are stable and loosely grouped. The mean direction is poorly defined (*A95*=21.8°) as a consequence of the low natural remanent magnetism intensity and incomplete resolution of more than one component. The mean direction is normal polarity and lies near the apparent field direction wander path between the 60 Ma and the present day direction. Within site scatter is probably due to low intensity and incomplete resolution of more than one component. The remanence carrier is ambiguous.

Summary (table 5.6 and fig. 5.20)

i. all nine sites have meta-stable or stable directions, although sites M21 and M22 did not have a high enough number of stable vectors from which to calculate a mean;

ii. several sites have more than one natural remanent magnetism component;

iii. 8 normal and 2 reversed polarity directions are identified; all directions are

a.

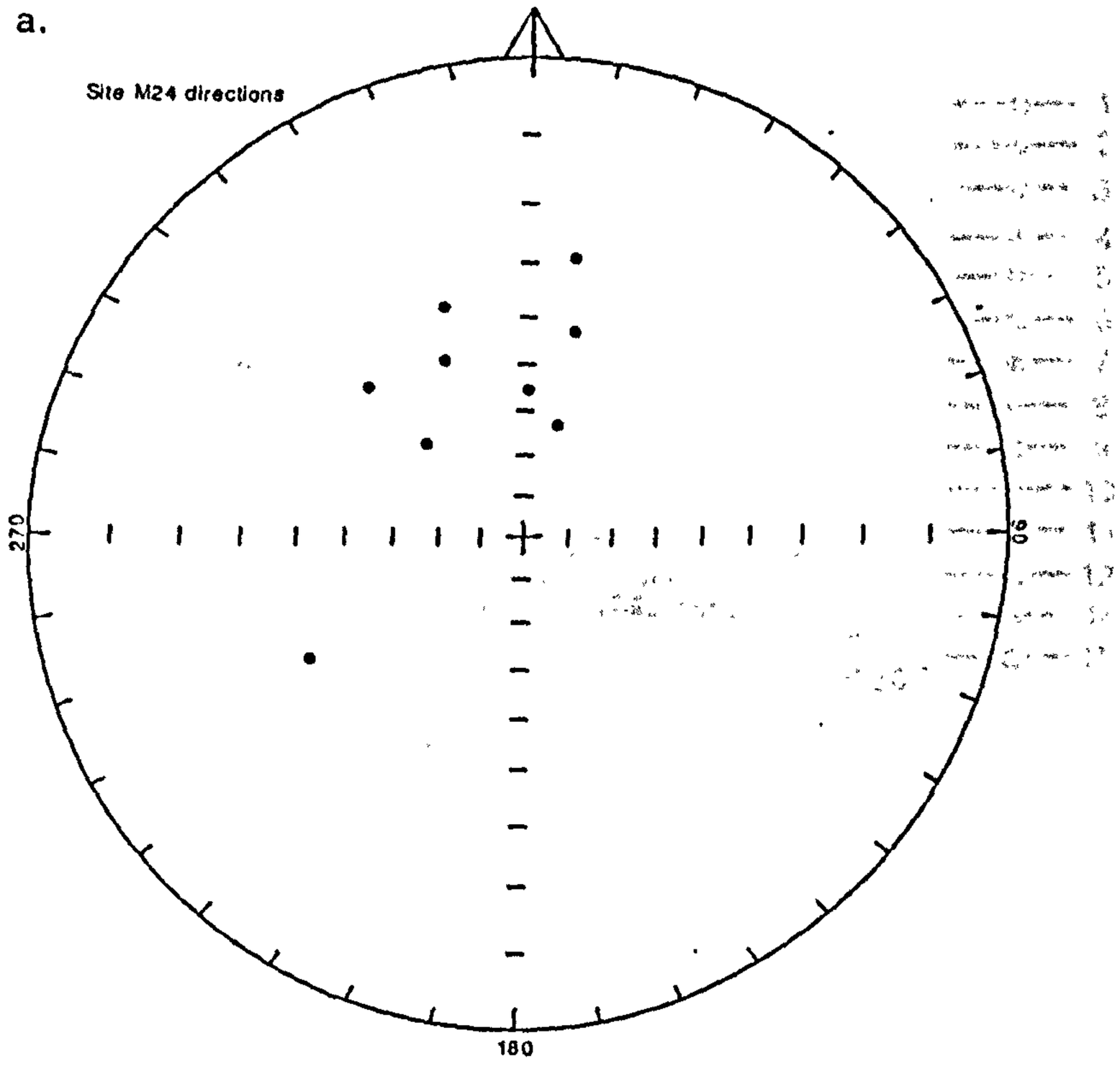

b.

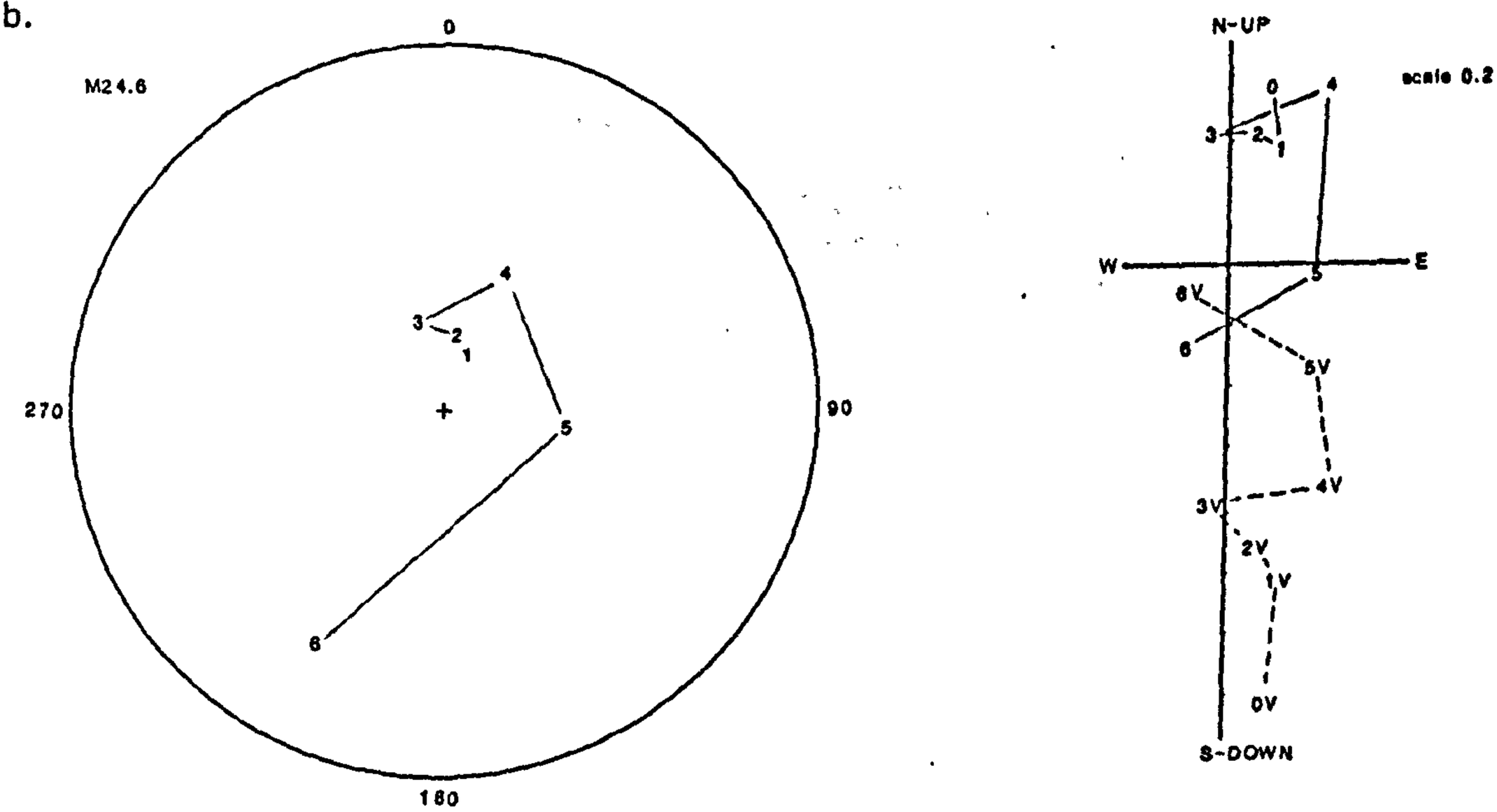

fig. 5.19 Summary of demagnetisation behaviour of samples from site M24. Natural remanent magnetism (NRM) intensity is given x $10^{-4}Am^{-1}$; susceptibility units x 10^{-6} GOe^{-1}
a. stereographic projection of stable sample directions; **b.** stereographic projection and accompanying orthogonal plot illustrating vector movement with progressive demagnetisation; **c.** NRM intensity change with increasing temperature illustrating variation of magnetic mineral content between samples; **d.** normalised NRM change with increasing temperature illustrating within-site variation; **e.** susceptibility variation with increasing temperature illustrating changes which occur due to mineralogical alteration.

c

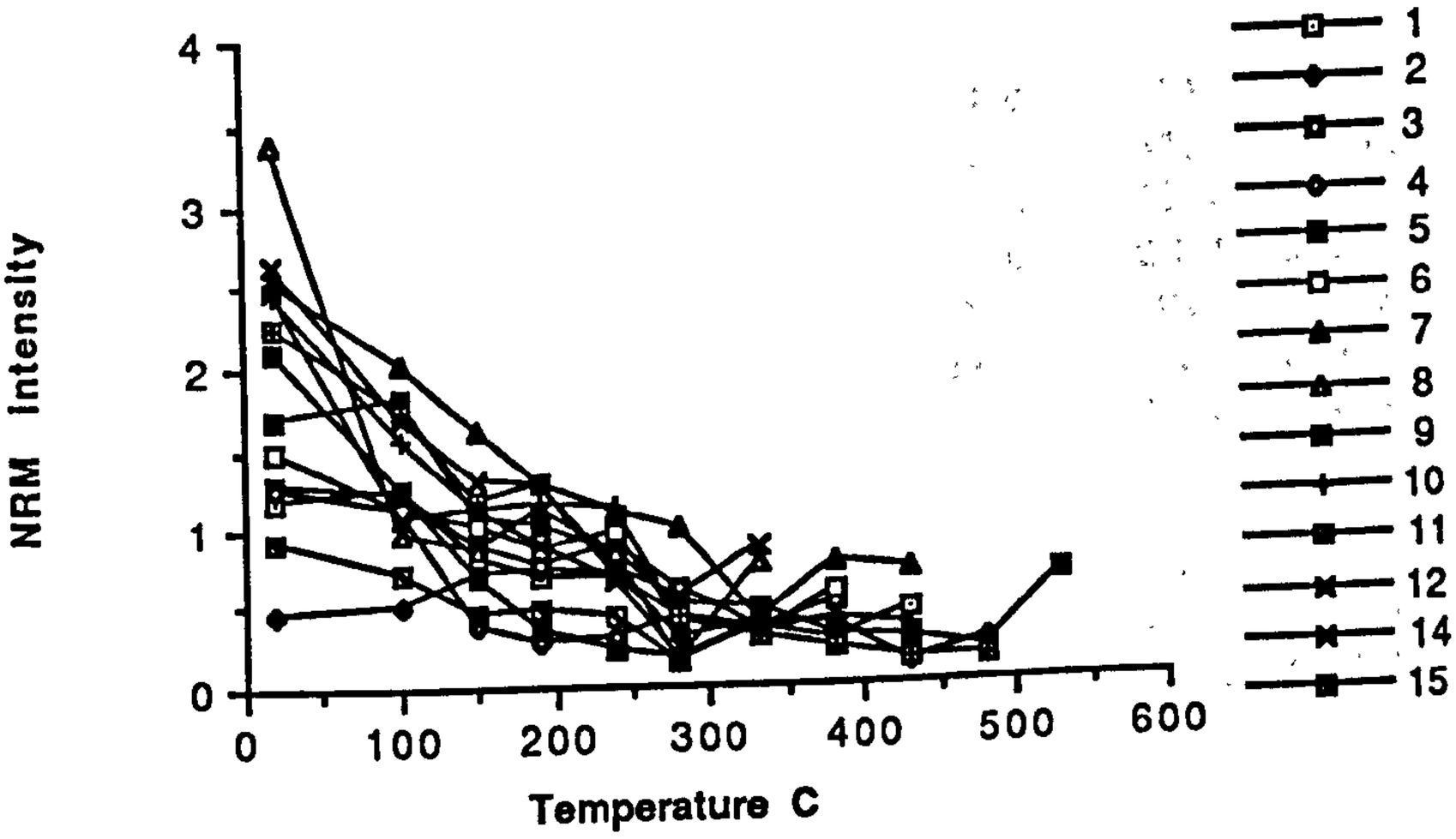
NRM Intensity
4
3
2
1
0
0
100
200
300
400
500
600
Temperature C
1
2
3
4
5
6
7
8
9
10
11
12
14
15

d

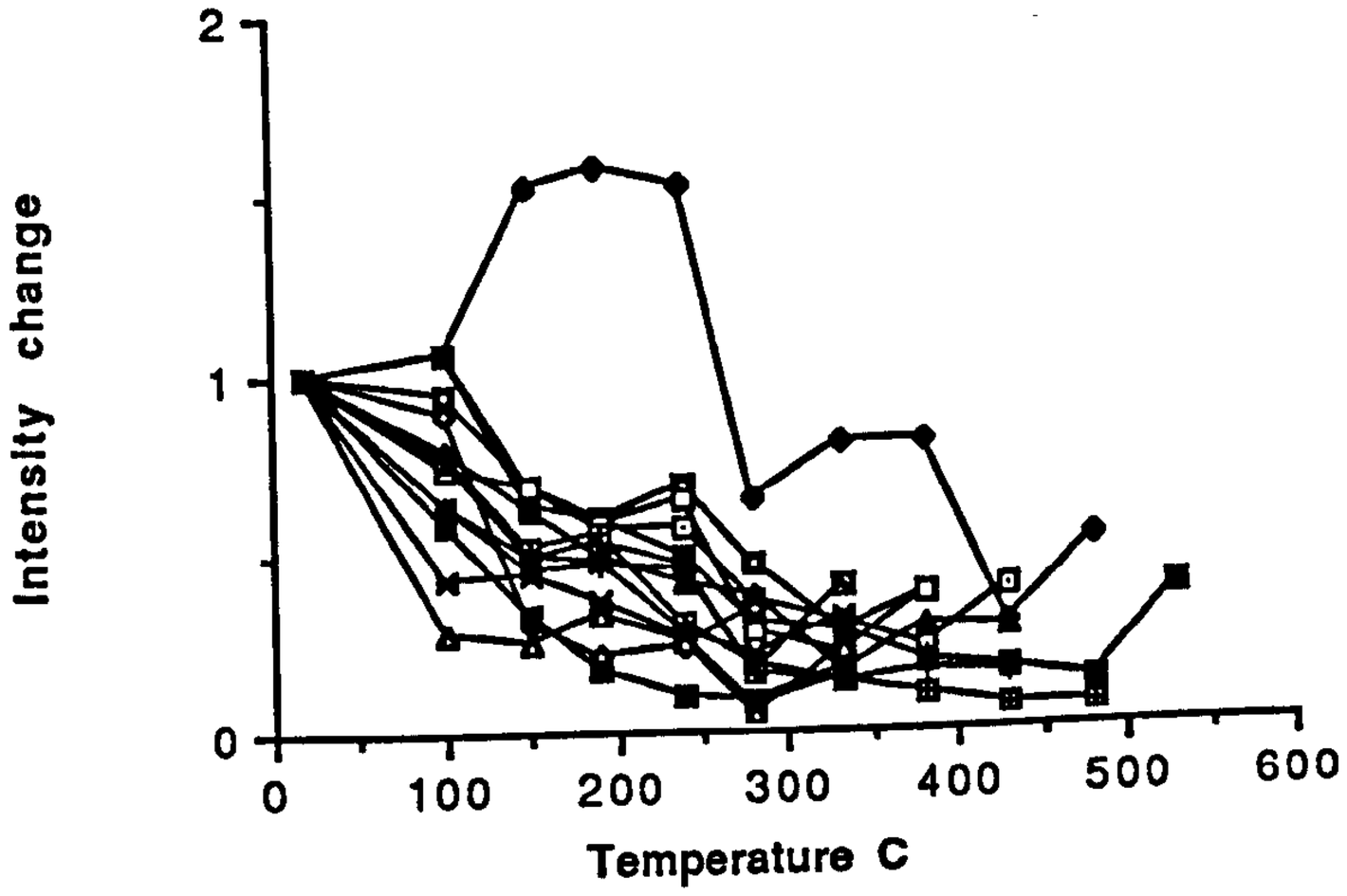
Intensity change
2
1
0
0
100
200
300
400
500
600
Temperature C

e

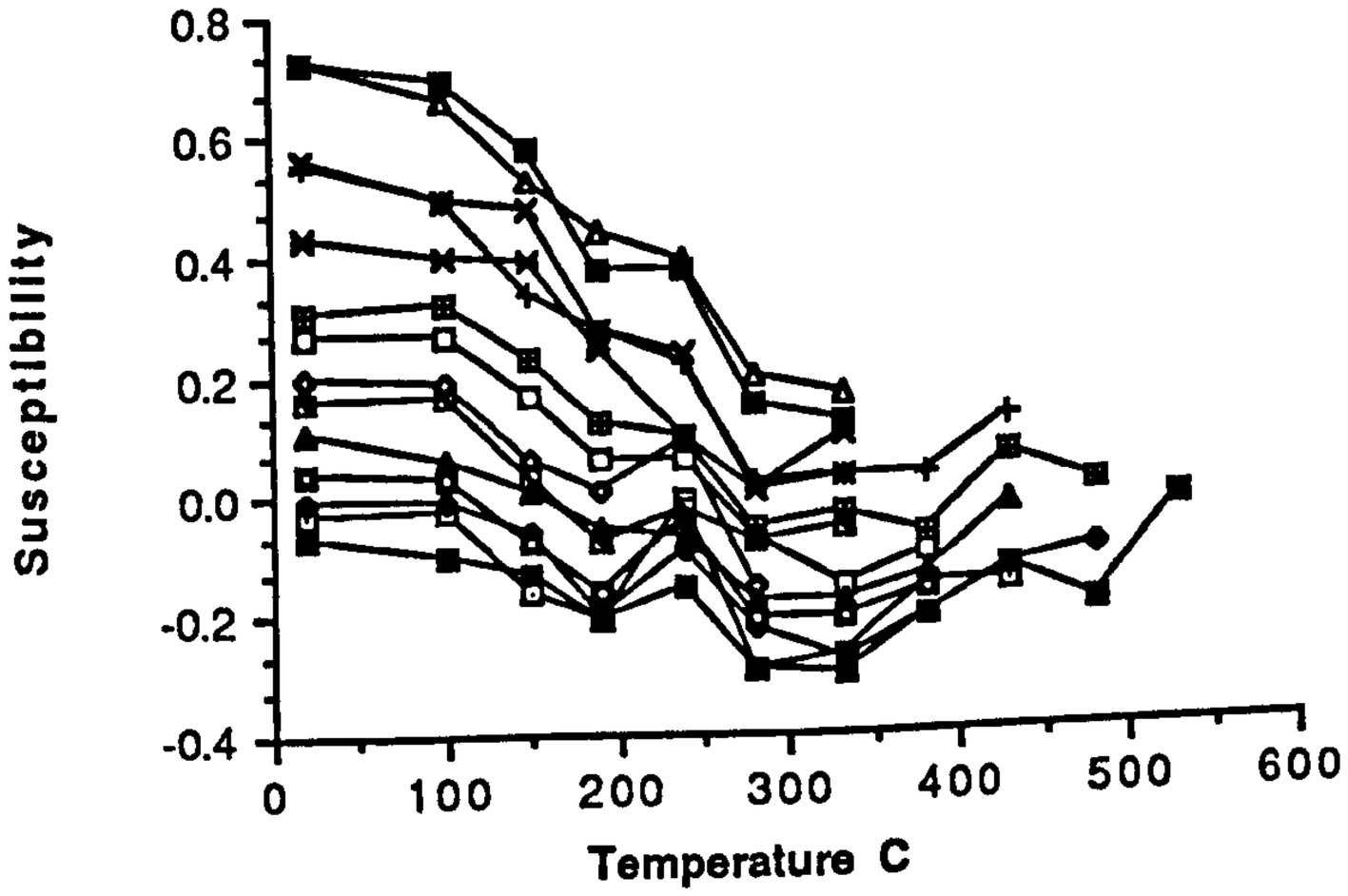
Susceptibility
0.8
0.6
0.4
0.2
0.0
-0.2
-0.4
0
100
200
300
400
500
600
Temperature C

site	stable proportion	N	site mean direction dec	inc	A95	pole(North) lat.	long.(E)	polarity
M8	6 of 10	6	353.6	31.6	19.8	74	98	N
M9	11 of 11	3	171.4	-28.8	12.4	41.9	86.4	R
		8	260.9	88.4	18.9	31.4	251.5	N
M10	14 of 14	7	6.6	59.4	16.9	80.2	286.3	N
		6	333.5	43.7	7.4	66	156.6	N
M11	8 of 10	7	220	67.7	15.7	0	231.1	N(R)
M20	11 of 12	8	174	-50.7	5.5	88.9	160.3	R
			280	62				N
M21	5 of 10	-	-	-	-	-	-	N
M22	3 of 3	-	-	-	-	-	-	N
M23	8 of 16	7	4.6	64.4	5.6	75.3	267.9	N
M24	12 of 14	8	356.3	55.2	21.8	85.2	216.7	N

site	intensity (max.)	susc. (max.)	blocking temperature C	magnetic minerals	interpreted age
M8	0.79	-0.6	100, 320, 480	G,P,H	Tertiary, 190my
M9	37.83	0.17	150, 350, 550	G,P	190my
				H	Tertiary?
M10	23.58	-0.3	150, 350, 500	G,P,H	140my-20my
				G,P,H	Tertiary
M11	1.43	-0.5	150, 350	G,P	ambiguous
M20	4.36	0.02	300	G,P,H	45my
					Tertiary
M21	0.82	-0.6	150, 390	G	Tertiary
M22	0.92	-0.6	110, 190	G	Tertiary
M23	8.01	0.81	100	G	210my, 20my
M24	3.39	0.56	100, 500	G,H	60my-40my

table 5.6 Summary of mean directions and other data for sites in the upper foreslope facies

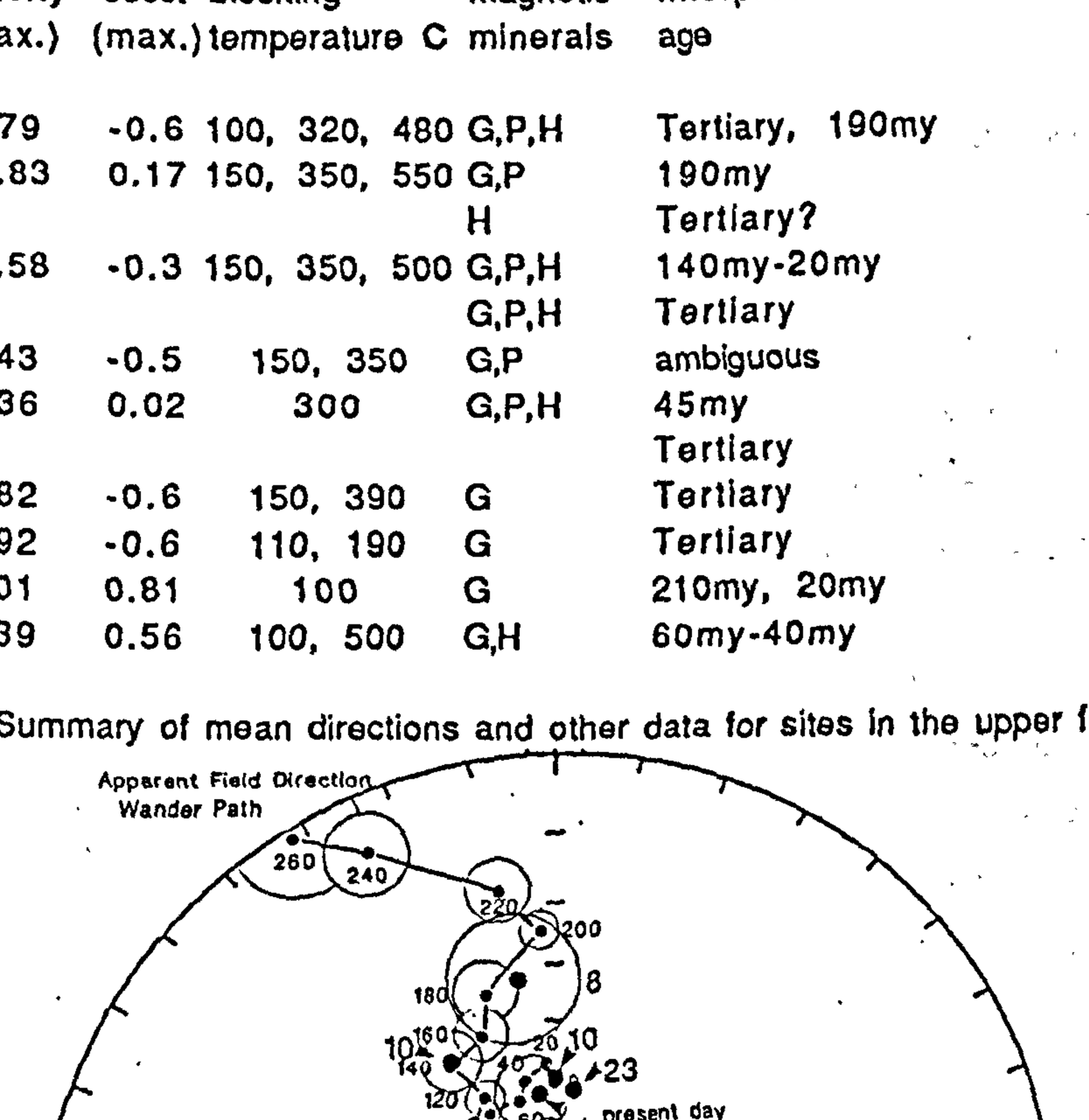

fig. 5.20 Stereographic projection of mean directions for sites in the upper foreslope facies

moderately to steeply inclined. Sites M9 and M20 have both reversed and normal polarity directions;

iv. goethite is ubiquitous and carries a viscous component;

v. haematite is the commonest magnetic carrier with pyrrhotite present in some samples;

vi. a range of dates for the acquisition of natural remanent magnetism are indicated: M8, 190 Ma, normal polarity; M9, 190 Ma, reversed polarity and Tertiary, reversed polarity??;M10, 155-20 Ma, normal polarity; M11, ambiguous, normal polarity; M20, ambiguous, normal polarity and 45-20 Ma, reversed polarity; M21, Tertiary, normal polarity; M22, ambiguous, normal polarity; M23, present day, normal polarity and 210 Ma, reversed polarity; M24, <60 Ma, normal polarity.

5.4.4 Lower foreslope facies

A summary of the demagnetisation behaviour for sites from the lower foreslope facies, and interpretations of vectors and magnetic mineralogy are as follows:

Site M4 (fig. 5.21) The maximum initial natural remanent magnetism intensity of $1.74 \times 10^{-4} Am^{-1}$ and susceptibility of -0.54 (volume units $\times 10^{-6} GOe^{-1}$; see appendix 4.2) indicate a low magnetic mineral content. Behaviour of intensity and susceptibility is uniform, with the exception of sample 11 which has significantly higher intensity. Demagnetisation in most samples is complete by 320°C, and by 550°C in a few samples. The vector directions form three groupings; group i. contains two vectors (samples 1 and 11) which have a normal polarity direction, intermediate between 60 Ma and present day. The vector is stable and clearly defined and demagnetises steadily. However, directional changes on the orthogonal plots are complicated and suggest that three or even four components are involved. These may be an artefact of low intensities and spurious remagnetisations, or may be a genuine mix of components. Group ii. contains four vectors (samples 14.1, 14.2, 16, and 18AF) which have equatorial directions. Again the vector is clearly defined but demagnetisation is incomplete. This is likely to be due to the low intensity of the natural remanent magnetism. One sample (10) has a direction intermediate between groups i. and ii. This may reflect a combination of the two vectors defined by these groups. The third group of vectors (samples 2, 4, and 5) also have a reversed equatorial direction, which is different by 70° declination from that of group ii. Sample 17 (AF) also yields a reversed direction. The direction of sample 13 is also equatorial and intermediate between groups ii. and iii

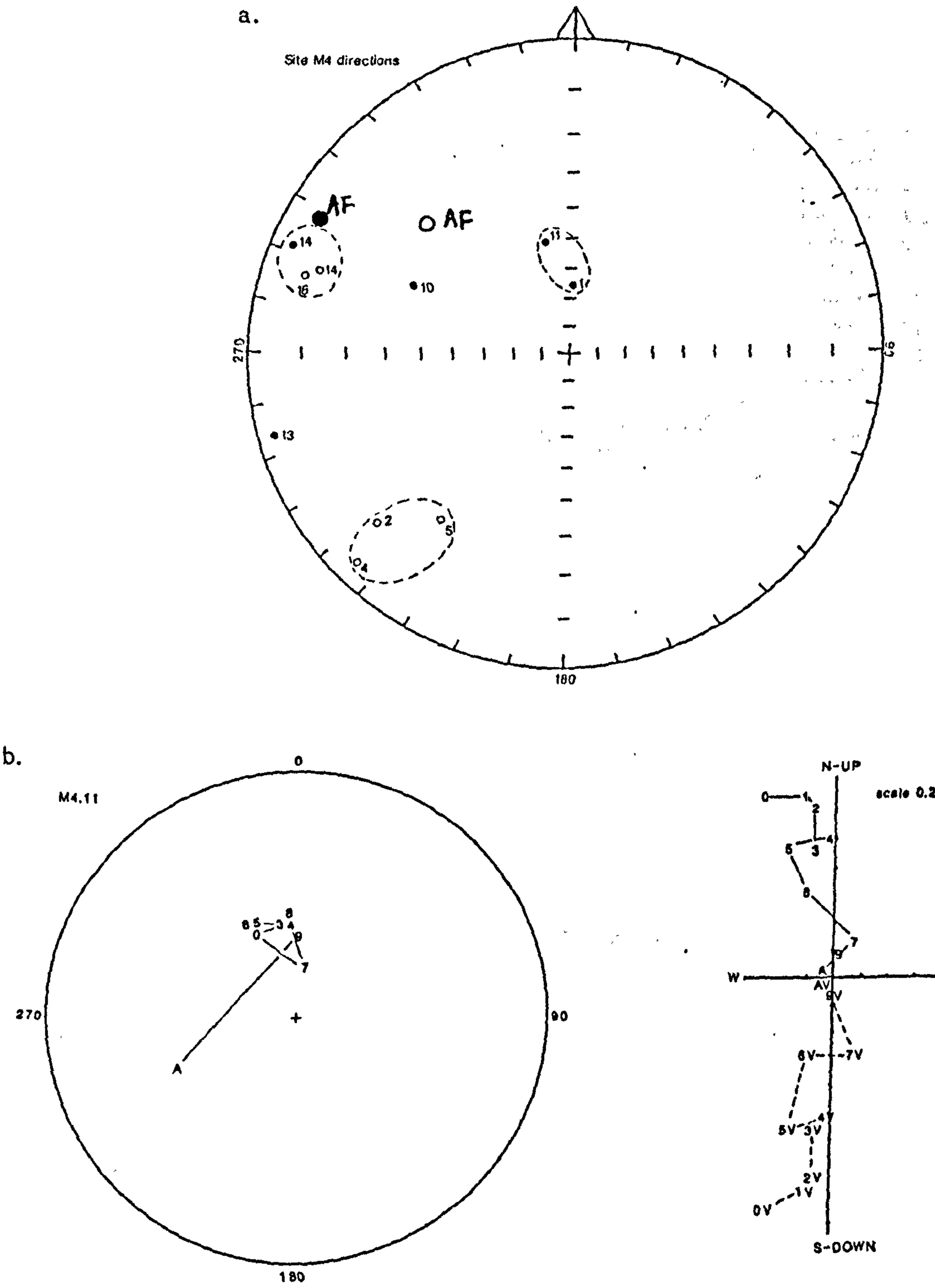

fig. 5.21 Summary of demagnetisation behaviour of samples from site M4. Natural remanent magnetism (NRM) intensity is given x $10^{-4}Am^{-1}$; susceptibility units x 10^{-6} GOe^{-1}.
a. stereographic projection of stable sample directions; **b.** stereographic projection and accompanying orthogonal plot illustrating vector movement with progressive demagnetisation; **c.** NRM intensity change with increasing temperature illustrating variation of magnetic mineral content between samples; **d.** normalised NRM change with increasing temperature illustrating within-site variation; **e.** susceptibility variation with increasing temperature illustrating changes which occur due to mineralogical alteration.

c

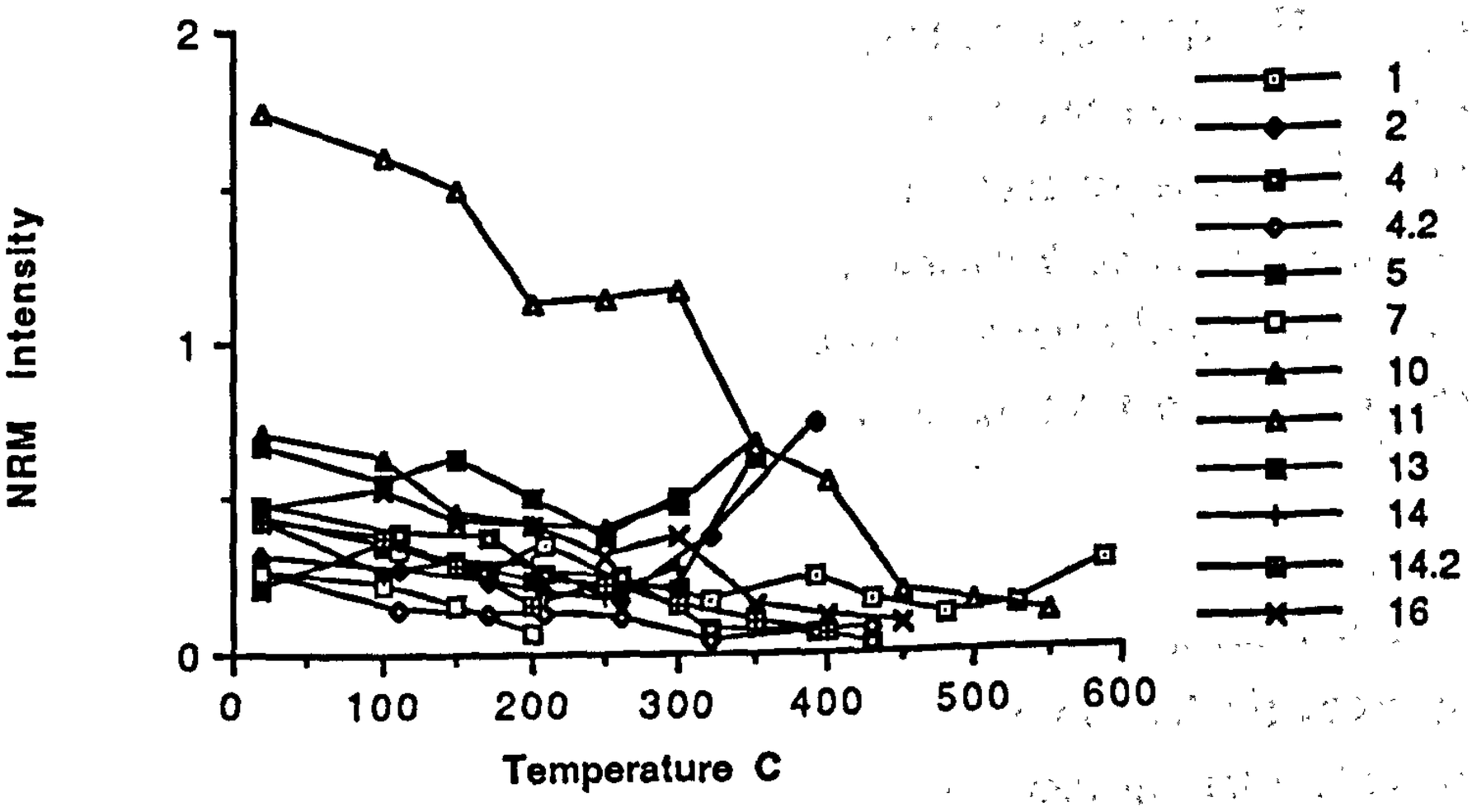
NRM Intensity
2
1
0
0
100
200
300
400
500
600
Temperature C
1
2
4
4.2
5
7
10
11
13
14
14.2
16

d

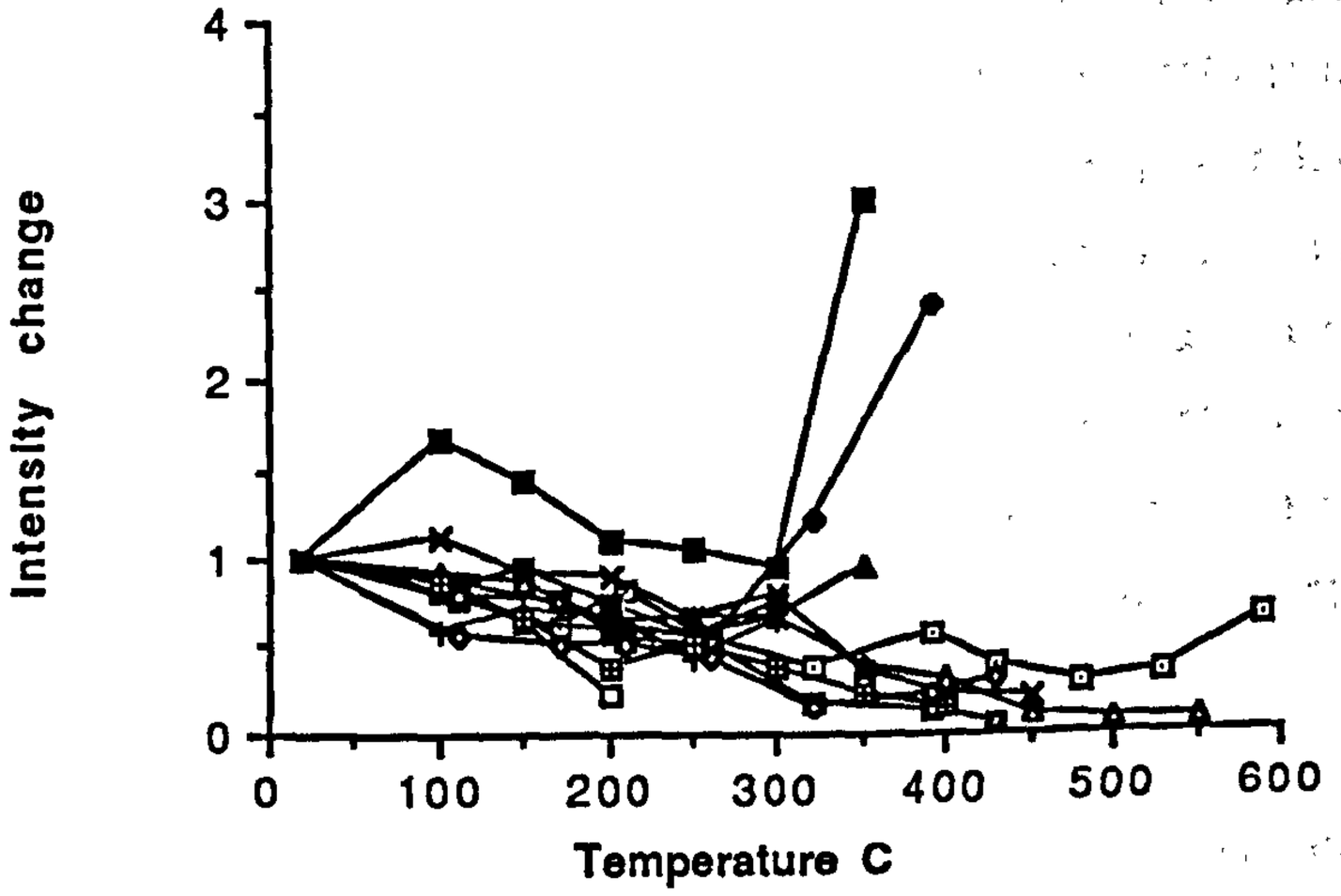
Intensity change
4
3
2
1
0
0
100
200
300
400
500
600
Temperature C

e

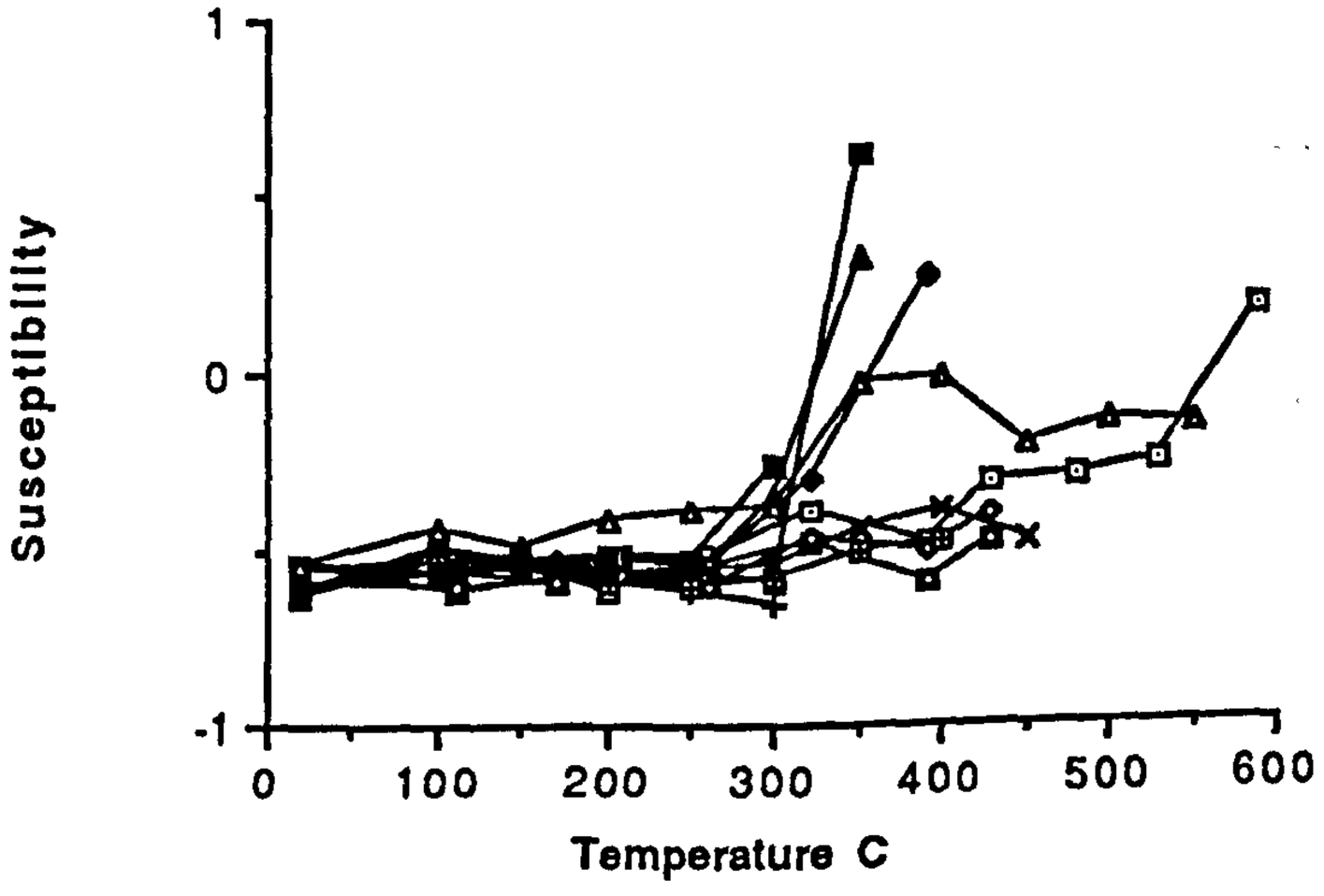
Susceptibility
1
0
-1
0
100
200
300
400
500
600
Temperature C

but has the same polarity. There appears to be a complicated overlap/mixing of vectors in samples from this site which suggests that some samples contain more than one natural remanent magnetism carrier. Only group I. vectors are interpretable in terms of the apparent field direction wander path; these have Tertiary-present day characteristics and higher natural remanent magnetism intensity. The remaining vectors have lower intensities and low inclinations and do not lie near the apparent field direction wander path. It may be that the intensity of these vectors is too low to be accurately measured and that they are being 'contaminated' by noise. However this seems unlikely as the vectors are well grouped. Alternatively, they could be approximations to a Permian direction, which is also equatorial, but with poorly defined declination.

Site M5 (fig. 5.22) The maximum initial natural remanent magnetism intensity of $3.10 \times 10^{-4} Am^{-1}$ and susceptibility of -0.35 (volume units $\times 10^{-6} GOe^{-1}$; see appendix 4.2) indicate a reasonable magnetic mineral content and that the mineral present is goethite or haematite. Within site scatter of intensity and susceptibility values is explained by variable total magnetic mineral content. All natural remanent magnetism is removed in the first heating step to 100°C, indicating that the natural remanent magnetism is viscous and caried by goethite. Site mean directions are meta-stable, but form a clearly defined group, which has high inclination and has normal polarity. The mean direction is close to the present day field direction. The largest intensity drop is from 20°C to 100°C but the direction remains little changed at higher temperatures. The fifth step (240°C) is of a different direction; this is spurious as demagnetisation is complete by this temperature.

Site M6 (fig. 5.23) Maximum initial natural remanent magnetism intensity of 18.89 $\times 10^{-4} Am^{-1}$ and susceptibility of -0.29 (volume units $\times 10^{-6} GOe^{-1}$; see appendix 4.2) indicate a high magnetic mineral content and that the natural remanent magnetism carrier is likely to be haematite. The range of natural remanent magnetism intensity values between samples reflects different quantities of magnetic minerals present in each sample. One sample shows a large increase in intensity and susceptibility at 300°C; this indicates the formation of magnetite from an iron sulphide phase due to the heating process. Normalised intensity change with progressive demagnetisation shows that the behaviour of samples within this site is consistent. Demagnetisation is complete by 450°C, suggesting that the natural remanent magnetism carrier is multi-domain, pseudo-single domain or impure. Vectors are well defined, stable to very stable, have low inclination and reversed directions and demagnetise steadily during both AF and

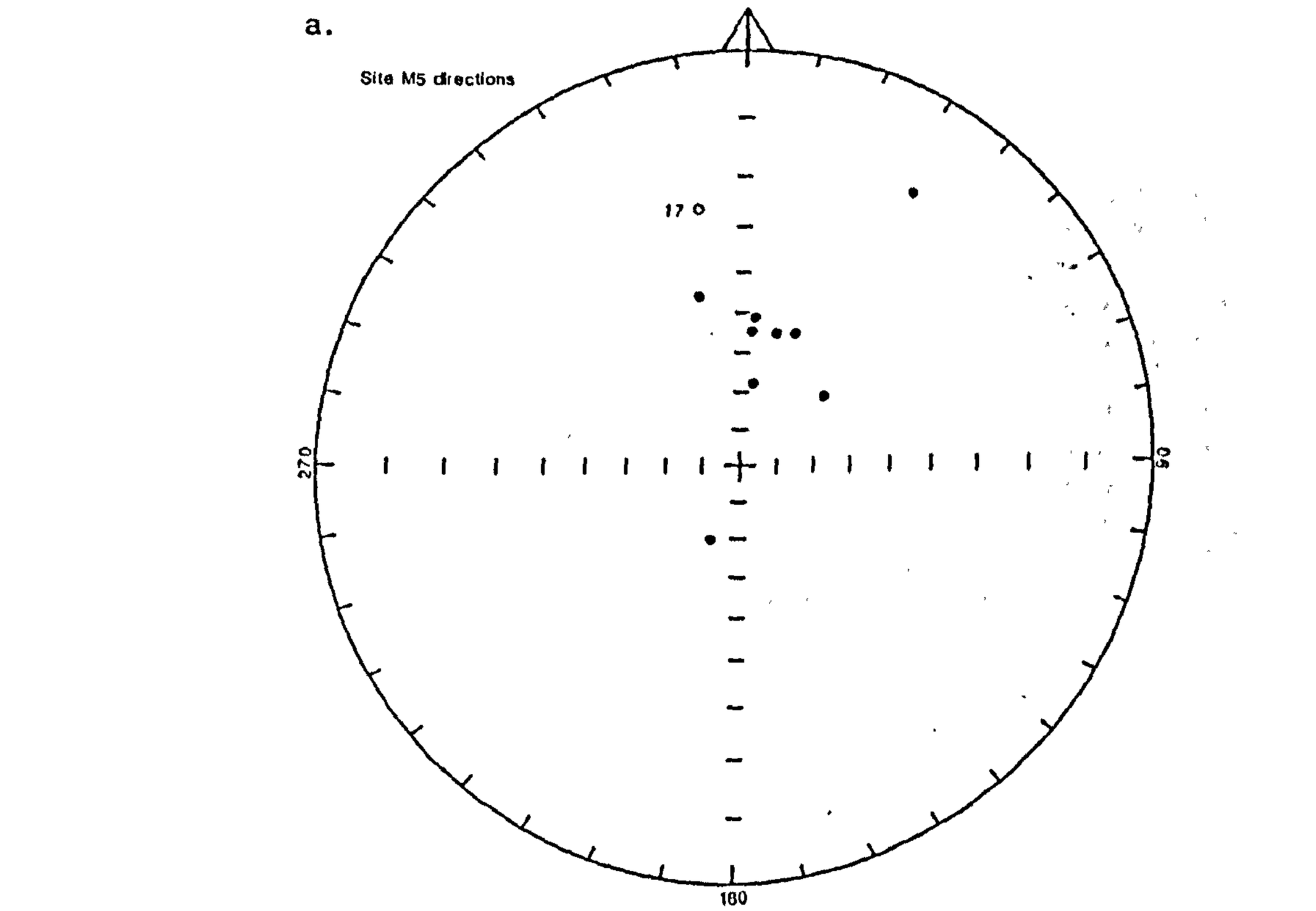

fig. 5.22 Summary of demagnetisation behaviour of samples from site M5. Natural remanent magnetism (NRM) intensity is given x $10^{-4}Am^{-1}$; susceptibility units x 10^{-6} GOe^{-1}
a. stereographic projection of stable sample directions; **b.** stereographic projection and accompanying orthogonal plot illustrating vector movement with progressive demagnetisation; **c.** NRM intensity change with increasing temperature illustrating variation of magnetic mineral content between samples; **d.** normalised NRM change with increasing temperature illustrating within-site variation; **e.** susceptibility variation with increasing temperature illustrating changes which occur due to mineralogical alteration.

c

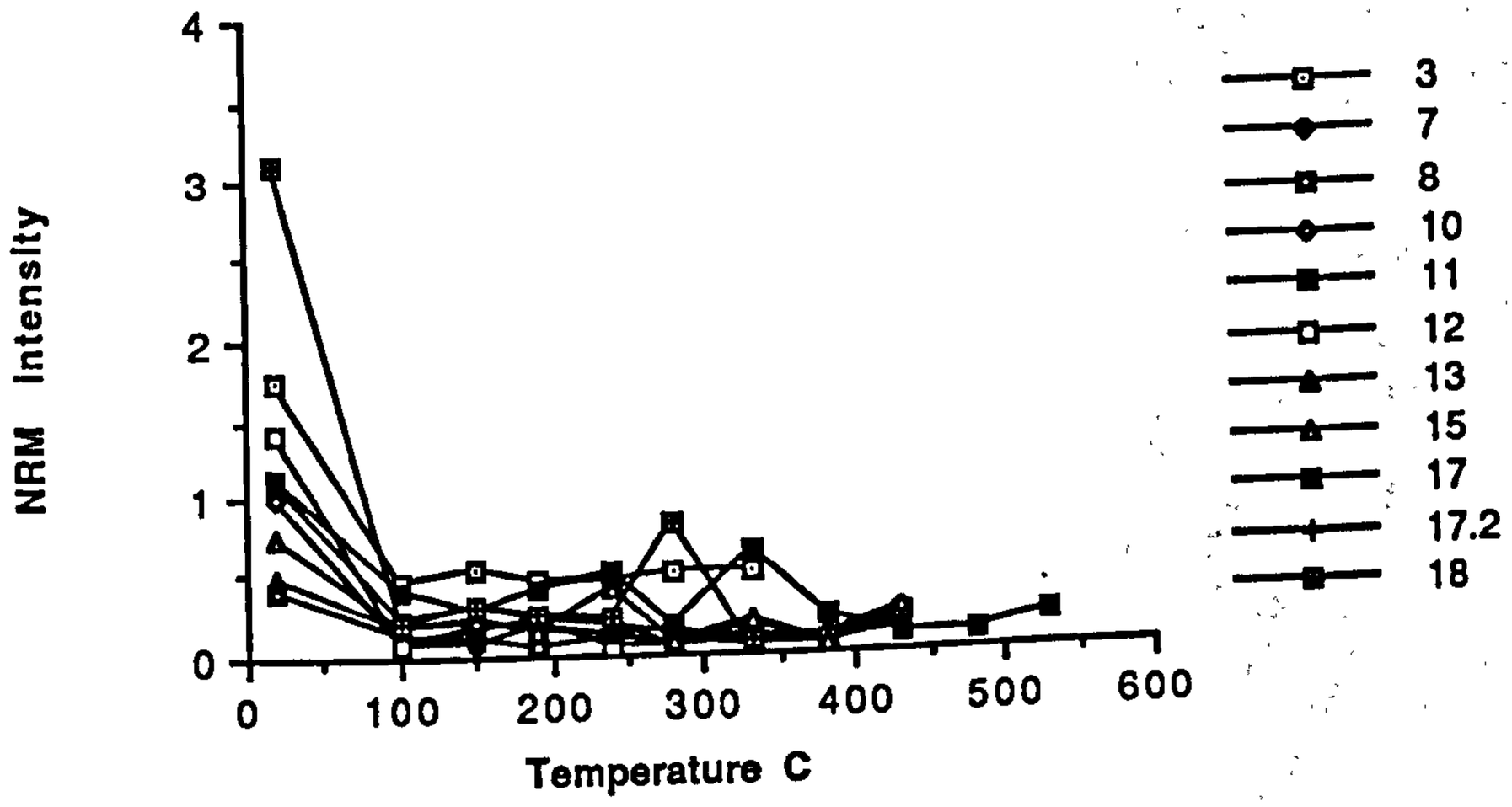
NRM Intensity
4
3
2
1
0
0
100
200
300
400
500
600
Temperature C
3
7
8
10
11
12
13
15
17
17.2
18

d

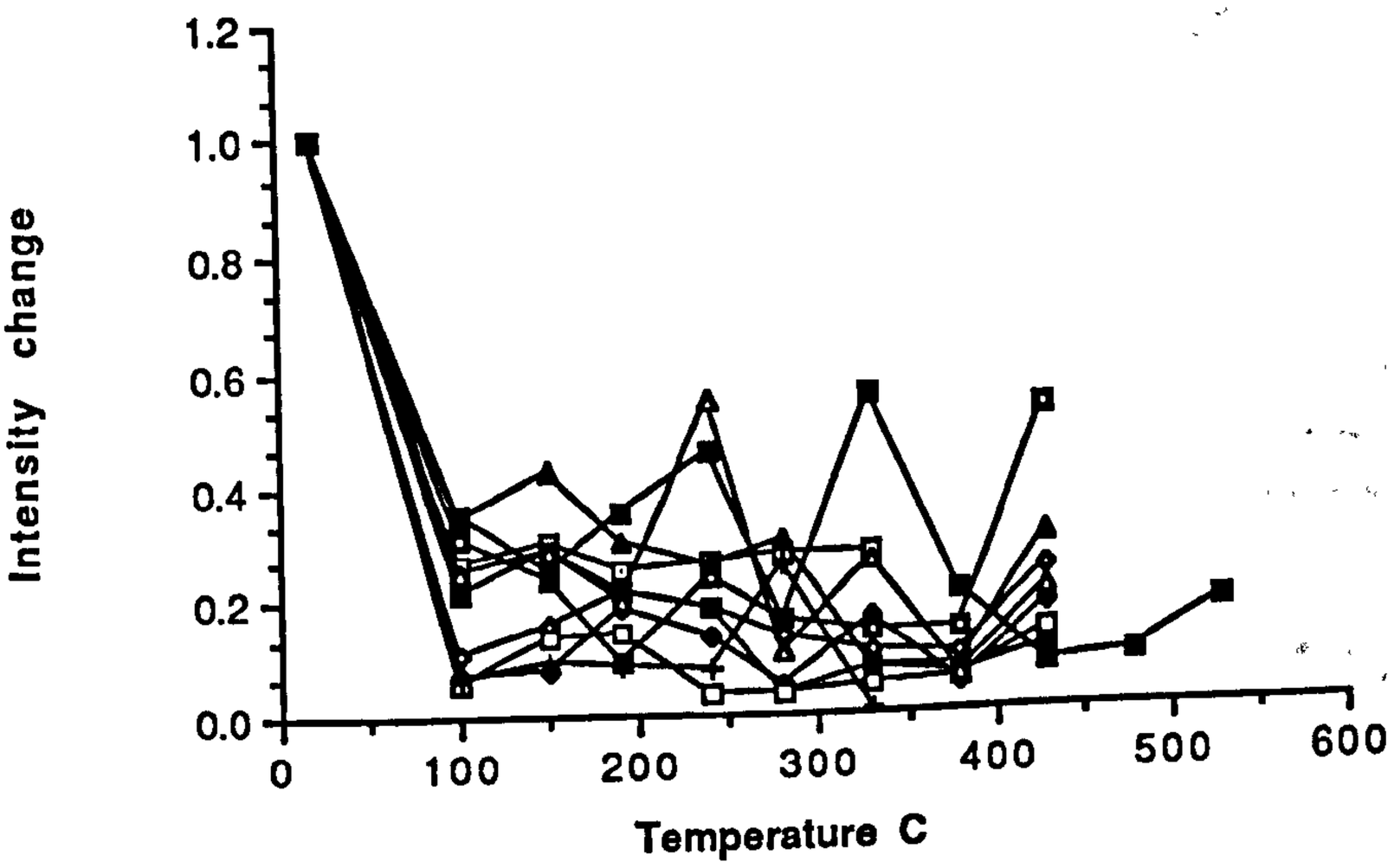
Intensity change
1.2
1.0
0.8
0.6
0.4
0.2
0.0
0
100
200
300
400
500
600
Temperature C

e

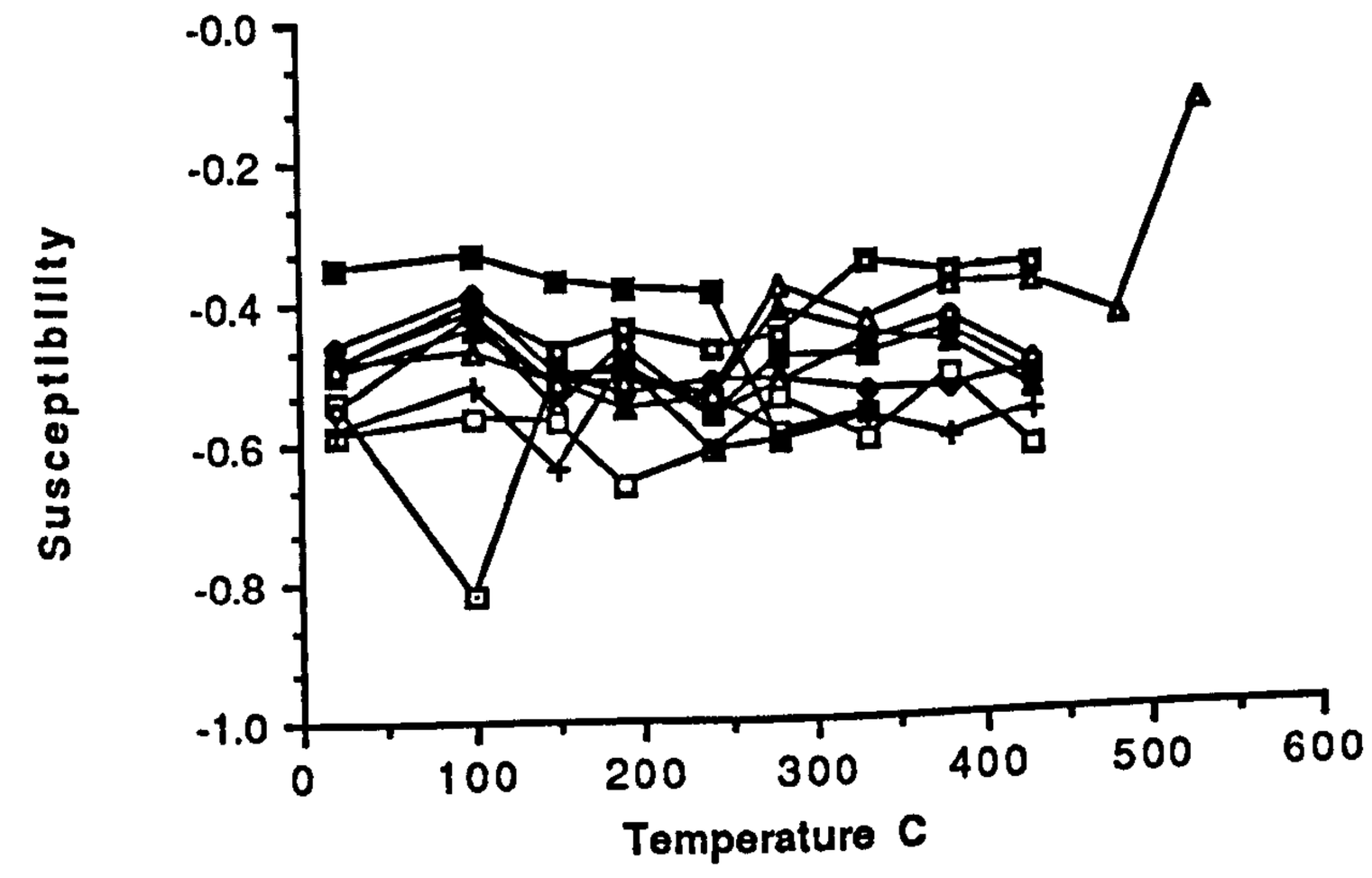
Susceptibility
-0.0
-0.2
-0.4
-0.6
-0.8
-1.0
0
100
200
300
400
500
600
Temperature C

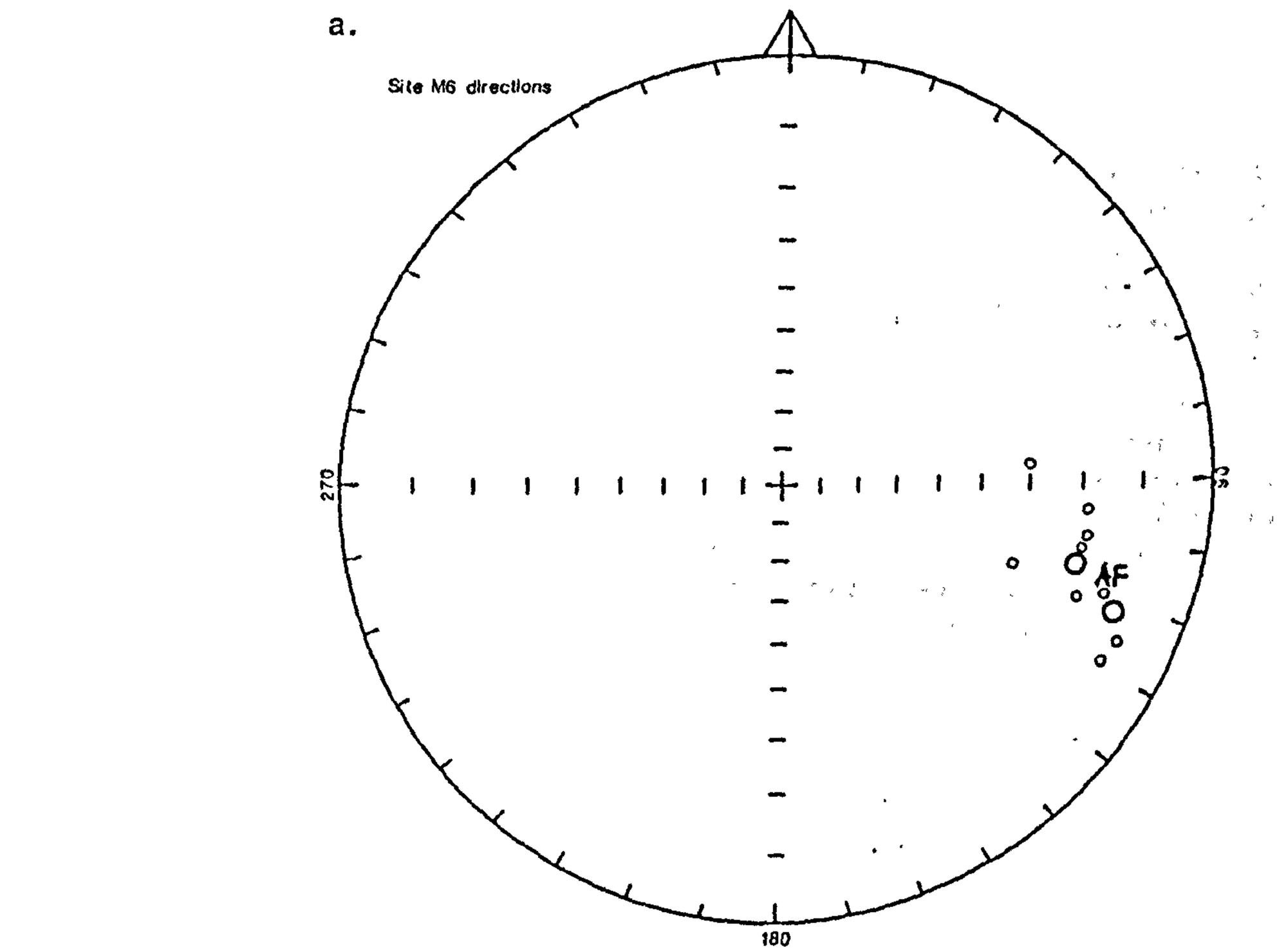

fig. 5.23 Summary of demagnetisation behaviour of samples from site M6. Natural remanent magnetism (NRM) intensity is given x $10^{-4}Am^{-1}$; susceptibility units x 10^{-6} GOe^{-1}.
a. stereographic projection of stable sample directions; **b.** stereographic projection and accompanying orthogonal plot illustrating vector movement with progressive demagnetisation; **c.** NRM intensity change with increasing temperature illustrating variation of magnetic mineral content between samples; **d.** normalised NRM change with increasing temperature illustrating within-site variation; **e.** susceptibility variation with increasing temperature illustrating changes which occur due to mineralogical alteration.

c

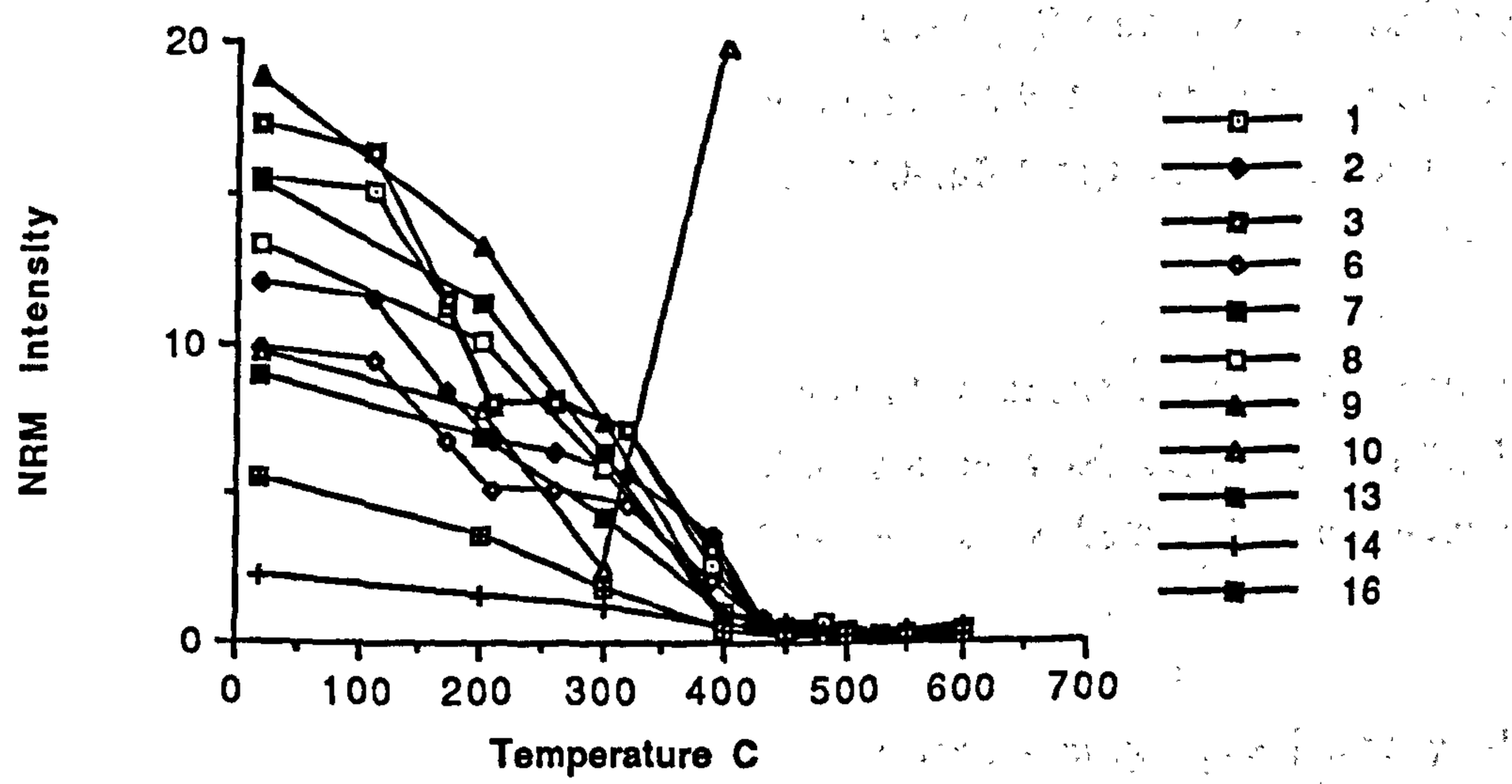
NRM Intensity
20
10
0
0
100
200
300
400
500
600
700
Temperature C
1
2
3
6
7
8
9
10
13
14
16

d

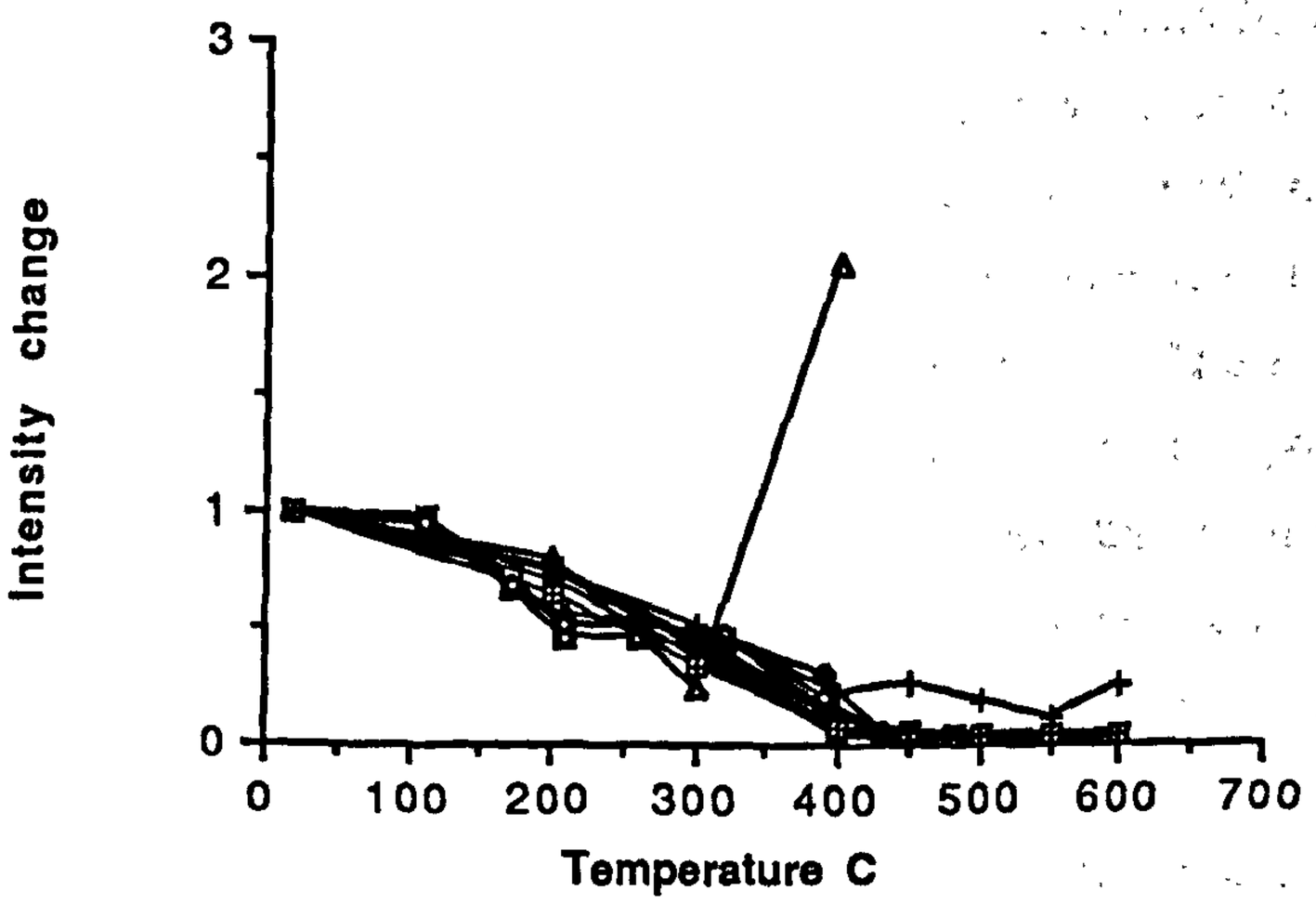
y change
Intensity
3
2
1
0
0
100
200
300
400
500
600
700
Temperature C

e

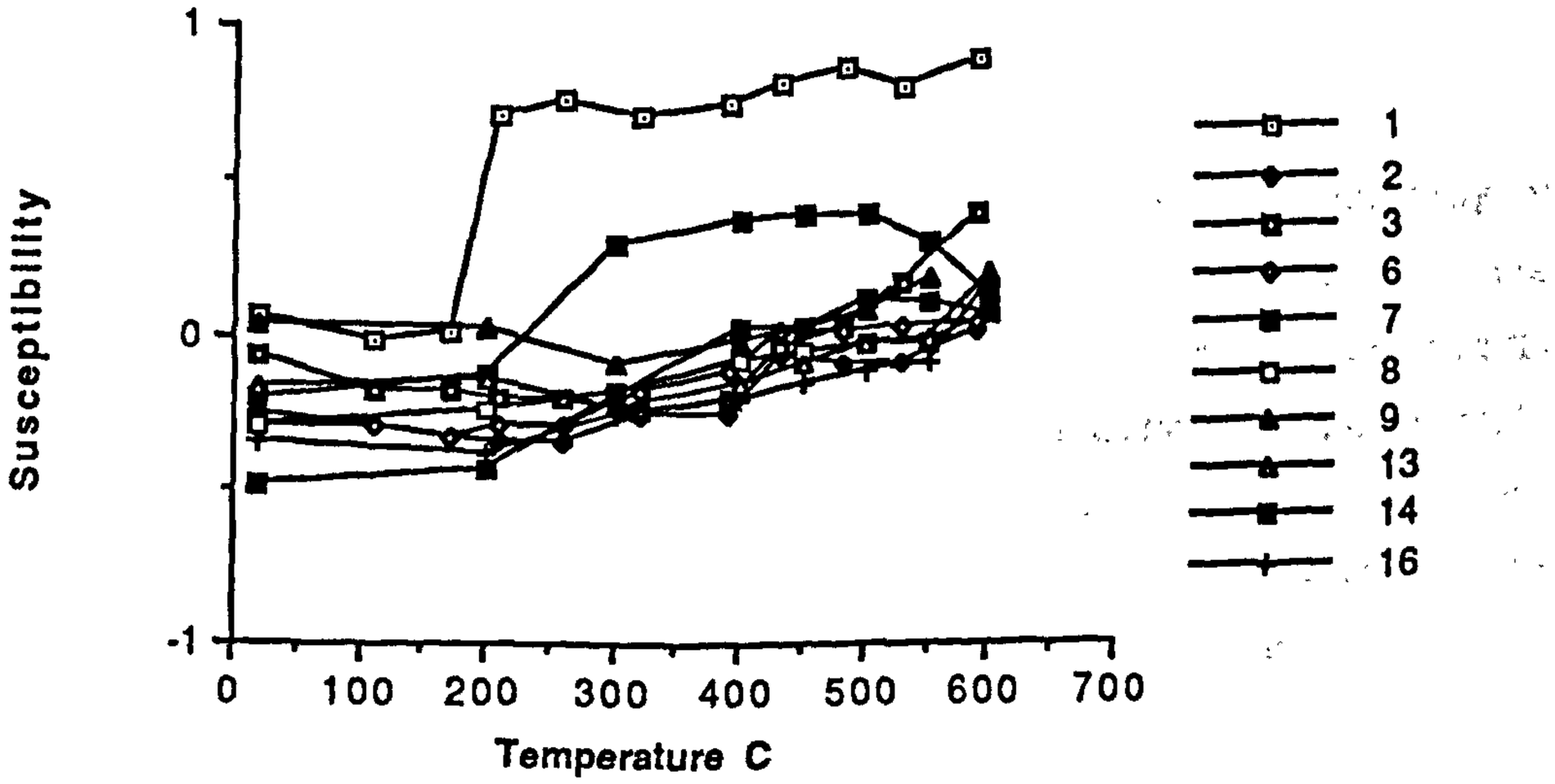
Susceptibility
1
0
-1
0
100
200
300
400
500
600
700
Temperature C
1
2
3
6
7
8
9
13
14
16

thermal demagnetisation. The site mean direction is well defined (*A95* = 8.2°) has shallow inclination and is reversed. It does not coincide with the apparent field direction wander path but differs in declination by > 65°. Goethite, haematite and pyrrhotite appear to carry natural remanent magnetism with basically the same directions. The direction defined has shallow inclination and is reversed and in these respects is similar to the apparent field direction wander path for 220-250 Ma; however it differs in declination by >65°.

Site M7 This site contained negligible quantities of magnetic minerals (maximum initial intensity of 0.37 x $10^{-4}Am^{-1}$ and initial susceptibility of -0.62 x $10^{-6}GOe^{-1}$ (see appendix 4.2) and yielded unstable directions after both AF and thermal demagnetisation.

Site M25 (fig. 5.24) The maximum initial natural remanent magnetism intensity of 0.72 x $10^{-4}Am^{-1}$ and susceptibility of -0.64 x $10^{-6}GOe^{-1}$(see appendix 4.2) indicate a very low magnetic mineral content. However, demagnetisation behaviour of samples is remarkably consistent (including AF demagnetised sample) and natural remanent magnetism intensity, susceptibility and vectors are very similar. Initial variability of direction and intensity reflects the removal of a viscous component by around 150°C or 10mT (*e.g.*, sample 15 AF) which is carried by goethite. The main natural remanent magnetism is demagnetised by 400°C-500°C which makes interpretation of the natural remanent magnetism carrier ambiguous. It may be impure, multi-domain or pseudo-single domain magnetite or haematite, although low susceptibility values suggests that haematite is more likely. Site directions are all reversed polarity and stable. Demagnetisation paths suggest the presence of two main components, one of which is more westerly in direction. A mix of these two vectors might explain the spread of site directions in this group. The mean direction is well defined but differs from the apparent field direction wander path by a declination of around 160°. This makes interpretation problematic.

Site M26 (fig. 5.25) The maximum initial natural remanent magnetism intensity of 1.25 x $10^{-4}Am^{-1}$ (sample 2) and susceptibility of 0.08 x $10^{-6}GOe^{-1}$(see appendix 4.2)) indicate a low magnetic mineral content. However, most samples have natural remanent magnetism intensity below 0.55 x $10^{-4}Am^{-1}$, indicating that they contain negligible amounts of magnetic minerals. All samples have unstable vectors except for sample 2, which has highest intensity, normal polarity and a present day direction. The demagnetisation path is erratic, but the direction is still clearly defined and similar to a

a.

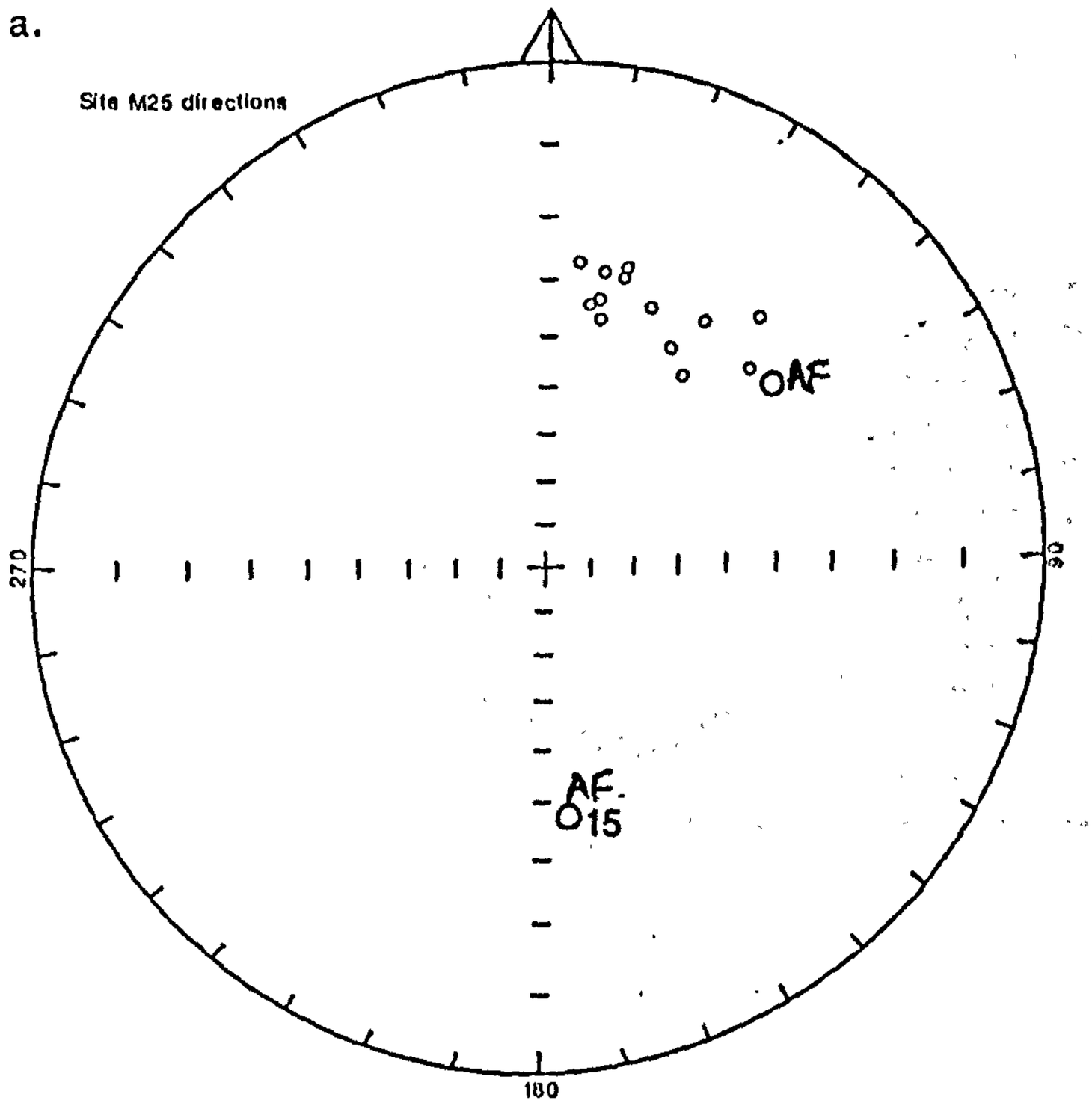

b.

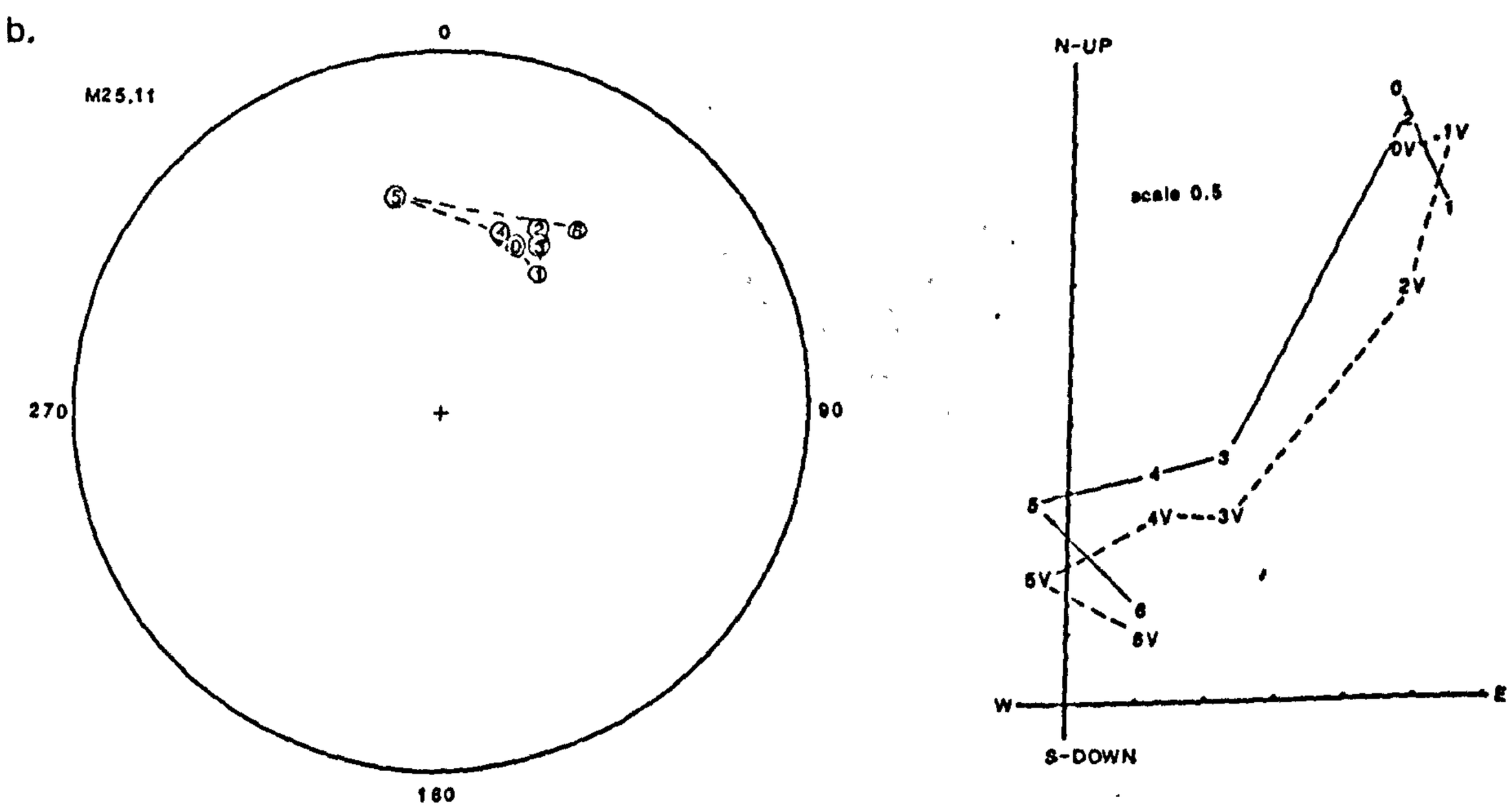

fig. 5.24 Summary of demagnetisation behaviour of samples from site M25. Natural remanent magnetism (NRM) intensity is given x $10^{-4}Am^{-1}$; susceptibility units x 10^{-6} GOe^{-1}

a. stereographic projection of stable sample directions; b. stereographic projection and accompanying orthogonal plot illustrating vector movement with progressive demagnetisation; c. NRM intensity change with increasing temperature illustrating variation of magnetic mineral content between samples; d. normalised NRM change with increasing temperature illustrating within-site variation; e. susceptibility variation with increasing temperature illustrating changes which occur due to mineralogical alteration.

c

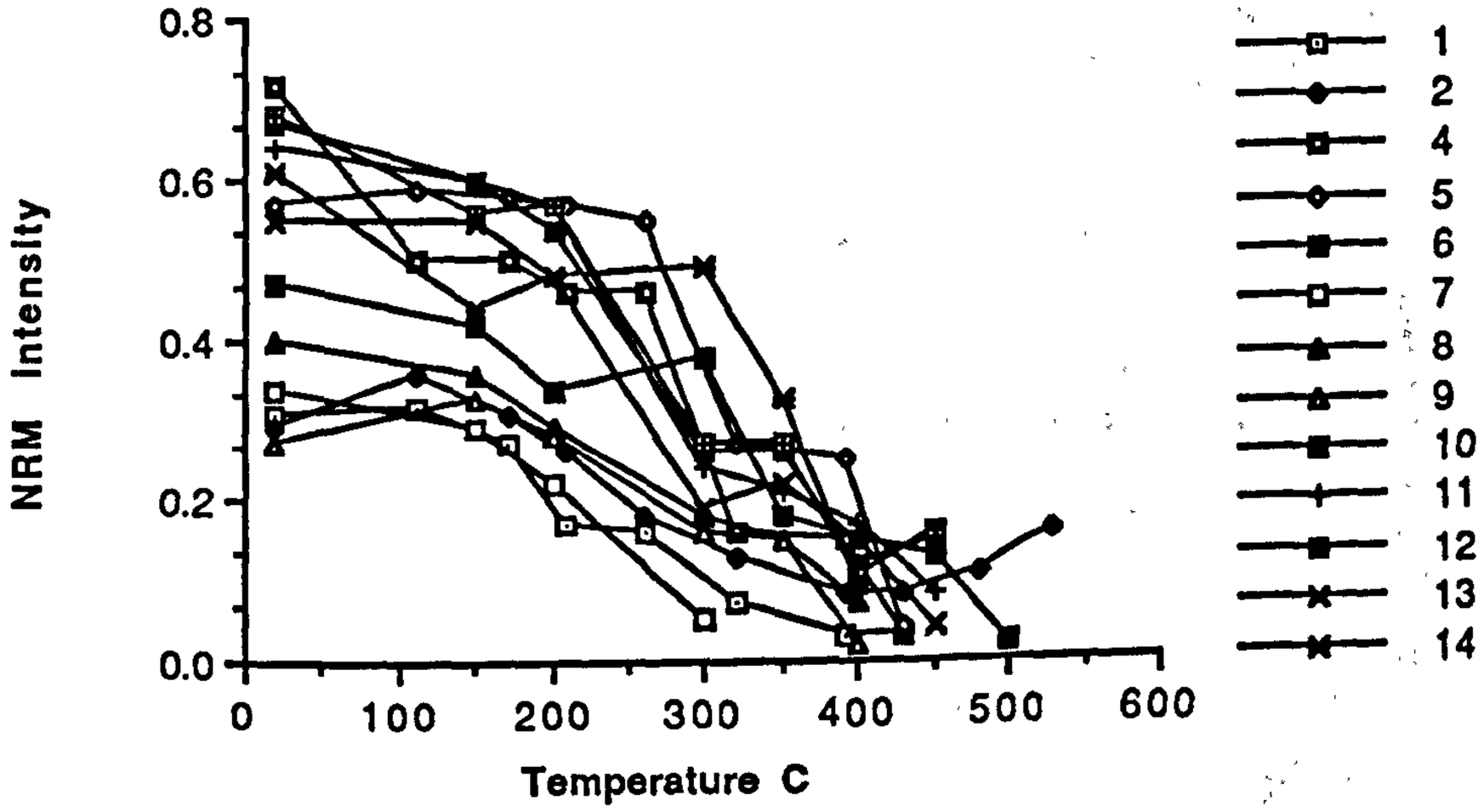
NRM Intensity
0.8
0.6
0.4
0.2
0.0
0
100
200
300
400
500
600
Temperature C
1
2
4
5
6
7
8
9
10
11
12
13
14

d

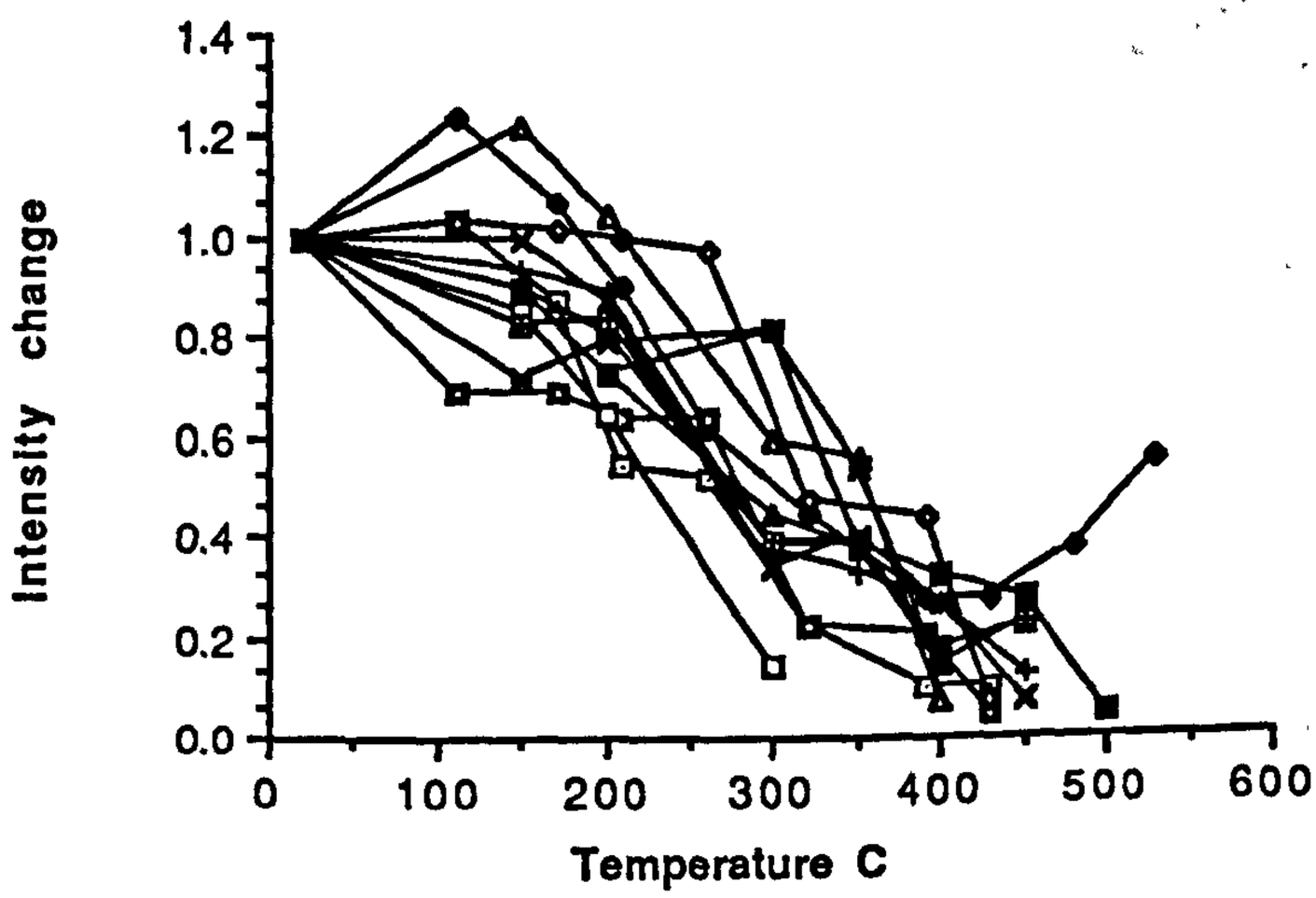
Intensity change
1.4
1.2
1.0
0.8
0.6
0.4
0.2
0.0
0
100
200
300
400
500
600
Temperature C

e

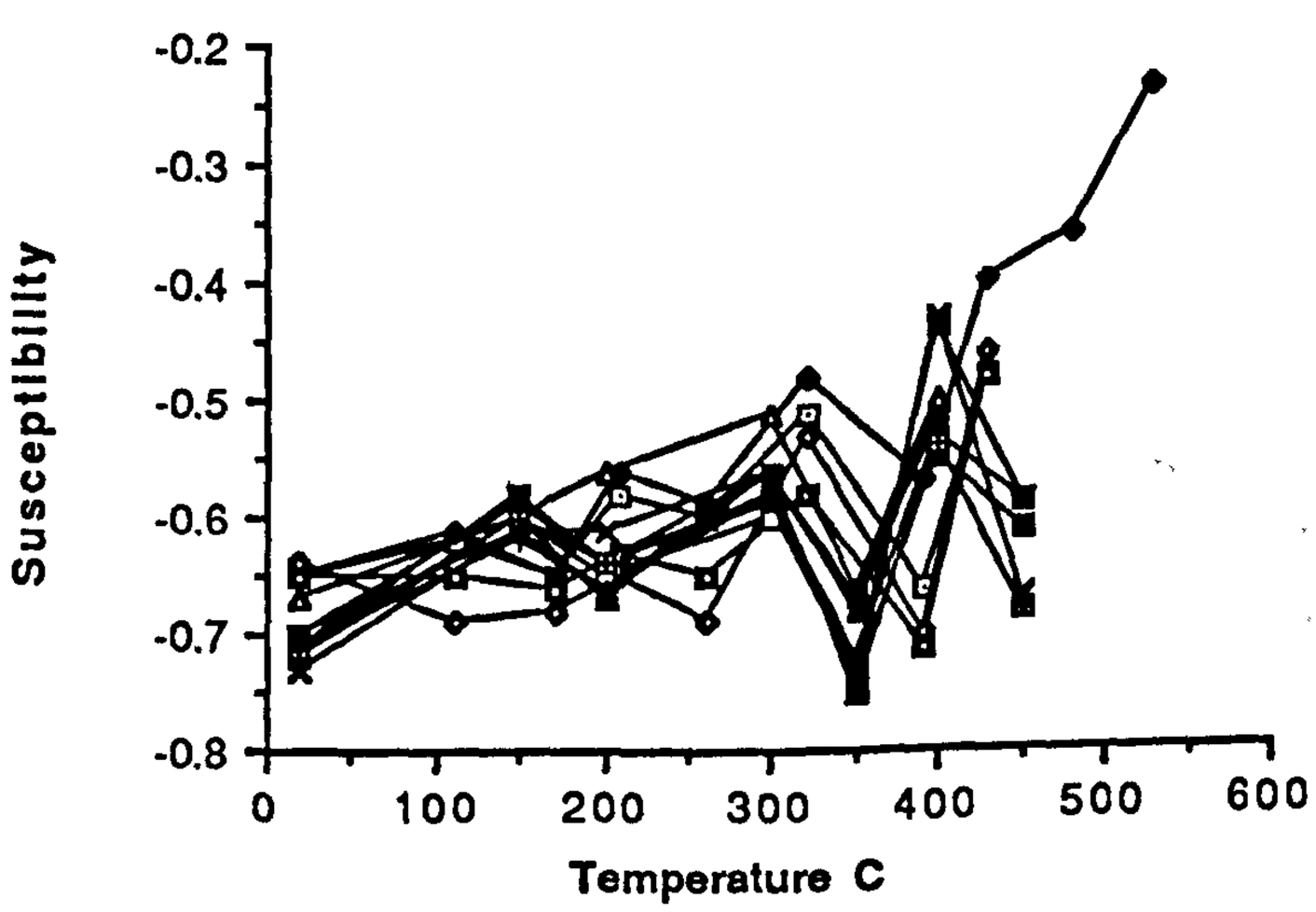
Susceptibility
-0.2
-0.3
-0.4
-0.5
-0.6
-0.7
-0.8
0
100
200
300
400
500
600
Temperature C

a.

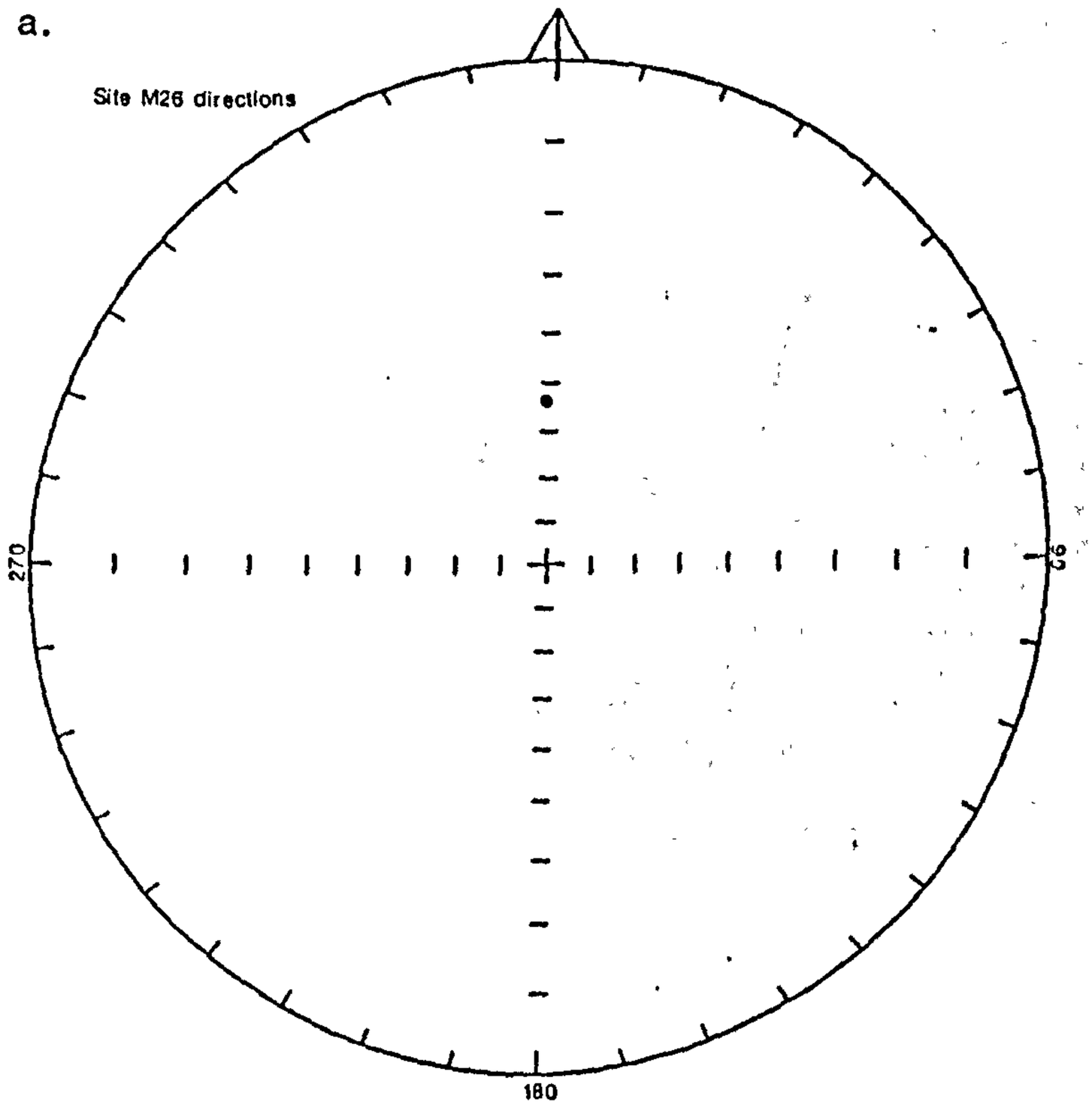

b.

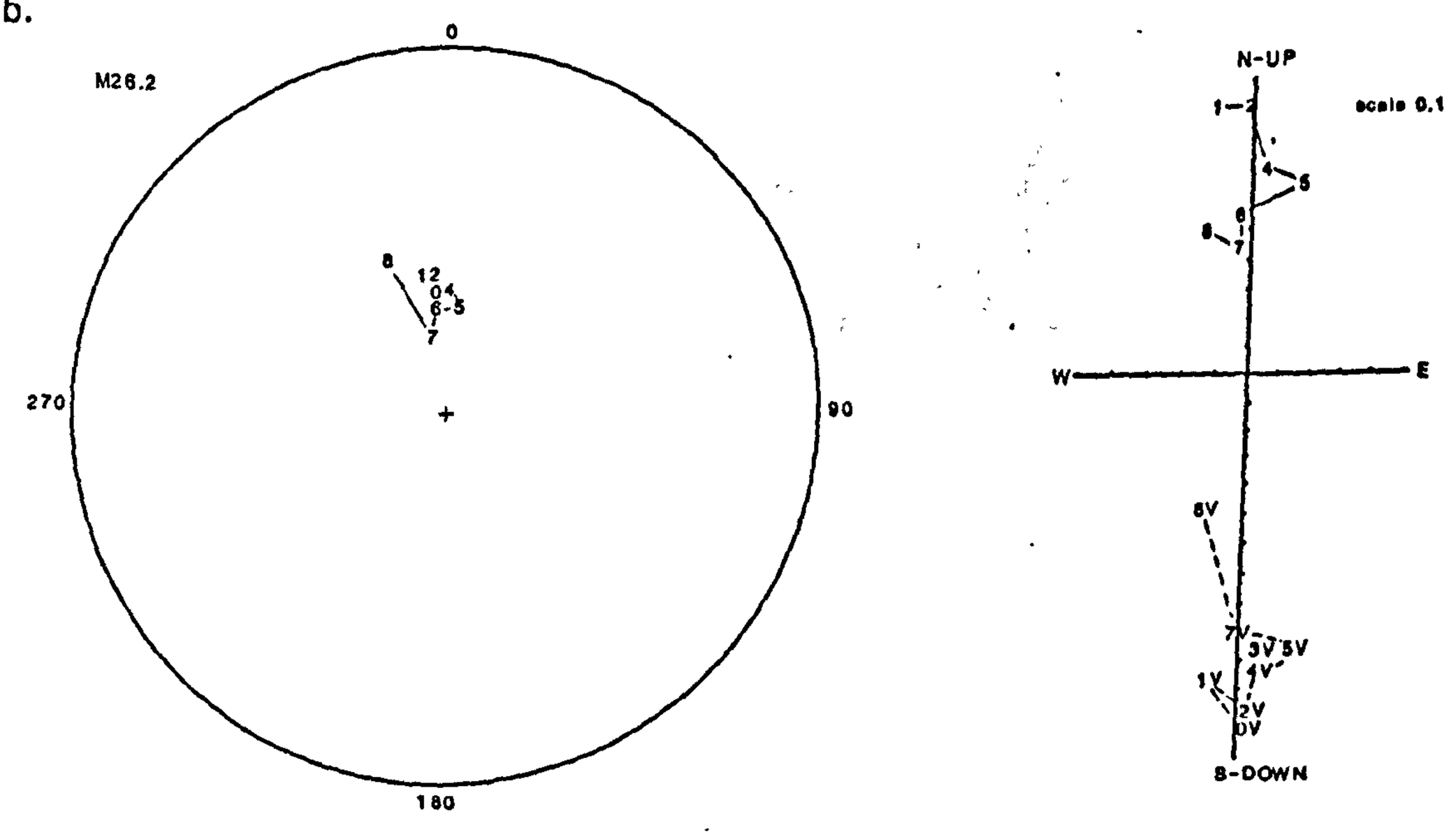

fig. 5.25 Summary of demagnetisation behaviour of samples from site M26. Natural remanent magnetism (NRM) intensity is given x $10^{-4}Am^{-1}$; susceptibility units x 10^{-6} GOe^{-1}
a. stereographic projection of stable sample directions; **b.** stereographic projection and accompanying orthogonal plot illustrating vector movement with progressive demagnetisation; **c.** NRM intensity change with increasing temperature illustrating variation of magnetic mineral content between samples; **d.** normalised NRM change with increasing temperature illustrating within-site variation; **e.** susceptibility variation with increasing temperature illustrating changes which occur due to mineralogical alteration.

c

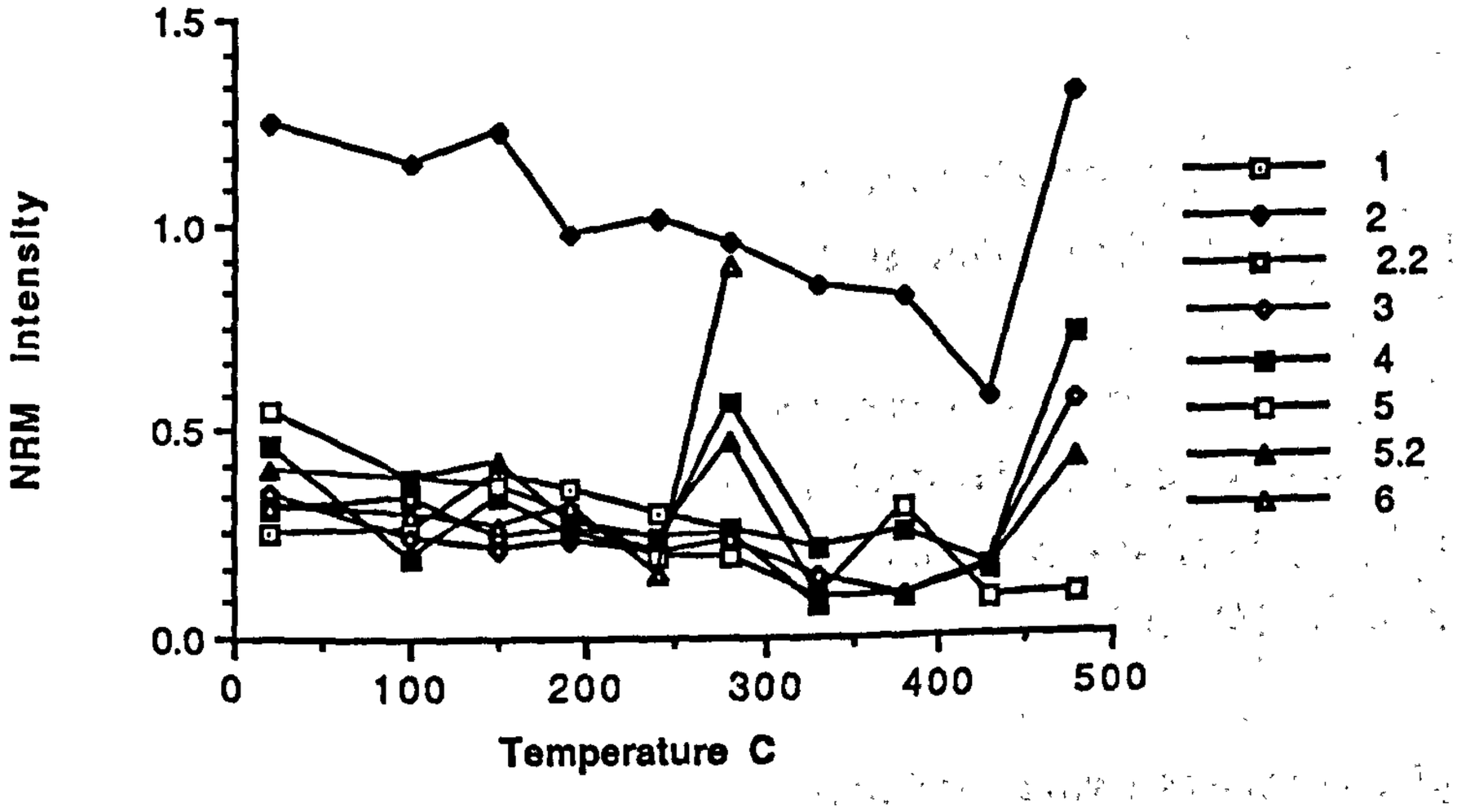
1.5
1.0
0.5
0.0
Intensity
NRM
0
100
200
300
400
500
Temperature C
1
2
2.2
3
4
5
5.2
6

d

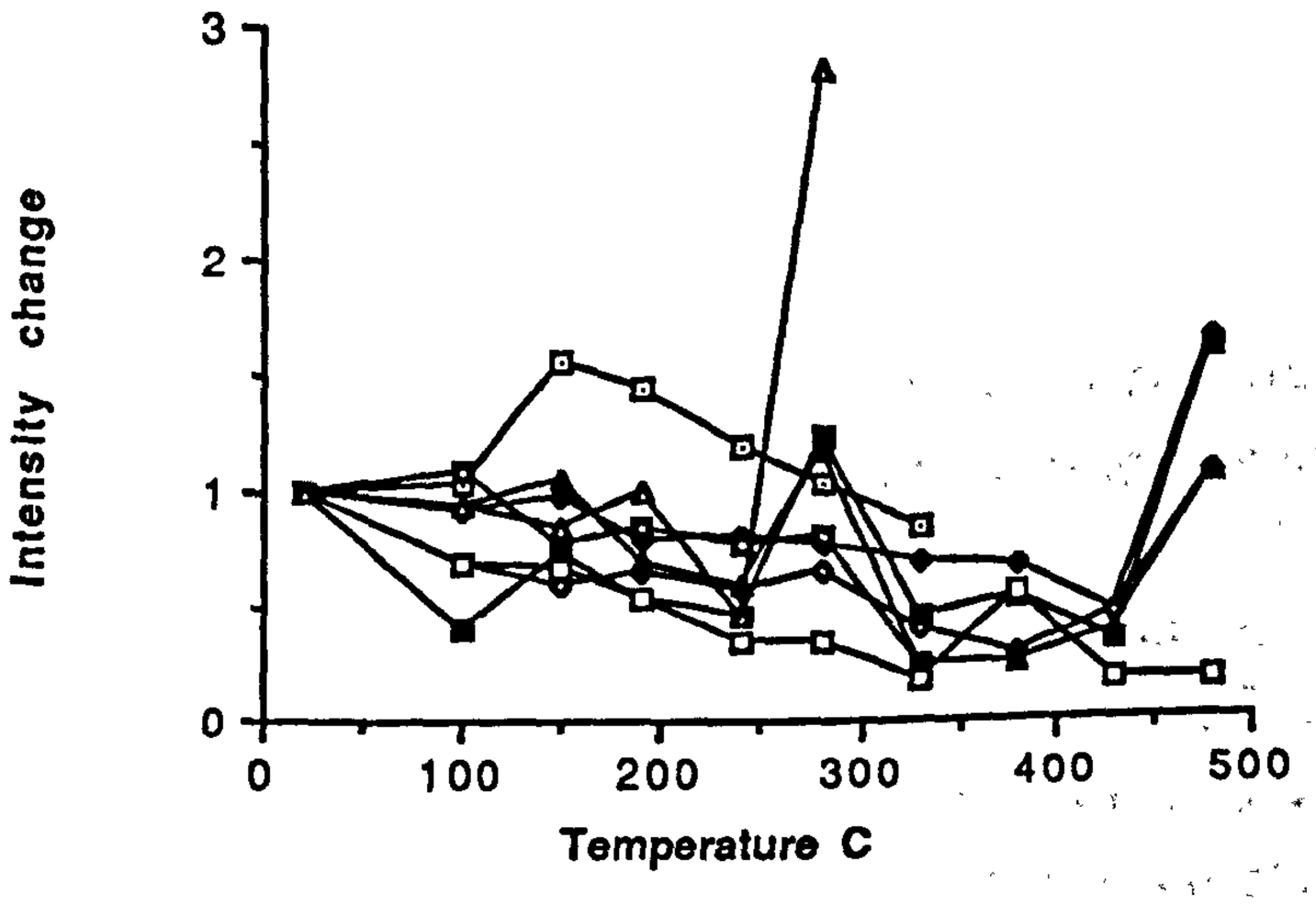
3
2
1
0
Intensity change
0
100
200
300
400
500
Temperature C

e

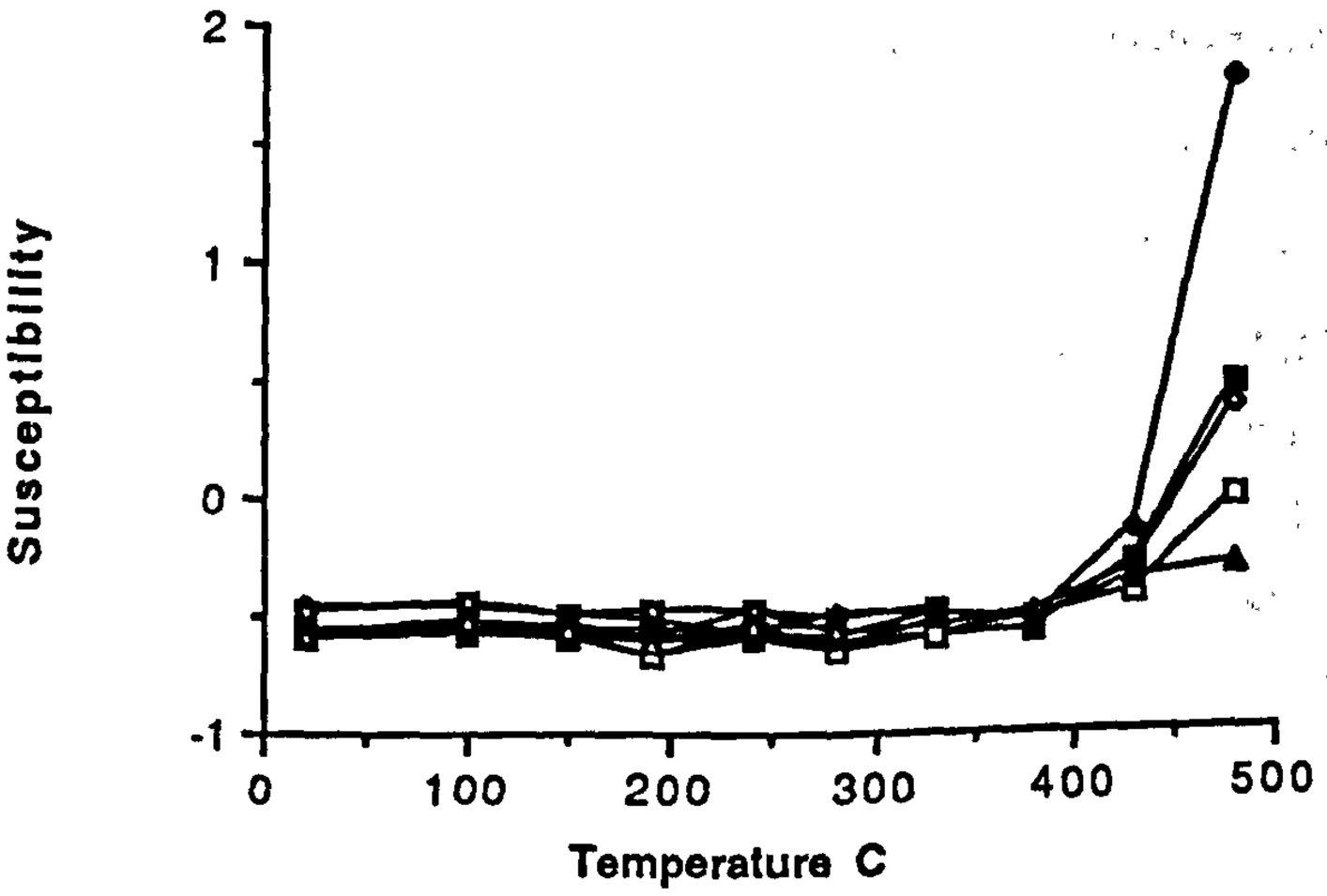
2
1
0
-1
Susceptibility
0
100
200
300
400
500
Temperature C

present day direction. Demagnetisation is complete by 430°C, which makes interpretation of the natural remanent magnetism carrier ambiguous. It may be impure, multi-domain or pseudo-single domain magnetite or haematite, although low susceptibility values suggests that haematite is more likely.

Summary (table 5.7 and fig. 5.26)

i. only 1 out of 6 sites has negligible magnetic mineral content;
ii. several sites have complex magnetisations with more than one magnetic component;
iii. goethite is ubiquitous and carries a viscous remanent magnetism;
iv. the directions are normal and reversed polarity; site M4, present day, normal polarity, ambiguous, reversed polarity; M5, present day, reversed polarity; M6, ambiguous, reversed polarity; M25, ambiguous, reversed polarity; M26, present day, normal polarity;
v. haematite is the main natural remanent magnetism carrier and has lower T_b than that of the pure phase.

5.4.5 Basin margin facies

A summary of the demagnetisation behaviour for sites from the basin margin facies, and interpretations of vectors and magnetic mineralogy are as follows:

Site M1 (fig. 5.27) The maximum initial natural remanent magnetism intensity of $4.85 \times 10^{-4} Am^{-1}$ and susceptibility of 0.34 (volume units $\times 10^{-6} GOe^{-1}$; see appendix 4.2) indicate moderate magnetic mineral content. There is very little within-site scatter of intensity or susceptibility to the extent that the plots of intensity and susceptibility superimpose. The magnetic carriers are goethite for the component with T_b of around 150°C and either magnetite or haematite (multi-domain, pseudo-single domain or impure) for the component with the higher T_b of 480°C. Site directions are clearly defined, consistent within the site and stable/meta-stable. An anti-parallel component is removed up to 150°C. Above this temperature the main natural remanent magnetism is demagnetised. The site mean direction is normal polarity, has moderate to steep inclination and lies close to the apparent field direction wander path for 80 - 60 Ma. The large increase in susceptibility at 480°C suggests the formation of a phase such as magnetite or haematite, or this could be the Hopkinson effect.

site	stable proportion	N	site mean direction dec	inc	A95	pole(North) lat.	long.(E)	polarity
M4	11 of 11	2	355	56		85	216	N
		2	288.3	-5.3		14	153	N
		3	222.5	-13.4	16.8	43.1	8.4	R
M5		9	8.7	58.9	8.6	79.6	295.4	N
M6	10 of 10	9	106.4	-18.2	8.2	188	164.6	R
M7	-	-	-	-	-	-	-	-
M25	13 of 13	13	21.9	-31.9	6.4	36.4	48.9	R
M26	1 of 8	1	358.6	54	3.5	87.2	230.4	N

site	intensity (max.)	susc. (max.)	blocking temperature C	magnetic minerals	interpreted age
M4	1.74	-0.54	100, 320, 550	M/H	60my
				M/H	ambiguous
				M/H	ambiguous
M5	3.1	-0.35	300	G	<20my
M6	18.89	-0.29	100, 450	G,P,H	220my-260my
M7	0.37	-0.62	-	-	
M25	0.72	-0.64	100, 500	G,M/H	ambiguous
M26	1.25	-0.55	100, 500	G,M/H	Tertiary

table 5.7 Summary of mean directions and other data for sites in the lower foreslope facies

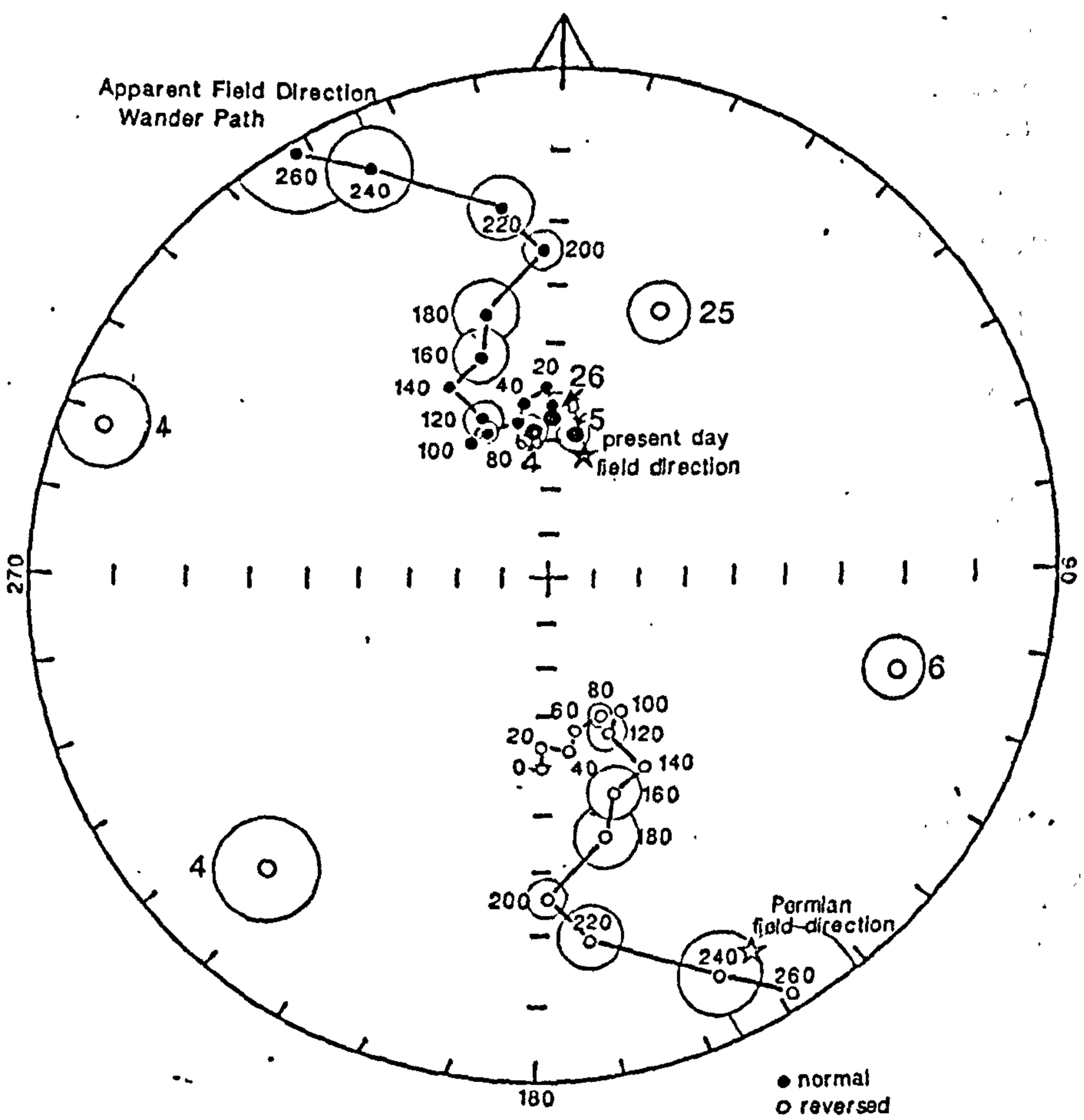

fig. 5.26 Stereographic projection of mean directions for sites in the lower foreslope facies

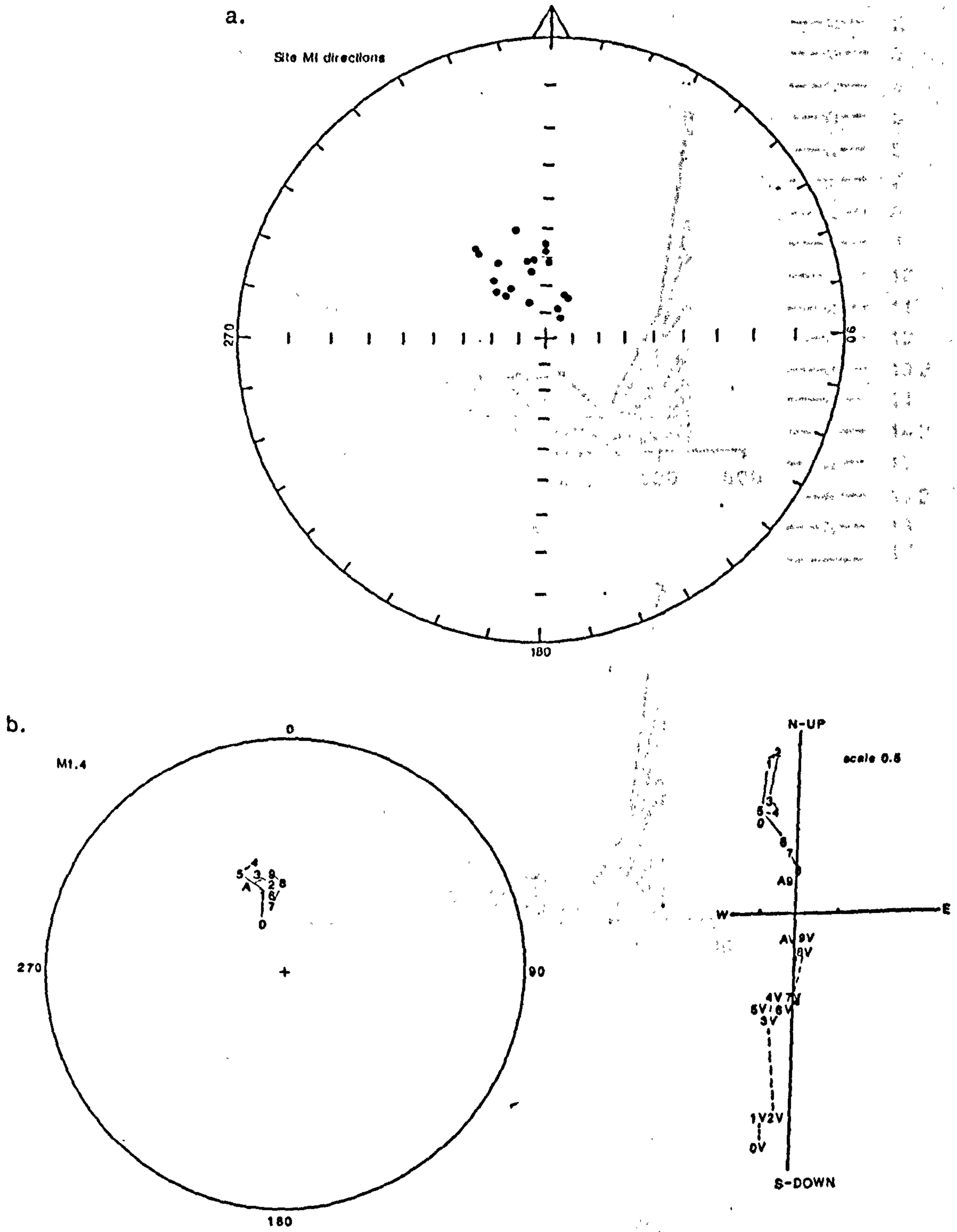

fig. 5.27 Summary of demagnetisation behaviour of samples from site M1. Natural remanent magnetism (NRM) intensity is given x $10^{-4}Am^{-1}$; susceptibility units x 10^{-6} GOe^{-1}.
a. stereographic projection of stable sample directions; **b.** stereographic projection and accompanying orthogonal plot illustrating vector movement with progressive demagnetisation; **c.** NRM intensity change with increasing temperature illustrating variation of magnetic mineral content between samples; **d.** normalised NRM change with increasing temperature illustrating within-site variation; **e.** susceptibility variation with increasing temperature illustrating changes which occur due to mineralogical alteration.

c

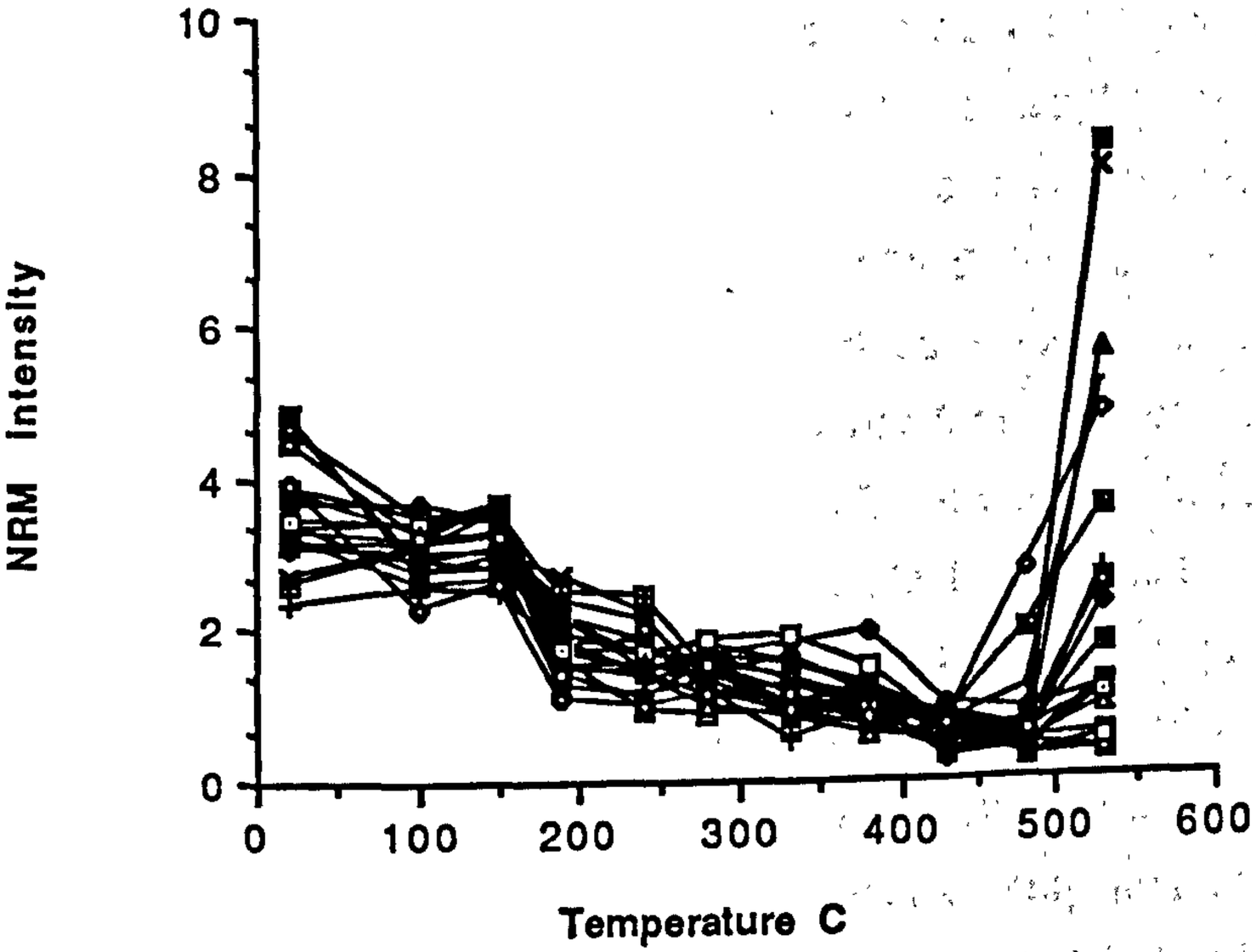
NRM Intensity
10
8
6
4
2
0
0
100
200
300
400
500
600
Temperature C

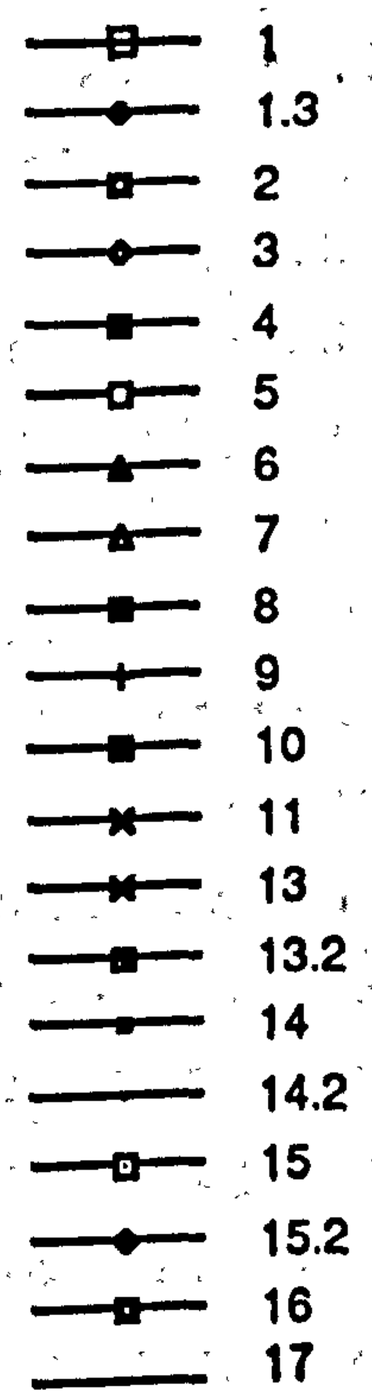
1
1.3
2
3
4
5
6
7
8
9
10
11
13
13.2
14
14.2
15
15.2
16
17

d

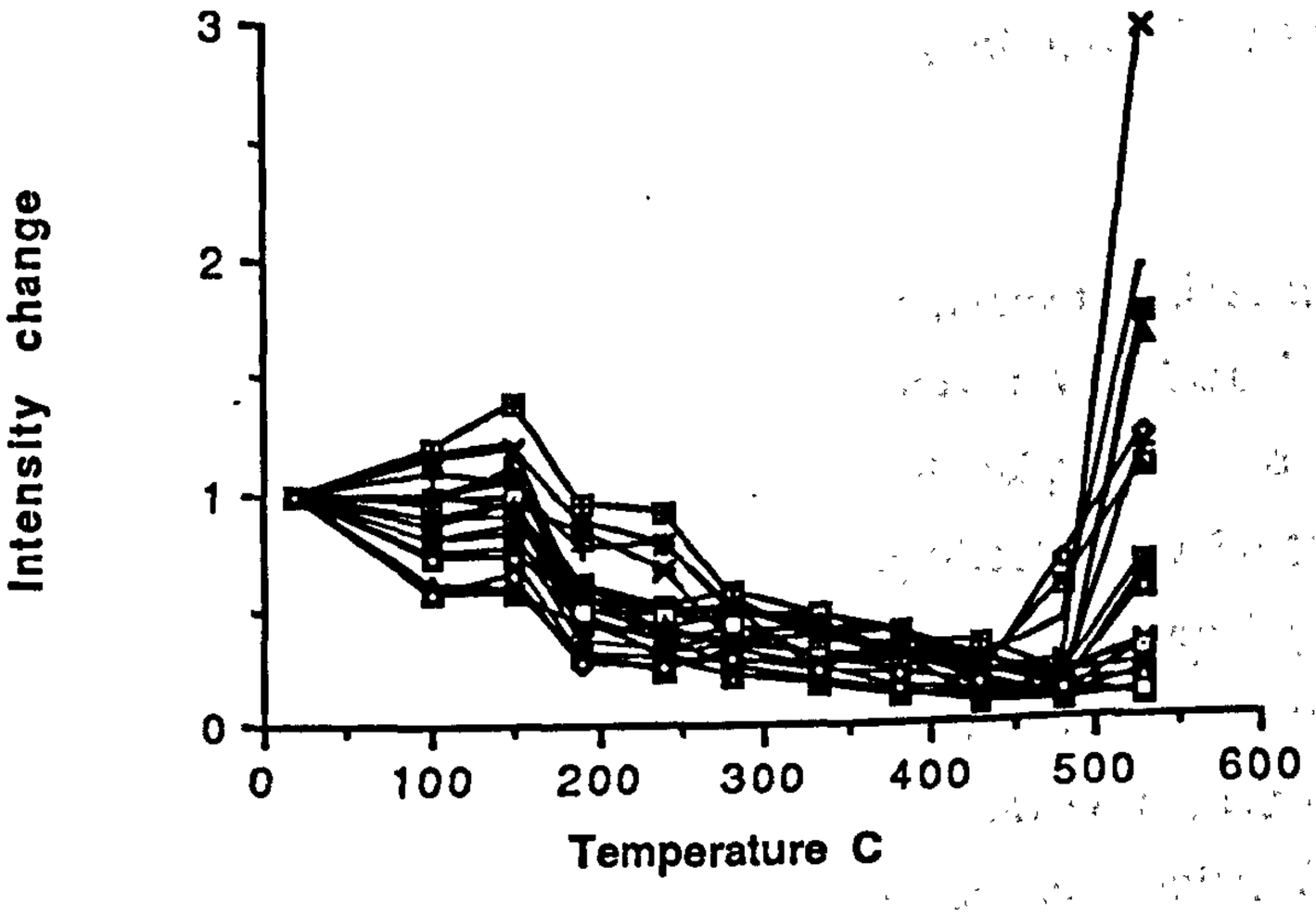
Intensity change
3
2
1
0
0
100
200
300
400
500
600
Temperature C

e

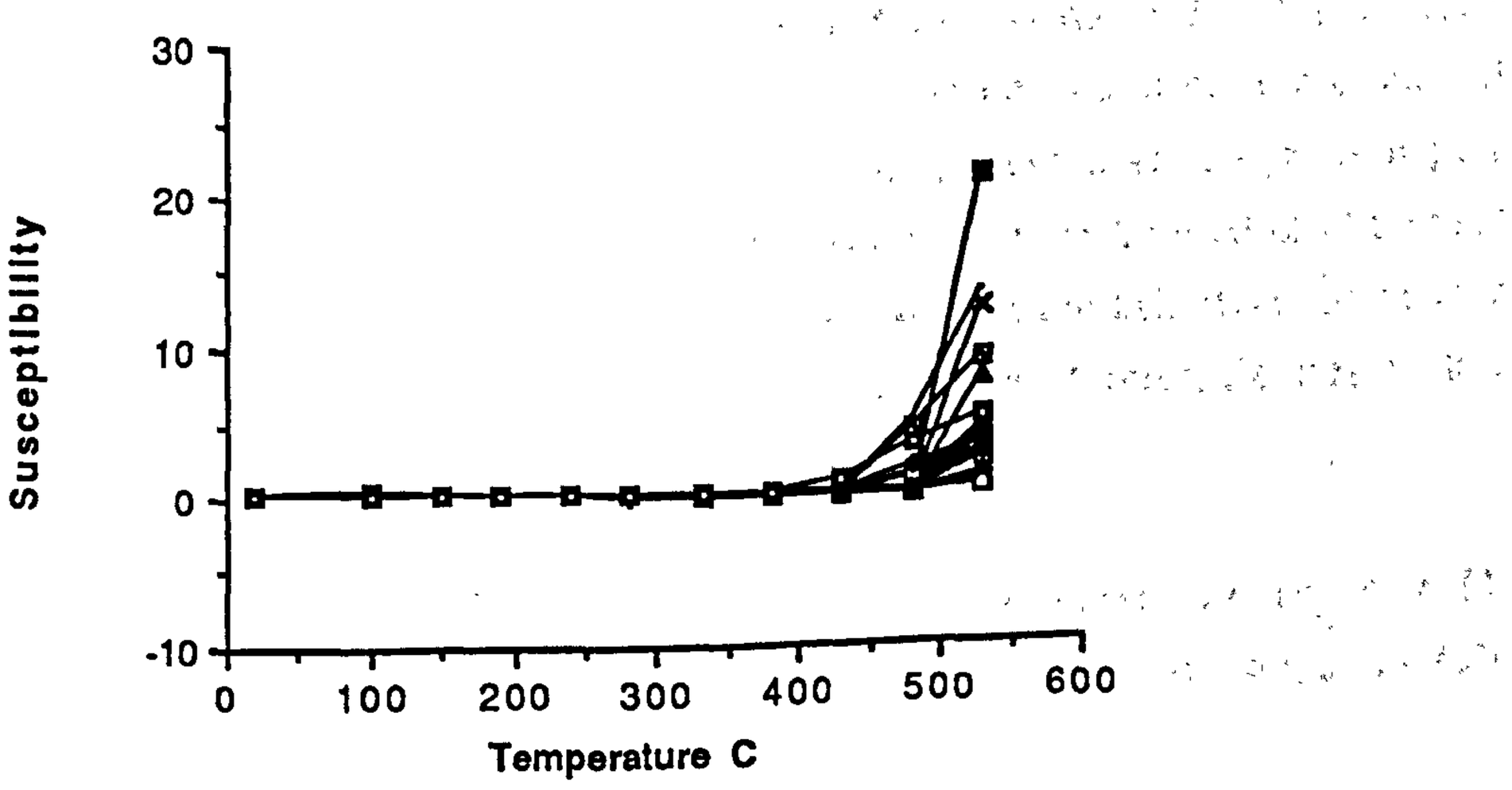
Susceptibility
30
20
10
0
-10
0
100
200
300
400
500
600
Temperature C

Site M2 (fig. 5.28) Maximum initial natural remanent magnetism intensity of 1.35 x $10^{-4}Am^{-1}$ and susceptibility of -0.07 (volume units x $10^{-6}GOe^{-1}$; see appendix 4.2) indicate that magnetic mineral content is low. There is little within site variation of susceptibility and intensity values. Increase of intensity and susceptibility at around 350°C -390°C represents the formation of magnetite or maghemite from the oxidation of pyrite or pyrrhotite. This suggests that the natural remanent magnetism carrier is pyrrhotite. Site directions are only defined up to 250°C. These are clearly defined and most have steep inclinations. The mean of these steep directions lies close to the present day field direction. Several site directions do not form part of this group but have equatorial inclinations (samples 1,4,11 and 14 AF). It may be that there is more than one natural remanent magnetism component. Sample 1 illustrates the demagnetisation of these components; the initial direction is similar to present day, but moves to an equatorial direction at higher temperatures. Within site variation of site directions seems to be due to the presence of more than one natural remanent magnetism component, the most stable of which is of normal polarity and approximates to the present day direction. The other component has an equatorial direction which is not on the apparent field direction wander path; this could be a displaced Permian direction or is otherwise unexplained.

Site M3 (fig. 5.29) Maximum initial natural remanent magnetism intensity of 1.52 x $10^{-4}Am^{-1}$ and susceptibility of 0.12 (volume units x $10^{-6}GOe^{-1}$; see appendix 4.2) indicate that magnetic mineral content is low. Intensity decreases steadily to around 350°C in most samples, which suggests that pyrrhotite may be the natural remanent magnetism carrier. Some samples lose all their natural remanent magnetism by around 100°C which indicates that goethite carries a viscous natural remanent magnetism in these samples. Susceptibility remains constant until above around 350°C, this indicates the oxidation of pyrite or pyrrhotite to magnetite or maghemite. There is a variety of vector behaviour with progressive demagnetisation and there is no consistency between samples. In all samples more than one component is involved, with a mixture of normal and reversed polarity components and the direction becomes reversed at higher temperatures. However, the inconsistency of the directions from both AF and thermal demagnetisation and the fact that no directions lie on the apparent field direction wander path, makes interpretation difficult. Site directions are uninterpretable due to low intensity and complex magnetisations.

Site M27 (fig. 5.30) Maximum initial natural remanent magnetism intensity of 5.41 x $10^{-4}Am^{-1}$ and susceptibility of -0.29 (volume units x $10^{-6}GOe^{-1}$; see appendix 4.2)

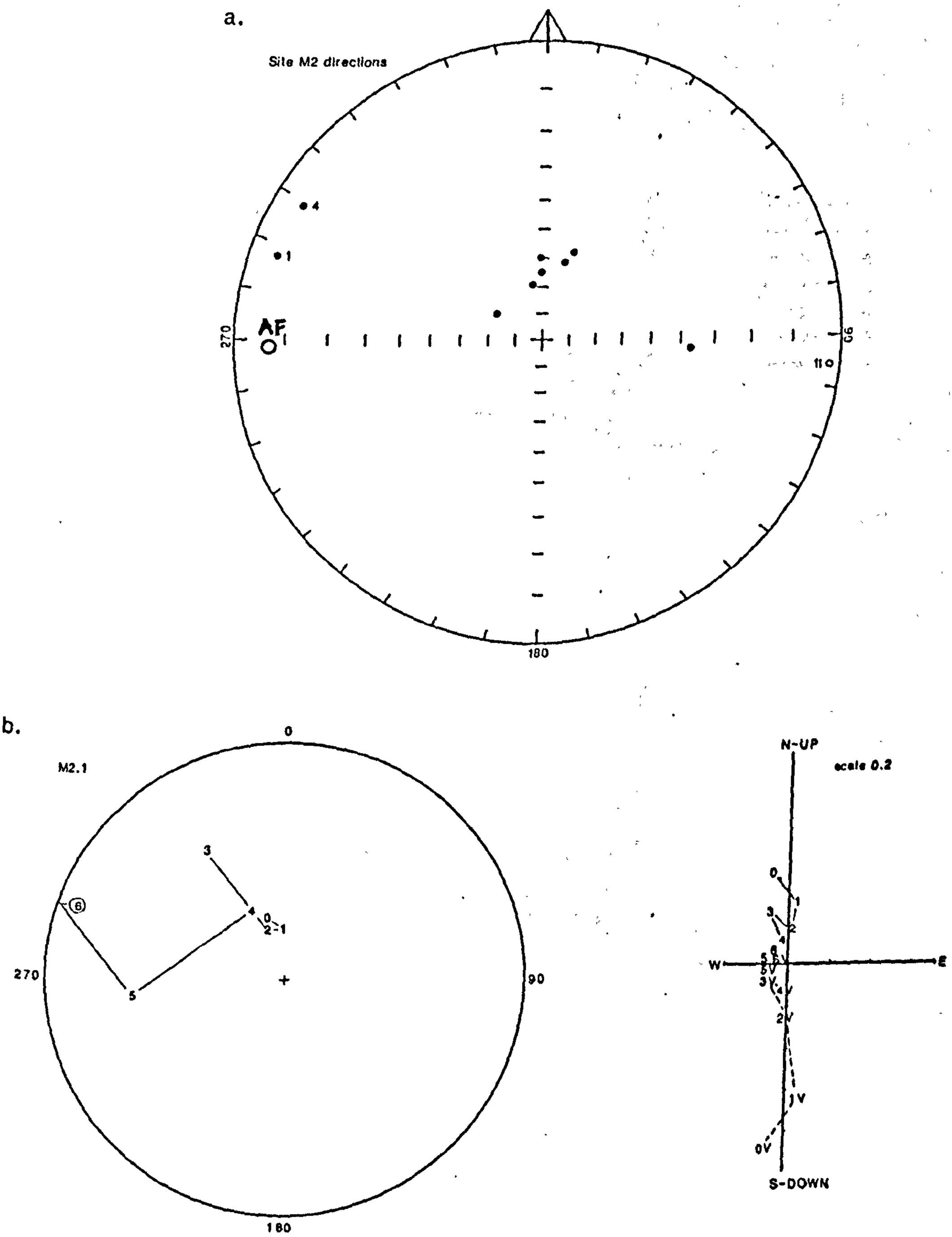

fig. 5.28 Summary of demagnetisation behaviour of samples from site M2. Natural remanent magnetism (NRM) intensity is given x $10^{-4}Am^{-1}$; susceptibility units x 10^{-6} GOe^{-1}
a. stereographic projection of stable sample directions; **b.** stereographic projection and accompanying orthogonal plot illustrating vector movement with progressive demagnetisation; **c.** NRM intensity change with increasing temperature illustrating variation of magnetic mineral content between samples; **d.** normalised NRM change with increasing temperature illustrating within-site variation; **e.** susceptibility variation with increasing temperature illustrating changes which occur due to mineralogical alteration.

c

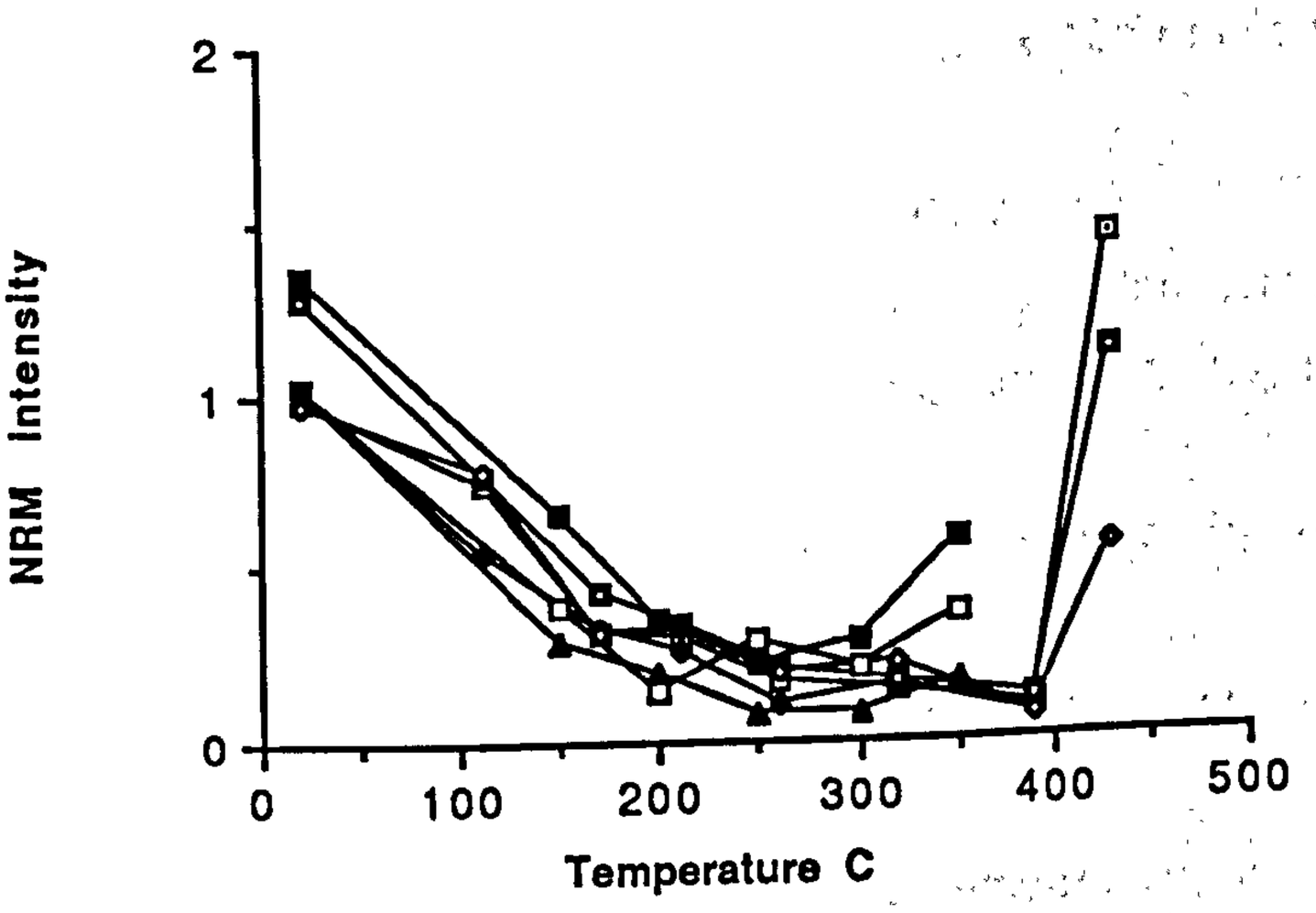
NRM Intensity
2
1
0
0
100
200
300
400
500
Temperature C
1
3
4
5
6
8
12

d

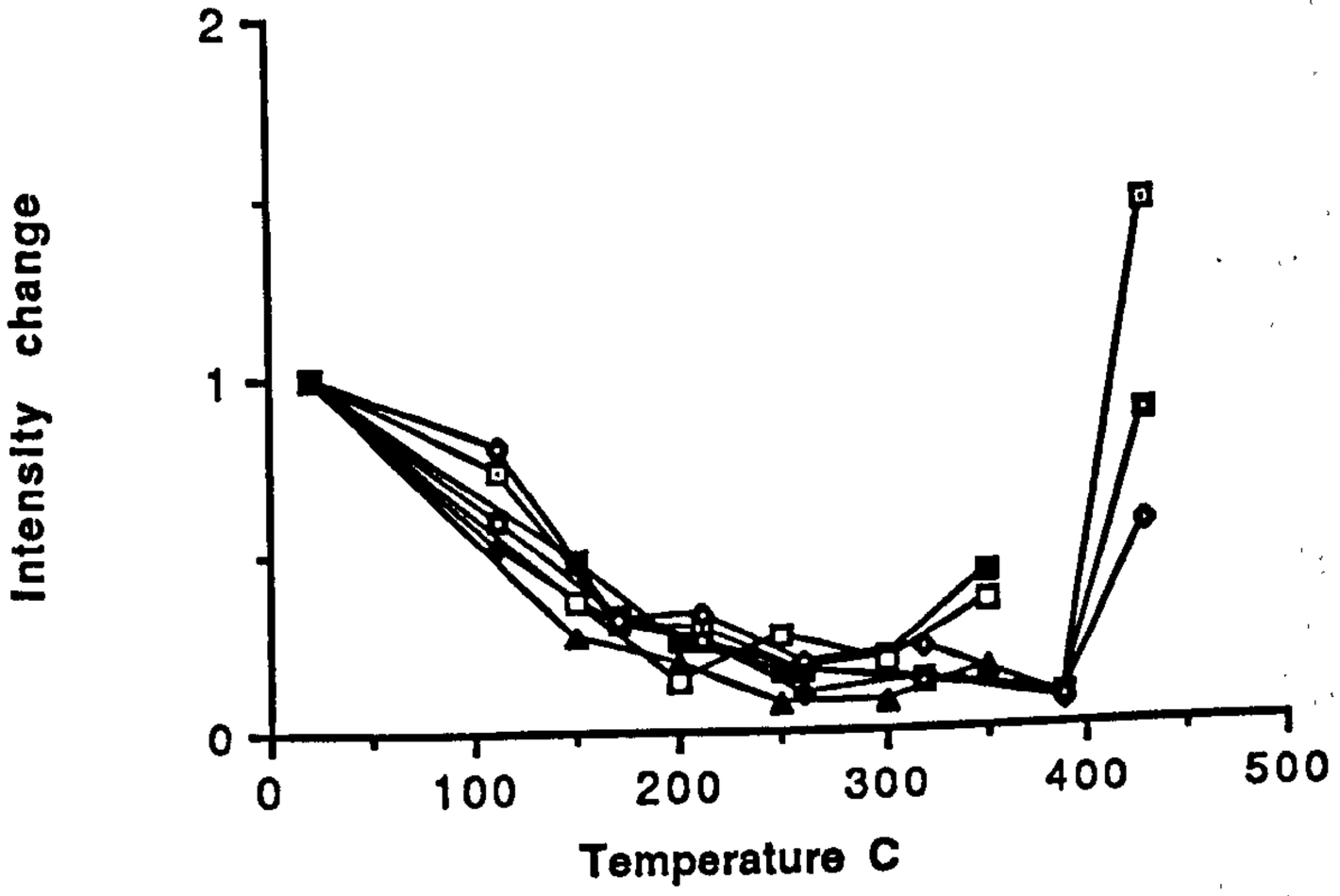
Intensity change
2
1
0
0
100
200
300
400
500
Temperature C

e

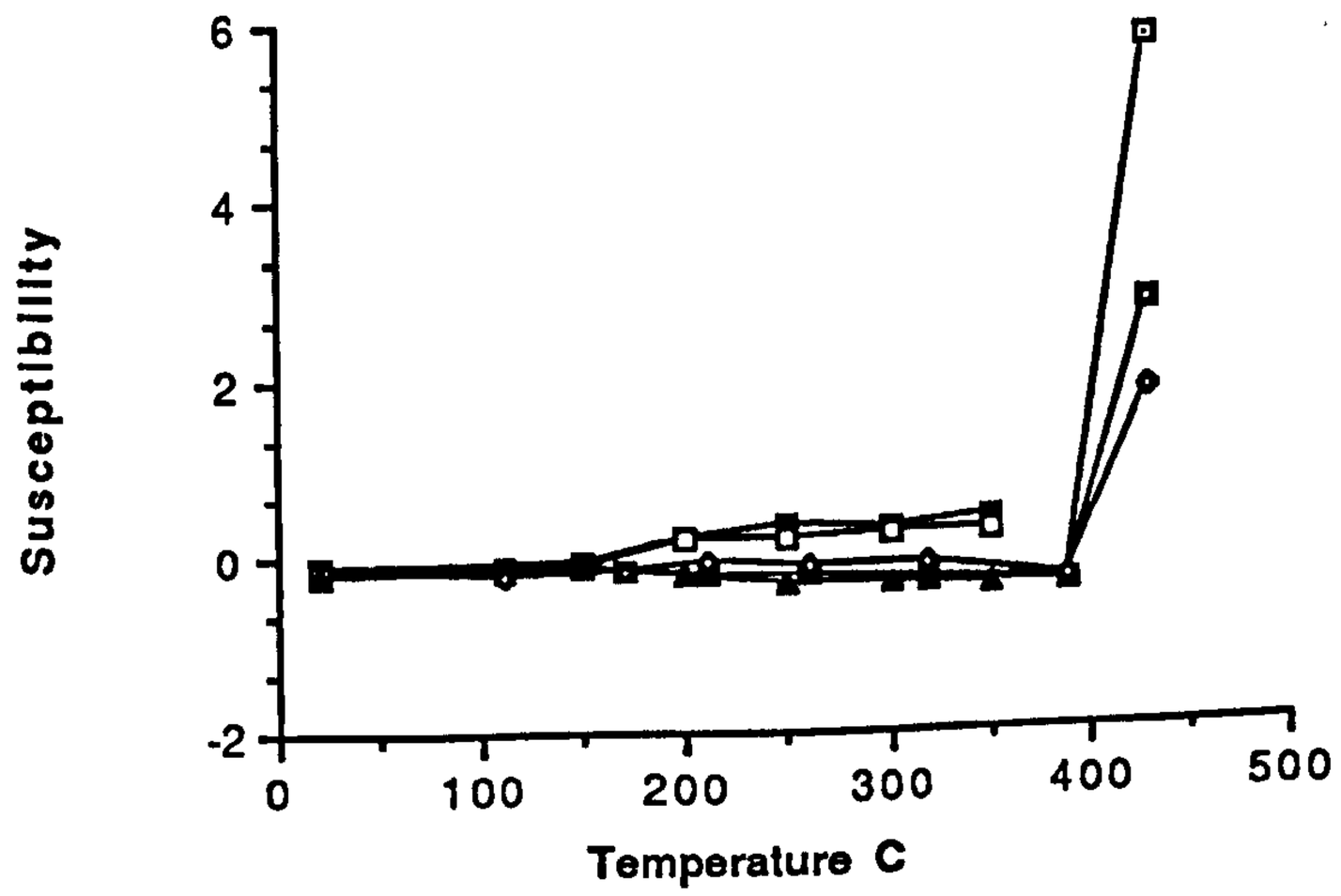
Susceptibility
6
4
2
0
-2
0
100
200
300
400
500
Temperature C

fig. 5.29 Summary of demagnetisation behaviour of samples from site M3. Natural remanent magnetism (NRM) intensity is given x $10^{-4}Am^{-1}$; susceptibility In units x 10^{-6} GOe^{-1}

a. stereographic projection of stable sample directions;

b. and **c.** stereographic projections and accompanying orthogonal plots illustrating vector movement with progressive demagnetisation for samples with different behaviour;

d. NRM intensity change with increasing temperature illustrating variation of magnetic mineral content between samples;

e. normalised NRM change with increasing temperature illustrating within-site variation;

f. susceptibility variation with increasing temperature illustrating changes which occur due to mineralogical alteration.

a.

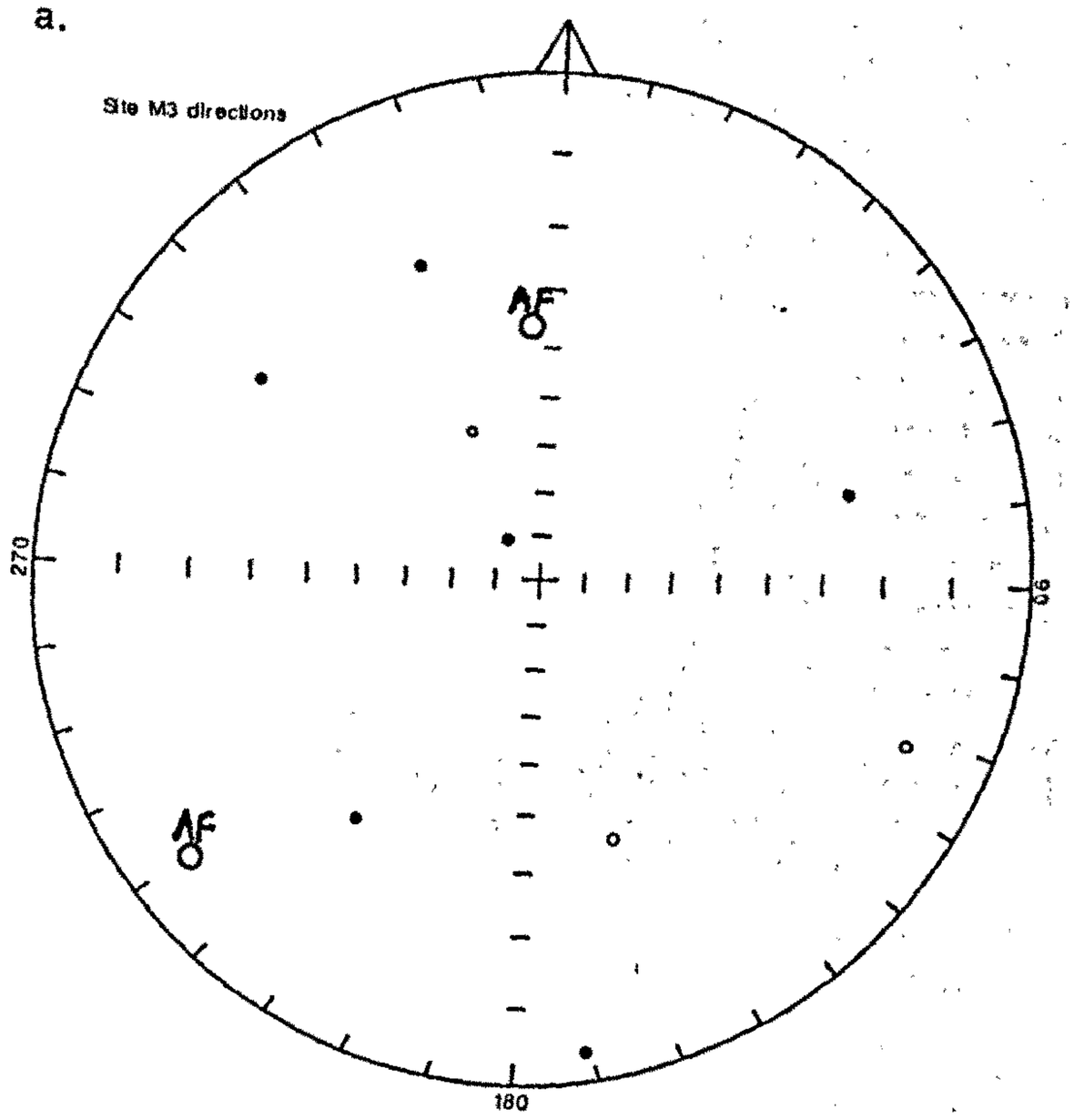
Site M3 directions
NF
270
90
180

b.

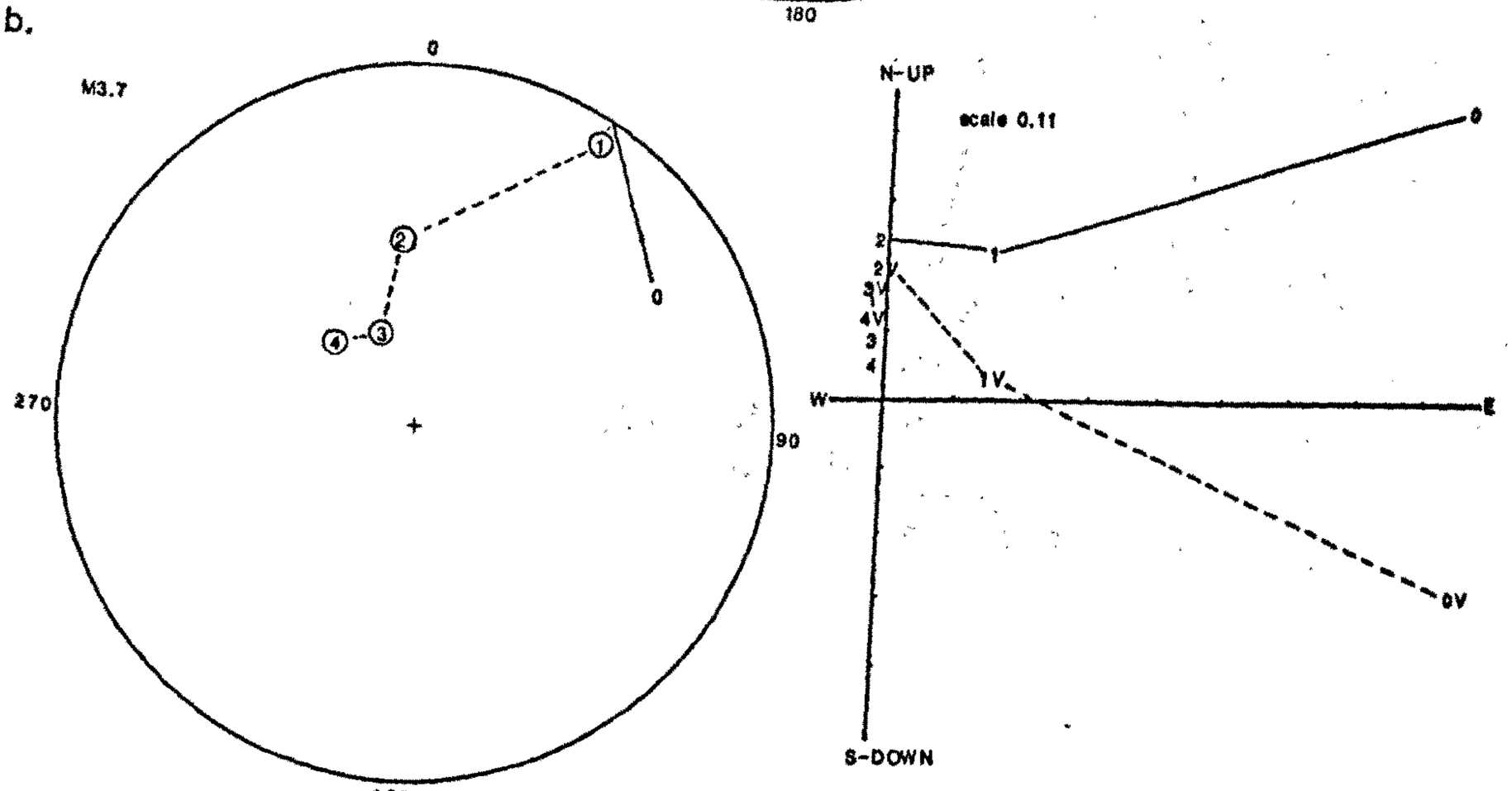
M3.7
0
90
180
270
N-UP
scale 0.11
W
E
S-DOWN

C.

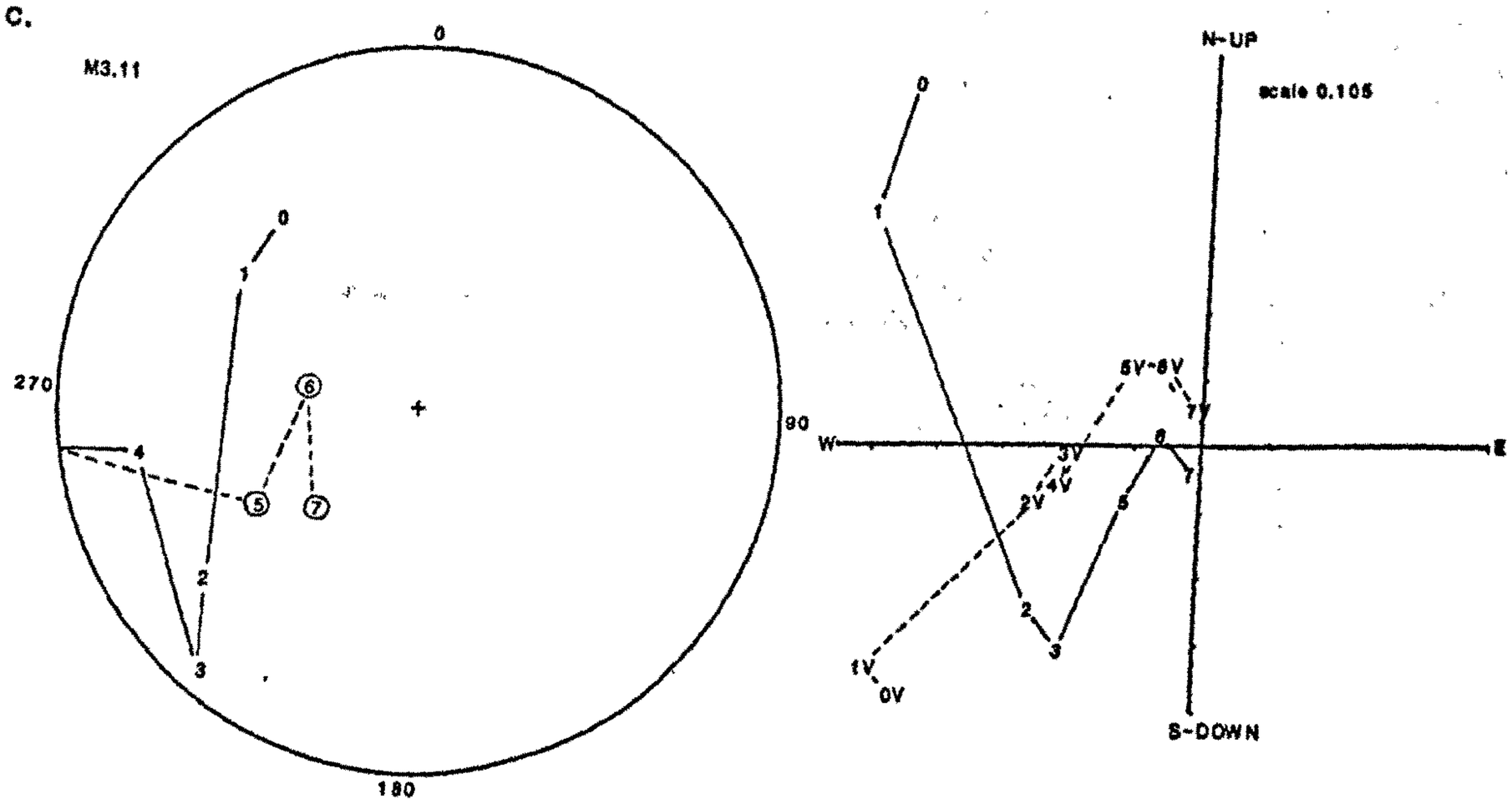
M3.11
0
90
180
270
N-UP
scale 0.105
W
E
S-DOWN

d

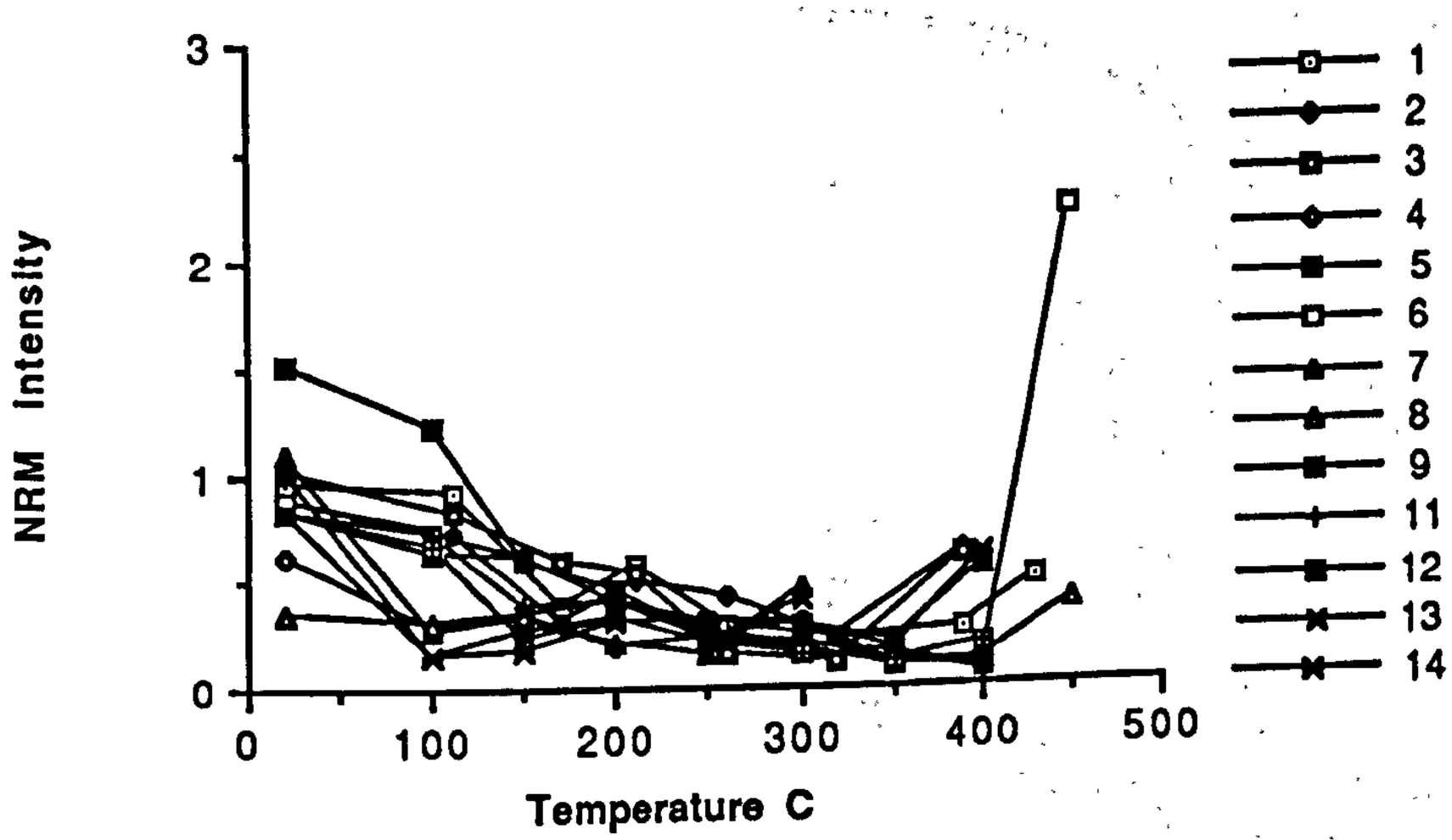
NRM Intensity
3
2
1
0
0
100
200
300
400
500
Temperature C
1
2
3
4
5
6
7
8
9
11
12
13
14

e

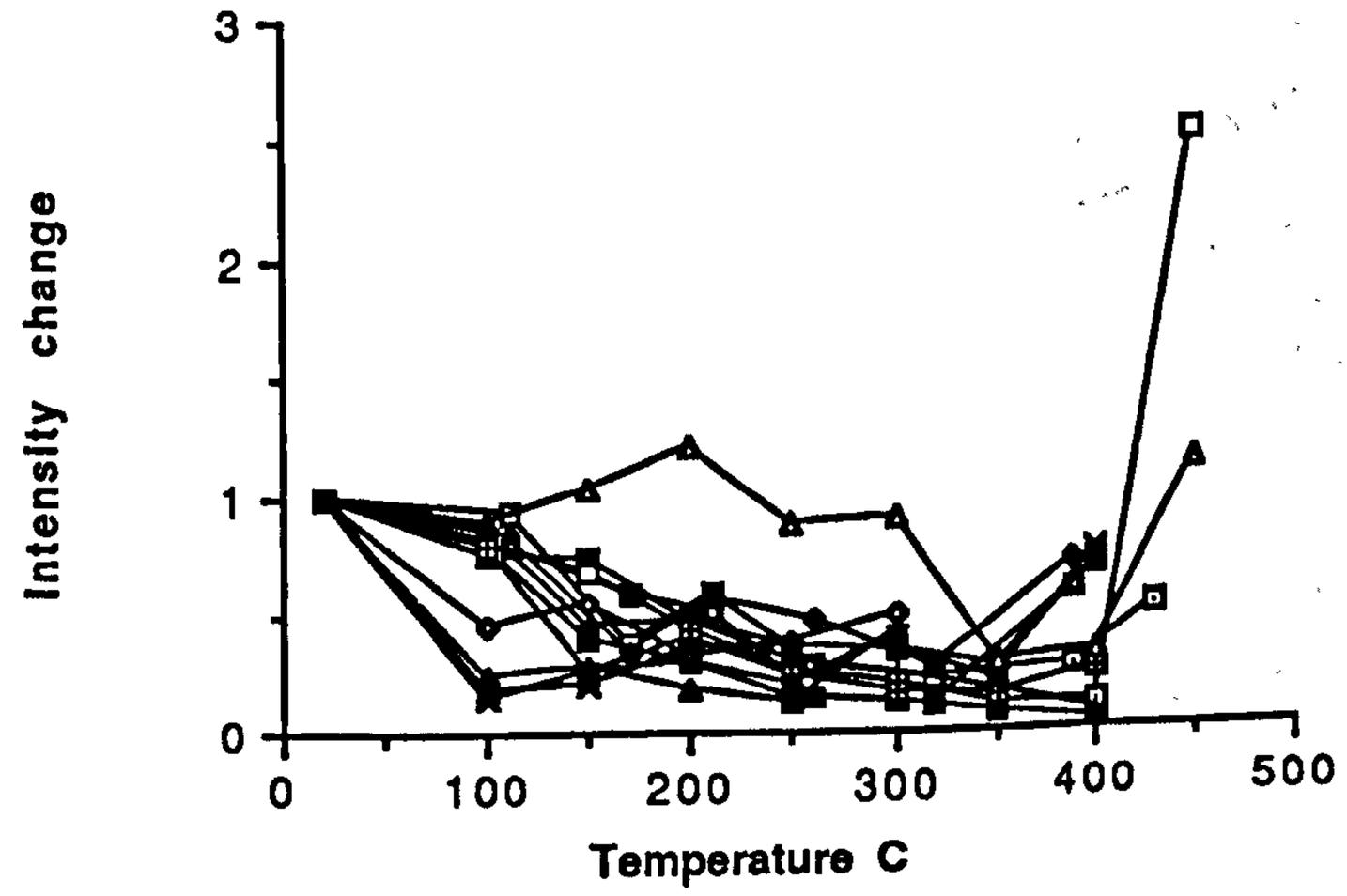
Intensity change
3
2
1
0
0
100
200
300
400
500
Temperature C

f

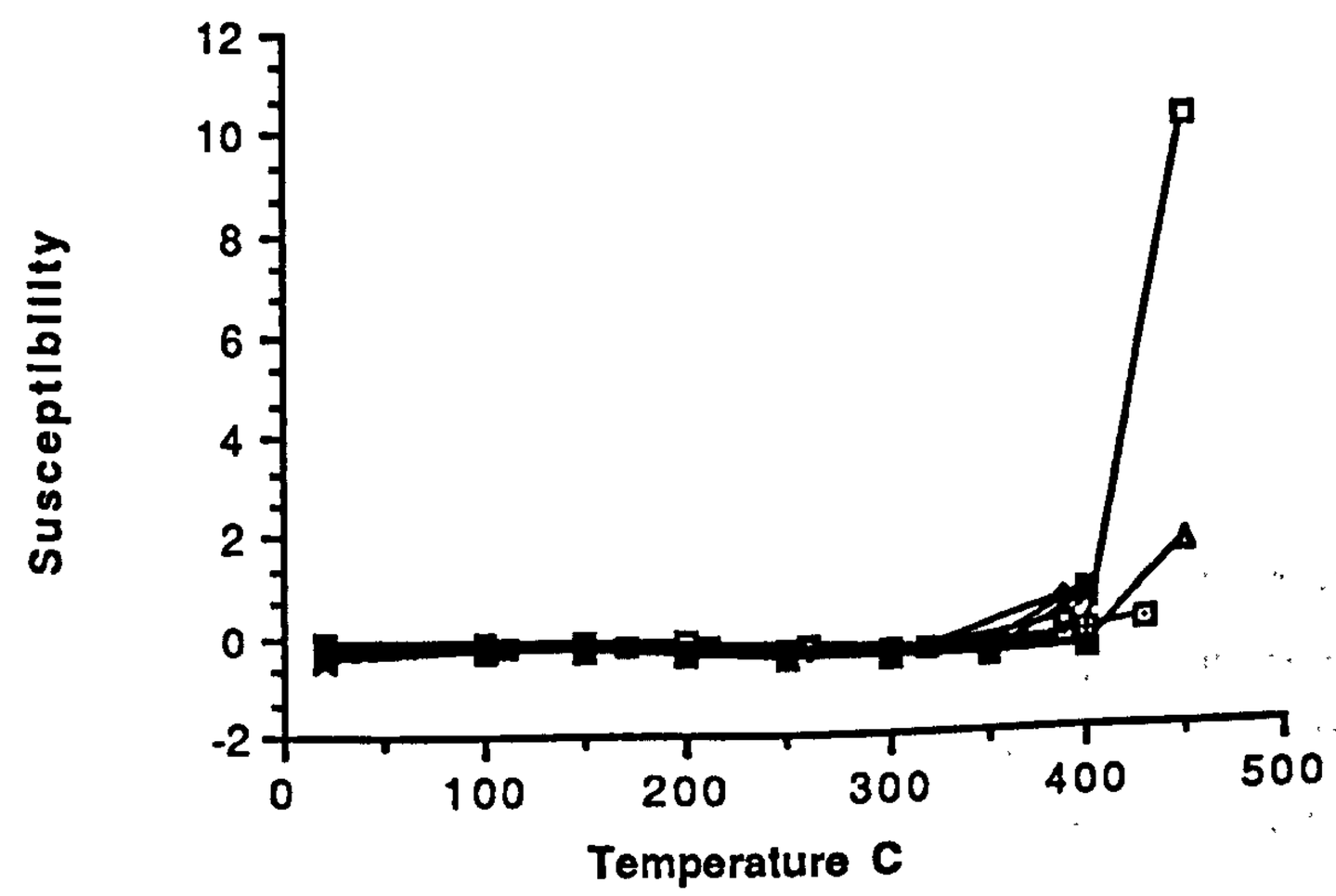
Susceptibility
12
10
8
6
4
2
0
-2
0
100
200
300
400
500
Temperature C

a.

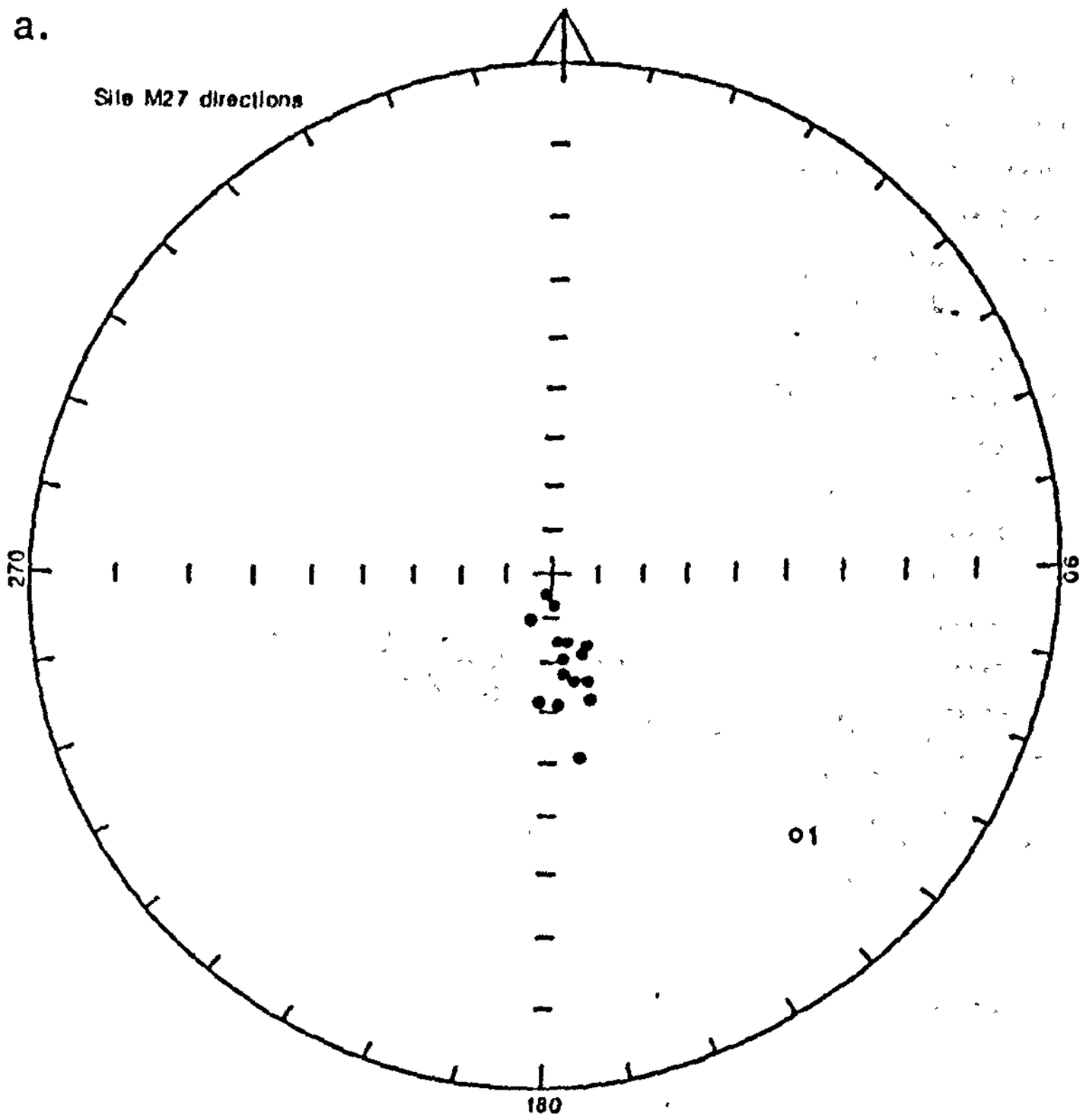

b.

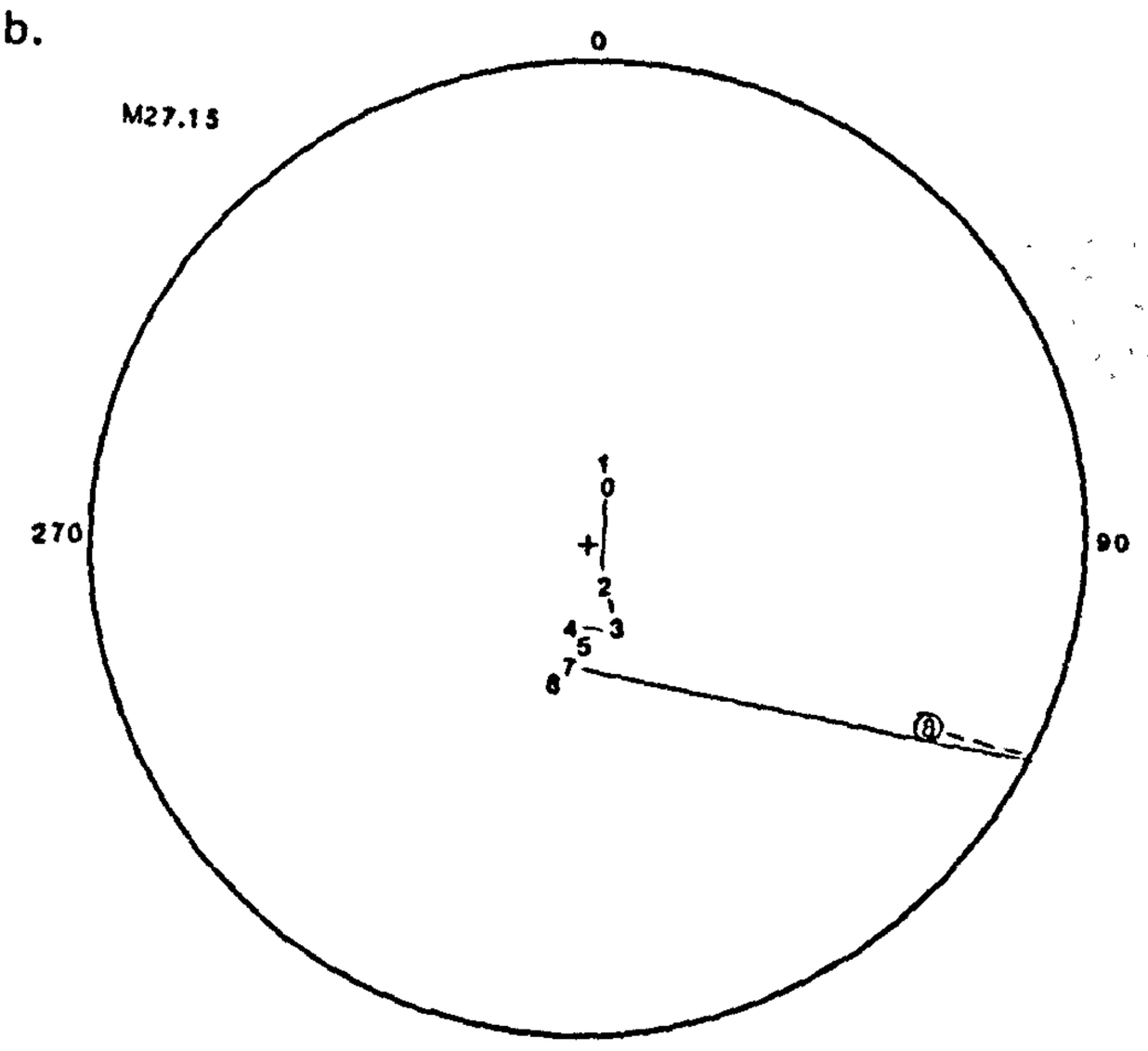

fig. 5.30 Summary of demagnetisation behaviour of samples from site M27. Natural remanent magnetism (NRM) intensity is given x $10^{-4}Am^{-1}$; susceptibility units x 10^{-6} GOe^{-1}.
a. stereographic projection of stable sample directions; **b.** stereographic projection and accompanying orthogonal plot illustrating vector movement with progressive demagnetisation; **c.** NRM intensity change with increasing temperature illustrating variation of magnetic mineral content between samples; **d.** normalised NRM change with increasing temperature illustrating within-site variation; **e.** susceptibility variation with increasing temperature illustrating changes which occur due to mineralogical alteration.

c

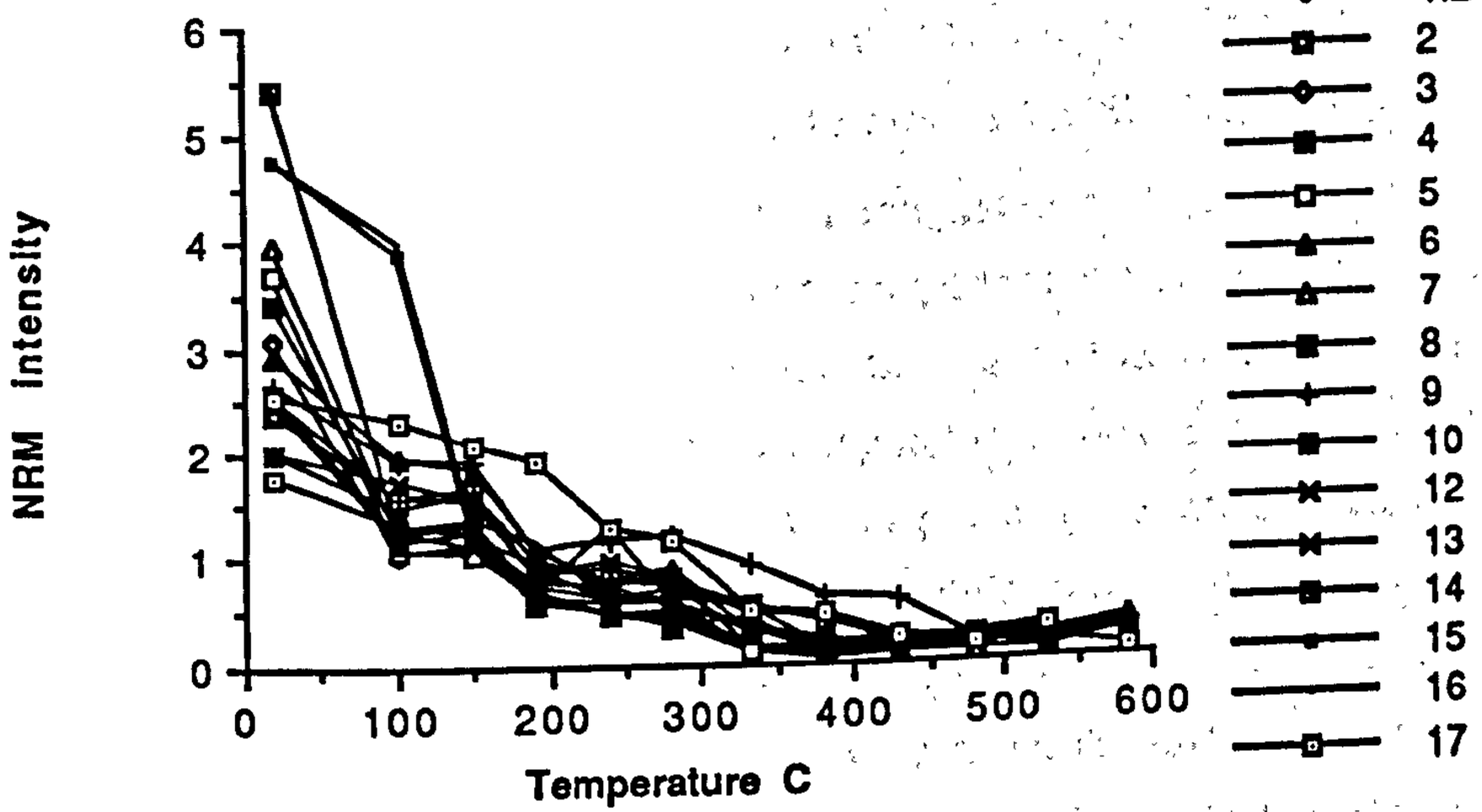
NRM Intensity
0
1
2
3
4
5
6
0
100
200
300
400
500
600
Temperature C
1
1.2
2
3
4
5
6
7
8
9
10
12
13
14
15
16
17

d

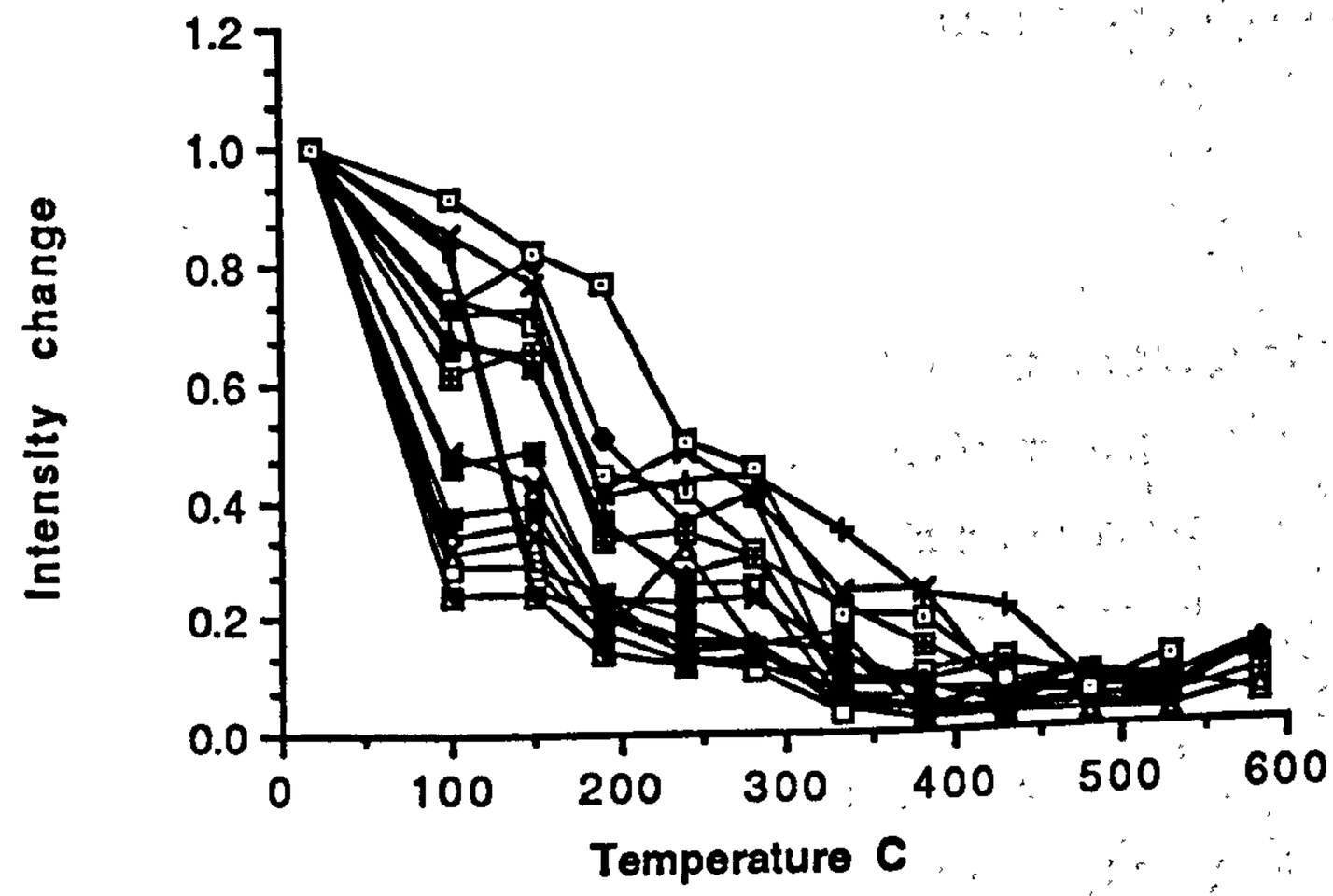
Intensity change
0.0
0.2
0.4
0.6
0.8
1.0
1.2
0
100
200
300
400
500
600
Temperature C

e

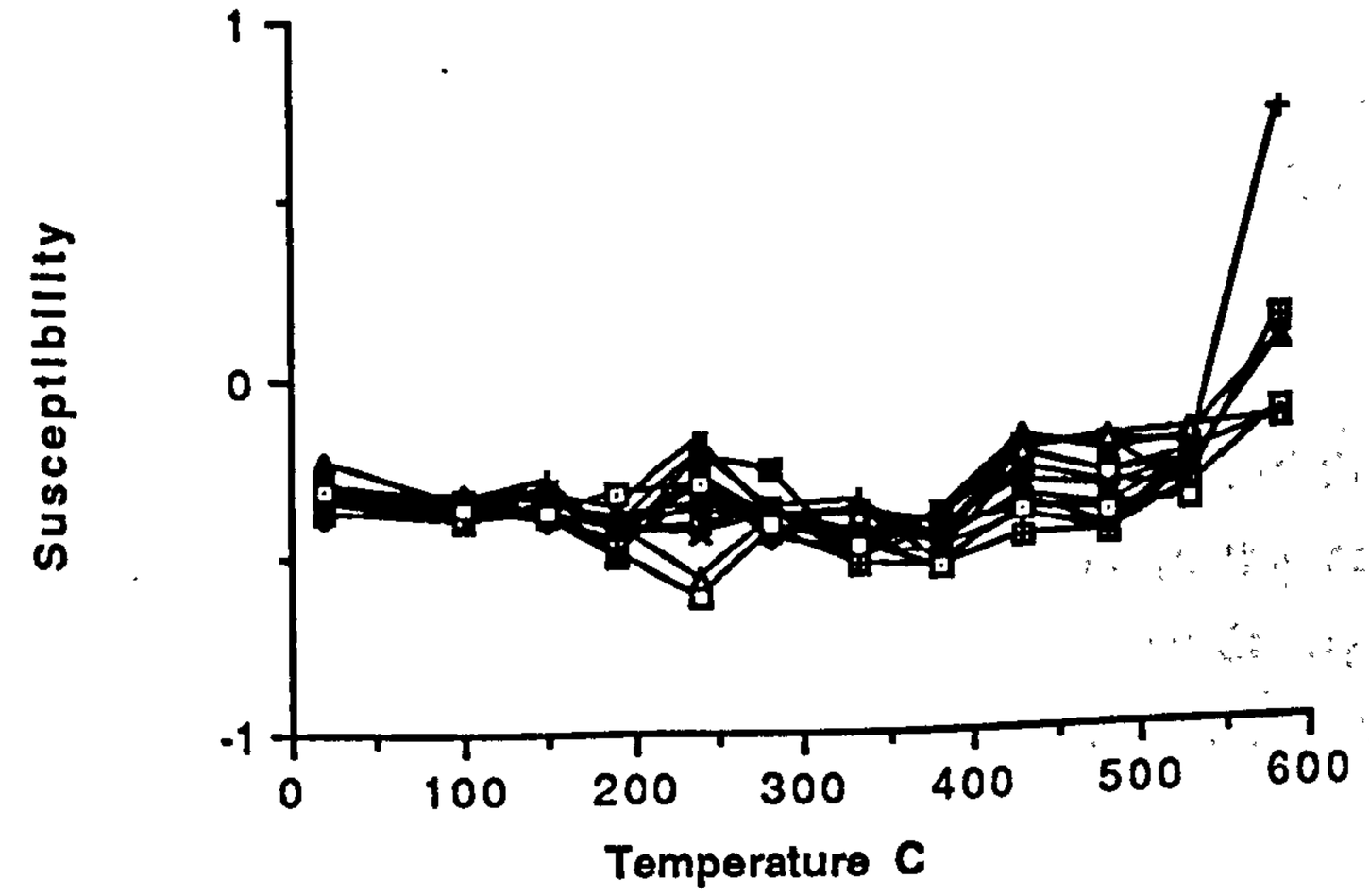
Susceptibility
-1
0
1
0
100
200
300
400
500
600
Temperature C

indicate that magnetic mineral content is moderate and that haematite is the likely natural remanent magnetism carrier. There is very little within site variation of intensity or susceptibility values with progressive demagnetisation. Some samples rapidly lose natural remanent magnetism intensity to around 150°C, this indicates the removal of a viscous natural remanent magnetism component carried by goethite. Above this temperature demagnetisation is gradual up to around 530°C. This T_b suggests that impure, multi-domain or pseudo-single domain magnetite or haematite may be the natural remanent magnetism carrier. The main component is near-vertical and normal polarity. The directions form a well defined group, the mean of which does not lie on the apparent field direction wander path. At high temperatures some samples have vectors which move to a reversed polarity, low inclination position. Sample 1 also has this vector defined even at lower temperatures. This site defines a reversed direction which has the same inclination as the apparent field direction wander path at 230 Ma, but differs in declination by 30°. This site contains two vectors, the end points of which are not fully resolved. This causes the site mean to be deflected from the apparent field direction wander path. The likely end-points are present day and 230 Ma in age.

Summary (table 5.8 and fig. 5.31)

i. 1 out of 4 sites has unresolved natural remanent magnetism directions; site M3 did not have stable natural remanent magnetism directions;

ii. several sites have more than one magnetic component;

iii. goethite commonly carries a viscous natural remanent magnetism;

iv. most directions are normal polarity and high inclination suggesting Tertiary age, although some reversed, shallow inclination directions are present in some samples;

v. pyrrhotite and impure, multi-domain or pseudo-single domain magnetite/haematite are the natural remanent magnetism carriers;

vi. pyrite/pyrrhotite is present in some samples.

5.4.6 Basin facies

Three sites were sampled for palaeomagnetic analysis in the basin facies; these were in Lamar limestone, L1 (the basinal equivalent to the section at McKittrick Canyon) and in the older strata of the Brushy Canyon and Cherry Canyon sandstones (sites BC1 and CC1 respectively). A summary of the demagnetisation behaviour for

site	stable proportion	N	site mean direction dec	inc	A95	pole(North) lat.	long.(E)	polarity
M1	20 of 20	20	341.6	67.8	5.4	66.8	224.7	N
M2	8 of 8	6	0	64.5	10.3	76.7	255.2	N
		4	299.7	-1.7	17.6	24.3	147.6	N
M3	7 of 13							
M27	17 of 17	16	169.5	69.7	4.5	4	81.4	N
		1						R

site	intensity (max.)	susc. (max.)	blocking temperature C	magnetic minerals	interpreted age
M1	4.85	0.34	100, 480	G,M/H	80my
M2	1.35	-0.07	350	P	<20my
M3	1.52	-0.12	100, 350		
M27	5.41	-0.29	100	G,H	Tertiary
			530	G,H	230 my

table 5.8 Summary of mean directions and other data for sites in the basin margin facies

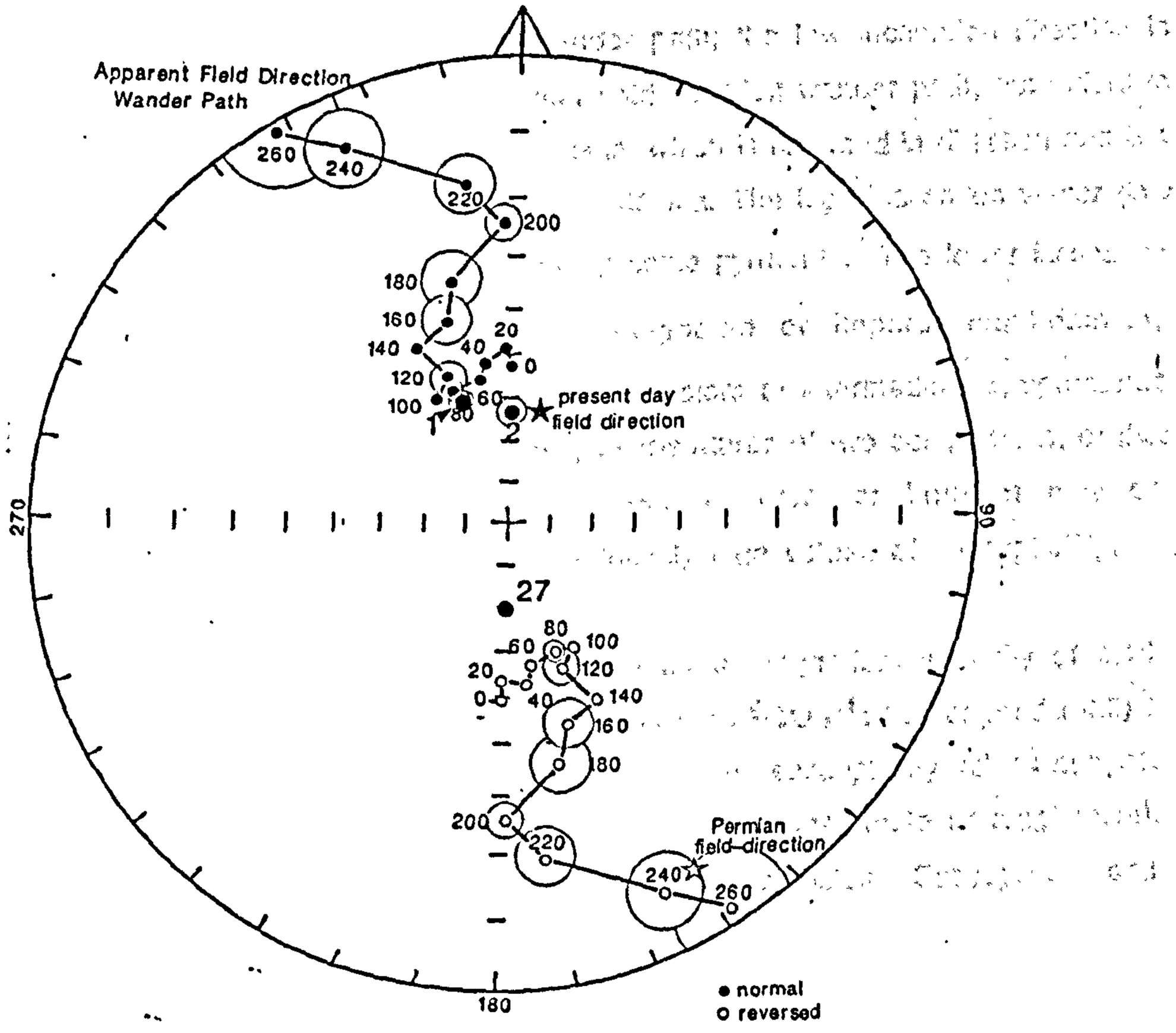

fig. 5.31 Stereographic projection of mean directions for sites in the basin margin facies

sites from the basin facies, and interpretations of vectors and magnetic mineralogy are as follows:

Site L1 (fig. 5.32) Maximum initial natural remanent magnetism intensity of 24.07 x $10^{-4}Am^{-1}$ and susceptibility of 1.78 (volume units x $10^{-6}GOe^{-1}$; see appendix 4.2) indicate high magnetic mineral content. There is little within site variation of intensity or susceptibility to the extent that graphs of intensity change from separate samples superimpose on each other. Two inflection points on the graph of normalised intensity change with progessive demagnetisation at 100°C and around150°C indicate that a low temperature, viscous remanent magnetism is carried by goethite and that another, slightly more stable natural remanent magnetism is also carried by goethite. Another inflection point at around 280°C suggests the demagnetisation of pyrrhotite. The presence of an iron sulphide phase is confirmed by the rapid increase in susceptibility above 330°C, which is due to the oxidation of pyrite/pyrrhotite to magnetite or maghemite. Demagnetisation of the remaining natural remanent magnetism is complete by 530°C. Site directions are normal polarity, well defined and stable. A mix of vectors is suggested by the movement of the vector from moderate to low inclinations with increasing demagnetisation steps. These are not easily resolved from the orthogonal projections so the end points *i.e.*, initial and final directions have been taken as best estimates of these vectors. The lower temperature direction is similar to a 180 Ma direction on the apparent field direction wander path; the low inclination direction is similar to a 245 Ma direction on the apparent field direction wander path, but differs in declination by 20°. One sample has an end point which is reversed in direction and lies on the apparent field direction wander path at 245 Ma. The high inclination vector (low T_b) is carried by goethite and also possibly by some pyrrhotite. The lower inclination (high T_b 590°C) direction is carried by magnetite or impure, multi-domain, pseudo-single domain haematite. The spread of vectors at intermediate temperatures suggests either overlap of a range of blocking temperatures of two components, or that the vectors were acquired over a long period of time, or both. It may be pyrite/pyrrhotite or magnetite that causes the initially high values of susceptibility.

Site CC1 (fig. 5.33) Maximum initial natural remanent magnetism intensity of 4.16 x $10^{-4}Am^{-1}$ and susceptibility of 6.56 (volume units x $10^{-6}GOe^{-1}$; see appendix 4.2)) indicate a reasonable magnetic mineral content. The high susceptibility values suggest that high susceptibility magnetic minerals (*e.g.*, pyrrhotite, magnetite or maghemite), or abundant paramagneitic minerals are present in these samples. Susceptibility and

a.

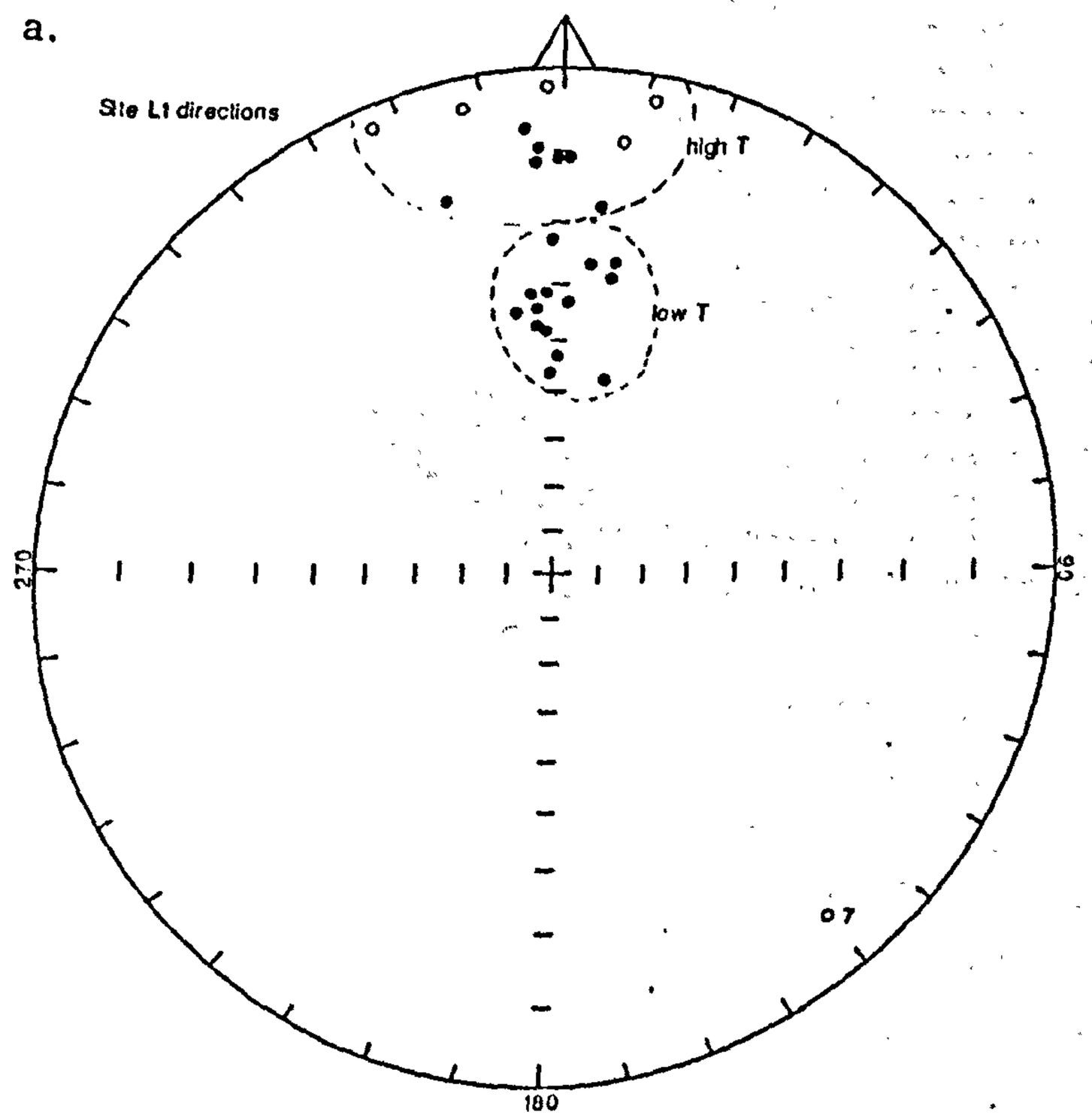

b.

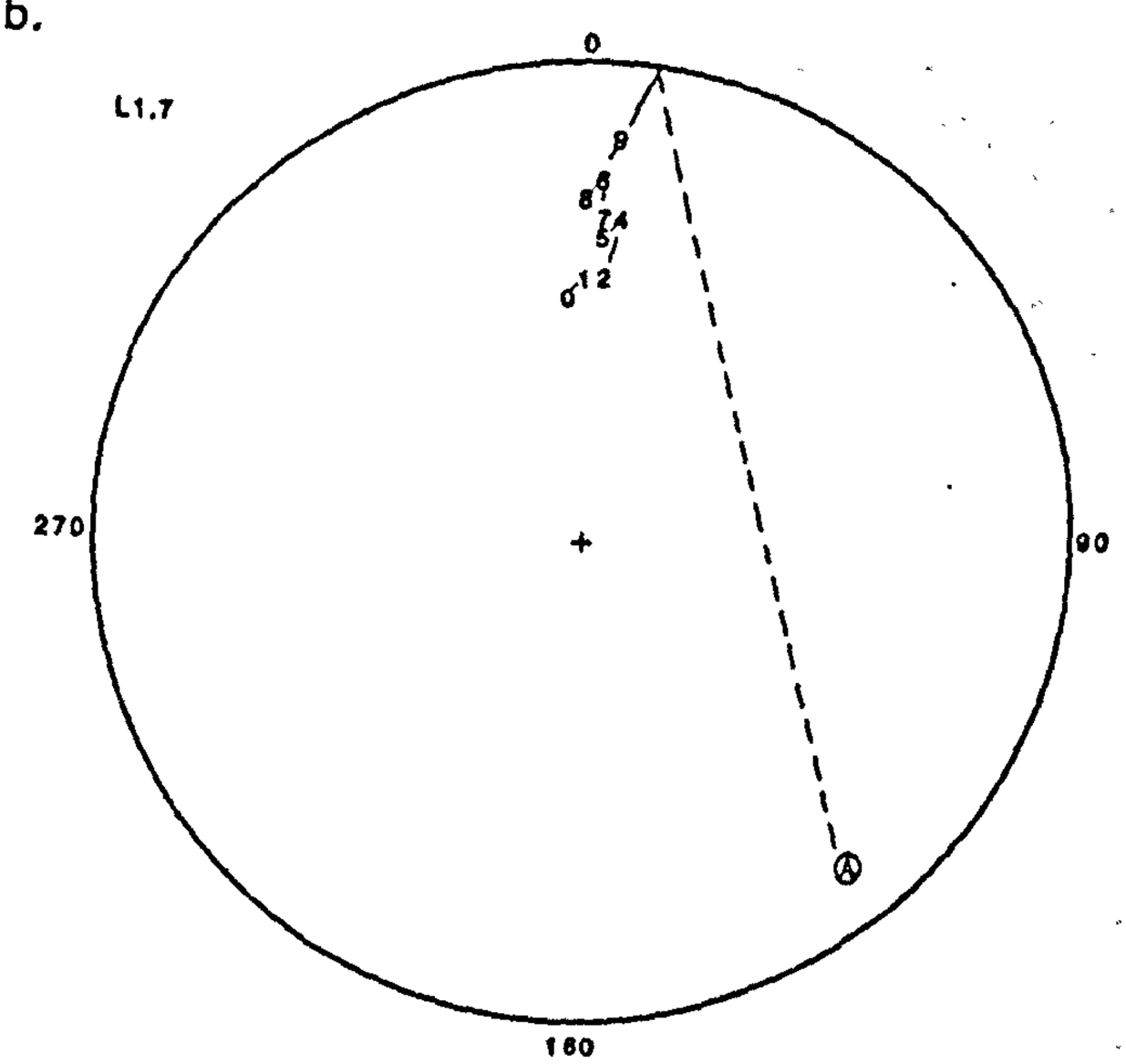

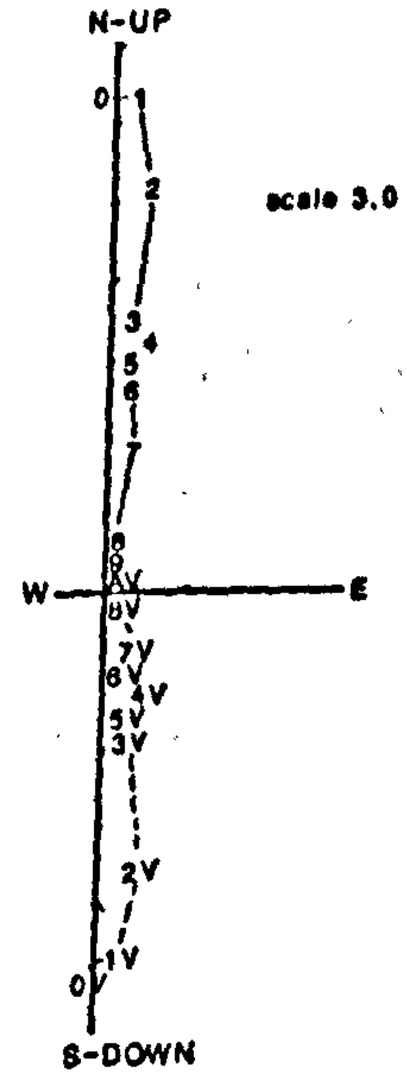

fig. 5.32 Summary of demagnetisation behaviour of samples from site L1. Natural remanent magnetism (NRM) intensity is given x $10^{-4}Am^{-1}$; susceptibility units x 10^{-6} GOe^{-1}
a. stereographic projection of stable sample directions; b. stereographic projection and accompanying orthogonal plot illustrating vector movement with progressive demagnetisation; c. NRM intensity change with increasing temperature illustrating variation of magnetic mineral content between samples; d. normalised NRM change with increasing temperature illustrating within-site variation; e. susceptibility variation with increasing temperature illustrating changes which occur due to mineralogical alteration.

c

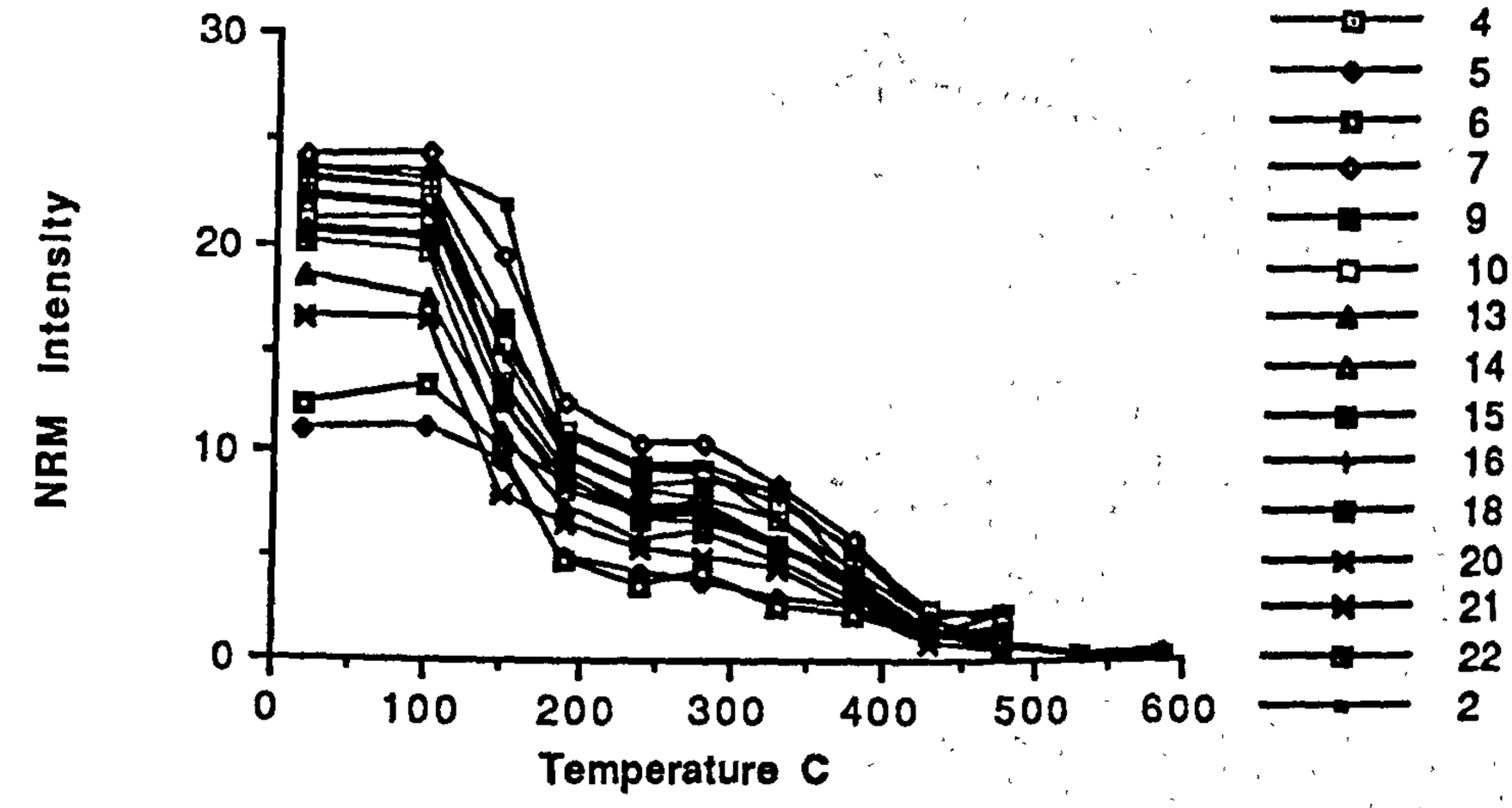
NRM Intensity
30
20
10
0
0
100
200
300
400
500
600
Temperature C
4
5
6
7
9
10
13
14
15
16
18
20
21
22
2

d

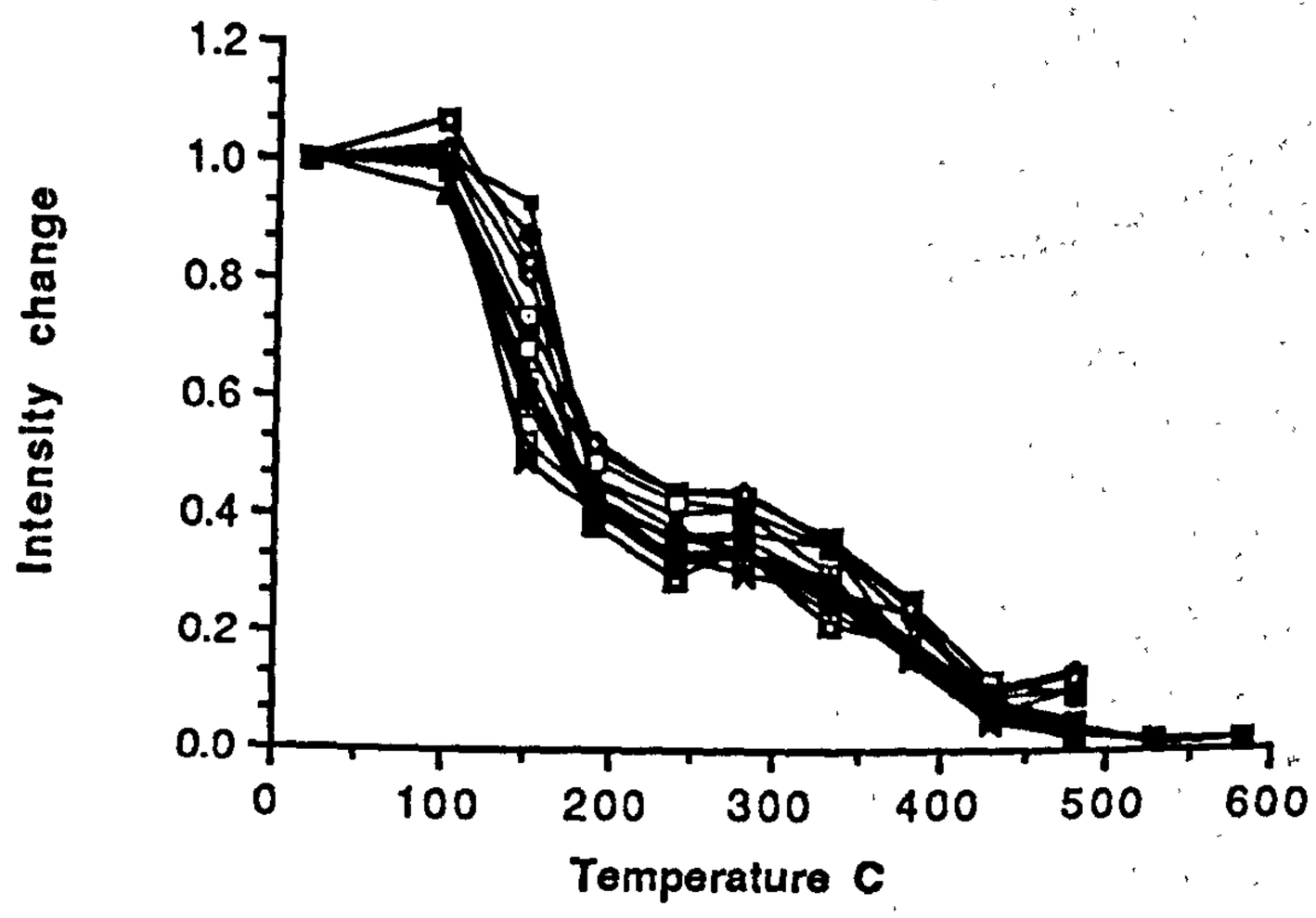
Intensity change
1.2
1.0
0.8
0.6
0.4
0.2
0.0
0
100
200
300
400
500
600
Temperature C

e

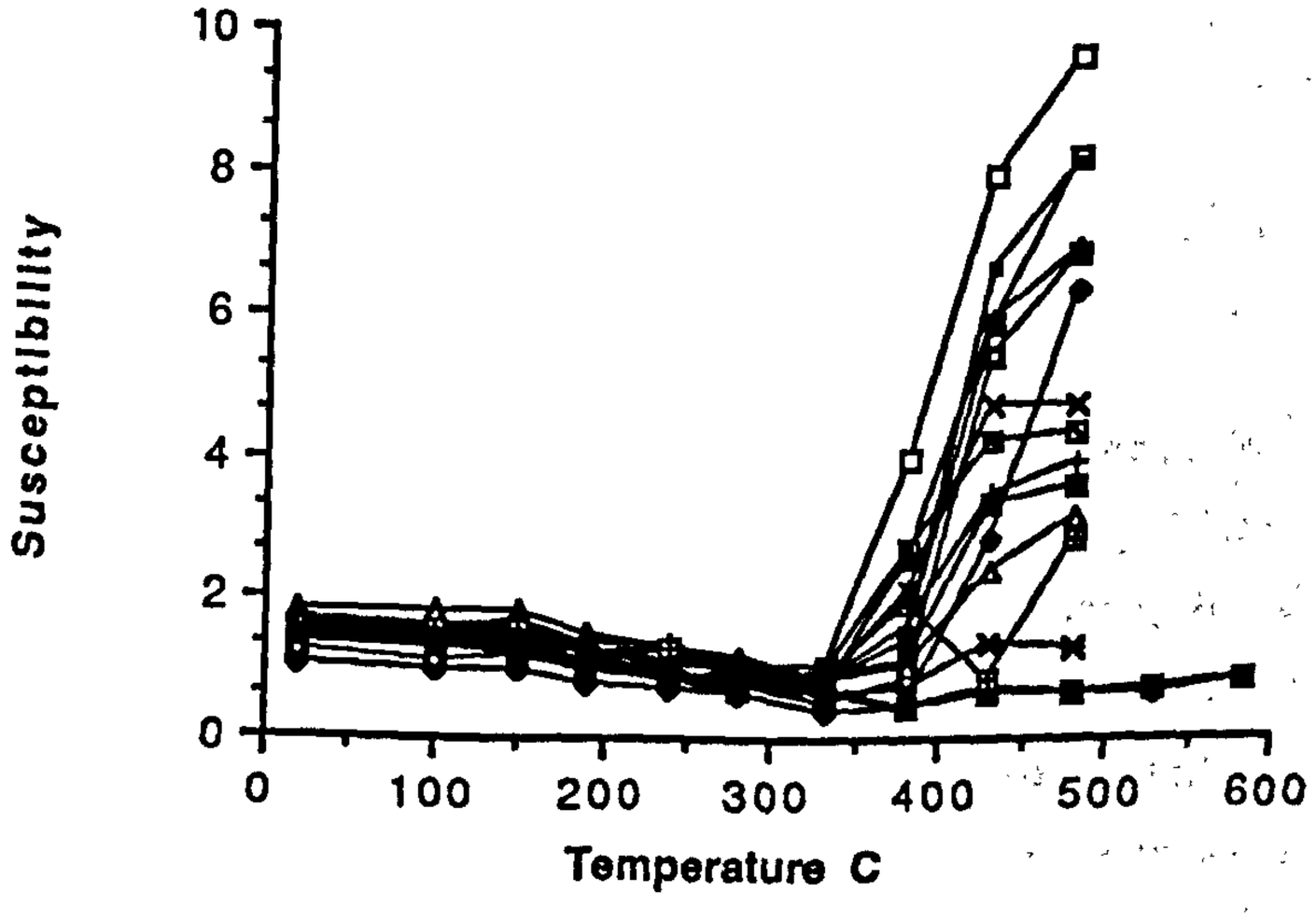
Susceptibility
10
8
6
4
2
0
0
100
200
300
400
500
600
Temperature C

a.

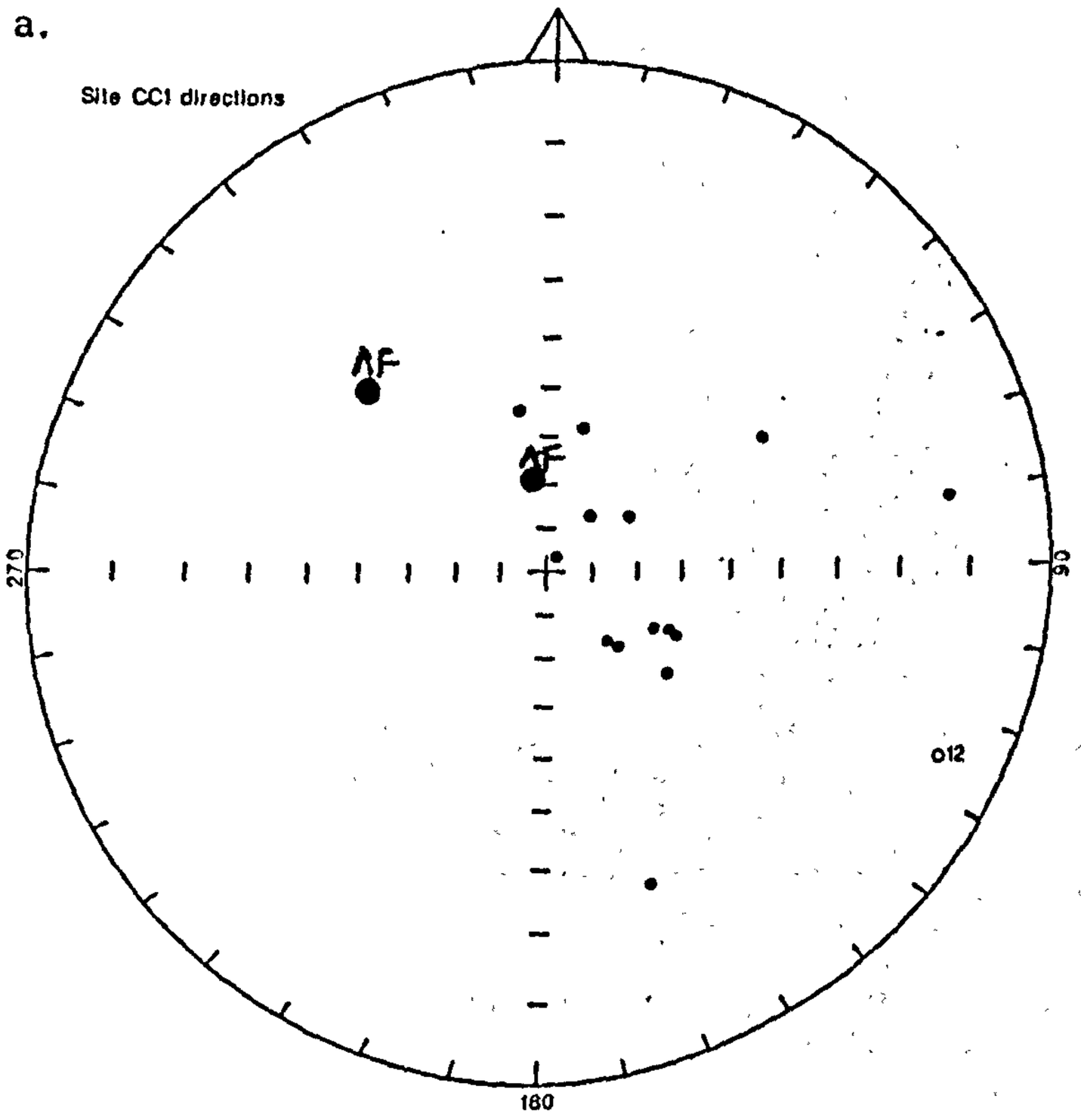

b.

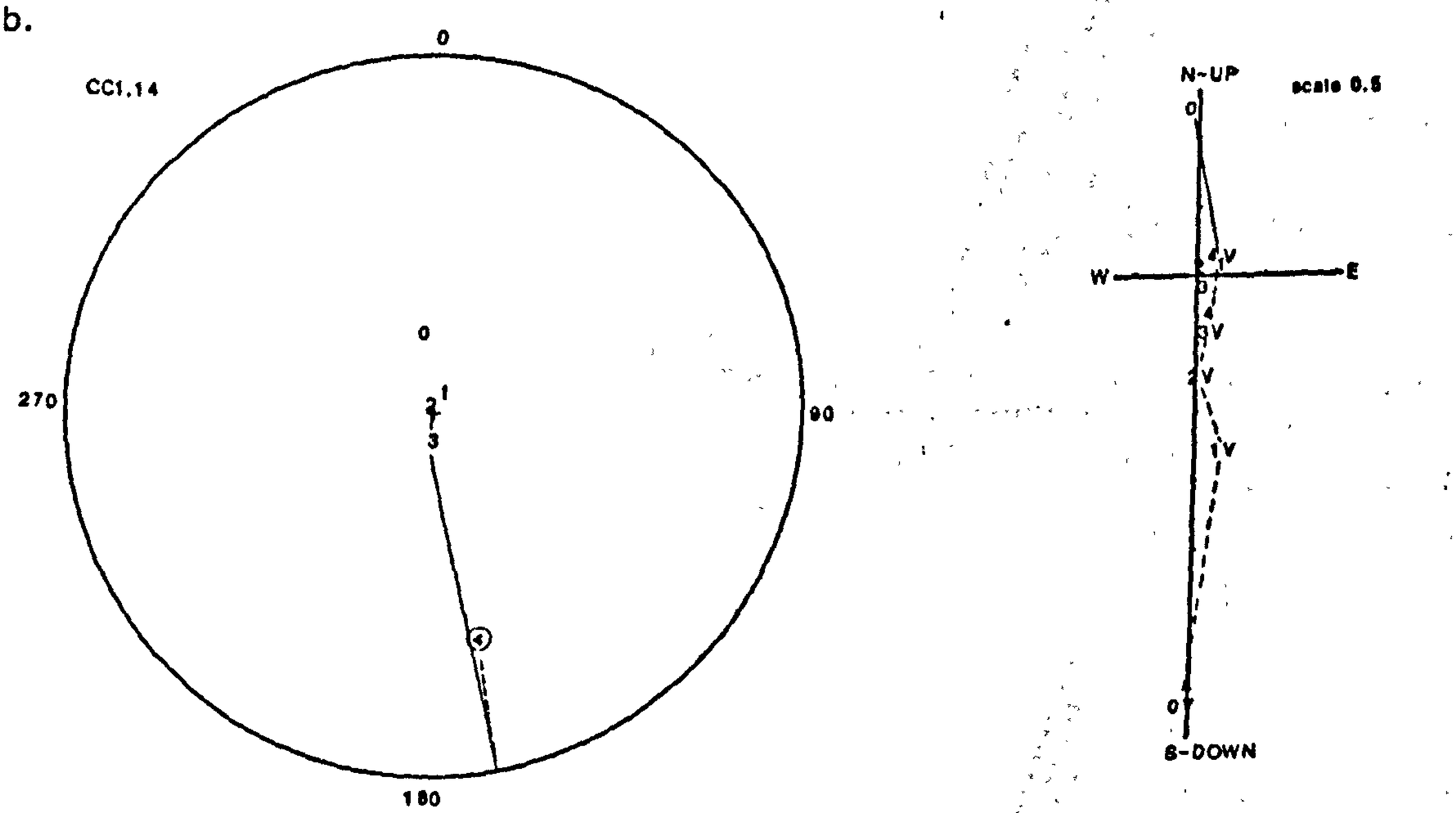

fig. 5.33 Summary of demagnetisation behaviour of samples from site CC1. Natural remanent magnetism (NRM) intensity is given x $10^{-4}Am^{-1}$; susceptibility units x 10^{-6} GOe^{-1}.
a. stereographic projection of stable sample directions; **b.** stereographic projection and accompanying orthogonal plot illustrating vector movement with progressive demagnetisation; **c.** NRM intensity change with increasing temperature illustrating variation of magnetic mineral content between samples; **d.** normalised NRM change with increasing temperature illustrating within-site variation; **e.** susceptibility variation with increasing temperature illustrating changes which occur due to mineralogical alteration.

c

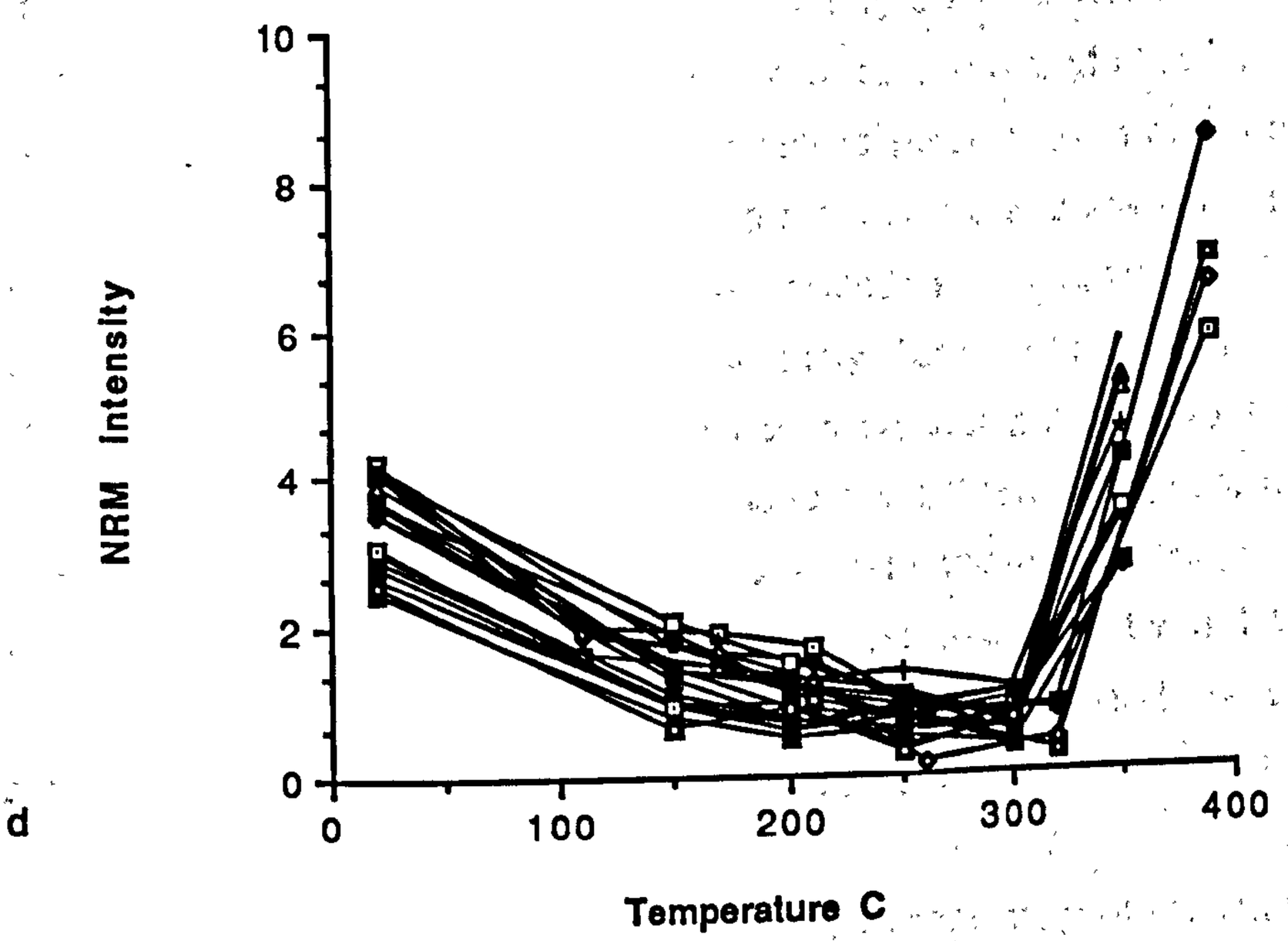
NRM Intensity
10
8
6
4
2
0
0
100
200
300
400
Temperature C

d

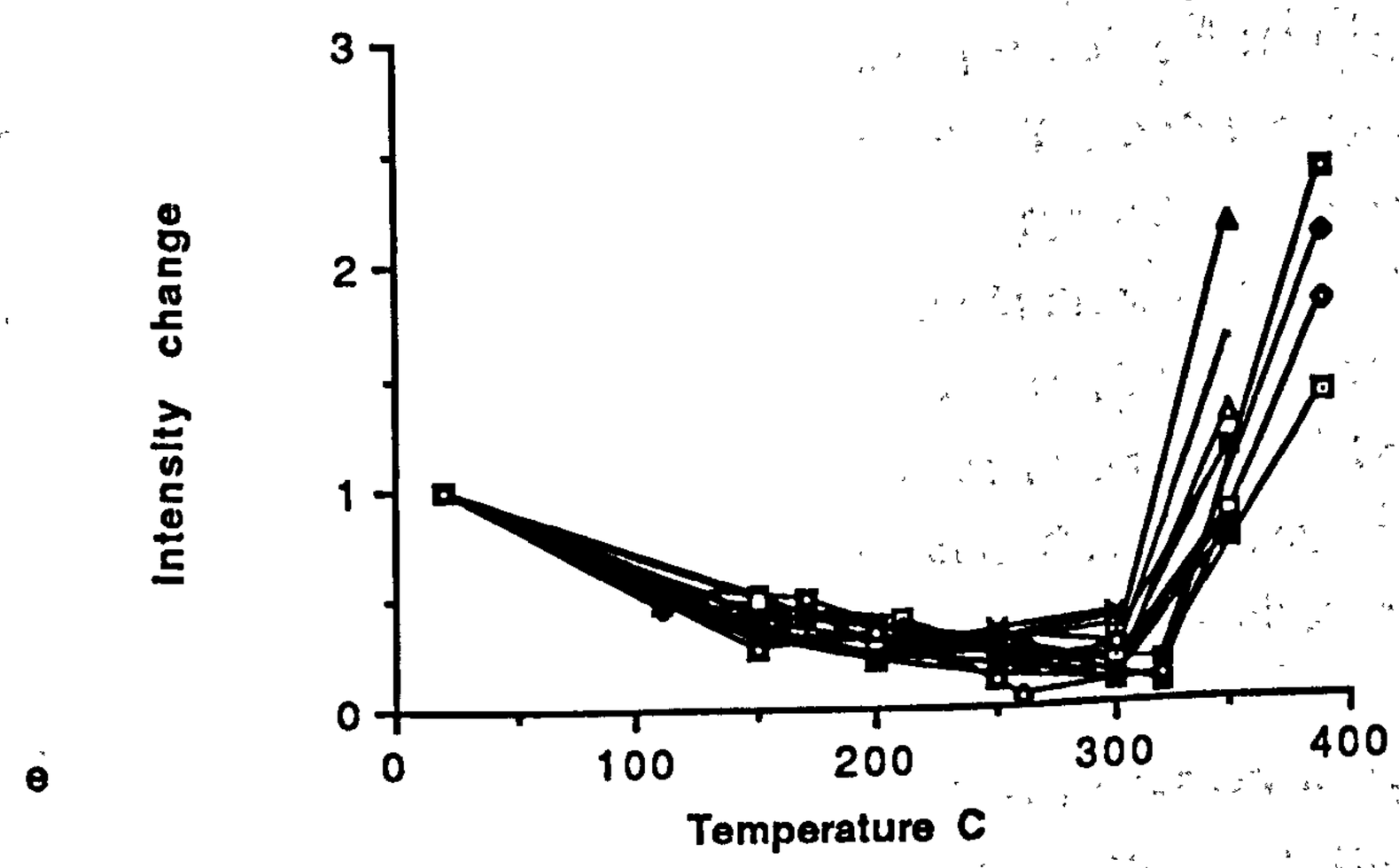
Intensity change
3
2
1
0
0
100
200
300
400
Temperature C

e

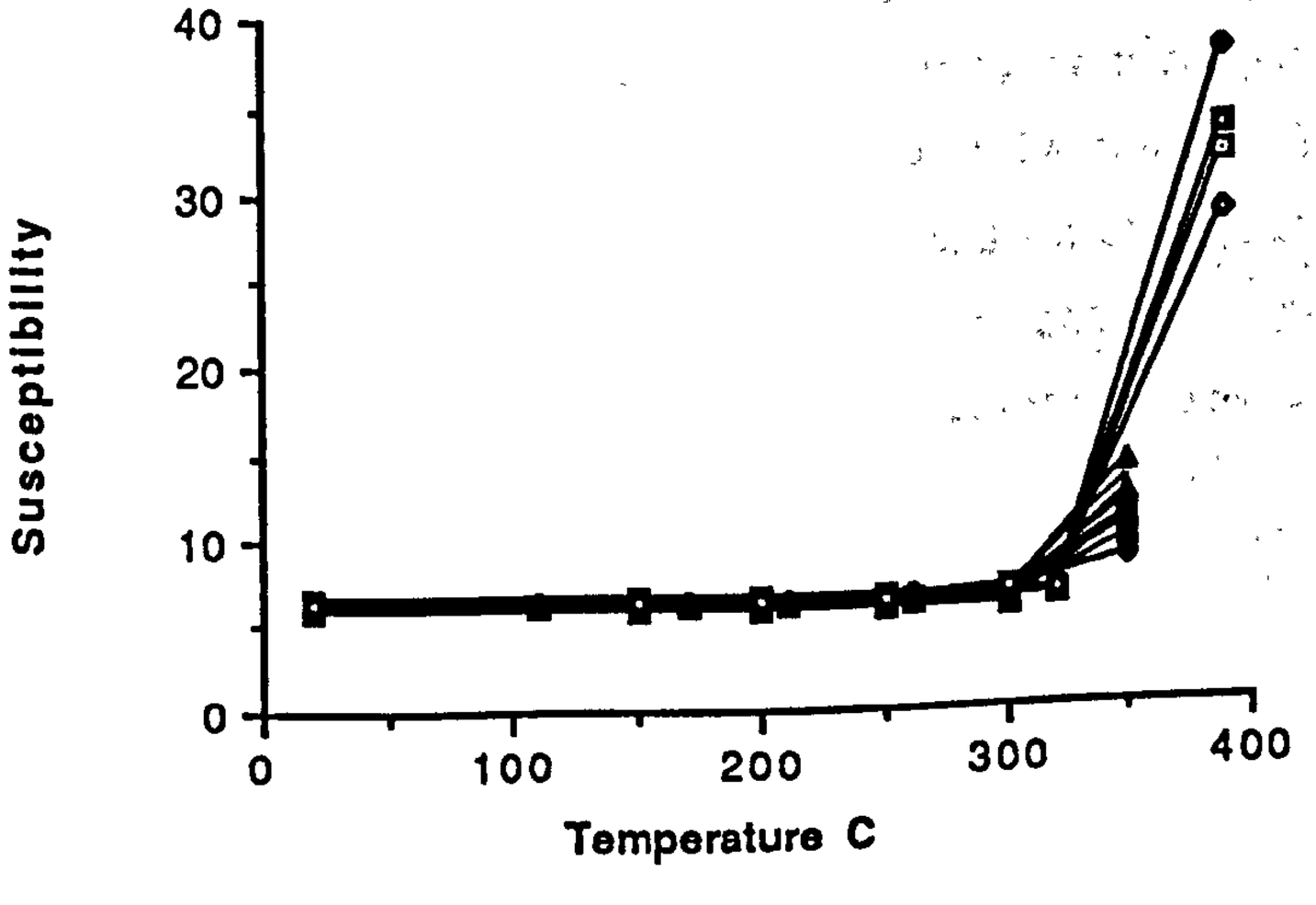
Susceptibility
40
30
20
10
0
0
100
200
300
400
Temperature C

intensity behaviour is so similar for all samples that a key is not given. Demagnetisation is complete by 320°C, at which temperature susceptibility increases rapidly. This implies that the natural remanent magnetism carrier is pyrrhotite. Vectors move across the centre of the stereographic projection with progressive demagnetisation (AF and thermal) and trend towards a reversed direction. This suggests a mix of two components but these are difficult to resolve, even on an orthogonal plot. Most site directions vary between stable and meta-stable and are normal polarity. Most form a grouping about the centre of the projection. Sample 12.2 has a reversed direction (116,-8) and this may be approximately Permian in age as the inclination is the same as that of the apparent field direction wander path at 245 Ma; however the declination is not well defined. Both directions are difficult to explain, and may not be completely resolved. Most directions have a high inclination suggesting a Tertiary origin. It is possible that the directions may be deflected by a fabric carried by paramagnetic minerals, the presence of which is suggested by the high initial susceptibility, and by incomplete resolution of vectors.

Site BC1 (fig. 5.34) Maximum initial natural remanent magnetism intensity of 6.82 x $10^{-4}Am^{-1}$ and susceptibility of 3.84 (volume units x $10^{-6}GOe^{-1}$; see appendix 4.2) indicate a reasonable magnetic mineral content. The high susceptibiity values suggest that high susceptibility magnetic minerals (*e.g.*, pyrrhotite, magnetite or maghemite), or abundant paramagneitic minerals are present in these samples. There is little within site variation of susceptibility and intensity behaviour. Demagnetisation is complete by 320°C, at which temperature susceptibility increases rapidly. This implies that the natural remanent magnetism carrier is pyrrhotite. Site directions are meta-stable and seem widely scattered after both AF and thermal demagnetisation. Most are normal polarity; those with reversed polarity have shallow inclinations. Two samples, one normal and one reversed, lie on the apparent field direction wander path at 245 Ma suggesting a Permian natural remanent magnetism origin. A cluster of several site directions has high inclination and lies close to the present day field direction. The remaining vectors are difficult to interpret in terms of the apparent field direction wander path; this may be due to the meta-stability of the site directions, and brings the validity of the other directions into question. Examination of an example of progressive demagnetisation shows that no stable end points are reached. A significant paramagnetic component is suggested by the high susceptibility; this may be due to pyrite and clays, as well as a lack of carbonate.

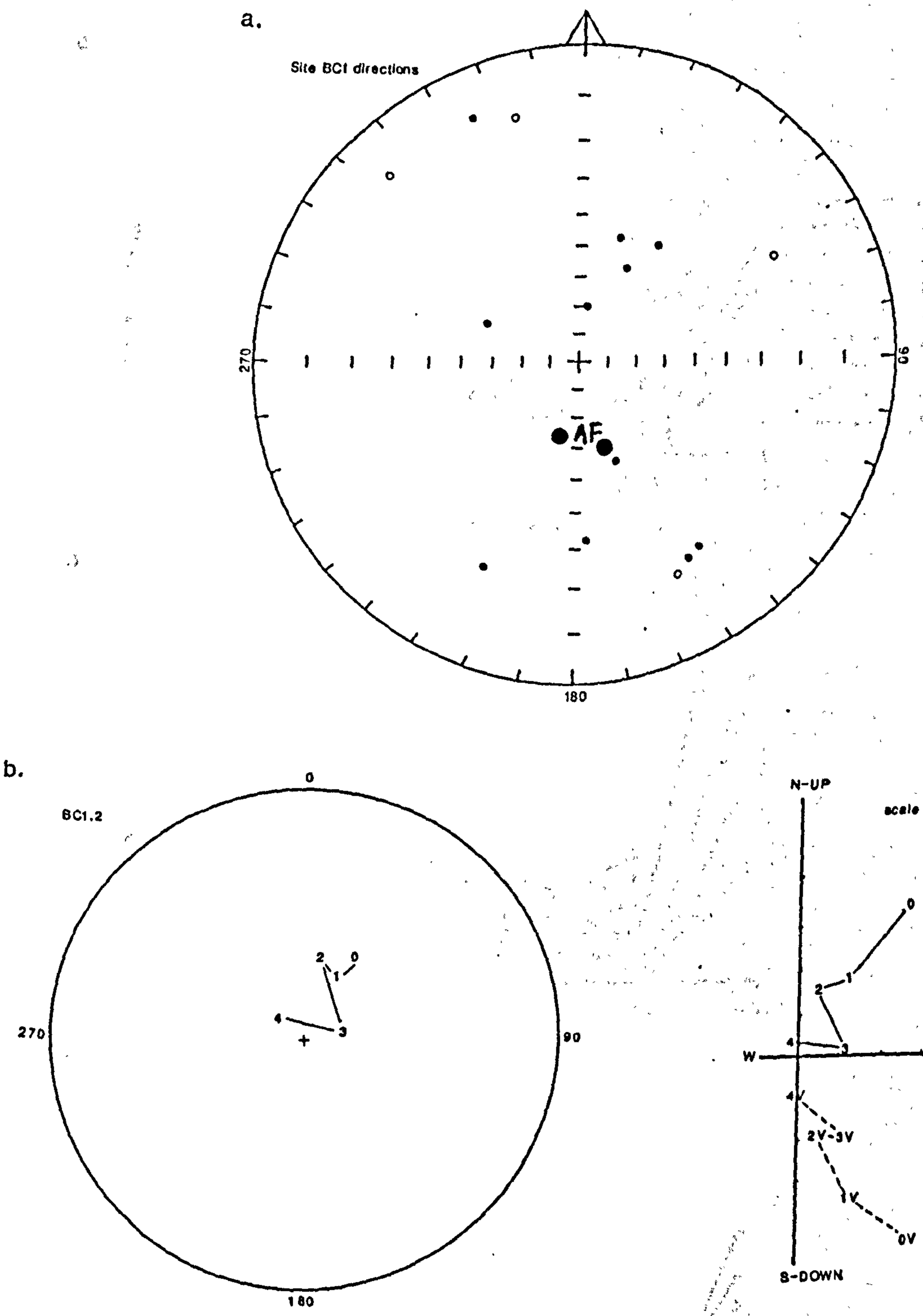

fig. 5.34 Summary of demagnetisation behaviour of samples from site BC1. Natural remanent magnetism (NRM) intensity is given x $10^{-4}Am^{-1}$; susceptibility units x 10^{-6} GOe^{-1}.
a. stereographic projection of stable sample directions; **b.** stereographic projection and accompanying orthogonal plot illustrating vector movement with progressive demagnetisation; **c.** NRM intensity change with increasing temperature illustrating variation of magnetic mineral content between samples; **d.** normalised NRM change with increasing temperature illustrating within-site variation; **e.** susceptibility variation with increasing temperature illustrating changes which occur due to mineralogical alteration.

c

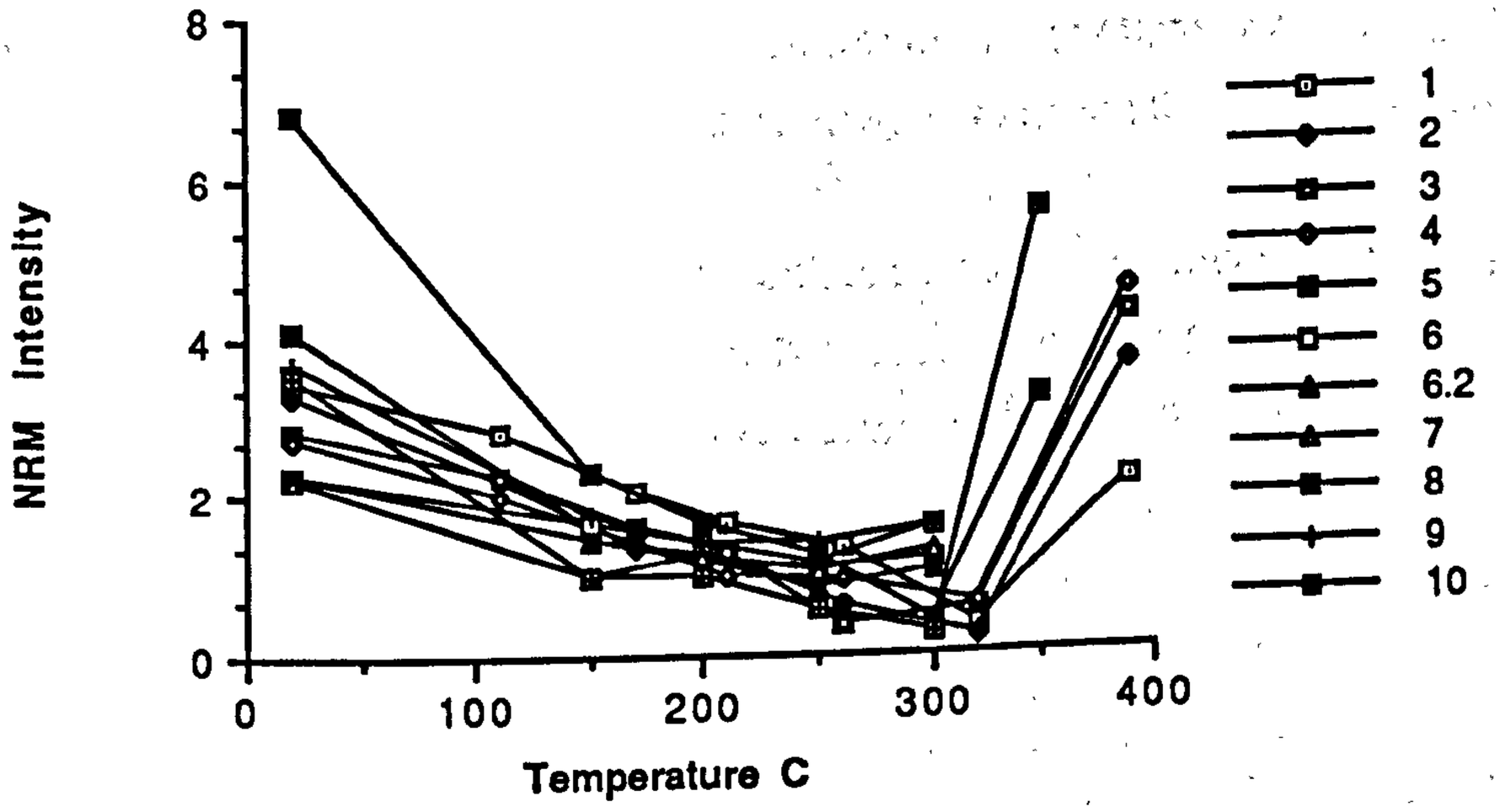
NRM Intensity
8
6
4
2
0
0
100
200
300
400
Temperature C
1
2
3
4
5
6
6.2
7
8
9
10

d

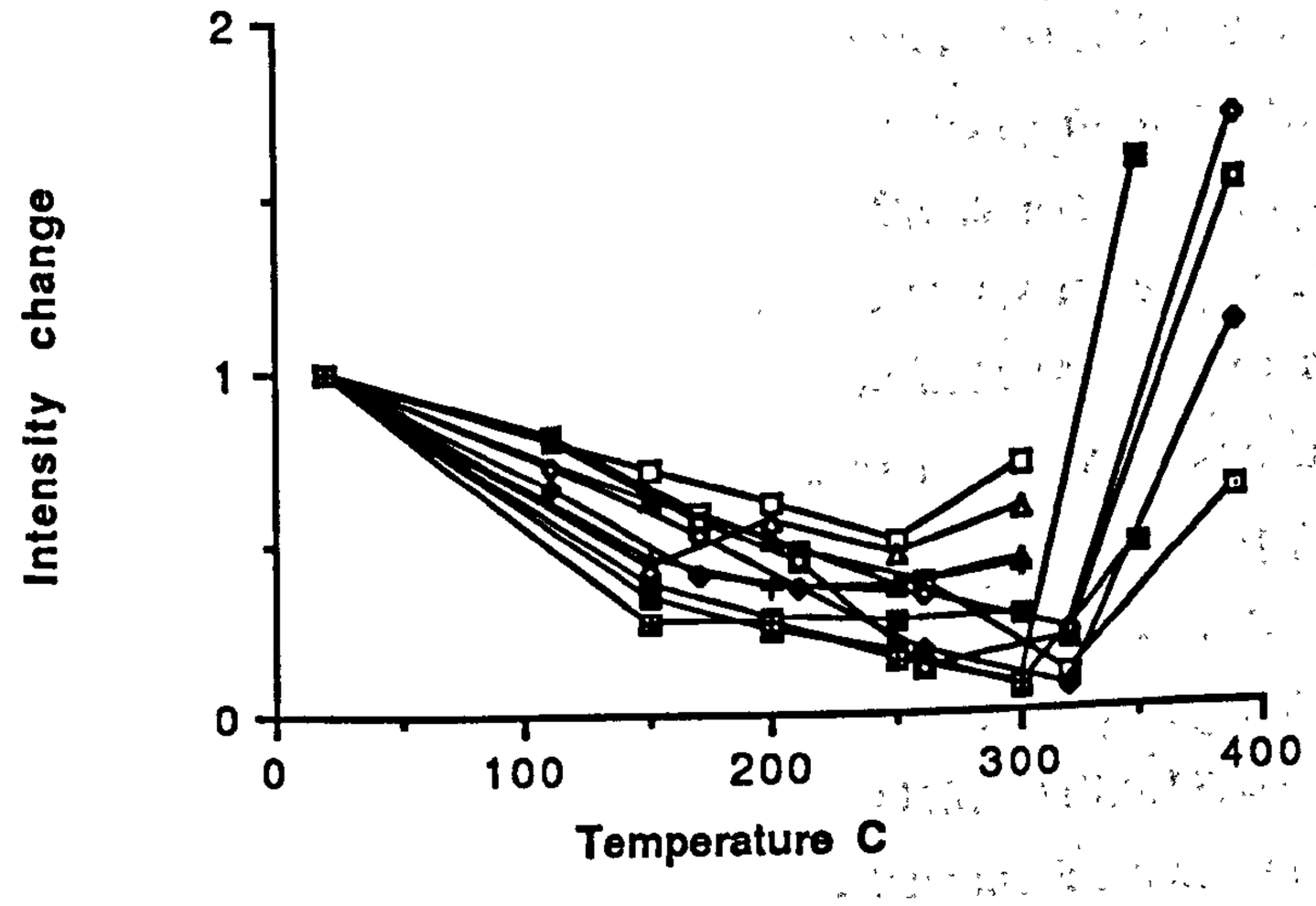
Intensity change
2
1
0
0
100
200
300
400
Temperature C

e

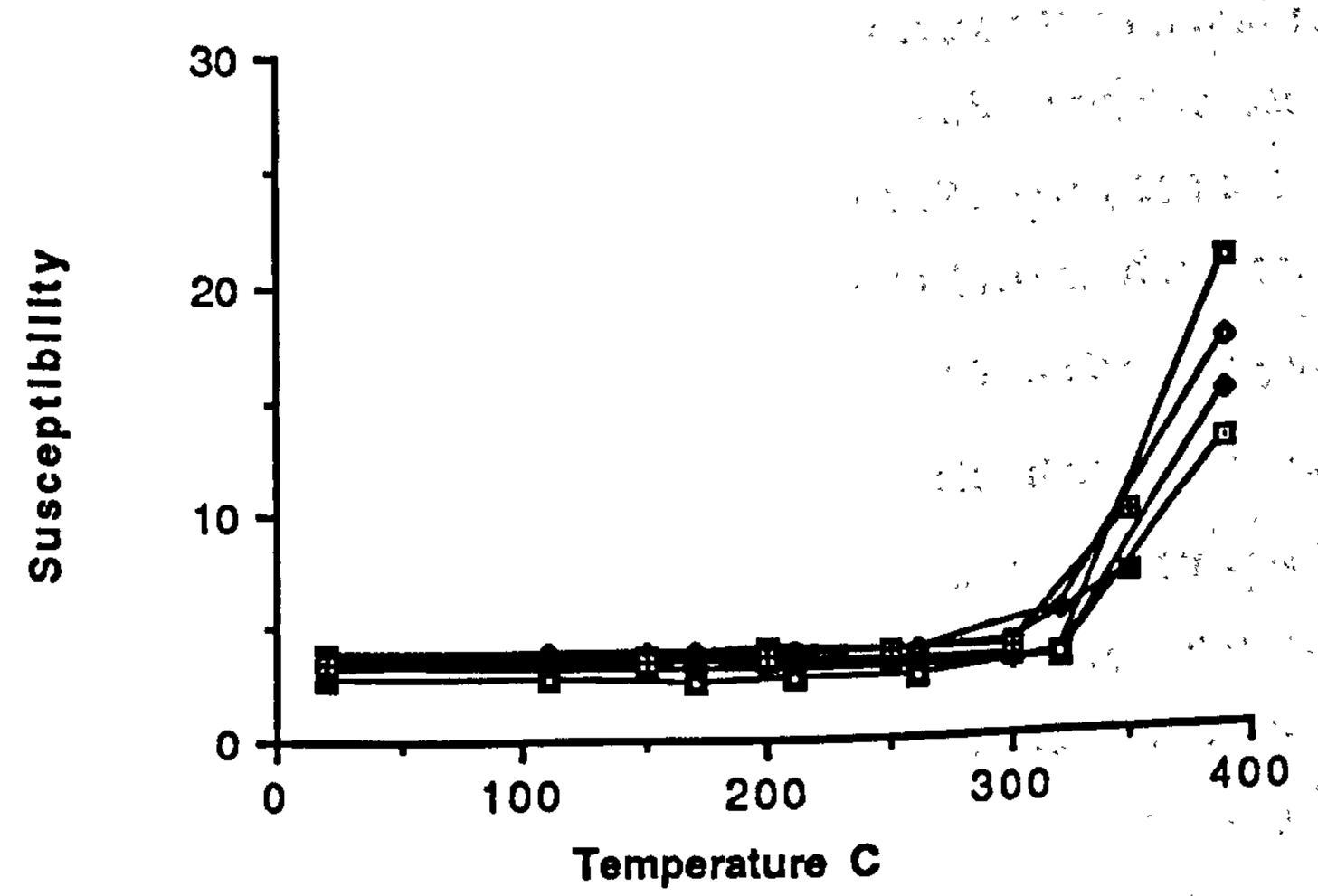
Susceptibility
30
20
10
0
0
100
200
300
400
Temperature C

Summary (table 5.9 and fig. 5.35)

i. all sites yield stable vectors;

ii. more than one magnetic component is present in most sites;

iii. pyrrhotite is the main natural remanent magnetism carrier; goethite, multi-domain, pseudo-single domain haematite magnetite/haematite and pyrite are also present;

iv. most directions are normal polarity although some are reversed polarity; L1, 180 Ma, 245 Ma, normal polarity; CC1, ambiguous, normal and reversed polarities; BC1, ambiguous, normal polarity, Tertiary?, normal polarity.

5.5 Discussion

5.5.1 Magnetic mineralogy

It is not necessarily the case that all the magnetic minerals present in a rock will carry a remanence. However, a correlation exists between initial intensity of remanence and bulk susceptibility which suggests that the majority of magnetic minerals present do also carry a natural remanent magnetism. Close examination of natural remanent magnetism intensity versus susceptibility values for individual sites (fig. 5.36 a,b,c and d) reveals two relationships. Firstly, these data show that individual sites can be defined by their natural remanent magnetism intensity versus susceptibility values. Secondly, three types of natural remanent magnetism intensity/susceptibility relationships are apparent and these are related to particular sites:

i. those sites with invariant range of natural remanent magnetism intensities and susceptibilities values (sites M2, M3, M4, M13, M15,M17,M18, M19, M21, M22, M25, M26 and M27; BC1 and CC1). This relationship indicates that the composition of samples from any one site is uniform. In most cases the natural remanent magnetism intensity and susceptibility values are *low* which indicates low magnetic mineral content. These low values also suggest that goethite or haematite are the remanence carriers. Intensity and susceptibility changes with thermal demagnetisation indicate the presence of goethite (T_b of 100°C to 150°C) and other phases (T_b of around 320°C and around 500°C). The T_b of 320°C indicates pyrrhotite; the T_b of around 500°C indicates that the remanence carrier is either an impure magnetite/haematite, or that the natural remanent magnetism is easily unblocked *i.e.*, that the grains are pseudo-single domain or multi-domain. Two notable exceptions to this group are sites CC1 and BC1 (fig.

site	stable proportion	N	site mean direction dec	inc	A95	pole(North) lat.	long.(E)	polarity
L1	14 of 14	14	356.8	4.9	7.5	60.3	81.8	N
	13 of 14	13	359.7	35.3	4.8	70.8	51	N
BC1	7 of 11	7	160.5	20.1	17.3	43	102.3	R
	4 of 11	4	23.9	53.5	15.5	70	333	N
CC1	13 of 13	13	95.7	72.9	12.3	12.9	290	N

site	intensity (max.)	susc. (max.)	blocking temperature C	magnetic minerals	interpreted age
L1	24.07	1.78	100, 590	G,P,M/H	245 my
					200my
BC1	6.82	3.84	320	P	?
				P	?
CC1	4.16	6.56	320	P	Tertiary?

table 5.9 Summary of mean directions and other data for sites in the basin facies

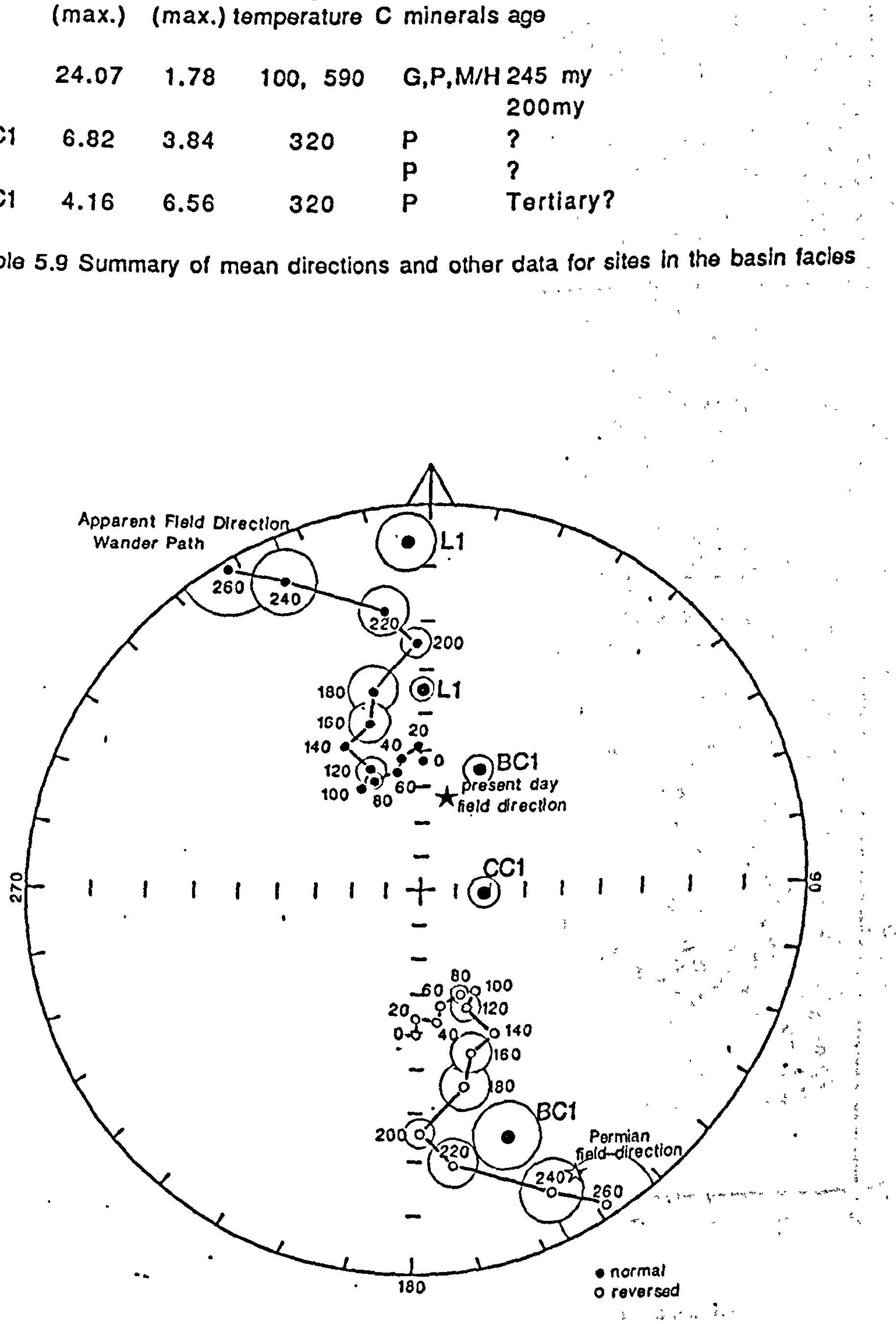

fig. 5.35 Stereographic projection of mean directions for sites in the basin facies

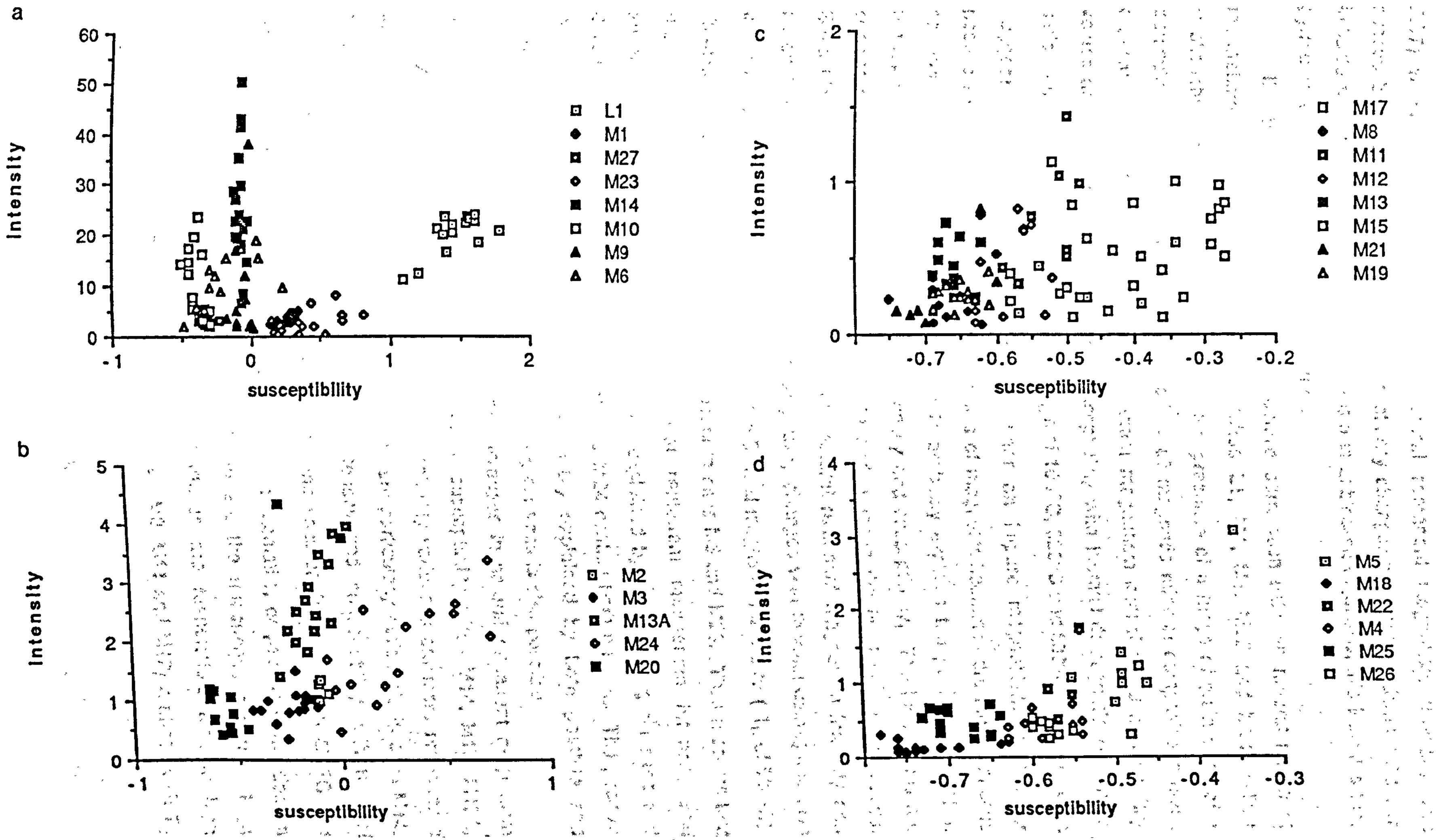

fig. 5.36 Summary graphs of initial intensity of natural remanent magnetism ($x10^{-4}Am^{-1}$) versus initial susceptibility for all sites (except BC1 and CC1) showing the within-site variation.

5.37) which have uniform but *high* natural remanent magnetism intensity and susceptibility values. Intensity and susceptibility changes with thermal demagnetisation indicate that the natural remanent magnetism is unblocked by 320°C; this indicates that pyrrhotite could be the remanence carrier.

ii. those sites which show a positive correlation between natural remanent magnetism intensity and susceptibility (sites L1, M1, M5, M23 and M24). This relationship could be explained by either the presence of a range of grain sizes of a particular magnetic mineral or by a variety of magnetic mineral compositions being present. Site L1 has high natural remanent magnetism intensity and susceptibility values and changes in intensity and susceptibility with thermal demagnetisation which indicate the presence of several phases (T_b's of 100°C, 320°C and 530°C). These values suggest that goethite, pyrrhotite and either an impure magnetite/haematite, or pseudo-single domain or multi-domain grains of magnetite/haematite are the remanence carriers. This range of magnetic minerals probably explains the positive correlation between natural remanent magnetism intensity and susceptibility. The high values are consistent with the presence of pyrrhotite and/or magnetite in significant quantities. Sites M1, M24, M23 and M5 have lower natural remanent magnetism intensity and susceptibility values. Intensity and susceptibility changes with thermal demagnetisation indicate the presence of goethite (T_b of 100°C) and magnetite/haematite (T_b of 500°C). Goethite is the only magnetic mineral present in sites M5 and M23. Thus it seems that the positive correlation between natural remanent magnetism intensity and susceptibility for sites M5 and M23 can be explained by a range of grain sizes and different quantities of goethite. Sites M1 and M24 contain both phases. The positive correlation for sites M24 and M1 is probably explained by both goethite and magnetite/haematite being present. A range of grain sizes is also possible.

iii. those sites which show large increases in natural remanent magnetism intensity values relative to small increases in susceptibility (sites M14, M10, M13A, M9, M6,M8, M11 and M12). The large susceptibility variations are more pronounced in some sites than in others. Large variations are particularly noticeable in sites M14, M13A, M10, M9 and M6. Changes in intensity and susceptibility with thermal demagnetisation indicate that the T_b for the remanence carrier is between 450°C and 550°C, indicating that either an impure magnetite/haematite, or pseudo-single domain or multi-domain grains of magnetite/haematite are the remanence carriers. High susceptibility values suggest that large particles are responsible for the high susceptibility values. In the remaining sites (*i.e.*, M8, M11 and M12) a phase with T_b of 320°C is identified; this indicates pyrrhotite.

Overall, samples fall into three main groups (fig. 5.37) which are related to lithology and facies:

group I. Sites BC1 and CC1 have high susceptibility values relative to natural remanent magnetism intensity values. This could reflect several factors, particularly that: i. they contain significant quantities of magnetic minerals with high susceptibilities such as magnetite or pyrrhotite and/or ii. they contain significant quantities of paramagnetic minerals such as ilmenite or garnet (table 5.2). These samples are from the basin facies and are siltstones.

group II. Site L1 has moderate natural remanent magnetism intensity and susceptibility values, suggesting that it contains either significant quantities of magnetic minerals and/or that these minerals have high initial susceptibility. This site is from the basin facies and is a micritic limestone.

group III. This group contains all sites from the Capitan shelf margin sampled in McKittrick Canyon and contains two groups; a. Sites M14, M10, M9, M13A, and M6 have high natural remanent magnetism intensity values relative to low, invariant susceptibility values. This probably reflects content of significant quantities of haematite; *i.e.*, a low susceptibility mineral capable of carrying a remanence. b. Remaining sites contain negligible quantities of magnetic minerals and have low natural remanent magnetism intensity and low susceptibility values.

5.5.2 Vectors

Any magnetic minerals deposited during sedimentation in Guadalupian times would have an Upper Permian natural remanent magnetism direction. This is subject to the proviso that no subsequent diagenetic changes have oxidised, reduced, removed the original magnetic mineral and overprinted the original natural remanent magnetism. Diagenesis of the sedimentary pile, from times immediately following deposition to uplift and modern weathering, may well cause changes in the original composition of the sedimentary rock, and cause the development of new mineral phases. Any magnetic minerals formed as a result of such diagenetic processes would be expected to have natural remanent magnetisation directions aligned with the ambient Earth's field at the time of formation of those phases *i.e.*, Upper Permian to present day directions.

Although many site mean directions are interpretable in terms of the apparent field direction wander path many site mean directions differ from expected directions. In almost all cases the *A95* values of all site mean directions are less than 10° (table 5.10). This clear definition of directions argues that these directions are significant, even if they are not readily explainable in conventional terms.

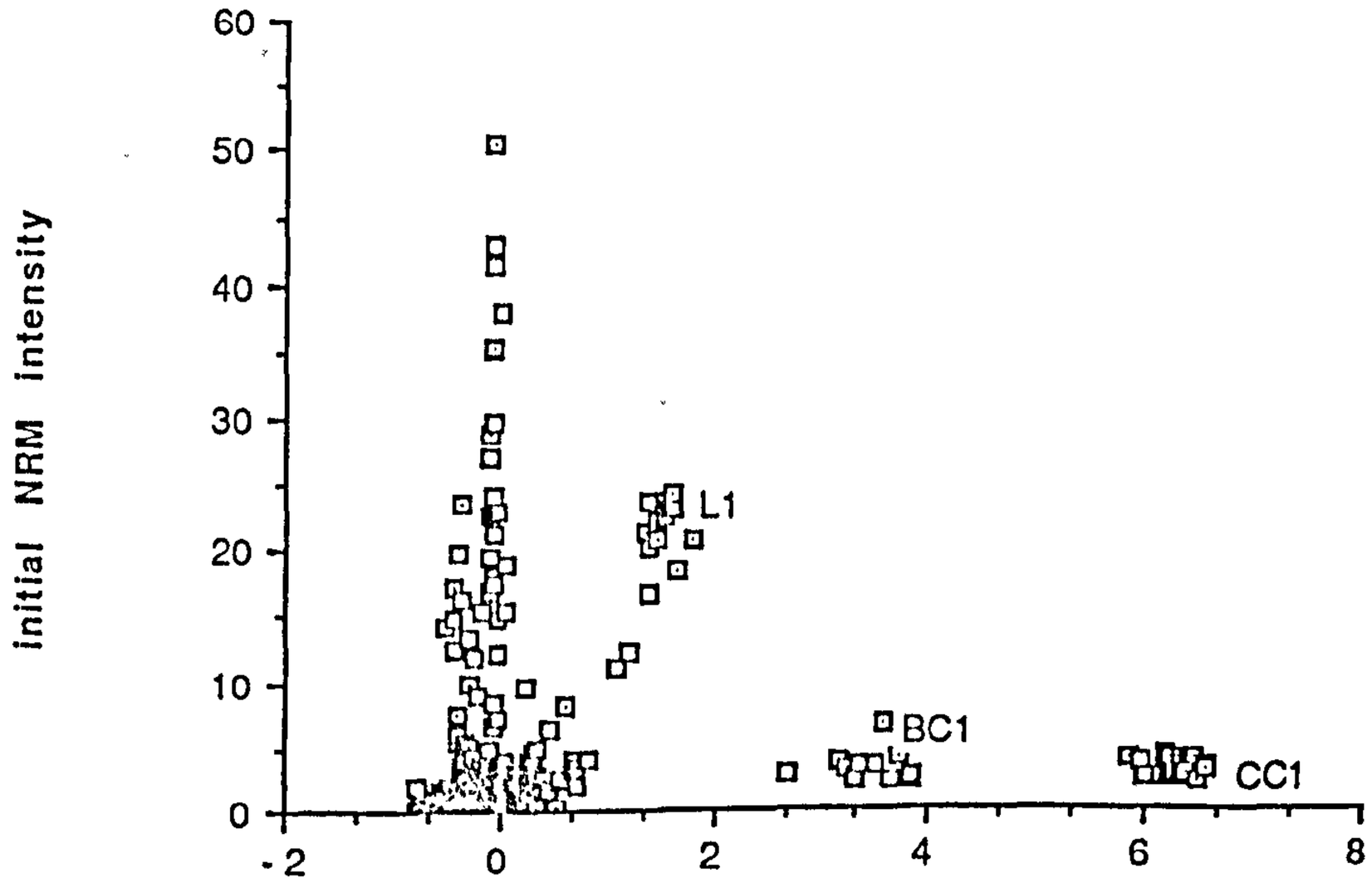

fig. 5.37 Summary diagram of the initial natural remanent magnetism ($x10^{-4}Am^{-1}$) versus initial susceptibility for all sites showing groupings according to facies/lithology.

facies	site	stable proportion	N	site mean direction dec	inc	A95	pole(North) lat.	long.(E)	polarity
back reef									
	M13	10 of 12	9	195	-30.1	9.6	69.1	31	R
	M13A	15 of 15	16	52.2	20.3	8.5			N
	M14	18 of 18	6	253	35.9	8.9	3	11	N(R)
	M15	14 of 14	14	255.9	41.8	10	2	193.9	N
	M16	0 of 4	4						
	M17	0 of 16	16						
	M18	0 of 13	13						
reef									
	M12								N(R)
	M19								N
upper foreslope									
	M8	6 of 10	6	353.6	31.6	20	74	98	N
	M9	11 of 11	3	171.4	-28.8	12	41.9	86.4	R
			8	260.9	88.4	19	31.4	251.5	N
	M10	14 of 14	7	6.6	59.4	17	80.2	286.3	N
			6	333.5	43.7	7.4	66	156.6	N
	M11	8 of 10	7	220	67.7	16	0	231.1	N(R)
	M20	11 of 12	8	174	-50.7	5.5	88.9	160.3	R
				280	62				N
	M21	5 of 10							N
	M22	3 of 3							N
	M23	8 of 16	7	4.6	64.4	5.6	75.3	267.9	N
	M24	12 of 14	8	356.3	55.2	22	85.2	216.7	N
lower foreslope									
	M4	11 of 11	2	355	56		85	216	N
			2	288.3	-5.3		14	153	N
			3	222.5	-13.4	17	43.1	8.4	R
	M5		9	8.7	58.9	8.6	79.6	295.4	N
	M6	10 of 10	9	106.4	-18.2	8.2	188	164.6	R
	M7								
	M25	13 of 13	13	21.9	-31.9	6.4	36.4	48.9	R
	M26	1 of 8	1	358.6	54	3.5	87.2	230.4	N
basin margin									
	M1	20 of 20	20	341.6	67.8	5.4	66.8	224.7	N
	M2	8 of 8	6	0	64.5	10	76.7	255.2	N
			4	299.7	-1.7	18	24.3	147.6	N
	M3	7 of 13							
	M27	17 of 17	16	169.5	69.7	4.5	4	81.4	N
			1						R
basin									
	L1		14	356.8	4.9	7.5	60.3	81.8	N
			13	359.7	35.3	4.8	70.8	51	N
	BC1		7	160.5	20.1	17	43	102.3	R
			4	23.9	53.5	16	70	333	N
	CC1		13	95.7	72.9	12	12.9	290	N

table 5.10 Summary of demagnetisation data and mean directions for all sites

site	intensity (max.)	susc. (max.)	blocking temperature C	magnetic minerals	interpreted age
BR					
M13	0.65	-0.62	110, 320	G,P,Mh,M/H	190my
M13A	3.97	0.05	110, 500	G,P,M/H	ambiguous
M14	50.34	-0.02	110, 500	G,M/H	ambiguous
M15	1.51	-0.27	110, 300	G,P,M/H	ambiguous
M16	0.21	-0.58			
M17	0.32	-0.33			
M18	0.17	-0.64			
R					
M12	0.82	-0.52	150, 300	G	Tertiary?
M19	0.36	-0.61	100, 240	G	Tertiary?
UFS					
M8	0.79	-0.6	100, 320, 480	G,P,H	190 my, Tertiary
M9	37.83	0.17	150, 350, 550	G,P	190my
				H	Tertiary?
M10	23.58	-0.29	150, 350, 500	G,P,H	140my-20my
				G,P,H	Tertiary
M11	1.43	-0.48	150, 350	G,P	ambiguous
M20	4.36	0.02	300	G,P,H	45my
					Tertiary
M21	0.82	-0.6	150, 390	G	Tertiary
M22	0.92	-0.55	110, 190	G	Tertiary
M23	8.01	0.81	100	G	210my, 20my
M24	3.39	0.56	100, 500	G,H	60my-40my
LFS					
M4	1.74	-0.54	100, 320, 550	M/H	60my
				M/H	ambiguous
				M/H	ambiguous
M5	3.1	-0.35	100	G	<20my
M6	18.89	-0.29	100, 450	G,P,H	220my-260my?
M7	0.37	-0.62			
M25	0.72	-0.64	100, 500	G,M/H	ambiguous
M26	1.25	-0.55		G,M/H	Tertiary
BM					
M1	4.85	0.34	100, 480	G,M/H	80my
M2	1.35	-0.07	350	P	<20my
M3	1.52	-0.12	100, 350		
M27	5.41	-0.29	100	G,H	Tertiary
			530	G,H	230 my
B					
L1	24.07	1.78	100, 590	G,P,M/H	245 my
					200my
BC1	6.82	3.84	320	P	?
				P	?
CC1	4.16	6.56	320	P	Tertiary?

table 5.11 Summary table of magnetic characteristics of sites in this study.
Abbreviations: G, goethite; P, pyrrhotite; Mh, maghemite; M, magnetite; H, haematite.

Site mean directions which differ from the expected directions

All site mean directions from sites from the back reef facies and some sites from basin, basin margin, lower and upper foreslope facies differ from the expected directions. However, patterns of similar directions are still apparent (fig. 5.39). Sites M9, M11, M20, M27 and CC1 all have normal polarity directions with high inclinations and similar declinations; sites M14 and M15 have normal polarity directions and declination of around 260° and inclination of 40°; sites M4, M6, M13A, M23 and BC1 all have low inclinations, but widely varied declinations and polarity.

Causes of discrepancy from expected directions

There are many reasons why measured directions may differ from the expected directions and these can be divided into several categories;

A. Error

acquisition of spurious remanence during the demagnetisation process
Stray fields may arise during the demagnetisation process, caused by insertion of the sample into the magnetometer, or anywhere else where a local magnetic field, however small, is concentrated (Tarling, 1985). This may be confused with the natural remanent magnetism directions. Contamination may also occur within the furnace because, even though great care was taken to ensure that the field in the furnace was zero, a small residual field may still have been present. Acquisition of spurious remanence during the demagnetisation process is a particular problem where the grain size of the natural remanent magnetism carrier is on the super-paramagnetic/pseudo-single domain threshold and where the natural remanent magnetism is weak. These spurious remanences may only take a few minutes to acquire, and are not stable for long (Tarling, 1983). However, they are often stable for the duration of the demagnetisation-measurement cycle. A range of final intensities might be expected in samples which have a low natural remanent magnetism intensity, due to the acquisiton of this type of remanence, with the *highest* spurious reading in the *first* sample to be measured after the heating-cooling process, and the *lowest* spurious intensity in the *last* sample to be measured, as this will have had the longest time to decay away. Evidence of this can be seen in samples from sites M1, M2, M12, M22 and M26, where the intensity of a spurious remanence at the final measurement correlates with the order of measurement of the samples. In site M19, an intensity rise occurs at 200°C, probably indicating the

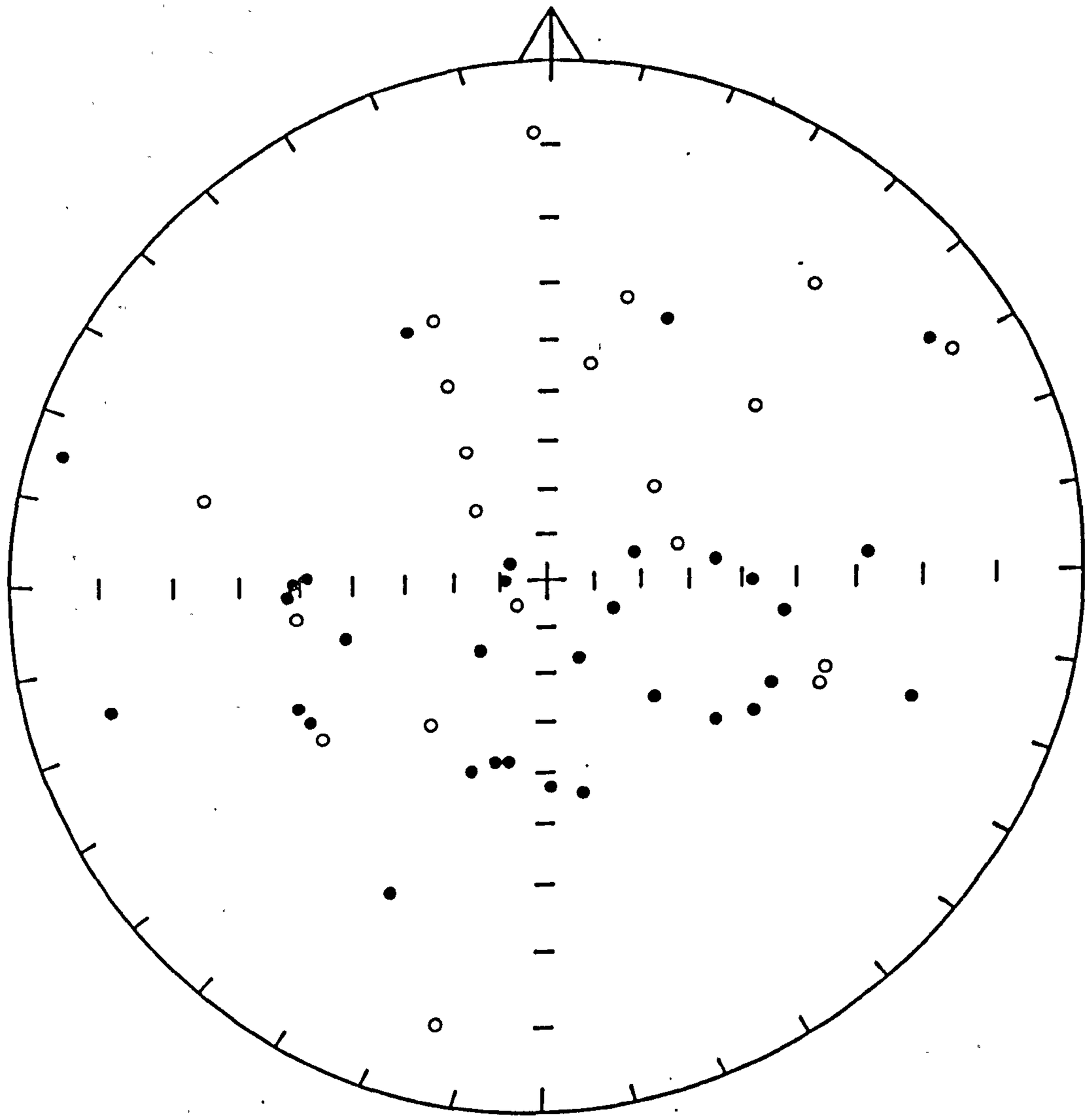

fig. 5.38 Stereographic projection of 52 measurements on the cryogenic magnetometer, of an empty sample holder showing the scatter of declinations and inclinations. The scatter does not appear random as normal directions with high inclination are commonest. This data is given in full in appendix 5.2.

formation of very-fine grained haematite from the destruction of goethite, which then acquired a spurious low remanence. In sites M3, M4 and M11 an intensity increases probably reflect the acquisition of a spurious remanence by newly formed magnetite or maghemite. Sites BC1 and CC1, show a rise in the final intensity consistent with the acquisition of a remanence carried by magnetite formed probably from the oxidation of pyrite or pyrrhotite.

Inaccurate and non-repeatable measurements Numerous measurements (52) were made of the sample holder without a sample in it, to see whether there was an obvious field inside the cryogenic magnetometer (fig. 5.38 and appendix 5.2). This showed that although directions are scattered, there seems to be a tendency for directions to have normal, steep inclination. However, during the process of measurement of natural remanent magnetism, the contribution from the empty sample holder was subtracted from the contribution from the sample. This should have reduced contamination of natural remanent magnetism directions.

In addition, some samples were measured several times (appendix 5.3) in order to assess the validity of measurements of natural remanent magnetism. Both the intensity and direction of the vector are statistically well defined. Even when few repeat measurements were made, visual inspection shows that direction and intensity of vectors is similar over these repeats, even for low intensities. Generally speaking, the higher the intensity of the natural remanent magnetism, the better the repeatability.

field orientation In order to minimise orientation errors numerous orientated drill-samples were collected in a *variety* of orientations in the field (section 1.4). This is therefore unlikely to be a source of error.

bedding correction No corrections have been attempted for bedding orientation. This is for several reasons: I. the tectonic tilt of strata is low with an average at 5°; ii. field relations were often not sufficiently clear for tectonic tilt of strata to be measured at all sites; iii. many strata, such as those of the foreslope facies, were not deposited horizontally. Also, the amount of post-depositional compaction is unclear, particularly in the foreslope facies, and is likely to have been variable (Chapter 2). Mean directions from all sites may deviate from their 'true' directions because of these factors, but the discrepancy is not likely to be greater than about 10°.

displaced strata Samples which have been moved since the time when they acquired their remanence would no longer have a remanence direction comparable with that of

Earth's past or present field. This may explain the discrepancy in the direction isolated from site M13A, relative to the expected directions, because site M13A is situated within a fracture zone (fig. 2.4 b,c,d). This implies that the block from which site M13A was sampled, has moved since the time at which it acquired its remanence.

overlap of T_b Where more than one component/direction contributes to the natural remanent magnetism the net vector moves continuously across a stereographic projection during progressive demagnetisation and the demagnetisation path on an orthogonal projection is curved. Resolution of the vectors may still be possible depending on the degree of overlap of the T_b spectra of the phases which carry the remanences. This is a source of ambiguity in sites M13A and L1.

human error is always possible, although care was taken at all stages!

B. Intrinsic magnetic mineral properties

relaxation time The relationship between grain size, T_b, blocking volume, and relaxation time for a given mineral is such that a natural remanent magnetism will only be preserved from the time of its acquisition to the present day, if the grain size is above a particular threshold and the blocking temperature has not been exceeded during the course of burial. If the natural remanence has been partially unblocked, or has 'relaxed', then the original natural remanence may be obscured by later remanences or be totally undetected. This can lead to omissions in the interpretation of the palaeomagnetic history and problems such as incomplete resolution of vectors, where more than one vector is carried by the sample.

magnetic isotropy A sample must be magnetically isotropic to ensure that the observed vectors accurately reflect the geognetic field under which they were acquired (Tarling, 1985). If there is preferred alignment of magnetic particles which have a shape anisotropy, then the natural remanent magnetism will tend to be acquired along the magnetically 'easy' direction. This will cause the true direction of the ambient geomagnetic field to deviate from the natural remanent magnetism direction if the orientation of this preferred alignment is at variance with the ambient field direction. This may be a source of error in samples from sites CC1, L1 and BC1 where strong compactional fabrics are developed, and possibly in other sites where forces such as

crystallographic growth during diagenesis, or depositional forces may have caused preferred alignment of magnetic minerals (chapter 4).

lightning Some high intensity natural remanent magnetistions may have been caused by lightning strike. When lightning strikes rocks, it effectively forms a strong line current and creates a circular field about the point of the strike. This can impart a strong isothermal remanent magnetisation to pre-existing magneic minerals in the rock, which is usually unstable (Piper, 1987). This is the likely cause of the magnetisations displayed by sites M14 and M15, and which are also located on a prominent outcrop.

C. geomagnetic assumptions

Palaeomagnetic interpretation relies on several assumptions and observations concerning Earth's magnetic field and its behaviour through time:

secular variation The geomagnetic field varies from the 'true' direction at certain instants of time, often by several degrees; this is known as secular variation. Secular variation occurs over a time period of 10^3 to 10^5 years. If the acquisition of remanence takes place during the entire period of secular variation, then one might expect the site mean direction to be an average of secular variation, and thus represent the 'true' field direction. If individual samples from a site acquired a natural remanent magnetism due to diagenetic processes at different stages of this secular variation, then it would be possible that the spread of directions from this site may reflect secular variation. If the natural remanent magnetism is acquired in less than the entire period of secular variation then the natural remanent magnetism direction will be at variance from the 'true' field direction. This would imply that the diagenetic 'event' which caused the growth of the magnetic mineral took place in less than 10^5 years.

geomagnetic field reversals Reversals of the geomagnetic field occur periodically. If the acquisition of remanence takes place over a period of time which either covers several reversals, or during a reversal, then the natural remanent magnetism direction may deviate from the 'true' direction due to the acquisition of composite magnetisations. This is a possible explanation for the site mean directions obtained from sites M11, M9, M27, M20 and CC1, which all have normal polarity and high inclinations and may therefore approximate to a Tertiary age, and for sites M13A, M6, BC1 and M4, which all have shallow inclinations and are normal or reversed polarity, suggesting a more equal

mix of normal and reversed polarity components. Alternatively, these directions could be explained by incomplete resolution of two (or more) components with opposite polarity, but not neccessarily acquired *during* reversal of Earth's field.

continental rotations and the apparent polar wander path Among the effects of plate tectonic movements are continental rotations, continental diplacements and igneous activity. Assessment of the timing of acquisiton of natural remanent magnetism assumes that the orientation of the area under study was the same as the orientation of the continental mass the apparent polar wander path of which is used for comparison of virtual poles. Possible errors arise in three ways; i. the majority of geomagnetic poles used to construct the apparent polar wander path are derived from the study of lavas in 'active' areas. Many of the pole positions used in the compilation of the apparent polar wander path are derived from rocks in the 'basin and range' province of the south-western USA. The degree of rotation/displacement of these areas through time, which would affect the conclusions of the position of the poles at these times, is not always clear. ii. This study area is on the margin of the 'basin and range' province (chapter 1) and the amount of rotation that *this* area has undergone in Tertiary times is uncertain. However, movement in the 'basin and range' province has been largely latitudinal extension rather than rotation and so the error incurred from these movements are likely to be minimal. Even so, there may be discrepancies between virtual poles calculated from sites in this study and the apparent polar wander path used (fig. 5.1). iii. there is more than one version of the apparent polar wander path and revisions are being made all the time.

The time-scale of 'normal' and 'reversed' polarity periods can be difficult to apply in that error is sometimes involved in establishing the age of the rocks sampled *i.e.*, there is usually an error bar associated with the dating of each reversal and these are not usually given.

Other reasons

It is assumed that a magnetic mineral deposited or growing in a magnetic field will aquire a natural remanent magnetism which is parallel with that field. The detailed characteristics of detrital remanent magnetisation (DRM) processes have been investigated in artificially re-deposited sediments (Irving and Major, 1964; Lovlie, 1974 and 1976) and inclination errors of about 20° were found. This suggested that magnetic particles were prohibited from aligning with the Earth's magnetic field by other factors, such as grain shape. In practice, these laboratory observations do not

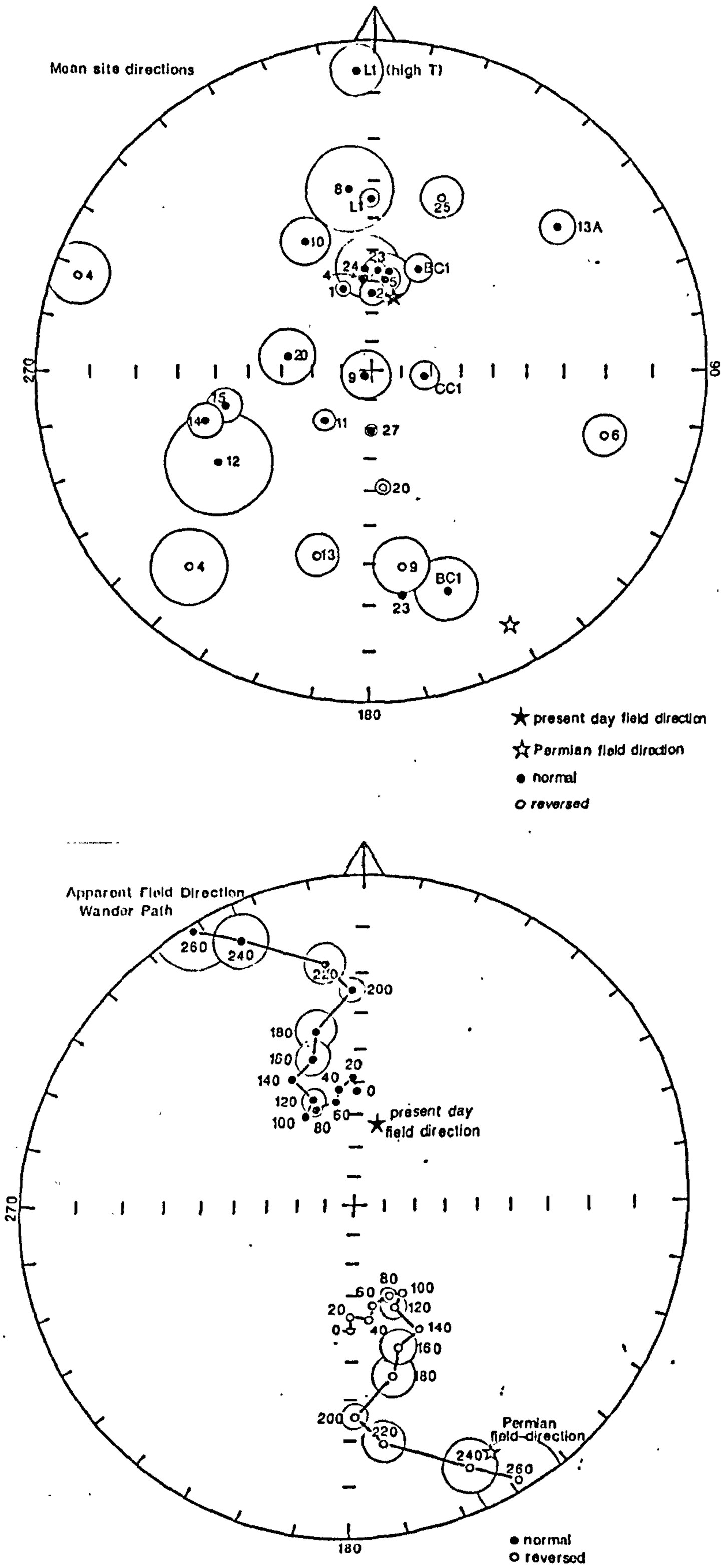

fig. 5.39 Summary stereographic projection of all site mean directions compared with the apparent field direction wander path. Normal directions are given as solid symbols, reversed directions are given as open circles. *A95* circles of confidence are given as large circles around each mean direction.

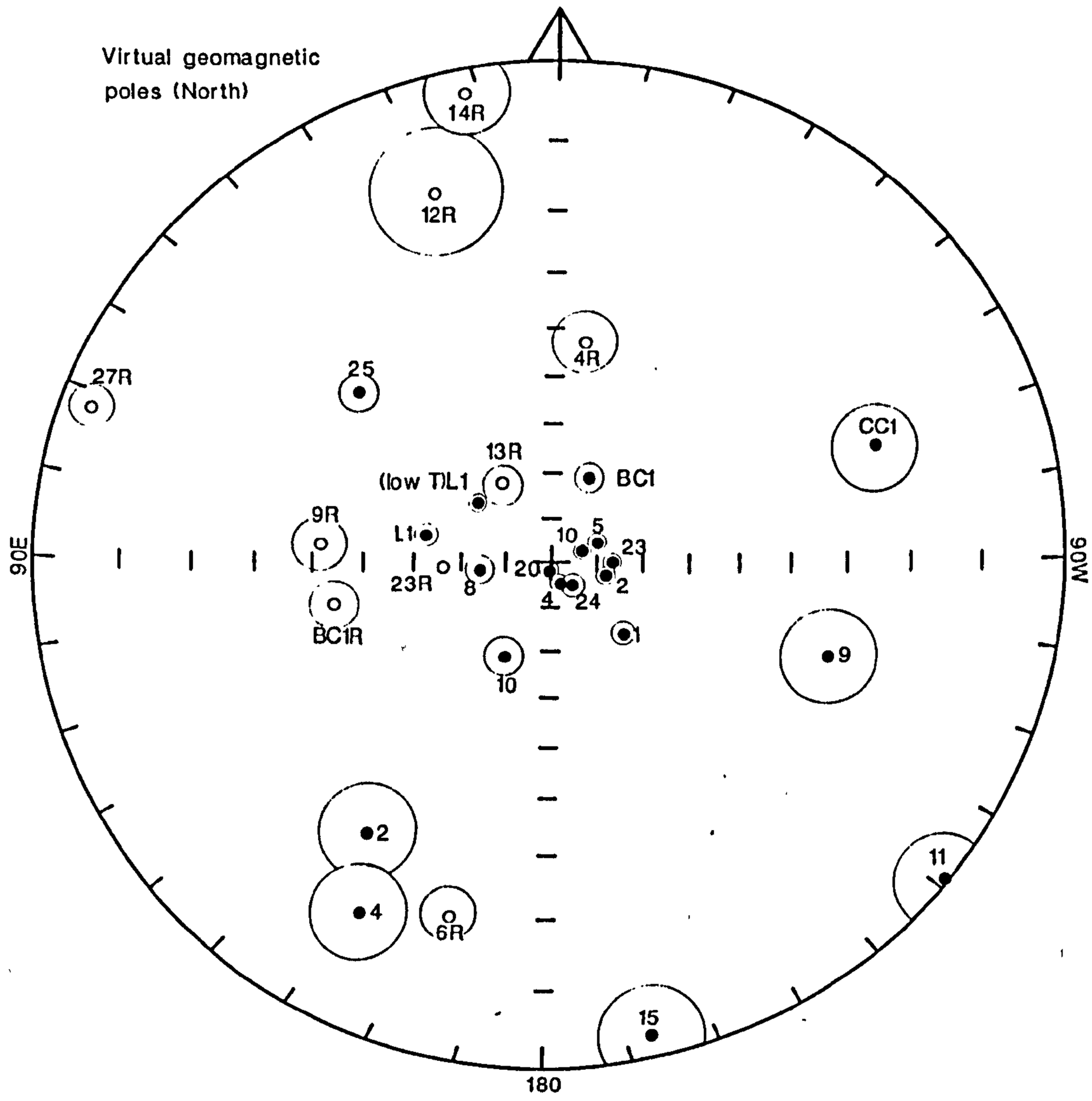

fig. 5.40 Summary stereographic projection of all site virtual poles. Normal directions are given as solid symbols, reversed directions are given as open circles. *A95* circles of confidence are given as large circles around each mean direction.

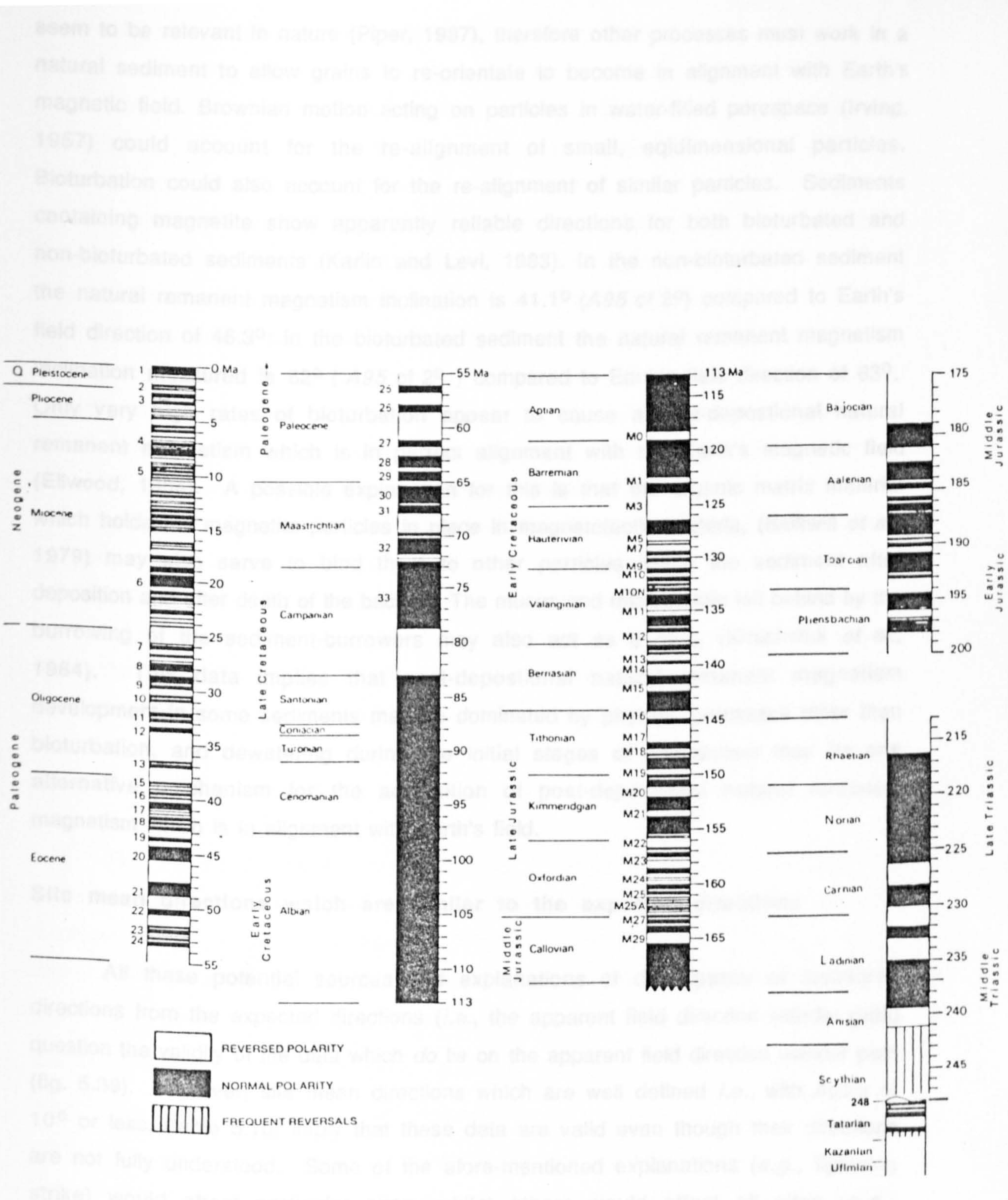

fig. 5.42 The geomagnetic polarity time scale for Permian times to the Cenozoic (Piper, 1987).

seem to be relevant in nature (Piper, 1987), therefore other processes must work in a natural sediment to allow grains to re-orientate to become in alignment with Earth's magnetic field. Brownian motion acting on particles in water-filled porespace (Irving, 1957) could account for the re-alignment of small, eqidimensional particles. Bioturbation could also account for the re-alignment of similar particles. Sediments containing magnetite show apparently reliable directions for both bioturbated and non-bioturbated sediments (Karlin and Levi, 1983). In the non-bioturbated sediment the natural remanent magnetism inclination is 41.1° (*A95* of 2°) compared to Earth's field direction of 46.3°; in the bioturbated sediment the natural remanent magnetism inclination measured is 62° (*A95* of 2°) compared to Earth's field direction of 63°. Only very high rates of bioturbation appear to cause a post-depostional natural remanent magnetism which is in perfect alignment with the Earth's magnetic field (Ellwood, 1984). A possible explanation for this is that the organic matrix material which holds the magnetite particles in place in magnetotactic bacteria, (Balkwill *et al.*, 1979) may also serve to bind them to other particles within the sediment after deposition and after death of the bacteria. The mucus and microprotein left behind by the burrowing of the sediment-burrowers may also act as a glue, (Kirschvink *et al.*, 1984). This data implies that post-depostional natural remanent magnetism development in some sediments may be dominated by physical processes other than bioturbation, and dewatering during the initial stages of compaction may be one alternative mechanism for the acquisition of post-depostional natural remanent magnetism which is in alignment with Earth's field.

Site mean directions which are similar to the expected directions

All these potential sources and explanations of discrepancy of measured directions from the expected directions (*i.e.*, the apparent field direction wander path) question the validity of the data which *do* lie on the apparent field direction wander path (fig. 5.39). However, site mean directions which are well defined *i.e.*, with *A95*'s of 10° or less, (table 5.10) imply that these data are valid even though their directions are not fully understood. Some of the afore-mentioned explanations (*e.g.*, lightning strike) would affect particular sites, whilst others would affect all sites (*e.g.*, continental rotations). After comparison with the apparent field direction wander path, virtual poles were calculated, for those sites from which a mean direction was isolated, (Piper, 1987) (fig. 5.40) in order that the site data could be compared to the established apparent polar wander path (fig. 5.41) and the time-scale of 'normal' and 'reversed' polarity periods (fig. 5.42).

Sites M1, M2, M4, M5, M10, M20, M23, M24, BC1

The mean site directions from these sites, except M20, form a cluster with inclinations ranging from 55° to 64° and declinations ranging from 342° to 24°; most cluster around zero declination. These directions have normal polarity and are well defined. Site M20 is similar to the above directions except that it has reversed polarity. The sites come from the basin, basin margin, lower and upper foreslope facies, and the interpreted magnetic carriers include pyrrhotite and goethite and haematite.

The site mean directions lie close to the apparent field direction wander path between 80 Ma (site M1) and the present day direction. Site M1 carries two vectors: one with normal polarity at around 80 Ma which suggests an Upper Cretaceous age, more specifically Santonian or Upper Campanian and one with reversed polarity at around 40 Ma which suggests natural remanent magnetism acquisition in the uppermost Eocene or in early Oligocene times. The remaining sites all have normal polarity and indicate an age somewhere between 20 Ma and present day. Their common polarity may be coincidental or may indicate that the natural remanent magnetism was acquired during the same period of normal polarity. There have been many periods of normal polarity during the last 20 Ma and the natural remanent magnetism could represent any of these, though perhaps the most likely is the present day field direction.

Sites M10, M8, L1and M9

The site mean directions for these sites lie on, or close to, the apparent field direction wander path. All are well defined, although the *A95* for site M8 is only 19.8°. A range of magnetic carriers is indicated, including pyrrhotite and magnetite/haematite and goethite. The sites are from the basin and upper foreslope facies. The best estimate of directions for site L1 suggests that low T_b and high T_b (480°C - 530°C) components are involved. The low T_b component, probably carried by goethite has a direction comparable with the apparent field direction wander path at 190 Ma. The high T_b component, probably carried by magnetite, has normal and reversed polarity, an inclination of 5° and a declination similar to that of the apparent field direction wander path at 245 Ma. This suggests that this vector was acquired during a period of mixed polarity. Comparison with the polarity time scale places the timing of this natural remanent magnetism as Ochoan/Scythian.

Sites M8 and M9 have directions of opposite polarity but similar age of 190 Ma. Site M13 also has a reversed direction similar to M9, but different in declination by

about 15°. Comparison with the polarity time scale indicates a Late Jurassic to Early Cretaceous age for natural remanent magnetism acquisition, a time when the Earth's field was reversing polarity frequently.

5.6 Conclusions and further work

The palaeomagnetic directions (table 5.10) derived from sites in this study indicate that most of the samples contain magnetic minerals in large enough quantities to be of use in palaeomagnetic studies even though they are carbonates and sandstones. Even samples with natural remanent magnetism intensity as low as 0.1 x $10^{-4}Am^{-1}$(*e.g.*, sites M12, M8 and M19) can give useful information; particularly when considered within the context of more reliable, higher intensity data. There is often little within site variation of vector directions, intensity or susceptibility behaviour with progressive demagnetisation, although absolute values usually vary between samples, and well-defined mean directions were obtained from most sites. Vectors isolated from both alternating field and thermal demagnetisation are also similar. However, although sites have well-defined mean directions, many of these directions differ from the expected directions *i.e.*, the past and present directions of the Earth's field for the study area. The main reasons for this are: the acquisition of spurious remanences during the demagnetisation process, especially for samples with weak natural remanences, and the overlap of blocking temperature spectra of natural remanences, acquired at different times by different magnetic minerals with a variety of grain sizes, during the course of diagenesis.

Natural remanent magnetisation intensity and susceptibility changes with thermal demagnetisation reveal the T_b spectra of the magnetic components present and aid the isolation of the components of the total natural remanent magnetism. These changes are also useful in constraining the mineralogy of the remanence carriers, as well as the range of grain sizes present. There is a range of mineralogy and domain size of natural remanent magnetism carriers within some sites and between sites (table 5.11). In some sites, within site variation reflects differences in magnetic carrier(s) and consequently in natural remanent magnetism direction(s). Natural remanent magnetism carriers are often ambiguous due to their blocking temperature spectra being lower than would be expected for pure magnetic mineral phases. Causes for this are probably related to the burial/thermal history of these strata and are discussed in chapter 6.

Goethite carries viscous natural remanent magnetism in samples from most sites (table 5.11). Pyrrhotite is a major natural remanent magnetism carrier; haematite is the other major carrier. Most of the natural remanent magnetisms have ages which are younger than Upper Permian *i.e.*, the stratigraphic age of the rocks, and are interpreted as chemical remanent magnetisms *i.e.*, they have diagenetic origins. Ages of around 200 Ma and 80 Ma to 20 Ma are indictated; the remainder of the ages are ambiguous or unresolved. The significance of these ages and explanation of the timing of natural remanent magnetism acquisition are related to the diagenetic history and are discussed in chapter 6.

There is apparently little relationship between age of natural remanent magnetism and facies, although there is a relationship between initial susceptibility versus intensity (table 5.11) and facies/lithological characteristics (fig. 5.37). These relationships are discussed in chapter 6.

Further work could be done on the isolation of vectors in cases where there is a clear overlap of more than one component and blocking temperature spectra, as indicated by Zijderveld projections of the data. Analysis of these vectors has not been developed to the fullest extent because of the volume of data involved in this study. Vectors unresolved after plotting on orthogonal plots could be replotted on stereographic projections in order to see if there was any convergence of circles of remagnetisation, thus indicating the directions of one of the end points (Collinson, 1983). This would only work if *a*. the sites selected displayed a combination of the same two vectors, and *b*. there is a dispersion of one component relative to the other component within these samples. Resolution of vectors could be improved by plotting site directions at intermediate temperatures and analysing any patterns that might be revealed in this way *i.e.*, observing the demagnetisation of site data in the dimensions of space and 'demagnetisation time'. No doubt some computer package somewhere could model this admirably, or one could be written!

Samples from some sites *e.g.*, site M20, could be demagnetised to higher temperatures in order to *completely* remove the natural remanent magnetisation.

Combined thermal and AF demagnetisation of samples from within the same site *e.g.*, thermal demagnetisation at lower temperatures and AF demagnetisation at later stages of demagnetisation, may enable better resolution of those vectors which became disguised by spurious remanences acquired due to mineralological changes resulting from the thermal demagnetisation process. Thermal demagnetisation in an oxygen-free atmosphere *e.g.*, nitrogen (g), would be interesting to compare with thermal demagnetisation in air, in order to compare mineralogical changes.

Isothermal remanent magnetism acquisition should be investigated in order to

identify the magnetic carriers with greater confidence than that derived from the demagnetisation data alone. This is particularly important because varitions in purity and domain size in the magnetic carriers, and temperature/duration of natural remanence acquisiton, can result in ambiguous T_b spectra (chapter 6).

All carbonate and silicate phases could be removed by dissolution in order to enable visual and physical examination *e.g.,* X-ray diffraction analysis, of the insoluble magnetic mineral residue. A potential problem for this is that a suitable solvent would have to be found that did not also remove, completely or in part, magnetic phases such as goethite.

Chapter 6. Discussion

'But if instead of hearing merely a symphonic mass of sound, we are able to isolate the themes as they enter, to see how one by one they are intricately woven together and by what magic new harmonies are produced, percieve the manifold subtle variations on a single theme, however disguised it may be, then the total effect is immeasurably enhanced.' W.G. Hoskins - The making of the English landscape; published by Hodder and Stoughton.

6.1 Introduction

In this chapter the results and interpretations from magnetic, palaeomagnetic, sedimentological and diagenetic studies (chapters 2,3,4, and 5) are integrated by relating these to the burial history of these strata. A knowledge of the burial and thermal history of the rocks is crucial to the understanding of: i. the movement of fluids during burial; ii. the chemical conditions prevailing during diagenesis; iii. the temperatures to which these rocks have been subjected; and iv. the timing/duration of particular phases of burial. Knowledge of these factors helps to constrain which magnetic minerals were likely to form during diagenesis and constrains the timing of the acquisition of natural remanent magnetism and its relaxation time as well as constraining the timing of certain diagenetic events.

6.2 Burial and thermal history

A burial curve, for strata of Mid-Upper Capitan age, has been estimated (fig. 1.5) by calculating amounts of deposition versus amounts of erosion and by incorporating information on the tectonic history of this area (Hills, 1984; Jones, 1953; Mazzullo, 1986). These data suggest that the strata of the Capitan shelf margin of upper-Mid Capitan and Upper Capitan age were buried to a maximum of about 1km, and that maximum burial was in the late Cretaceous. Periods of erosion took place during the Lower/Middle Triassic, the Jurassic and from the late-Cretaceous to the present day. All these periods of erosion were probably accompanied by the influx of meteoric waters into the strata of the Capitan shelf margin. The dip of the Delaware Basin has been eastwards since at least the end of the Cretaceous, and probably since 80 Ma (Hills,

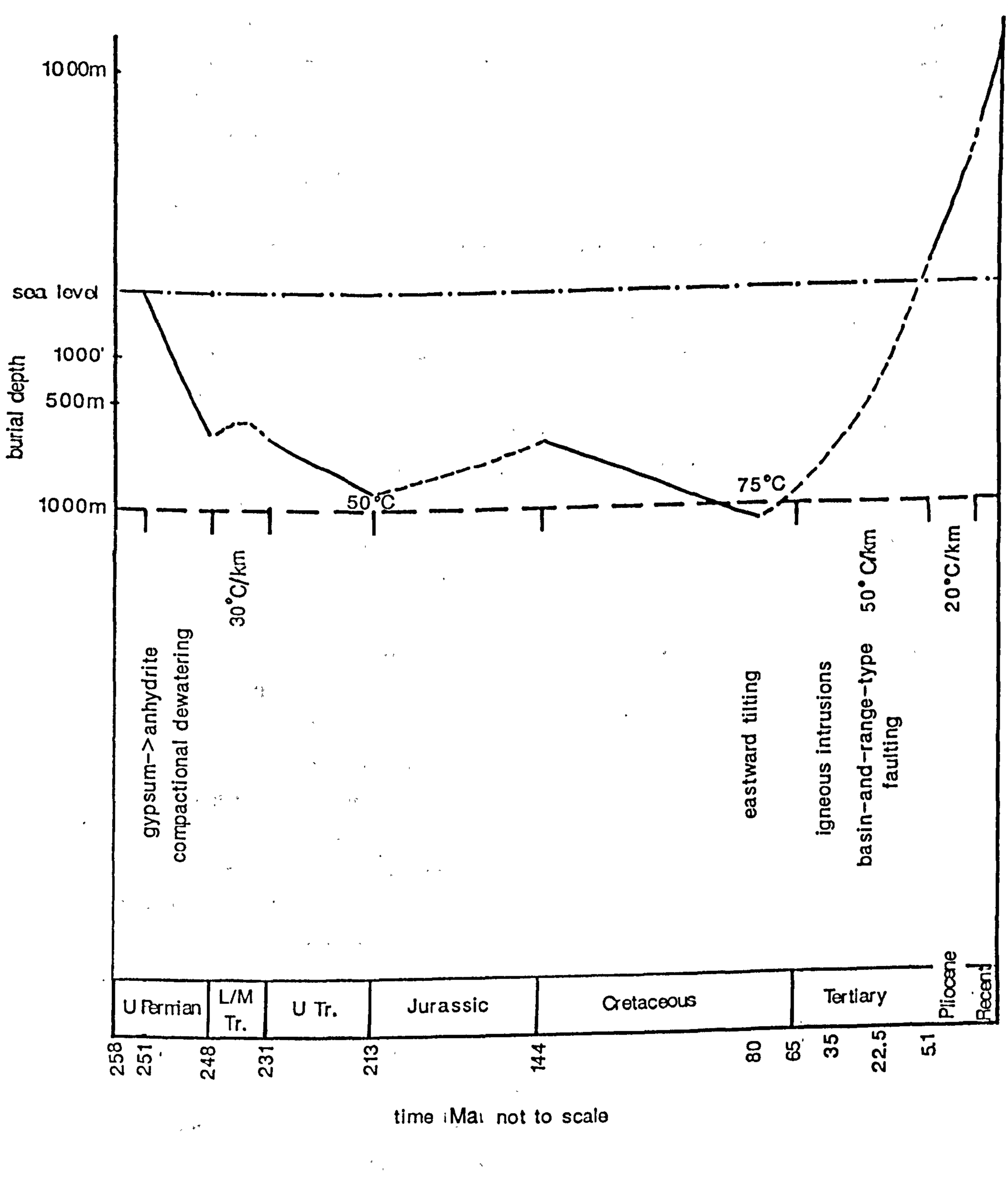

fig. 6.1 Summary diagram of the thermal history, superimposed on the burial curve, for strata of upper Middle to Upper Capitan age. The main aspects of basin evolution are also shown. The surface temperature is taken as 25°C. Geothermal gradients are taken from Tissot and Welte (1978), Barker and Halley (1986) and Barker and Pawlewicz (1989).

1984; Hiss, 1980). This eastward tilting would have allowed recharge down the depositional dip of the strata (Hiss, 1980; Mazzullo, 1986). In Tertiary times uplift has been very rapid and the Delaware Basin was probably elevated to above sea level by 35 Ma (Hills, 1984). Uplift of a further 1200m or so, brought the rocks of the western Delaware Basin to their present elevation; this period of uplift was associated with higher heat flow, igneous activity and block-faulting (fig. 6.1) which accompanied the basin-and-range-type extension in the south-western United States.

The thermal history of the Delaware Basin has been estimated by compiling data from fluid inclusions and mean random vitrinite reflectance (Barker and Halley, 1986; Mazzullo, 1986; Barker and Pawlewicz, 1989) and direct down-hole measurements (Mazzullo, 1986). The present day geothermal gradient for the western Delaware Basin has been measured down-hole at 18 - 21°C/km (Mazzullo, 1986) and at 20°C/km (Geothermal survey of North America subcommittee, 1976). The geothermal gradient in the Palaeozoic has been estimated from a variety of data as being around 30°C/km (Tissot and Welte, 1978). Fluid inclusion studies of sphalerite from a core in the eastern part of the Delaware Basin indicated that these sphalerites were precipitated from fluids at a temperature 40 - 50°C hotter than could have been expected from burial depths and normal heat flow at the end of the Cretaceous or in the early Tertiary (Mazzullo, 1986). A source of fluids from the (hotter) basin was inferred to explain these high formation temperatures. However, there is evidence from a variety of sources that the geothermal gradient was significantly higher during Tertiary times, than during the Palaeozoic or than the present day geothermal gradient. Mean random vitrinite reflectance data from over 40 wells in the western Delaware Basin suggest that the geothermal gradient was 40°C/km. This heating post-dated eastward-tilting of the basin and has been interpreted as related to higher heat flow associated with the emplacement of igneous intrusions during the Tertiary (Barker and Halley, 1989). Fluid inclusion data from blocky calcite cements in the Capitan reef at McKittrick Canyon indicate that this cement formed from fluids at a temperature of about 75°C and thus a geothermal gradient of 50°C/km has been estimated for the Tertiary (Barker and Halley, 1986). This cement is interpreted as being one of the last cements precipitated in the Capitan shelf margin (chapter 3 and Barker and Pawlewicz, 1986). Other evidence for high heat flow affecting the Capitan shelf margin is the presence of dickite in fractures associated with the late calcite spar (chapter 3). This data infers that the maximum temperature to which the strata of the Capitan shelf margin, of upper-Mid Capitan and Upper Capitan age were subjected to, due to burial, was around 75°C and that the period of maximum geothermal gradient occurred around 35 Ma (fig. 6.1).

6.3 Diagenetic events and the paragenetic sequence

The diagenetic events which have affected the Capitan shelf margin in the western part of the Delaware Basin (chapter 3) can be related to the burial and thermal history of the region (fig. 3.41 and fig. 6.2). Syndepositional and early reflux dolomitisation (Adams and Rhodes, 1960), associated with the earliest phase of draw-down which accompanied the desiccation of the Delaware Basin, caused dolomitisation of back reef facies and foreslope strata before significant burial. Anhydrite occluded the primary porosity of the Capitan shelf margin left after the precipitation of marine cements and replacement by anhydrite occurred on early burial, due to the infilling of the Delaware Basin by the Castile Formation and associated fluid movement. Some of the calcium sulphate may have been originally precipitated as gypsum. The transformation of gypsum to anhydrite on burial is thought to take place at around 500m (Murray, 1964) although these relationships are not well known. The petrographic evidence of replacive textures, indicates that anhydrite replaced carbonates in the Capitan shelf margin. This required burial to several hundred metres and the continued input of calcium sulphate-laden fluids, in order to maintain the volume originally taken up by the gypsum after its replacement by anhydrite, and for anhydrite to replace the host carbonate. This suggests that fluid movement continued on further burial *i.e.*, beneath the Castile Formation. The continued flushing of calcium sulphate-laden fluids during Castile times caused further dolomitisation which was pervasive and fabric destructive, particularly in parts of the lower foreslope, where replacement by anhydrite was taking place. The upper part of the foreslope and the back reef facies also contain some replacive anhydrite textures; these strata were several hundred metres of depositional relief higher then the lower foreslope facies and were therefore not buried to the depths required for the transformation of gypsum to anhydrite until later in the burial history. The Salado Formation overlies the Castile Formation and is composed mainly of halite rather than anhydrite, especially in the upper parts of the formation, although magnesite, dolomite and polyhalite are also present. Traces of magnesite have been suggested in parts of the lower foreslope facies but halite pseudomorphs have not been found; this suggests that the porosity and permeability in the Capitan shelf margin strata had been reduced to such an extent by anhydrite cementation, that they were effectively sealed *before* the deposition of the upper (halite) part of the Salado Formation.

There is no petrographic evidence of diagenetic events affecting the rocks of the Capitan shelf margin until the large-scale dissolution of anhydrite started, concomitant with the formation of the calcite spars. At 80 Ma tectonic activity started to affect the Delaware Basin and the basin was tilted eastwards, rapidly uplifted and affected by

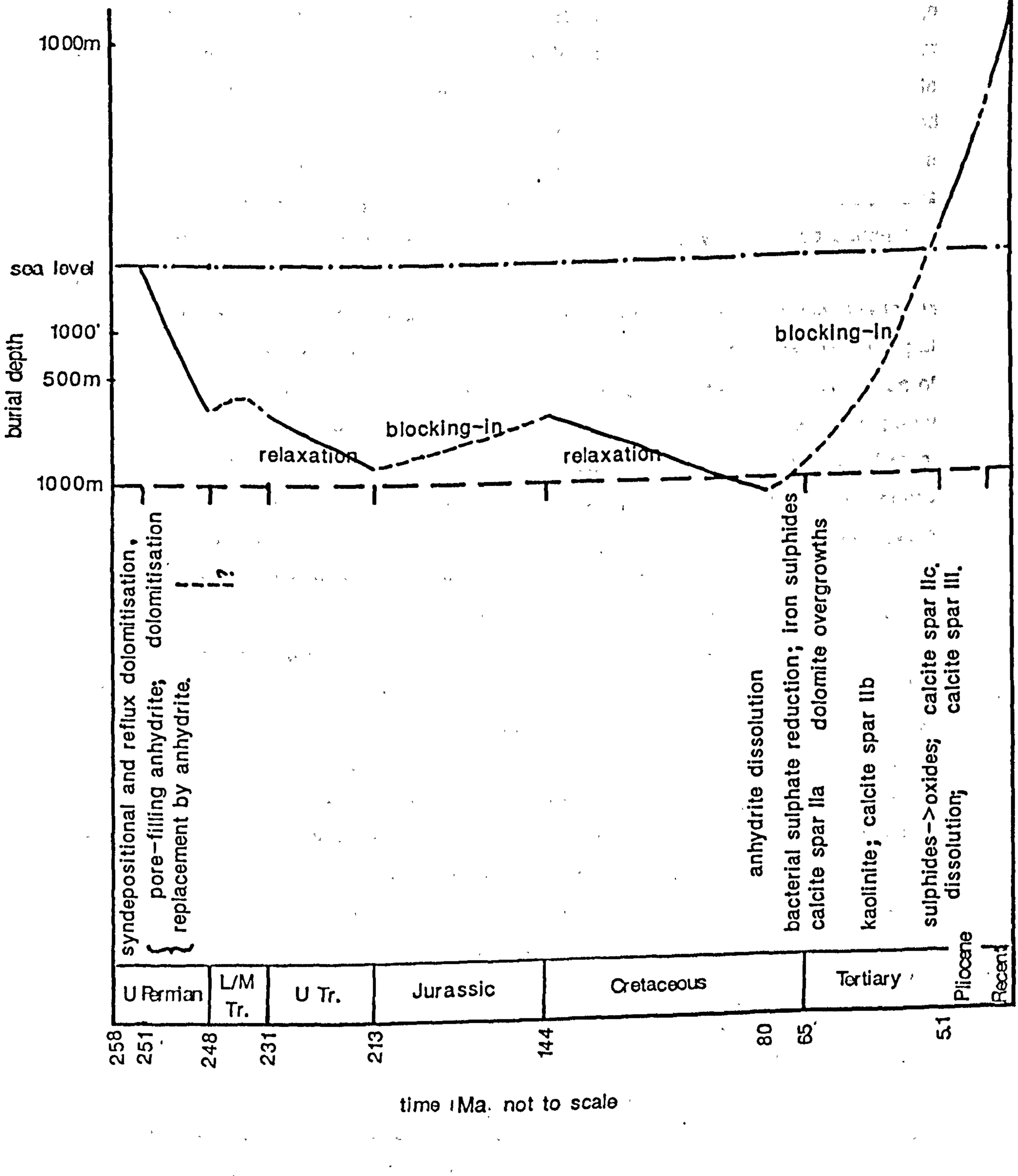

fig. 6.2 The main diagenetic events which have affected the Capitan shelf margin related to the burial and thermal history of the region.

basin-and-range-type faulting and higher heat flow (fig. 6.1). Meteoric water flowed down-dip from recharge areas in the mountains which were forming around the margins to the basin (fig. 1.4) (Hiss, 1980; Mazzullo, 1986). The continuous input of large volumes of meteoric water down-dip caused the dissolution of the anhydrite, under reducing conditions. Several diagenetic phases were associated with this anhydrite dissolution. Meteoric waters transported sulphate-reducing bacteria which caused sulphate reduction and calcitisation of some small quantities of anhydrite and the formation of spar IIa, and the concomitant formation of iron sulphides (pyrite/pyrrhotite). Dolomite overgrowth cements also probably developed during this phase.

Faulting started at 22.5 Ma and was accompanied by higher heat flow due to the emplacement of igneous intrusions (fig. 6.1). The rate of meteoric water input increased greatly after the period of faulting. After this faulting the rate of dissolution of anhydrite probably exceeded the rate of the calcitisation of anhydrite by bacterial sulphate reduction and some fracturing of the strata occurred, due to partial collapse, particularly in the lower foreslope facies. There was not enough time for the phase change from anhydrite to gypsum to occur on uplift before dissolution had taken place and anhydrite is still present in the subsurface (Garber *et al.*, 1989).

Kaolinite is found in pores in the backreef and foreslope facies and dickite is found in association with calcite spar IIb in fractures in the basin margin facies. This period of kaolinite/dickite formation took place following the development of the dolomite overgrowths and following fracturing. Kaolinite/dickite formation requires acidic conditions and dickite indicates elevated temperatures. The presence of dickite rather than kaolinite in the basin margin facies only, is consistent with the higher temperatures which would be expected in the basin margin facies which is around 600m topographically below the shelf crest and has therefore been buried deeper than the shelf crest. The development of the acidic conditions necessary for the development of kaolinite/dickite were associated with the mixing of this new influx of meteoric water with waters rich in hydrogen sulphide resulting from bacterial sulphate reduction and causing the formation of sulphuric acid and possibly also hydrocarbon migration. The reduction of sulphate by bacteria may have been enhanced by the migration of hydrocarbons from the basin at this time (Barker and Halley, 1986).

The meteoric waters brought in large volumes of calcium carbonate in oxygenated solution, resulting from the uplift, erosion and dissolution of the exposed surface of the Capitan shelf. This calcium carbonate precipitated as spar IIb and spar IIc, in pore spaces left after the dissolution of anhydrite and was accompanied by the oxidation of iron sulphides to haematite. Spar IIa is interpreted as resulting from the calcitisation of

anhydrite under reducing conditions; there is no reason to suppose that spar IIb precipitated from waters with a different composition. Minor dissolution of calcite spar IIb and kaolinite formation occurred prior to the precipitation of calcite spar IIc and spar III and suggests that reducing and acidic conditions continued to prevail.

Dissolution and compositional zoning of the calcite spars, seen under cathodoluminescence, indicates that the pH and redox conditions and the composition of the meteoric water, from which the calcite spars were precipitated, varied with time. The controls on these factors are the rate of flow, the residence time and the contribution from diagenetic reactions. These were controlled by the rate of dissolution of the anhydrite which opened up pore space and caused fracturing; bacterial sulphate reduction and the migration of H_2S-rich fluids up-dip coming in to contact with oxygenated groundwaters and causing the formation of dilute sulphuric acid. Sulphate reducing bacteria require hydrocarbons in order to metabolise sulphate and the source of these hydrocarbons may have been from the petroleum generated due to the heating of the Western Delaware Basin by igneous intrusions at around 35 Ma (Barker and Halley, 1986). The presence of native sulphur and minerals containing traces of arsenic, barium, copper, zinc, lead, molybdenum in mines and caves around the Capitan shelf margin (Hill, 1989) argues for some input of fluids from the basin. The mechanism for the production of the large caves found in the Capitan shelf margin has been interpreted as resulting from sulphuric acid production due to bacterial sulphate reduction associated with the movement of hydrocarbons (DuChene, *cited in* Jagnow, 1986; Hill, 1987). Another explanation for the development of acidic conditions is the oxidation of pyrite/pyrrhotite to haematite which is a acid-generating reaction. In the oxic environment, pyrite (and other iron sulphides) will oxidise to haematite according to the equation:

$$FeS_2(s) + 15/4\ O_2(aq) + H_2O(l) \rightarrow Fe(OH)_3(s) + 2\ H_2SO_4(aq)$$

In nature this reaction is not simple and the ultimate driving force is the availability of dissolved atmospheric oxygen, derived from recharge of meteoric waters (Berner, 1981). Only small quantities of iron sulphides has been found, and although this mechanism may explain the small-scale corrosion of spar IIb, it is unlikely to explain the dissolution of the large cavern systems found in the Capitan shelf margin.

6.4. Timing of magnetic mineral formation and the acquisition of natural remanent magnetism

The magnetic characteristics of the rocks studied from the Capitan shelf margin are dependent on the origins of the magnetic minerals as well as on the chemical and thermal history of these strata. The magnetic minerals present in these rocks could have been derived from eroded rocks and *deposited* during the Guadalupian, or could have been formed by *biogenic* or *diagenetic* processes during the subsequent burial and diagenesis of the rocks of the Guadalupe Mountains. The origins, occurrence and characteristics of magnetic minerals in carbonate sediments are discussed in chapter 3. The magnetic minerals which have been identified from magnetic studies (chapter 5), and which carry a natural remanent magnetism, are interpreted as pyrrhotite, magnetite/haematite and goethite; maghemite is also indicated, but is much less common (*N.B.*, pyrite is also considered here because of its potential for diagenetic alteration to magnetic minerals).

The timing of natural remanent magnetism acquisition is dependent on temperature (the blocking temperature) and is also dependent on grain size for very small grains (chapter 5). When a magnetic mineral is growing, it can only retain a magnetic moment when it has grown to certain size *i.e.*, through its blocking volume. Rapid diagenetic changes *e.g.*, the influx of large volumes of meteoric water causing the reduction and dissolution of anhydrite and associated diagenetic reactions, cause the formation of small grains which can grow through their blocking volume if the diagenetic reactions proceed for long enough.

The minerals which have been interpreted as magnetite/haematite (chapter 5) have not been unequivocally identified as either magnetite or haematite because they have blocking temperature spectra lower than expected for pure, single domain minerals (table 5.11). Lower blocking temperature spectra indicate that the magnetic minerals either have an impure composition (Piper, 1987) or that the magnetisation that they carry was acquired over a long period of time at lower temperatures (Pullaiah *et al.*, 1975). Clay minerals have been found as inclusions within some haematite, and electron microprobe analysis also indicates the presence of some Al and Si (chapter 3) in haematite. Petrographic examination indicates that some haematite crystals are up to 1cm in length; these grains would be multi-domain and domain sizes within these grains could be large and viscous 'soft' behaviour could result.

Blocking curves have been developed (fig. 6.3) which show the theoretical relationship between the duration of heating at the temperature at which the natural remanent magnetism is *blocked in to* the grain, with the blocking temperature and length

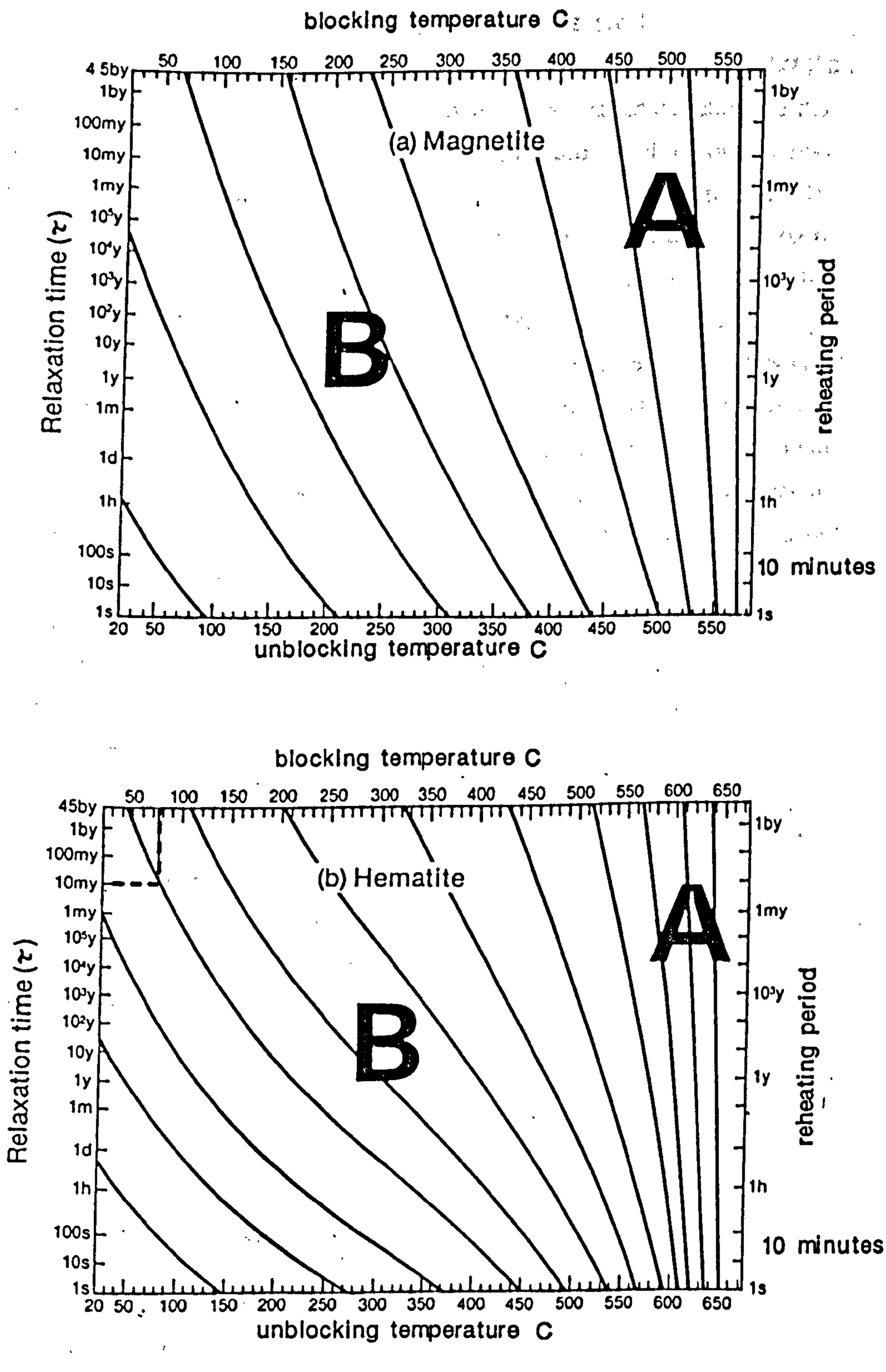

fig. 6.3 Blocking curves for a. haematite and b. magnetite (Pullaiah *et al.*, 1975) showing the relationship between temperature/duration for the *blocking-in* of natural remanent magnetism versus the temperature/duration for the *unblocking* of natural remanent magnetism.

of time required to *unblock* this natural remanent magnetism (Pullaiah, *et al.*, 1975). The overall relationship is that individual blocking temperatures are lowered and their collective range is broadened during prolonged heating. These blocking curves predict the result of a purely physical effect and do not take account of the diagenetic changes that affect rocks on burial, and reservations have been expressed on their quantitative application (Piper, 1987). However, the blocking curves suggest that *e.g.*, for haematite, a natural remanent magnetism which is unblocked at 450°C, after heating of the sample in the laboratory for 10 minutes, could have been blocked in to that haematite at *for example*, 95°C for 1my or 75°C for 10 Ma. The ambiguous mineral, which has been hitherto referred to as magnetite/haematite (chapter 5), has a blocking temperature of between 450°C and 590°C when heated for 10 minutes. The burial and thermal history of the Capitan shelf margin (fig. 6.1) indicates that the maximum burial temperature probably did not exceed 75°C and that the temperature did not exceed 50°C for most of the burial history. This information, on the maximum burial temperature and the temperature/duration required to unblock the natural remanent magnetism, can then be applied to the blocking curve. These curves suggest that the maximum blocking temperature possible for haematite from rocks in this study is around 480°C, given that these rocks are 255 Ma old and have not been heated to temperatures greater than 50°C for most of their burial history. The blocking curves indicate that if the ambiguous mineral is haematite with a blocking temperature of 450°C, then the magnetisation could have been acquired by heating to 75°C for 10 Ma, or by heating to lower temperatures for a longer duration. Blocking temperatures of up to 590°C have been identified and these cannot be explained by the effects of prolonged heating described by these blocking curves, assuming that the curves are applicable to all magnetites and haematites.

6.4.1 Magnetite

Magnetite has not been unequivocally identified in the magnetic studies although its presence is suggested from the relationship between blocking temperature and the blocking curves (fig. 6.3) in sites M15, M12 and M20, and from intensity/susceptibility relations in site L1 (basin facies). However, in this site, the blocking temperature is lower than expected for pure magnetite; this suggests that the magnetite is impure. This indicates that the magnetite does not have a biogenic origin. Magnetite has been identified petrographically from the Brushy Canyon siltstone in the basin facies, and this magnetite exhibits exsolution lamellae of ilmenite (fig. 3.40)

which indicates that it formed by crystallisation from a melt and was derived from weathering and transport of continental igneous rocks. Magnetite formed in igneous rocks is commonly rich in titanium, and these factors suggest that the magnetite found in site L1 is detrital, titanium-rich magnetite. The natural remanent magnetism directions from site L1 indicates that some of the remanence was acquired around 245 Ma *i.e.*, shortly after deposition. This age of remanence acquisition supports the interpretation that this magnetite was detrital.

If *diagenetic* magnetite was present and it had formed when the temperature of burial was 50°C or less *i.e.*, up to 80 Ma, then it would be expected to have a blocking temperature of 280°C or less. If magnetite had formed *since* the higher geothermal gradient developed in the last 80 my or so *i.e*, maximum temperature of 75°C, then it would be expected to have a blocking temperature of 300°C or less. Blocking temperatures of 300°C were identified from samples in sites M15 (back reef facies), M12 (reef facies) and M20 (upper foreslope facies) and these magnetisations could therefore have been acquired by the formation of diagenetic magnetite within the last 80 my. Carbonates which contain hydrocarbons or bitumen may contain associated magnetite (McCabe *et al.*, 1985; McCabe *et al.*,1987; Benthien and Elmore, 1987). Bitumen is commonly derived from the microbial degradation of liquid crude oil and it has been suggested, (Elmore *et al.*, 1987; McCabe *et al.*, 1987), that the magnetite results from microbial activity though no direct evidence has been found (although the discovery of a dissimilatory iron-reducing anaerobic bacterium which produces magnetite as a metabolic by-product (Lovley *et al.*, 1987), and the discovery that this bacterium can oxidise an aromatic hydrocarbon anaerobically (Lovley *et al.*, 1989), makes this proposed association more plausible). Other alternatives for the formation of diagenetic magnetite are the oxidation of iron sulphides such as framboidal pyrite or the reduction of precursor oxides, or the release of iron from iron-rich carbonate phases as a result of other diagenetic changes (McCabe *et al.*, 1987).

However, pyrrhotite *also* has a blocking temperature of 320°C and so it is possible that the blocking temperature of 300°C could be carried by pyrrhotite. In order to assess whether the natural remanent magnetism in sites M15, M12 and M20 is carried by magnetite or pyrrhotite, the chemical conditions of the formation waters must be examined. During the period when magnetite may have formed *i.e.*, since 80 Ma, anhydrite was being dissolved and calcitised under reducing condititions and H_2S and HCO_3 were being produced. Magnetite could form under these conditions as long as conditions were also alkaline (fig. 6.4). Pyrite and pyrrhotite will form under more reducing and more alkaline conditions (fig. 6.4). The stability fields of magnetite and

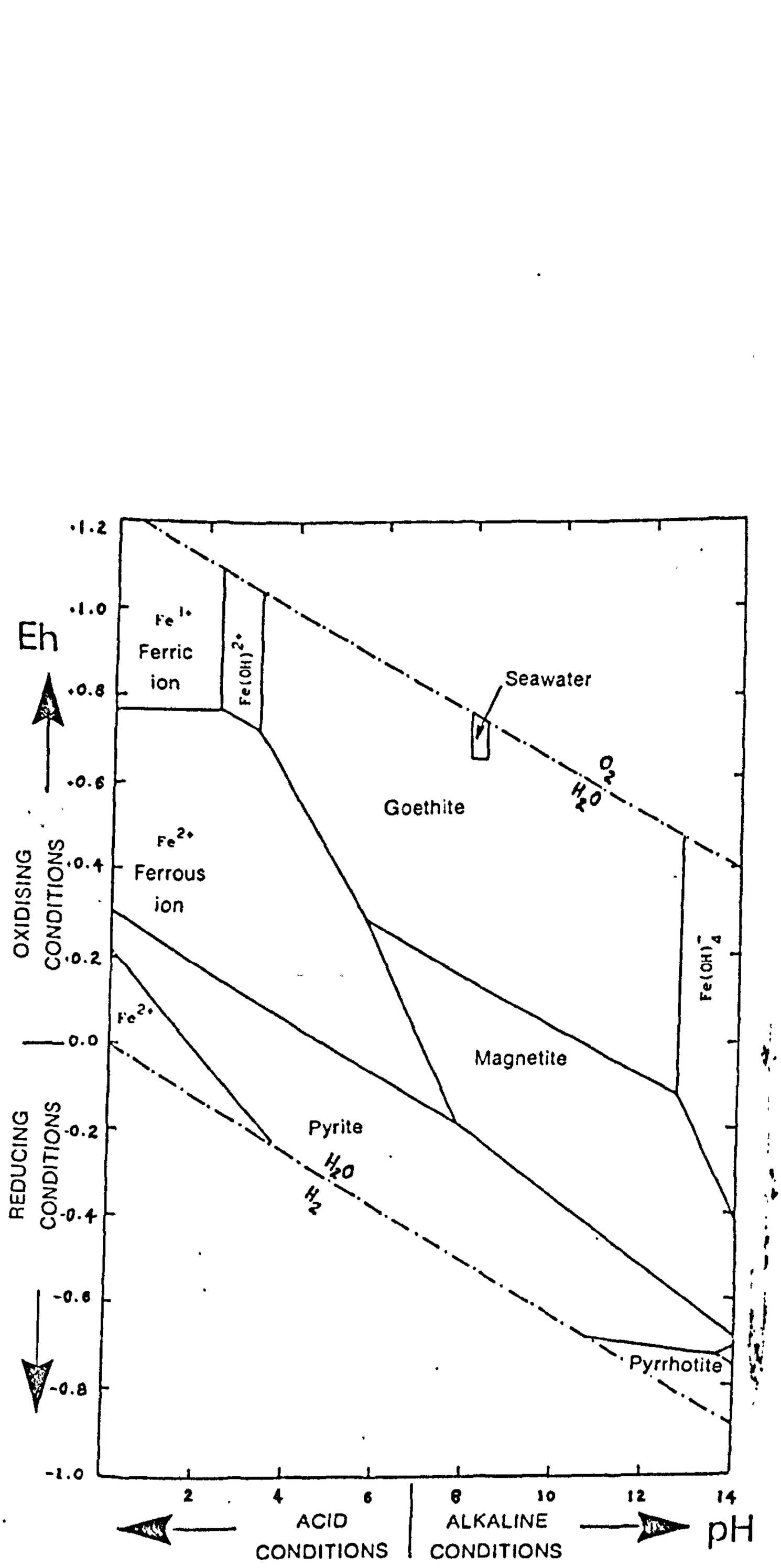

fig. 6.4 The stability fields of iron sulphides, magnetite and goethite in the presence of water (Henshaw and Merrill, 1980).

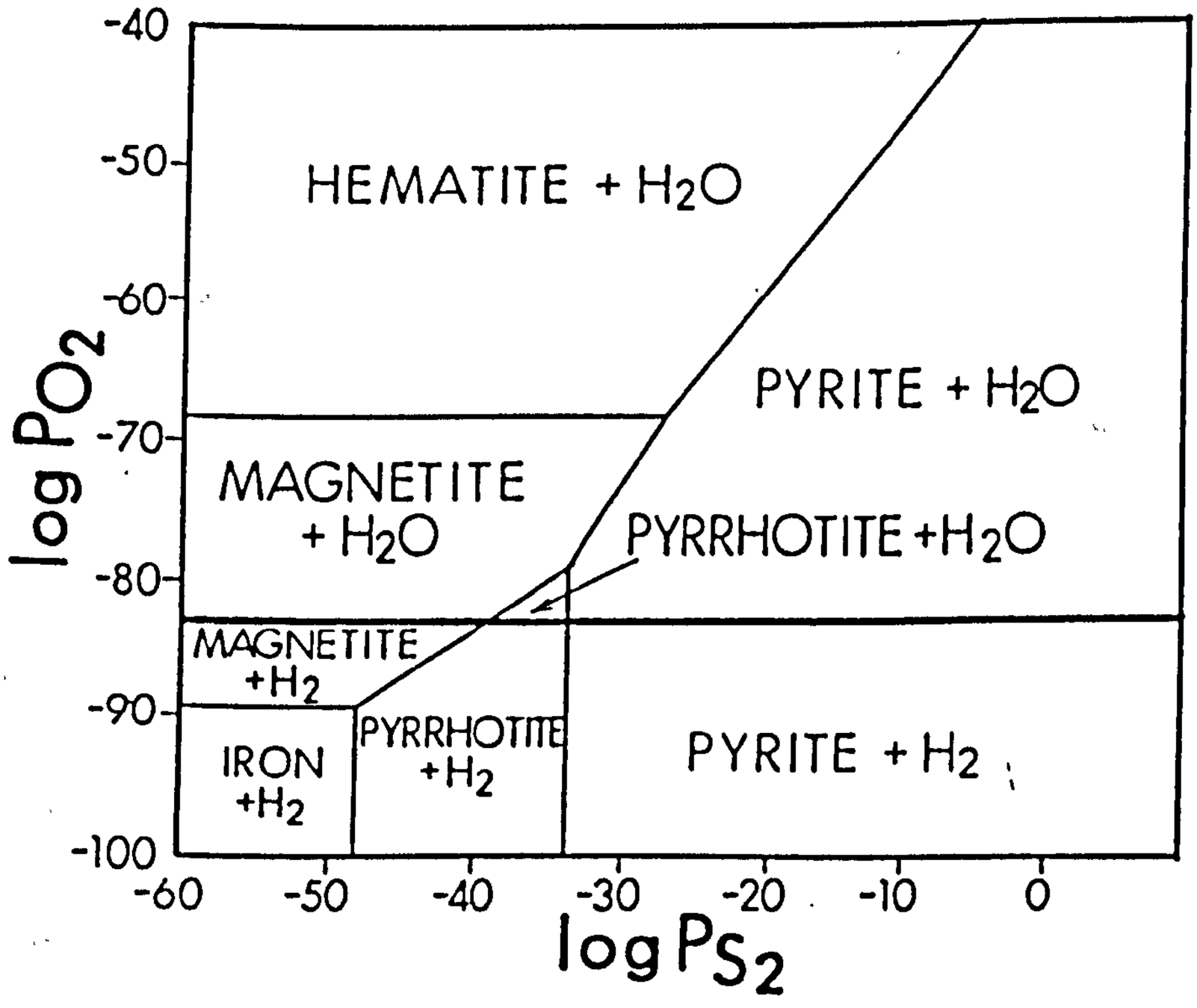

fig. 6.5 The stability fields of haematite, magnetite, pyrite and pyrrhotite as functions of the partial pressure of oxygen (P_{O_2}) and the partial pressure of sulphur (P_{S_2}) at 25°C and 1 atm. (Machel, in review). Diagenetic environments are aqueous and therefore plot above the H_2/H_2O boundary.

pyrrhotite as functions of partial pressures of O_2 and S_2 (fig. 6.5) indicate that the stability field of pyrrhotite is small, and that only small fluctuations in conditions would cause the formation of magnetite or pyrite instead of pyrrhotite. Whether pyrrhotite or magnetite formed is therefore still not unequivocally resolved although magnetite is more likely.

The chemical conditions of the pore waters present in the Capitan shelf margin during its burial are not known, however the rapid influx of meteoric water, in an effectively open system, during the Tertiary and especially since 22.5 Ma, would tend to encourage pyrite or magnetite formation rather than the formation of pyrrhotite. Pyrrhotite would be more likely to form under a more closed system, when conditions would be more reducing. Such conditions are more likely to have prevailed during the period between the input of meteoric waters (and associated sulphate reducing bacteria) during the early Jurassic and the late Cretaceous, when uplift began.

6.4.2 Iron sulphides

Pyrrhotite and pyrite, and other iron sulphides such as marcasite, were difficult to distinguish in both petrographic studies and from rock magnetic studies, because many of their properties are similar. Although pyrite and some pyrrhotite are non-magnetic they can oxidise to form haematite or iron hydroxides and are therefore important to consider. Iron sulphide minerals, pyrrhotite/pyrite, have been interpreted from magnetic studies as being present in rocks from sites in all the facies belts of the Capitan shelf margin *i.e.*, M13, M13A and M15 in the back reef facies, sites M8, M9, M10, M11 and M20 in the upper foreslope facies, site M2 in the basin margin facies, and sites L1, BC1 and CC1 in the basin facies (table 5.11).

Petrographic evidence indicates that anhydrite occluded most porosity in the Capitan shelf margin until the influx of meteoric waters in Tertiary times caused the dissolution and reduction of this anhydrite. The burial/thermal history of the Capitan shelf margin (fig. 1.5 and 6.1) indicates that the maximum burial temperature of these strata was around 75°C, at around 35 Ma, which is not hot enough for thermo-chemical sulphate reduction to have occurred and implies that reduction of anhydrite took place by bacterial sulphate reduction. These bacteria were introduced within meteoric water. Iron (and other metal) sulphides such as pyrrhotite, marcasite and pyrite, magnetite and HCO_3^-, H_2S are the by-products of the the reactions involved in the reduction of sulphate in the form of anhydrite or gypsum. There is no petrographic evidence for the

formation of magnetite. However, iron sulphide pseudomorphed some of the anhydrite (fig. 3.38 and pers. comm., G.M. Harwood, 1989; Machel, in press) and also precipitated around the margins of some pores (fig. 3.22c).

Where pyrrhotite (magnetite) is the carrier of the natural remanent magnetism many of the natural remanence directions are ambiguous (sites M13A, M11 and BC1) and difficult to interpret in terms of the apparent field direction wander path (chapter 5). Of those sites which contain possible pyrrhotite, only the site from the basin facies (site L1) has a natural remanent magnetism direction which suggests an Upper Permian age (245 Ma). Site mean directions from sites M13, M9, M10, M23 have natural remanent magnetism interpreted to be carried by pyrrhotite and with ages ranging from 210 Ma to 140 Ma. Pyrrhotite (or magnetite) commonly forms as a by-product of sulphate reduction assuming that there are iron ions available. These ages and the magnetic mineralogy suggest that a period of sulphate reduction and concomitant pyrrhotite formation may have occurred during initially during the upper Permian and again during Jurassic times. Uplift, associated with erosion and non-deposition and the possible influx of meteoric water, occurred during the Jurassic, from 213 to 144 Ma. Input of meteoric water containing bacteria could have caused minor sulphate reduction during this time. There is no other evidence for diagenetic events affecting the Capitan shelf margin at this time, or any other time until the late Cretaceous/early Tertiary.

Framboidal, opaque iron minerals occur in the micritic limestones and siltstones from the basin margin and basin facies respectively. Early diagenetic pyrite formation by bacterial sulphate reduction and oxidation of sedimentary organic matter is a common process in normal marine sediments below the sediment/water interface, where conditions are anoxic (Berner, 1984) and the pyrite formed in this way commonly has a framboidal form. This pyrite forms because of the ubiquity of organic matter and the availability of sea water sulphate. The opaque, framboids found in the basin margin and basin facies rocks may represent early diagenetic pyrite formed in this way. Sites M2 (basin margin facies) and CC1 (basin facies) have natural remanent magnetism interpreted to be carried by pyrrhotite and with 20 my and Tertiary ages respectively. This suggests that the framboidal mineral may be pyrrhotite formed as a result of anhydrite reduction in the Tertiary. Framboidal pyrite has also been reported as forming as a result of bacterial sulphate reduction of anhydrite by Machel (in press).

6.4.3 Haematite and goethite

Haematite occurs in several habits and associations in the rocks of the Capitan shelf margin and has been identified from both petrographic and magnetic studies.

Furthermore, there is petrographic and magnetic evidence that the haematite which occurs as well-developed crystals up to 500μm in diameter and as minute framboids in calcite spar, formed from the oxidation of iron sulphides during and after the reduction and dissolution of anhydrite. Iron sulphide oxidising to haematite is currently found in the subsurface at the margin between calcitised and non-calcitised anhydrite (fig.3.22); haematite is also found to be replacing iron sulphide at outcrop (fig. 3.38). Haematite and pyrrhotite are commonly found to carry natural remanent magnetism of different ages within the same site. Pyrrhotite and haematite have been identified together in sites M9, M10, M20 and M6. In all these sites one natural remanent magnetism is 210 - 140 Ma old and the other is 45-20 Ma old (except M6 which is less well defined). Where this occurs, the pyrrhotite yields an age between 210 Ma to 140 Ma and the haematite yields an age of 45 Ma or 20 Ma or Tertiary. However, it is not unequivocally the case that some pyrrhotite does not also have a mid-Tertiary age in some sites. These data suggest that the *majority* of pyrrhotite formed after a period of meteoric water influx during the Jurassic and that the period of meteoric water influx at around 20my due to continued uplift and faulting, caused most pyrrhotite, whether of Jurassic or Tertiary age, to oxidise to haematite.

Haematite and goethite have been identified as present, *without* pyrrhotite, in sites M14 (backreef facies), M19 (reef facies), M21, M22, M23, M24 (upper foreslope facies), M4, M5, M25 and M26 (lower foreslope facies) and M27 (basin margin facies). These natural remanent magnetism directions have ambiguous ages, or are dated at between 80 and 20 my old, or have high inclinations which have been interpreted as likely to be Tertiary (table 5.11 and chapter 5). These data, and the prevalence of haematite in calcite spar, suggest that the haematite formed from the complete oxidation of pyrite/pyrrhotite.

Haematite also occurs as euhedral crystals (up to 500μm in diameter) in silicified shell fragments (fig. 3.34) in the basin margin facies only. One site from the basin margin facies (site M27) contains haematite which has a natural remanent magnetism which was acquired 230 Ma. It may be that this haematite formed 230 Ma.

The haematite which has acicular morphology and is associated with pore-space and the goethite, are likely weathering products of iron-bearing minerals.

6.5 Intensity/susceptibility relationships with geology

A graph of maximum initial natural remanent magnetism intensity versus maximum initial susceptibility (fig. 6.6) indicates that there is an overall relationship between intensity/susceptibility and facies/lithology. Sites from basinal siltstones have

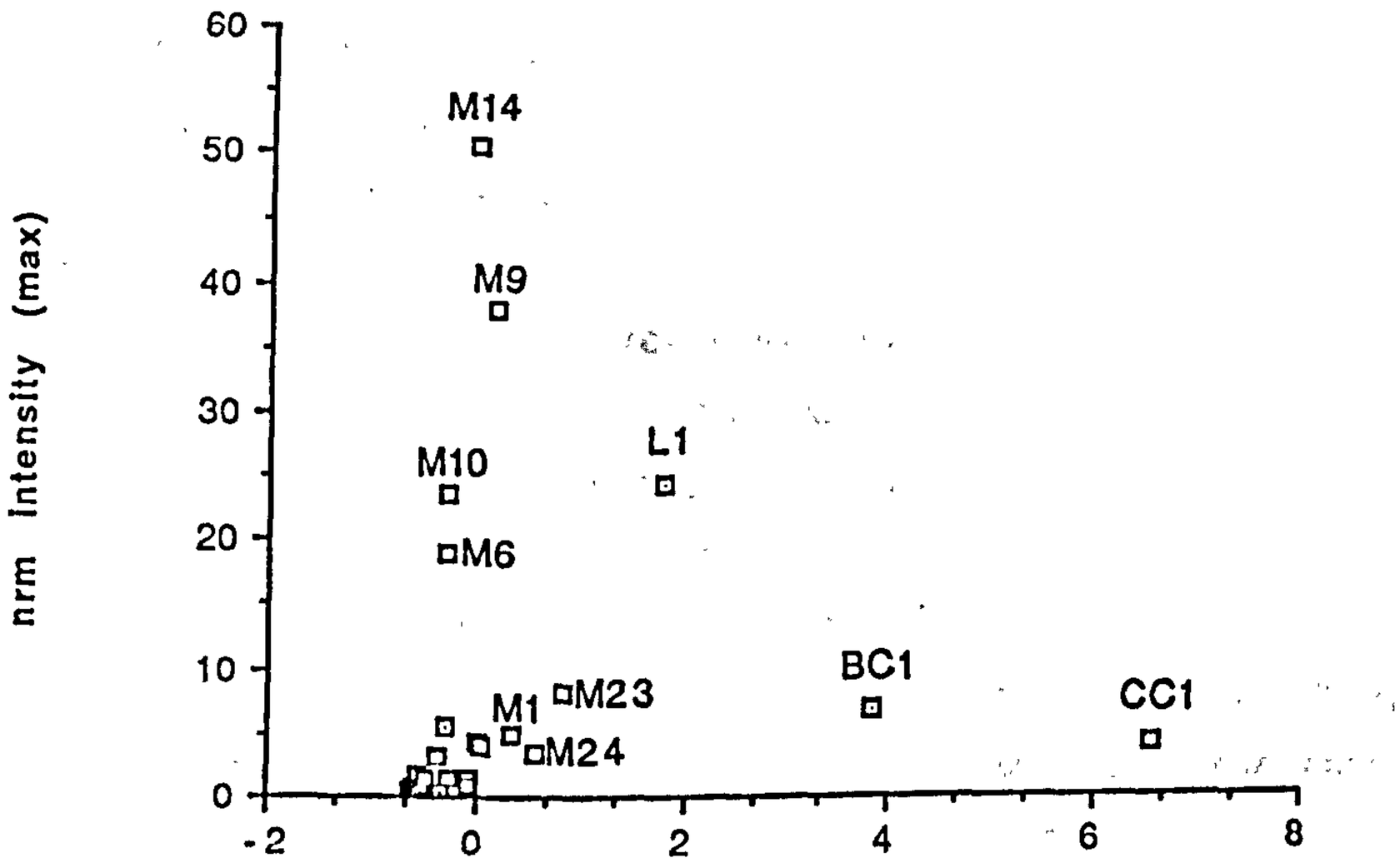

fig. 6.6 Graph of initial natural remanent magnetism intensity ($10^{-4}Am^{-1}$) versus initial susceptibility for sites.

higher susceptibility than the sites in the Capitan shelf margin, and the site from the basinal limestone also plots in a distinct field and has high intensity and susceptibility. Sites with siltstone lithology (sites M9, M14, M23 and M24) from the Capitan shelf margin have higher intensity and susceptibility values than sites with carbonate lithology, and sites from the basin margin facies tend to have higher intensity and susceptibility values than sites from the reef, back reef and foreslope facies. Sites M10 and M6 have high intensity values related to the large proportions of haematite present in these samples.

The siltstone lithologies would be expected to have higher intensity and susceptibility because of the input of detrital grains of minerals with high susceptibility *e.g.*, rutile, garnet and other paramagnetic minerals; also, many silt grains would have been coated with 'desert varnish' composed of various oxides and clays. Sites in the basin margin facies (M1, M2, M3 and M27) and the site in basinal limestone (L1) represent condensed sequences, relative to the other facies of the Capitan shelf margin, and therefore might be expected to contain relatively larger proportions of detrital paramagnetic minerals; site L1 also contains detrital magnetite. Sites from these facies would probably also have originally contained more early diagenetic pyrite, and bacterial reduction of sulphate, derived from anhydrite, could have proceeded for a longer time in these facies thus producing more iron sulphides, than the other facies of the Capitan shelf margin. Most other sites have low intensity and susceptibility values, and the site with the lowest values (sites M18, M19, M17, M16, M21) are those which were cemented early by marine cements and which are not dolomitised.

6.6 Summary and conclusions

The chemical conditions of the pore waters present in the Capitan shelf margin during it's burial are not known, however the rapid influx of meteoric water, in an effectively open system, during the Tertiary and especially since 22.5 Ma, would tend to encourage pyrite or magnetite formation rather than the formation of pyrrhotite. Pyrrhotite would be more likely to form under a more closed system, when conditions would be more reducing. Such conditions are more likely to have prevailed during the period between the input of meteoric waters (and associated sulphate reducing bacteria) during the early Jurassic, and the late Cretaceous when uplift began.

These interpretations of the timing of mineral formation help to explain the ambiguous directions derived from some sites in this study. If sulphate reduction and concomitant pyrite/pyrrhotite/magnetite formation have been occurring to some degree in the strata of the Capitan shelf margin since Jurassic times, and if the natural remanent magnetism acquired by the magnetic grains has been partially to totally overprinted by the alteration of those sulphides to haematite and goethite, then overlap of blocking temperature spectra would be expected and this would lead to the potential for incomplete resolution of >1 vector.

A summary of the evolution of the Capitan shelf margin, as elucidated from sedimentologic, diagenetic and magnetic studies, is as follows (fig. 6.7):

a. Mid-Upper Capitan times were characterised by:

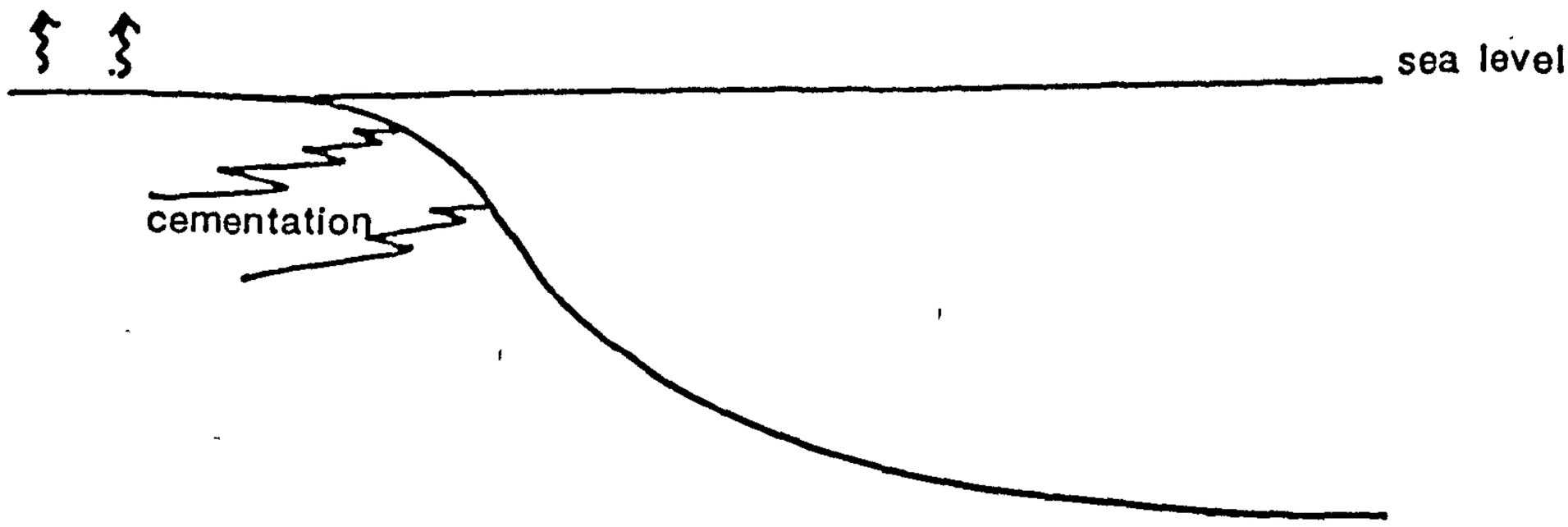

- a tropical/arid climate;
- high evaporation;
- high carbonate productivity;
- syndepositional selective dolomitisation;
- rapid cementation of the reef, back reef and upper foreslope facies;
- progradation and aggradation of the Capitan shelf margin.

The shelf crest was subjected to periodic emergence, there was considerable downslope movement of carbonate debris and compaction occurred in the lower foreslope, basin margin and basin facies. The basin margin and basin facies were also bioturbated.

b. **Upper Capitan times *i.e.*, late Lamar limestone equivalent** were characterised by:

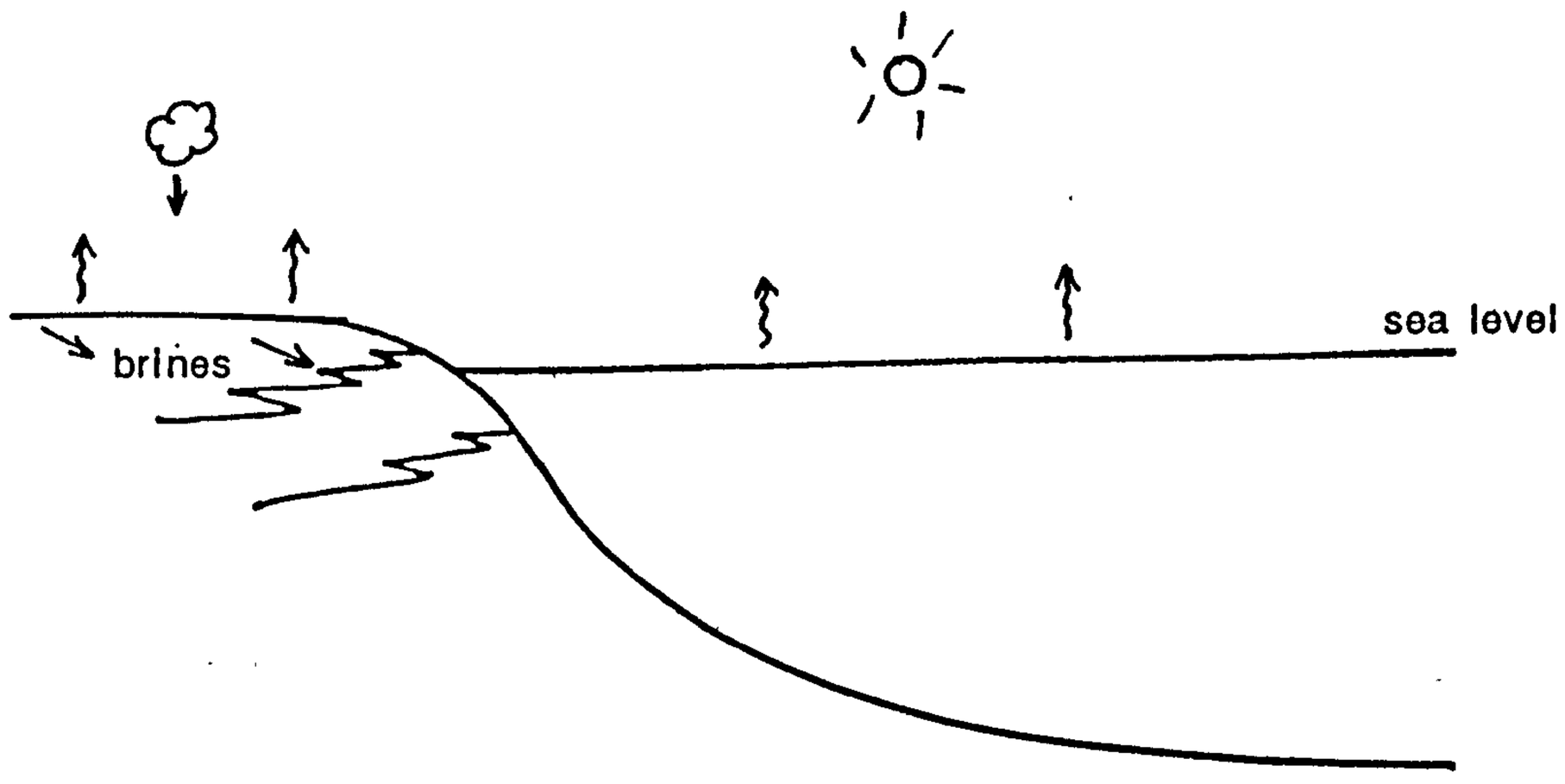

- an arid climate;
- high evaporation;
- exposure of the shelf and no carbonate productivity;
-drawdown of evaporatively-concentrated formation waters from the shelf and reflux dolomitisation;
- partial dissolution of aragonite.

Progradation and aggradation of the Capitan shelf margin ceased, the Delaware basin became restricted and the upper, laminated, non-bioturbated part of the Lamar limestone was deposited.

c. **Early Castile times** were characterised by:

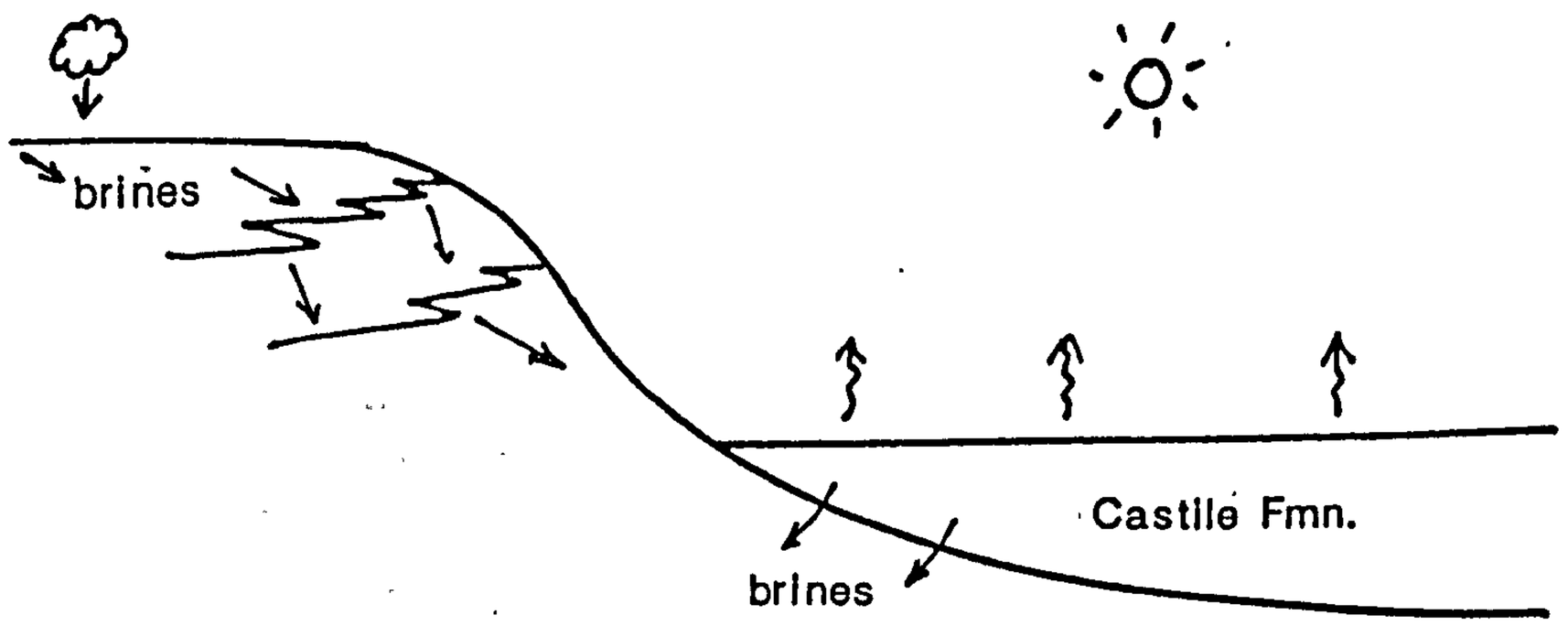

- an arid climate;
- desiccation of the Delaware Basin;
- the start of the deposition of the Castile formation;
- continued drawdown of calcium sulphate-laden fluids;
- reflux dolomitisation by these fluids;
- pervasive dolomitisation of the lower foreslope facies;
- passive pore-filling by calcium sulphate in the lower foreslope facies.

d. **Later Castile times** were characterised by:

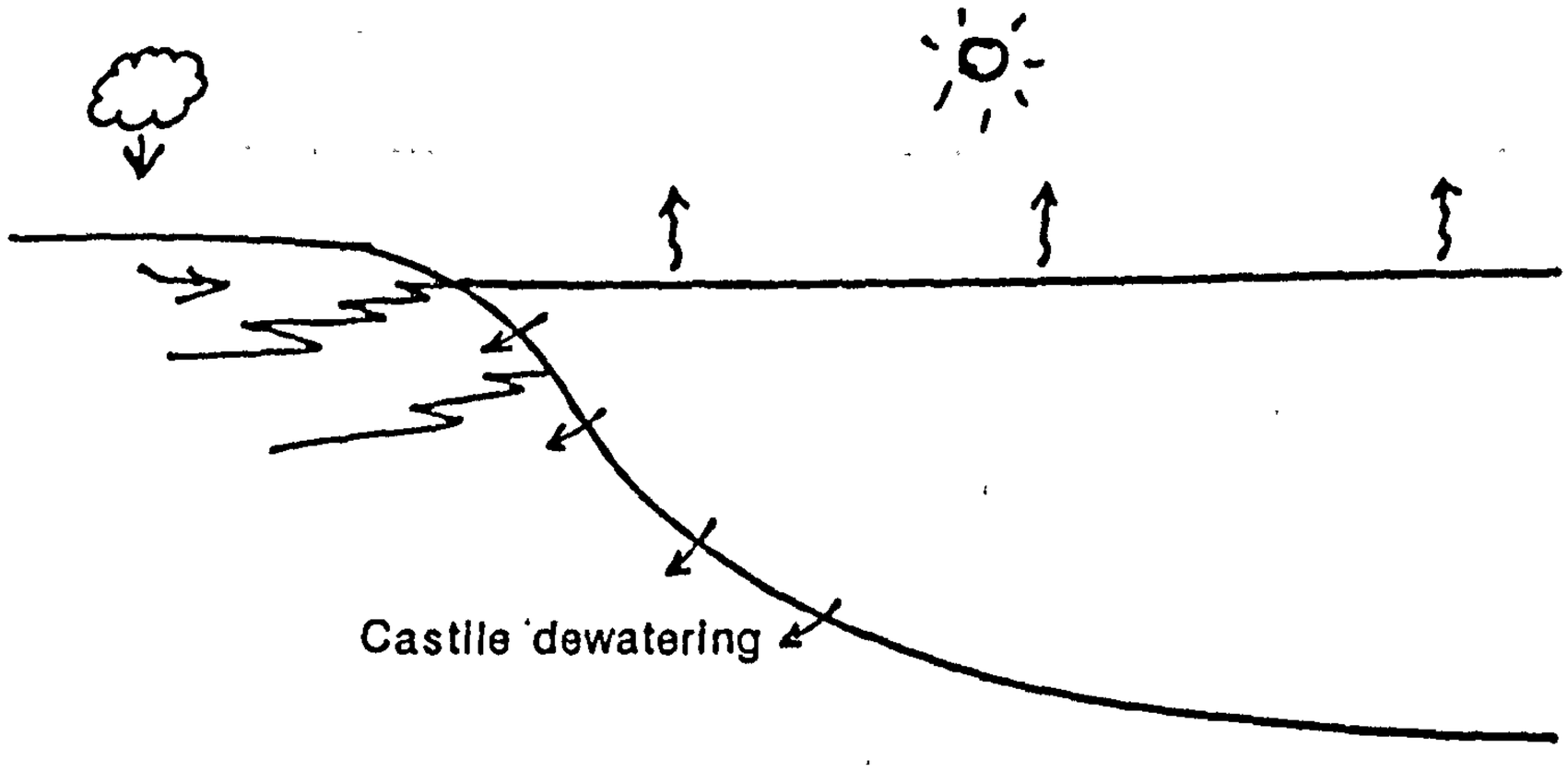

- an arid climate;
- deposition of most of the Castile formation;
- compaction of the Castile formation and movement of these brines into the Capitan shelf margin;
- pervasive dolomitisation of the foreslope facies and passive pore-filling calcium sulphate in the upper foreslope facies;
- replacive anhydrite in the lower foreslope facies.
- minor sulphate reduction, with concomitant pyrrhotite formation, may have occurred at this time.

e. **Salado times** were characterised by:

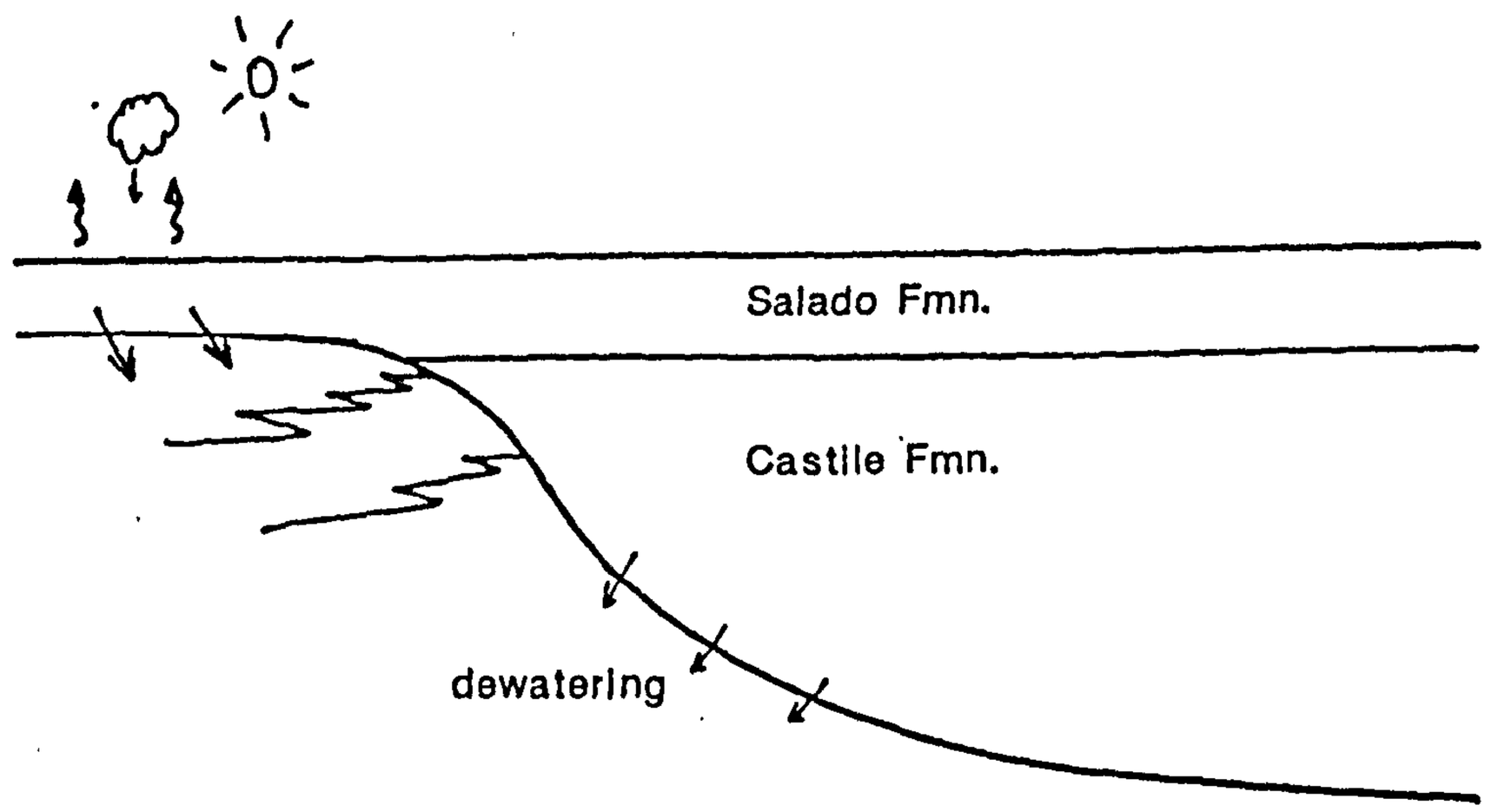

- an arid climate;
- significantly reduced porosity and permeability due to cementation by anhydrite;
- early burial of the Capitan shelf margin;
- compaction of the Castile formation and the expulsion of brines into the Capitan shelf margin;
- replacive anhydrite in the upper parts of the Capitan shelf margin.

f. **Jurassic times** were characterised by:

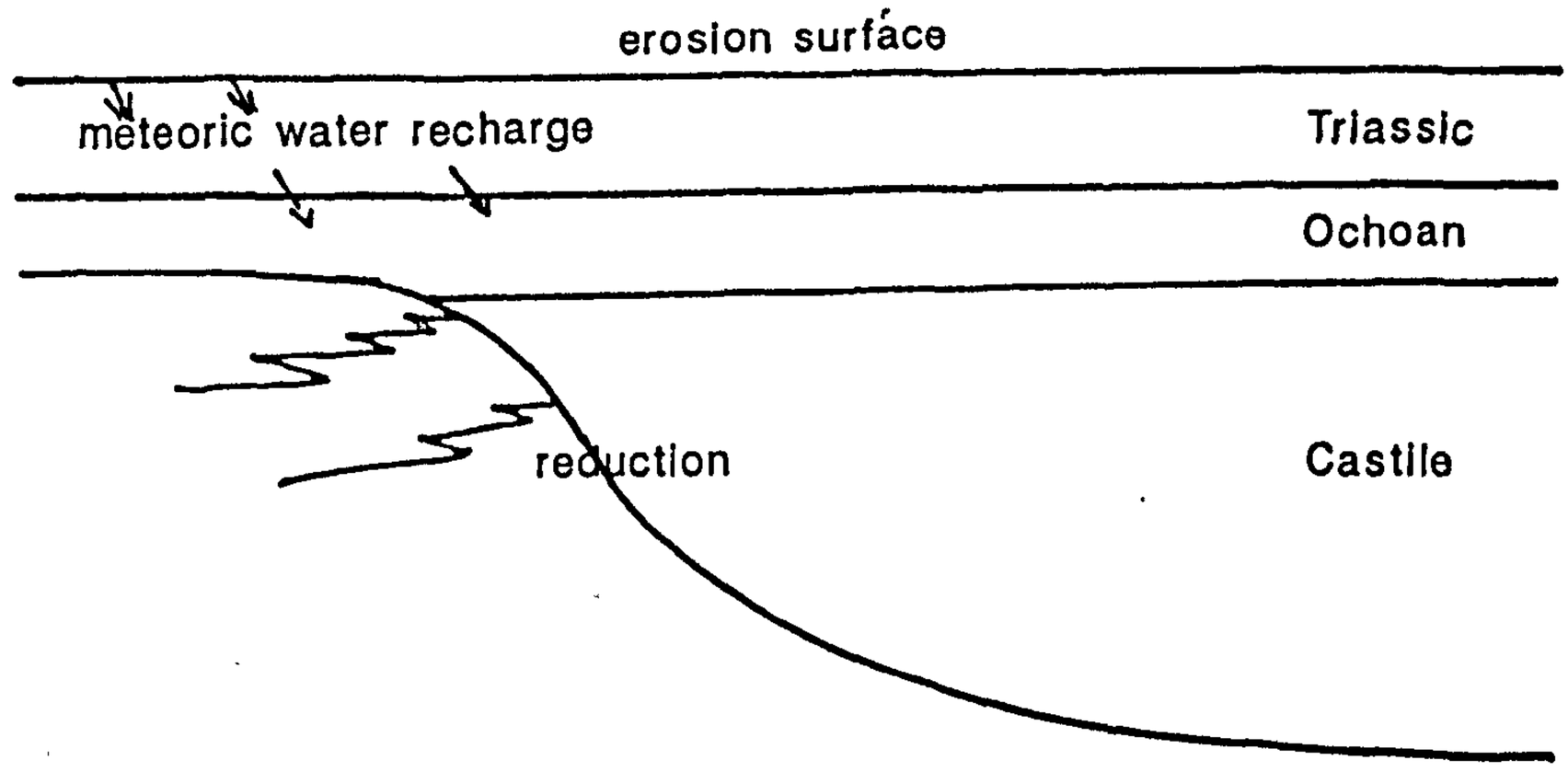

- non-deposition;
- erosion and uplift;
- input of some meteoric water and some sulphate reducing bacteria;
- minor reduction of anhydrite by bacteria and the formation of pyrrhotite.

g. **Upper Cretaceous times (80 m.y.a.)** were characterised by:

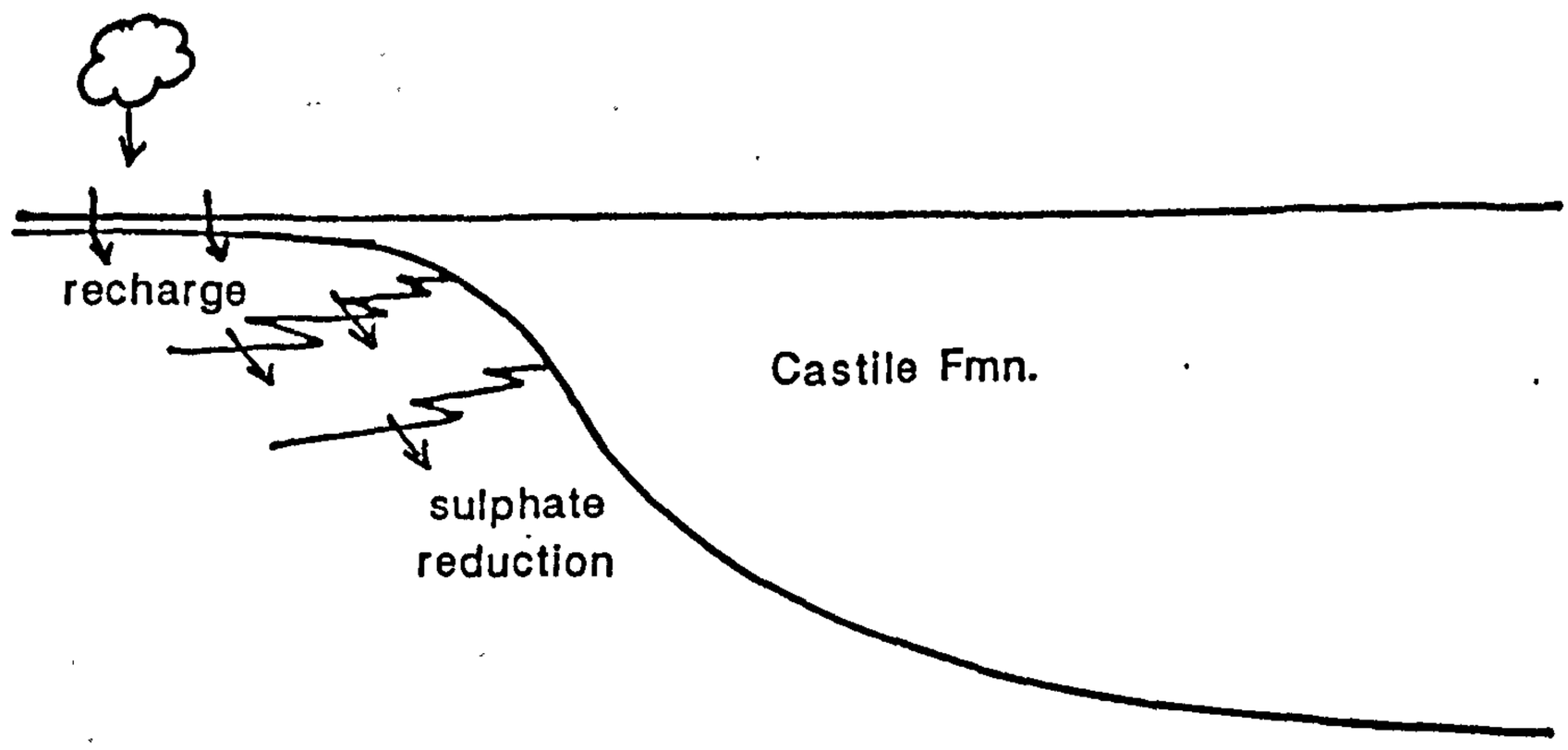

- a temperate climate;
- eastward tilting and uplift of the Delaware basin;
- development of a regional aquifer and meteoric recharge in a relatively closed system;
- reduction of anhydrite by sulphate reducing bacteria;
- minor pyrrhotite/pyrite formation;
- dolomite overgrowths and kaolinite formation;
- minor calcitisation of anhydrite and formation of calcite spar IIa.

h. Oligocene times (35 m.y.a.) were characterised by:

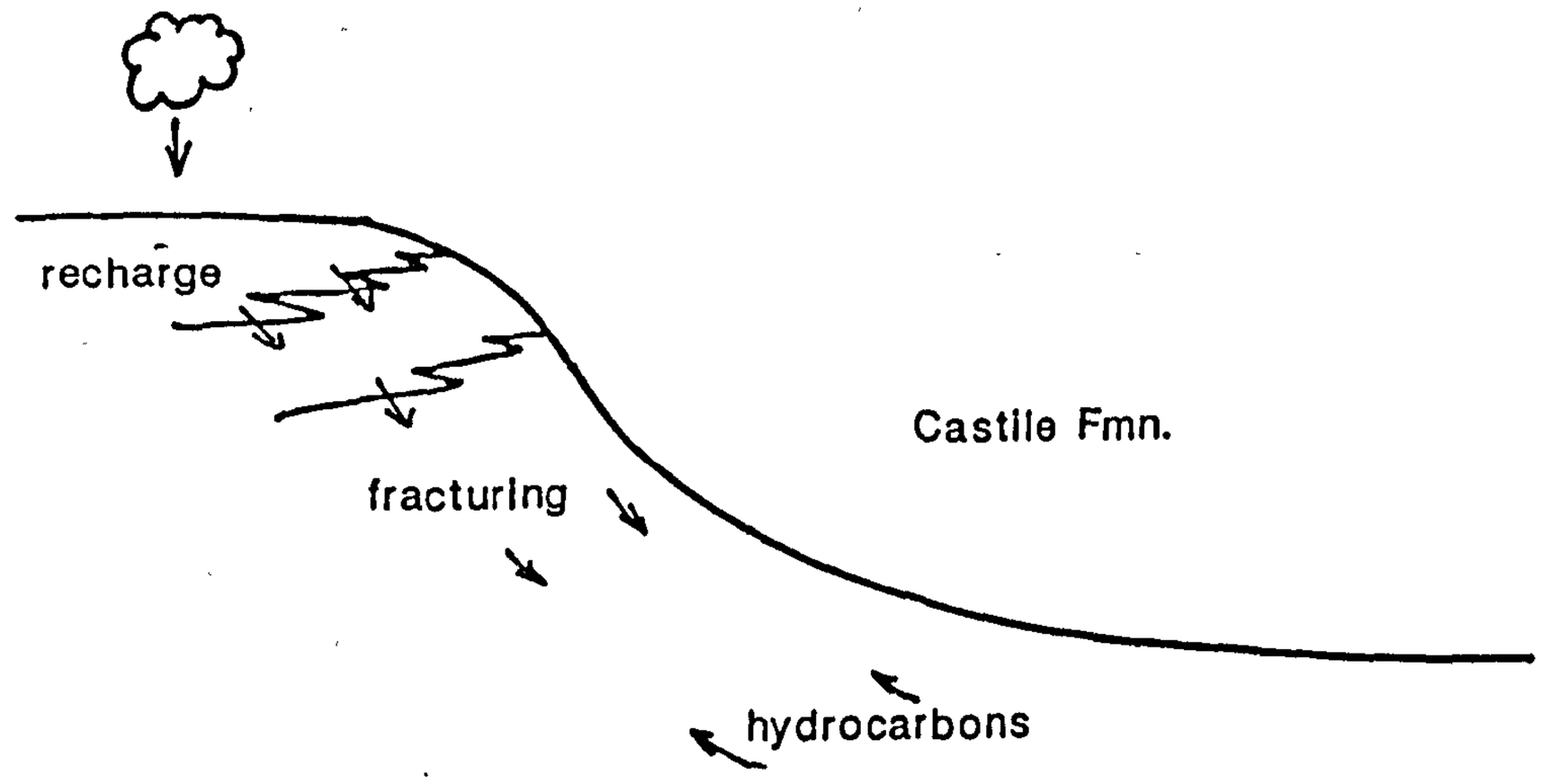

- a temperate climate;
- high heat flow and a geothermal gradient of up to 50°C/km;
- uplift of mountains;
- meteoric water recharge;
- some anhydrite dissolution, minor fracturing and the precipitation of calcite spar IIb;
- enhanced sulphate reduction due to renewed pulse of hydrocarbons from the basin ?;
- kaolinite/dickite formation;
- minor magnetite and pyrite formation.

i. **Miocene times (22.5 m.y.a.)** were characterised by:

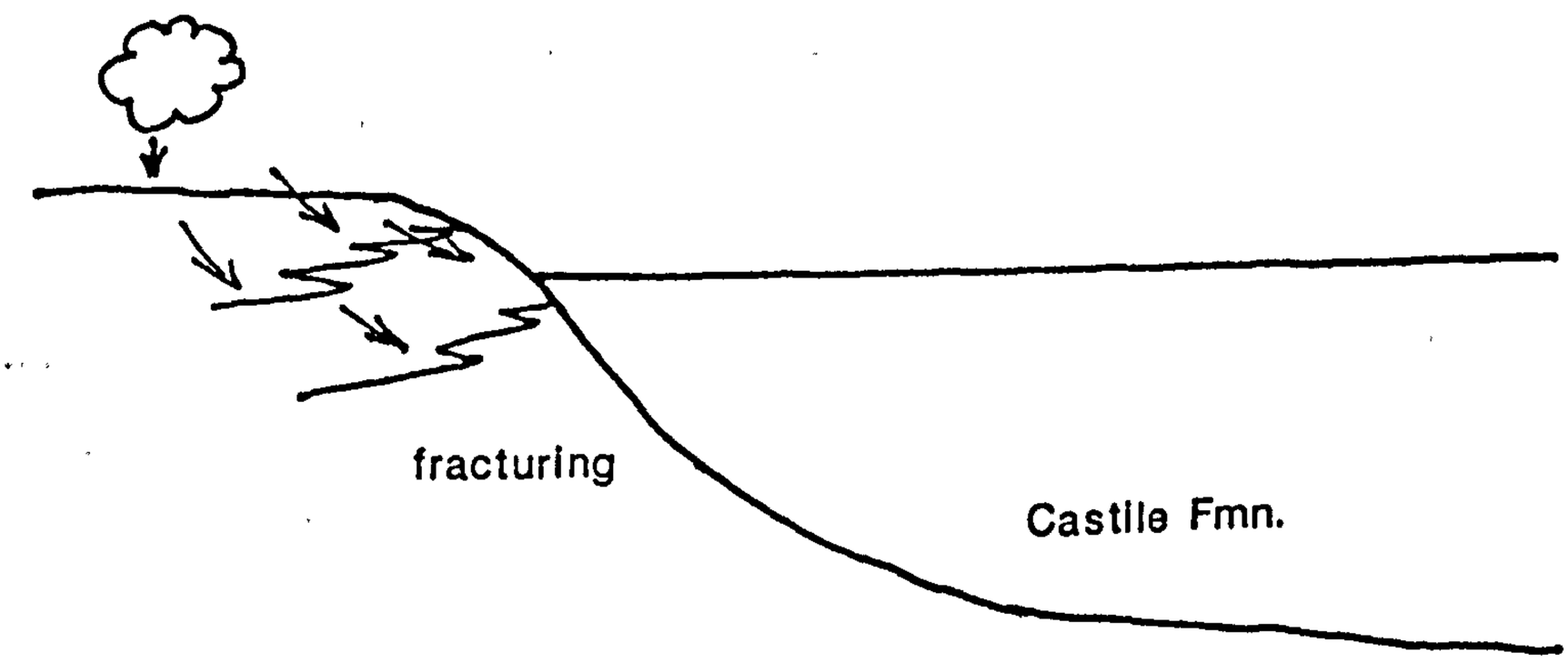

- a temperate climate;
- faulting;
- establishment of an open meteoric system;
- dissolution of anhydrite from the Capitan shelf margin and consequent fracturing;
- precipitation of calcite spars IIc and III;
- oxidation of iron sulphides to haematite and goethite.

The results and interpretations from this study have illustrated several points. The main conclusions and suggestions for further work, from the sedimentological, diagenetic and magnetic/palaeomagnetic studies, have been given at the end of each chapter respectively.

The complex nature of magnetisations in these carbonate sedimentary rocks has highlighted the need for careful sampling and magnetic analysis of carbonate rocks. The importance of an integrated approach towards understanding the palaeomagnetic characteristics of carbonate sedimentary rocks has been shown, in that diagenetic processes and the burial/thermal history of these strata controlled the formation of the magnetic minerals for the rocks of the Capitan shelf margin. However, the magnetic study of carbonates is hindered by the time-consuming process of demagnetisation of large numbers of samples, their measurement on a cryogenic magnetometer, and the analysis of large volumes of data. Any way of reducing the time involved in making these measurements, such as the development of new magnetometers which operate at liquid nitrogen temperatures or room temperature, and the computerisation of parts of the demagnetisation process and the data analysis process, would greatly enhance the feasability of magnetic studies of carbonates.

The potential for the dating of diagenetic events by relating magnetic characteristics to the diagenetic/burial/thermal history of these strata has been demonstrated. The main control on the formation of magnetic minerals was the presence of anhydrite and its subsequent dissolution or calcitisation. The formation of magetite/pyrrhotite by bacterial sulphate reduction of the anhydrite was associated with the input of meteoric water. Further input of meteoric water caused the oxidation of these minerals to haematite and goethite.

In order to be able to relate the magnetic mineralogy more closely to the diagenetic/burial history, the chemical conditions which prevailed during diagenesis/burial must be better constrained. If the chemical condititions for the formation of the magnetic minerals were better understood, then isotopic studies might be informative because the geochemical characteristics of the diagenetic phases may vary due to such processes as sulphur and carbon isotope fractionation.

Magnetic studies on rock-cores taken from the numerous wells in the Delaware Basin would also be informative, particularly if the orientation of these cores was known. Such data could then be integrated with diagenetic studies to further constrain studies of basin evolution.

Adams, J.E. and Rhodes, M.L., 1960. Dolomitisation by seepage refluxion. Amer. Assoc. Petrol. Geol. Bull., 44; 1912-1921.

Addison, F.T. 1982. A magnetic study of diagenesis in carbonate sediments. Ph.D thesis, Univ. Newcastle, U.K., 221 pp.

Addison, F.T., Turner, P. and Tarling, D.H., 1985. Magnetic studies of the Pendleside limestone: evidence for remagnetisation and late-diagenetic dolomitisation during a post-Asbian normal event. J. geol. soc. Lond. 142, 983-994.

Alderman, A.R. and Skinner, H.C.W., 1957. Dolomite sedimentation in the south-east of Australia. Am. jour. Sci., 225; 561-567.

Anderson, G.M. and Garven, G., 1987. Sulfate-sulfide-carbonate associations in Mississippi-Valley-Type lead-zinc deposits. Econ. Geol., 82; 482-488.

Babcock, J.A., 1974. The role of algae in the formation of the Capitan limestone (Permian, Guadalupian), Guadalupe Muntains, West Texas and New Mexico. PhD thesis, Univ. of Wisconsin, Madison, 241 pp.

Babcock, J.A., 1977. Calcareous algae, organic boundstones and the genesis of the Upper Capitan Limestone (Permian, Guadalupian), Guadalupe Mountains, West Texas and New Mexico. *in*; Upper Guadalupian Facies. Permian Reef Complex, Guadalupe Mountains, New Mexico and West Texas, 1977 field conference guidebook. (ed. Hileman, M.E. and Mazzullo, S.J.) Permian Basin Section - Soc. Econ. Paleont. Miner. publ. 77-16; 3-44.

Babcock, L.C., 1974. Conodont paleoecology of a Guadalupian (Permian) shelf to basin sequence, Permian reef complex, West Texas and New Mexico. Geol. Soc. Amer. abstacts with programs, p. 489.

Babcock, L.C., 1977. Life in the Delaware Basin. The palaeoecology of the Lamar limestone. *in*; Upper Guadalupian Facies. Permian Reef Complex, Guadalupe Mountains, New Mexico and West Texas, 1977 field conference guidebook. (ed. Hileman, M.E. and Mazzullo, S.J.) Permian Basin Section - Soc. Econ. Paleont. Miner. publ. 77-16; 3-44.

Badiozamani, K., 1973. The Dorag dolomitisation model application to the middle Ordovician of Wisconsin. Jour. Sed. Petrol. , 43; 965-984.

Baker, P.A. and Kastner, M., 1981. Constraints on the formation of sedimentary dolomite. Science, 213; 214-216.

Balkwill, D.L., Maratea, D. and Blkemore, R.D., 1979. Ultrastructure of a magnetotactic spirillium. J. Bacteriol., 141; 1399-1408.

Barker, C.E. and Pawlewicz, M.J., 1989. Renewed petroleum generation related to Tertiary intrusions and increased heat flow, Western Permian Basin, Texas and New Mexico. Amer. Assoc. Petrol. Geol. Bull. 73; 331.

Barker, C.E., and Halley, R.B., 1986. Fluid inclusion, stable isotope and vitrinite reflectance: evidence for the thermal history of the Bone Spring Limestone, South Guadalupe Mountains, Texas. Soc. Econ. Paleont. Mineral: Spec. publ. in 'Roles of organic matter in diagenesis'. (ed.) D.O. Gautier, p. 189-203.

Bathurst, R. G. C., 1971. Carbonate sediments and their diagenesis. Elsevier, Amsterdam. 620 pages.

Bazylinski, D.A., Frankel, R.B., Jannnasch, H.W., 1988. Anaerobic magnetite production by a marine, magnetotactic bacterium: Nature, 334; 518-519.

Bell, P.E., Mills, A.L. and Herman, J.S., 1987. Biogeochemical conditions favouring magnetite formation during anaerobic iron reduction. Applied Environmental Microbiology, 53; 2610-2616.

Benthien, R.H. and Elmore, R.D., 1987. Origin of magnetisation in the Phosphoria Formation at Sheep Mountain, Wyoming: a possible relationship with hydrocarbons. Geophys. Res. Lett. 14; 323-326.

Berner, R. A. 1981. A new geochemical classification of sedimentary environments. Jour. Sed. Petrol. . 51; 359-365.

Berner, R. A., 1984. Sedimentary pyrite formation - an up-date., Geochim. Cosmochim. Acta. , 48; 605-615.

Blakemore, R.P., 1975, Magnetotactic bacteria. Science, 190; 377-379.

Blakemore, R.P., Short, K.A., Bazylinski, D.A., Rosenblatt, C. and Frankel, R.B., 1985. Geomicrobiol. J., 4; 53-71.

Borer, J.M. and Harris, P.M., 1989. Depositional facies and cycles in Yates formation outcrops, Guadalupe Mountains, New Mexico. in; Soc. Econ. Paleont. Miner. core workshop, no. 13: subsurface and outcrop examination of the Capitan shelf margin. (ed.) Harris, P.M. and Grover, G.A. p. 305-318.

Candelaria, M.P., 1985. Inferred tectonic control of Permian hemicyclic sandstone-carbonate sedimantation, Northwestern Shelf, Delaware basin, New Mexico. *in*: Permian carbonate-clastic sedimentology, Guadalupe Mountains. Analogues for shelf and basin reservoirs. Permian Basin Section - Soc. Econ. Paleont. Miner. ann. field trip. (ed.) Beard, C.

Chang, S.R. and Kirschvink, J.L., 1987. Biogenic magnetite as a primary remanence carrier in limestone deposits. Phys. Earth Planet. Ints.,46; 289-303.

Chilingar, G.V., Zenger, D.H., Bissell, H.J., and Wolf, K.H., 1979. Dolomites and dolomitisation. Chapt. 7 in developments in sedimentology 25A. Diagenesis in sediments and sedimentary rocks, Elsevier. p. 423-525.

Cisowski, S.M. and Fuller, M., 1987. The generation of magnetic anomalies by combustion metamorphosm of sedimentary rock, and its significance to hydrocarbon exploration. Bull. geol. Soc. Am., 99; 21-29.

Collinson, D.W., 1983. Methods in rock magnetism and palaeomagnetism: techniques and instrumentation. Chapman and Hall, New York. 503pp.

Creer, K.M. and Sanver, M., 1967. The use of the suncompass. *In;* Methods in palaeomagnetism. ed. Collinson, D.W. *et al.*, Elsevier, Amsterdam. p. 11-15.

Cys J.M., Toomey, D.F., Brezina, F.L., Greenwood, E., Groves, D.B., Klement, K.W., Kullmann, J.D., McMillan, T.L., Scmidtt, V., Sneed, E.D. and Wagner, L.H., 1977. The Capitan reef- evolution of a concept; *in*: Upper Guadalupian Facies, Permian Reef Complex, Guadalupe Mountains, New Mexico and West Texas, 1977 Field Conference Guide Book. Permian Basin Section - Soc. Econ. Paleont. Miner. publ. 77-16 (eds. Hileman, M.E. and Mazzullo, S.J.), p. 201-322.

Dana, E.S., 1892. The system of mineralogy. (ed.) Palache, C., Berman, H. and Frondel, C., seventh edition vol. II. John Wiley and sons.

Darke, G., 1989. An investigation of the use of palaeomagnetic techniques in a carbonate terrane, Capitan reef complex, southwestern USA. *In*: *Soc. Econ. Paleont. Miner. core workshop, no. 13: subsurface and* outcrop examination of the Capitan shelf margin. (ed.) Harris, P.M. and Grover, G.A. p. 415-422.

Darke, G. and Harwood, G.M., 1990. Time-constraints of sulphate-related diagenesis, Capitan reef complex, West Texas and New Mexico. abst. Amer. Assoc. Petrol. Geol. Bull. June 1990.

Deer, W.A., Howie, R.A. and Zussman, J., 1966. An introduction to the rock-forming minerals. Longman and sons. 528 pages.

DuChene, H.R., *cited in*; Jagnow, D.H., 1986. Observations on previous hypotheses and some new ideas on cavern formation in the Guadalupe

Mountains; in; Jagnow, D.H. and DuChene, H.R., (eds.) geology fieldtrip guidebook, National Speleological Covention, Tulsa, New Mexico. p 85-102.

Dunham, R.J., 1962. Classification of carbonate rocks according to depositional texture, in: Ham W.E., (ed). Classification of carbonate rocks. Amer. Assoc. Petrol. Geol. Bull., 108-121.

Dunham, R.J., 1972. Capitan Reef, New Mexico and Texas: facts and questions to aid interpretation by group discussion. Permian Basin Section - Soc. Econ. Paleont. Miner. spec. publ. 72-14.

Dunlop, D.J. 1979. On the use of Zijderveld vector diagrams in multicomponent paleomagnetic studies. Phys. Earth Planet. Ints. 20, 12-24.

Ellwood, B.B., 1984. Anisotropy of magnetic susceptibility; empirical evaluation of instrumental precision. Geophys. Res. Lett., 11; 645-648.

Ellwood, B.B., 1984. Bioturbation: some effects on remanent magnetisation acquisition. Geophys. Res. Lett., 11; 653-655.

Elmore, R.D., Dunn, W. and Peck, C., 1985. Absolute dating of dedolomitisation by means of palaeomagnetic techniques. Geology; 13, 558-561.

Elmore, R.D., Engel, M.H., Crawford, L., Nick, K., Imbus, S. and Sofer, Z., 1987. Evidence for a relationship between hydrocarbons and authigenic magnetite. Nature. 325; 428-430.

Elmore, R.D., Imbus, S.W., Lewis, C.A., Crawford, L., and Enger, M.H., 1987. Application of palaeomagnetic methods for dating hydrocarbon migration events. Abst. 13th international meeting on organic geochemistry, Venice.

Endo, R., 1959. Stratigraphical and paleontological studies of the later Palaeozoic calcareous algae in Japan. *in*; XIV: fossil algae from the Nyugawa Valley in the Hida Massif; Saitama Univ. Sci. Rpt. ser. B., 3; 177-217.

Erdlac, R.J., 1984. Reactivation of a Pre-Cambrian feature during Palaeozoic time. *in*: Geologic evolution of the Permian Basin, a symposium. Permian Basin Section - Soc. Econ. Paleont. Miner. , p 13-14.

Fischer, A.G. and Sarnthein, M., 1988. Airborne silts and dune derived sands in the Permian of the Delaware Basin. J. Sediment. Petrol. 58, 637-643.

Fisher, R.A., 1953. Dispersion on a sphere. Proc. R. soc. Lond., A217; 295-305.

Fishman, N.S., Reynolds, R.L., Hudson, M.R. and Vito, F.N., 1989. Source of anomalous magnetisation in an area of hydrocarbon potential: petrologic evidence from Jurassic Preuss sandstone, Wyoming-Idaho thrust belt. Amer. Assoc. Petrol. Geol. Bull., 73; 182-194.

Foex, G., 1957. Contantes selectionees; diamagnetisme et paramagnetisme; *en*: tables de constantes et donees numeriques. 7; 317p. Masson, Paris.

Folk, R.L. and Land, L.S., 1975. Mg/Ca ratio and salinity: two controls over the crystallisation of dolomite. Amer. Assoc. Petrol. Geol. Bull., 59; 60-68.

Folk, R.L., and Pittman, J.S., 1971. Length-slow chalcedony: a new testament for vanished evaporites. J. Sediment. Petrol. 41, 1045-1058.

Frank, J.R., 1981. Dedolomitisation in the Taum Sauk limestone (Upper Cambrian), south-east Missouri. Jour. Sed. Petrol. , 51; 7-17.

Frank, J.R., Carpenter, A.B. and Oglesby, T.W., 1982. Cathodoluminescence and composition of calcite cement in the Taum Sauk limestone (Upper Cambrian), Southeast Missouri. Jour. Sed. Petrol. 52; 631-638.

Frankel, R.B., Blakemore, R.P. and Wolfe, R.S., 1979. Magnetite in freshwater magnetotactic bacteria. Science, 203, 1355-1356.

Garber, R.A., Grover, G.A. and Harris, P.M., 1989. Geology of the Capitan shelf margin - subsurface data from the Northern Delaware Basin. *in*; Soc. Econ. Paleont. Miner. core workshop, no. 13: subsurface and outcrop examination of the Capitan shelf margin. (ed.) Harris, P.M. and Grover, G.A. p. 3-272.

Given, R.K. and Lohmann, K.C., 1986. Isotopic evidence for the early meteoric diagenesis of the reef facies, Permian Reef Complex of West Texas and New Mexico. Jour. Sed. Petrol. 56;183-193.

Given, R.K. and Lohmann, K.C., 1985. Derivation of the original isotopic composition of Permian marine cements. Jour. Sed. Petrol. , 55; 430-439.

Goree, W.B. and Fuller, M.D., 1976. Magnetometers using RF-driven SQUID's and their applications in rock magnetism and paleomagnetism. Rev. Geophys. Space Phys., 14; 591-608.

Gose, W.A. and Kyle, J.R., 1988. Palaeomagnetic studies of salt domes. aAmer. Assoc. Petrol. Geol. Bull., 72; 190.

Griffiths, D.H., King, R.F., Rees, A.I. and Wright, A.E., 1960. The remanent magnetism of some recent varved sediments. Proc. R. Soc., A256; 359-383.

Griffiths, S.H., King, R.F. and Wright, A.E., 1957. Some field and laboratory studies of the depositional remanence of Recent sediments. Adv. Phys. 6; 306-316.

Hailwood, E.A. and Folaml, S.L., 1984. Magnetic fabric of Quaternary, Tertiary and Cretaceous sediments from the Goban Spur. IPOD leg 90 - implications for sediment transport processes. *In*: De Graciansky, P.C. *et al.*, (eds.), Initial reports of the DSDP, 80; 415-421. Washington.

Hamilton, N. and Rees, A.I., 1970. The use of magnetic fabric in palaeocurrent estimation. *In*: Runcorn, S.K. (ed.). Palaeogeophysics: New York Academic Press. p. 445-464.

Hamilton, N., 1967. The efect of magnetic and hydrodynamic control on the susceptibility anisotropy of redeposited silts. J. Geol. 75; 738-743.

Hamilton, N., 1979. Preliminary magnetic studies of Lower Cretaceous sediments from DSDP site 397, northwest African continental margin. *In*: von Rad, U., *et al.*, (eds), Initial reports of the DSDP, 47; 481-482.

Handford, C.R., Kendall, A.C., Prezbindowski, D.R. Dunham, J.B. and Logan, B.W., 1984. Salina margin tepees, pisoliths and aragonite cements, Lake MacLeod, Western Australia: their significance in interpreting ancient analogues. Geology, 12: 523-527.

Hanshaw, B.R. and Back, W. and Deike, R.G., 1971. A geochemical hypothesis for dolomitisation by ground-water. Econ. Geol., 66;710-724.

Hanshaw, B.R. and Back, W., 1979. Major geochemical processes in the evolution of carbonate aquifer systems. J. Hydrol., 43; 287-312.

Hardie, L.A., 1987. Perspectives; a critical view of some current views of dolomitisation. Jour. Sed. Petrol. 57; 166-183.

Harland, W.B., Cox, A.V., Llewellyn, P.G., Smith, A.G. and Walters, R., 1982. A geologic time scale. Cambridge Univ. press. 131 pages.

Harms, J.C. and Williamson, C.R., 1988. Deep-water density current deposits of the Delaware Mountain Group (Permian), Delaware Basin, Texas and New Mexico. Amer. Assoc. Petrol. Geol. Bull. 72; 299-317.

Harris, P.M., Garber, R.A. and Grover, G.A., 1988. Upper Permian Capitan reef: revision of outcrop model. Amer. Assoc. Petrol. Geol. Bull.. abstr. ann. conv. 1988.

Harwood, G.M. and Coleman, M.L., 1983. Isotopic evidence for U.K. Upper Permian mineralisation by bacterial reduction of evaporites. Nature, 301; 597-599.

Hayes, P.T., 1964. Geology of the Guadalupe Mountains, New Mexico. Geol. Surv. Professional paper 446, 69pp.

Hemming, N.G., Meyers, W.J and Grams, J.C., 1989. Cathodoluminescence in calcites: the role of Fe and Mn as deduced from electron probe and spectro-photometric measurements. Jour. Sed. Petrol. , 59; 404-411.

Henshaw, P.C. and Merrill, R.T., 1980. Magnetic and chemical changes in marine sediments. Rev. Geophys. Space Phys., 483-504.

Heydari, E., Moore, C.H. and Sassen, R., 1988. Late burial diagenesis driven by thermal degradation of hydrocarbons and thermochemical sulfate reduction: Upper Smackover carbonates, South East Mississippi salt basin. Amer. Assoc. Petrol. Geol. Bull., 72; 197.

Hileman, M.E. and Mazzullo, S.J., 1977 (eds). Upper Guadalupian facies: Permian reef complex, Guadalupe Mountains, New Mexico and West Texas. 1977 field conference guidebook. Permian Basin Section - Soc. Econ. Paleont. Miner. publ. 77-16.

Hills, J.M., 1984. Structural evolution of the Permian Basin of West Texas and New Mexico. Permian Basin Section - Soc. Econ. Paleont. Miner. symposium, Midland, Texas, April 25.

Hiss, W.L., 1980. Movement of groundwater in Permian Guadalupian aquifer systems, suotheastern New Mexico and western Texas. *In*: Dickenson, P.W. and Hoffer, J.M., (eds.), Trans-Pecos region, southeastern New Mexico, west Texas: New Mexico Geol. Soc. 31st field trip guidebook, p. 289-294.

Horak, R.L., 1984. Sequential tectonism and hydrocarbon distribution in the Permian Basin. *In*: Structural evolurion of the Permian Basin. Permian Basin Section - Soc. Econ. Paleont. Miner. , publ. p. 14-15.

Horak, R.L., 1985. Trans-Pecos tectonism and its effects on the Permian Basin. Permian Basin Section - Soc. Econ. Paleont. Miner. , publ. 85-81. (ed.) Dickenson, P. and Muehlberger, W.R., p. 81-87.

Horton, R.A., Geissman, J.W. and Tschauder, R.J., 1984. Palaeomagnetism and rock magnetism of the Mississippian Leadville (carbonate)

formation and implications for the age of sub-regional dolomitisation. Geophys. Res. Lett., 11; 649-652.

Hounslow, M.W., 1985. Magnetic fabric arising from paramagnetic phyllosilicate minerals in mudrocks. Jour. Geol. Soc. Lond. ; 142; 995-1006.

Hounslow, M.W., 1987. Magnetic fabric characteristics of bioturbated wave-produced grain orientations in the Bridport-Yeovil sands (Lower Jurassic) of Southern England. Sedimentology; 34, 117-128.

Hsu, K.J. and Siegenthaler, C., 1969. Preliminary experiments and hydrodynamic movement induced by evaporation and their bearing on the dolomite problem. Sedimentology, 12; 11-25.

Hull, J.P.D., 1957. Petrogenesis of Permian Delaware Mountain sandstones, Texas and New Mexico. Amer. Assoc. Petrol. Geol. Bull., 41; 278-307.

Hurley, N.F. and Van der Voo, R., 1987. Palaeomagnetism of Upper Devonian reefal limestones, Canning Basin, Western Australia. bGeol. Soc. Amer. 98, 138-146.

Hurley, N.F., 1978. Facies mosaic of the lower Seven Rivers Formation (Permian), North McKittrick Canyon, Guadalupe Mountains , New Mexico. MS thesis, Univ. Wisconsin, Madison, Wisconsin. 198 pages.

Hurley, N.F., 1979. Seaward primary dip of 'fall-in' beds, lower Seven Rivers formation(Permian), Guadalupe Mountains , New Mexico. Amer. Assoc. Petrol. Geol. Bull., 63; 471.

Irving, E,. 1957. The origin of the palaeomagnetism of the Torridonian sandstones of northwest Scotland. Phil. Trans. Roy. Soc. Lond., A250; 100-110.

Irving, E. and Irving, G.A.,1982. Apparent polar wander paths; Carboniferous to Cainozoic and the assembly of Gondwana. Geophys. surveys, 5, 141-188.

Irving, E. and Major, A., 1964. Post-depositional detrital remanent magnetisation in a synthetic sediment. Sedimentology; 3; 135-143.

Irving, E. and Park, J.K., 1973. Palaeomagnetism of metamorphic rocks: errors owing to intrinsic anisotropy. Geophys. J. R. astro. Soc., 34; 489-493.

Jacka, A.D., 1974. Replacement of fossils by length-slow chalcedony and associated dolomitisation. Jour. Sed. Petrol. , 44; 421-427.

James, N.P. and Ginsburg, R.N., 1979. The seaward margin of the Belize Barrier and atoll reefs. Spec publ. No. 3 of the I.A.S. publ. Blackwell Scientific Publications.

James, N.P., Ginsburg, R.N., Marszalek, D.S., and Choquette, P.W. 1976. Facies and fabric specificity of early subsea cements in shallow Belize (British Honduras) Reefs. Jour. Sed. Petrol. 46, 523-544.

James, N.P., Wray, J.L. and Ginsburg, R.N., 1988. Calcification of encrusting aragonitic algae, (*Peysonneliaceae*); implications for the origin of late Palaeozoic reefs and cements; Jour. Sed. Petrol. 58, 291-303.

Johnson, J.H., 1942. Permian lime-secreting algae from the Guadalupe Mountains, New Mexico. bsga,, 53;195-216.

Johnson, R.J.E., van der Voo, R. and Lowrie, W., 1984. Palaeomagnetism and late diagenesis of Jurassic carbonates from the Jura Mountains, Switzerland and France. bGeol. Soc. Amer. 95, 478-488.

Jones, T.S., 1953. *Stratigraphy of the Permian Basin of west Texas.* West Texas Geol. Soc., Midland, Tx, 63 pages.

Karlin, R. and Levi, S., 1983. Diagenesis of magnetic minerals in recent hemipelagic sediments. Nature, 303; 327-330

Karlin, R., Lyle, M. and Heath, G.R., 1987. Authigenic magnetite formation in suboxic marine sediments. Nature; 326; 490-493.

Kendall, A.C. and Harwood, G.M., 1989. Shallow-water gypsum in the Castile formation - significance and implications. *In*: Soc. Econ. Paleont. Miner. core workshop, no. 13: subsurface and outcrop examination of the Capitan shelf margin. (ed.) Harris, P.M. and Grover, G.A., p. 451-459.

Kendall, C., 1969. An environmental reinterpretation of the Permian evaporite/carbonate shelf sediments of the Guadalupe Mountains. bGeol. Soc. Amer. 80, 2503-2526.

Khan, M.A., 1962. The anisotropy of magnetic susceptibility of some igneous and metamorphic rocks. Jour. Geol. r, 67; 2873-2885.

King, P.B. 1948 Geology of the Southern Guadalupe Mountains, Texas. U.S.G.S. prof. paper, 215, 183 pages.

King, P.B., 1942. The Permian of West Texas and southeastern New Mexico. Amer. Assoc. Petrol. Geol. Bull., 26; 535-736.

King, R.F., 1955. The remanent magnetism of artificially deposited sediments. Mon. Not. R. astr. Soc. Geophys. Suppl., 7; 115-134.

Kirkland, B.L. and Chapman, R.L., 1989. Paleoecology of the Permian green alga *Mizzia (Dasycladaceae)*. abstr. In fieldtrip notes: the

Capitan reef complex, west Texas and New Mexico, Permian Basin Section - Soc. Econ. Paleont. Miner. seminar, 1989.

Kirschvink, J.L., 1980. The least-squares line and plane and the analysis of palaeomagnetic data. Geophys. J. R. astr. Soc. 62; 699-718.

Kirschvink, J.L. and Chang. S-B.R., 1984. Ultrafine-grained magnetite in deep-sea sediments: possible bacterial magnetofossils. Geology, 12; 559-562.

Kirschvink, J.L. and Lowenstam, H.A., 1979. Mineralisation and magnetisation of chiton teeth: palaeomagnetic, sedimentologic and biologic implications of organic magnetite. Earth and Planet. Sci. Lett. 44; 193-204.

Lang, W.T.B., 1937. The Permian formations of the Pecos valley of New Mexico and Texas. Amer. Assoc. Petrol. Geol. Bull., 21; 833-898.

Lee, M.R. and Harwood, G.M., In press. Dolomite calcitisation and cement zonation related to uplift of the Raisby formation (Zechstein carbonate), north-east England. Sedimentary Geology, In press (1989).

Lohmann, K.C. and Meyers, W.J., 1977. Microdolomite inclusions in cloudy prismatic calcites: a proposed criterion for former high-magnesian calcites. Jour. Sed. Petrol. , 47; 1075-1088.

Loope, D.B. and Watkins, D.K., 1989. Pennsylvanian fossils replaced by red chert: early oxidation of pyritic precursor. Jour. Sed. Petrol. , 59; 375-386.

Loucks, V. and Elmore, R.D., 1986. Absolute dating of dedolomitisation and the origin of magnetisation in the Morgan Creek Limestone, central Texas. bGeol. Soc. Amer. , 97; 486-496.

Lovley, D.R., Baedecker, M.J., Lonergan, D.J., Cozzarelli, I.M., Phillips, E.J.P. and Siegel, D.I., 1989. Oxidation of aromatic contaminants coupled to microbial iron-reduction. Nature, 339; 297.

Lovley, D.R., Stolz, J.F., Nord, G.L., Phillips, E.J.P., 1987. Anaerobic production of magnetite by a dissimilatory iron-reducing micro-organism. Nature, 330; 252-254.

Lovlie, R., Lowrie, W. and Jacobs M., 1971. Magnetic properties and mineralogy of four deep-sea cores. Earth and Planet. Sci. Lett. 15, 157-168.

Lovlie, R., 1974. Post-depositional remanent magnetisation in a redeposited deep-sea sediment. Earth and Planet. Sci. Lett. 21; 315-320.

Lovlie, R., 1976. The intensity pattern of post-depositional remanence acquired in some marine sediments deposited during a reversal of the external magnetic field. Earth and Planet. Sci. Lett., 30; 209-214.

Lowenstam, H.A., 1981. Science, 244; 126-130.

Lowrie, W. and Heller F., 1982. Magnetic properties of marine limestones. Rev. Geophys. Space. Phys., 20; 171-192.

Lowrie, W.,and Hirt, A.M., 1987. Anisotropy of magnetic susceptibility in the Scalia Rossa pelagic limestone. Earth and Planet. Sci. Lett. 82; 349-356.

Machel, H.G., 1986. Early lithification, dolomitisation and anhydritisation of Upper Devonian Nisku buildups, subsurface of Alberta, Canada *in*: "Reef diagenesis". (ed.) Scroeder, J.H. and Purser, B.H.

Machel, H.G., 1989 (in press). Relationships between sulfate reduction and oxidation of organic compounds, to carbonate diagenesis, hydrocarbon accumulations, salt domes and metal sulfide deposits. Carbonates and Evaporites, in press.

Machel, H.G., 1989 (in review). Causes and distribution of magnetic anomalies with hydrocarbon accumulations. (paper under review, Soc. Petrol. Eng., spec. publ.)

Maher, B.A. and Taylor, R.M., 1988. Formation of ultra-fine-grained magnetite in soils. Nature, 336; 368-370.

Mann, S., Frankel, R.B. and Blakemore, R.P., 1984. Structure and morphology and crystal growth of bacterial magnetite. Nature, 310; 405-407.

Maslov, V.P., 1956. Fossil calcareous algae of the USSR. Akad. Nauk. SSSR, Inst. Geol. Nauk., Trudy, 160; 301 pages.

Matsuda, T., Endo, J., Osakabe, N. and Tonomuta, A., 1983. Morphology and structure of biogenic magnetite particles. Nature, 302; 411-412.

Mazzullo, S.J. and Cys, J.M., 1977. Submarine cements in Permian boundstones and reef-associated rocks, Guadalupe Mountains West Texas and SE New Mexico *in*: Permian Basin Section - Soc. Econ. Paleont. Miner. , publ. 77-16, p. 151-200.

Mazzullo, S.J. and Cys, J.M., 1978. *Archaeolithoporella*-boundstones and marine aragonite cements, Permian Capitan Reef, New Mexico and Texas, USA. N. Jahrbuch F. Geologie u. Palaontologie, Monatshefte, 10; 600-611.

Mazzullo, S.J. and Cys, J.M., 1979. Marine aragonite and seafloor growths and cements in Permian phylloid algal mounds, Sacramento Mountains, New Mexico. Jour. Sed. Petrol. 49; 917-937.

Mazzullo, S.J. and Hedrick, C.L., 1985. Road log and locality guide: lithofacies, stratigraphy, and depositinal models of the back reef, Guadalupian section (Queen, Seven Rivers, Yates and Tansill Formations). *in*: Permian Basin Section - Soc. Econ. Paleont. Miner. ann. field trip notes 85-24. (ed.) Beard, C.

Mazzullo, S.J., 1980. Calcite pseudospar replacive of marine acicular aragonite and implications for aragonite cement diagenesis. Jour. Sed. Petrol. 50; 409-422.

Mazzullo, S.J., 1986. *Mississippi Valley-type sulfides in Lower Permian* dolomites, Delaware Basin, Texas: implications for basin evolution. Amer. Assoc. Petrol. Geol. Bull.. 70; 943-952.

Mazzullo, S.J., Mazzullo, J. and Harris, P.M., 1985. Eolian origin of *Quartzose Sheet Sands in Permian Shelf facies, Guadalupe* Mountains. Permian Basin Section - Soc. Econ. Paleont. Miner. field-trip symposium notes. p. 71 (ed.) Beard, C.

Mazzullo, S.J., Bischoff, W.D. and Hedrick, C.L., 1989. Stacked Island facies in Tansill outer-shelf platform, Dark Canyon, Guadalupe Mountains, New Mexico. *in*: Soc. Econ. Paleont. Miner. core workshop, no. 13: subsurface and outcrop examination of the Capitan shelf margin. (ed.) Harris, P.M. and Grover, G.A., p. 287-294.

M^{c}Bride, E.F., 1987. Diagenesis in the Maxxon sandstone (Early Cretaceous), Marathon region, Texas: a diagenetic quartz-arenite. Jour. Sed. Petrol. , 57; 98-107.

M^{c}Cabe, C., Jackson, M. and Ellwood, B.B., 1985. Magnetic anisotropy in the Trenton limestone: *results of a new technique, anisotropy of* anhysteretic susceptibility. Geophys, Res. Lett. , 12; 333-336.

M^{c}Cabe, C., Sassen, R. and Saffer, B., 1987. Occurrence of secondary magnetite within biodegraded oil. Geology, 15; 7-10.

M^{c}Cabe, C., van der Voo, R., Peacor, D.R., Scotese, C.R. and Freeman, R., 1983. Diagenetic magnetite carries ancient yet secondary remanence in some Palaeozoic sedimentary carbonates. Geology, 11; 221-223.

M^{c}Cabe, C., van der Voo, R., Wilkinson, B.H. and Devaney. K., 1985. A mid/late Silurian palaeomagnetic pole from limestone reefs of the

late Wabash Formation. Indiana, USA. Jour. Geol. r., 90; 2959-2965.

McManus, K.M. and Hanor, J.S., 1987. Pyrite and pyrrhotite cementation of Tertiary sediments flanking the west Hackberry salt dome: Cameron Parish, Louisiana. Soc. Econ. Palaont. Miner. mid-year meeting, abst. p. 56.

Meissner, F.F., 1972. Cyclic sedimentation in middle-Permian strata of the Permian Basin. In; Cyclic sedimentation in the Permian Basin. West Texas Geol. Soc., p. 203-232.

Melim, L.A. and Scholle, P.A., 1989. Dolomitisation model for the fore-reef facies of the Permian Capitan formation, Guadalupe mountains, Texas-New Mexico. *in*: Soc. Econ. Paleont. Miner. core workshop, no. 13: subsurface and outcrop examination of the Capitan shelf margin. (ed.) Harris, P.M. and Grover, G.A., p. 407-414.

Miller, J., 1988. Cathodoluminescence microscopy. *in*: Techniques in sedimentoloogy. (ed.) Tucker, M. p. 171-190.

Mruk, D.H., 1985. Cementation and dolomitisation of the Capitan limestone (Permian), McKittrick Canyon, West Texas. MS thesis, Univ. of Colorado, Boulder, Co., 155 pages.

Mruk, D.H., 1989. Diagenesis of the Capitan limestone, Upper Permian, McKittrick Canyon, West Texas. *in*: Soc. Econ. Paleont. Miner. core workshop, no. 13: subsurface and outcrop examination of the Capitan shelf margin. (ed.) Harris, P.M. and Grover, G.A., p. 387-406.

Murray, R.C., 1964. Origin and diagenesis of gypsum and anhydrite. Jour. Sed. Petrol. 34; 512-523.

Mutti, M. 1989. Diagenesis associated with an outer shelf, intraformational erosion surface, Upper Yates, Permian, West Texas. in: Permian Basin Section - Soc. Econ. Paleont. Miner. fieldtrip seminar notes, April, 1989.

Neese, D.A. and Schwartz, A.H., 1977. Facies mosaic of the Upper Yates and Lower Tansill formations, Walnut and Rattlesnake canyons, Guadalupe Mountains, New Mexico. *in*: Permian Basin Section - Soc. Econ. Paleont. Miner. publ. 77-16. p. 437-450.

Newell, N.D., Rigby, J.K., Fischer, A.G., Whiteman, A.J., Hickox, J.E. and Bradley, J.S., 1953. The Permian reef complex of the Guadalupe Mountains region, Texas and New Mexico. W.H. Freeman and Co., San Fransisco, 236 pages.

Noel, M.,1983. The magnetic remanence and anisotropy of susceptibility of cave sediments from Agen Allwedd, South Wales. Geophys. J. R. astr. Soc., 72; 557-570.

Nordstrom, D.K., 1982. Aqueous pyrite oxidation and the consequent formation of secondary iron minerals. *in*: Acid sulfate weathering. Soil science soc. of America spec. publ., 10. (ed.) Kittrick, J.A.

Nye, J.F., 1969. Physical properties of crystals; their representation by tensors and matrices. publ. Oxford at the Clarendon Press. 322 pp.

Owens, W.H. and Bamford, D., 1976. Magnetic, seismic and other anisotropic properties of rock fabrics. Phil. trans. Roy. Soc. Lond., A283; 55-68.

Owens, W.H. and Rutter, E.H., 1978. The development of magnetic susceptibility anisotropy through crystallographic preferred orientation in a calcite rock. Phys. Earth Planet Inst. 16; 215-222.

Perarnau, A. and Tarling, D.H., 1985. Thermal enhancement of magnetic fabric in Cretaceous sandstones. Jour. Geol. Soc. Lond. , 142; 1029-1034.

Petersen, N and von Dobeneck, T., 1986. Fossil bacterial magnetite in deep sea sediments from the South Atlantic. Nature, 320. 611-615.

Pierre, C. and Rouchy, J.M., 1988. Carbonate replacements after sulfate evaporites in the Middle-Miocene of Egypt. Jour. Sed. Petrol. , 58; 446-456.

Piper, D.J.A., 1987. Palaeomagnetism and the continental crust. Open University Press, 434 pages.

Pray, L.C. and Esteban, M., (eds.), 1977. Upper Permian Guadalupian Facies, Permian reef complex, Guadalupe Mountains, New Mexico and West Texas, Field conference guidebook, v. 2. Permian Basin Section - Soc. Econ. Paleont. Miner. , 77-16, 194 pages.

Pray, L.C., 1989. Lateral variability of the Capitan reef complex, West Texas and New Mexico. *in*: Soc. Econ. Paleont. Miner. core workshop, no. 13: subsurface and outcrop examination of the Capitan shelf margin. (ed.) Harris, P.M. and Grover, G.A., p. 273-278.

Pullaiah, G., Irving, E., Buchan, K.L. and Dunlop, D.J. 1975. Magnetisation changes caused by burial and uplift. Earth and Planet. Sci. Lett., 28; 133-143.

Rathore, J.S., 1975. Studies of magnetic susceptibility in rocks. Ph.D thesis, University of Newcastle upon Tyne, UK.

Reeckmann, S.A., 1985. Geology of the foreslope to basinal transition, Permian Reef Complex, McKittrick Canyon, Guadalupe Mountains. Exxon Production Research Co. special report. EPR. 125Ex. 85. Dec. 1985.

Rees, A.I., 1961. The effect of water currents on the magnetic remanence and anisotropy of susceptibility of some sediments. Geophys. J. R. astr. Soc. 5; 235-251.

Rees, A.I., 1965. The use of anisotropy of magnetic susceptibility in the estimation of sedimentary fabric. Sedimentology, 4; 252-271.

Rees, A.I., 1966. The effect of depositional slopes of the anisotropy of magnetic susceptibility of laboratory deposited sand Jour. Geol. 74; 856-857.

Reynolds, R.L., Fishman, N.S., Hudson, M.R., Karachewski, J.A. and Goldhaber, M.B., 1985. Magnetic minerals and hydrocarbon migration: evidence from Cement (Oklahoma), North Slope (Alaska) and the Wyoming-Idaho-Utah thrust belt. Am. Geophys. Union. trans., 66; 867.

Rochette, P., 1987. Magnetic susceptibility of the rock matrix related to magnetic fabric studies. Observatoire de Grenoble, LGIT-IRIGM, BP 68, 38402, St. Martin d'Heres, Grenoble. 13 p. *in*: J. struct. geol., 9; 1015-1020.

Rochette, P., 1988. Inverse magnetic fabric in carbonate-bearing rocks. Earth and Planet. Sci. Lett., 90; 229-237.

Ross, C.A., and Ross, J.R.P., 1987. Late Palaeozoic sea levels and depositional sequences. *in*: Ross, C and Haman, D. (eds). Timing and depositional history of eustatic sequences, constraints on seismic stratigraphy: Cushman Foundation for Foramaniferal Research. spec. pub. 24; 137-149.

Sarg, J.F. and Pray, L.C., 1984. Unconformities and depositional sequences of seismic stratigraphic scale (Permian) of Western Guadalupe Mountains, Texas. Soc. Econ. Palaont. Miner. ann mid-year meeting abst., p.71.

Sarg, J.F., 1977. Sedimentology of the carbonate-evaporite facies transition of the Seven Rivers Formation (Guadalupian-Permian) in SE New Mexico. in 1977 guidebook, Permian Basin Section - Soc. Econ. Paleont. Miner. publ. 77-16. p. 451-478.

Sarg, J.F., 1981. Petrology of the carbonate-evaporite facies transition of the Seven Rivers formation (Guadalupian, Permian), south-east New Mexico. Jour. Sed. Petrol. 51; 73-96.

Sassen, R., Chinn, E.W., Kyle, J.R. and M^{c}Cabe, C., 1987. Recent hydrocarbon degradation and sulfate reduction in salt-dome cap rock at Damon Mound, Brazoria Co., Texas. Soc. Econ. Palaont. Miner. mid-year meeting, abstr., p. 75.

Schmidt, V., 1977. Inorganic and organic reef growth and subsequent diagenesis in the Permian Capitan Reef Complex. Guadalupe Mountains, Texas and New Mexico. *In*: Upper Guadalupian facies, Permian Reef Complex, Guadalupe Mountains, New Mexico and West Texas,. 1977 field conference guidebook. Permian Basin Section - Soc. Econ. Paleont. Miner. , publ 77-16, (eds. Hileman, M.E and Mazzullo. S.J.), 93-132.

Schmitt, J.G. and Boyd, D.W., 1981. Patterns of silicificationin Permian pelycopods and brachiopods from Wyoming. Jour. Sed. Petrol. 51; 1297-1308.

Scholle, P.A. and Melim, L.A., 1988. Evaporites and dolomites in Permian (Guadalupian), Capitan fore-reef carbonates, Delaware Basin Margin, West Texas and New Mexico. Abst. Geol. Soc. Amer. Denver Colorado; p. A211.

Scotese, C.R., Barnbach, R.K., Barton, C., van der Voo, R. and Ziegler, A.M., 1979. Palaeozoic base maps. Jour. Geol. 87; 217-277.

Shinn, E.A. and Ginsburg, R.N., 1964. Formation of Recent dolomite in Florida and the Bahamas. Amer. Assoc. Petrol. Geol. Bull., 48; 547.

Shumard, G.G., 1860. Observations of the geological formations of the country between the Rio Pecos and Rio Grande in New Mexico. St. Louis Acad. Sci. Trans. 1; 280 pages.

Siedlecka, A., 1972. Length-slow chalcedony and relicts of sulphates - evidence of evaporite environments in the Upper Carboniferous and Permian beds of Bear Island, Svalbard, Jour. Sed. Petrol. ; 42; 812-816.

Silver, B.A. and Todd, R.G., 1969. Permian cyclic strata, northern Midland and Delaware basins, West Texas and south-east New Mexico. Amer. Assoc. Petrol. Geol. Bull., 53; 2223-2251.

Smith, D.B., 1974. Sedimentation of Upper Artesia (Guadalupian) cyclic shelf deposits of northern Guadalupe mountains, New Mexico. Amer. Assoc. Petrol. Geol. Bull., 58;1699-1730.

Stacey, F.D., 1960. Magnetic anisotropy of igneous rocks. Jour. Geol. r, 65; 2429-2442.

Stephenson, A., Sadikun, S. and Potter, D.K., 1986. A theoretical and experimental comparison of the anisotropies of magnetic

susceptibility and remanence in rocks and minerals. Geophys. J. R. astr. Soc. 84; 185-200.

Stoltz. J.F., Chang, S.R and Kirschvink, J.L. 1987. The effect of magnetotactic bacteria on the magnetic properties of marine sediments. *in*: Crick, R.E. (ed), Proceedings of the fifth international symposium on biomineralisation, Chicago University Press, in press.

Stoltz. J.F., Chang, S.R and Kirschvink, J.L. ,1986. Magnetotactic bacteria and single domain magnetite in hemipelagic sediments. Nature, 321; 849-851.

Tarling, D.H. and Symons, D.T.A., 1967. A stability index of remanence in palaeomagnetism. Geophys. J. R. astr. Soc., 12; 443-448.

Tarling, D.H., 1983. Palaeomagnetism: principles and applications in geology, geophysics and archaeology. Chapman Hall; 379 pages.

Tarling, D.H., 1985. Problems in Palaeozoic palaeomagnetism. J. Geodynamics, 3; 87-103.

Tissot, B.P. and Welte, D.H., 1978. Petroleum formation and occurrence. New York, Springer-Verlag. 538 pages.

Toomey, D.F. and Cys, J.M., 1977. Rock/biotic relationships of the Permian Tansill-Capitan facies exposed on the north side of the entrance to Dark Canyon, Guadalupe Mountains, south-east New Mexico. Permian Basin Section - Soc. Econ. Paleont. Miner. , publ. 77-16. p.151-200.

Torres de Aranjo, F.F., Pines, M.A., Frankel, R.B. and Bicudo, C.E.M., 1986. Magnetite and magnetotaxis in algae. Biophysical Journal, 50; 375-378.

Towe, K.M. and Moench, T.T., 1981. Electron-optical characterisation of bacterial magnetite. Earth and Planet. Sci. Lett., 52; 213-220.

Turner, P. and Archer, R., 1975. Magnetisation history of the Lower Old Red Sandstone for the Gamrie Outlier. Earth and Planet. Sci. Lett., 27; 240-250.

Turner, P., 1975. Depositional magnetisation of Carboniferous Limestone from the Craven Basin of Northern England. Sedimentology, 22; 563-581.

Turner, P. and Ixer, R.A., 1977. Diagenetic development of unstable and stable magnetisation in the St. Bees sandstone (Triassic of northern England). Earth and Planet. Sci. Lett., 34; 113'124.

Turner, P., Vaughan, D.J. and Whitehouse, K.I., 1978. Dolomitisation and mineralisation of the Marl slate (NE England). Mineral deposita 13; 245-358.

Tyrrell, W.W., 1964. Palaeontology and stratigraphy of near-reef Tansill-Lamar strata, Guadalupe Mountains, Texas and New Mexico. *in*: Geology of the Capitan Reef Complex, Culberson Co., Texas, and Eddy Co. New Mexico. Roswell Geol. Soc., guidebook, 66-82.

Tyrrell, W.W., 1969. Criteria useful in interpreting environments of unlike but time-equivalent carbonate units (Tansill-Capitan-Lamar), Capitan Reef Complex, West Texas and New Mexico. *in*: 'Depositional environments in carbonate rocks' Soc. Econ. Palaont. Miner. spec. publ. 14;

Uyeda, S., Fuller, M.D., Belshe, J.C and Girdler, R.W., 1963. Anisotropy of magnetic susceptibility of rocks and minerals. Jour. Geol. r 68; 279-291.

Vaughan, D.J. and Turner, P., 1980. Diagenesis, magnetisation and mineralisation of the Marl Slate. *in*: The Zechstein Basin, with emphasis on carbonate sequences . (ed.) Fuchtbauer, H. and Peryt, T. p. 73-90. 'Contributions to Sedimentology' no. 9.

Williamson, C.R. 1979. Deep sea sedimentation and stratigraphic traps. Bell Canyon Formation (Permian), Delaware Basin. Permian Basin Section - Soc. Econ. Paleont. Miner. publ. 79-18 Sulliven, N.M., *(ed)*.

Wisniowiecki, M.J., van der Voo, R., M^cCabe, C. and Kelly, W.C., 1983. A Pennsylvanian palaeomagnetic pole from the mineralised late Cambrian Bonnterre Formation, SE Missouri. Jour. Geol. r 88; 6540-6548.

Worm, H.U. and Banerjee, S.K., 1987. Rock magnetic signature of the Cretaceous-Tertiary boundary. Geophys, Res. Lett. , 14; 1083-1086.

Yurewicz, D.A., 1976. Sedimentology, palaeoecology and diagenesis of the massive facies of the Lower and Middle Capitan Limestone. unpubl. PhD. thesis, Univ of Wisconsin, Madison, 278 pp.

Yurewicz, D.A., 1977. The origin of the massive facies of the Lower and Middle Capitan limestone (Permian), Guadalupe Mountains, Texas and New Mexico. in: Permian Basin Section - Soc. Econ. Paleont. Miner. publ. 77-16. (eds.) Hileman, M.E. and Mazzullo, S.J., p. 45-92.

Zenger, D.H. and Dunham, J.B., 1980. Concepts and models of dolomitisation - an introduction. Soc. Econ. Palaont. Miner. spec publ. 28. 320 pp.

Zijderveld, J.D.A., 1967. AC demagnetisation of rocks: analysis of results. *in*: Methods in palaeomagnetism. (ed.) Collinson, D.W., *et al.*, Elsevier. p. 254-286.

List of Appendices

Appendix 3.1 Methods and techniques employed during diagenetic studies

All thin sections were crafted by Trevor Whitfield to a thickness of 20μm. Samples were impregnated with 'Orasol Blue GN' pigment in resin (styrene monomer) prior to section making, in order to be able to distinguish porosity from any holes generated in the section making process. The polished sample surface was glued to a glass slide using 'Permabond' epoxy resin. The section was then ground down to 20μm and polished using 0.3μm polishing alumina. The sections were not etched or stained. Average section area was 20 x 30mm.

Some stained acetate peels were made in order to distinguish calcite and dolomite (Dickson, 1966). Samples were cut and polished until the surface was able to give a good reflection. The surface was then washed with dilute detergent solution, then etched for 10 seconds in 0.5% HCl. The samples were then stained in a combination stain of alizarin red-S and potassium ferricyanide (0.6 alizarin red-S in 300cc of 0.5% HCl plus 4g. of potassium ferricyanide in 200cc of 0.5% HCl) for between 60 and 90 seconds, then rinsed with distilled water and left to dry. The surface was then flooded with acetone and a sheet of acetate 'rolled' onto the surface. This was left to harden, then peeled off, trimmed and mounted between two glass slides.

A Nikon Labophot-PO1 polarising microscope with reflected light facility was used for all petrography. Photographs were taken using an Olympus OM4 SLR camera with an autowinder and auto-shutter release mechanism. A 'varimagni-finder' was used to achieve optimum focusing.

A Technosyn Ltd (Cambridge) CL unit 200 was used, in conjunction with a Nikon Labophot-microscope for all cathodoluminescence work. The operating conditions were a vacuum of 0.65 to 0.55 Torr and a gun current of 160-190 microamps. Standard polished thin sections were used, sometimes including thin sections which had been carbon coated for electron mocroprobe studies. This thin coating does not impede the electron beam (Miller,1988). Care was taken to keep the sample surface clean and dry. Samples were placed on a glass slide supported on an X-Y moving carriage, enabling them to be moved in any X-Y direction beneath the microscope stage. The samples were then sealed in an evacuated sample chamber, bombarded with an electron beam, and their cathodoluminescence observed.

The electron microprobe equipment used in this study was a CAMECA microprobe; (Edinburgh University Geology Dept). Samples were placed on an X-Y stage in an evacuated chamber and bombarded with an electron beam (accelerating voltage of 8kV, magnification multiplier of 1.3, filament temperature set at 1.5). The electron beam had a 10μm square raster size. When the sample area was less than this raster size, a spot beam of 2μm diameter was used. The intensities the characteristic X-ray spectra produced were calibrated by comparison with spectra generated from a set of standards (table A3.1). A verification of a standard (andradite) was carried out at each specimen change and after each break in the sample run *i.e.*, about every two hours. Normal

polished thin sections were used. The thin sections were prepared for microprobe analysis by immersion in an ultrasonic bath of petroleum ether for 30 minutes. They were then carefully dried and placed in a carbon-coating device and coated with a thin, uniform coating of vaporised carbon. The ends of each thin-section were then painted with an aqueous suspension of carbon in order to allow a good electrical connection between the surface of the rock sample and the electron microprobe stage. After preparation all thin sections were stored in a sealed desiccator to keep them clean and dry. All electron microprobe analyses are given in appendix 3.2.

element	standard	wt.% element	beam	counts/sec	m	R_B	T_B
Mg	periclase	60.32	9.5	9495	16.57	6.47	30
Sr	celestite	47.70	9.8	3805	8.14	28.03	30
Ca	wollastonite	34.32	9.5	4186	12.84	13.07	30
Fe	pure metal	100.00	9.7	5480	5.65	8.8	30
Na	jadeite	11.34	9.8	723	6.51	3.2	30
Si	wollastonite	24.00	10.0	5261	21.9	20.67	60
K	orthoclase	12.40	9.5	1192	10.18	7.33	30
Mn	pure metal	100.00	9.7	4837	4.98	5.0	30
Al	sapphire	52.91	9.5	11846	23.59	11.87	30
S	synthetic	17.46	9.5	563	3.41	2.07	30
Ti	rutile	59.95	9.5	1344	2.36	2.93	30

where: T_B = count time on background

R_B = count rate on background

m = counts/second/(wt% element in standard x beam)

Table A3.1 Summary table giving details of standards used in electron microprobe analysis of elements.

element	99.9% detection limit (wt.%)	95.0% detection limit (wt.%)
Mg	0.083	0.055
Sr	0.346	0.230
Ca	0.152	0.099
Fe	0.286	0.189
Na	0.147	0.099
Si	0.075	0.052
K	0.142	0.093
Mn	0.246	0.164
Al	0.076	0.050
S	0.228	0.151
Ti	0.393	0.260

where: 99.9% detection limit = $3/m \times \sqrt{(R_B / T_B)}$

and 95.0% detection limit = $2/m \times \sqrt{(R_B / T_B)}$

Table A3.2 Summary table of detection limits for element-content analysed using electron microprobe.

Appendix 3.2 Electron microprobe analyses for all samples.

i. These data are the weight% oxide values *measured* by the electron microprobe.

ii. The 95% and 99% detection limits for the electron microprobe used are given in appendix 3.1.

iii. In this appendix the values which lie **above** the **95%** detection limit of the microprobe are shown in **bold** type.

iv. All measurements, including those below the 95% detection limit, are listed in order that: *i.* measured values of zero may be distinguished from other measured values and *ii.* these data *could* be related to the 99.9% detection limit. However, this listing does **not** imply that precision of the microprobe used was *necessarily* better than 95%.

v. These data are given to 2 significant figures. This has been done on the recommendation of G.M. Harwood (thesis supervisor), Pete Hill (microprobe laboratory, Edinburgh University) and following conventional proceedures apparent from papers on carbonate cement analysis published in recognised journals (*e.g.* The Society of Economic paleontologists and Mineralogists).

Key to abbreviations:

sm	spot mode
cc	calcite spar (sometomes followed by classification name)
cc(i)	inclusion-rich calcite spar
m	micrite
d	dolomite
d o'g	dolomite overgrowth cement
emc	early marine cement (isopachous)
dmc	dolomitised early marine cement (isopachous)
b	bioclast
db	dolomitised bioclast
ALP	*Archaeolithoporella* laminae
k	kaolinite/dickite
h	haematite
f	feldspar
s	siliciclastic silt grain

Appendix 3.2

element	1	2	3	4	5	6	7	8	9	10
MgO	**0.54**	**21.07**	**21.06**	**0.45**	**20.98**	**0.35**	**0.35**	**0.42**	**0.08**	**0.13**
SrO	0.03	0.00	0.02	0.02	0.02	0.08	0.05	0.04	0.06	0.04
CaO	**0.57**	**31.10**	**31.82**	**56.05**	**31.47**	**56.21**	**56.20**	**56.26**	**56.75**	**56.56**
FeO	**73.94**	0.08	0.05	0.03	0.03	0.03	0.00	0.02	0.04	0.00
Na2O	0.09	0.10	0.03	0.02	0.07	0.02	0.02	0.00	0.04	0.04
SiO2	**3.42**	0.03	0.03	0.03	0.02	0.00	0.03	0.02	0.01	0.00
K2O	0.02	0.02	0.01	0.01	0.01	0.00	0.01	0.01	0.00	0.01
MnO	0.00	0.00	0.05	0.00	0.00	0.04	0.04	0.05	0.05	0.05
Al2O3	**0.60**	**0.28**	**0.21**	0.00	**0.20**	0.03	0.03	0.00	0.01	0.00
SO3	0.09	0.46	0.06	0.00	**0.44**	**0.19**	**0.18**	0.03	0.02	0.04
TiO2	0.00	0.00	0.02	0.03	0.00	0.05	0.03	0.05	0.02	0.14
total	79.30	53.13	53.34	56.64	53.25	57.00	56.94	56.88	57.09	57.01
	h	g	ccII	g	cclll	cclll	ccII	ccII	cclll	ccII

element	11	12	13	14	15	16	17	18	19	20
MgO	**0.04**	**0.21**	**0.43**	**0.44**	**0.13**	**0.28**	**0.30**	**0.30**	**0.19**	**0.36**
SrO	0.03	0.06	0.03	0.06	0.05	0.05	0.05	0.04	0.03	0.03
CaO	**56.80**	**56.31**	**55.90**	**56.23**	**56.50**	**56.38**	**56.48**	**56.05**	**56.15**	**56.46**
FeO	0.00	0.00	0.00	0.00	0.03	0.04	0.00	0.01	0.00	0.01
Na2O	0.02	0.00	0.03	0.03	0.03	0.03	0.04	0.03	0.00	0.00
SiO2	0.00	0.00	0.00	0.01	0.02	0.01	0.01	0.01	0.01	0.00
K2O	0.01	0.01	0.02	0.02	0.00	0.02	0.00	0.01	0.03	0.01
MnO	0.02	0.02	0.10	0.04	0.02	0.00	0.01	0.02	0.06	0.03
Al2O3	0.00	0.00	0.03	0.03	0.00	0.02	0.02	0.00	0.01	0.02
SO3	0.04	**0.28**	0.05	0.00	0.05	0.02	0.00	0.01	0.02	0.05
TiO2	0.00	0.06	0.00	0.00	0.05	0.00	0.00	0.01	0.00	0.05
total	56.96	56.95	56.59	56.87	56.89	56.84	56.91	56.49	56.50	57.01
	ccII	ccII	ccII	ccII	ccII	ccII	ccII	ccII	ccII	ccII

element	21	22	23	24	25	26	27	28	29	30
MgO	**0.43**	**0.34**	**0.31**	**0.31**	**0.32**	**0.35**	**0.37**	**0.34**	**0.36**	**0.38**
SrO	0.03	0.03	0.03	0.06	0.03	0.02	0.03	0.03	0.03	0.01
CaO	**56.20**	**56.24**	**56.33**	**56.38**	**56.46**	**55.84**	**56.20**	**56.20**	**55.46**	**56.29**
FeO	0.04	0.02	0.00	0.00	0.00	0.02	0.04	0.00	0.00	0.03
Na2O	0.01	0.05	0.02	0.02	0.03	0.04	0.00	0.02	0.01	0.04
SiO2	0.02	0.02	0.00	0.01	0.00	0.02	0.00	0.01	0.01	0.02
K2O	0.03	0.01	0.02	0.00	0.02	0.04	0.02	0.02	0.02	0.04
MnO	0.03	0.06	0.06	0.06	0.04	0.01	0.02	0.07	0.08	0.02
Al2O3	0.01	0.00	0.01	0.03	0.01	0.00	0.01	0.01	0.00	0.00
SO3	0.04	0.01	0.05	0.03	0.02	0.02	0.06	0.03	0.05	0.02
TiO2	0.00	0.06	0.02	0.06	0.00	0.05	0.00	0.00	0.00	0.00
total	56.84	56.85	56.85	56.96	56.92	56.41	56.74	56.72	56.01	56.85
	ccII	ccII	ccII	ccII	ccII	ccII	ccII	ccII	ccII	ccII

element	31	32	33	34	35	36	37	38	39	40
MgO	**0.31**	**0.41**	**21.76**	**21.53**	**21.53**	**0.10**	**0.08**	**0.09**	**0.13**	**0.06**
SrO	0.04	0.03	0.00	0.05	0.03	0.00	0.03	0.02	0.05	0.04
CaO	**56.35**	**56.89**	**31.27**	**31.76**	**31.54**	**33.48**	**57.47**	**57.45**	**57.27**	**57.71**
FeO	0.00	0.03	0.01	0.02	0.00	**26.64**	0.02	0.00	0.01	0.01
Na2O	0.04	0.00	0.09	**0.12**	0.05	0.00	0.01	0.02	0.00	0.01
SiO2	0.02	0.02	0.03	0.04	0.02	**36.49**	0.00	0.00	0.01	0.00
K2O	0.02	0.00	0.01	0.01	0.01	0.00	0.03	0.02	0.02	0.00
MnO	0.05	0.03	0.04	0.03	0.04	**0.41**	0.02	0.04	0.03	0.00
Al2O3	0.02	0.00	**0.09**	**0.18**	**0.11**	**1.77**	0.02	0.01	0.01	0.02
SO3	0.08	0.02	0.09	**0.27**	0.04	0.00	0.03	0.06	0.01	0.02
TiO2	0.00	0.08	0.06	0.00	0.01	0.07	0.03	0.01	0.02	0.01
total	56.93	57.50	53.43	54.00	53.38	98.96	57.74	57.71	57.55	57.89
	ccII	ccII	d	dmc	dmc	dmc	cclll	cclll	cclll	cclll

back reef facies: site MT74l

Appendix 3.2

element	41	42	43	44	45	46	47	48	49	50
MgO	0.12	0.32	0.14	0.45	0.41	0.40	0.30	20.24	20.23	7.28
SrO	0.01	0.02	0.05	0.03	0.01	0.03	0.02	0.02	0.00	0.00
CaO	57.00	56.66	57.32	56.99	55.68	55.73	56.00	31.29	31.07	13.54
FeO	0.03	0.00	0.00	0.00	0.02	0.00	0.01	0.05	0.06	0.08
Na2O	0.00	0.01	0.01	0.02	0.02	0.00	0.02	0.14	0.10	0.16
SiO2	0.00	0.01	0.00	0.02	0.00	0.00	0.01	0.02	0.05	0.84
K2O	0.01	0.01	0.01	0.03	0.01	0.01	0.02	0.02	0.04	0.08
MnO	0.04	0.02	0.01	0.01	0.02	0.03	0.07	0.00	0.02	0.02
Al2O3	0.00	0.01	0.01	0.02	0.02	0.00	0.01	1.15	1.11	3.98
SO3	0.03	0.00	0.03	0.02	0.00	0.02	0.00	0.33	0.79	8.81
TiO2	0.02	0.00	0.00	0.09	0.00	0.03	0.02	0.00	0.00	0.05
total	57.27	57.07	57.58	57.67	56.20	56.25	56.47	53.26	53.46	34.83
	cclll	ccll	ccll	ccll	ccll	ccll	ccll	d	d	dmc

element	51	52	53	54	55	56	57	58	59	60
MgO	5.56	21.40	12.97	18.13	0.15	21.27	11.15	21.30	0.79	0.94
SrO	0.00	0.01	0.02	0.01	0.06	0.02	0.00	0.00	0.03	0.00
CaO	9.99	31.21	27.20	28.65	56.11	31.75	27.43	32.01	0.60	0.62
FeO	0.06	0.04	0.09	0.06	0.03	0.01	0.05	0.04	70.86	70.85
Na2O	0.13	0.03	0.25	0.32	0.00	0.07	0.49	0.03	0.11	0.08
SiO2	1.13	0.03	0.58	0.23	0.01	0.00	0.36	0.00	3.73	3.66
K2O	0.04	0.00	0.21	0.13	0.01	0.02	0.23	0.00	0.01	0.01
MnO	0.03	0.03	0.00	0.02	0.03	0.02	0.04	0.04	0.17	0.22
Al2O3	0.73	0.02	2.75	5.93	0.00	0.13	4.98	0.06	0.79	0.68
SO3	10.04	0.00	0.18	0.21	0.06	0.12	0.27	0.08	0.14	0.09
TiO2	0.06	0.00	0.03	0.00	0.00	0.00	0.05	0.03	0.04	0.07
total	27.77	52.77	44.29	53.68	56.46	53.41	45.05	53.59	77.27	77.20
	dmc	d	dmc	dmc	ccll	d	dmc	d	h	h

element	61	62	63	64	65	66	67	68	69	70
MgO	0.55	21.24	0.48	20.78	21.92	7.90	20.87	21.69	0.03	0.12
SrO	0.02	0.04	0.03	0.01	0.02	0.03	0.01	0.00	0.05	0.02
CaO	55.64	32.05	55.65	31.34	31.60	23.70	31.44	31.38	57.12	57.36
FeO	0.53	0.02	0.01	0.01	0.06	0.08	0.07	0.09	0.02	0.02
Na2O	0.02	0.05	0.03	0.03	0.04	0.10	0.15	0.01	0.04	0.00
SiO2	0.02	0.00	0.02	0.00	0.03	0.37	0.01	0.03	0.03	0.01
K2O	0.01	0.01	0.01	0.01	0.00	0.07	0.03	0.03	0.01	0.00
MnO	0.00	0.04	0.05	0.03	0.03	0.01	0.05	0.03	0.01	0.01
Al2O3	0.02	0.17	0.02	0.09	0.05	2.58	0.30	0.03	0.00	0.03
SO3	0.07	0.01	0.00	0.23	0.03	1.24	1.03	0.09	0.00	0.00
TiO2	0.04	0.02	0.02	0.00	0.04	0.04	0.00	0.02	0.00	0.00
total	56.92	53.78	56.33	52.52	53.81	36.12	53.96	53.39	57.30	57.57
	cclll	dmc	ccll	d	d	dmc	d	d	ccll	ccll

element	71	72	73	74	75	76	77	78	79	80
MgO	0.27	15.58	10.29	21.71	21.79	21.24	0.65	0.50	0.49	10.95
SrO	0.03	0.01	0.02	0.01	0.03	0.04	0.00	0.02	0.00	0.03
CaO	56.78	26.50	24.27	31.34	31.80	32.13	55.85	56.01	55.95	27.32
FeO	0.00	0.08	0.10	0.06	0.02	0.04	0.04	0.05	0.00	0.01
Na2O	0.00	0.41	0.36	0.01	0.00	0.00	0.01	0.04	0.04	0.29
SiO2	0.03	0.37	0.62	0.00	0.03	0.00	0.00	0.00	0.02	0.36
K2O	0.01	0.19	0.14	0.00	0.01	0.00	0.00	0.01	0.02	0.25
MnO	0.02	0.02	0.01	0.06	0.03	0.01	0.00	0.02	0.00	0.00
Al2O3	0.01	4.55	18.53	0.03	0.08	0.06	0.03	0.02	0.00	4.47
SO3	0.01	0.21	0.29	0.03	0.03	0.00	0.02	0.02	0.02	0.20
TiO2	0.03	0.00	0.00	0.01	0.04	0.00	0.00	0.00	0.00	0.03
total	57.19	47.92	54.64	53.28	53.85	53.51	56.59	56.70	56.54	43.91
	ccll	dmc	dmc	d	d	d	ccll	ccll	ccll	dmc

back reef facies: site MT74l

Appendix 3.2

element	81	82	83	84	85	86	87	88	89	90
MgO	10.24	1.79	4.28	15.58	0.30	0.52	0.33	0.30	0.40	0.41
SrO	0.01	0.00	0.00	0.01	0.06	0.02	0.01	0.03	0.07	0.05
CaO	20.84	4.79	11.29	20.02	56.42	56.35	55.95	56.26	56.18	56.18
FeO	0.11	0.07	0.02	0.05	0.02	0.00	0.03	0.03	0.02	0.00
Na2O	0.72	0.33	0.24	0.38	0.03	0.00	0.01	0.00	0.04	0.00
SiO2	0.59	84.35	24.93	2.17	0.02	0.03	0.00	0.00	0.00	0.00
K2O	0.38	0.18	0.13	0.17	0.02	0.02	0.01	0.01	0.01	0.02
MnO	0.02	0.03	0.01	0.00	0.03	0.00	0.02	0.03	0.03	0.05
Al2O3	10.38	5.20	3.38	4.84	0.00	0.02	0.00	0.02	0.00	0.00
SO3	0.29	4.73	6.19	3.38	0.01	0.00	0.00	0.03	0.00	0.02
TiO2	0.00	0.00	0.08	0.00	0.00	0.00	0.07	0.05	0.08	0.00
total	43.59	101.47	50.52	46.84	56.91	56.96	56.41	56.77	56.84	56.73
	dmc(sm)	dmc(sm)	dmc(sm)	dmc(sm)	cclll	cclll	cclll	cclll	cclll	cclll

element	91	92	93	94	95	96	97	98	99	100
MgO	0.46	0.40	0.23	0.18	0.26	0.40	0.42	0.21	0.24	0.45
SrO	0.01	0.03	0.02	0.05	0.03	0.04	0.02	0.02	0.03	0.03
CaO	55.66	56.24	55.80	56.89	55.98	55.78	56.07	56.62	56.29	56.16
FeO	0.02	0.00	0.00	0.00	0.02	0.01	0.00	0.02	0.00	0.01
Na2O	0.03	0.01	0.00	0.02	0.00	0.00	0.01	0.02	0.02	0.02
SiO2	0.00	0.01	0.03	0.00	0.00	0.02	0.00	0.01	0.02	0.00
K2O	0.02	0.01	0.02	0.03	0.02	0.01	0.01	0.01	0.01	0.01
MnO	0.02	0.05	0.01	0.05	0.01	0.04	0.03	0.00	0.05	0.02
Al2O3	0.02	0.01	0.03	0.00	0.02	0.00	0.02	0.01	0.00	0.01
SO3	0.00	0.00	0.02	0.02	0.01	0.04	0.01	0.03	0.05	0.04
TiO2	0.00	0.00	0.02	0.00	0.05	0.00	0.00	0.00	0.00	0.04
total	56.24	56.75	56.17	57.24	56.40	56.33	56.58	56.94	56.70	56.78
	cclll	cclll	cclll	cclll	cclll	cclll	cclll	cclll	cclll	cclll

element	101	102	103	104	105	106	107	108	109
MgO	1.33	0.53	0.29	0.17	0.39	20.84	20.79	21.39	0.10
SrO	0.06	0.06	0.06	0.01	0.03	0.02	0.03	0.02	0.01
CaO	55.24	56.23	56.83	48.78	56.37	32.20	32.60	31.83	56.75
FeO	0.01	0.03	0.03	0.00	0.00	0.05	0.04	0.07	0.02
Na2O	0.00	0.04	0.02	0.00	0.02	0.03	0.02	0.04	0.01
SiO2	0.01	0.02	0.02	0.01	0.00	0.41	0.05	0.34	0.01
K2O	0.02	0.01	0.01	0.00	0.01	0.06	0.00	0.04	0.00
MnO	0.03	0.04	0.04	0.00	0.01	0.01	0.00	0.05	0.04
Al2O3	0.04	0.01	0.00	0.01	0.01	0.30	0.17	0.26	0.02
SO3	0.01	0.03	0.03	0.01	0.03	0.04	0.07	0.02	0.00
TiO2	0.07	0.00	0.10	0.00	0.01	0.07	0.00	0.00	0.03
total	56.81	56.99	57.43	48.98	56.89	54.03	53.77	54.06	56.99
	mc	mc	mc	ccl	ccl	g	g	g	ccl

back reef facies: site MT74l

Appendix 3.2

element	1	2	3	4	5	6	7	8	9	10
MgO	0.33	0.61	0.65	0.78	0.64	0.56	0.57	0.33	0.30	0.43
SrO	0.07	0.04	0.05	0.06	0.05	0.02	0.04	0.02	0.05	0.06
CaO	57.94	56.58	56.79	57.08	57.20	54.00	57.09	57.55	57.09	57.11
FeO	0.00	0.01	0.00	0.00	0.01	0.04	0.00	0.02	0.00	0.00
Na2O	0.00	0.02	0.02	0.01	0.00	0.02	0.00	0.05	0.00	0.02
SiO2	0.00	0.02	0.02	0.00	0.02	0.01	0.00	0.02	0.01	0.00
K2O	0.00	0.00	0.00	0.01	0.00	0.01	0.01	0.01	0.02	0.01
MnO	0.00	0.01	0.02	0.00	0.02	0.05	0.02	0.04	0.02	0.03
Al2O3	0.03	0.00	0.02	0.00	0.02	0.01	0.03	0.01	0.00	0.03
SO3	0.01	0.00	0.00	0.00	0.02	0.01	0.00	0.02	0.00	0.03
TiO2	0.00	0.00	0.00	0.00	0.03	0.08	0.00	0.06	0.00	0.00
total	58.37	57.58	57.53	57.94	58.01	54.84	57.75	58.13	57.48	57.73
	cc	cc	cc	cc	cc	cc	cc	cc (I)	cc(I)	cc

element	11	12	13	14	15	16	17	18	19	20
MgO	0.36	0.14	0.21	0.32	0.35	0.27	0.37	0.30	0.18	0.16
SrO	0.05	0.09	0.07	0.02	0.02	0.04	0.02	0.05	0.09	0.06
CaO	57.03	57.47	57.61	47.64	47.51	56.43	47.46	57.74	57.92	56.93
FeO	0.02	0.01	0.00	0.00	0.00	0.02	0.00	0.02	0.00	0.02
Na2O	0.02	0.02	0.02	0.01	0.04	0.03	0.04	0.03	0.00	0.02
SiO2	0.00	0.00	0.03	0.01	0.00	0.04	0.03	0.00	0.01	0.03
K2O	0.00	0.00	0.01	0.01	0.01	0.01	0.00	0.00	0.00	0.00
MnO	0.02	0.01	0.02	0.01	0.03	0.03	0.05	0.02	0.02	0.02
Al2O3	0.03	0.27	0.00	0.01	0.63	1.16	0.02	0.00	0.02	0.00
SO3	0.04	0.07	0.08	0.04	0.08	0.13	0.05	0.08	0.11	0.06
TiO2	0.00	0.00	0.02	0.00	0.00	0.04	0.01	0.01	0.00	0.04
total	57.55	58.07	58.05	48.07	48.67	58.20	48.04	58.24	58.34	57.35
	cc	cc	cc	cc	cc	cc	cc	cc	cc	cc

element	21	22	23	24	25	26	27	28	29	30
MgO	0.21	0.18	0.39	0.78	0.81	0.20	0.32	0.20	0.40	0.50
SrO	0.06	0.07	0.04	0.08	0.05	0.03	0.07	0.06	0.02	0.01
CaO	57.40	57.55	57.50	56.89	56.91	57.90	57.62	57.98	43.75	57.26
FeO	0.03	0.00	0.02	0.04	0.00	0.04	0.03	0.00	0.01	0.00
Na2O	0.00	0.05	0.04	0.03	0.04	0.02	0.06	0.06	0.16	0.03
SiO2	0.02	0.02	0.02	0.01	0.00	0.00	0.01	0.02	1.78	0.01
K2O	0.01	0.01	0.02	0.00	0.00	0.01	0.00	0.00	0.02	0.00
MnO	0.03	0.03	0.04	0.02	0.02	0.02	0.01	0.02	0.04	0.05
Al2O3	0.01	0.15	0.01	0.02	0.46	0.00	0.03	0.02	1.06	0.00
SO3	0.07	0.05	0.02	0.06	0.03	0.00	0.03	0.03	2.74	0.02
TiO2	0.00	0.00	0.00	0.00	0.00	0.05	0.06	0.06	0.00	0.02
total	57.84	57.97	58.11	57.92	58.32	58.27	58.22	58.45	49.99	57.91
	cc	cc	cc	cc	cc	cc	cc	cc	cc	cc

element	31	32	33	34	35	36	37	38	39	40
MgO	0.22	0.19	0.30	0.24	0.23	7.14	0.25	0.41	2.31	0.65
SrO	0.08	0.07	0.07	0.06	0.04	0.04	0.05	0.04	0.06	0.05
CaO	57.57	57.56	57.89	58.10	56.86	49.09	58.04	44.51	54.58	57.26
FeO	0.00	0.03	0.04	0.05	0.06	0.03	0.05	0.01	0.01	0.01
Na2O	0.03	0.01	0.03	0.02	0.04	0.03	0.00	0.06	0.00	0.00
SiO2	0.00	0.00	0.03	0.00	0.00	0.00	0.02	0.01	0.03	0.00
K2O	0.00	0.01	0.01	0.00	0.00	0.02	0.00	0.00	0.01	0.01
MnO	0.03	0.03	0.04	0.01	0.02	0.02	0.06	0.03	0.02	0.04
Al2O3	0.02	0.00	0.00	0.01	1.24	0.01	0.04	0.20	0.13	0.01
SO3	0.02	0.07	0.05	0.01	0.11	0.03	0.02	0.03	0.20	0.04
TiO2	0.00	0.00	0.03	0.03	0.03	0.06	0.00	0.05	0.04	0.02
total	57.95	57.97	58.48	58.52	58.63	56.47	58.53	45.35	57.40	58.09
	cc	cc	cc	cc	cc(I)	cc (I)	cc (I)	cc (I)	cc (I)	cc (I)

Upper foreslope facies: site MT60

Appendix 3.2

element	41	42	43	44	45	46	47	48	49	50
MgO	0.31	0.79	0.20	0.14	0.14	0.33	0.51	0.12	0.41	0.38
SrO	0.01	0.01	0.82	0.04	0.03	0.05	0.05	0.04	0.04	0.05
CaO	49.18	55.66	57.64	58.11	58.08	57.80	57.52	57.77	54.87	57.68
FeO	0.00	0.00	0.00	0.01	0.00	0.03	0.00	0.04	0.04	0.02
Na2O	0.05	0.04	0.03	0.00	0.00	0.02	0.03	0.03	0.04	0.02
SiO2	0.00	0.13	0.01	0.00	0.00	0.02	0.03	0.00	0.07	0.01
K2O	0.00	0.01	0.01	0.00	0.00	0.01	0.00	0.01	0.01	0.00
MnO	0.03	0.03	0.02	0.00	0.07	0.03	0.05	0.01	0.02	0.00
Al2O3	0.04	2.85	0.04	0.00	0.03	0.00	0.02	0.00	2.79	0.02
SO3	0.04	0.02	0.44	0.02	0.00	0.00	0.00	0.00	0.05	0.02
TiO2	0.00	0.04	0.00	0.02	0.05	0.00	0.00	0.03	0.02	0.02
total	49.65	59.58	59.20	58.34	58.40	58.30	58.19	58.05	58.34	58.22
	cc (i)	cc (i)	cc (i)	cc (i)	cc (i)	cc (i)	cc (i)	cc (i)	cc (i)	cc (i)

element	51	52	53	54	55	56	57	58	59	60
MgO	0.54	0.24	0.17	20.63	0.18	11.67	0.15	0.20	0.22	0.20
SrO	0.04	0.00	0.03	0.01	0.08	0.01	0.05	0.02	0.02	0.01
CaO	56.94	48.21	58.11	32.70	58.19	41.24	57.96	57.46	57.80	58.45
FeO	0.00	0.00	0.00	0.00	0.04	0.03	0.02	0.03	0.04	0.04
Na2O	0.02	0.02	0.02	0.04	0.00	0.05	0.00	0.05	0.04	0.02
SiO2	0.00	0.00	0.02	0.01	0.02	0.04	0.02	0.00	0.01	0.01
K2O	0.00	0.00	0.01	0.00	0.01	0.01	0.00	0.01	0.00	0.01
MnO	0.02	0.02	0.04	0.00	0.02	0.01	0.02	0.01	0.00	0.01
Al2O3	0.02	0.01	0.03	1.53	0.05	0.08	0.08	0.00	0.02	0.05
SO3	0.17	0.05	0.04	0.02	0.06	0.09	0.00	0.04	0.01	0.01
TiO2	0.00	0.00	0.00	0.00	0.00	0.02	0.00	0.05	0.00	0.06
total	57.74	48.55	58.46	54.95	58.64	53.25	58.30	57.86	58.16	58.85
	cc (i)	cc (i)	cc (i)	dmc	m	m	m	m	m	m

element	61	62	63	64	65	66	67	68	69	70
MgO	0.26	0.40	0.25	0.35	0.38	0.35	0.32	0.33	0.26	0.30
SrO	0.01	0.05	0.01	0.02	0.04	0.04	0.03	0.04	0.05	0.03
CaO	57.87	57.49	49.57	57.39	57.87	58.30	47.73	57.45	57.15	48.25
FeO	0.00	0.00	0.00	0.05	0.00	0.02	0.00	0.04	0.00	0.00
Na2O	0.00	0.03	0.03	0.01	0.02	0.04	0.00	0.02	0.03	0.00
SiO2	0.02	0.01	0.01	0.00	0.00	0.03	0.00	0.00	0.00	0.01
K2O	0.00	0.01	0.00	0.01	0.00	0.01	0.01	0.01	0.00	0.01
MnO	0.04	0.02	0.05	0.00	0.01	0.01	0.00	0.06	0.04	0.00
Al2O3	0.01	0.02	0.21	0.00	0.00	0.01	0.01	0.00	0.00	0.01
SO3	0.02	0.03	0.02	0.04	0.04	0.03	0.05	0.02	0.05	0.04
TiO2	0.03	0.02	0.01	0.01	0.05	0.02	0.02	0.00	0.00	0.00
total	58.25	58.07	50.15	57.88	58.41	58.86	48.16	57.97	57.59	48.64
	m	cc	cc	cc	cc	cc	cc	cc	cc	cc

element	71	72	73	74	75	76	77	78	79	80
MgO	0.31	0.69	0.53	0.62	0.95	0.28	0.39	0.51	0.59	0.67
SrO	0.06	0.07	0.03	0.05	0.05	0.03	0.00	0.01	0.04	0.04
CaO	57.99	57.31	58.04	48.24	56.85	57.64	47.77	47.27	56.79	56.42
FeO	0.01	0.00	0.02	0.03	0.02	0.04	0.01	0.00	0.00	0.01
Na2O	0.06	0.00	0.05	0.06	0.04	0.01	0.12	0.03	0.01	0.02
SiO2	0.01	0.00	0.00	0.00	0.02	0.02	0.02	0.01	0.03	0.00
K2O	0.00	0.00	0.02	0.01	0.00	0.00	0.01	0.00	0.01	0.01
MnO	0.00	0.03	0.03	0.00	0.04	0.02	0.13	0.01	0.05	0.03
Al2O3	0.00	0.02	0.01	0.00	0.05	0.95	0.14	0.00	1.22	0.02
SO3	0.05	0.02	0.04	0.00	0.01	0.03	0.00	0.00	0.06	0.00
TiO2	0.00	0.00	0.03	0.00	0.00	0.00	0.00	0.00	0.05	0.04
total	58.50	58.14	58.80	49.02	58.03	59.01	48.58	47.84	58.85	57.25
	cc	cc (i)	cc (i)	cc (i0	cc (i)	cc (i)	cc (i)	cc (i)	cc (i)	cc (i)

Upper foreslope facies: site MT60

Appendix 3.2

element	81	82	83	84	85	86	87	88	89	90
MgO	**0.51**	**0.56**	**0.25**	**0.21**	**0.73**	**0.13**	**0.30**	**0.36**	**0.47**	**0.36**
SrO	0.06	0.04	0.04	0.04	0.03	0.04	0.06	0.08	0.02	0.04
CaO	**56.59**	**46.39**	**53.68**	**56.17**	**48.90**	**56.92**	**56.66**	**56.86**	**47.12**	**46.43**
FeO	0.00	0.00	0.01	0.02	0.00	0.01	0.00	0.02	0.02	0.02
Na2O	0.00	0.01	**0.12**	0.06	**0.12**	0.03	0.02	0.01	0.03	0.02
SiO2	0.00	0.00	**0.06**	0.00	**0.13**	0.00	0.01	0.00	0.00	0.00
K2O	0.00	0.00	0.05	0.00	0.03	0.02	0.02	0.00	0.01	0.01
MnO	0.01	0.01	0.03	0.06	0.03	0.02	0.00	0.01	0.03	0.01
Al2O3	0.03	0.01	**5.40**	0.01	**10.02**	0.02	0.00	0.01	0.03	0.00
SO3	0.01	0.02	0.05	0.00	**0.32**	0.02	0.10	0.06	0.06	0.03
TiO2	0.05	0.04	0.04	0.00	0.00	0.00	0.07	0.03	0.00	0.01
total	57.27	47.07	59.72	56.57	60.31	57.22	57.23	57.43	47.78	46.93
	cc (i)	cc	cc (i)	cc (i)	cc (i)	cc (i)	cc	cc	cc	cc

element	91	92	93	94	95	96	97	98	99	100
MgO	**0.36**	**0.40**	**0.30**	**0.20**	**0.18**	**0.23**	**2.95**	**0.20**	**16.33**	**0.38**
SrO	0.02	0.07	0.06	0.06	0.09	0.04	0.02	0.03	0.03	0.04
CaO	**46.94**	**56.65**	**56.71**	**46.39**	**56.50**	**56.71**	**50.74**	**57.16**	**38.20**	**56.45**
FeO	0.00	0.05	0.01	0.00	0.01	0.00	0.05	0.03	0.02	0.03
Na2O	0.01	0.00	0.02	0.00	0.01	0.02	0.03	0.04	0.05	0.04
SiO2	0.00	0.02	0.02	0.00	0.02	0.01	0.02	0.00	0.00	0.00
K2O	0.01	0.00	0.02	0.01	0.00	0.02	0.01	0.01	0.01	0.01
MnO	0.03	0.02	0.01	0.00	0.01	0.04	0.05	0.00	0.03	0.03
Al2O3	0.02	0.03	0.03	0.00	0.01	**0.20**	**0.55**	0.07	**0.16**	0.02
SO3	0.06	0.00	0.04	0.10	0.10	0.05	0.04	0.03	0.01	0.02
TiO2	0.00	0.00	0.02	0.04	0.02	0.00	0.04	0.00	0.00	0.00
total	47.45	57.24	57.22	46.80	56.95	57.32	54.53	57.57	54.83	57.02
	cc	cc	cc	cc	cc	cc (i)	cc (i)	emc	dmc	cc

element	101	102	103	104	105	106	107	108	109	110
MgO	**0.19**	**10.71**	**0.24**	**0.12**	**18.90**	**1.09**	**0.61**	**0.73**	**0.67**	**0.62**
SrO	0.03	0.02	0.02	0.03	0.05	0.04	0.05	0.03	0.05	0.05
CaO	**57.29**	**40.25**	**57.06**	**57.11**	**34.84**	**55.71**	**56.43**	**56.73**	**56.62**	**56.97**
FeO	0.00	0.03	0.00	0.00	0.04	0.01	0.05	0.00	0.00	0.01
Na2O	0.00	0.04	0.03	0.00	0.06	0.04	0.00	0.02	0.00	0.04
SiO2	0.01	0.02	0.00	0.00	0.00	0.02	0.00	0.02	0.00	0.01
K2O	0.02	0.01	0.01	0.00	0.00	0.01	0.00	0.01	0.01	0.01
MnO	0.01	0.02	0.01	0.02	0.03	0.04	0.03	0.06	0.03	0.05
Al2O3	**0.08**	**0.15**	0.02	0.00	**0.53**	**1.67**	0.02	0.01	0.00	0.04
SO3	0.03	0.05	0.04	0.04	0.10	0.00	0.00	0.00	0.01	0.01
TiO2	0.00	0.00	0.00	0.00	0.00	0.06	0.06	0.00	0.05	0.10
total	57.66	51.28	57.43	57.33	54.54	58.67	57.25	57.61	57.45	57.89
	emc	m	m	emc	dmc	c	c	cc	cc	cc

element	111	112	113	114	115	116	117	118	119	120
MgO	**0.65**	**0.64**	**0.51**	**0.56**	**0.21**	**0.26**	**0.39**	**0.22**	**0.15**	**19.36**
SrO	0.05	0.05	0.05	0.04	0.03	0.02	0.00	0.03	0.03	0.00
CaO	**56.61**	**56.81**	**56.45**	**56.66**	**56.36**	**57.09**	**57.29**	**57.59**	**57.93**	**35.31**
FeO	0.01	0.02	0.00	0.00	0.00	0.01	0.02	0.00	0.00	0.02
Na2O	0.02	0.02	0.01	0.02	0.05	0.02	0.04	0.00	0.03	0.07
SiO2	0.02	0.02	0.03	0.00	0.03	0.01	0.05	0.00	0.00	0.03
K2O	0.01	0.00	0.01	0.02	0.01	0.01	0.00	0.01	0.01	0.01
MnO	0.02	0.00	0.00	0.02	0.06	0.02	0.00	0.02	0.06	0.00
Al2O3	0.02	0.01	**1.44**	**0.30**	**1.81**	0.02	0.04	0.02	0.00	**0.14**
SO3	0.02	0.01	0.04	0.03	0.06	0.00	0.01	0.01	0.03	0.07
TiO2	0.00	0.01	0.01	0.06	0.00	0.00	0.00	0.01	0.01	0.05
total	57.44	57.60	58.55	57.72	58.61	57.46	57.84	57.90	58.25	55.06
	cc	cc	cc (i)	cc (i)	cc (i)	cc (i)	cc (i)	cc	cc	dmc

Upper foreslope facies: site MT60

Appendix 3.2

element	121	122	123	124	125	126	127	128	129	130
MgO	**0.37**	**0.11**	**0.54**	**0.25**	**0.23**	**0.22**	**19.09**	**18.72**	**18.51**	**19.13**
SrO	0.02	0.03	0.04	0.05	0.04	0.03	0.00	0.02	0.03	0.00
CaO	**57.05**	**57.54**	**56.70**	**57.51**	**57.69**	**47.66**	**29.77**	**33.90**	**26.35**	**29.09**
FeO	0.05	0.01	0.00	0.00	0.01	0.00	0.02	0.01	0.01	0.03
Na2O	0.00	0.00	0.02	0.01	0.05	0.02	0.03	0.04	0.04	0.00
SiO2	0.00	0.01	0.03	0.01	0.01	0.00	0.00	0.01	0.02	0.01
K2O	0.01	0.01	0.00	0.01	0.00	0.00	0.00	0.00	0.01	0.01
MnO	0.00	0.00	0.02	0.01	0.02	0.00	0.02	0.00	0.03	0.03
Al2O3	0.04	0.00	**1.61**	**0.65**	**0.06**	**0.50**	**0.06**	**0.07**	**0.10**	**0.19**
SO3	0.04	0.02	0.02	0.03	0.01	0.00	**0.18**	0.01	**0.24**	**0.17**
TiO2	0.02	0.00	0.00	0.00	0.00	0.02	0.06	0.00	0.03	0.02
total	57.60	57.74	58.97	58.51	58.11	48.44	49.23	52.77	47.36	48.67
	cc (i)	cc	cc (i)	cc (i)	cc (i)	cc (i)	b	b	b	b

element	131	132	133	134	135	136	137	138	139	140
MgO	**16.67**	**19.44**	**18.63**	**0.35**	**12.44**	**15.13**	**0.20**	**0.14**	**0.20**	**0.78**
SrO	0.03	0.03	0.00	0.04	0.03	0.03	0.01	0.02	0.00	0.03
CaO	**25.86**	**33.25**	**35.91**	**56.89**	**37.82**	**34.75**	**57.28**	**57.38**	**46.30**	**54.88**
FeO	0.02	0.00	0.02	0.02	0.03	0.04	0.00	0.03	0.03	0.02
Na2O	0.02	0.02	0.00	0.04	**0.13**	0.04	0.03	0.00	0.04	0.06
SiO2	0.03	0.01	0.00	0.01	0.03	0.00	0.03	0.04	0.01	0.00
K2O	0.01	0.01	0.00	0.01	0.01	0.01	0.00	0.01	0.02	0.01
MnO	0.03	0.04	0.00	0.00	0.01	0.02	0.02	0.04	0.01	0.00
Al2O3	**0.09**	**0.08**	**0.05**	**0.25**	**0.26**	**0.26**	0.00	**0.20**	0.03	**0.06**
SO3	0.53	0.01	0.08	0.04	0.08	0.11	0.00	0.02	0.00	0.02
TiO2	0.06	0.03	0.05	0.04	0.00	0.00	0.00	0.00	0.00	0.00
total	43.35	52.91	54.74	57.68	50.84	50.38	57.57	57.88	46.65	55.86
	b	b	b	emc	dmc	dmc	m	m	m	cc (i)

element	141	142	143	144	145	146	147	148	149	150
MgO	**0.44**	**0.21**	**0.25**	**0.28**	**0.32**	**0.73**	**0.51**	**0.21**	**0.58**	**0.64**
SrO	0.06	0.08	0.06	0.06	0.07	0.06	0.05	0.04	0.07	0.03
CaO	**56.92**	**57.52**	**57.21**	**47.33**	**56.58**	**56.23**	**50.84**	**57.25**	**56.77**	**47.56**
FeO	0.02	0.00	0.00	0.00	0.00	0.04	0.04	0.03	0.00	0.01
Na2O	0.00	0.03	0.01	0.00	0.00	0.03	0.00	0.00	0.00	0.02
SiO2	0.02	0.00	0.01	0.01	0.02	0.02	0.01	0.02	0.00	0.00
K2O	0.00	0.01	0.01	0.00	0.00	0.01	0.01	0.01	0.01	0.01
MnO	0.03	0.00	0.07	0.03	0.00	0.03	0.01	0.02	0.02	0.00
Al2O3	**0.05**	0.01	0.00	0.00	0.01	0.02	0.01	**0.38**	0.01	0.00
SO3	0.01	0.08	0.06	0.07	0.03	0.03	0.03	0.01	0.00	0.04
TiO2	0.00	0.00	0.06	0.01	0.07	0.09	0.00	0.00	0.00	0.00
total	57.56	57.93	57.73	47.79	57.10	57.29	51.51	57.95	57.45	48.30
	cc (i)	cc	cc	cc	cc	cc	cc	cc	cc	cc

Upper foreslope facies: site MT60

Appendix 3.2

element	1	2	3	4	5	6	7	8	9	10
MgO	0.28	0.27	0.35	0.61	0.33	0.26	0.28	0.38	0.69	0.33
SrO	0.03	0.04	0.07	0.03	0.02	0.04	0.01	0.05	0.03	0.03
CaO	54.68	55.20	54.99	55.01	55.73	55.68	56.11	55.09	54.61	55.46
FeO	0.01	0.00	0.06	0.00	0.00	0.01	0.03	0.00	0.01	0.01
NaO2	0.07	0.03	0.00	0.02	0.00	0.04	0.02	0.00	0.05	0.04
SiO2	0.03	0.00	0.03	0.01	0.00	0.02	0.02	0.02	0.12	0.00
K2O	0.02	0.00	0.00	0.01	0.00	0.01	0.00	0.02	0.01	0.00
MnO	0.04	0.02	0.00	0.00	0.01	0.03	0.00	0.01	0.04	0.00
Al2O3	0.27	0.06	0.17	0.49	0.00	0.01	0.02	0.03	1.67	0.00
SO3	0.04	0.08	0.11	0.14	0.01	0.03	0.03	0.19	0.05	0.01
TiO2	0.00	0.02	0.03	0.00	0.03	0.07	0.00	0.03	0.08	0.03
total	55.45	55.71	55.82	56.32	56.13	56.19	56.49	55.83	57.36	55.92
	ALP	cc(l)	cc(l)	cc(l)	cc	cc	cc	cc(l)	cc(l)	cc(l)

element	11	12	13	14	15	16	17
MgO	0.28	0.28	0.32	0.28	0.26	0.42	0.25
SrO	0.00	0.02	0.03	0.01	0.01	0.07	0.05
CaO	54.93	55.49	53.77	54.12	54.37	53.66	53.78
FeO	0.02	0.02	0.00	0.02	0.03	0.03	0.04
NaO2	0.00	0.03	0.03	0.03	0.01	0.06	0.02
SiO2	0.00	0.01	0.01	0.00	0.00	0.03	0.00
K2O	0.01	0.01	0.02	0.01	0.01	0.01	0.01
MnO	0.01	0.07	0.02	0.02	0.00	0.02	0.02
Al2O3	0.02	0.03	0.30	0.02	0.02	0.19	0.06
SO3	0.03	0.00	0.09	0.09	0.00	0.02	0.01
TiO2	0.00	0.00	0.00	0.00	0.05	0.00	0.00
total	55.29	55.95	54.59	54.58	54.77	54.51	54.23
	cc(l)	cc	cc(l)	cc(l)	cc	cc(l)	ALP

element	1	2	3	4	5	6	7	8	9	10
MgO	0.33	0.43	18.68	9.18	18.84	4.83	1.15	1.72	0.52	0.45
SrO	0.03	0.02	0.01	0.00	0.04	0.00	0.00	0.00	0.03	0.05
CaO	56.55	56.19	28.64	16.50	29.37	6.54	0.00	0.00	56.57	56.52
FeO	0.03	0.02	0.34	0.38	0.33	2.23	2.72	3.00	0.00	0.04
Na2O	0.00	0.00	0.08	0.11	0.06	0.59	0.59	0.80	0.01	0.02
SiO2	0.01	0.02	4.01	6.03	3.46	37.48	47.41	48.05	0.02	0.01
K2O	0.01	0.01	0.49	0.75	0.39	6.10	7.71	7.58	0.03	0.01
MnO	0.01	0.00	0.02	0.01	0.00	0.02	0.04	0.01	0.03	0.00
Al2O3	0.02	0.00	2.80	4.02	2.27	26.95	33.03	32.69	0.00	0.01
SO3	0.03	0.03	0.22	4.74	0.10	0.11	0.02	0.01	0.00	0.05
TiO2	0.03	0.00	0.10	0.06	0.04	0.34	0.30	0.38	0.00	0.00
total	57.04	56.71	55.39	41.77	54.88	85.18	92.96	94.24	57.21	57.16
	cc	cc	m	m	m	f	f	f	cc	cc

element	11	12	13	14	15	16	17	18	19	20
MgO	14.42	21.37	21.19	21.23	12.12	5.03	0.07	0.31	0.80	0.18
SrO	0.03	0.00	0.01	0.02	0.01	0.00	0.02	0.07	0.06	0.06
CaO	40.85	32.64	32.75	33.06	20.98	6.59	57.44	56.29	55.71	56.68
FeO	0.17	0.15	0.30	0.05	0.13	2.85	0.00	0.03	0.06	0.00
Na2O	0.01	0.00	0.01	0.03	0.06	0.23	0.00	0.03	0.04	0.03
SiO2	0.40	0.04	0.14	0.10	1.83	36.35	0.00	0.34	0.44	0.04
K2O	0.04	0.01	0.02	0.02	0.08	4.63	0.01	0.03	0.06	0.01
MnO	0.00	0.05	0.00	0.06	0.02	0.00	0.00	0.02	0.04	0.03
Al2O3	0.25	0.12	0.17	0.09	3.50	21.83	0.02	0.15	0.31	0.02
SO3	0.02	0.01	0.05	0.03	6.11	0.52	0.03	0.06	0.06	0.01
TiO2	0.05	0.00	0.00	0.02	0.04	0.82	0.00	0.09	0.01	0.01
total	56.25	54.39	54.64	54.71	44.86	78.82	57.60	57.43	57.57	57.07
	d	d	d	d	d	d	cc	cc	cc	cc

Lower foreslope facies: site MT33 and site MT39

Appendix 3.2

element	1	2	3	4	5	6	7	8	9	10
MgO	1.67	0.16	1.67	0.27	0.93	20.96	0.18	20.62	11.38	7.75
SrO	0.03	0.04	0.03	0.04	0.02	0.02	0.03	0.02	0.03	0.03
CaO	49.65	58.52	57.47	58.40	57.76	31.16	52.59	31.21	40.11	45.87
FeO	0.04	0.00	0.00	0.00	0.00	0.01	0.00	0.02	0.00	0.01
Na2O	0.13	0.00	0.01	0.04	0.00	0.02	0.04	0.01	0.06	0.04
SiO2	0.01	0.00	0.01	0.05	0.01	0.00	0.01	0.03	0.01	0.00
K2O	0.01	0.01	0.01	0.00	0.00	0.00	0.01	0.01	0.01	0.01
MnO	0.00	0.02	0.00	0.00	0.02	0.03	0.03	0.01	0.01	0.03
Al2O3	0.06	0.12	0.28	0.00	0.00	0.03	0.14	0.18	0.07	0.12
SO3	0.00	0.00	0.00	0.00	0.02	0.23	0.01	0.17	0.00	0.03
TiO2	0.00	0.04	0.01	0.00	0.07	0.02	0.00	0.00	0.00	0.00
total	51.61 mc	58.90 mc	59.47 mc	58.80 mc	58.83 mc	52.48 A	53.04 mc	52.27 g	51.68 mc	53.88 mc

element	11	12	13	14	15	16	17	18	19	20
MgO	19.98	4.63	3.44	2.19	5.04	0.24	0.42	0.14	0.35	0.63
SrO	0.03	0.03	0.02	0.05	0.01	0.01	0.03	0.11	0.05	0.03
CaO	29.70	51.07	55.18	56.41	53.30	56.58	53.42	58.69	47.20	48.35
FeO	0.01	0.04	0.00	0.04	0.01	0.00	0.01	0.02	0.03	0.01
Na2O	0.02	0.03	0.05	0.01	0.09	0.09	0.05	0.02	0.02	0.01
SiO2	0.03	0.02	0.02	0.01	0.02	0.01	0.00	0.02	0.00	0.00
K2O	0.00	0.00	0.01	0.01	0.00	0.01	0.00	0.00	0.00	0.00
MnO	0.00	0.03	0.00	0.03	0.00	0.00	0.00	0.04	0.03	0.03
Al2O3	0.62	0.04	0.07	0.01	0.09	0.02	0.20	0.01	0.01	0.00
SO3	0.37	0.05	0.00	0.13	0.03	0.00	0.00	0.02	0.01	0.00
TiO2	0.00	0.05	0.00	0.00	0.01	0.00	0.03	0.14	0.00	0.03
total	50.58 g	55.99 g	58.78 m	58.89 m	58.59 mc	56.91 mc	54.16 mc	59.20 ccl	47.68 ccll	49.09 ccll

element	21	22	23	24	25	26	27	28	29	30
MgO	0.45	0.20	0.33	0.39	0.28	0.44	0.43	0.28	0.15	0.11
SrO	0.03	0.06	0.05	0.03	0.01	0.03	0.02	0.03	0.02	0.02
CaO	58.62	58.34	58.75	53.92	56.96	58.57	58.25	55.66	58.98	58.70
FeO	0.03	0.00	0.01	0.00	0.03	0.00	0.00	0.00	0.01	0.01
Na2O	0.02	0.00	0.03	0.01	0.06	0.04	0.03	0.06	0.00	0.00
SiO2	0.00	0.01	0.00	0.00	0.02	0.00	0.02	0.04	0.02	0.00
K2O	0.00	0.00	0.00	0.00	0.01	0.01	0.00	0.01	0.00	0.00
MnO	0.03	0.00	0.02	0.00	0.02	0.00	0.00	0.04	0.04	0.04
Al2O3	0.02	0.14	0.04	0.44	0.47	0.03	0.02	0.36	0.05	0.05
SO3	0.01	0.06	0.00	0.04	0.06	0.03	0.12	0.00	0.00	0.06
TiO2	0.03	0.00	0.00	0.00	0.00	0.00	0.03	0.00	0.00	0.00
total	59.25 ccll	58.81 ccll	59.23 ccll	54.82 ccl	57.92 ccl	59.15 ccl	58.92 mc	56.47 mc	59.26 mc	58.98 ccl

element	31	32	33	34	35	36	37	38	39	40
MgO	0.51	7.35	4.04	5.27	19.91	14.14	20.39	9.77	8.50	4.06
SrO	0.04	0.01	0.03	0.02	0.02	0.01	0.03	0.04	0.00	0.01
CaO	50.22	51.85	54.97	53.09	31.52	28.49	32.53	48.78	50.07	51.07
FeO	0.00	0.00	0.01	0.02	0.01	0.01	0.03	0.00	0.02	0.01
Na2O	0.00	0.02	0.01	0.04	0.04	0.03	0.00	0.02	0.00	0.19
SiO2	0.02	0.00	0.00	0.04	0.03	0.02	0.01	0.01	0.02	0.03
K2O	0.00	0.00	0.01	0.00	0.01	0.00	0.00	0.00	0.01	0.02
MnO	0.01	0.04	0.01	0.00	0.02	0.00	0.00	0.01	0.03	0.02
Al2O3	0.04	0.15	0.02	0.01	0.19	0.62	0.06	0.27	0.13	0.28
SO3	0.00	0.04	0.03	0.00	0.25	0.58	0.14	0.01	0.03	0.03
TiO2	0.00	0.01	0.00	0.00	0.00	0.00	0.00	0.07	0.07	0.00
total	50.83 ccl	59.48 mc	59.12 mc	58.50 mc	51.99 g	43.89 g	53.19 g	58.98 mc	58.87 mc	55.70 mc

lower foreslope facies: sample MT30

Appendix 3.2

element	41	42	43	44	45	46	47	48	49	50
MgO	0.10	14.54	3.12	0.12	0.19	0.20	18.36	0.14	0.25	10.75
SrO	0.06	0.02	0.03	0.02	0.02	0.02	0.01	0.00	0.03	0.03
CaO	58.58	38.59	56.36	59.63	59.23	50.24	28.58	59.18	58.80	44.16
FeO	0.04	0.06	0.01	0.04	0.00	0.02	0.02	0.00	0.01	0.01
Na2O	0.13	0.07	0.00	0.04	0.00	0.07	0.03	0.03	0.03	0.06
SiO2	0.03	0.01	0.01	0.00	0.01	0.00	0.02	0.03	0.02	0.45
K2O	0.01	0.00	0.00	0.01	0.01	0.01	0.02	0.01	0.01	0.01
MnO	0.01	0.00	0.02	0.05	0.03	0.00	0.02	0.04	0.00	0.02
Al2O3	0.14	0.02	0.01	0.00	0.04	0.07	0.32	0.03	0.04	0.51
SO3	0.00	0.03	0.03	0.03	0.00	0.00	0.67	0.00	0.00	0.59
TiO2	0.04	0.00	0.06	0.02	0.00	0.01	0.00	0.00	0.00	0.00
total	59.11	53.34	59.64	59.60	59.52	50.64	48.04	59.46	59.16	56.58
	mc	mc	mc	mc	mc	mc	g	mc	mc	mc

element	51	52	53	54	55	56	57	58	59	60
MgO	17.86	7.81	4.44	8.22	5.44	2.57	10.43	0.10	0.32	0.26
SrO	0.00	0.02	0.01	0.03	0.02	0.03	0.02	0.01	0.04	0.05
CaO	26.84	50.19	54.46	50.48	49.01	56.10	48.04	59.42	58.92	48.90
FeO	0.03	0.47	0.00	0.00	0.03	0.00	0.20	0.02	0.00	0.03
Na2O	0.30	0.01	0.04	0.00	0.06	0.01	0.00	0.00	0.04	0.02
SiO2	0.01	0.06	0.01	0.01	0.00	0.01	0.01	0.00	0.01	0.00
K2O	0.02	0.00	0.00	0.00	0.01	0.02	0.01	0.01	0.01	0.00
MnO	0.04	0.04	0.01	0.05	0.02	0.01	0.00	0.00	0.02	0.00
Al2O3	0.34	0.17	0.03	0.04	0.07	0.46	0.02	0.00	0.02	0.00
SO3	0.48	0.04	0.01	0.04	0.01	0.06	0.09	0.00	0.00	0.01
TiO2	0.00	0.06	0.00	0.01	0.00	0.00	0.07	0.03	0.00	0.06
total	45.65	58.86	59.04	58.88	54.66	59.28	58.89	59.59	59.38	49.32
	g	mc	mc	mc	mc	mc	mc	ccl	ccl	ccll

element	61	62	63	64	65	66	67	68	69	70
MgO	0.39	0.16	0.05	0.43	0.50	0.38	0.21	0.23	0.31	0.53
SrO	0.03	0.03	0.04	0.05	0.05	0.03	0.03	0.07	0.08	0.01
CaO	59.18	59.10	58.97	58.33	58.77	58.81	59.33	59.05	50.23	55.33
FeO	0.00	0.01	0.02	0.01	0.00	0.02	0.00	0.01	0.00	0.03
Na2O	0.02	0.04	0.00	0.03	0.05	0.01	0.00	0.00	0.00	0.00
SiO2	0.03	0.07	0.00	0.00	0.00	0.00	0.02	0.00	0.00	0.02
K2O	0.00	0.01	0.01	0.00	0.00	0.00	0.00	0.00	0.00	0.00
MnO	0.05	0.02	0.02	0.02	0.02	0.02	0.00	0.00	0.00	0.00
Al2O3	0.13	0.21	0.04	0.00	0.02	0.00	0.01	0.01	0.03	0.11
SO3	0.00	0.03	0.05	0.07	0.00	0.03	0.07	0.01	0.01	0.00
TiO2	0.00	0.03	0.00	0.00	0.00	0.00	0.00	0.03	0.54	0.00
total	59.82	59.72	59.54	58.95	59.40	59.30	59.67	59.40	51.19	56.03
	ccl	ccl	ccl	ccl	ccl	ccll	ccll	ccll	ccll	ccll

element	71	72	73	74	75	76	77	78	79	80
MgO	0.47	0.40	0.28	0.63	0.61	0.59	0.62	0.58	0.60	0.18
SrO	0.03	0.00	0.07	0.06	0.02	0.03	0.06	0.03	0.03	0.00
CaO	59.29	50.91	57.28	58.54	58.62	58.73	58.84	58.36	48.11	59.55
FeO	0.00	0.00	0.01	0.00	0.00	0.00	0.02	0.01	0.00	0.02
Na2O	0.00	0.02	0.00	0.01	0.03	0.00	0.00	0.03	0.04	0.03
SiO2	0.00	0.02	0.02	0.00	0.03	0.01	0.02	0.01	0.02	0.00
K2O	0.01	0.00	0.00	0.00	0.01	0.00	0.00	0.00	0.01	0.01
MnO	0.02	0.04	0.01	0.05	0.04	0.00	0.00	0.01	0.02	0.00
Al2O3	0.02	0.01	0.00	0.01	0.00	0.01	0.01	0.02	0.03	0.00
SO3	0.02	0.01	0.01	0.02	0.01	0.00	0.00	0.02	0.00	0.03
TiO2	0.04	0.06	0.00	0.09	0.03	0.04	0.04	0.00	0.00	0.14
total	59.90	51.47	57.69	59.40	59.39	59.42	59.61	59.05	48.84	59.96
	ccll	ccll	ccll	ccll	ccll	ccll	ccll	ccll	ccll	ccll

lower foreslope facies: sample MT30

Appendix 3.2

element	81	82	83	84	85	86	87	88	89	90
MgO	0.02	0.42	0.34	0.41	0.18	9.35	14.39	12.61	16.20	18.81
SrO	0.00	0.00	0.05	0.00	0.03	0.02	0.00	0.01	0.00	0.01
CaO	0.34	59.30	59.52	49.00	59.44	49.35	28.32	45.54	21.78	27.39
FeO	0.00	0.01	0.04	0.01	0.00	0.02	0.02	0.00	0.03	0.00
Na2O	0.15	0.04	0.00	0.02	0.03	0.03	0.06	0.01	0.07	0.06
SiO2	0.01	0.02	0.01	0.01	0.02	0.00	0.05	0.00	0.06	0.03
K2O	0.02	0.01	0.00	0.00	0.01	0.01	0.00	0.01	0.03	0.02
MnO	0.00	0.02	0.02	0.03	0.01	0.06	0.01	0.00	0.01	0.05
Al2O3	0.10	0.11	0.01	0.00	0.02	0.04	0.35	0.03	0.53	0.18
SO3	16.62	0.01	0.02	0.00	0.02	0.04	0.33	0.04	0.28	0.35
TiO2	0.00	0.00	0.00	0.05	0.10	0.05	0.07	0.00	0.00	0.00
total	17.27	59.94	60.01	49.53	59.84	58.97	43.60	58.25	38.98	46.89
	hole	ccll	ccll	ccl	mc	mc	g	g	g	g

element	91	92	93	94	95	96	97	98	99	100
MGO	8.13	10.44	20.32	14.64	21.00	0.79	0.14	0.98	0.23	20.22
SrO	0.02	0.04	0.02	0.02	0.00	0.01	0.02	0.03	0.00	0.03
CaO	50.42	46.08	30.60	30.35	31.83	58.67	47.96	58.27	48.34	34.24
FeO	0.00	0.05	0.00	0.00	0.24	0.05	0.00	0.01	0.00	0.02
Na2O	0.02	0.04	0.01	0.03	0.06	0.02	0.07	0.05	0.16	0.03
SiO2	0.02	0.00	0.01	0.03	0.03	0.00	0.01	0.03	0.01	0.02
K2O	0.00	0.00	0.02	0.01	0.00	0.00	0.00	0.01	0.00	0.01
MnO	0.02	0.01	0.02	0.00	0.03	0.01	0.01	0.01	0.02	0.00
Al2O3	0.01	0.07	0.19	0.26	0.07	0.04	0.01	0.44	0.01	0.15
SO3	0.00	0.01	0.42	0.19	0.12	0.07	0.00	0.05	0.00	0.22
TiO2	0.07	0.06	0.00	0.06	0.00	0.00	0.00	0.02	0.07	0.04
total	58.71	56.78	51.60	45.58	53.39	59.66	48.22	59.90	48.84	54.99
	g	g	g	g	g	mc	mc	mc	mc	g

element	101	102	103	104	105
MGO	16.19	9.18	4.14	10.36	0.08
SrO	0.02	0.02	0.01	0.01	0.03
CaO	40.23	49.53	53.03	48.66	49.62
FeO	0.02	0.00	0.02	0.04	0.05
Na2O	0.01	0.02	0.03	0.03	0.15
SiO2	0.02	0.02	0.03	0.03	0.00
K2O	0.00	0.00	0.01	0.02	0.02
MnO	0.01	0.03	0.00	0.00	0.02
Al2O3	0.10	0.07	0.04	0.17	0.03
SO3	0.08	0.01	0.01	0.03	0.00
TiO2	0.02	0.05	0.02	0.00	0.00
total	56.70	58.93	57.34	59.34	50.00
	g	g	g	g	ccll

lower foreslope facies: sample MT30

Appendix 3.2

element	1	2	3	4	5	6	7	8	9	10
MgO	0.08	21.43	21.4	0.5	21.29	0.53	0.64	21.45	0.61	0.58
SrO	0	0.04	0.03	0.01	0.04	0.03	0.02	0.02	0.02	0.02
CaO	57.89	32.51	33.06	56.2	33.3	57.48	57.47	33.14	56.67	56.69
FeO	0.02	0.00	0.03	0.01	0.01	0.03	0.00	0.01	0.01	0.01
Na2O	0.02	0.09	0.05	0.03	0.02	0.03	0.00	0.01	0.00	0.00
SiO2	0.01	0.03	0.01	0.00	0.02	0.01	0.01	0.02	0.00	0.00
K2O	0.02	0.02	0.00	0.01	0.01	0.01	0.01	0.01	0.00	0.00
MnO	0.01	0.00	0.01	0.02	0.01	0.03	0.04	0.01	0.02	0.07
Al2O3	0.00	0.11	0.12	0.04	0.20	0.01	0.00	0.18	0.00	0.01
SO3	0.00	0.31	0.06	0.00	0.02	0.05	0.00	0.06	0.00	0.04
TiO2	0.02	0.00	0.00	0.00	0.00	0.01	0.00	0.00	0.00	0.00
total	58.06	54.53	54.75	56.81	54.93	58.20	58.20	54.90	57.34	57.43
	ccll	dmc	dmc	ccll	dmc	ccll	ccll	dmc	ccll	ccll

element	11	12	13	14
MgO	16.94	28.08	16.24	21.77
SrO	0.00	0.01	0.01	0.03
CaO	29.77	28.01	30.62	32.72
FeO	0.03	0.00	0.09	0.05
Na2O	0.07	0.13	0.07	0.12
SiO2	0.60	0.81	0.37	0.03
K2O	0.01	0.03	0.02	0.00
MnO	0.00	0.02	0.02	0.03
Al2O3	1.19	3.33	9.83	0.09
SO3	0.06	0.10	0.09	0.55
TiO2	0.00	0.00	0.01	0.00
total	48.67	60.53	57.37	55.39
	dmc	dmc (sm)	m (sm)	dmc (sm)

element	1	2	3	4	5	6	7	8	9	10
MgO	21.98	21.66	0.10	21.93	0.29	21.13	0.53	0.21	0.14	0.18
SrO	0.02	0.00	0.02	0.03	0.03	0.03	0.02	0.07	0.04	0.11
CaO	32.61	32.56	57.24	32.14	58.06	33.15	57.53	58.45	47.94	57.04
FeO	0.12	0.07	0.00	0.01	0.02	0.01	0.01	0.00	0.02	0.02
Na2O	0.05	0.04	0.02	0.06	0.00	0.00	0.00	0.03	0.05	0.05
SiO2	0.02	0.02	0.00	0.00	0.01	0.01	0.01	0.02	0.01	0.00
K2O	0.00	0.01	0.00	0.01	0.00	0.01	0.00	0.01	0.00	0.01
MnO	0.03	0.03	0.05	0.06	0.00	0.01	0.03	0.02	0.04	0.01
Al2O3	0.06	0.18	0.01	0.09	0.03	0.09	0.00	0.02	0.00	0.02
SO3	0.07	0.08	0.01	0.00	0.02	0.05	0.00	0.07	0.06	0.03
TiO2	0.08	0.01	0.05	0.05	0.00	0.01	0.04	0.01	0.00	0.07
total	55.04	54.63	57.49	54.37	58.44	54.50	58.17	58.89	48.30	57.53
	db	db	cc	c	cc	db	cc	cc	cc	cc

element	11	12	13	14	15
MgO	0.15	20.94	0.55	18.08	14.88
SrO	0.05	0.03	0.03	0.03	0.01
CaO	57.38	30.72	56.73	28.94	34.48
FeO	0.00	0.00	0.00	0.04	0.01
Na2O	0.04	0.04	0.03	0.02	0.03
SiO2	0.01	0.05	0.00	0.05	0.00
K2O	0.00	0.01	0.00	0.02	0.00
MnO	0.05	0.01	0.02	0.05	0.01
Al2O3	0.02	0.35	0.00	0.30	0.16
SO3	0.12	0.09	0.00	0.26	0.13
TiO2	0.04	0.08	0.06	0.01	0.02
total	57.87	52.29	57.42	47.78	49.75
	cc	d	cc	cc	cc

Upper foreslope facies: site MT102b and site MT117

Appendix 3.2

element	1	2	3	4	5	6	7	8	9	10
MgO	0.22	0.27	0.21	1.74	0.24	0.38	0.47	0.50	0.52	0.27
SrO	0.02	0.04	0.02	0.00	0.03	0.01	0.01	0.05	0.04	0.04
CaO	56.19	56.29	56.77	6.13	56.69	56.75	56.49	56.52	56.13	56.38
FeO	0.01	0.04	0.05	0.00	0.00	0.02	0.02	0.04	0.01	0.02
Na2O	0.01	0.01	0.03	0.14	0.02	0.04	0.00	0.05	0.00	0.02
SiO2	0.02	0.00	0.02	2.38	0.01	0.02	0.00	0.01	0.02	0.00
K2O	0.01	0.00	0.00	0.03	0.01	0.00	0.01	0.00	0.01	0.00
MnO	0.00	0.00	0.02	0.05	0.01	0.01	0.05	0.05	0.01	0.02
Al2O3	0.02	0.00	0.02	0.46	0.00	0.00	0.00	0.00	0.01	0.00
SO3	0.02	0.05	0.01	12.35	0.03	0.00	0.04	0.00	0.01	0.03
TiO2	0.01	0.00	0.01	0.00	0.00	0.00	0.03	0.14	0.05	0.05
total	56.53	56.69	57.16	23.28	57.03	57.22	57.12	57.24	56.80	56.82
	cc	cc	cc	cc(l)	cc	cc	cc	cc	cc	cc

element	11	12	13	14	15	16	17	18	19	20
MgO	0.18	0.21	0.14	0.36	18.00	18.09	16.41	21.69	21.57	0.07
SrO	0.05	0.10	0.03	0.04	0.01	0.01	0.02	0.00	0.01	0.02
CaO	56.41	56.66	56.91	56.39	26.87	26.75	23.60	31.35	31.58	57.11
FeO	0.00	0.00	0.02	0.02	0.01	0.43	0.27	0.03	0.04	0.00
Na2O	0.00	0.04	0.00	0.00	0.17	0.11	0.11	0.06	0.03	0.01
SiO2	0.04	0.02	0.01	0.00	0.08	0.02	0.05	0.02	0.02	0.01
K2O	0.01	0.01	0.01	0.01	0.05	0.04	0.04	0.00	0.01	0.00
MnO	0.02	0.03	0.02	0.05	0.02	0.00	0.03	0.00	0.01	0.01
Al2O3	0.01	0.05	0.05	0.02	0.89	0.50	0.54	0.06	0.02	0.00
SO3	0.06	0.03	0.00	0.00	0.05	0.17	0.23	0.04	0.03	0.00
TiO2	0.00	0.00	0.02	0.05	0.01	0.01	0.03	0.04	0.03	0.00
total	56.77	57.15	57.20	56.94	46.24	46.12	41.33	53.30	53.34	57.22
	cc	cc	cc	cc	cc	m	m	m	cc(l)	cc(l)

element	21	22	23	24	25	26	27	28	29
MgO	0.38	0.38	0.22	0.33	0.61	0.32	0.43	0.25	21.83
SrO	0.03	0.02	0.02	0.02	0.03	0.00	0.00	0.04	0.01
CaO	56.46	48.94	56.52	56.90	56.18	55.77	17.03	1.85	31.52
FeO	0.01	0.01	0.00	0.02	0.00	0.01	50.71	71.19	0.01
Na2O	0.01	0.04	0.02	0.03	0.03	0.02	0.08	0.08	0.04
SiO2	0.00	0.00	0.01	0.01	0.00	0.01	1.81	2.32	0.02
K2O	0.01	0.00	0.00	0.00	0.00	0.01	0.02	0.03	0.01
MnO	0.00	0.01	0.00	0.02	0.01	0.00	0.00	0.00	0.00
Al2O3	0.02	0.00	0.03	0.02	0.11	0.04	0.90	1.25	0.05
SO3	0.02	0.01	0.04	0.05	0.05	0.06	0.07	0.09	0.07
TiO2	0.04	0.00	0.00	0.00	0.00	0.00	0.08	0.15	0.01
total	56.97	49.41	56.87	57.39	57.01	56.22	71.12	77.24	53.57
	cc	cc	cc	cc	cc	cc	h	h	cc

element	1	2	3	4	5	6	7	8	9
MgO	0.03	0.02	0.02	0.02	0.53	0.50	0.01	0.37	0.47
SrO	0.00	0.00	0.00	0.00	0.04	0.03	0.00	0.08	0.01
CaO	0.06	0.12	0.11	0.11	55.65	54.49	0.17	55.99	56.28
FeO	0.03	0.03	0.00	0.02	0.28	0.32	0.03	0.02	0.09
Na2O	0.02	0.01	0.02	0.00	0.02	0.00	0.02	0.01	0.02
SiO2	50.70	50.09	50.74	50.08	0.02	0.02	50.15	0.06	0.01
K2O	0.00	0.03	0.01	0.01	0.01	0.00	0.03	0.01	0.00
MnO	0.02	0.00	0.00	0.00	0.04	0.08	0.01	0.00	0.03
Al2O3	40.62	40.13	40.86	40.07	0.02	0.01	40.47	0.06	0.08
SO3	0.02	0.00	0.00	0.05	0.03	0.02	0.00	0.11	0.03
TiO2	0.05	0.00	0.05	0.02	0.09	0.02	0.00	0.06	0.00
total	91.55	90.43	91.81	90.37	56.71	55.49	90.90	56.75	57.03
	k	k	k	k	cc	cc	k	m	cc

Upper foreslope facies: site M22; Basin margin facies: site MC34

Appendix 3.2

element	1	2	3	4	5	6	7	8	9	10
MgO	0.22	0.20	2.54	20.75	21.15	21.98	21.47	22.67	0.55	0.58
SrO	0.05	0.05	0.02	0.00	0.05	0.01	0.02	0.00	0.00	0.00
CaO	54.61	54.61	7.92	31.27	31.42	30.91	30.69	29.20	12.58	1.45
FeO	0.02	0.01	60.54	0.09	0.03	0.00	0.03	0.01	56.02	70.61
Na2O	0.00	0.01	0.09	0.04	0.02	0.00	0.06	0.01	0.02	0.00
SiO2	0.00	0.02	2.63	0.00	0.01	0.00	0.00	0.00	3.04	2.99
K2O	0.00	0.01	0.03	0.01	0.01	0.00	0.00	0.01	0.02	0.01
MnO	0.00	0.00	0.03	0.00	0.03	0.02	0.00	0.04	0.05	0.03
Al2O3	0.01	0.02	0.51	0.05	0.17	0.09	0.11	0.05	0.47	0.37
SO3	0.06	0.06	0.05	0.03	0.03	0.04	0.03	0.06	0.07	0.03
TiO2	0.00	0.00	0.05	0.00	0.04	0.02	0.06	0.04	0.00	0.02
total	54.97	54.99	74.39	52.23	52.94	53.08	52.47	52.08	72.83	76.07
	cc	cc	h	d	d	d o'g	d o'g	d o'g	h	h

element	11	12	13	14	15	16	17	18	19	20
MgO	20.68	21.04	20.68	21.92	0.59	0.63	20.66	0.09	0.56	0.67
SrO	0.01	0.01	0.01	0.00	0.01	0.00	0.02	0.03	0.05	0.04
CaO	31.78	31.01	32.48	30.88	54.68	54.95	31.48	54.93	54.79	54.31
FeO	0.01	0.00	0.02	0.06	0.01	0.02	0.00	0.00	0.00	0.01
Na2O	0.03	0.02	0.05	0.02	0.00	0.01	0.02	0.02	0.04	0.02
SiO2	0.01	0.00	0.00	0.00	0.02	0.00	0.02	0.00	0.01	0.01
K2O	0.00	0.00	0.00	0.00	0.01	0.01	0.00	0.01	0.01	0.02
MnO	0.02	0.02	0.05	0.03	0.04	0.00	0.01	0.00	0.03	0.03
Al2O3	0.09	0.13	0.01	0.04	0.01	0.03	0.05	0.01	0.00	0.02
SO3	0.03	0.01	0.02	0.03	0.01	0.04	0.06	0.00	0.00	0.07
TiO2	0.00	0.00	0.00	0.00	0.00	0.05	0.00	0.03	0.02	0.03
total	52.66	52.24	53.33	52.98	55.38	55.75	52.32	55.15	55.50	55.21
	d o'g	d	d	d	cc	cc	d	cc	cc	cc

element	21	22	23	24
MgO	0.10	21.09	1.26	0.96
SrO	0.04	0.03	0.00	0.00
CaO	48.55	28.53	0.46	0.44
FeO	0.03	0.05	70.39	69.82
Na2O	0.02	0.01	0.06	0.04
SiO2	0.00	0.00	3.19	3.05
K2O	0.00	0.00	0.03	0.01
MnO	0.04	0.00	0.01	0.05
Al2O3	0.00	0.01	0.47	0.47
SO3	0.00	0.02	0.07	0.08
TiO2	0.06	0.00	0.00	0.00
total	48.84	49.76	75.95	74.91
	cc	d	h	h

element	1	2	3	4	5	6	7	8
MgO	0.38	1.02	0.36	0.31	0.29	0.27	0.19	0.28
SrO	0.03	0.04	0.00	0.02	0.04	0.03	0.01	0.02
CaO	57.79	57.52	56.65	56.98	56.55	56.13	50.17	56.89
FeO	0.01	0.00	0.01	0.02	0.07	0.00	0.05	0.00
Na2O	0.06	0.05	0.03	0.02	0.06	0.00	0.15	0.05
SiO2	0.01	0.14	0.01	0.01	0.00	0.00	0.12	0.01
K2O	0.02	0.03	0.01	0.00	0.00	0.00	0.05	0.03
MnO	0.02	0.00	0.07	0.02	0.02	0.05	0.00	0.04
Al2O3	0.06	0.14	0.24	0.02	0.01	0.00	5.14	0.00
SO3	0.01	0.07	0.02	0.00	0.01	0.01	0.09	0.03
TiO2	0.06	0.02	0.03	0.02	0.01	0.00	0.03	0.00
total	58.44	59.04	57.42	57.42	57.04	56.50	55.98	57.34
	m	m	emc	cc sp lc	cc sp lc	cc sp lc	emc	emc

Lower foreslope facies: site M6i; Back reef facies: site MT74ii

Appendix 3.2

element	1	2	3	4	5	6	7	8	9	10
MgO	0.79	0.77	0.82	1.01	0.64	0.49	0.55	0.52	0.55	0.48
SrO	0.00	0.00	0.00	0.00	0.00	0.05	0.03	0.02	0.05	0.03
CaO	0.60	0.52	0.75	0.54	0.72	57.70	56.97	56.77	56.88	56.97
FeO	73.00	73.76	72.33	72.46	72.75	0.07	0.81	0.37	0.01	0.02
Na2O	0.17	0.12	0.11	0.12	0.12	0.03	0.08	0.05	0.04	0.08
SiO2	3.56	3.00	3.19	3.61	2.84	0.02	0.05	0.01	0.03	0.02
K2O	0.03	0.02	0.04	0.05	0.00	0.02	0.02	0.01	0.02	0.00
MnO	0.04	0.02	0.04	0.04	0.01	0.00	0.01	0.05	0.00	0.02
Al2O3	0.68	0.46	0.53	0.65	0.33	0.00	0.00	0.02	0.00	0.01
SO3	0.08	0.19	0.17	0.15	0.11	0.03	0.00	0.06	0.00	0.02
TiO2	0.02	0.06	0.05	0.06	0.05	0.01	0.00	0.02	0.08	0.01
total	78.96	78.91	78.02	78.67	77.56	58.41	58.51	57.92	57.66	57.66
	h	h	h	h	h	∝	∝	∝	∝	∝

element	11	12	13	14	15	16	17	18	19	20
MgO	0.47	21.85	0.11	0.09	0.55	0.49	0.38	0.14	21.60	21.36
SrO	0.04	0.03	0.02	0.04	0.03	0.04	0.04	0.03	0.04	0.01
CaO	57.43	32.21	57.36	57.99	57.08	55.01	57.45	57.48	31.67	31.98
FeO	0.00	0.12	0.00	0.02	0.01	0.03	0.05	0.04	0.01	0.05
Na2O	0.03	0.06	0.05	0.04	0.08	0.05	0.09	0.08	0.06	0.14
SiO2	0.03	0.01	0.06	0.03	0.00	0.02	0.01	0.00	0.17	0.04
K2O	0.00	0.01	0.01	0.01	0.01	0.00	0.00	0.02	0.01	0.03
MnO	0.03	0.00	0.00	0.01	0.02	0.00	0.02	0.10	0.01	0.02
Al2O3	0.01	0.04	0.23	0.02	0.01	0.02	0.01	0.03	0.26	1.04
SO3	0.06	0.04	0.05	0.05	0.03	0.01	0.03	0.00	0.00	0.07
TiO2	0.00	0.00	0.01	0.00	0.02	0.00	0.00	0.01	0.00	0.03
total	58.08	54.35	57.89	58.28	57.83	55.67	58.06	57.93	53.83	54.76
	∝	d	∝	∝	∝	∝	∝	∝	d o'g	d

element	21	22	23	24	25	26	27	28	29	30
MgO	0.20	0.43	0.22	0.12	0.54	21.96	22.19	2.53	18.85	0.02
SrO	0.02	0.02	0.01	0.04	0.02	0.01	0.01	0.04	0.01	0.00
CaO	57.31	57.52	57.63	57.54	57.61	32.82	31.77	55.14	36.65	0.11
FeO	0.03	0.01	0.01	0.00	0.00	0.05	0.00	0.01	0.00	0.00
Na2O	0.03	0.04	0.07	0.06	0.06	0.05	0.06	0.07	0.08	0.04
SiO2	0.01	0.00	0.01	0.02	0.00	0.08	0.04	0.04	0.03	102.12
K2O	0.02	0.03	0.01	0.00	0.02	0.01	0.01	0.01	0.01	0.01
MnO	0.04	0.02	0.03	0.04	0.03	0.02	0.02	0.06	0.00	0.00
Al2O3	0.00	0.00	0.00	0.01	0.03	0.12	0.08	0.02	0.02	0.03
SO3	0.02	0.03	0.00	0.01	0.03	0.01	0.03	0.06	0.05	0.02
TiO2	0.00	0.02	0.02	0.02	0.04	0.05	0.01	0.01	0.01	0.02
total	57.67	58.12	58.01	57.87	58.37	55.17	54.22	57.99	55.70	102.37
	∝	∝	∝	∝	∝	d	d	∝III	d	s

element	31	32	33	34
MgO	21.83	0.51	0.44	21.97
SrO	0.05	0.03	0.02	0.02
CaO	31.52	56.83	57.39	32.92
FeO	0.18	0.02	0.04	0.02
Na2O	0.10	0.06	0.09	0.04
SiO2	0.55	0.01	0.00	0.04
K2O	0.07	0.01	0.00	0.00
MnO	0.22	0.01	0.00	0.05
Al2O3	0.32	0.01	0.03	0.07
SO3	0.17	0.01	0.04	0.03
TiO2	0.00	0.04	0.01	0.01
total	55.00	57.53	58.06	55.19
	∝III	∝III	∝III	d

Lower foreslope facies: site MT19

Appendix 4.1

20 repeat measurements of bulk (axial) susceptibility of a sample with negative susceptibility and a sample with positive susceptibility.

sample M25.1.1	sample CC1.2.2
-0.65	6.18
-0.71	6.16
-0.68	6.19
-0.71	6.16
-0.64	6.18
-0.66	6.18
-0.68	6.20
-0.68	6.20
-0.72	6.20
-0.73	6.23
-0.70	6.25
-0.68	6.21
-0.68	6.24
-0.67	6.21
-0.70	6.27
-0.69	6.23
-0.68	6.26
-0.66	6.24
-0.67	6.26
-0.65	6.25
mean = -0.68	mean = 6.22
standard deviation = 0.024	standard deviation = 0.03

Appendix 4.2 Summary table of repeat measurements of anisotropy of susceptibility using a Minisup. Samples are from back reef and reef facies in the 'scenic loop' (SL; Carlsbad Caverns National Park); shelf facies from Rocky Arroyo (RA); basinal facies sandstones and limestones from sites on the highway US62/180 (RL); back reef, reef and foreslope and basin margin facies from the 'reef trail' in McKittrick Canyon (MC). D=declination; I=inclination; K=principal susceptibilities (volume units x 10^{-6}GOe^{-1}). L=linearity ($L=K_{max}/K_{int}$); F=foliation ($F=K_{int}/K_{min}$); P=planarity ($P=K_{max}/K_{min}$).

N.B., to convert volume units x 10^{-6}GOe^{-1} to volume SI units, multiply values by 4Π.

sample	measurement		Kmax	Kint	Kmin	Kmean
RL1.4.1	1	D	92.7	184.4	336.4	0.73
Bone Spring		I	6.7	13.1	75.4	
limestone	2	D	117.2	230.7	345.3	
basin facies		I	38.6	26.4	40	
	summary	D	103.5	206.5	343.1	
		I	23.1	21.3	57.7	
		N	2	2	2	
				st. dev		
		L	1.2032	0.0341		
		P	1.2904	0.0068		
		F	1.073	0.0359		
		q	1.2143	0.3031		

sample	measurement		Kmax	Kint	Kmin	Kmean
RL2.1.4	1	D	259	357.4	114.6	2.38
Brushy Canyon		I	27	15.9	57.9	
sandstone	2	D	265.2	173.7	72.3	
basin facies		I	20	4.1	69.4	
	summary	D	262.2	115.4	98	
		I	23.5	78.3	65.1	
		N	2	2	2	
				st. dev		
		L	1.0428	0.0264		
		P	1.1032	0.0054		
		F	1.0582	0.0219		
		q	5786	0.394		

sample	measurement		Kmax	Kint	Kmin	Kmean
RL3.2.1	1	D	104.1	358	232.9	2.47
Cherry Canyon		I	28.8	27	48.6	
sandstone	2	D	113.9	199.3	25.6	
basin facies		I	-2.3	64.8	25.1	
	summary	D	109.3	340.7	341.1	
		I	13.3	69.2	69.2	
		N	2	2	2	
				st. dev		
		L	1.0331	0.006		
		P	1.0895	0.01		
		F	1.0546	0.0039		
		q	0.4829	0.0443		

sample	measurement		Kmax	Kint	Kmin	Kmean
RL3.6.1	1	D	108.4	265.2	1.2	2.34
Cherry Canyon		I	44.7	40.6	16.7	
sandstone	2	D	102.3	210	10.2	
basin facies		I	6.4	69.5	19.4	
	summary	D	104.9	242	5.7	
		I	25.6	56.9	18.1	
		N	2	2	2	
				st. dev		
		L	1.0592	0.0218		
		P	1.0952	0.012		
		F	1.0341	0.01		
		q	0.9433	0.3239		

Appendix 4.2; repeat (Minisup) measurements

sample	measurement		Kmax	Kint	Kmin	Kmean
RL6.13.1.3	1	D	223.1	185.2	104.1	1.69
turbidite		I	57.4	-26.7	17.1	
Rader Slide	2	D	51.6	182.7	113.5	
basin facies		I	-43	-35	26.8	
	summary	D	73.5	184	108.6	
		I	36.9	-30.8	22	
		N	2	2	2	
				st. dev.		
		L	1.0712	0.0037		
		P	1.142	0.024		
		F	1.0661	0.019		
		q	0.7407	0.1048		

sample	measurement		Kmax	Kint	Kmin	Kmean
RL7.2.1	1	D	69.3	322.8	216	1.2
Lamar lst.		I	42.2	17.5	42.5	
basin facies	2	D	96	324.5	210	
		I	38.9	39.4	26.7	
	summary	D	83	323.5	212.7	
		I	41.3	28.5	34.6	
		N	2	2	2	
				st. dev.		
		L	1.1256	0.0301		
		P	1.2241	0.0367		
		F	1.0875	0.0042		
		q	0.8706	0.0998		

sample	measurement		Kmax	Kint	Kmin	Kmean
RL8.1.1	1	D	152.1	324.3	59.2	-1.08
gypsum		I	38.3	51.4	3.9	
Castile Fmn.	2	D	154.3	305	59.6	
basin facies		I	22.5	64.4	11.3	
	summary	D	153.3	316.4	59.4	
		I	30.4	58.3	7.6	
		N	2	2	2	
				st. dev.		
		L	0.9143	0.0304		
		P	0.8145	0.0026		
		F	0.8913	0.0273		
		q	0.5224	0.2453		

sample	measurement		Kmax	Kint	Kmin	Kmean
RL8.2.2	1	D	159	309.5	54.9	-1.1
gypsum		I	41.9	44.1	15.3	
Castile Fmn.	2	D	171.5	317.3	50	
basin facies		I	71.9	15.1	9.8	
	summary	D	162.7	314	52.4	
		I	57.1	29.6	12.5	
		N	2	2	2	
				st. dev.		
		L	0.945	0.0131		
		P	0.8052	0.0246		
		F	0.8524	0.0377		
		q	0.2872	0.1289		

Appendix 4.2; repeat (Minisup) measurements

sample	measurement		Kmax	Kint	Kmin	Kmean
MC3.1.1	1	D	263.6	169.5	35.1	-1
grainstone		I	14.7	15.8	68.1	
back reef	2	D	278.3	185.4	54.2	
facies		I	13.2	12.2	71.9	
	summary	D	271	177.5	43.8	
		I	14.1	14.1	70.2	
		N	2	2	2	
				st. dev.		
		L	0.8571	0.0205		
		P	0.775	0.0236		
		F	0.9042	0.0061		
		q	0.8035	0.0364		

sample	measurement		Kmax	Kint	Kmin	Kmean
MC3.2.1	1	D	259.3	160.3	46.1	-1
grainstone		I	29.6	15.7	55.7	
back reef	2	D	265.6	168.5	22.9	
facies		I	14.6	25.3	60.3	
	summary	D	262.6	164.3	35.3	
		I	22.1	20.5	58.5	
		N	2	2	2	
				st. dev.		
		L	0.8488	0.0537		
		P	0.7451	0.0072		
		F	0.8798	0.0639		
		q	0.7607	0.4472		

sample	measurement		Kmax	Kint	Kmin	Kmean
MC12.1.1	1	D	23.2	117.7	274.7	-1.05
boundstone		I	9.3	25.2	62.9	
reef facies	2	D	15.9	116	262.9	
		I	16	31.4	53.9	
	summary	D	19.6	116.9	268.1	
		I	12.7	28.3	58.6	
		N	2	2	2	
				st. dev.		
		L	0.9035	0.0222		
		P	0.744	0.003		
		F	0.8237	0.0173		
		q	0.3704	0.1048		

sample	measurement		Kmax	Kint	Kmin	Kmean
MC12.2.2	1	D	23	288.3	134.7	-1.05
boundstone		I	10.7	24.4	63.2	
reef facies	2	D	40.1	137.4	276.1	
		I	17.2	22.4	61.2	
	summary	D	19.6	116.9	268.1	
		I	12.7	28.3	58.6	
		N	2	2	2	
				st. dev.		
		L	0.9035	0.0222		
		P	0.744	0.003		
		F	0.8237	0.0173		
		q	0.3704	0.1048		

Appendix 4.2; repeat (Minisup) measurements

sample	measurement		Kmax	Kint	Kmin	Kmean
MC18.1.3	1	D	167.6	81.1	196.8	-0.96
grainstone		I	-18.8	9.6	68.7	
upper foreslope	2	D	173.7	90.2	233.8	
facies		I	-14.8	23.1	62.1	
	summary	D	170.7	85.16.4	66.5	
		I	-16.8	2	2	
		N	2	217.7		
				st. dev.		
		L	0.9541	0.0268		
		P	0.8457	0.0218		
		F	0.8869	0.0421		
		q	0.3357	0.2323		

sample	measurement		Kmax	Kint	Kmin	Kmean
MC18.4.1	1	D	26.6	260.9	138.3	-0.96
grainstone		I	32.5	42.6	30.2	
upper foreslope	2	D	172.4	97.4	247	
facies		I	-15.7	42.4	43.4	
	summary	D	111.6	178.4	185.8	
		I	26.2	81.1	51.9	
		N	2	2	2	
				st. dev.		
		L	0.8329	0.0629		
		P	0.7363	0.0829		
		F	0.8827	0.0329		
		q	0.7643	0.0304		

sample	measurement		Kmax	Kint	Kmin	Kmean
MC21.1.1	1	D	239.5	36.9	128.8	-0.91
grainstone		I	72.3	16.2	6.3	
upper foreslope	2	D	295.1	70.5	166.7	
facies		I	63.7	19.3	17	
	summary	D	272.9	53.6	147.4	
		I	70.3	18.5	12.3	
		N	2	2	2	
				st. dev.		
		L	0.8165	0.0595		
		P	0.7555	0.0244		
		F	0.9266	0.0377		
		q	1	0		

sample	measurement		Kmax	Kint	Kmin	Kmean
MC21.2.1	1	D	247.3	35.1	128.2	-1.03
grainstone		I	70	17	9.9	
upper foreslope	2	D	305	41.3	131.7	
facies		I	74.6	1.6	15.2	
	summary	D	272.2	38.3	129.9	
		I	74.3	9.3	12.6	
		N	2	2	2	
				st. dev.		
		L	0.85	0.0047		
		P	0.7393	0.0181		
		F	0.8698	0.0258		
		q	0.6741	0.1152		

Appendix 4.2; repeat (Minisup) measurements

sample	measurement		Kmax	Kint	Kmin	Kmean
MC27.1.1	1	D	178.9	252.9	151.8	-0.9
wackestone		I	27	9.5	49.5	
lower	2	D	357.7	267.3	175	
foreslope		I	24.4	1.1	65.6	
facies						
	summary	D	314.6	260.1	160.8	
		I	88.2	5.3	58.2	
		N	2	2	2	
				st. dev.		
		L	0.8375	0.0421		
		P	0.7569	0.0011		
		F	0.8675	0.042		
		q	0.6054	0.2905		

sample	measurement		Kmax	Kint	Kmin	Kmean
MC27.2.1	1	D	14	105.1	207	-0.84
wackestone		I	16.1	3.5	73.4	
lower	2	D	7.4	268	153.8	
foreslope		I	29.9	16	55.3	
facies						
	summary	D	10.9	179.5	171	
		I	23	48.9	66.5	
		N	2	2	2	
				st. dev.		
		L	0.9375	0.0884		
		P	0.8022	0.0345		
		F	0.8577	0.0441		
		q	0.3333	0.4714		

sample	measurement		Kmax	Kint	Kmin	Kmean
MC34.1.1	1	D	180.2	24	113.2	-0.42
Lamar lst.		I	78.8	10.2	-4.3	
basin margin	2	D	207.3	125.6	36.5	
facies		I	71.4	-2.7	18.3	
	summary	D	197.1	75.3	76	
		I	75.5	59	8.9	
		N	2	2	2	
				st. dev.		
		L	0.6118	0.0347		
		P	0.4921	0.0655		
		F	0.8026	0.0616		
		q	0.8939	0.15		

sample	measurement		Kmax	Kint	Kmin	Kmean
MC34.4.1	1	D	226.7	144.5	55.2	-0.4
Lamar lst.		I	74.1	-2.1	15.7	
basin margin	2	D	112	271.2	5.3	
facies		I	62.7	25.7	8.4	
	summary	D	147.9	202	29.9	
		I	77.1	24.8	13.3	
		N	2	2	2	
				st. dev.		
		L	0.7348	0.0133		
		P	0.5664	0.0711		
		F	0.7718	0.1106		
		q	0.662	0.3012		

Appendix 4.2; repeat (Minisup) measurements

sample	measurement		Kmax	Kint	Kmin	Kmean
MC35.1.1	1	D	299.2	129.1	33.7	-0.43
Lamar lst.		I	42.2	47.3	4.7	
basin margin	2	D	139.2	320.4	50.3	
facies		I	74.6	15.3	-0.5	
	3	D	311.4	138.5	48.3	
		I	80	10.1	1.2	
	summary	D	294.5	126.9	44.1	
		I	75.8	59	1.9	
		N	3	3	3	
				st. dev.		
		L	0.7997	0.1144		
		P	0.6277	0.0348		
		F	0.7925	0.0869		
		q	0.6038	0.4675		

sample	measurement		Kmax	Kint	Kmin	Kmean
MC35.3.1	1	D	189	321.6	53.5	-0.35
Lamar lst.		I	75.3	9.9	10.5	
basin margin	2	D	177.9	119.7	30.7	
facies		I	78.9	-5.8	9.3	
	3	D	296.3	117.6	27.3	
		I	61.6	28.3	0.4	
	summary	D	243.1	97.12	37	
		I	79.7	27.6	6.9	
		N	3	3	3	
				st. dev.		
		L	0.7668	0.0355		
		P	0.5385	0.0502		
		F	0.7003	0.0792		
		q	0.4477	0.1608		

sample	measurement		Kmax	Kint	Kmin	Kmean
MC35.4.1	1	D	155.6	307.2	38.5	-0.29
Lamar lst.		I	76.5	11.8	6.2	
basin margin	2	D	149.2	323.9	55	
facies		I	63.7	26.1	2.1	
	summary	D	151.4	315.2	46.7	
		I	70.1	19.2	4.2	
		N	2	2	2	
				st. dev.		
		L	0.5174	0.0247		
		P	0.3836	0.0089		
		F	0.7418	0.0184		
		q	0.8194	0.071		

sample	measurement		Kmax	Kint	Kmin	Kmean
MC36.1.1	1	D	320	184.5	94.3	0.19
Lamar lst.		I	86	3	2.7	
basin margin	2	D	13.2	198	107.8	
facies		I	76.5	13.5	1	
	summary	D	1.6	191.1	101.1	
		I	81.9	8.3	1.9	
		N	2	2	2	
				st. dev.		
		L	2.0833	0.1179		
		P	-4.643	11.819		
		F	-2.071	5.558		
		q	0.8533	0.264		

Appendix 4.2; repeat (Minisup) measurements

sample	measurement		Kmax	Kint	Kmin	Kmean
MC36.2.1	1	D	356.6	167.5	84.4	0.19
Lamar lst.		I	29.1	60.5	-3.9	
basin margin	2	D	230.8	13.1	108.9	
facies		I	64.1	20.9	14.4	
	summary	D	326.7	36.6	96.5	
		I	62.8	66.5	5.3	
		N	2	2	2	
				st. dev.		
		L	1.3709	0.0255		
		P	5.9617	2.4749		
		F	4.3333	1.8856		
		q	0.4023	0.0698		

sample	measurement		Kmax	Kint	Kmin	Kmean
SL1.6.1	1	D	10.9	251.4	280.8	0.1
grainstone		I	1.4	87	-2.6	
teepee	2	D	356.6	229.9	279.3	
back reef		I	24.4	52.7	-26.4	
facies						
	summary	D	3.9	231.6	280.1	
		I	13	70	-14.1	
		N	2	2	2	
				st. dev.		
		L	0.9167	3.8891		
		P	0.2888	0.6386		
		F	-0.563	1.3258		
		q	0.9039	0.0213		

sample	measurement		Kmax	Kint	Kmin	Kmean
SL1.8.1	1	D	294.8	355	210.6	-0.65
grainstone		I	-14	63.2	22.4	
teepee	2	D	5.7	221.9	116.4	
back reef		I	46	38	18.9	
facies						
	summary	D	323.5	256.3	162.8	
		I	19.3	68.3	28.9	
		N	2	2	2	
				st. dev.		
		L	0.8082	0.0458		
		P	0.6654	0.009		
		F	0.8249	0.0577		
		q	0.6438	0.2756		

sample	measurement		Kmax	Kint	Kmin	Kmean
SL2.2.1	1	D	15.6	112.8	203	-0.5
pisolite		I	80.3	1.1	9.6	
back reef	2	D	50.5	173.3	135.1	
facies		I	14.2	64.8	-20.5	
	summary	D	45.5	129.8	-6.5	
		I	47.9	2	2	
		N	2	170		
				st. dev.		
		L	0.851	0.0721		
		P	0.744	0.0321		
		F	0.8758	0.0366		
		q	0.6957	0.3689		

Appendix 4.2; repeat (Minisup) measurements

sample	measurement		Kmax	Kint	Kmin	Kmean
SL2.4.1	1	D	62.2	207.1	131.6	-0.29
pisolite		I	47	37.2	-18.4	
back reef	2	D	40	213.5	124.7	
facies		I	64.7	25	-2.6	
	summary	D	53.7	210.5	128	
		I	56.3	31.5	-10.5	
		N	2	2	2	
				st. dev.		
		L	0.7185	0.0567		
		P	0.5533	0.0211		
		F	0.7724	0.0318		
		q	0.6513	0.1668		

sample	measurement		Kmax	Kint	Kmin	Kmean
SL2.5.1	1	D	83.6	228.8	163.5	-0.29
pisolite		I	30.5	54.3	-16.7	
back reef	2	D	91.8	348	213.3	
facies		I	22.6	29.6	51.1	
	summary	D	87.8	307	182.9	
		I	26.6	59.3	18.8	
		N	2	2	2	
				st. dev.		
		L	0.369	0.0206		
		P	0.3436	0.0033		
		F	0.9323	0.044		
		q	1.6324	0.2221		

sample	measurement		Kmax	Kint	Kmin	Kmean
SL2.8.1	1	D	67.8	226.6	137.3	-0.56
pisolite		I	79.2	10.2	-3.9	
back reef	2	D	331.7	133.1	225.5	
facies		I	67.7	21.2	6.5	
	summary	D	359.1	181.5	181.3	
		I	78	22.3	1.8	
		N	2	2	2	
				st. dev.		
		L	0.7471	0.1138		
		P	0.6836	0.1108		
		F	0.9143	0.0091		
		q	1.1216	0.172		

sample	measurement		Kmax	Kint	Kmin	Kmean
SL2.9.1	1	D	249.7	88.9	15.5	-0.19
pisolite		I	54.1	34.2	27.6	
back reef	2	D	273.6	169	31.1	
facies		I	21.5	32.3	49.5	
	summary	D	264.4	129.5	22.1	
		I	38.4	40.6	38.8	
		N	2	2	2	
				st. dev.		
		L	0.4885	0.252		
		P	0.3663	0.1007		
		F	0.8035	0.2083		
		q	1.1109	0.8884		

Appendix 4.2; repeat (Minisup) measurements

sample	measurement		Kmax	Kint	Kmin	Kmean
RA1.1.1	1	D	300.4	86.4	195.8	-0.33
Azotea dolomite		I	38.6	46.1	17.6	
shelf	2	D	303	173.7	46.3	
facies		I	26	52.3	25.2	
	3	D	297.7	120.9	28.5	
		I	29.2	60.8	1.3	
	4	D	47.7	165.4	272.7	
		I	36.8	31.3	37.1	
	5	D	67.4	170.9	269	
		I	50.9	10.8	37.1	
	summary	D	333.7	149.3	316.8	
		I	51.7	45.5	62.3	
		N	5	5	5	
		A95	51.7	34.1	90	
				st. dev.		
		L	0.5522	0.2959		
		P	0.407	0.1357		
		F	0.8031	0.1551		
		q	1.019	0.7502		

sample	measurement		Kmax	Kint	Kmin	Kmean
RA1.2.1	1	D	32.5	135.4	285.7	0.1
Azotea dolomite		I	15.2	39.4	46.7	
shelf	2	D	177	66.8	289.2	
facies		I	22.8	39.3	42.1	
	summary	D	88.5	131.8	281.5	
		I	42.2	35.6	48	
		N	2	2	2	
				st. dev.		
		L	1.2081	0.0365		
		P	4.3809	2.2673		
		F	3.6667	2.022		
		q	0.2743	0.0811		

sample	measurement		Kmax	Kint	Kmin	Kmean
RA1.4.1	1	D	279.7	105.5	13.3	0.18
Azotea dolomite		I	51.4	38.5	2.8	
shelf	2	D	285.3	55.7	184.6	
facies		I	23.9	55.8	23.1	
	3	D	76.3	290.6	177.2	
		I	31.9	53	16.8	
	4	D	198.2	47.9	294	
		I	25.2	61.5	12.4	
	5	D	167.9	52	260.7	
		I	9.1	69.9	17.7	
summary		D	210.4	56.4	248	
		I	57.2	69.3	35.4	
		N	5	5	5	
		A95	85.6	33.6	90	
				st. dev.		
		L	1.4649	0.2962		
		P	4.3278	2.5251		
		F	2.8278	1.1982		
		q	0.5627	0.2624		

Appendix 4.2; repeat (Minisup) measurements

summary of sample directions derived from thermal demagnetisation

M 1

sample	N	range		SI	kappa	A95	DA	dec	Inc
1.1	7	20	330	1.6	53	8.4	4.2	347	61
1.3	3	190	280	2.8	570	3.2	5.6	317	63
2.1	5	100	280	2.5	223	5.1		25	75
	3	380	480				4	306	60
3.1	10	20	480	1.6	36	8.1		31	74
4.1	10	100	530	3.2	152	3.9	4.2	346	50
5.1	3	190	280	2.2	361	6.5		322	50
6.1	10	20	480	1.4	27	9.4		317	70
7.1	8	20	380	1.4	35	9.4		40	81
8.1	3	20	150	1.7	141	10.4		338	76
	3	190	280				8.9	352	69
8.2	3	150	240	2.5	468	5.7		314	66
9.1	3	100	190	3.1	705	4.6		327	58
10.1	4	100	240	4.7	1026	2.9		356	58
	6	150	380				5.6	350	55
11.1	9	100	480	2	71	6.2		322	50
	10	100	530				5.6	353	49
13.1	4	100	240	3.1	144	6.4		348	65
13.2	3	100	190	2.3	390	6.3		27	78
14.1	3	100	190	3.6	960	4		1	68
	3	150	240				0.8	354	61
14.2	5	190	280	3.8	497	3.4		325	69
15.1	8	100	430	2.4	112	5.3		0	64
	3	240	330				1.4	324	37
16.1	6	100	330	2.9	243	4.3		3	65
	3	150	240				4.6	29	64
17.1	7	100	380	2				306	73
	3	150	240				3.4	7	69

M 2

sample	N	range		SI	kappa	A95	DA	dec	Inc
1.1	3	20	170	2.5	274	7		352	68
3.1	3	20	170	1.8	136	11		19	55
4.1	3	20	170	1.1	54	17		0	64
	3	210	320				9.4	300	6
6.1	4	20	250				1.6	93	37
11.1	6	150	400				1.8	95	-2

not including 3 samples

M 3

sample	N	range		SI	kappa	A95	DA	dec	Inc
1.1	3	20	390				2.7	171	3
3.1	3	26	390				8	113	-11
	3	0	170				6	311	78
6.1	5	20	450				4.8	214	29
7.1	3	240	150				6	74	25
9.1	3	20	150				6	303	21

not including 9 samples

appendix 5.1

M 4

sample	N	range		SI	kappa	A95	DA	dec	inc
4.1	5	20	260	2.8	210	5.3	9	224	-4
10.1	5	20	250	1.7	86	8.3		293	34
11.1	6	20	300	3.1	231	4.4		347	51
13.1	3	20	150	2.8	386	6.3		253	3
14.1	5	20	250	2.7	208	5.3		291	4
14.2	4	20	200	1.2	52	12.9		288	-11
16.2	5	20	250	1.1	32	13.6		286	-9

not including 5 samples

M 5

sample	N	range		SI	kappa	A95	DA	dec	inc
3.1	4	20	190	1.5	84	10.1		23	53
	3	20	150				4.2	10	39
7.1	3	20	150				4.9	7	39
10.1	3	20	150				3.6	349	45
12.1	3	20	150				5.5	3	48
15.1	3	20	150				8.4	65	81
18.1	3	20	150				1.3	3	55

not including 4 samples

M 6

sample	N	range		SI	kappa	A95	DA	dec	inc
1.1	8	20	240	3.2	167	4.3	<6	120	-10
2.1	8	20	430	6.4	662	2.2	<3	110	-13
3.1	8	20	430	4	252	3.5	<2	115	-9
6.1	7	20	390	3.8	244	3.6	<2	112	-17
7.1	4	20	400	2.4	100	9.2	<4	96	-19
8.1	4	20	400	3.7	238	6	<1	110	-30
9.1	3	20	300	5.5	703	4.7	<1	103	-19
13.1	6	20	500	2.3	73	7.9	<1	101	-18
14.1	6	20	500	1.3	24	14.1	<8	87	-30

not including 1 sample

M 8

sample	N	range		SI	kappa	A95	DA	dec	inc
1.1	3	190	280	1.3	117	11.5		343	22
2.1	5	100	280	1.2	55	10.4		16	51
	3	20	150				6	76	43
3.1	9	20	430	1.1	19	12.4		353	40
8.1	3	100	190	2.2	356	6.5		10	14

not including 8 samples

M 9

sample	N	range		SI	kappa	A95	DA	dec	Inc
1.1	4	20	210	1.4	64	11.6		22	80
2.1	6	20	320	1	23	14.3		212	72
3.1	4	20	210	2.6	225	6.1		18	59
	3	260	390				4	98	33
4.1	6	20	300	1.2	32	12.1		141	68
6.1	9	20	500	1.8	44	7.8		237	81
7.1	7	20	400	1.8	56	8.1		302	63
8.1	3	20	200	6.1	1366	3.3		180	3
9.1	9	20	500	5.5	415	2.5		203	49
10.1	9	20	500	5.8	466	2.4		163	-28
12.1	9	20	500	4.6	290	3		171	-32

not including 2 samples

M 10

sample	N	range		SI	kappa	A95	DA	dec	Inc
1.1	7	20	390	1.3	29	11.4	<5	202	29
	3	20	170				4.5	327	72
3.1	10	20	150	1.4	25	9.8	<3	328	42
4.1	4	110	260	5.7	1425	2.4	<3	339	37
5.1	8	20	430	1.7	47	8.2	<7	340	32
6.1	3	300	400	5.2	1803	2.9		268	64
7.1	4	20	350	5.2	544	3.9	<4	303	62
8.1	4	20	350	5.5	609	3.7	<4	345	35
9.1	6	20	450	4.7	333	3.7		346	41
11.1	6	20	450	7.5	864	2.3		358	42
12.1	7	20	500	8.4	935	2.2		1	56
13.1	7	20	500	3.4	159	4.8		304	53
14.1	6	20	450	5	375	3.5		12	53
15.1	6	20	450	10.2	1601	1.7		17	59
16.1	3	20	300	19.1	8560	1.3		82	54

M 11

sample	N	range		SI	kappa	A95	DA	dec	Inc
1.1	3	20	150	2.3	270	7.5		178	83
	3	190	280				3.6	292	85
3.1	3	20	240	1.2	43	11.9		255	47
	3	280	380				2.6	253	18
4.1	4	20	240	2.3	164	6		337	31
7.1	3	20	150	2.1	216	8.4		232	50
	3	280	380				7.7	297	35
8.1	4	20	190	2.3	210	6.4		213	53
	3	190	280				6.8	229	53
12.1	4	20	190	1.2	52	12.8		235	68
13.1	4	20	190	1.7	208	8.7		131	77
14.1	4	20	190	1.5	84	10.1		178	69

not including 2 samples

M12

sample	N	range		SI	kappa	A95	DA	dec	inc
3.1	4	100	240	1	44	14		18	39
9.1	4	100	240	2.5	288	5.4		218	30
10.1	5	20	240	3	265	4.7		259	-13
	3	330	430				8.5	252	-11
11.1	3	100	190	3.3	814	4.3		223	-7
	4	150	280				6	212	-7
12.1	4	100	240	1.4	98	9.3		245	31
13.1	6	100	330	2.7	233	5.1		228	46
	3	190	280				3.7	233	47
14.1	4	20	190	1.4	79	10.4		263	23

not including 5 samples

M13

sample	N	range		SI	kappa	A95	DA	dec	inc
2.1	5	20	260	1.6	74	9	<4	48	-54
3.1	10	20	530	1.2	20	11.1		215	-35
5.2	4	20	210	2.2	173	7		199	-36
6.1	10	20	530	1.1	17	12.2	<4	199	-27
7.1	3	20	200		61	15.9		180	-48
9.1	4	20	300	1.9	10	25.3		190	-20
10.1	3	20	200	3.6	466	5.7		182	-36
12.1	3	20	200	3.5	444	5.9	<6	189	-36
14.1	3	20	200	1.8	117	11.5	7	185	-7
15.1	4	20	300	1.4	49	13.3		204	-21
	7	20	450				2	197	-31

not including 2 samples

M13A

sample	N	range		SI	kappa	A95	DA	dec	inc
1.1	3	170	260	2.2	346	6.6		69	6
2.1	3	210	320	2.6	404	6.1		51	34
3.1	6	170	430	3	222	4.5		54	17
4.1	5	110	320	2.4	186	5.6		57	15
5.1	6	20	350	2.2	98	6.8		60	17
7.1	6	100	400	1.6	54	9		63	6
8.1	5	20	300	2	94	7.9		55	15
9.1	5	20	300	1.2	35	13		56	30
10.1	5	20	300	1.1	26	15		59	19
12.1	3	100	250	2	171	9.7		61	11
13.1	8	20	450	1.8	52	7.8		63	6
14.1	8	20	450	1.6	37	9.3		54	6
14.2	7	20	400	2	71	7.2		44	24
16.1	6	20	350	1.4	38	11		39	17

M14

sample	N	range		Sl	kappa	A95	DA	dec	Inc
2.1	4	240	380	19.4	17574	0.7		269	41
	5	430	585				1.1	272	40
3.1	4	240	380	15.8	11694	0.8		308	16
	3	480	585				0.4	309	17
4.1	6	190	430	16.2	7192	0.8		342	-5
	4	480	585				0.8	338	-1
5.1	3	240	330	26.2	49932	0.6		242	44
	4	480	585				0.2	244	43
6.1	3	240	330	25.3	46603	0.6		260	28
	7	280	585				1.8	260	28
8.1	4	240	380	14.3	9620	0.9		252	35
	4	330	480				1.8	244	35
10.1	5	280	480	9	2672	1.5		322	-7
	4	430	585				1.3	323	-8
11.1	4	240	380	12.7	7508	1.1		8	-6
	5	330	530				1.8	9	-5
12.1	3	280	380	24.8	40330	0.6		248	38
	6	380	585				1.7	248	37
12.2	7	190	480	17.2	6707	0.7		246	27
	4	430	585				1.5	247	26
13.1	4	240	380	12.8	7729	1		276	8
	3	430	530				0.5	276	7
14.1	5	190	380	14.9	7682	1.2		287	-12
	3	430	530				3.7	293	-9
15.1	4	240	380	9	3822	1.5		345	-45
	7	240	530				4.8	338	-48
17.1	7	20	330	5.5	635	2.4		256	-7
	5	430	585				1.3	257	-10
18.1	4	190	330	17	13501	0.8		239	-22
	10	190	585				2.7	239	-22
18.2	6	240	480	5.7	889	2.2		268	-47
	5	430	585				1.9	268	-50
19.1	4	330	480	17.8	13919	0.8		227	-5
	11	150	585				3.2	229	-5
20.1	3	330	430	23.3	35545	0.7		262	-21
	4	430	585					231	-21

M15

sample	N	range		SI	kappa	A95	DA	dec	Inc
1.1	3	20	170	3.9	671	4.8		249	27
2.1	7	20	390	2.1	80	6.8		250	37
3.1	3	110	210	3	595	5.1		258	32
4.1	3	210	320	3.7	832	4.3		252	29
4.2	4	20	300	5.1	616	3.7		250	36
5.1	6	20	400	2.3	44	6.9		266	43
7.1	4	20	300	1.8	77	10.5		261	50
8.1	6	20	400	3.6	227	4.5		256	43
9.1	4	20	300	2.6	163	7.2		263	54
11.1	7	20	450	1.5	33	10.7		261	40
12.1	3	20	200	7.9	2287	2.6		261	64
12.2	7	20	450	1.5	33	10.7		257	59
13.1	7	20	450	1	15	15.8		246	44
14.1	3	20	200	1.5	77	14.1		311	70

M19

sample	N	range		SI	kappa	A95	DA	dec	Inc
2.1	3	190	280	1.2	106	12.1		359	-31
3.1	3	20	150	1	47	18.1		97	76
	3	100	190				7.1	84	19
7.1	3	20	150	1.2	75	14.1		10	39
9.1	3	20	150	1.7	151	10.1		12	75
11.1	3	20	150	1.7	143	10.3		14	74

not including 10 samples

M20

sample	N	range		SI	kappa	A95	DA	dec	Inc
1.1	4	20	210	2.1	158	7.3		269	60
2.1	6	20	320	3.8	308	3.8		167	-48
4.1	10	20	530	1.9	47	7.1		182	-46
5.1	4	20	250	1.6	70	11.1		150	-14
6.1	9	20	500	2	57	6.9		170	-64
7.1	4	20	250	3.8	413	4.5		258	61
8.1	5	150	350	2.5	202	5.4		181	-47
9.1	8	20	450	3.5	185	4.1		173	-57
12.1	8	20	450	5.1	394	2.8		173	-47
13.1	10	20	550	2.4	70	5.8		167	-54
14.1	10	20	550	3.7	169	3.7		176	-42

M22

sample	N	range		SI	kappa	A95	DA	dec	Inc
1.1	5	100	280	1.8				9	48
2.1	5	20	240	1.6				63	52
3.1	4	20	190	1.5				8	32

M23

sample	N	range		SI	kappa	A95	DA	dec	Inc
5.1	3	20	150				4.8	6	62
6.1	3	20	150				5.1	357	57
7.1	3	100	200	1.9	224	8.2		184	2
8.2	3	20	200				5.3	32	75
11.2	3	20	150				3.9	5	65
12.1	5	20	150				6	358	65

not including 10 samples

M24

sample	N	range		SI	kappa	A95	DA	dec	Inc
1.1	3	20	150	2.9	418	6		1	56
	3	240	330				8.4	68	50
3.1	3	150	240	1.5	161	9.7		239	38
4.1	3	20	150	1.2	74	14.5		335	47
	3	190	280				7	323	0
5.1	4	20	190	1.8	114	11.6		341	36
	3	100	190				6.5	11	48
6.1	3	20	150	3.3	554	5.2		18	68
	3	100	190				8.5	95	45
7.1	4	20	190	2.8	295	5.4		13	43
	3	20	150				3.9	347	35
8.1	3	20	150				8.1	2	49
10.1	4	20	190	1.5	82	10.2		315	59
	4	20	190				6.1	347	47
11.1	3	20	150	1.6	125	11.1		315	42

M25

sample	N	range		SI	kappa	A95	DA	dec	Inc
1.1	6	20	320	1.4	44	1.02		33	-30
2.1	6	20	320	1.6	58	8.9		22	-32
4.1	6	110	390	2.5	144	5.6		15	-27
5.1	7	20	390	2.2	89	6.4		11	-28
6.1	5	20	350	1.8	68	9.4		12	-36
7.1	3	20	200	2.5	225	8.2		36	-40
8.1	5	20	350	1.6	50	11		15	-28
9.1	6	20	400	1.4	33	11.9		9	-34
10.1	7	20	450	1	15	16		6	-27
11.1	5	20	350	2.7	149	6.3		30	-37
12.1	4	150	350	2.5	203	6.5		10	-33
13.1	7	20	450	1.4	32	10.9		46	-31
14.1	3	20	200	1.2	50	17.6		41	-24

M26

sample	N	range		SI	kappa	A95	DA	dec	Inc
2.1	5	20	240	4	262	4.1		1	55
3.1	4	190	330	1.3	84	10.1		46	26
5.1	3	100	190	1.5	163	9.7		22	37
5.2	5	20	240	1	35	13.6		13	64

not including 5 samples

M27

sample	N	range		Sl	kappa	A95	DA	dec	inc
1.1	3	150	240	2	293	7.2		153	70
	3	430	530				3.1	137	-20
1.2	3	100	190	5.5	2180	2.6		170	49
2.1	5	100	280	2.3	190	5.6		165	74
	6	150	380				6.8	172	71
3.1	5	100	280	1.2	50	11		173	83
	3	190	280				7.9	185	35
4.1	5	100	280	1.7	110	7.3		173	74
	3	280	380				5.9	187	79
5.1	3	100	190	1.7	199	8.8		184	86
	3	20	150				2.4	30	55
7.1	3	100	190	2.9	211	5		173	67
	3	100	190				6	166	62
8.1	5	100	280	2.3	191	5.6		161	63
	4	150	280				7.4	170	59
9.1	6	100	330	5.1	752	2.4		159	70
	3	100	190				7.3	166	70
10.1	3	100	190	4.2	1266	3.5		161	60
	3	20	150				4	19	51
12.1	3	100	190	7.6	4178	1.9		176	64
	3	330	430				2.7	173	78
13.1	5	100	280	2.5	227	5.1		167	61
	3	20	150				2.2	28	52
14.1	5	100	280	3.6	466	3.5		201	79
	3	20	150				0.5	12	51
15.1	4	240	380	2	188	6.7		184	61
	3	100	190				1.4	8	60
16.1	4	150	280	1.9	178	6.9		167	65
	3	100	190				1.9	19	57
17.1	5	150	330	4.7	801	2.7		171	75
	4	150	280				5.4	151	76

L1

sample	N	range		SI	kappa	A95	DA	dec	inc
2.1	3	20	150	1.6	137	10.6		12	35
4.1	3	20	150	2.3	257	7.7		4	40
	4	100	240				8.2	356	54
5.1	3	150	240	2.6	496	5.5		15	17
	3	150	240				3.8	17	23
6.1	3	20	150	3.4	600	5		16	45
	3	100	190				3.3	26	50
7.1	5	240	430	4.2	602	3.1		4	23
	12	100	585				6.6	3	32
9.1	4	240	380	4	1172	3.6		7	22
	4	280	430				1.8	10	29
10.1	3	190	280	4.6	1547	3.1		15	15
	3	330	430				3.1	11	24
13.1	3	20	150	2.1	226	8.2		0	43
	3	100	190				3.8	347	50
14.1	5	150	330	2.2	182	5.7		7	18
	3	100	190				2.5	6	39
15.1	4	150	280	3.5	614	3.7		3	26
	5	20	240				5.2	350	40
16.1	5	150	330	2.4	209	5.3		9	14
	4	100	240				6	3	34
18.1	5	150	330	2.3	189	5.6		0	16
	4	100	240				4.2	0	38
20.1	4	150	280	2.3	268	5.6		5	19
	4	100	240				4.3	1	37
21.1	5	190	380	2.8	268	4.7		356	8
	4	100	240				2.7	347	41
22.2	3	150	240	6	2628	2.4		352	23
	3	100	190				4.5	358	39

BC1

sample	N	range		SI	kappa	A95	DA	dec	inc
1.1	3	260	390				8.7	146	20
	3	20	170				8.9	34	43
2.2	3	260	390				5.7	158	29
	3	20	170	1.2	65	23		27	54
3.1	3	260	390				7.1	107	-12
	5	20	260				6.1	18	46
4.1	3	260	390				7	149	18
6.1	4	250	300	1	40	15		150	19
19.1	3	150	250	1.1	83	14		62	-21

not including 4 samples

CC1

sample	N	range		SI	kappa	A95	DA	dec	Inc
1.1	3	20	170	2.7	330	6.8		119	62
	3	20	170				6.2	130	55
1.3	4	20	210	1.5	74	11		115	59
2.2	3	20	170	2.1	9	9		115	46
3.3	3	20	170	2.4	242	7.9		117	57
4.1	5	20	300	1.4	44	11.7		136	66
4.3	5	20	300	1.7	66	9.5		139	68
7.1	3	20	200				8	14	57
7.2	3	150	250				9.8	59	36
8.2	3	20	200				8.1	351	54
10.3	3	150	250				5.3	80	12
12.2	3	20	250				9.7	116	-8

not including 8 samples

AF demagnetisation data mT

sample	N	range		SI	kappa	A95	DA	dec	Inc
M2.14	3	40	60				1.7	271	-7
M3.15	3	0	10				7.9	232	-9
M3.16	3	5	20				4	349	37
M4.17	3	5	20				3.2	310	-31
M4.18	3	5	20				9.5	293	7
M6.17	4	0	20	1	347	4.9		113	-12
	4	10	40				1	114	-19
M6.18	3	50	70	1.1	376	6.4		37	30
	4	0	20	0.8	210	6.4		103	-14
	3	10	30				0.7	109	-20
M9.15	3	60	100	2	657	4.8		316	84
	3	70	100				1.9	300	85
M9.16	3	5	20				4.5	42	55
M10.17	4	0	20	3.9	6223	1.6		105	40
	6	10	60				1.9	108	37
M10.18	4	5	30	1.6	691	3.5		108	53
	7	10	70				2.4	111	50
M13A.6	3	0	10				2.7	50	7
M13A.11	8	10	100	1.4	146	4.6		358	51
	3	0	10				5	74	-6
M15.15	3	10	30				5.3	298	48
M20.11	10	0	100	1.2	97	4.9		173	-42
	3	70	100				9.2	164	-45
	3	30	50				5	205	-5
M20.20	3	60	100	1.8	506	5.5		164	-35
	3	70	100				3.9	163	-35
	3	40	60				6.1	76	4
M23.14	7	0	50	0.9	115	5.7		348	51
M23.17	4	20	50	2.5	1365	2.5		12	60
M25.15	3	10	30				4.8	56	-37
	3	0	10				0.3	174	39
BC1.11.1	3	0	10				5	212	63
BC1.11.2	3	0	10				4.6	156	60
CC1.18.2	3	10	30				7.7	349	68
	3	0	10				7.9	315	42

declination	inclination	intensity
329	-59	0.03
274	41	0.04
137	57	0.05
254	10	0.06
253	-31	0.06
192	52	0.03
108	-33	0.03
74	-62	0.04
236	-83	0.02
71	71	0.02
66	-8	0.04
285	-23	0.03
162	70	0.07
15	-32	0.04
180	47	0.04
111	-34	0.03
10	-45	0.06
171	45	0.06
49	-36	0.03
358	-8	0.05
131	46	0.07
97	29	0.03
41	-17	0.02
23	33	0.01
194	-9	0.02
123	41	0.04
57	11	0.04

declination	inclination	intensity
49	-60	0.08
299	81	0.02
219	-53	0.04
337	-32	0.03
114	75	0.06
332	33	0.03
257	48	0.03
-39	-39	0.07
206	24	0.04
225	70	0.06
225	-44	0.05
271	80	0.03
244	35	0.02
109	20	0.06
271	39	0.03
268	38	0.09
237	-37	0.01
98	43	0.05
315	-68	0.05
239	35	0.09
201	48	0.03
196	52	0.03
90	50	0.04
114	40	0.04
286	4	0.05
83	56	0.08

appendix 5.2 Measurements on the cryogenic magnetometer of an empty sample holder

Appendix 5.3a

	BC1.1.1	
declination	inclination	intensity
147	37	2.04
146	38	1.99
148	41	2
144	39	1.97
145	40	2.02
147	39	2.03
150	43	1.99
143	43	1.98
147	42	2.05
147	43	1.96
	mean	n=10
146.4	40.5	mean=2.00
k=908	a95=1.6	s.d=0.03

appendix 5.3a 10 repeat measurements of natural remanent magnetism for one sample

sample	treatment (mT)	declination	inclination	intensity
BC1.11.1	50	230	46	0.57
		228	45	0.57
		231	47	0.61
BC1.11.2	50	241	51	0.38
		252	62	0.38
		234	69	0.28
CC1.17.2	50	162	-17	0.42
		157	-17	0.47
		159	-18	0.52
M4.18.2	60	184	38	0.13
		203	30	0.17
		201	48	0.17
		219	10	0.18
M6.17.1	60	244	63	0.3
		236	53	0.33
		231	59	0.38
		200	53	0.33
		203	46	0.27
		202	57	0.3
M6.18.1	60	314	51	0.67
		318	47	0.69
		303	51	0.67
		303	54	0.68
M9.15.1	60	203	65	2.07
		204	65	2.12
		184	63	1.74
		185	62	1.77
M9.16.1	60	1	68	1.9
		0	66	1.88
		3	67	1.85
		8	58	1.29
		7	58	1.27
M131.11.1	60	257	64	1.05
		262	67	1.09
		256	66	1.16
		254	64	1.11
M6.17.1	70	206	36	0.26
		194	42	0.22
		193	57	0.26

appendix 5.3b Repeat measurements of samples after AF demagnetisation